

# **Mineral Matter and Ash in Coal**



A C S   S Y M P O S I U M   S E R I E S   **301**

# Mineral Matter and Ash in Coal

**Karl S. Vorres**, EDITOR  
*Argonne National Laboratory*

Developed from a symposium sponsored by  
the Division of Fuel Chemistry  
at the 188th Meeting  
of the American Chemical Society,  
Philadelphia, Pennsylvania,  
August 26-31, 1984

Publication Date: April 2, 1986 | doi: 10.1021/bk-1986-0301.fw001



American Chemical Society, Washington, DC 1986



### Library of Congress Cataloging-in-Publication Data

Mineral matter and ash in coal.  
(ACS symposium series, ISSN 0097-6156; 301)

“Developed from a symposium sponsored by the Division of Fuel Chemistry at the 188th meeting of the American Chemical Society, Philadelphia, Pennsylvania, August 26-31, 1984.”

Bibliography: p.  
Includes index.

I. Coal—Analysis—Congresses.

I. Vorres, Karl Spyros, 1937- . II. American Chemical Society. Division of Fuel Chemistry. III. Series.

TP325.M567 1986 662.6'22 86-3556  
ISBN 0-8412-0959-6

Copyright © 1986

American Chemical Society

All Rights Reserved. The appearance of the code at the bottom of the first page of each chapter in this volume indicates the copyright owner's consent that reprographic copies of the chapter may be made for personal or internal use or for the personal or internal use of specific clients. This consent is given on the condition, however, that the copier pay the stated per copy fee through the Copyright Clearance Center, Inc., 27 Congress Street, Salem, MA 01970, for copying beyond that permitted by Sections 107 or 108 of the U.S. Copyright Law. This consent does not extend to copying or transmission by any means—graphic or electronic—for any other purpose, such as for general distribution, for advertising or promotional purposes, for creating a new collective work, for resale, or for information storage and retrieval systems. The copying fee for each chapter is indicated in the code at the bottom of the first page of the chapter.

The citation of trade names and/or names of manufacturers in this publication is not to be construed as an endorsement or as approval by ACS of the commercial products or services referenced herein; nor should the mere reference herein to any drawing, specification, chemical process, or other data be regarded as a license or as a conveyance of any right or permission, to the holder, reader, or any other person or corporation, to manufacture, reproduce, use, or sell any patented invention or copyrighted work that may in any way be related thereto. Registered names, trademarks, etc., used in this publication, even without specific indication thereof, are not to be considered unprotected by law.

PRINTED IN THE UNITED STATES OF AMERICA



# ACS Symposium Series

## M. Joan Comstock, *Series Editor*

### *Advisory Board*

**Harvey W. Blanch**  
University of California—Berkeley

**Alan Elzerman**  
Clemson University

**John W. Finley**  
Nabisco Brands, Inc.

**Marye Anne Fox**  
The University of Texas—Austin

**Martin L. Gorbaty**  
Exxon Research and Engineering Co.

**Roland F. Hirsch**  
U.S. Department of Energy

**Rudolph J. Marcus**  
Consultant, Computers &  
Chemistry Research

**Vincent D. McGinniss**  
Battelle Columbus Laboratories

**Donald E. Moreland**  
USDA, Agricultural Research Service

**W. H. Norton**  
J. T. Baker Chemical Company

**James C. Randall**  
Exxon Chemical Company

**W. D. Shults**  
Oak Ridge National Laboratory

**Geoffrey K. Smith**  
Rohm & Haas Co.

**Charles S. Tuesday**  
General Motors Research Laboratory

**Douglas B. Walters**  
National Institute of  
Environmental Health

**C. Grant Willson**  
IBM Research Department

# FOREWORD

The ACS SYMPOSIUM SERIES was founded in 1974 to provide a medium for publishing symposia quickly in book form. The format of the Series parallels that of the continuing ADVANCES IN CHEMISTRY SERIES except that, in order to save time, the papers are not typeset but are reproduced as they are submitted by the authors in camera-ready form. Papers are reviewed under the supervision of the Editors with the assistance of the Series Advisory Board and are selected to maintain the integrity of the symposia; however, verbatim reproductions of previously published papers are not accepted. Both reviews and reports of research are acceptable, because symposia may embrace both types of presentation.

## PREFACE

**M**INERAL CONSTITUENTS OF COAL and the changes these minerals undergo on heating in different environments are of scientific and commercial interest. This interest warrants a thorough discussion of the nature of mineral matter in coal.

This volume is the product of a symposium given at the 188th National Meeting of the American Chemical Society. As is probably the case for many symposia, the symposium upon which this book is based came as a result of a number of discussions among some of the session chairmen and the symposium chairman over a period of years. Many of the Division of Fuel Chemistry's symposia dealt with a number of aspects of coal, but none in recent memory have dealt with the mineral matter in a comprehensive manner. This significant constituent affects almost every application of this abundant resource. From these thoughts came an interest in developing a symposium that would cover all of the important aspects in sufficient detail so that the current thinking in the field could be reasonably represented. In addition, it was intended that the whole subject be developed in a logical manner, assuming that there is a logical manner.

With these goals in mind, the matter of organizing individual sessions led to the approach of inviting a speaker to provide an introduction to each session, such that the novice in this part of the symposium activity could be quickly introduced to the area and be able to follow the talks in that session. The speakers that followed would then talk about particular topics of significance.

The sequence of session topics was chosen to be similar to that which could be used in a text on the subject of the chemistry of mineral matter and ash in coal. An introductory session described what the mineral matter is, where mineral matter comes from, the chemical constituents that are present, the manner in which the constituents vary among the different coal deposits, and the special nature of some of the deposits, such as volcanic materials.

The second session dealt with the effects of high temperatures on mineral matter and the conversion of that material to a variety of forms dependent on the temperature and history, such as slag, deposits, fly ash, or just ash. This session was intended to deal with the observations of the properties at high temperatures in the laboratory and the efforts to correlate these observations with some knowledge of the composition of the mineral matter or ash.

The third session dealt with efforts to reverse the perspective and begin with the materials that are present in the mineral matter and then try to predict the behavior that would be observed. A wide range of properties are of interest, and a number of papers covered thermodynamic properties and also the physical properties related to flow and thermal effects such as conductivity.

The fourth session looked at the question "What does the owner or operator of large equipment that consumes coal observe because of the mineral matter?" Because most of the coal consumed in the United States is used to generate steam in electric power generation facilities, the major purpose of the coal is to provide heat energy in boilers. The problems are associated with the accumulation of deposits on the walls or tubes inside the boiler. In some cases these materials are hot and flow from the walls as a slag, whereas in other cases the mineral matter undergoes a series of changes leading to the formation of deposits on the tubes.

The fifth session looked at the possibility that there may be some desirable aspects associated with the mineral matter in the coal. The mineral matter may be a catalyst for some of the current or future uses of coal. Specifically, the mineral matter could have some effect on combustion and also on future synthetic fuels efforts that could provide either gaseous or liquid fuels.

The final session responded to the question "If the mineral matter is in the coal, what can be done to remove the mineral matter?" This session dealt with a number of techniques to physically remove the mineral matter in processes called coal cleaning. These processes involve crushing and in some cases pulverizing to fine and even ultrafine sizes to permit the liberation of the mineral matter from the coal. An efficient separation requires removal of mineral matter with a minimum removal of the desirable combustible material.

One of the goals for this volume is to provide the type and quality of chapters that will endure or stand the "test of time" such that the book will be cited for years to come. It is hoped that the efforts that have gone into this work will achieve this goal.

As in any large undertaking such as this book, many people are involved. Expressions of thanks and appreciation go to many who helped plan the individual sessions, the session chairmen. Each of the authors deserves thanks for contributing to the individual presentations and to the further revisions that led to the chapters in this book. Thanks also go to the many reviewers who read and commented on the manuscripts to bring out additional points for the clarity and improved quality of the manuscripts. The American Chemical Society staff have been very helpful in their many ways.

Acknowledgment is made to the donors of The Petroleum Research Fund, administered by the American Chemical Society, for partial travel support for K. C. Mills and Erich Raask.

Additional thanks go to Beth Mustari and the late Katherine Archambeault for their typing assistance. My wife, Nancy, deserves appreciation for patience through many hours of paperwork with less than the usual attention that she is accustomed to having. Last, and by no means least, I thank the U.S. Department of Energy, Office of Basic Energy Science, Chemical Sciences Division, whose support has made my participation possible.

KARL S. VORRES  
Chemistry Division  
Argonne National Laboratory  
Argonne, IL 60439

November 4, 1985

# Chemistry of Mineral Matter and Ash in Coal: An Overview

Karl S. Vorres

Chemistry Division, Argonne National Laboratory, Argonne, IL 60439

Coal contains significant and variable amounts of largely incombustible mineral matter. This mineral matter primarily includes clays, shales, pyrite, quartz, calcite and lesser amounts of other materials, depending on the chemical and mineralogical composition. It occurs in many forms and sizes, which may be seen by the naked eye or occur in micron-sized particles that require an optical or electron microscope to observe. Coal is usually burned in combustion equipment, liberating hot gases and also heating the mineral matter to temperatures of 2000°F and above. The different forms of the mineral matter can and do interact to bring about new chemical materials with a variety of properties. This volume describes the nature of the mineral matter, its occurrence, composition, sources, and the effects of heating this material in terms of the chemical and physical properties of mineral matter and deposits. These effects are observed both experimentally and in the operation of boilers and other coal utilization equipment. The properties may be predicted with suitable models and a certain amount of data from simpler systems. The deposition of mineral matter or ash in boilers is a major concern in the design of coal-burning equipment and the major reason for the forced outages of these units. Under certain conditions, there can be beneficial effects from certain kinds of mineral matter in the coal, and these are explored. Finally, there are approaches that can be taken to reduce the mineral matter content of the coal from the original values. The extent of the reduction depends on the nature of the coal, the need for reduction, and the premium price that can be obtained for the cleaned coal.

This volume is divided into six sections, corresponding to the six sessions in the Symposium on Chemistry of Mineral Matter and Ash in Coal presented to the Fuel Chemistry Division at the American Chemical Society National Meeting in Philadelphia in August, 1984. These six sessions were intended to provide a forum for the six major areas indicated above. Each section contains chapters dealing with the subject area. The nature of the mineral matter in coal is discussed in the first section. The second

section examines the experimental information available from a variety of high temperature measurements on the coal ash. By contrast, the third section examines the approaches to predict the properties of high temperature coal ash from a knowledge of the chemical composition and an understanding of the thermodynamics of these and similar systems. The fourth section looks at the problems caused by the mineral matter that are being experienced by the owners and operators of coal-burning equipment. These problems are primarily related to the deposition of coal ash and the interactions of the mineral matter to provide material of different compositions than the original mineral species. The fifth section examines the potential benefits derived from the presence of the mineral matter in the coal. Some of the species may catalyze certain coal conversion processes such as liquefaction. Other species, such as sodium, may catalyze combustion itself. Finally, since the mineral matter is generally not desired, a number of utilities are willing to pay a premium price to have the mineral matter content reduced. The closing section explores technology to remove the mineral matter from coal. Taken together these topics should provide an understanding of the nature of the mineral matter and ash. In addition the study provides insights into the current methods of dealing with the inorganic constituents of coal and suggests useful directions for further research.

The nature of the mineral matter in coal is discussed in the initial chapters. The mineral matter present in coal includes the mineral matter present in the living plants which were altered over time to produce the coal material. In addition, mineral matter has been added through the effects of subsidence and the subsequent addition of sedimentary material, and the accumulation of airborne dust or other inorganic material. Volcanic eruptions have contributed substantial mineral matter in limited areas. Furthermore, during the coalification process, water has usually percolated through the coal seams and provided additional mineral matter as well as altered the matter that was present.

The nature of the coal mining process is such that some of the floor and roof of the seam may be included in the product with normal use of the mining equipment. The mineral matter content can then vary depending not only on the material present in the coal but also depending on the material directly above or below the seam and the care taken in mining.

The effects of the mineral matter depend on the chemical and mineralogical composition. Many standard analytical techniques are available to quantify the elements present in the mineral species. These include silicon, aluminum, iron, calcium, magnesium, sodium, potassium, titanium and others. The elements are usually reported as oxides, because the oxide anion is the predominant one in fly ash. However, the mineral species are not usually simple oxides, but very frequently are tied up in the different mineral forms as more complex aluminosilicates or other species as indicated above. A variety of techniques is used to identify the mineral matter.

Usually low-temperature ashing (LTA) techniques are used to remove the combustible matter to provide a sample of mineral material which has undergone minimal change from that in the original coal. The LTA technique involves the use of a low-pressure, low-temperature oxygen plasma to oxidize the combustible material away from the grains of mineral matter in the coal. Even though this technique is the most gentle in common use, some changes have been observed in the mineral matter when LTA has been used. The presence of pyrite and calcite in the coal sample has led to the observation of some sulfated calcium species.

In the normal preparation of a coal ash sample for analysis, the coal is heated to 700-750°C for sufficient time to burn off the carbonaceous matter. These temperatures and times are sufficient to permit interaction among the more reactive species, and lead to changes from the materials which have been observed from LTA studies on the same coal.

Petrographic examination under the microscope can provide identification of the material, and can be complemented with techniques such as x-ray diffraction (XRD) to identify crystalline minerals. The quantitative measure of the relative amounts of the minerals is a somewhat controversial subject due to some of the limitations of the techniques. However the comparison of the results from a number of laboratories has led to the conclusion that no one XRD method is superior to all others. Repeated attempts to compare results between different laboratories has led to the consensus that the technique is semi-quantitative.

The types of mineral matter found in a particular deposit depend on the geography of the deposit. Those deposits found in the eastern part of the United States have mineral matter which is rich in clay, quartz and pyrite. As a result utilities which burn eastern higher-sulfur coals must now use equipment which can reduce the sulfur oxides which are released. The deposits in the western parts of the U.S. frequently have mineral matter characterized by high calcite and sodium and lower clay and pyrite contents. The low sulfur content and some inherent ability to capture liberated sulfur oxides with calcium compounds has led to the use of the low sulfur western coals for a growing part of the U.S. power generation market.

The composition of the mineral matter in a particular coal seam is affected by the geologic conditions surrounding the deposit. A marine, brackish or freshwater environment will alter the chemistry of the deposit and the nature of the mineral species which are found with the coal. Higher sulfur contents are usually associated with the presence of a marine environment during part of the coalification process.

The properties of coal ash reflect the changes that have taken place in the mineral matter through some heating process. As a result of heating the different mineral forms may have undergone decomposition (as with carbonates, hydrates), or solid-state



reaction (as quartz with other species to form silicates) or heterogeneous reaction (as pyrite with air to form iron oxides). The changes in chemical composition cause changes in the physical properties as well. The reactions do not all proceed at the same rate. In general the thermal decomposition reactions will proceed rapidly. The heterogeneous reactions proceed at an intermediate rate, which may vary with time if a layer with low permeability for the reacting gas is generated. The rate will decrease with time under these circumstances. The slowest reactions involve the conversion of two solid phases to some new material. This reaction proceeds through the diffusion of some mobile species across the interface between two adjacent particles. This reaction can be augmented by the formation of a liquid phase which can act as a solvent for a reactive species. The alkalis can be released if they are in an active form and act as a flux, or agent for the formation of a lower melting point phase. The reactions will proceed measurably faster under these conditions.

The melting properties and viscosity of molten coal ash have been the subject of continuing work. They are not a simple function of the composition. The properties are used in attempting to predict the problems that might be encountered with a particular coal in an operating boiler with a specific design. A number of correlations have been developed, but have had limited application. One of the problems has been a lack of complete understanding of the role of the acids and bases. These terms are used in many of the correlations of the melting behavior with composition of the coal ash.

The acids include the oxides of silicon, aluminum and titanium. The bases include the oxides of iron (iron is mostly present as basic  $\text{FeO}$ ), calcium, magnesium, sodium and potassium. Taken together these elements make up virtually all of the cations found in the high temperature mineral matter. The molten coal ash is a polymer of the acidic species silica and alumina. The average molecular weight of the polymeric species depends on the presence of chain terminating species or bases. The terminating species is the oxide ion associated with the base. The viscosity depends on the average molecular size of the polymer. For example the addition of a base to an acidic eastern coal ash will reduce the viscosity over a period of time as the polymeric species are gradually reduced in size.

A reasonably complete understanding of the behavior of molten slags also requires an understanding of the composition, gaseous environment (oxidizing or reducing), loss of volatile species, existence of several immiscible liquid phases, thermal history and interaction with the container.

Workers are developing the theoretical understanding of the behavior of molten coal ash systems. This activity proceeds from a consideration of the energy effects upon mixing the constituent oxides and a description of the non-ideal behavior of systems containing polymers of varying size. The models of polymer chemistry are being applied to these higher temperature systems.

The high temperature data available on coal slags is limited, and the work required to obtain additional data is expensive and time consuming. Therefore it has become more desirable to develop suitable models of high temperature behavior to avoid the time and cost involved in acquiring additional information. The models are needed for rapid estimation of properties and testing of operating strategies to permit continual operation of a boiler with new fuels or a fuel with varying mineral matter compositions.

The work done with coal ash involves silica-rich systems which are not unique to coal. The same types of materials are found in steel-making slags, volcanic magmas, and some fluxes, glasses and refractories. The behavior of these systems is, not surprisingly, similar to and consistent with the behavior of coal slags. The data on these systems may then be used to test models which have been developed for coal ash. Similarly the understanding of coal ash systems can be augmented by using models developed for these other materials. Work with fluxes demonstrates the ability of materials containing fluoride to form low-melting phases. This is consistent with the hypothesis of the base as an anion donor, and the ability of the anions to diminish the size of the silica-type polymer in melts containing these species.

Other work with volcanic magmas has demonstrated the significance of the crystallites which appear as the molten material cools. A sharp transition in the Arrhenius plot of log of viscosity versus reciprocal absolute temperature was observed as the volume of crystallites approached 30% of the total volume. This transition has been observed in coal ash systems. The composition of the solid phases or crystallites can be interpreted by comparison with phase equilibrium diagrams of related simpler systems.

The continuing efforts to generate electric power more efficiently have led to further studies of magnetohydrodynamic power generation. This approach involves the use of an ionizable vapor which is passed through a strong magnetic field at high velocities. The current produced in this way is used to augment normal steam generation. The efficiency depends on the amount of potassium vapor that can be maintained in the system in contact with the slag derived from the coal being burned. Studies of these slags have added to the understanding of the interactions of alkalis with slags.

The problems with the commercial use of coal are usually due to the mineral matter present in the coal. Over 80% of the coal used in the United States is burned in boilers to generate steam for electric power production. In the combustion process, the mineral matter is released and in a few seconds traverses the furnace and subsequent parts on the way to the smokestack. If most of the mineral matter has a relatively high ash fusion temperature, this material, termed flyash, moves through the furnace parts to some equipment designed to remove the fine particles. If the ash fusion temperature is not relatively high then the small particles

become soft and sticky. They can impinge on the walls and the tubes of the furnace cavity to produce deposits. The presence of the flyash and deposits reduces heat transfer and steam generation, impedes gas flow through the furnace cavity, causes physical damage to the parts, and corrodes as well as erodes internal parts of the furnace.

The problems with coal ash are most often associated with deposits in boilers. The sticky material may accumulate on the walls of the large furnace cavity. This process is usually referred to as slagging. The large furnaces have suspended tubes in them. Deposits form and grow on these tubes in a process called fouling. Sometimes these deposits grow to a point at which the operation of the boiler must be terminated, called a forced outage, for cleaning of the walls and/or tubes.

The accumulation of these deposits may be partially due to deformation and adhesion of soft, highly viscous particles as they impinge on hot metal surfaces. Studies have shown that an initial process involving the formation of a low melting phase on the surface of tubes provides a kind of glue which permits deposits to accumulate. The low melting materials that are associated with the formation of the initial layers include alkali sulfates and iron or aluminum sulfates. A succession of stages seems to be involved in the formation of the hard deposits which can not be easily removed. The presence of two immiscible liquid phases derived from oxide and sulfate materials has been observed, indicating multiple mechanisms for deposit formation.

A variety of techniques have been used to model the deposition processes. Frequently a small furnace will be built to provide controlled combustion and careful monitoring of the conditions. The coal is burned and the ash is allowed to impinge on tubes. The increase in deposit weight is noted as a function of time under different conditions. This approach has been helpful and is useful if variations in ash chemistry are the most significant variables. In some furnaces, the aerodynamics are also quite important and cannot usually be scaled. It is also possible to model the effects of impinging ash-like particles by substituting glasses of known fusion or viscosity properties for the coal ash type materials.

As was indicated above, the nature of the mineral species is quite important in determining whether a given coal will be difficult to burn continually in a particular boiler. The reactions between the species and the speed with which they can form new low melting phases, or release volatile species which can form low melting species, usually determine the severity of the problems.

To date, no universally accepted tool to predict fouling and slagging from coal ash compositions has been developed. Information about the performance of particular coals is frequently not widely available for a variety of reasons. When the information is available from both commercial and small scale studies then

correlations can be proposed between performance in the small and large scale equipment. The use of these correlations, when accurate, permit the designer or operator to avoid problems before they are allowed to occur. Statistical studies have been employed to establish which ones are the most important.

Coal ash is not always a deleterious material for a process. In coal liquefaction, it has been observed that the rate is increased in the presence of pyrite. In gasification, the rate is increased in the presence of alkalis. There is limited data available on the effects of materials on combustion. Although interest in synthetic fuels from coal is quite limited at present, there is an interest in developing the technical capability to permit the production of more premium fuel types from less desirable ones. The conversion of solid coal to liquid fuels has been a very demanding process in terms of the pressures and, to some extent, the temperatures that have been used. Catalysts have been required in all cases. The catalysts have been poisoned by the sulfur and other species in the mineral matter. As a result, catalyst costs and replacement rates can be quite high. A cheap, naturally occurring catalyst that came with the coal would be of significant interest. Pyrite seems to be such a material.

Finally, one can ask "What can be done to remove the mineral matter from the coal?" The answer is that several processes can be used to reduce the mineral matter. The extent and cost of removal usually dictate the cleaning process that is chosen. Generally, a large part of the coal that is mined for electric power production is "cleaned" or physically processed to remove part of the mineral matter by initially crushing the coal and then density separation of the coal from the mineral matter. This is especially true when the run-of-mine coal contains more than about 15% mineral matter. In the physical separation a dense fraction and light fraction, or several of these, are obtained. Since some combustible matter is present in the denser fractions, the process results in an energy loss. The quality of the separation also depends upon the differences in the surface properties of the coal and mineral matter as well as the density differences. The mineral species and clays can vary in such a way that the typical cleaning process steps apparently function inconsistently and reject a significant amount of combustible material with the mineral fractions. In order to minimize the loss, it is necessary to crush and grind the coal in such a way that there are particles of mineral matter free from attached coal. The complete separation usually requires grinding to smaller and smaller particle sizes. This concept has been carried to very fine grinding, capable of giving particles finer than 15 microns. Mineral matter separation has improved but becomes very sensitive to coal and mineral surface properties. Improved cleaning has yielded coal with ash concentrations of the order of a tenth of a per cent.

Coal cleaning is based on a knowledge of the mineral species that must be removed. The cleaning plant is a series of circuits that separate different fractions and provide for recombination of

certain ones to maximize the yield of a quality product, and minimize losses of combustible material. The performance of the circuits will change as the feed streams vary. The act of cleaning takes out some of the mineral matter, leaving a portion of the mineral matter yet to be removed. This remaining matter may be enriched or depleted in certain parts of the original matter and lead to performance different than that which would be expected on the basis of the original material. There is a need to remain aware of the composition of the different streams in the cleaning plant. The analytical techniques that have been used are difficult to carry out quickly enough and cheaply enough for easy modification of the circuits. Recently the technique of automated image analysis has been developed so that it may find application in solving this problem.

Chemical treatment of coal has also been used to further reduce the mineral matter content. Usually the physical techniques mentioned earlier are used to reduce the inorganic sulfur species (mostly pyrite) to a very low level. Since there is a great concern about the sulfur contents of coal, and the organic sulfur content exceeds the permissible standards for many high-sulfur coals, non-physical or chemical techniques have been tried to further reduce the sulfur content. Strong caustic reagents are used most often to remove the more refractory sulfur forms.

The removal of both mineral matter and sulfur species to very low values would provide premium solid fuels and possibly new chemical feedstocks. Several techniques are being explored to achieve these goals. The mineral matter in a physically cleaned coal can be further reduced by the solubilization of the aluminosilicate minerals. This can technically be accomplished with the use of alkaline and then acid treatments. A variety of studies are under way to define the conditions required for effective removal of the mineral matter and establish the amount of sulfur reduction that can be accomplished. Others involve the use of fine grinding to liberate the coal from the mineral matter. Then an agglomerant is used to separate the coal matter from the aqueous phase containing suspended mineral matter. A new approach uses microwave energy to selectively decompose the clays into species that can be solubilized and removed. Still another technique involves treatment with carbon dioxide to reduce the particle size and permit the liberation of the mineral matter. Over the next few years these will be studied further and it is hoped that coal will become available in a form with less of these interesting, but not entirely desirable mineral species.

It is hoped that this volume will serve as a further stimulus to workers in and outside of the field of coal mineral matter and ash chemistry. We all benefit from the work of others to extend our current knowledge and can help make coal not only an abundant fuel, but also a more convenient and desirable resource as well.

RECEIVED November 12, 1985

## Mineral Matter in Illinois and Other U.S. Coals

Richard D. Harvey and Rodney R. Ruch

Illinois State Geological Survey, Champaign, IL 61820

This review (1) describes and classifies the geological, physical, and chemical occurrences of mineral matters in coal; (2) summarizes analytical methods used to characterize the mineral matter; and (3) compares the mineral-matter composition of Illinois coals with that of other U.S. coals.

In Illinois coals the organic constituents generally vary vertically within seams by a factor of 2 to 3; many elements also vary laterally within the same seam. Similarly, variations are substantial from one seam to another within the Illinois Basin. There is a considerable overlap, however, in compositional ranges of coals from different U.S. basins. On a regional basis, the material variability of many elements, such as sulfur and chlorine, is the result of geological processes. Low-sulfur coals mined in many western states, southern West Virginia, southwestern Virginia, and eastern Kentucky underlie strata deposited from fresh water; whereas many high-sulfur seams underlie strata deposited from sulfate-bearing brackish or marine waters.

Because of the high variability of coal, samples from all prospective deposits need to be analyzed. Methods for analysis of inorganic elements in coal are generally precise, but methods for quantitative analysis of mineral phases need to be improved.

Mineral matter is generally considered to be the sum total of all inorganic minerals (discrete phases) and elements that are present in coal (1). Thus, all elements in coal except organically combined C, H, O, N, and S are classified by this definition as mineral matter. This adequately classifies most inorganic elements in coals, those that are structurally bound within various minerals, but some other elements are also combined in the organic matter. For bituminous coals such elements include B, Be, Br, Ge, Sb, and V (2-5); for lower rank coals much of the Ca is combined as an organic salt. In

addition, many other elements are combined in both the organic and the mineral matter fractions.

The chemistry of coal is further complicated by the fact that the organic elements, except nitrogen, also occur in one or more mineral constituents: carbon in carbonates; hydrogen in absorbed water and as hydroxide in clay minerals; oxygen in water, quartz and other simple oxides, clay minerals, carbonates, sulfates, and other trace minerals; and sulfur in pyrite, related sulfides, and sulfates. For scientific and technological purposes, it is important to know the organic-inorganic associations of the elements in coals being studied or used in industrial processes.

Characterization of the mineral matter in coal is important for a number of reasons. Because of the way coal must be mined, the mine-run product always includes some rock material other than coal, thereby contributing mineral matter to the mine product. Miners of a thin seam usually have to remove some roof and floor strata. Irregular bodies of roof shale or other rocks frequently occur within coal seams and inevitably become part of the mine product. Some coal seams grade upwards to shale coal or coaly shales so that there is no clear-cut boundary between coal and the roof rocks. In addition, many coal seams contain one or more mineral partings of various thickness so that miners must include these in the mine product. It is best for mining and sales purposes if the amounts, types, and characteristics of these rock materials be known prior to mining in order to properly design the mine and preparation plant.

While it has long been known that mineral matter is an important design factor for utility and other large boilers (6-8), consumer pressure for low electric bills coupled with more stringent regulations of sulfur emissions are causing utilities to seek more efficient operation of existing coal-fired power plants. Thus, there is renewed interest and concern with such problems as slagging and fouling of boilers (9-16).

Slagging is the accumulation of mineral matter in a fused and hardened form on the walls and other surfaces in the furnace of boilers. Slagging reduces heat transfer and causes excessive temperature of the exhaust gases as they exit the furnace. The net effect of slagging is to add maintenance costs for boiler operation as it damages the metal parts on which the slag forms. Blocks of slag have been known to grow to over 5 feet thick in the top of furnaces and eventually to fall of their own weight, knocking out the bottom of the furnace. Availability of the boiler for generating electric power is significantly reduced by severe slagging.

Fouling is the accumulation of mineral-derived ash on the superheater and reheater tubes in the convective (heat exchanger) section downstream from the furnace. Fouling restricts the flow of exhaust gases and impedes heat transfer through superheater tube walls and thereby reduces the amount of steam generated.

Abrasion of metal parts inside the boiler is a third deleterious effect of ash particles produced by some coals. Ash particles that are especially hard will cause excessive abrasion

when they impinge on the furnace and boiler surfaces. At plants where abrasion is serious, it causes frequent shut-downs.

A fourth important factor that increases outages and maintenance costs is the corrosive effects of alkali elements, especially sodium, which is associated with chlorine in certain coals. The specific damage to boilers by chlorine is not well known, but this mineral constituent clearly causes excessive rates of corrosion to coal handling equipment.

Thirty-four minor and trace elements are of potential environmental concern (17). Sulfur is the element of major concern due to its abundance in flue gases from some coal-burning plants and its subsequent contribution to "acid rain." Sulfur as acidic ions of sulfate can also contribute to pollution of surface water and groundwater. Other elements of greatest concern are As, B, Cd, Pb, Hg, Mo, and Se. With the exception of B and Se, these elements are strongly associated with mineral matter in the coal and are concentrated in waste piles from coal preparation plants. If the waste disposal site is not constructed as a closed system, pollution of nearby groundwater is possible. Boron and Se may contribute to the pollution risk as they are associated with both mineral and organic components. On the other hand, certain coal-mine wastes have potential for recovery of valuable metals such as zinc and cadmium (18).

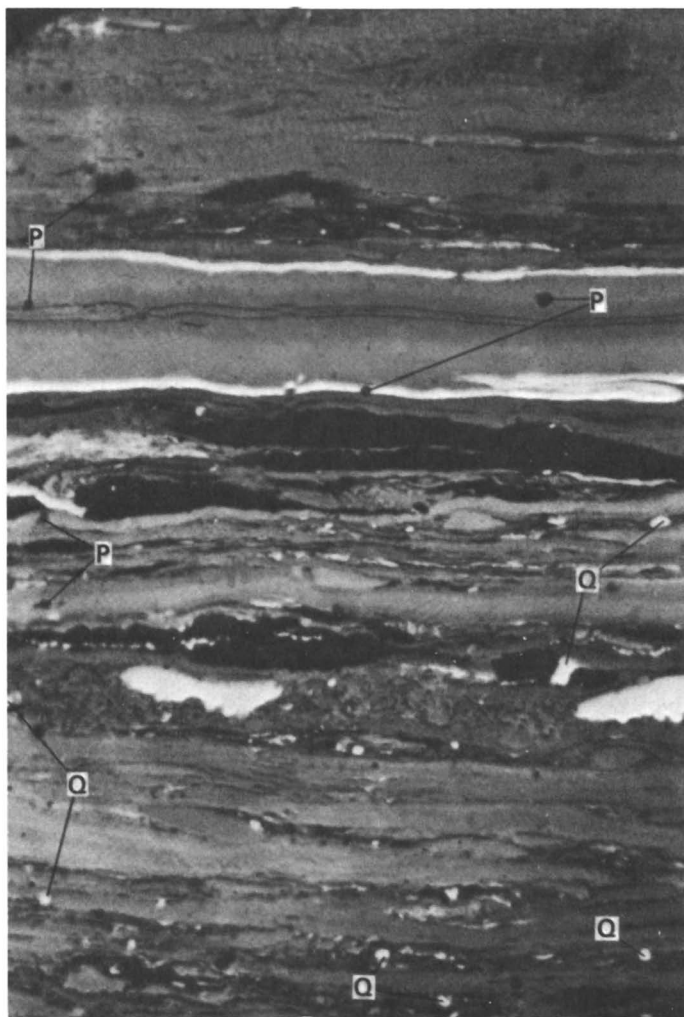
Geological studies of the distribution (or variation) of mineral matter in a local area, such as a large mine, as well as regionally over the extent of a commercial seam, enable useful predictions of the concentrations of some inorganic elements important to coal quality. Geological processes that formed the seam operated over extensive areas; therefore, patterns of elemental distribution enable quality parameters of the coal bed to be predicted in some unexplored areas (5,19-24).

### Coal Geology

Coal is a brown to black, combustible, sedimentary rock composed principally of consolidated and chemically altered plant remains (25)(Figure 1). The original plants grew abundantly in ancient swamps and their remains accumulated as peat on the swamp floor, mostly under water, which restricted decomposition of the plant debris. Commercial thicknesses of coal are thought to have required possibly a century or more of unusually consistent climatic and hydrologic conditions to allow for the deposition of the required thickness of peat. Studies have shown that peat: coal (bituminous) thickness ratios range from about 3:1 to 30:1 (26).

Coal seams in the United States that are of minable thickness and quality range in age from the Pennsylvanian to the Tertiary geologic periods (Figure 2). A rough estimate suggests that two-thirds to three-quarters of the coal produced to date in the United States has been bituminous coal from Pennsylvanian strata mined from seams in the Appalachian, Illinois, and Western Interior Basins (Figure 3). Most of the remainder has been lignite and subbituminous coal mined from Tertiary and





0.5 50  $\mu\text{m}$

Figure 1. Thin section of a coal in transmitted light sliced normal to bedding showing layered structure of plant debris and disseminated grains (2-4  $\mu\text{m}$ ) of quartz (Q) and pyrite (P).

Yrs (10 <sup>6</sup> )	Geologic Period	Lignite	Sub-bituminous	Bituminous			Anthracite
				High volatile	Medium volatile	Low volatile	
50	Tertiary	western					
100	Cretaceous	western states					
150	Jurassic			MT			
200	Triassic			VA			
250	Permian			TX, OH, PA, WV			
300	Pennsylvanian			East of Great Plains			
350	Mississippian			Widely scattered and limited coals			

Figure 2. Geologic age (period) and rank of coal deposits in North America, after Cady (27).

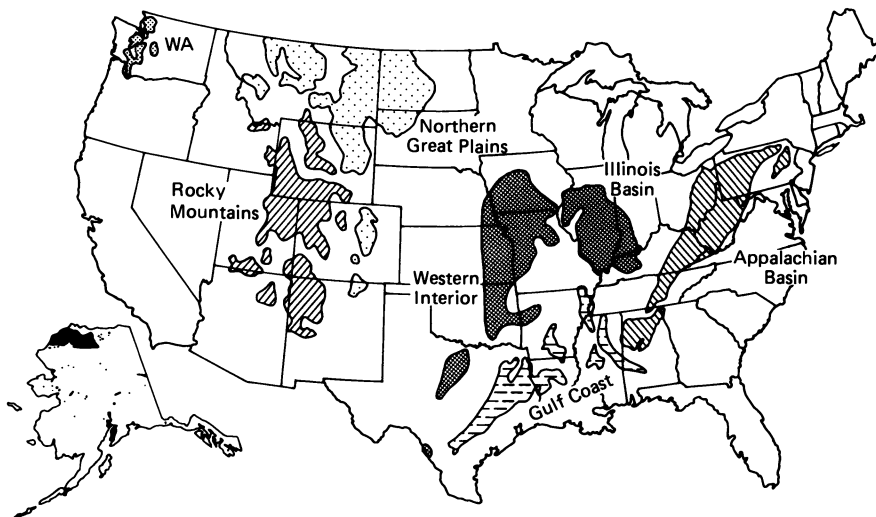


Figure 3. Coalfields of the United States (28,29).

Cretaceous strata in the northern Great Plains, the Rocky Mountains (including central Utah and northeastern Arizona), Washington, Texas and Alaska. In recent years production from these Tertiary and Cretaceous deposits has greatly increased. For example, between 1972 and 1982 the production from these deposits in Wyoming increased from an annual tonnage of about 10 million to nearly 110 million, while production in Illinois decreased from about 65 to 61 million tons.

Origin of Coal Seams. By analogy to present-day deposits and to the lithologic character of associated strata, the ancient coal seams formed in vast peat swamps. The swamps were located on coastal plains, often on, or adjacent to, major river deltas. Some of the swamps might have been 200 to 400 miles across. Over a period of many centuries the swamp land slowly subsided while maintaining a dense forest at or near sea level. Layer upon layer of fallen vegetation was converted to peat. Mineral matter was introduced into the swamps, mainly by rivers, as suspended mud and dissolved ionic species during storms that flooded the swamp, by sea water during wind storms, and by distant volcanic eruptions that rained dust onto the swamp. Some inorganic elements were drawn into plant tissues through their roots from the swamp water and peaty soil; this material is known as "inherent" mineral matter (30) in the final coal. Ultimately the swamp was drowned by rivers or sea water from which sand and mud were deposited onto the dying forest. Peats covered with seawater were injected with sulfate, but those covered by thick and impermeable river muds (fresh water) remained more or less free of sulfate.

More often than not, once a peat swamp was established on a coastal plain or delta and later covered by sediments due to land subsidence, a second swamp was established in the same region by cyclic changes in sea level and re-establishment of swamp-type vegetation. In this way, multiple layers of peat and subsequently of coal were formed.

Coalification. The transformation of peat into coal was a slow and complex process that began with bacterial reduction of plant debris during the peat stage (Figure 4). As the peat was progressively buried under hundreds of feet of sediments, it was compacted; its inherent moisture was progressively forced out by the pressure of overlying sediments and by heat from the earth's interior. Methane and CO<sub>2</sub> were released or entrapped within pores of the compacted organic debris. Several chemical processes briefly described as peatification, humification, gelification, and vitrification, altered the roots, bark, and other cellulose and lignin bearing debris to vitrinite--the most abundant maceral comprising bituminous coals (Figure 4). Plant spores, cuticles, and resins and other lipid components were incorporated into peat and these are classified as the liptinite group of macerals. Various oxidized (charred or fusinized) debris are classified as inertinites (Figure 4). With increasing coalification (rank), these macerals become increasingly enriched in carbon so that all macerals in anthracite have essentially the same properties as inertinite.

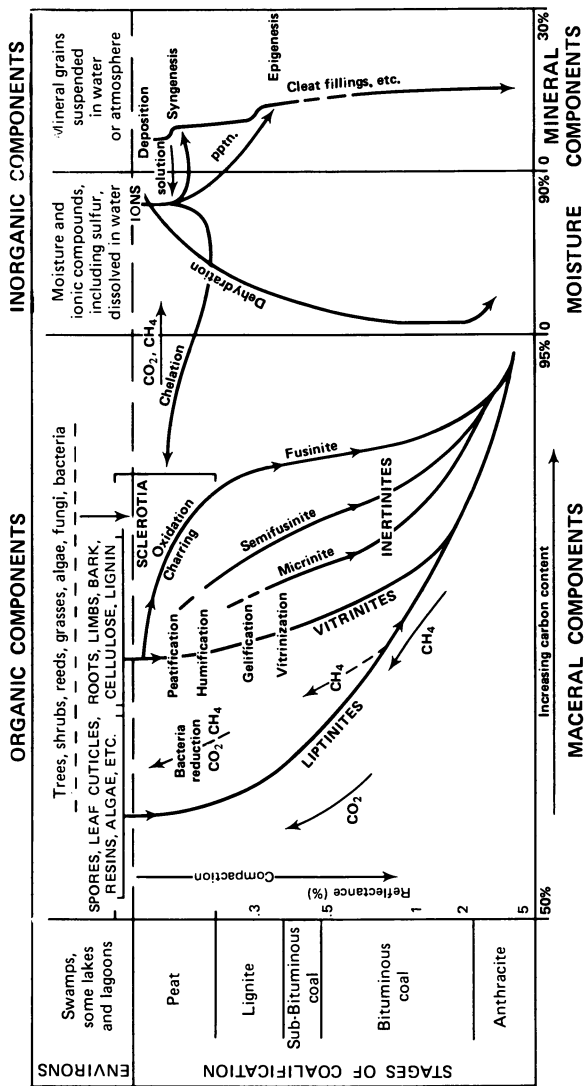


Figure 4. Diagrammatic representation of coalification processes involving the conversion of plant debris to various macerals, and those involving moisture and genetic processes of mineral matter.

Because of the complexity of the coalification processes, different measures are used to define different levels of rank (Table I): high moisture, low heating value, and non-agglomerating character of the coal define the rank (group) within the lignite and subbituminous classes; and volatile matter (or fixed carbon) define the various groups of rank in the bituminous and anthracite classes. In addition to these properties, the reflectance of vitrinite, carbon content of the coal (dry, mineral matter free), and some other properties change proportionately as rank increases (Table I).

### Mineral Occurrences in Coal Seams

Over 125 different minerals have been reported in coal (32); however, only about 25 have been recognized as occurring in significant amounts (Table II). Minerals in coal occur as discrete grains or flakes or aggregates in one of five physical modes (31): (1) as microscopically disseminated inclusions within macerals; (2) as layers or partings wherein fine-grained clay minerals usually predominate; (3) as nodules including lenticular and spherical concretions; (4) as fissures, including cleat and other fracture or void fillings; (5) as rock fragments—megascopic masses of rock material found within the coal bed as a result of faulting, slumping, or related disturbances. This classification is useful in that the removal of minerals from coal in preparation plants is strongly influenced by the mineral's physical mode of occurrence. Fine-grained quartz, clay, and pyrite disseminated within macerals are least susceptible to removal by physical cleaning methods; whereas rock fragments and minerals in layered, nodular, and fissure modes break free and are more easily removed.

Origin of Mineral Matter. A genetic classification of mineral matter provides the best means to predict the quality of coal in areas ahead of mining and exploration. We consider three main genetic processes to be responsible for minerals in coal: detrital deposition, syngensis, or epigenesis (see the right side of Figure 4). Detrital grains were introduced into the swamp by rivers, tidal (storm) waves, and wind (volcanic dusts). Syngenetic minerals were formed during the peat stage of coal formation, before the peat was "lithified" to lignite. Three different subclasses of syngenetic minerals can be distinguished on theoretical grounds.

- (a) minerals formed by crystallization of inorganic elements that were incorporated into the tissues of the living plants (the inherent mineral matter referred to above).
- (b) minerals formed by bacterial reduction of aqueous sulfates by crystal growth in microscopic pores within the plant remains.
- (c) mineralization around nuclei or other centers, forming nodules; these include coal balls (permineralized peat) and other plant replacement forms.

It is rarely possible to unequivocally distinguish type (a)

TABLE 1  
ASTM Classification of Coals by Rank (in Box) and Corresponding Rank Parameters Not Used in the ASTM Classification

ASTM Class	ASTM group	Heating value		Agglomerating (d,mmf)	% VM (d,mmf)	% R Oil max. (vitrinite)	% Moisture (moist,mmf)	% C (d,mmf)	% O (d,mmf)	% H (d,mmf)	FSI
		Btu/lb (moist,mmf)	MJ/kg (moist,mmf)								
Peat		3,000-4,000*	7.0-9.3	No	62-72	0.2-0.4	50-95	50-65	30-42	5-7	
Lignite	Lignite B	Undefined-6,300*	-14.6	No	40-65	0.2-0.4	45-60*	55-73	23-35		
Subbituminous	Lignite A	6,300-8,300*	14.6-19.3	No			31-50*				
	Subbituminous C coal	8,300-9,500*	19.3-22.1	No			25-38*				
Bituminous	Subbituminous B coal	9,500-10,500*	22.1-24.4	No	35-55	0.3-0.7	20-30*	60-80*	15-28*	4.5-6.0	
	Subbituminous A coal	10,500-11,500*	24.4-26.7				18-25*				
	High volatile C bit. coal	10,500-13,000*	26.7-30.2		35-55	0.4-0.7	10-25*	76-83*	8-18*	1-5	
	High volatile B bit. coal	13,000-14,000*	30.2-32.5	Yes	35-50	0.5-0.8*	5-12*	80-84*	7-12*	2-7	
Anthracitic	High volatile A bit. coal	>14,000	>32.5		31-45	0.6-1.2*	1-7*	78-88*	6-10*	4-9	
	Med. volatile bit. coal				22-31*	1.0-1.7*	<1.5	84-91	4-9	7-9	
	Low volatile bit. coal				14-22*	1.5-2.0*	<1.5	87-92	3-5	1-9	
	Semianthracite				8-14*	1.8-2.6*	<1.5	89-93*	3-5*	3-5*	
	Anthracite	>14,000	>32.5	No	2-8*	2.2-5.0*	0.5-2	90-97*	2-4*	2-4*	
	Meta-anthracite				<2	>4.5*	1-3	>94*	1-2*	1-2*	

\* Air dried.

\* Well-suited for rank discrimination in range indicated.

\* Moderately well-suited for rank discrimination.

Reproduced with permission from Ref. 31. Copyright 1984, Plenum Press.

Table II. Minerals Frequently Occurring in Coals, Their Stoichiometric Compositions, Relative Abundances, and Modes of Occurrences

Mineral	Composition	Common minor and trace element associations	Frequency of occurrence in coal seams	Concentration in min. matter	Chief occurrences Physical*	Genetic**
Clay minerals						
illite (sericite)	$KAl_2(AlSi_3O_{10})(OH)_2$	Na, Ca, Fe, Li, Ti, Mn, F & other lithophile elements	Common	Abundant	D, L	d, s(?)
smectite (including mixed layered)	$Al_2Si_4O_{10}(OH)_2 \cdot H_2O$		Common	Abundant	D, L	d, s(?)
kaolinite group	$Al_2Si_2O_5(OH)_4$ $Mg_5Al_4(AlSi_3O_{10})(OH)_8$		Common	Abundant	L, F	d, e, s(?)
Sulfides						
pyrite	$FeS_2$ (isometric)	As, Co, Cu, & other chalcophile elements	Rare-common	Variable	D, N, F	s, e
marcasite	$FeS_2$ (rhombohombic)		Rare-moderate	Trace	D(?)	D(?)
pyrrhotite	$Fe_{1-x}S$		Rare	Trace	D	s(?)
sphalerite	$ZnS$		Rare	Minor-trace	F	e
galena/chalcocopyrite	$PbS/CuFeS_2$	Rare	Trace	F	F	e
Carbonates						
calcite	$CaCO_3$	Mn, Zn, Sr	Rare-common	Abundant	N, F	e, s
dolomite (ankerite)	$CaMg(CO_3)_2$		Moderate	Trace	N, L	N, L
siderite	$FeCO_3$		Rare	Minor	N	s, e
Oxides						
quartz	$SiO_2$	--	Common	Abundant	D, L, N	d, s(?)
magnetite/hematite	$Fe_3O_4/Fe_2O_3$	Mn, Ti	Common	Minor-trace	N	s
rutile & anatase	$TiO_2$	--	Common	Trace	D	d(?)
Others						
goethite/limonite	$FeOOH$	Mn, Ti	Common	Trace	N	w
feldspar	$K(Nz)AlSi_3O_8$	Ca	Moderate	Trace	D, L	d
zircon	$ZrSiO_4$	--	Moderate	Trace	D	d
sulfates: gypsum	$CaSO_4 \cdot 2H_2O$	--	Moderate	Minor	D, F	w
barite	$BaSO_4$	Na, Sr, Pb	Rare	Minor	F	e
szomolnokite	$FeSO_4 \cdot H_2O$	--	Rare	Trace	D	w
apatite	$Ca_5(PO_4)_3(F, Cl, OH)$	Mn, Ce, Sr, U	Moderate	Trace	D	d, s(?)
halite	$NaCl$	K, Mg	Rare	Trace	D	e

\*D=disseminated, L=layers (partings), N=nodules, F=fissures (cleat). First listed is the most common occurrence.  
 \*\*d=diagenetic, s=syngenetic, e=epigenetic, w=weathering. First listed is the most common occurrence; ? indicates there is divergence of opinion about the genetic occurrence.

syngenetic minerals from fine-grained detrital forms, especially quartz silt and certain clay minerals. There is much debate on this topic. Cecil et al. (33) postulates that most quartz and clay minerals in low-ash coals are crystallized phases of elements originally amorphous within the plant tissues as inherent mineral matter. On the other hand, Finkelman (34) and Davis et al. (35) interpret most such mineral forms as detrital in origin. The microscopically observed layered form of many quartz and clay mineral grains leads to the conclusion that high proportions of quartz and clay are of detrital origin. We, therefore, assign a detrital origin to these minerals in Table II.

Ultra-small crystallites of other mineral phases disseminated within macerals are judged syngenetic; these include the sub-micrometer-sized crystals of kaolinite and illite observed by Strehlow et al. (36) and of kaolinite and pyrrhotite observed by Wert and Hsieh (37).

Epigenetic minerals are those found as fillings of fissures and voids and as products of weathering or oxidation. Cleat-filling calcite, pyrite, and kaolinite, the most abundant minerals in this class, formed after the peat was lithified (coalified). For most coals, this type of mineralization took place after the coal was well lithified (Figure 4).

Freshly mined coal rarely exhibits oxidation, but if coal is exposed to oxidative weathering some forms of pyrite or marcasite, especially the nodular forms, rapidly oxidize to iron sulfates. For completeness, these alteration products are included in the epigenetic occurrences as proposed by Mackowsky (38). Some forms of pyrite are known to oxidize in situ to Szomolnokite ( $\text{FeSO}_4 \cdot \text{H}_2\text{O}$ ) prior to exposure to the atmosphere (39).

The pH of the ancient swamp was an important factor controlling mineral matter in coal. A condition of low pH reduces iron to the ferrous state, causes leaching of acid soluble phases, and retards sulfate reducing bacteria, thereby inhibiting fermentation (33). In addition, the pH of the muddy waters that overlie peat deposits may affect the peat in the same manner (40).

### Composition of Minerals in Coal

Of prime importance to gaining detailed knowledge of the behavior of minerals in a coal during various stages of combustion or other use are the abundance and composition of each mineral phase in the coal. The behavior of minerals and the derived ash depends primarily on the properties of the minerals in the coal, rather than on the concentration of the metal oxides in the ash, as is commonly reported. Few analyses of individual minerals separated from coal are available (30, 41). This is due to the extreme difficulty of separating the different minerals from coal in sufficient quantity for separate analysis. At present the best available estimates of the compositions of minerals in coal are the well known stoichiometric formulas (Table II).

The application of computer-controlled microprobe methods



has provided valuable data on the major elements in coal minerals (42-44), but the detection limits for the minor and trace elements within the mineral grains by this method are usually too high for quantitative determinations of these elements.

The pioneering work of Palmer (45) included the successful separation and analysis of major and trace elements in 13 different grain-size and density fractions of the low temperature ash from five samples of coal and coal products. Palmer's results showed good mass balance and remarkably good agreement with the stoichiometric composition of illite, kaolinite, pyrite, calcite, quartz, and other minerals. Palmer's trace element results are in good agreement with Goldschmidt's (46) lithophilic, chalcophilic, and biophilic associations (Table II). The extent to which Palmer's results can be applied to coal seams other than those studied is uncertain.

### Samples

A laboratory sample submitted for analysis must be representative of the original material for which information is desired; and its source, location, and seam must be identified. Proper sampling procedures are required from the initial collection to the final stage of grinding sample splits. Gluskoter et al. (1) and Damberger et al. (31) summarize the procedures for sampling and discuss the problems involved. Channel samples are most commonly taken to evaluate the quality of coal seams according to procedures described by Schopf (47), Swanson and Huffman (48), and Gluskoter et al. (1).

### Chemical Methods of Analysis

Chemical methods for the elemental characterization of mineral matter in coal have been extensively developed and reported. The most utilized methods include X-ray fluorescence (XRF), atomic absorption spectroscopy (AAS), activation analysis (AA), optical emission spectroscopy (OES) and inductively coupled plasma (ICP), mass spectroscopy (MS). Less frequently used techniques include ion-selective electrode (ISE), proton induced X-ray emission (PIXE), and ion chromatography (IC). In different laboratories each of these methods may be practiced by using one of several optional approaches or techniques. For instance, activation analysis may involve conventional thermal neutron activation analyses, fast neutron activation analysis, photon activation analysis, prompt gamma activation analysis, or activation analysis with radio chemical separations. X-ray fluorescence options include both wave-length and/or energy dispersive techniques. Atomic absorption spectroscopy options include both conventional flame and flameless graphite tube techniques.

At present elements in coal can be determined with acceptable accuracy and precision with proper choice of analytical procedure and sample pretreatment technique. Multi-element standards and numerous consensus samples are now readily

available for comparison and calibration (49). Coal chemists tend to utilize multi-element techniques such as XRF, ICP, AA, AAS, and MS where maximum characterization of both major and trace elements is desired. Some methods such as AAS, ICP, OES, and ISE generally require that coal samples be properly ashed and pretreated prior to analyses. Ash and pretreatment necessitates consideration of volatility losses (50). Methods such as AA, XRF, and PIXE can readily be utilized on whole coal without ashing or extensive pretreatment.

It is beyond the scope of this section to describe each analytical method and to list its advantages, disadvantages, and specific applications. For these details readers are referred to Gluskoter et al. (1), Damberger et al. (31), and Schultz (51).

### Mineralogical Methods of Analysis

There are numerous definitive methods available for characterizing the minerals in coal. The more prevalent methods are briefly described below.

X-ray Diffraction. X-ray diffraction is the most extensively developed and universally applied method for characterization of minerals in coal and other rocks. This method is capable of giving quantitative results of major minerals in coal, coal ash, and coal-related materials accurate to about  $\pm 5-7$  percent absolute (52). Quantitative X-ray diffraction is difficult. A general overview of the method with many references is provided by Herzenberg (53).

Electron Microscopy. Scanning electron microscopy and energy-dispersive X-ray microanalysis can be effectively used in combination to provide both structural and elemental information about individual mineral particles in coal and other materials (42,53-55). Transmission electron microscopy has the advantage of higher resolution (56,57) allowing more detailed characterization of mineral inclusions.

Thermal Analyses. Thermal techniques such as differential thermal analysis, thermal gravimetric analysis, and derivative thermogravimetric analysis have been successfully applied to characterizing various minerals in coal (58). The methods are based on measurements of weight loss or heat transfer during phase changes at temperatures from ambient to over 1000° C. Since each mineral undergoes certain phase changes at a definite temperature (or range of temperatures), it is possible to detect specific minerals in mixtures. A monograph detailing application of various thermal techniques to coal, coal-related materials, and other substances has been prepared by Earnest (59).

Infrared Spectroscopy. A least-squares curve-fitting approach with Fourier transform infrared spectroscopy (FT-IR) appears to be an effective method for mineralogical analysis. A study by Painter et al. (60) demonstrated that the method is rapid

relative to other techniques and the results were in good agreement with those obtained from other analytical methods. Conventional infrared spectroscopy has also been successfully used to analyze minerals in coal (61).

Mössbauer Spectroscopy. Mössbauer spectroscopy has been found to be a valuable tool in identifying the multiple iron species found in coal and coal-related materials (62,63). A combination of Mössbauer spectroscopy and FT-IR has been used to study the low temperature oxidation of minerals in bituminous coal (64).

ESCA. Electron spectroscopy for chemical analysis (ESCA) has been demonstrated to be effective in analyzing major elements in coal or ash surfaces having different chemical environments (65). Sulfur can be detected as the sulfide or sulfate. Carbon can be detected as graphite, carbonyl, carboxyl, or hydrocarbon.

Low Temperature Ashing. Radio-frequency excited low-temperature ashing (LTA) of coal has been extensively utilized to prepare samples for mineralogical analysis (24,66,67). The technique selectively removes the carbonaceous material leaving mineral matter essentially unaltered. The percent residue (%LTA) provides the best determination of the total mineral matter in a coal sample. A new low-temperature ashing technique involving glow discharge (68) permits faster ashing and less mineral change.

#### Variation of Mineral Matter in Illinois Basin Coals

Coal, by virtue of its origin, is quite heterogeneous; its mineral content varies considerably both vertically and laterally within coal seams. Vertical variation has resulted from changes through time in the content of mineral detritus introduced into the peat swamp, in the pH, and to some extent in the species of vegetation that inhabited the swamp at any one place or time. This variation has been measured by determining the differences in mineral content in different layers or benches of the seam at particular places. Lateral variation has been measured by analysis of the whole coal seam (channel samples) from one locality to another.

Variations Between Benches of the Herrin (No. 6) Coal. Variations of mineral matter in bench samples collected from the Herrin Coal seam at five different mines in Illinois were reported by Gluskoter et al. (3). The total mineral matter (%LTA) varied between benches at one site from 9.2 to 26.5 percent (Figure 5). The variations of several mineral components at the same site are also shown in this figure. The amount of arsenic is related to or is a function of the amount of pyrite. Organic sulfur, silica, and calcium contents varied only a little. Molybdenum ranged from 1 to 49 ppm and was concentrated at the top and bottom of the coal seam (Figure 6). At four of the five sites analyzed, Ge and Mo were enriched in the top and bottom benches.

A comprehensive bench study was undertaken to evaluate the

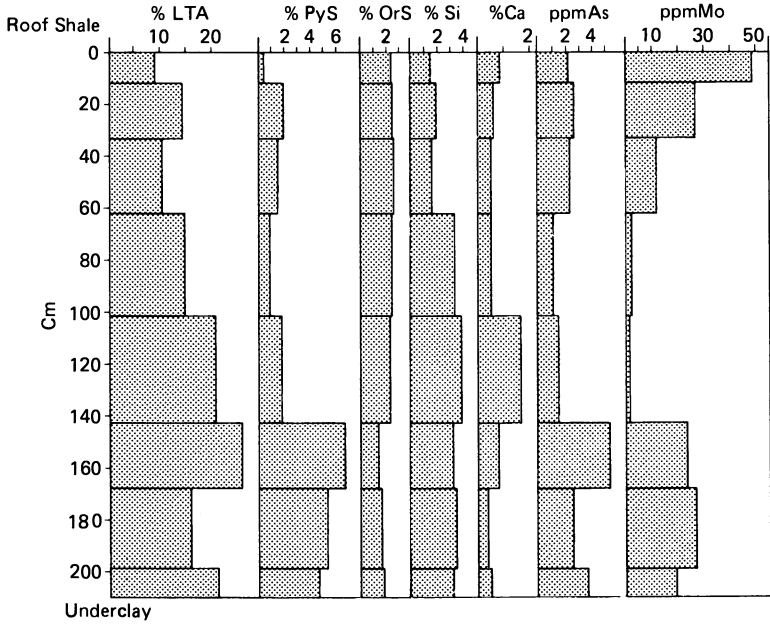


Figure 5. Variation of low temperature ash (LTA), pyritic sulfur (PyS) and other inorganic constituents in benches of the Herrin (No. 6) Coal at one site (compiled from Gluskoter et al. (3)).

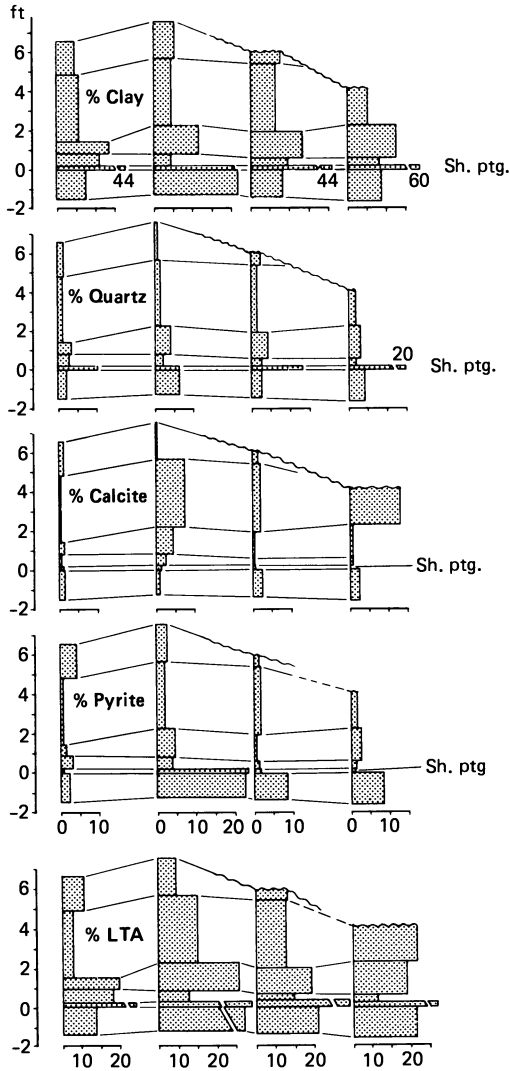


Figure 6. Variation in mineral constituents in six benches along a traverse (4 sites) in one mine, Herrin (No. 6) Coal (5).

variations of minerals within the seam along a 700-foot traverse in one operating mine. Five to six benches were sampled at four sites along the traverse that crossed a major change in the type of roof shale. The seam was overlain at two of the sites by a black shale of marine origin and at the other two sites by a gray shale of nonmarine (probably fluvial) origin.

Identification and correlation of petrologic benches within the coal seam by Johnson (69) provided a basis for detailed study of the minerals in the coal (5). The variation of the minerals is distinctly correlated along the traverse (Figure 6).

Excluding the major shale parting, the ratio of the maximum/minimum concentration for different benches along the traverse varies considerably. In general, the ratio varies for ash from 2 to 5 and for Si from 1 to 4; but for pyritic S and Fe it varies from 3 to 15, and for many trace elements such as As, Mo, V, U, and Zr it varies up to 20 or more.

Mineral Variation of Channel Samples From the Herrin and Springfield Coals in the Illinois Basin. Both the Herrin Coal (No. 6 in Illinois, No. 11 in Kentucky) and the Springfield Coal (No. 5 in Illinois and Indiana, No. 9 in Kentucky) extend over much of the Illinois Basin Coal Field. These two seams account for more than 90 percent of the coal produced and about 75 percent of the remaining resources in the field.

A large number (226) of localities in these two seams from throughout the basin were sampled and analyzed for their mineral and trace element contents. The minerals were separated from the coal by LTA and this residue was quantitatively analyzed by X-ray diffraction methods (5). The variability of both seams is shown by the contrasting means and ranges of the mineral composition in the several regions of the Basin. In each of the regions considered all mineral components varied by several percentage points. The quantity of clay minerals (total of kaolinite, illite and mixed layer clay minerals) has the greatest variation, 5 to 16% for the Herrin (Table III) and 3 to 19% for the Springfield (Table IV). The lower mean pyrite content of the Herrin in south central Illinois is significant. Pyrite is lower in this region, as is the total sulfur, because of the thick nonmarine shale that overlies the seam in this area. Each of the other mineral phases also tends to have a low concentration in this region as well. Pyrite content of the Springfield Coal is also lowest in south central Illinois (Table IV) for the same reason. Both quartz and calcite contents in this seam are low in southwestern Indiana and in western Kentucky. Calcite and quartz contents of both the Herrin and Springfield Coals show the least variation, with a standard deviation of 1 percent or less over the entire basin.

Systematic variation of an inorganic constituent in a seam throughout the entire basin is best illustrated by results of chlorine (Figure 7). Chlorine and Na contents in the Herrin seam are closely associated with these elements in groundwater. The increasing Cl and Na content of the seam with depth is a function of the increasing salinity of groundwater with depth in the Illinois Basin. This variability of Cl and Na with depth also applies to the deeper Springfield Coal (5).

Table III. Mineralogical Composition of Herrin Coal in Various Regions of the Illinois Basin\*

Type of mineral	Illinois										Kentucky		Entire Illinois Basin
	North-west	Central	South-west	South Central	Southern part of SE	Northern part of SE	Kentucky		Entire Illinois Basin				
							5	4		4	4		
No. of Samples	7	5	6	5	4	4	4	4	61				
LTA (%)	Mean 17.5	16.1	16.4	11.5	18.1	19.5	11.9	15.8	15.8				
	SD 1.7	3.1	0.7	0.9	0.8	2.8	1.8	3.2	3.2				
	Range 15.6-20.9	12.4-19.5	15.4-17.2	10.7-12.9	17.5-19.1	17.1-22.7	9.8-13.8	9.3-25.6	9.3-25.6				
Quartz (%)	Mean 2.7	2.7	2.4	1.7	2.5	2.6	1.2	2.4	2.4				
	SD 0.8	0.8	0.3	0.6	0.4	0.5	0.4	0.9	0.9				
	Range 1.4-3.8	1.7-3.6	2.1-2.8	1.0-2.2	2.1-3.0	2.2-3.4	0.7-1.7	0.7-5.4	0.7-5.4				
Calcite (%)	Mean 2.3	1.2	1.2	1.0	1.2	0.8	0.9	1.3	1.3				
	SD 1.4	0.3	0.7	0.2	0.4	0.5	0.8	0.8	0.8				
	Range 1.0-5.2	0.8-1.7	0.9-2.0	0.8-1.3	0.6-1.6	0.3-1.4	0.0-1.9	0.1-5.2	0.1-5.2				
Pyrite (%)	Mean 2.8	3.6	3.5	1.5	3.3	5.9	3.2	3.1	3.1				
	SD 0.3	1.2	0.8	0.7	1.7	3.8	1.4	1.7	1.7				
	Range 2.3-3.3	2.5-5.5	2.2-4.5	1.0-2.7	1.6-5.0	3.6-11.6	2.0-5.0	0.3-11.6	0.3-11.6				
Clay Minerals (%)	Mean 9.7	8.7	9.1	7.2	11.2	10.2	7.5	9.1	9.1				
	SD 2.5	2.2	0.8	0.8	1.2	2.7	1.1	2.4	2.4				
	Range 7.6-13.5	5.0-10.5	8.9-10.0	6.7-8.6	9.8-12.3	6.8-13.3	6.4-9.3	5.0-16.3	5.0-16.3				

\*All samples represented the whole coal seam exclusive of major mineral partings, if present (face channel samples).

Table IV. Mineralogical Composition of the Springfield Coal in Various Regions of the Illinois Basin\*

Type of mineral	Illinois				Indiana		Kentucky		Entire Illinois Basin
	North-west	South-west	South-Central	South-Southeast	North-Southeast	South-West	Western	6	
No of Samples	4	4	5	5	5	7	6	6	46
LTA (%)	Mean 15.8 SD 1.0	15.0 1.4	13.2 1.5	15.8 7.3	14.3 3.3	15.6 5.2	14.2 2.2	14.2 2.2	15.1 3.5
Range	14.9-17.2	13.0-16.4	10.7-14.0	9.8-28.1	11.0-19.0	11.4-26.3	12.3-17.2	12.3-17.2	9.8-28.1
Quartz (%)	Mean 3.1 SD 0.6	2.6 1.2	1.8 0.6	2.3 0.8	2.0 0.9	1.7 1.0	1.7 0.6	1.7 0.6	2.2 0.9
Range	2.1-3.8	1.8-4.3	1.2-2.8	1.3-3.4	1.2-3.6	1.1-3.7	1.2-2.7	1.2-2.7	1.0-4.5
Calcite (%)	Mean 2.3 SD 0.5	1.9 3.0	1.6 1.1	1.1 0.7	1.1 0.8	0.9 0.8	0.9 0.3	0.9 0.3	1.4 1.0
Range	1.9-3.0	0.5-4.9	0.6-2.9	0.5-2.3	0.3-1.7	0.2-2.4	0.6-1.3	0.6-1.3	0.2-4.9
Pyrite (%)	Mean 3.1 SD 0.8	3.5 1.2	2.8 1.0	5.4 7.2	4.6 2.8	3.9 1.9	4.0 0.9	4.0 0.9	3.9 2.6
Range	2.6-4.3	2.1-5.0	1.6-4.3	0.5-18.0	2.5-9.3	1.7-7.9	3.2-5.3	3.2-5.3	0.5-18.0
Clay Minerals (%)	Mean 7.3 SD 1.1	7.1 3.4	6.9 1.9	7.0 3.5	6.6 0.8	9.2 5.2	7.5 1.1	7.5 1.1	7.7 2.6
Range	6-9	3-11	5-9	4-13	6-7	4-19	6-9	6-9	3-19

\*All samples represented the whole coal seam exclusive of major mineral partings, if present (face channel samples).



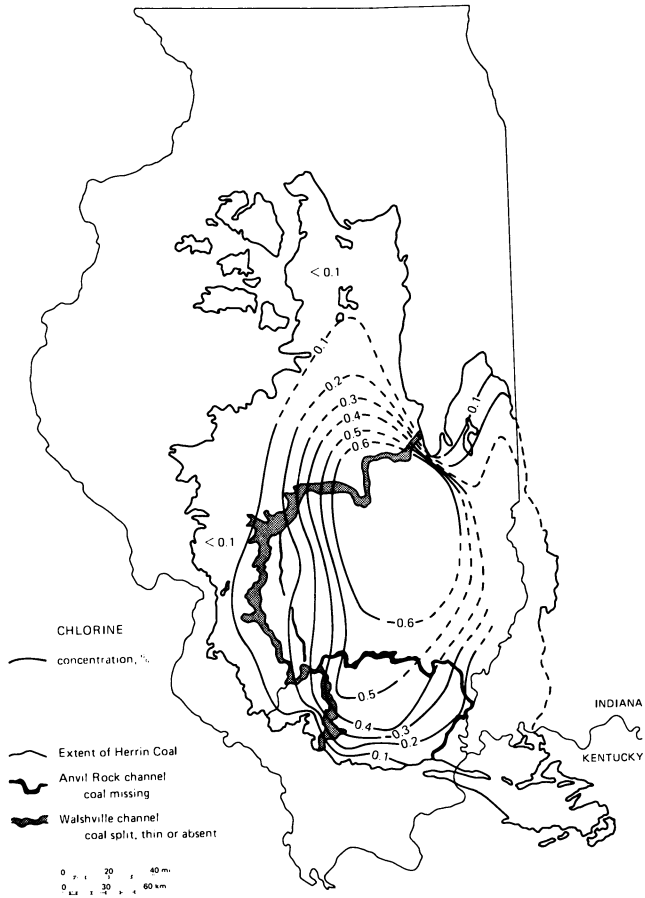


Figure 7. Areal distribution of chlorine in the Herrin Coal (5).

Variability Between Coal Seams in the Illinois Basin. The variability of mineral matter between different seams in the Illinois Basin other than the Springfield and Herrin seams has not been extensively studied. Assuming the ash content is a first approximation to the total mineral matter, a compilation by Weir (70) of the ash contents of Indiana Coals (Figure 8) illustrates the ranges and the means for 13 different major seams and groups of seams by formation. The ash content generally varies within a range of 15 percent or more for each seam. The seams in the uppermost Pennsylvanian strata (McLeansboro Group) have the greatest average ash content (28%).

#### Comparisons of Mineral Matter in Other U.S. Coals

Minerals. Few analyses of the mineral contents are available despite the abundance of elemental analyses expressed as oxides of high temperature ashes (71,72). Sprunk and O'Donnell (30) described and illustrated the microscopic occurrences of minerals in many U.S. coals, especially kaolinite, pyrite, calcite, siderite, and quartz. O'Gorman and Walker (73) quantitatively identified 14 different mineral phases in dull durain and clarain layers in 12 samples from mines in Kentucky, Pennsylvania, West Virginia, North Dakota, and Wyoming.

Accurate and detailed comparisons of mineral contents in coals from all U.S. coal fields will require years of coordinated work to generate the needed analytical data. To date, there are insufficient data and deficiencies in the precision of the mineral data. Standardized methods of analysis are needed. Finkleman et al. (74) described the first attempt toward this goal. At this time, only rudimentary comparisons of minerals in coals from different fields can be made, preferably based on analyses made in a single laboratory, using consistent sampling and analytical methods.

Gluskoter et al. (3) studied the trace elements in some 40 or more samples of coal from mines in eastern and western coal fields; we have determined the mineral phases in these and a few additional samples. These results and those of the two main Illinois coals are summarized in Table V. Based on this limited number of samples, the following comparisons can be made:

- (a) Total mineral matter, expressed by LTA, is highest in the three samples from the northern part (Iowa) of the Western Interior Basin. Several other coal seams occurring in other parts of this basin in Iowa, Oklahoma, and Arkansas, are known to contain much lower ash contents than suggested by the three samples reported here.
- (b) The average pyrite content is low (< 1%) in samples from various seams in the Northern Great Plains, the southern part of Central Appalachian Basin (the Pocahontas seam in southern West Virginia), and the Black Mesa Basin. Nonmarine strata overlie most seams in these areas. The pyrite content was highest in samples from Iowa, the Illinois Basin, and the Pittsburgh (No. 8) seam in the Central Appalachian Basin. Seams in the Warrior Basin of Alabama exhibit a wide variation in pyrite content.

Table V. Mineral Composition of Channel Samples from Some U.S. Coal Basins\*

Basin State(s)	Northern Great Plains		Western Interior (northern part)		Illinois Basin		Central Appalachian Basin			
	ND, MT, WY	IA	IL, IN, W-KY	Southern WV	Northern WV, PA					
No. of Samples	23		3		107		3		6	
Seam(s)	Beulah, Noonan, Couteau Mammouth, Rosebud Hanna (No. 24), Canyon E Canyon D, Anderson		Cliffland Ladssdale		Herrin Springfield		Pocahontas (No.4)		Pittsburgh (No.8)	
LTA	13 (7-27)		28 (23-34)		16 (9-28)		13 (13-14)		14 (10-15)	
Pyrite	<1 (0-2)		8 (7-9)		2 (<1-12)		<1 (<1-1)		4 (2-5)	
Quartz	2 (<1-6)		4 (1-7)		2 (<1-5)		1 (<1-3)		2 (1-2)	
Calcite	<1 (0-3)		4 (1-7)		1 (<1-5)		<1 (0-<1)		1 (<1-3)	
Clay†	11 (4-25)		13 (9-16)		9 (3-19)		11 (10-12)		8 (6-9)	
Others	sulfates chlorite		nil		sulfate marcasite		siderite dolomite		siderite feldspar	
Basin	Black Mesa						Southern Appalachian			
State(s)	AZ						AL(Warrior B.)		TN	
No. of Samples	3						6		4	
Seam (s)	Red (Mepo)						Johnson Clemants Blue Creek		Pewee Red Ash	
LTA	9 (5-12)						17 (11-18)		12 (10-16)	
Pyrite	<1 (<1)						2 (<1-6)		1 (<1-1)	
Quartz	2 (2-3)						2 (<1-4)		1 (<1-2)	
Calcite	<1 (0-1)						<1 (0-1)		nil	
Clay†	6 (0-1)						14 (10-21)		11 (9-14)	
Others	nil						siderite, apatite sericite		nil	

\*Mean (range) in weight percent of the dry coal.

†Content of clay minerals determined by difference.

- (c) Calcite occurred in some samples from all basins tested except those from Tennessee (Southern Appalachian Basin). Despite the similarity in range of calcite contents from the other basins, samples from Iowa (Western Interior) and the Illinois Basin average higher than others.
- (d) Quartz content was rather similar in samples from the different basins. The few samples from Iowa were most enriched with quartz.

These results are in good agreement with those of Glick and Davis (75) who made a comprehensive statistical analysis of the inorganic constituents in 335 whole-seam samples (The Pennsylvania State University Coal Sample Bank). In addition to those minerals listed here in Table V, Glick and Davis distinguished gypsum (all sulfates) and kaolinite. They found the content of kaolinite was mostly less than 15% of the minerals extracted by LTA in coals from the Western Interior Basin and the Illinois Basin as compared to coals from the Appalachian and western basins where kaolinite mostly comprised more than 15 percent of the LTA.

Minor Elements. Glick and Davis (75) documented the variation of five of the minor elements in coal ash, expressed as oxides, by plotting the concentration on triangular diagrams. The ash composition is remarkably similar for coal samples from five major coal provinces (Figure 9). Some samples from the Western Interior Province (Iowa) contain relatively large amounts of  $Fe_2O_3$ ,  $CaO$ , and  $MgO$ ; some from the Rocky Mountain Province (Western Wyoming, Colorado, Utah, New Mexico, and Arizona) are enriched in  $SiO_2$ ; and some from the Appalachian Basin are enriched in  $Al_2O_3$ . However, there is a very large area on the triangular diagram where samples from all provinces exhibit overlapping composition (Figure 9).

Compilations by Swanson et al. (76) and Harvey et al. (5) provide a basis to compare the average concentrations of other minor elements in U.S. coals (Table VI). The following generalizations can be drawn from these compilations:

- (a) Sulfur is distinctly lower in western coals, higher in Illinois Basin coals, and intermediate in Appalachian coals. On the average, sulfur is lowest in coals from the Rocky Mountains and next to lowest in lignites from the Northern Great Plains.
- (b) Iron tends to be lowest in Rocky Mountain coals (mostly subbituminous but also some lignite and bituminous coals). Changes in iron appear to follow those of sulfur because part of the iron is in pyrite.
- (c) Calcium tends to be highest in Northern Great Plains lignites and lowest in bituminous coals in the Appalachian region.
- (d) Magnesium tends to be highest in coals from the Rocky Mountains and lowest in the those from the Illinois Basin.
- (e) Sodium and chlorine tend to be highest in coals from the Illinois Basin.

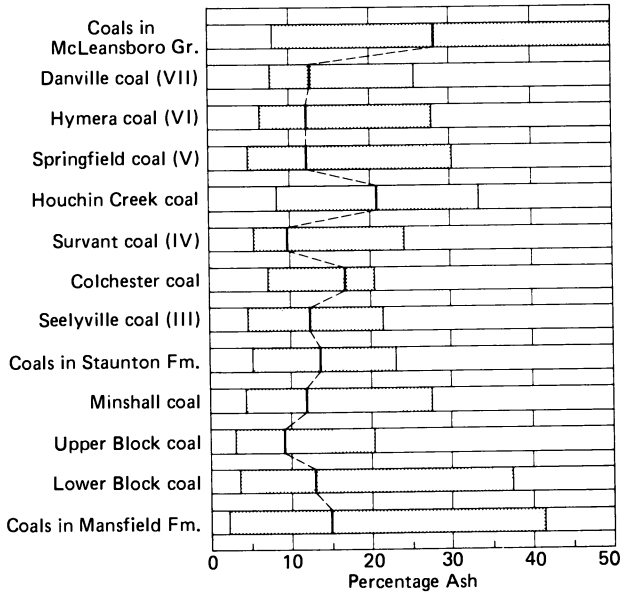


Figure 8. Range in value and mean value of percentage of ash in Indiana Coals, dry basis, after Wier (70).

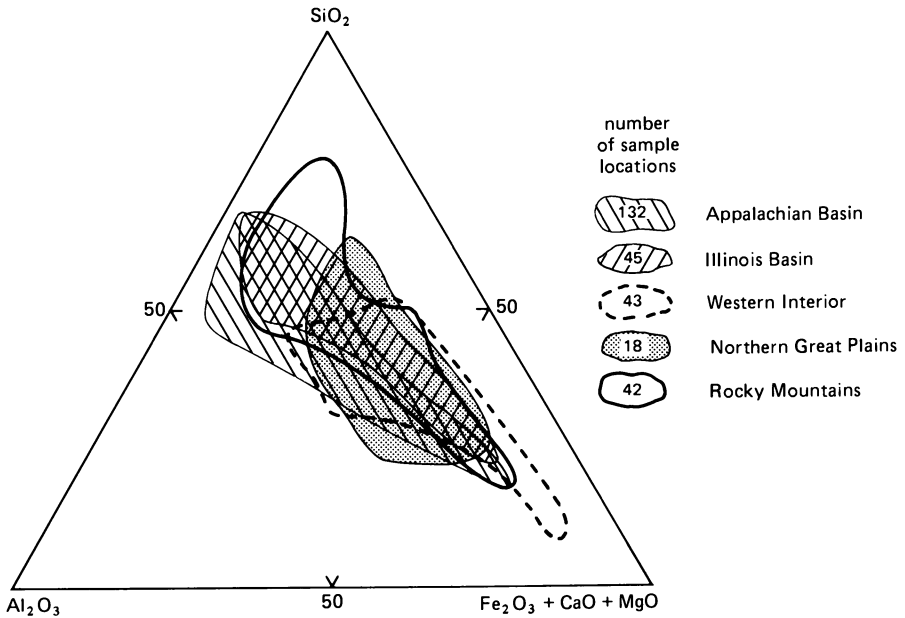


Figure 9. Variation of principal inorganic constituents in coal ash from various U.S. coal basins and regions (compiled from Glick and Davis (75)).

Table VI. Concentrations of Minor Elements in Some U. S. Coals\*

	Rocky Mtns. †		Northern Great Plains †		Illinois Basin †		Appalachian Region †	
	Mean	Range	Mean	Range	Mean	Range	Mean	Range
No. of Samples	124	93	118	331				
Si	2.5	.19-23.	1.4	.17-5.6	2.6	1.2-5.8	2.7	.22-25.0
Al	1.2	.17-13.	0.7	.18-2.5	1.3	0.64-3.0	1.6	.19-10.5
Ca	0.6	.08-2.1	1.0	.49-1.9	0.7	.05-2.7	0.12	<.02-2.0
Mg	1.0	.015-.76	0.26	.116-.45	0.05	nil-0.17	0.07	.007-1.1
Na	0.1	.003-.664	0.18	.008-.67	0.74	0.01-.41	0.03	.025-.24
K	0.08	.003-1.7	0.04	.006-.37	0.18	0.06-.64	0.23	.008-2.4
Fe	0.45	.094-4.2	0.75	.025-8.9	1.9	0.35-6.8	1.9	.059-9.3
Ti	0.06	.011-.54	0.04	.012-.13	0.07	.03-.15	0.09	.011-.49
S	0.7	.2-5.1	1.6	.2-4.9	3.5	.76-8.4	2.4	.5-15.0
Cl	<.02	nil-.09	<.01	nil-.03	0.17	nil-.77	<.02	nil-.065

\*Weight percent in dry coal.

†Rocky Mtns: Arizona, Colorado, New Mexico, Utah, southwestern Wyoming; Swanson et al. (76).  
 Northern Great Plains: North Dakota, Montana, northeastern Wyoming; Swanson et al. (76).  
 Illinois Basin: Illinois, Indiana, western Kentucky; Harvey et al. (5).  
 Appalachian Region: Alabama, eastern Kentucky, Maryland, Ohio, western Pennsylvania, Tennessee, Virginia, West Virginia; Swanson et al. (76).

Trace Elements. The mean concentrations of selected trace elements in some U.S. coals are listed in Table VII in order of decreasing average abundance in Illinois Basin coals. In the different regions, the elements decrease in abundance in nearly the same order with the notable exceptions of Zn and Sr. Zinc occurs in some channel samples from mines in Illinois in amounts up to 800 ppm, which results in a higher mean concentration of zinc in Illinois Basin coals as compared to western and Appalachian coals. Strontium averages unusually low in abundance in Illinois Coals. The boron content is also high in Illinois Basin coals because of the apparent saturation of the original peat deposit by sea water during the early stage of coalification. It is of interest that the mean concentration of Pb, Cr, Ni, and As are 3 to 5 times as high in Appalachian and Illinois Basin coals as in the two western regions (Table VII). This difference for Cr is tempered by the similarity of this element's range in the different regions, yet even the ranges for Pb, Ni, and As are notably lowest in the western coals.

### Summary

The suite of minerals occurring as impurities in U.S. coals of commercial quality is moderately consistent; this suite includes quartz, calcite, pyrite, various clay minerals including kaolinite, illite, and varieties of illite-smectite mixed-layer clay minerals. The weathering of pyrite produces some sulfate minerals in many coals. Several other minerals are present in most coals in trace amounts.

Pyrite contents vary most; and the largest percentage of pyrite occurs as nodules and/or fissures along cleat joints in the coal. This variation is largely explained by the variable geological conditions that prevailed during the time the original beds of peat were buried. If the peat was buried by muds deposited from fresh water rivers or lakes, little sulfur was introduced into the peat; whereas if the peat was buried by muds from sulfate-bearing sea water, considerable sulfur was introduced.

Western coals tend not to contain calcite, but are enriched in calcium associated with the organic matter. Calcite in Illinois Basin coals occurs in cleat joints and in nodules within the coal seams; kaolinite is also abundant along these joints. Because of these occurrences, the concentrations of calcite, kaolinite, and pyrite in cleaned coal products from this basin are much reduced compared to that of the mine-run material.

Uncommon mineral phases in trace amounts are difficult to detect by routine methods, but these minerals result in measurable amounts of trace elements in coals (32). These trace mineral phases may be quite important in engineering processes utilizing coal.

Inorganic elements in ash from all U.S. coal fields vary significantly, and each deposit must be analyzed to obtain sufficiently accurate assessment of their abundance. Some coal seams show uncommon enrichments in some metallic elements,

Table VII. Concentrations of Some Trace Elements in Some U. S. Coals\*

	Rocky Mtns.		Northern Great Plains		Illinois Basin		Appalachian Region	
	Mean	Range	Mean	Range	Mean	Range	Mean	Range
	No. of Samples 124		93		118		331	
Zn	9.9	1-130	25.6	1.1-86.3	248.	0.2-5300	20.	1.5-1072
Ba	200.	3-700	500.	15-2000	140.	5-2666	100.	7-700
B	70.	10-150	70.	30-200	118.	15-225	30.	1-100
Zr	20.	3-70	15.	3-50	35.	nil-133	50.	2-300
Sr	100.	15-700	150.	15-700	34.	<10-236	100.	7-700
V	15.	2-100	10.	1.5-50	31.	1.4-140	20.	2-150
Pb	5.5	.9-19	5.3	1.4-42.1	28.	nil-206	15.1	1-70
Cr	5.	.5-70	5.	.7-30	18.4	7-60	20.	<.5-70
Ni	3.	.7-20	3.	.7-20	18.	2-46	15.	1.5-300
Cu	9.1	1.5-100	8.3	2.4-22	12.5	4.6-66.5	24.	1.2-911
As	2.	< 1-50	3.	< 1-30	11.	1-151	27.	0.5-357
Co	2.	.3-10	2.	< .5-7	5.3	1.6-18	7.	0.5-300
U	1.6	<.2-24	.9	<.2-2.9	1.5	nil-9.3	1.4	<.2-11
Hg	.6	.01-1.5	.09	<.01-.5	.16	.03-.71	.24	.01-3.3

\*Parts per million in dry coal. The states in the different regions and corresponding sources for data are given in Table VI.



notably iron in some Western Interior coals, silicon in some Rocky Mountain coals, and aluminum in some Appalachian coals.

We recommend future research on mineral matter in coals be directed toward improving the methods to more accurately determine the mineral composition. Lower detection limits for trace minerals are needed, as is better precision for quantitative determinations. Standard methods of analysis of mineral phases in coal would assist in this work. Future research utilizing computer-assisted SEM, accompanied by X-ray fluorescence analysis, should be increasingly applied to provide much needed data on minerals in coals. Lastly, we recommend research be undertaken to identify mineral variability in coal seams within local areas. Although some geological factors have been identified that control the variation of some inorganic elements in coals, much additional work needs to be done on this topic. Multidisciplinary studies by chemists and geologists would likely reveal useful geological controls of mineral variations that are not now recognized. Success in these types of studies would greatly improve our ability to predict the quality of coal from untested areas of the seam.

#### Literature Cited

1. Gluskoter, H. H.; Shimp, N. F.; Ruch, R. R. In "Chemistry of Coal Utilization" 2nd suppl.; Elliott, M. A. Ed.; John Wiley & Sons: New York, 1981; pp. 369-424.
2. Zubovic, P. In "Environmental Deposits of Fuel Conversion Technology, II"; Ayer, F. A. Compiler; U.S. EPA-600/2-76-169, 1976, pp. 47-63.
3. Gluskoter, H. J.; Ruch, R. R.; Miller, W. B.; Cahill, R. A.; Dreher, G. B.; Kuhn, J. K. "Trace Elements in Coal: Occurrence and Distribution"; Ill. St. Geol. Survey, Circ. 499, 1977.
4. Kuhn, J. K.; Fiene, F. L.; Cahill, R. A.; Gluskoter, H. J.; Shimp, N. F. "Abundance of Trace and Minor Elements in Organic and Mineral Fractions of Coal"; Ill. St. Geol. Survey, EGN 88, 1980.
5. Harvey, R. D.; Cahill, R. A.; Chou, C. L.; Steele, J. D. "Mineral Matter and Trace Elements in the Herrin and Springfield Coals, Illinois Basin Coal Field"; Final Report, EPA-CR806654 (EPA-600/7-84-036), Ill. St. Geol. Survey, 1983.
6. Barkley, J. F. "The Sulphur Problem in Buring Coal"; U.S. Bur. Mines, Tech. Pap. 436, 1928.
7. Babcock & Wilcox. "Steam/its generation and use"; Babcock & Wilcox, New York, 1972, 15-1-22.
8. Reid, W. T. In "Chemistry of Coal Utilization", 2nd supp.; Elliot, M.A. Ed.; John Wiley & Sons: New York, 1981; 1387-1445.
9. Hensel, R. P.; Skowyra, R.S. Tappi 1976, 60, 101-5.
10. Bryers, R. W.; Taylor, T. E. J. Engng. for Power 1976, 528-39.
11. Bryers, R. W. J. Engng. for Power 1979, 506-15.
12. Vorres, K. S. J. Engng. for Power 1979, 101, 497-9.
13. Vaninetti, G. E.; Busch, C. F. J. Coal Quality 1982, 1, 22-31.

14. Pader, D. W.; Duzy, A. F. Coal Mining and Processing 1982, 19, 72-8.
15. Kurgan, G. J.; Balestrino, J. M.; Daley, J. R. "Coal Combustion By-products Utilization Manual, Volume 1: Evaluating the Utilization Option"; Michael Baker, Jr., Inc., Beaver, PA for EPRI, 1984.
16. Coal Industry Advisory Board Committee on Coal Quality and Ash Characteristics, G. Blackmore, Chairman: Old Ben Coal Co., Lexington, KY, 1984.
17. U.S. National Committee for Geochemistry "Trace Element Geochemistry of Coal Resource Development Related to Environmental Quality and Health"; National Academy Press, Washington, D.C., 1980.
18. Cobb, J. D.; Steele, J. D.; Treworgy, C. G.; Ashby, J. F. "The Abundance of Zinc and Cadmium in Sphalerite-bearing Coals in Illinois"; Ill. St. Geol. Survey, IMN 74, 1980.
19. Williams, E.G.; Keith, M. L. Economic Geology 1963, 58, 720-29.
20. Gluskoter, H. J.; Rees, O. W. "Chlorine in Illinois Coal"; Ill. St. Geol. Survey, Circ. 372, 1964.
21. Gluskoter, H. J.; Simon, J. A. "Sulfur in Illinois Coals"; Ill. St. Geol. Survey, Circ. 432, 1968.
22. Babu, S. P.; Barlow, J. A.; Craddock, L. L.; Hildalgo, R. V.; Friel, E. "Suitability of West Virginia Coals to Coal-Conversion Processes"; West Virginia Geological and Economic Survey, Coal-Geology Bull. 1, 1973.
23. Rao, C.P.; Gluskoter, H. J. "Occurrence and Distribution of Minerals in Illinois Coals"; Ill. St. Geol. Survey, Circ. 476, 1973.
24. Cecil, C. B.; Stanton, R. W.; Dulong, F. T. "Geology of Contaminants in Coal: Phase I Report of Investigations" U. S. Geol. Survey; Open-File Report 81-953A, 1981.
25. American Society for Testing and Materials, "Annual Book of ASTM Standards, Section 5, Petroleum Products, Lubricants, and Fossil Fuels"; ASTM: Philadelphia, 1983; D2797, pp. 375-9.
26. Ryer, T. A.; Langer, A. W. J. Sedimentary Petrology 1980, 50, 987-92.
27. Cady, G. H. In "Encyclopedia of Science and Technology"; McGraw-Hill: New York, 1971; Vol. 3, p. 245.
28. Trumbull, J. V. A. "Coal Fields of the United States, exclusive of Alaska", Sheet 1, U.S. Geol. Survey; Map scale 1:5,000,000, 1960.
29. Barnes, F. F. "Coal Fields of Alaska", Sheet 2, U. S. Geol. Survey; Map scale 1:5,000,000, 1961.
30. Spunk, G. C.; O'Donnell, H. J. "Mineral Matter in Coal"; U. S. Bur. Mines, Tech. Pap. 648, 1942.
31. Damberger, H. H.; Harvey, R. D.; Ruch, R. R.; Thomas, J. R. In "The Science and Technology of Coal and Coal Utilization"; Cooper, B. R.; Ellingson, W. A., Eds.; Plenum Press: New York, 1984; pp. 7-45.
32. Finkleman, R. B. Ph.D. Thesis, University of Maryland, College Park, 1980.
33. Cecil, C. B.; Stanton, R. W.; Dulong, F. T.; Renton, J.

- J. In "Atomic and Nuclear Methods in Fossil Energy Research"; Filby, R. H.; Carpenter, B. S.; Ragaini, R. C., Eds.; Plenum Publ. Corp.: New York, 1982; pp. 323-35.
34. Finkelman, R. B. Geol. Soc. America Abstracts with Program. 1981, 13, 451.
  35. Davis, A.; Russell, S. J.; Rimmer, S. M.; Yeakel, J. D. Int. J. Coal Geology 1984, 3, 293-314.
  36. Strehlow, R. A.; Harris, L. A.; Yust, C. S. Fuel 1978, 57, 185-186.
  37. Wert, C. A.; Hsieh, K. C. In "Proc. Int. Conf. on Coal Science"; Düsseldorf 7-9.9; Verlag Glueckauf GmbH, 1981, pp. 780-85.
  38. Stach, E.; Mackowsky, M.-Th.; Teichmüller, R. "Stach's Textbook of Coal Petrology", 3rd ed., Gebrüder Borntraeger, Berlin, 1982; pp. 153-170.
  39. Raymond, R., Jr.; Bish, D. L.; Godey, R. In "Mineral Matter in Peat"; Raymond, R., Jr.; Andrejko, M. J., Eds.; Los Alamos Natl. Lab.; LA-9907-OBES, 1983, pp. 159-67.
  40. Hatch, J. R. In "Cameron Volume on Unconventional Mineral Deposits"; Shank, W. C. III, Ed.; SME-AIME: New York, 1983, pp. 89-98.
  41. Ball, C. G. "Mineral Matter of No. 6 Bed Coal at West Frankfort, Franklin County, Illinois"; Ill. St. Geol. Survey, R.I. 33, 1935.
  42. Moza, A. K.; Strickler, D. W.; Austin, L. G. In "Scanning Electron Microscopy/1980/IV"; SEM Inc.; AMF O'Hare (Chicago); pp. 91-96.
  43. Huggins, F. E.; Kosmack, D. A.; Huffman, G. P.; Lee, R. J. In "Scanning Electron Microscopy/1980/I"; SEM Inc., AMF O'Hare (Chicago), 1980; pp. 531-40.
  44. Huggins, F. E.; Huffman, G. P.; Lin, M. C. Int. J. Coal Geology 1983, 3, 157-182.
  45. Palmer, C. A. Ph.D. Thesis, Washington State University, Pullman, 1983.
  46. Goldschmidt, V. M. "Geochemistry"; Muir, A., Ed.; Clarendon Press: Oxford, 1954, pp. 24-26.
  47. Schopf, J. M. "Field Description and Sampling of Coal Beds"; U.S. Geol. Survey, Bull. 1111-B, 1960.
  48. Swanson, V. E.; Huffman, C., Jr. "Guidelines for Sample Collecting and Analytical Methods Used in the U.S. Geological Survey for Determining Chemical Composition of Coal"; U.S. Geol. Survey, Circ. 735, 1976.
  49. Gladney, E. S. "Compilation of Elemental Concentration Data for NBS biological and Environmental Standard Reference Materials"; LA-8438MS Informal Report, July 1980, pp. 14-20.
  50. Doolan, K. J.; Turner, K. E.; Mills, J. C.; Knott, A. C.; Ruch, R. R. "Volatilities of Inorganic Elements in Coals During Ashing"; Australian Nat. Energy Research Dev. and Demo. Program, Proj. Grant 80/0220, Final Report, 1983.
  51. Schultz, H.; Wells, A. W.; Mima, M. J. Analytical Chemistry 1985, 57, 268R-278R.
  52. Russell, S. J.; Rimmer, S. M. In "Analytical Methods for Coal and Coal Products"; Kan, C., Jr.; Academic Press: New York, 1979; pp. 133-162.

53. Herzenberg, C. L. "Application Potential of Advanced Instrumental Methods for On-Line Automated Composition Analysis of Solid/Liquid Fossil Energy Process Materials Volume III: Non-Nuclear Methods"; Argonne National Lab. ANL/FF-83-22, 1984.
54. Ruch, R. R.; Gluskoter, H. J.; Shimp, N. F. "Occurrence and Distribution of Potentially Volatile Trace Elements in Coal"; Ill. St. Geol. Survey, EGN 72, 1974.
55. Minnis, M. M. Amer. Assoc. Petrol. Geol. Bull. 1984, 68, 744-52.
56. Wert, C. A.; Hsieh, K. C. In "Scanning Electron Microscopy/1983/III"; SEM Inc., AMF O'Hare (Chicago), 1983; pp. 1123-36.
57. Allen, R. M.; VanderSande, J. B. Fuel 1984, 63, 24-29.
58. O'Gorman, J. V.; Walker, P. L., Jr. Fuel 1973, 52, 71-79.
59. Earnest, C. M. "Thermal Analysis of Clays, Minerals and Coal"; Perkin-Elmer: Norwalk, CT, 1984, pp. 49-78.
60. Painter, P. E.; Rummer, S. M.; Snyder, R. W., Davis, A. Applied Spectroscopy 1981, 35, 102-6.
61. Estep, P. A.; Kovach, J. J.; Karr, C., Jr. Analytical Chemistry 1968, 40, 358-63.
62. Smith, G. V.; Liu, J-H.; Saporoschenko, M. Fuel 1978, 57, 41-45
63. Montano, P. A.; Magn. Reson. Rev. 1981, 7, 175-96.
64. Lin, M. C.; Huggins, F. E.; Huffman, G. P.; Lowenhaupt, D. E. Preprints American Chemical Society, Div. Pet. Chem. 1983, 28, 1196-1202.
65. Brown, J. R.; Kronberg, B. I.; Fyfe, W. S. Fuel 1981, 60, 439-46.
66. Gluskoter, H. J. Fuel 1965, 44, 285-91.
67. Miller, R. N.; Yarzab, R. F.; Given, P. H. Fuel 1979, 58, 4-10.
68. Adolphi, P.; Storr, M. Fuel 1985, 64, 151-55.
69. Johnson, P. J. M.S. Thesis, University of Illinois, Urbana, 1979.
70. Wier, C. E. "Coal Resources of Indiana"; Ind. Geol. Survey, Bull. 42-I, 1973.
71. Selvig, W. A.; Gibson, F. H.; "Analyses of Ash from United States Coals"; U.S. Bur. Mines, Bull. 567, 1956.
72. Abernathy, R. F.; Peterson, M. J.; Gibson, F. H. "Major Ash Constituents in U. S. Coals"; U.S. Bur. Mines, R. I. 7240, 1969.
73. O'Gorman, J. V.; Walker, P. L. Jr. Fuel 1971, 50, 135-51.
74. Finkleman, R. B.; Fiene, F. L.; Miller, R. H. Simon, F. O. "Interlaboratory Comparison of Mineral Constituents in a Sample from the Herrin (No. 6) Coal Bed from Illinois"; U.S. Geol. Survey, Circ. 932, 1984.
75. Glick, D. C.; Davis, A. "Variability in the Inorganic Content of United States' Coals--A Multivariate Statistical Study"; Final Report-Part 10, DOE Contract DE-AC22-80PC30013, Penn. State University, 1984.
76. Swanson, V. E.; Medlin, J. H.; Hatch, J. R.; Coleman, G. H.; Wood, D. S.; Woodruff, S. D.; Hildebrand, R. T. "Collection, Chemical Analysis, and Evaluation of Coal Samples in 1975"; U.S. Geol. Survey, Open-File Report 76-468, 1976.

RECEIVED August 1, 1985

## Geologic Controls on the Inorganic Composition of Lower Kittanning Coal

Susan M. Rimmer<sup>1</sup> and Alan Davis<sup>2</sup>

<sup>1</sup>Department of Geology, University of Kentucky, Lexington, KY 40506

<sup>2</sup>Department of Geosciences, The Pennsylvania State University, University Park, PA 16802

Lateral trends in mineral composition of the Lower Kittanning seam can be related to depositional environments. Syngenetic pyrite formation occurred in areas where the overlying shales indicate brackish conditions existed; marcasite formed epigenetically. Quartz content increases towards a northern source area which is coincident with a basement high. Kaolinite, the major clay component, is predominantly authigenic and increases towards the margins of the depositional basin where it was stable in the low pH, freshwater areas of the peat swamp. Illite/mica is mostly detrital (as indicated by the high-temperature polytype) and increases towards the center of the basin due to its greater stability in marine-influenced environments. Low expandable clay contents are consistent with the level of metamorphism experienced by this coal.

The mineral composition of coal is the result of physical, chemical and biological processes acting on the system from the time of peat accumulation, through burial and subsequent increase in metamorphic level, to the present. With respect to origin, inorganic constituents may be classified as detrital (those transported into the peat swamp) or authigenic (those formed within the environment). Mackowsky (1) further differentiates between syngenetic minerals, formed during the accumulation of peat, and epigenetic minerals, which formed later.

In recent years, the question has been raised as to whether most of the silicate minerals in coal are derived from inorganic substances originally contained within peat-forming plants (2-4), or from sources outside the peat swamp (5-6).

Studies of modern peat-forming environments have emphasized the importance of detrital influx (6-7), syngenetic formation of pyrite (8) and biogenic silica (7,9), and *in-situ* mixing with underlying sediments (7,10) to account for mineral constituents in peat. Within

the peat environment unstable detrital clays, such as smectite and illite, may undergo alteration or dissolution (6,11), whereas kaolinite may form authigenically (2,12). In addition, biogenic silica dissolves, possibly contributing to later authigenic clay formation (6,9); in coals, authigenic kaolinite in cleats is common (13-14). Clays may also form by alteration of volcanically-derived material within the peat swamp (15-16).

Whereas many authors have emphasized the great contribution of detritus to the mineral content of some coals, such as the Waynesburg (5), the existence of coals with little or no identifiable detrital input, such as the Indiana Block coal (17), has led other authors (3-4) to suggest that the inorganic portion of swamp plants is an important source of ash constituents in the coal (including quartz and clays). It is suggested that this is particularly important in the case of low-ash, commercial-quality coals (2). A recent cathodoluminescence study indicates that most of the quartz that is intimately mixed with the organic portion of the coal (i.e. not associated with attrital coal layers) is indeed authigenic, and probably derived from constituents originally contained in the plants (18).

It appears, therefore, that several origins are possible for minerals in peat and coal, including detrital influx, biogenic input, and precipitation either during or after peat accumulation, including some contribution from inorganic substances derived from plants. Various studies have attempted to relate inorganic composition to conditions that existed at the time of peat accumulation. Pyrite has been associated with marine and brackish conditions (8,19), and the pyrite content of coal has been related to roof lithologies which reflect those conditions (20-21). Clay assemblages in coals and underclays also have been related to depositional environment (14,22).

The purpose of this paper is to describe variability in the inorganic content of the Lower Kittanning coal seam in western Pennsylvania and attempt to explain the distribution of minerals, taking into consideration depositional environment and level of metamorphism. The Lower Kittanning peat accumulated on a delta plain; as the sea transgressed from the west, the peat was later covered by the Lower Kittanning Shale. Fossil invertebrates in this shale unit indicate freshwater, brackish and marine conditions existed across the study area (23). Structural features of the basin may have strongly influenced sedimentation (24). During accumulation of Lower Kittanning sediments and peat, the greatest amount of subsidence is believed to have occurred in the western and southwestern parts of western Pennsylvania, where the basement is now more deeply buried, leaving the edges of the basin topographically higher (24). Bouguer gravity and sediment thickness data provide support for this increased subsidence. Basement highs, also indicated by gravity anomalies, represent a second control on sedimentation. Such a high exists in the north-central part of western Pennsylvania and may have supplied detrital material to the swamp, supplementing a predominantly eastern sediment source. Additional controls on sedimentation appear to be active folds and local variations in paleotopography (24).

### Sampling and Methods

Forty-three channel samples of the Pennsylvanian-age Lower Kittanning coal (Kittanning Formation, Allegheny Group) were collected in western Pennsylvania. Samples are representative of the three suggested depositional environments (Figure 1) and also of the increase in rank from high volatile B bituminous in the west to low volatile bituminous in the southeast. Chemical analyses included major and minor elements, total sulfur and sulfur forms. Low-temperature ashes (LTA's) were obtained according to procedures described by Gluskoter (25). X-ray diffraction analysis of LTA's provided qualitative, quantitative (for quartz and pyrite), and semi-quantitative (for clays in the less than 2 micron fraction) data using procedures modified from Russell and Rimmer (26). Kaolinite was quantified using infra-red spectroscopy. Mineral composition was also calculated by normative techniques modified by Rimmer (12) from methods used by earlier workers (27-28).

The spatial distribution of these mineral constituents was assessed by contouring and by trend surface analysis. One problem that must be addressed in a study such as this, is whether the density of data points is sufficient to justify the description of trends across the basin, or is local variability in the constituents too great. Application of trend surface analysis permitted a statistical assessment of basinal trends, and indicated the extent of local variation. In this paper, contour maps are presented to show important basinal trends; trend surface analysis indicated that these trends were statistically significant. Details of the trend surface technique and complete data are described in Rimmer (12).

### Results and Discussion

The major mineral components of this coal are quartz, pyrite (and marcasite), and clays (predominantly kaolinite and illite/mica, with minor amounts of expandable clays).

Pyrite and Marcasite. High sulfide concentrations are found towards the central part of the study area, particularly where the overlying shales indicate brackish conditions existed on the southeastern side of the basin (Figure 2). This observation supports a similar finding by Guber (29), rather than the conclusion of other workers that higher pyrite contents are associated with marine rocks (20). Factors influencing the distribution of sulfur in peat and coals include availability of iron and sulfate, and pH. Sulfate is thought to be introduced by marine and brackish waters (8). Recent work on pyrite distribution in the Florida Everglades (30) indicates high pyrite contents are associated with brackish conditions rather than marine, and this has been related to the availability of iron in the different environments. In freshwater, iron is transported in organic colloids which flocculate quickly upon entering brackish water, resulting in a higher availability of iron in the brackish environment (31). In addition, some iron may also be transported into the swamp by detrital clays which also flocculate upon entering the swamp. Acidity is also a factor, as much of the pyrite appears to form as a by-product of sulfate-reducing bacteria (8). Compared

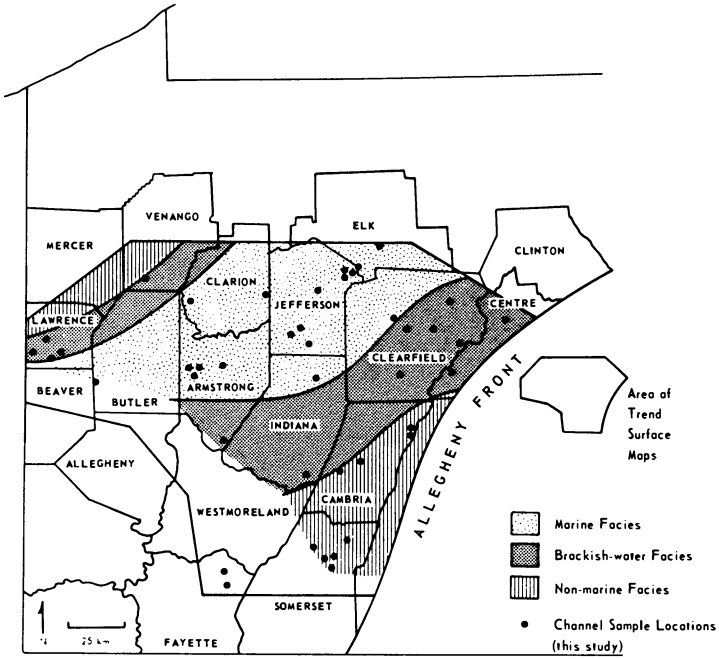


Figure 1. Distribution of Lower Kittanning coal samples in western Pennsylvania in relation to suggested environments of deposition for the overlying shale.

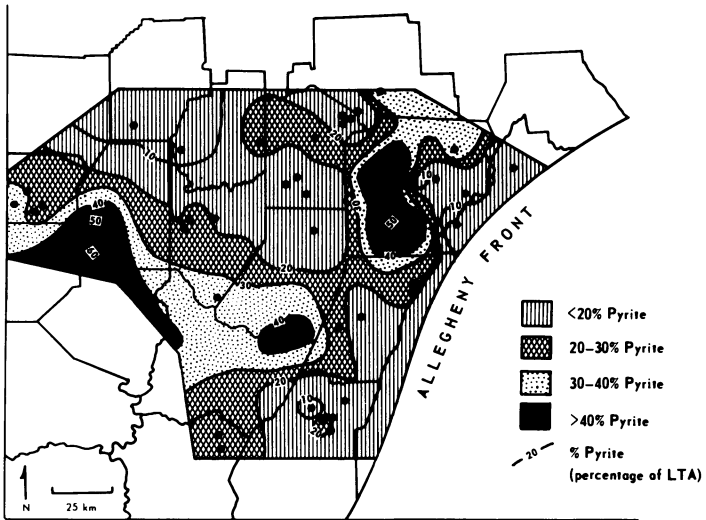


Figure 2. Pyrite content of the Lower Kittanning seam (% LTA basis, as determined by x-ray diffraction analysis).



to the more acidic freshwater environments, higher levels of microbial activity would occur in the neutral to basic pH conditions associated with brackish or marine waters.

In the case of the Lower Kittanning seam, therefore, whether iron was transported in organic-rich colloids or was associated with clays, iron availability would tend to be higher in those areas which received an influx of freshwater and detritus. The brackish zone in the southeastern part of the basin thus represents an optimization of iron and sulfate availability and pH level of the swamp waters.

The discussion thus far has assumed a syngenetic origin for the pyrite. Observations of sulfide morphology suggest that at least some of the sulfide may be epigenetic. Edwards and Baker (32) showed that pyrite forms in marine environments whereas marcasite forms under more acidic conditions. Recent experimental work has shown that pyrite forms at a pH of 5.0, whereas marcasite forms at a pH of 3.5 (33). The occurrence of marcasite in what apparently are marine facies may therefore indicate subsequent acidification.

In the Lower Kittanning seam, marcasite occurrence does not appear to be closely related to depositional environment. Coal samples associated with freshwater, brackish and marine facies contain both pyrite and marcasite. Marcasite is absent or only a minor constituent in low-sulfide (less than 20%, LTA basis) samples. If these coals had formed in an acidic swamp environment, a dominance of marcasite over pyrite might have been expected. In fact, marcasite is more abundant in high-sulfide coals. A possible explanation is that the marcasite is epigenetic, and its presence indicates an increase in the acidity of the interstitial waters following burial. This interpretation of the epigenetic nature of marcasite in the Lower Kittanning seam is supported by petrographic observations. For example, marcasite frequently occurs in sulfide masses, such as spherules which may represent recrystallized framboids, or as cell infillings.

Quartz. In this seam, quartz content tends to be relatively low, with many samples containing less than 15% (Figure 3). High quartz contents (15-20% and above) are observed in the north-central part of the region, in Clarion and Jefferson Counties, and in several isolated areas along the eastern edge of the field area, such as Centre County. Low quartz contents occur in a zone extending from the south and southeast towards the northwest, and in Clearfield County.

The distribution of quartz may provide clues as to the origin of this mineral in the Lower Kittanning seam. Quartz may have been transported into the peat swamp by water and wind (detrital), or may have precipitated within the swamp, possibly from silica that was originally contained in the swamp plants. Some of the quartz grains observed in this study were 30-50 microns in size, and most grains were concentrated in attrital coal bands. Both of these observations suggest that much of the quartz in the Lower Kittanning is of detrital origin.

Williams and Bragonier (24) suggested a basement high, situated in the north-central part of western Pennsylvania, was a control on sedimentation during the Pennsylvanian. It is possible that quartz-rich sediments were shed from this topographic high into the

peat swamp. Transportation of sediment within a swamp is restricted by the filtering effect of the vegetation (7). It would be unlikely, therefore, that detrital quartz would be dispersed evenly throughout the swamp, but rather it would concentrate close to the source area. The irregular distribution of quartz along the eastern margin of the basin again reflects a detrital influx. Sediment entering the swamp from the east was predominantly clay, with minor influxes of quartz occurring locally.

Holbrook (34) observed that quartz content of the Lower Kittanning underclay was highest directly over clastic wedges in Clarion and Jefferson Counties and over another wedge in Lawrence County. This coincides with areas of high quartz content in the Lower Kittanning coal itself. Quartz-rich sediment from the north may have continued to be received by these areas during peat accumulation. Alternatively, mixing of the underlying sediments with the lower peat layers, perhaps aided by bioturbation, may have occurred; however, the vertical distribution of quartz in the seam (12) does not support this hypothesis.

Clay Minerals. Clay minerals may be transported into the swamp during peat accumulation (detrital), precipitate from solutions rich in aluminum, silicon and various cations (syngenetic and epigenetic), or may form by the alteration of other minerals either within the swamp or during burial (transformation and/or diagenesis) (6).

The Lower Kittanning coal contains kaolinite (well-crystallized), illite/mica and expandable clays. Low total clay contents are observed in the center of the study area, where the coal is rich in pyrite, and in the north-central region where high quartz contents are observed. High total clay contents are seen on the northwestern and eastern margins of the basin. Because clay mineral data are presented as a percentage of the low-temperature ash, variations in the quartz and pyrite contents influence the proportionate distribution of the clays. To avoid this problem, the relative amounts of individual clay minerals in the clay (less than 2 micron) fraction were examined. As this size fraction contains only clays, variations in quartz and pyrite do not influence the results.

Kaolinite content increases towards the margins of the basin (Figure 4), whereas illite and expandable clays increase towards the center of the basin (not illustrated). The distribution of kaolinite in the Lower Kittanning seam closely resembles that found in the underclay. Holbrook (34) related high kaolinite content of the Lower Kittanning underclay to topographic highs, where kaolinite enrichment resulted from subaerial leaching. Thus, high kaolinite contents are found along the margins of the basin and in other areas which exhibited positive relief. Comparison with data presented in Holbrook (34) suggests that many of the coal samples which contain more kaolinite overlie kaolinite-rich underclays. This is particularly true in the north, northwest and southeast. Mixing of peat with the underlying sediment could have increased the kaolinite content in these areas. Sharp contacts were observed between coal and underclay, but evidence of such intermixing could be obscured during compaction.

In a study of clay mineral variations in underclays in the Illinois Basin, Parham (22,35) suggested that differential

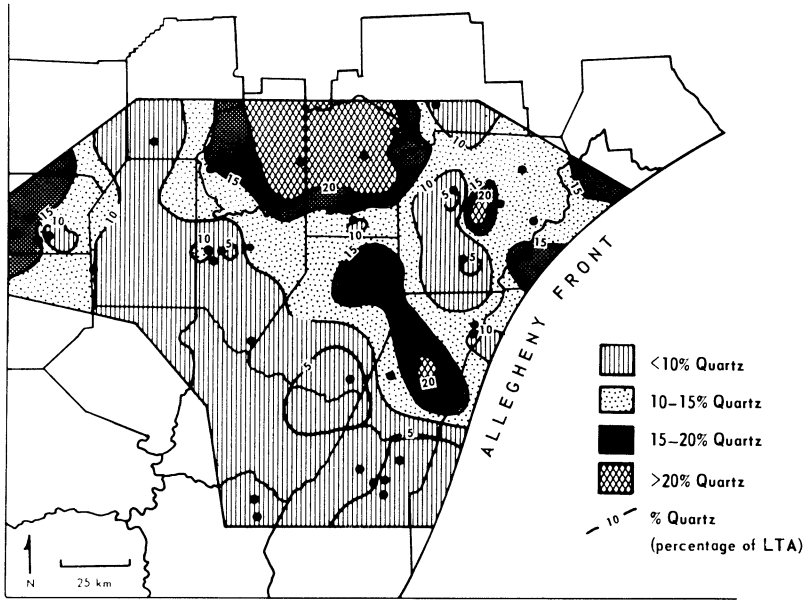


Figure 3. Quartz content of the Lower Kittanning seam (% , LTA basis, as determined by x-ray diffraction analysis).

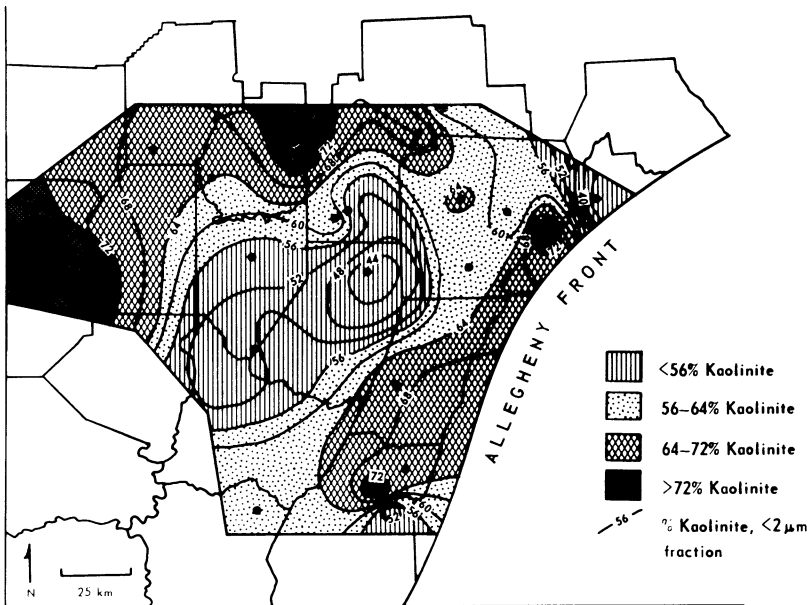


Figure 4. Kaolinite content of the Lower Kittanning seam (% of the less than 2 micron fraction).

flocculation across the depositional basin resulted in higher kaolinite contents towards the basin margins, whereas illite and expandable clay contents increase towards the center of the basin. According to this theory, some authigenic formation or regrading of illite would also take place. Holbrook (34) argued against this process for the Lower Kittanning underclay on the basis that most of the mica he observed was the 2M<sub>1</sub> polytype, which forms only at temperatures far in excess of those experienced during burial of these sediments, thus any mechanism that involved formation of mica within the basin would not be valid. Similarly, the 2M<sub>1</sub> illite/mica polytype is present in the Lower Kittanning<sup>1</sup> coal, particularly in clay partings and high-ash samples (4,12). In some samples, polytype identification was difficult, however, owing to the degraded nature of this mineral which resulted in broad diffraction peaks. The presence of degraded illite/mica is not surprising because, under the conditions that existed within the peat swamp and during burial, leaching by organic acids would most likely have occurred.

Alternatively, the distribution of clays in this coal can be explained in terms of the chemical conditions that existed in the swamp environment. A comparison of Figures 1 and 4 shows that kaolinite occurs in areas which may have been influenced by freshwater conditions; illite and expandable clay contents are generally higher in areas of the basin which may have experienced more brackish conditions. Under the acidic conditions that existed in the freshwater swamps, kaolinite would be the stable clay mineral, forming either from solution or as the alteration product of incoming sediment. The high degree of crystallinity of this kaolinite suggests *in situ* formation which could result from either of these mechanisms (12). Towards the center of the basin, neutral pH conditions existed and illite/mica was less altered than in the more acidic freshwater conditions. This trend would have been even more pronounced with the onset of the marine invasion. Alteration of the illite/mica still proceeded to some extent, producing degraded illites and expandable clays. Around the margins of the swamp, influxes of sediment, now represented by clay partings within the coal, introduced illite/mica-rich sediments, thus accounting for some of the local decreases in kaolinite content.

To examine further the influence of peat-swamp chemistry on the clays, the composition of the clay fraction of the coal samples was compared to that of floor, roof, and parting samples. Coal samples tend to be enriched in kaolinite compared to other sample types (Table I). Floor rocks tend to have the highest expandable clay contents, whereas roof rocks have the highest illite/mica contents. If it is assumed that the composition of the roof shales is the closest representation of parent mineralogy available, the clay sediments entering the depositional basin included considerable amounts of illite/mica, moderate amounts of kaolinite, relatively small amounts of expandable clays, and some chlorite. Whereas some modifications may have taken place since deposition of the clays in the roof shales, they probably have been affected less by the organic acids than the clays in the underclays, coals or partings. The presence of chlorite in the roof rocks suggests that acidic

conditions have not been experienced, because this mineral is usually unstable in such environments.

Table I. Clay Composition of the Less Than 2 Micron Fraction of Coals and Associated Sediments: Summary Statistics.

Sample Type	Sample Size (n)	Kaolinite + Chlorite		Illite/Mica		Expandable Clays	
		$\bar{x}$	s	$\bar{x}$	s	$\bar{x}$	s*
Coals	28	62.2	12.58	23.6	8.03	14.1	8.55
Floors	18	42.2	11.53	33.7	12.45	23.9	8.94
Roofs	16	31.2	11.03	50.4	12.71	18.3	10.00
Partings	4	43.5	17.89	41.5	9.88	15.0	8.16

\* n = Number of Samples;  $\bar{x}$  = Mean; s = Standard Deviation

Acidic conditions within the peat swamp, particularly in the freshwater areas, would favor the formation and/or preservation of kaolinite. This would result in the observed enrichment in kaolinite within the coal relative to the surrounding sediments. Relatively low illite/mica contents are observed in the coals, possibly due to alteration of this clay to expandable clays and ultimately to kaolinite. The transition from expandable clays to kaolinite has been observed in the Snuggedy Swamp by Staub and Cohen (11).

The inorganic partings within the coal have slightly higher illite contents; however, very few samples were examined and the results must be interpreted with care. Most of the clay in these partings is detrital rather than the result of *in situ* formation, as suggested by the presence of 2M<sub>1</sub> illite/mica and the low degree of crystallinity of the kaolinite. This is in contrast to most of the kaolinite within the coal which is probably authigenic.

The floor rocks contain larger amounts of expandable clays compared to the coals and roof rocks. Kaolinite is less abundant than in the coals, but more so than in the roofs. Only one sample contained any chlorite. These observations are consistent with alteration of underlying sediment by organic acids as suggested by Rimmer and Eberl (36). Acting on a typical sedimentary clay assemblage, such as that observed in the roof shales, organic acids would leach the clays resulting in the destruction of chlorite and the gradual alteration of illite to expandable clays. As suggested by the slight increase in kaolinite, this alteration may have progressed to kaolinite. Alteration of clays in the floor rocks is less severe than was experienced by clays within the peat swamp itself; thus, the floor rocks have lower kaolinite contents than the coals.

A final control on clay mineral composition is the extent of metamorphism experienced by the coals. With the increase in rank exhibited by this coal across the study area, certain diagenetic changes might be expected. Whereas no consistent trends in the type of expandable clays was observed, a general lack of smectite and expandable clays was noted. These clays do occur in lower rank bituminous coals, such as those in the Illinois Basin (14). Thus, it appears that thermal maturity (coal rank) may help explain the absence of smectite and the paucity of mixed-layer expandable clays in the Lower Kittanning coal and associated sediments, but no distinct relationship was found between the amount of expandable clays and rank.

The most significant control on clay mineral composition, therefore, appears to be chemical conditions within the swamp which produced alteration of a parent material that included illite/mica, kaolinite, and lesser amounts of chlorite and expandable clays. Within the acidic freshwater environments, alteration of other clays to kaolinite may have occurred, in addition to the precipitation of kaolinite from solution. In brackish or marine conditions, kaolinite formation was not favored, resulting in a relative increase in illite/mica content. Some illite may have formed diagenetically, but the presence of the high-temperature polytype indicates a detrital origin for most of this clay mineral. Regrading of degraded illites may have also taken place in potassium-rich marine or brackish waters. Local increases in expandable clays along the edges of the swamp may reflect chemical alteration of mica-rich sediments introduced into the peat swamp.

### Summary

The distributions of minerals within the Lower Kittanning seam can be related to depositional environment. Pyrite content is highest in areas which may have experienced brackish conditions. This distribution reflects the availability of iron and sulfur, and pH conditions within the swamp. Whereas much of the pyrite formed syngenetically, observations of sulfide modes of occurrence suggest that marcasite formed epigenetically.

The relatively high quartz contents observed towards the north of the study area reflect the influx of quartz-rich detritus from a topographic high in that area. Most of the detritus entering the basin from the east was clay-rich; however, local influxes of quartz may have occurred periodically.

Chemical conditions within the peat swamp influenced the clay mineral assemblage. Kaolinite is enriched towards the margins of the depositional basin; an authigenic origin in acidic freshwater conditions is proposed for much of this clay. Illite/mica is primarily detrital, as indicated by the presence of the high-temperature polytype. An increase in illite/mica towards the center of the basin reflects the greater stability of this clay in a marine-influenced environment. The level of metamorphism of the coal (rank) may explain the paucity of expandable clays.

### Acknowledgments

The authors acknowledge U.S. Department of Energy Contract Number DE-AC22-80PC30013 for financial support of the research presented here. Additional support was provided by the Pennsylvania State University Cooperative Program in Coal Research and by the Phillips Petroleum Foundation.

### Literature Cited

1. Mackowsky, M-Th. In "Coal and Coal-Bearing Strata"; Murchison, D.; Westoll, T.S., Eds.; American Elsevier: New York, 1968; pp. 325-345.
2. Cecil, C.B.; Stanton, R.W.; Dulong, F.T.; Ruppert, L.F.; Renton, J.J. In "Mississippian-Pennsylvania Boundary in the Central Part of the Appalachian Basin, Part 1: Southwestern Virginia-Southern West Virginia"; Englund, K.J.; Henry, T.W., Eds.; Geol. Soc. Amer. Field Guide, 1981; pp. 175-177, 192-194.
3. Renton, J.J.; Cecil, C.B. In "Carboniferous Coal Short Course and Guidebook, Vol. 3"; Donaldson, A.C.; Presley, M.K.; Renton, J.J., Eds.; AAPG Seminar: Morgantown, W.Va., 1980; pp. 103-128.
4. Renton, J.J.; Cecil, C.B.; Stanton, R.; Dulong, F. In "Carboniferous Coal Short Course and Guidebook, Vol. 3"; Donaldson, A.C.; Presley, M.K.; Renton, J.J., Eds.; AAPG Seminar: Morgantown, W.Va., 1980, pp. 57-101.
5. Finkelman, R.B. Geol. Soc. Amer. Abstr. Progr., 1981, 7, p. 450.
6. Davis, A.; Russell, S.J.; Rimmer, S.M.; Yeakel, J.D. Int. J. Coal Geol. 1984, 3, 293-314.
7. Otte, L.J. Geol. Soc. Am. Ann. Mtg. Abstr. Progr., 1984, p. 185.
8. Casagrande, D.J.; Siefert, K.; Berschinski, C.; Sutton, N. Geochim. Cosmochim. Acta 1977, 41, 161-167.
9. Andrejko, M.J.; Raymond, R. Jr.; Cohen, A.D. In "Mineral Matter in Peat: Its Occurrence, Form, and Distribution"; Raymond, R. Jr.; Andrejko, M.J., Eds.; Proc. Workshop, Los Alamos Natl. Lab.: Los Alamos, New Mexico, 1983; pp. 25-37.
10. Andrejko, M.J.; Cohen, A.D.; Raymond, R. Jr. In "Mineral Matter in Peat: Its Occurrence, Form, and Distribution"; Raymond, R. Jr.; Andrejko, M.J. Eds.; Proc. Workshop, Los Alamos Natl. Lab.: Los Alamos, New Mexico, 1983; pp. 3-24.
11. Staub, J.R.; Cohen, A. J. Sed. Pet. 1978, 48, 203-210.
12. Rimmer, S.M. Ph.D. Thesis, The Pennsylvania State University, University Park, 1985.
13. Ball, C.G. Econ. Geol. 1934, 29, 757-776.
14. Gluskoter, H.G. J. Sed. Pet. 1967, 37, 205-214.
15. Bohor, B.F.; Pollastro, R.M.; Phillips, R.E. 27th. Ann. Clay Min. Conf. Prog. Abstr., 1978, p. 47.
16. Bohor, B.F.; Triplehorn, D.M. In "Coal and Coal-Bearing Rocks of Eastern Kentucky"; Cobb, J.C.; Chestnut, D.R., Jr.; Hester, N.C.; Hower, J.C., Eds., Geol. Soc. Amer. Field Trip Guide, 1981; pp. 49-54.
17. Finkelman, R.B. Ph.D. Thesis, University of Maryland, College Park, 1981.

18. Ruppert, L.F.; Cecil, C.B.; Stanton, R.W. J. Sed. Pet. 1985, 55, 334-339.
19. Spackman, W.; Cohen, A.D.; Given, P.H.; Casagrande, D.J. "A Field Guide to Aid in the Comparative Study of the Okefenokee Swamp and the Everglades-Mangrove Swamp-Marsh Complex of Southern Florida"; The Pennsylvania State University Coal Research Section Short Course, University Park, PA., 1976.
20. Williams, E.G.; Keith, M.C. Econ. Geol. 1963, 58, 720-729.
21. Kravits, C.M.; Crelling, J.C. Int. J. Coal Geol. 1981, 1, 195-212.
22. Parham, W.E. Proc. Int. Clay Conf., 1966, pp. 135-145.
23. Williams, E.G. J. Paleontol. 1960, 34, 908-922.
24. Williams, E.G.; Bragonier, W.A. In "Carboniferous of the Southeastern United States"; Briggs, G., Ed.; SPECIAL PAPER 148, Geological Society of America, pp. 135-152.
25. Gluskoter, H.G. Fuel 1965, 44, 285-291.
26. Russell, S.J.; Rimmer, S.M. In "Analytical Methods for Coal and Coal Products, Vol. III"; Karr, C. Jr., Ed.; Academic Press: New York, 1979; pp. 133-162.
27. Pollack, S. Fuel 1979, 58, 76-78.
28. Given, P.H.; Weidon, D.; Suhr, N. "Investigation of the Distribution of Minerals in Coal by Normative Analysis"; Tech. Rept. 2, Pennsylvania State University to U.S. Dept. Energy, Rept. No. FE-2494-TR-2, 1980.
29. Guber, A.L. Proc. Int. Geol. Congress, 1972, 24, pp. 389-396.
30. Cohen, A.D.; Spackman, W.; Dolsen, P. In "Mineral Matter in Peat: Its Occurrence, Form and Distribution"; Raymond, R. Jr.; Andrejko, M.J., Eds.; Proc. Workshop, Los Alamos Natl. Labs.: Los Alamos, New Mexico, 1983; pp. 87-112.
31. Sholkovitz, E.R.; Boyle, E.A.; Price, N.B. Earth and Planet. Sci. Newsletter 1978, 40, 130-136.
32. Edwards, A.B.; Baker, G. J. Sed. Pet. 1951, 21, 34-46.
33. Murowchick, J.B.; Barnes, H.L. Geol. Soc. Amer. Abstr. Progr. 1983, 15, p. 649.
34. Holbrook, P.W. Ph.D. Thesis, The Pennsylvania State University, University Park, 1973.
35. Parham, W.E. Ph.D. Thesis, University of Illinois, Urbana, 1962.
36. Rimmer, S.M.; Eberl, D.D. Clays and Clay Miner. 1982, 30, 422-430.

RECEIVED August 1, 1985



# Semiquantitative Determination of Coal Minerals by X-ray Diffractometry

John J. Renton

Department of Geology, West Virginia University, Morgantown, WV 26506

The most commonly employed analytical procedure for the quantification of minerals in coal is x-ray diffraction analysis of the low temperature ash. The magnitudes of the Bragg intensities used to evaluate mineral abundances are affected by inherent compositional and/or structural variations characteristic of a number of the common minerals found in coal and by non-random crystallite orientation within the sample mount. The subsequent variations in Bragg intensities cause the Bragg intensity-mineral abundance relationship to depart from linearity and result in errors of determination of mineral abundances of  $\pm 10$  percent or more. The procedure must therefore be considered only semi-quantitative.

The purpose of this paper is to present and support the argument that abundance estimates of the minerals in coal based upon x-ray diffraction (XRD) data can only be considered semi-quantitative with expected errors of determination of 10 percent or more of the reported values. The compositional and physical characteristics of the low temperature ash components of coal relative to the preparation and mounting of ash for XRD analysis also affect the precision of analyses.

## Minerals in Coal

The minerals commonly found in coal are listed in Table I. In the average coal, clay minerals may constitute up to 60 weight percent of the mineral matter (1-2). Quartz is usually the second most abundant mineral, with up to 20 weight percent being common. The carbonate minerals (calcite, siderite and to a lesser extent, dolomite and ankerite) and the iron disulphide minerals (pyrite and marcasite) make up, on the average, up to 10 weight percent of each group. Sulphate minerals of calcium and iron and the feldspar minerals are commonly present but rarely in concentrations of more than a few weight percent. Except for unusual cases such as the

Table I  
COMMON COAL MINERALS

Major	Silicates	Clay Minerals	Kaolinite <sup>1</sup>	$Al_2Si_2O_5(OH)_4$		
			Illite	a		
			Mixed Layer	b		
			Chlorite	$(MgFeAl)_6(SiAl)_4O_{10}(OH)_8$		
			Quartz	$SiO_2$		
Minor	Carbonates	Carbonates	Calcite	$CaCO_3$		
			Dolomite	$(Ca, Mg)(CO_3)_2$		
			Ankerite	$Ca(Fe, Mg)CO_3$		
			Siderite	$FeCO_3$		
			Disulfides	Disulfides	Pyrite	$FeS_2$ (cubic)
					Marcasite	$FeS_2$ (orthorhombic)
			Sulfates	Sulfates	Coquimbite	$Fe_2(SO_4)_3 \cdot 9H_2O$
					Szomolnokite	$FeSO_4 \cdot H_2O$
					Gypsum	$CaSO_4 \cdot 2H_2O$
					Bassanite	$CaSO_4 \cdot 1/2H_2O$
Anhydrite	$CaSO_4$					
Jarosite	$KFe_3(SO_4)_2(OH)_6$					
Feldspars	Feldspars	Plagioclase	$(NaCa)Al(AlSi)Si_2O_8$			
		Orthoclase	$KAlSi_3O_8$			

<sup>a</sup> Illite has a composition similar to muscovite -  $KAl_2(Si_3Al)O_{10}(OH)_2$ , except for less K<sup>+</sup> and more  $SiO_2$  and  $H_2O$ .

<sup>b</sup> Mixed layered clays are usually randomly interstratified mixtures of illitic lattices with montmorillonitic and/or chloritic lattices.

sulphide rich coals of the northern Illinois Basin, the occurrence of the other minerals in concentrations exceeding a few percent is rare. It must, however, be kept in mind that the mineralogy of the inorganic portion of coal shows systematic variation both geographically and locally reflecting the geochemistry of the original peat forming environment (3). As a result, "average" values of concentration may have little practical meaning.

Most coals considered for conversion processes such as liquifaction, and thereby those of prime interest to chemists, are generally high in ash (>10 weight percent) and sulfur (>1 weight percent). In such coals, illite would invariably be the dominant clay material, constituting, in some coals, up to half or more of the mineral content. Most of the sulfur contained in these coals will be in the form of pyrite although marcasite may be locally dominant (4).

#### Quantification by X-ray Diffraction

The most commonly employed quantitative XRD procedure used to evaluate the concentration of mineral components in a multicomponent mixture of minerals compares the Bragg intensity data of unknowns to those generated from a suite of known standard samples. Mineral specimens are acquired to represent each of the minerals expected in the unknowns. The specimens are ground to a uniformly small size (less than 44 microns) and mixed together in concentrations which represent the range of concentrations expected for each mineral. An internal standard such as calcium fluoride, aluminum oxide or powdered aluminum is usually added in order to monitor and correct for variations in sample absorption and instrumental variables. Working curves are then prepared by plotting the ratio of intensity (preferably integrated intensity) of the Bragg reflection chosen to quantify the mineral to that chosen for the standard versus the weight percent of the mineral in the standard samples.

This procedure will provide analyses of high precision provided certain basic assumptions are met: (1) the composition and crystallinity (degree of ordering) of the individual minerals in the unknowns are both REASONABLY constant from sample to sample and (2) the composition and crystallinity of the standard minerals chosen for the preparation of the standard samples REASONABLY duplicate the composition and crystallinity of the respective minerals in the unknowns. The purpose of the following discussion is to demonstrate that, in the case of coal minerals, neither of the above assumptions is valid and as a result, any such quantitative procedure will reflect the inherent degree of departure from these basic assumptions and will therefore be semi-quantitative. Other procedures using data normalized to the total integrated intensity and quantification procedures utilizing weighting factors based upon standard chemical formulae for the minerals can be used but with no improvement in quantitative errors (5-6).

Illite and pyrite were specifically cited in the above discussion to make a point relative to the precision and accuracy with which coal minerals can be quantified by XRD. First, illite is NOT a mineral. Illite is "...a general term for the clay mineral constituents of argillaceous sediments belonging to the mica group"

(7). To a clay mineralogist, the term illite is synonymous with variability in both composition and crystallinity (8). The situation is even further complicated by the fact that much of the material in coal referred to as "illite" is actually an illite dominated mixed layered clay wherein the illite lattices are randomly interstratified with  $14\text{\AA}$  clay lattices; usually chlorite. This mixing of clay mineral lattices further adds to the inherent variability in both composition and crystallinity of the illitic material. The constitution of "illite" can therefore be expected to vary significantly from sample to sample. It should be quite apparent from the above discussion that no "standard" illite exists that could be used to represent illite in standard samples.

The iron disulphides may represent 10 weight percent or more of high ash-high sulfur coal ashes. Usually, pyrite is the major disulphide. Pyrite occurs in coal in a number of morphological forms and sizes (9). Not only does the pyrite in coal vary in morphology and size but also in stoichiometry and crystallinity. Studies have been conducted in the author's laboratory on cut and polished surfaces of coal blocks wherein the blocks have been exposed to the atmosphere and the pyrites observed over a period of time. Some pyrite grains, the euhedral forms (those that show definite crystal faces), remain bright and show little tendency to react. The massive forms of pyrite, on the other hand, show a wide variation in apparent reactivity, with crystals of iron sulfates being observed to form on some pyrite surfaces within a matter of hours and in some cases, within minutes.

Another study involved the quantification of pyrite in different coal lithotypes. Coals are described megascopically based upon the degree of bright and dull banding. Zones are delineated within the coal and designated as a "lithotype" based on the relative percentage of bright and dull bands within the zone (10). Dominantly bright bands are called "VITRAIN", dull bands, "DURAIN" and those intermediate between the two; "CLARAIN". Although the designation as to lithotype is solely made depending upon megascopic description, the lithotypes differ in basic maceral composition as illustrated by some data for the Waynesburg Coal shown in Table II.

TABLE II. Maceral Composition of Lithotypes of the Waynesburg Coal

Lithotype	%Vitrinite	%Exinite	%Inertinite	%Mineral Matter
Vitrain	93.1	1.8	2.4	2.7
Clarain	84.2	4.4	5.6	5.8
Durain	43.4	17.8	24.9	13.9

The low temperature ash of each lithotype was submitted to XRD analysis. The integrated intensities of each of the selected analytical Bragg reflections selected for the individual minerals were summed for all minerals present in each sample to give a "total integrated intensity". This value was then divided into the integrated intensity of the pyrite analytical Bragg reflection to give the "percent of total integrated intensity". The data are summarized in Figure 1. It is apparent that there is a systematic relationship between the composition/crystallinity of the pyrite and the basic organic makeup of the coal. Most important is the

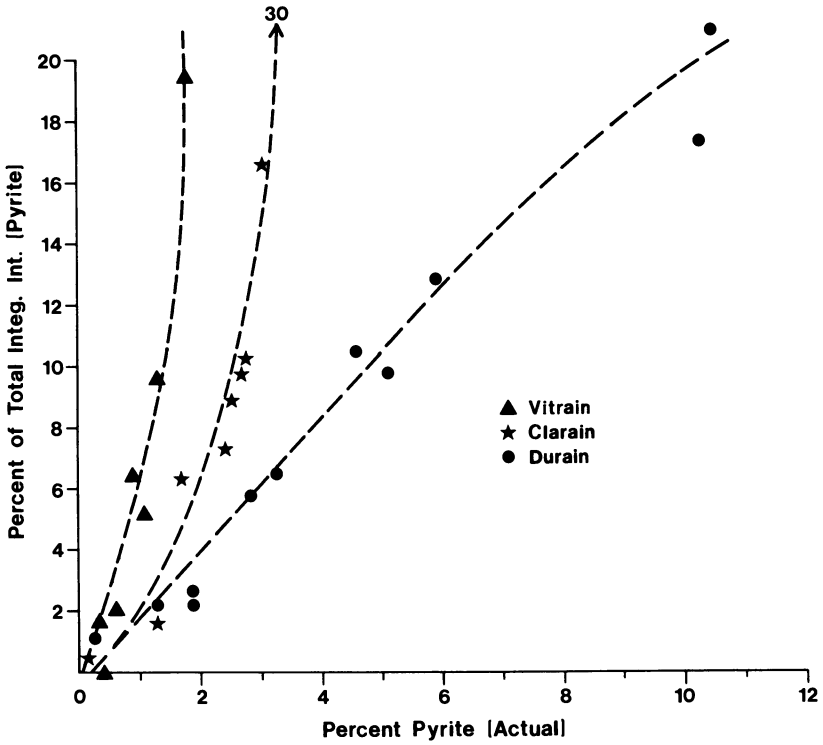


Figure 1. Relationship between actual percent pyrite and percent of total integrated intensity for Pyrite Bragg Reflection for various coal lithotypes.

observation that equal concentrations of pyrite give different intensity responses. Volume for volume, the pyrite contained within the bright coal (vitrain) showing significantly higher Bragg intensities than the pyrite contained in the duller coals.

To compound the problem, marcasite for reasons unknown to the author does not show the intensity response, volume for volume, as does pyrite. It has been the author's experience that coals that have been shown by optical examination to contain marcasite in significant concentrations show almost no indication of the mineral being present on a diffractogram generated from the low temperature ash.

It must be apparent from the above discussion that a number of variables other than concentration affect the intensities of mineral patterns as observed on a diffractogram. Inasmuch as they cannot be monitored and compensated for mathematically, these variations must be reflected in the error of determination. This would be true regardless of the quantification procedure employed. The conclusion, therefore, is that the inherent variability in composition and/or crystallinity that exists within the major mineral components of the low temperature ashes of coal will be reflected in the statistical error of determination and that error will be of sufficient magnitude to preclude the use of the term "quantitative" to describe the procedure. Therefore, any procedure using x-ray diffraction to determine the minerals in coal must be considered semi-quantitative at best.

#### Sample Preparation and Mounting

Any procedure for the preparation and mounting of coal low temperature ashes for XRD analysis MUST take two properties of the material into account: (1) minerals exist which react with water to produce acidic solutions (the iron disulphides) which in turn dissolve acid soluble components such as calcite and (2) the clay minerals, by virtue of exceptionally well developed (001) cleavage surfaces, have a dominant platy crystal form. The significance of the first attribute is that the ashes cannot be placed in water thereby precluding certain sample preparation techniques such as dispersion in water followed by vacuum mounting on filters or ceramic blocks. The second characteristic, possession of a platy crystal form, precludes the attainment of the theoretically required randomly oriented sample. Those who work with the clay minerals, realizing a random sample cannot be prepared and that the clay particles will deposit in preferred orientation, purposely prepare and mount the samples such that the preferred orientation of the individual platelets is maximized and thereby minimize any variations in diffraction intensity due to variations in particle alignment within the sample. The orientation of the clay platelets parallel to the sample surface positions the "C" crystallographic axis perpendicular to the sample surface. Because the diagnostic interplanar spacing for the clay minerals is along the "C" crystallographic direction, such an orientation is ideal for clay mineral identification. The simplest method to mount a low temperature ash for XRD analysis is to press the ash onto the surface of a pellet prepared from the coal from which the ash was derived.

Future Prospects

A few years ago, an ad hoc group of workers interested in coal minerals, The Mineral Matter in Coal Group, prepared and distributed a round-robin low temperature ash to ten laboratories. Each laboratory was to prepare, mount and quantify the mineral components in the ash by their respective XRD techniques. The data were then compared. Even though a wide variety of techniques was used for each phase of the analysis, with the exception of the clay mineral estimates made by one laboratory (significantly lower than the others) and the pyrite estimate made by another (too high), the data compared reasonably well. The averages of all the submitted estimates are summarized in Table III.

TABLE III. Results of Round-Robin L.T.A. Analysis

Mineral	Ave. Conc.		Coeff. of Variation
	WT%	STD Dev.	
Illite+Mixed Layer	30	7.07	0.24
Kaolinite	18	4.85	0.27
Quartz	21	6.31	0.30
Calcite	10	3.59	0.36
Pyrite	18	4.93	0.27

Another objective of the exercise was to discuss the results and procedures used and come to some agreement on a "standard" procedure for sample preparation, mounting and quantification that would be acceptable to all the workers. The agreement that was reached was that no agreement would be forthcoming on any of the phases of the analysis. With no one procedure demonstrably better than the other, each laboratory was expected to maintain their own procedure. As long as a procedure is scientifically and analytically sound and reflects a thorough understanding of the characteristics of minerals contained in coal and the requirements and limitations of x-ray diffraction, one procedure will probably be as good as another but none will be better than semi-quantitative.

With all its shortcomings, x-ray diffraction is still the best and most practical method for the estimation of the abundance of the individual minerals in coal.

Literature Cited

1. Renton, J.J., 1982, in "Coal Structure", R. Meyers ed., Academic Press, p. 283-326.
2. Renton, J.J., 1978, Energy Sources, Vol. 43, No. 2, p. 91-112.
3. Renton, J.J., Cecil, C.B., 1979, in "Carboniferous Coal Guide-book", Donaldson, A.C., Presley, M.W., Renton, J.J., eds., West Virginia Geological and Economic Survey, Morgantown, WV, p. 103-128.
4. King, H.M., 1978, Masters Thesis, Dept. of Geology, West Virginia University.
5. Renton, J.J., 1977, U.S. Dept. of Energy, MERC/CR-77/10, 20pp.
6. Renton, J.J., 1979, U.S. Dept. of Energy, MERC/CR-79/5, 22pp.
7. Grim, R.E., et al, 1937, Amer. Min., Vol. 22, pp. 813-829.

8. Brown, G., 1961, Mineralogical Soc. of London, Clay Mineral Group, London, 544pp.
9. Grady, W.C., 1977, AIME Transactions, Vol. 262, p. 268-274.
10. Stopes, M.C., 1919, Proc. Roy Soc. B., 90, p. 470-487, London.

RECEIVED August 1, 1985



## Factors Influencing Major, Minor, and Trace Element Variations in U.S. Coals

Peter C. Lindahl<sup>1</sup> and Robert B. Finkelman<sup>2</sup>

<sup>1</sup>Analytical Chemistry Laboratory, Chemical Technology Division, Argonne National Laboratory, Argonne, IL 60439

<sup>2</sup>Reservoir and Facies Division, Exxon Production Research Company, Houston, TX 77001

This general review of factors influencing major, minor, and trace element variations in U.S. coals provides an interpretation of coal inorganic elemental data found in the literature. Variations due to ash-related, rank-related, geochemical, and geological factors are discussed.

Although chemical analyses exist for thousands of coal samples, more data will be required to elucidate elemental trends within coal basins and to help decipher the geological and geochemical controls on their distribution and mode of occurrence. However, increased numbers of analyses will not necessarily provide all the answers. With an uncritical accumulation of data, we run the risk of ending up information rich but knowledge poor.

The purpose of this paper is to provide a critical interpretation of coal inorganic elemental data in the literature. Several valuable compilations of elemental data exist for U.S. coal (1-4). We have borrowed freely from these compilations to illustrate their value in elucidating just one aspect of coal geochemistry: the factors influencing inorganic elemental variations.

The concentrations of specific elements can be useful indicators of some coal quality characteristics. Huggins et al. (5) and Reid (6) demonstrated that the aluminum, silicon, potassium, calcium, magnesium, and sodium values of a coal ash can be used to estimate ash fusion temperature. The Si/Al ratio of coal ash has been used as an indicator of the abrasiveness of a coal. Sodium is a major contributor to boiler fouling and metal corrosion and contributes to agglomeration in fluidized-bed reactors. Trace elements are generally defined as those elements with concentrations below 0.1 wt. % (1000 ppm). Despite concentrations in the parts-per-million range, certain trace elements can have a significant impact on coal

utilization. For example, Be and the chalcophile elements, As, Cd, Hg, Pb, and Se, which are released during coal combustion or leached from coal waste products, can present significant environmental hazards; halogens such as Cl and F can cause severe boiler corrosion; and volatilized Ni, Ti, or V can cause corrosion and pitting of metal surfaces. On the positive side, some trace elements (e.g., Ge, Zn, U, and Au) may eventually prove to be economic by-products of coal utilization, while other elements (e.g., B) may be useful in helping to understand depositional environments and to correlate coal seams (7,8).

In early studies of major, minor, and trace elements in coal (9-13), coal ash was analyzed using emission spectroscopy. Recent studies (3,4,14,15) have employed several quantitative multielement instrumental methods. The instrumental methods used at the Illinois State Geological Survey and the United States Geological Survey are shown in Table I. Because a particular analytical technique is better suited for certain elements than for others, a combination of methods is usually necessary to determine all elements of interest. Methods for determining inorganic elements in coal must be accurate and precise. In addition, if possible, they should determine a large number of elements of interest simultaneously, require relatively little sample preparation, be capable of automation, produce an output compatible with computerized data processing, and be rapid.

Inorganic element concentrations in coal show variations from a microscopic to a worldwide scale. From a resource evaluation perspective, the most significant variations occur within and between coal seams and basins. The rest of the paper will discuss factors that cause these variations.

## Discussion

Ash Related Variations. The amount of ash in a coal is a major factor influencing inorganic element content. In general, trace element concentrations increase as ash content increases. This relationship reflects the fact that most inorganic elements in coal are associated with minerals (7). Figures 1 and 2 illustrate this relationship for K in eastern Kentucky coals and for Ti in coals from the Uinta Region in Colorado.

The above relationship also holds when comparing inorganic element concentrations among coal basins. Table II compares major, minor, and trace element data for coals from the Black Mesa Field, the Powder River Region, and the San Juan Region. As shown in Table II, the concentrations of the following elements increase as the ash contents of the coals increase: Si, Al, Na, K, Cu, Th, V, Li, Pb, and Se. The reason for the variation of these elements with ash content is that most of these elements are, or were, associated with the detrital silicate minerals, i.e., those minerals brought into the depositional basins during the formation of the coals. Chemical alteration of minerals within the coal basin can remobilize some elements, which then precipitate as nonsilicate minerals, e.g., Cu and Pb, as sulfides or selenides (16). The good

Table I. Instrumental Methods Used in Coal Analysis by the Illinois State Geological Survey (ISGS) and the United States Geological Survey (USGS)

Instrumental Method	Element(s) Determined	
	ISGS <sup>a</sup>	USGS <sup>b</sup>
Atomic Absorption Spectrophotometry	Ni, Zn, Pb, Cu, Cd	Mg, Na, Cd, Cu, Li Mn, Pb, Zn, Hg
Ion-Selective Electrode	F	F
Neutron Activation Analysis	Rb, Cs, Ba, Ga, In As, Sb, Se, I, Sc, Hf, Ta, W, La, Ce, Sm, Eu, Tb, Dy, Lu, Th, U, Yb, Na, K, Br, Fe	As, Sb, Se, Na, Cs, W, Eu, Fe, Hf, Sc, Tb, Ba, Rb, La, Yb, Br, Ta, Ca, Lu, Co, Th, Nd, Cr, Zn, Sm
Emission Spectrometry - Direct Reader	Be, Ge, Zr, Cr, Co, Mo, Ni, Zn, B, Sr, V, Cu, Cd	
Emission Spectrometry - Photographic	Be, Ge, Zr, Cr, Co, Mo, Ag, Sn, Ni, Zn, Pb, V, Cu, Mn	B, Ga, Ni, Zr, Ba, Ge, Sc, Be, La, Sr, Co, Mo, V, Cr, Nb, Y
X-ray Fluorescence	Na, K, Br, Fe, Cl, Mg, Ca, Al, Si, P, Ti, V	Al, Si, Ca, S, Fe, Ti, K, Cl, P

<sup>a</sup>Data from Reference 3.

<sup>b</sup>Data from Reference 14.

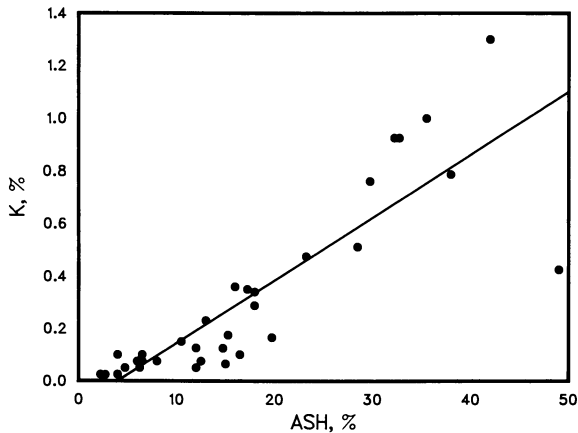


Figure 1. Relationship between K concentration in the coal and ash content for 34 coals from Eastern Kentucky.  $R = 0.86$ .

Data from reference 1.

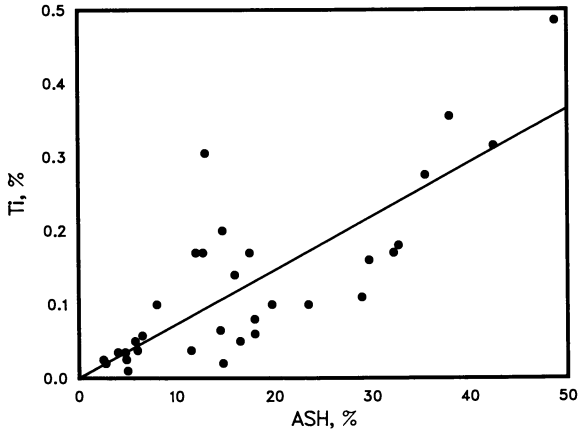


Figure 2. Relationship between Ti concentration in the coal and ash content for 34 coals from the Uinta region.  $R = 0.86$ . Data from reference 1.

Table II. Concentrations of Selected Elements in Coal Samples from Black Mesa (Arizona), Powder River (Wyoming), and San Juan (New Mexico) Regions<sup>a</sup>

	Black Mesa	Powder River	San Juan
Ash, %	8.0	9.9	21.1
Si, %	1.1	1.5	5.4
Al, %	0.69	0.78	2.7
Ca, %	0.78	1.1	0.67
Mg, %	0.1	0.2	0.1
Na, %	0.09	0.1	0.2
K, %	0.04	0.05	0.16
Fe, %	0.31	0.54	0.54
Ti, %	0.05	0.04	0.11
Cu, ppm	5.5	11.2	13.3
Th, ppm	2.2	4.3	5.9
Zn, ppm	5.6	20	15.1
Cr, ppm	3	7	5
Ni, ppm	2	5	3
V, ppm	7	15	20
Mn, ppm	9.7	51	29
Li, ppm	3.9	5.9	19.7
Pb, ppm	2.7	5.6	13.1
Se, ppm	1.6	1.7	2
Ba, ppm	300	300	300
Sr, ppm	150	200	100
Nb, ppm	1.5	1.5	3
Zr, ppm	15	15	50

<sup>a</sup>Data from Reference 4; results are calculated on a moisture-free coal basis (mf coal).

correlation between element concentration and ash content indicates that most elements have remained within the coal basin despite remobilization (17).

Elements not increasing in concentration with ash content are generally those with (a) organic affinities (Ca, Mg, Sr, Ba); (b) sulfide affinities (Fe, Zn); (c) carbonate affinities (Ca, Mn, Mg); or (d) sulfate affinities (Ba, Sr, Ca). Sulfides, carbonates, and sulfates are generally epigenetic phases, that is, they precipitate in the cleats and fractures subsequent to coalification. Presence of epigenetic phases affects element concentration more than ash content. The concentrations of Zr and Nb would be expected to increase with ash content, because these elements are usually associated with the detrital compounds of coal. The reason that this behavior is not apparent in Table II may be the poor resolution of the technique (emission spectrographic analysis) used to obtain the data.

**Rank-Related Variations.** Several elements exhibit a distinct variation in concentration with coal rank. Table III illustrates the general decrease in concentration of alkaline-earth elements (Mg, Ca, Sr, Ba), Na, and B with increasing coal rank. It is generally accepted that these elements are associated with organic functional groups (e.g., carboxylic acids) in low-rank coals. With increasing coal rank, these groups are destroyed, thus mobilizing organically associated inorganic trace elements.

Table III. Rank-Related Variations<sup>a</sup>

	Anthracite	Bituminous	Subbituminous	Lignite
Ca, %	0.07	0.33	0.78	1.2
Mg, %	0.06	0.08	0.18	0.31
Na, %	0.05	0.04	0.10	0.21
B, ppm	10	50	70	100
Ba, ppm	100	100	300	300
Sr, ppm	100	100	100	300

<sup>a</sup>Data from Reference 1; mf coal.

An organic association has been proposed for other trace elements, such as Be, Sb, Ge, U, and some halogens (3,18). Finkelman (17) suggests that organic association of these elements is significant mainly for low-rank, low-ash coals. Concentrations of organically bound elements in coal can decrease with increasing amount of detritus (Figure 3).

**Variations Due to Geochemical Factors.** Geochemical factors, such as Eh and pH of the peat environment, as well as the environment during and subsequent to coal formation, can have dramatic effects on inorganic element content. The effect of these geochemical

factors can be seen in Table IV, in which selected data for Appalachian and Interior Province coals are compared. Coals from both areas are similar in rank and ash content, but the Interior Province coals have significantly higher contents of all six elements. The higher content of Ca is perhaps due to carbonate mineralization (high pH), whereas that of Fe, Cd, Pb, and Zn is attributable to sulfide mineralization (low Eh). The higher content of B in the Interior Province may be attributable to greater marine influence (high salinity).

Table IV. Concentrations of Selected Elements in Coal Samples from Appalachian and Interior Coal Basins

	Appalachian <sup>a</sup>	Interior <sup>b</sup>
Ash, %	13.3	15.7
Ca, %	0.12	1.2
Fe, %	1.9	3.3
Cd, ppm	0.7	7.1
Pb, ppm	15.3	55
Zn, ppm	20	373
B, ppm	30	100

<sup>a</sup>Data from Reference 2; mf coal.

<sup>b</sup>Data from Reference 4; mf coal.

The occurrence of cleat-filling sphalerite and galena in the Interior Province coals is a classic example of how epigenetic mineralization can affect trace element content (19). Dramatic intra- and interseam variations are common. Cobb et al. (20) report that zinc content from benches of the Herrin (No. 6) coal varied from 20 to 14,900 ppm.

Variations Due to Geologic Factors. Ash chemistry is another important factor affecting elemental variations. Its influence is, however, generally more subtle than the other factors. In Table V the contents of selected elements are compared for Appalachian Province coals and Wasatch Plateau coals. Both are bituminous coals with similar ash contents. However, with a few exceptions, the content of the elements in the Wasatch coals is lower than those of Appalachian coals. The lower content of chalcophile elements in Wasatch coals may be due to a lower pyrite content. The lower concentration of lithophile elements (e.g., Li, Zr, Nb, Th, Sc, Y) but higher Si content may reflect a higher quartz content in the detrital component of Wasatch coals; this, in turn, may be a reflection of differences in the mineralogy of the source rocks. Volcanic ash, which is prevalent in some of our western coals can have a significant impact on ash chemistry.

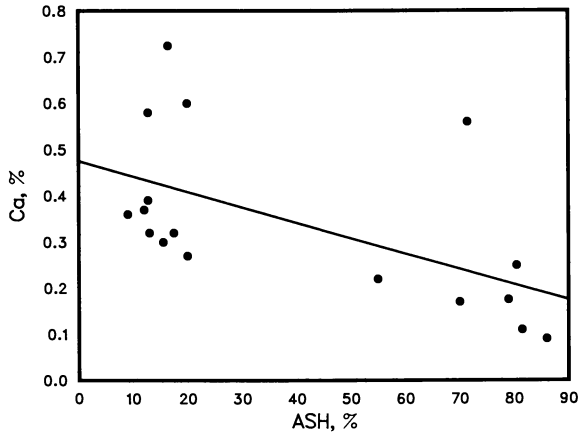


Figure 3. Relationship between Ca concentration in the coal and ash content for 17 coals and shales from the Emery Coal Field.  $R = -0.57$ . Data from reference 18.

Table V. Concentrations of Selected Elements in Coal Samples from Appalachian Province and Wasatch Coal Field

	Appalachian <sup>a</sup>	Wasatch <sup>b</sup>
Ash, %	13.3	11.3
Ca, %	0.12	0.41
Fe, %	1.9	0.26
Si, %	2.7	3.0
Cd, ppm	0.7	0.06
Li, ppm	27.6	16
Pb, ppm	15.3	5.8
U, ppm	1.4	1.2
Zn, ppm	20	11
B, ppm	30	100
Nb, ppm	5	0.3
Ni, ppm	15	5
Zr, ppm	50	30
As, ppm	27	0.8
Cu, ppm	24	9.3
F, ppm	80	67
Th, ppm	4.9	1.8
Ba, ppm	100	70
Co, ppm	7	1.5
Cr, ppm	20	10
Mo, ppm	3	0.7
Sc, ppm	5	3
V, ppm	20	15
Y, ppm	10	7

<sup>a</sup>Data from Reference 8; mf coal.

<sup>b</sup>Data from Reference 21; mf coal.

Other Factors Affecting the Inorganic Element Content. Other factors that could modify the ash chemistry or the availability of inorganic elements include the salinity of waters in contact with the coal or peat, the type of chemical weathering process (arid vs. humid), and hydrologic conditions (Br and Cl may be especially sensitive to this factor). In general, these factors are still poorly understood. Marginal enrichment and coal thickness are additional factors that can affect the inorganic element content.

### Concluding Comments

In this paper, we made several broad generalizations regarding factors that influence major, minor, and trace element variations in U.S. coals. Examples were chosen to illustrate specific points; we do not deny the probability of alternate explanations. We urge that in any interpretative work these generalizations be applied carefully.

A critical evaluation of existing elemental data of coal would probably result in identification of anomalous values and elimination of suspect data. Several questions might be answered by such an evaluation; for example, do the two K values in the high-ash region of Figure 1 deviate significantly from the trend of the other data because of analytical errors or recording errors? Are they legitimate geochemical anomalies?

The nature of inorganic element variations, for whatever cause, highlights the need to more judiciously select representative samples for reliable quantitative analyses. Statistical techniques, such as principal component analysis, should help in resolving the influence of the factors affecting major, minor, and trace element variations in coal. We encourage analytical chemists and geologists to interact closely because this is one of the best ways to improve the quality of analytical methodology and data, and geological interpretation.

It is hoped that this paper will encourage more detailed study of factors influencing inorganic element variations in coals.

### Acknowledgment

Portions of the work by PCL were supported by the U.S. Department of Energy, Office of Basic Energy Sciences, Division of Chemical Sciences under contract W-31-109-Eng-38.

### Literature Cited

1. Swanson, V. E., Medlin, J. H., Hatch, J. R., Coleman, S. L., Wood, G. H., Jr., Woodruff, S. D., Hildebrand, R. T. Geol. Surv. Open-File Rep. (U.S.) 1976, No. 76-468.



2. Zubovic, P., Oman, C., Coleman, S. L., Bragg, L., Kerr, P. T., Kozey, K. M., Simon, F. O., Rowe, J. J., Medlin, J. H., Walker, F. E. Geol. Surv. Open-File Rep. (U.S.) 1979, No. 79-665.
3. Gluskoter, H. J., Ruch, R. R., Miller, W. G., Cahill, R. A., Dreher, G. B., Kuhn, J. K. Circ.-Ill. State Geol. Surv. 1977, No. 499.
4. Hatch, J. R., Swanson, V. E. Resour. Serv. (Colo. Geol. Surv.) 1977, 1 (Geol. Rocky Mt. Coal-Symp., 1976), 143-164.
5. Huggins, F. E., Kosmack, D. A., Huffman, G. P., Fuel, 1981, 60, 577-584.
6. Reid, W. T., in Chemistry of Coal Utilization, 2nd Supp. Vol. M. A. Elliot, Edt., J. Wiley and Sons, Inc., New York, 1981, 1389-1445.
7. Finkelman, R. B., Geol. Surv. Open-File Rep. (US) 1981, No. 81-99.
8. Swaine, D. J. In "The Significance of Trace Elements in Solving Petrogenetic Problems and Controversies," Theophrastus Publications S.A.; Athens, Greece, 1983; p. 521-532.
9. Abernethy, R. F., Peterson, M. J., Gibson, F. H. Bur. Mines Rept. Inv. (U.S.) 1969, No. 7281.
10. Zubovic, P., Stadnichenko, T., Sheffey, N. B. Geol. Surv. Bull. (U.S.) 1961, No. 1117-A.
11. Zubovic, P., Stadnichenko, T., Sheffey, N. B. Geol. Surv. Bull. (U.S.) 1964, No. 1117-B.
12. Zubovic, P., Stadnichenko, T., Sheffey, N. B. Geol. Surv. Bull. (U.S.) 1966, No. 1117-C.
13. Zubovic, P., Sheffey, N. B., Stadnichenko, T. Geol. Surv. Bull. (U.S.) 1967, No. 1117-D.
14. Swanson, V. E., Huffman, J. C. Geol. Surv. Circ. (U.S.) 1976, No. 735.
15. Ruch, R. R., Gluskoter, H. J., Shimp, N. F. Environ. Geol. Notes (Ill. State Geol. Surv.) 1974, No. 72.
16. Cecil, C. B., Stanton, R. W., Allshouse, S.C., Finkelman, R. B., and Greenland, L. P., Prepr. Pap. - Am. Chem. Soc., Div. Fuel Chem. 1979, 24(1), 230-235.
17. Finkelman, R. B. "Proceedings," Basic Coal Science Workshop, Houston, TX, Dec. 1981; Energy Resources Co., Inc.: Cambridge, MA, 1982; 69-90.
18. Miller, R. N., Given, P. H. State College, PA, 1978, DOE Report FE-2494-TR-1.
19. Hatch, J. R., Gluskoter, H. J., Lindahl, P. C. Econ. Geol. 1976, 71, 613-624.
20. Cobb, J. C., Masters, J. M., Treworgy, C. G., Helfinstine, R. J. Ill. Mineral Note 1979, No. 71.
21. Hatch, J. R., Affolter, Davis, F. D. Spec. Stud.-Utah Geol. Miner. Surv. 1979, No. 49, 69-102.

RECEIVED January 24, 1986

## Elemental Distribution and Association with Inorganic and Organic Components in North Dakota Lignites

F. R. Karner, H. H. Schobert, S. K. Falcone, and S. A. Benson

Energy Research Center, University of North Dakota, University Station, Grand Forks, ND 58202

Elemental associations in Beulah-Zap and Kinneman Creek lignites have been evaluated by: 1) spatial patterns of vertical distribution of elements within seams; 2) behavior in chemical fractionation tests; 3) microprobe evidence of distribution in coal components; 4) inorganic and organic affinities determined by correlation with ash content; and 5) correlation with ionic potential data. Si, Sc, Ti, V, Cr, Co, Br, Y, Zr, Sb, Cs, La, Ce, Sm, Eu, Yb, Th and U are inorganically associated with mineral phases and are typified by concentration at the margins of coal seams, relative insolubility, and positive correlation with ash content. Na, Mg, Ca, Sr and Ba are organically associated with carbonaceous components and are typified by concentration within the central part of seams, high ion-exchangeability, and low correlation with ash content. Al, S, K, Mn, Fe, Cu, Zn, As and Se occur in significant amounts in both inorganic and organic components.

The associations of major, minor, and trace elements in lignite-bearing strata of the Fort Union Region present a challenge in understanding their geochemical relationships and history. In an earlier work (1), the spatial patterns of elemental distribution within a lignitic sedimentary sequence were examined and were related to factors of accumulation of plant materials and to the depositional and post-depositional influx of inorganic matter. In this study, two beds, the Kinneman Creek and the Beulah-Zap, which are part of the Sentinel Butte Formation (Paleocene) of North Dakota, were compared to determine elemental distribution and association with specific coal components. The inorganic elements in lignites are distributed as ions adsorbed on the organic acid groups, as coordinated species, and in detrital and authigenic

minerals. The distribution of elements is determined by natural processes, and, therefore, is expected to be systematic even though complex.

The methods used to qualitatively identify the interrelationships of major, minor, and trace elements include examining the spatial patterns of distribution of elements within a stratigraphic sequence (1), consideration of results of chemical fractionation procedures (2), and direct study of the distribution of elements by microprobe techniques (3). Evaluation of the organic and inorganic affinities (4-5) of the elements correlated these methods with theoretical considerations based on ionic potentials and allowed broad characterization of elements into inorganic, organic and combined inorganic-organic associations.

### **Methods and Procedures**

The samples were collected from freshly exposed faces within open pit mines. The lignite, lignite overburden, and underclay were collected from two pits at the Beulah Mine where lignite is mined from the Beulah-Zap bed and from the Kinneman Creek bed in the Center mine. The sample collection procedures have been summarized by Karner (6) and Benson (7).

The lignite samples collected at various intervals within the stratigraphic sequence were subjected to the following analyses: proximate, ultimate, heating value, ash analysis, and trace element analysis by neutron activation analysis (NAA) (8) and x-ray fluorescence (XRF) (9). Minerals in the coal and the associated sediments were determined by x-ray diffraction and by scanning electron microscopy and electron microprobe analysis. A split from a bulk sample was examined by chemical fractionation to selectively extract inorganic constituents based on their bonding in the coal. The chemical fractionation procedure involves extracting the coal with 1M ammonium acetate to remove soluble and ion-exchangeable inorganic components. The coal is subsequently extracted with 1M hydrochloric acid to remove elements present as carbonates, oxides, or coordinated species. The extracts and residues from the chemical fractionation procedure are analyzed by a combination of NAA, XRF, inductively coupled argon plasma (ICAP), and atomic absorption spectroscopy (AA).

Direct determination of inorganic elements associated with macerals and lithotypes was based on an electron microprobe study of coal microcomponents (3) using energy dispersive x-ray analysis to determine the presence of elements and their ratios as well as variation at three locations in the Beulah-Zap seam.

### **Results**

**Patterns of Elemental Distribution.** The major, minor, and trace element abundances and the lithology of the stratigraphic sequence are summarized in Tables I and II for the Beulah coals. The data from the Center Mine is given in Karner and others (1) where the spatial distribution of elements in the seam was described as fitting into several patterns. In this study the classification of elemental distribution patterns includes: 1) Concentration at

Table I. Elemental Analysis of a Stratigraphic Sequence Containing Two Lignite Seams at the Beulah Mine, North Dakota. Results in parts per million on a dry coal basis determined by neutron activation analysis unless indicated otherwise.

Height, m <sup>+</sup>	Lithology	% Ash <sup>++</sup>	Na	Mg	Al	Si <sup>*</sup>	P <sup>**</sup>	S <sup>*</sup>	K	Ca
-0.3	Clay	--	1964	10364	84699	321210	289	2992	10062	3398
0.0	Lignite	17.0	7767	722	8394	17290	683	11980	530	6888
0.1	Lignite	8.47	14348	678	1935	3830	332	9790	<500	6101
0.5	Lignite	7.30	3479	642	2584	4190	271	6310	<500	7249
0.9	Lignite	22.20	753	1598	27082	22070	420	17820	1908	2191
1.0	Clay	--	1821	13741	113270	295900	0	7932	13269	3720
1.6	Clay	--	2159	12454	111945	307701	0	3343	13585	2559
1.7	Lignite	10.80	3991	671	9428	12670	305	8520	<500	7062
2.1	Lignite	7.20	7497	707	5192	4920	467	7770	<500	5281
2.6	Lignite	7.60	9482	717	4542	4950	362	8040	713	6206
2.9	Lignite	7.10	6598	731	3431	2820	572	7910	<500	6031
3.3	Lignite	7.40	6988	571	3886	4260	345	9780	<500	3973
3.4	Lignite	5.60	6692	564	2664	1600	352	7660	<500	4615
3.6	Lignite	15.28	6583	3386	7312	20170	346	5920	<500	8261
4.2	Lignite	6.40	5907	472	4308	4750	580	11440	<500	12635
4.8	Lignite	12.0	5631	1242	9554	10490	348	87000	<500	8927
5.1	Lignite	9.10	5561	914	5937	5110	425	119104	<500	6423
6.3	Clay	--	4385	14031	88995	293117	0	1214	15654	4983
7.3	Silt	--	3440	14605	88403	288425	134	3019	9177	2880
7.5	Chert	--	464	3800	13052	56211	0	9369	<1000	1709
7.8	Sand	--	4084	9826	49621	250031	0	2931	7608	27085
8.9	Clay	--	1771	14771	81163	287669	196	4544	4162	6110

Height, m†	Sc	Ti	V	Cr	Mn	Fe	Co	Cu	Zn	As	Se
-0.3	11.7	3574	99.1	65.8	177	24853	5.90	<150	66.1	2.5	<0.20
0.0	11.8	829	66.1	36.6	44.3	15358	5.52	58.5	19.8	21.8	1.42
0.1	2.06	207	4.28	5.12	42.2	6580	3.97	<10	<25	22.5	0.69
0.5	4.86	<100	6.24	6.49	40.1	2561	1.71	11.6	<25	2.17	0.55
0.9	10.6	438	148	39.3	57.1	26129	13.0	<25	91.9	374	4.28
1.0	15.0	4211	205	91.3	95.5	15258	18.0	<150	<30	24.1	<0.20
1.6	16.1	4560	181	94.4	98.3	11929	2.68	<150	94.4	6.66	4.12
1.7	10.8	125	25.0	16.1	36.4	3100	1.94	52.6	32.8	11.5	0.43
2.1	0.85	119	3.73	2.87	41.4	1502	1.21	<25	8.8	3.55	<0.10
2.6	0.75	140	2.73	2.91	45.6	1467	1.08	<25	<25	5.18	0.52
2.9	1.65	226	5.19	3.11	46.2	1489	0.71	47.5	7.0	2.22	1.00
3.3	0.54	59.4	2.87	2.46	30.7	6193	0.99	<25	<30	31.5	0.39
3.4	0.34	<100	1.89	1.26	36.1	1035	1.12	<25	<25	0.66	0.32
3.6	0.80	502	1.74	4.35	58.1	2928	0.60	<25	<25	4.37	0.59
4.2	2.44	77.8	6.20	8.58	26.6	8711	5.23	<25	20	21.2	1.27
4.8	6.07	121	5.08	6.48	78.5	2821	1.45	<25	19	3.45	0.56
5.1	11.5	196	34.4	9.33	70.4	2405	3.01	<10	<25	7.03	<0.20
5	15.5	3647	177	81.0	212	22282	17.0	<150	<30	14.8	<0.20
6.3	13.9	3630	144	64.3	735	27448	12.0	<150	<30	2.63	<0.20
7.3	12.0	3082	136	56.5	1000	28123	11.0	<150	<30	2.75	<0.20
7.5	12.1	<1000	73.3	18.9	8046	273475	2.74	<300	<200	<0.50	<0.20
7.8	8.29	2426	72.5	55.6	611	15853	8.65	<150	51.8	6.09	0.54
8.9	4.5	4017	134	68.1	738	35592	12.0	<150	<30	2.48	3.22

Continued on next page

Table I. Continued

Height, m <sup>†</sup>	Br	Rb	Cd	Sb	Cs	Ba	La	Ce	Sm	E	Yb	U
-0.3	1.10	86.00	<2.50	0.65	4.96	786	32.18	48.7	2.51	1.36	1.59	1.91
0.0	1.70	12.00	<1.00	4.61	5.50	746	8.07	19.8	1.31	0.71	2.22	2.09
0.1	4.98	<5.00	<1.00	<0.05	<0.02	756	1.29	8.46	1.42	0.36	1.37	0.50
0.5	1.69	<5.00	<1.00	0.04	<0.05	1114	2.95	9.21	1.04	0.46	1.62	0.23
0.9	3.28	16.00	<1.00	5.74	4.56	683	45.36	71.9	8.29	1.95	1.38	3.32
1.0	0.77	108	2.17	1.78	8.10	676	32.2	41.1	2.45	1.13	1.20	3.47
1.6	0.76	126	2.50	1.35	10.00	644	36.3	45.3	2.58	0.98	1.60	2.34
1.7	1.73	3.26	1.20	1.33	1.49	1005	2.49	8.32	1.05	0.49	1.41	1.86
2.1	1.18	<5.00	<1.00	0.12	<0.05	988	9.75	14.6	0.52	0.21	0.40	0.41
2.6	1.25	<5.00	<1.00	0.28	<0.05	1158	3.75	6.98	0.35	0.12	0.38	0.36
2.9	1.29	<5.00	<1.00	0.04	<0.05	1284	11.36	15.9	0.43	0.11	0.41	0.56
3.3	0.45	1.42	0.65	<0.01	0.16	844	0.84	<1.00	0.17	0.07	0.11	0.23
3.4	0.53	<5.00	<1.00	0.03	0.12	1041	0.58	1.66	0.17	0.06	0.07	<0.10
3.6	0.46	<5.00	<1.00	0.21	<0.05	2122	2.07	4.07	0.42	0.26	0.63	0.50
4.2	0.55	5.18	<1.00	0.34	1.15	3045	7.47	39.3	0.63	0.55	0.42	0.24
4.8	1.24	<5.00	<1.00	0.29	0.34	1749	4.06	9.69	0.81	0.37	1.11	0.90
5.1	1.16	<5.00	<1.00	0.60	<0.02	226	3.52	6.77	0.82	0.43	1.39	2.08
5	<0.50	115	<2.90	1.52	8.50	811	36.3	52.5	2.73	1.11	1.72	2.88
6.3	<0.50	90.00	<2.50	1.04	5.31	813	35.0	45.6	3.28	1.30	1.83	1.28
7.3	0.89	77.80	<2.50	0.63	4.35	613	28.3	39.4	2.54	1.06	1.17	2.30
7.5	0.89	<10.00	<2.50	0.19	0.40	274	11.7	<10.0	1.27	0.40	1.09	<0.20
7.8	0.25	50.60	<2.50	0.49	2.98	725	26.7	36.5	2.65	1.18	1.26	1.54
8.9	1.12	87.00	<2.50	0.73	5.28	851	25.6	46.7	2.63	1.43	1.81	1.75

<sup>†</sup>Height from base of first seam.

<sup>‡</sup>Ash on a moisture-free basis.

\*XRF of bulk samples.

\*\*XRF of ashed lignite and XRF of bulk non-lignite samples.

both margins of the seam, 2) concentration at the base of the seam, 3) concentration at the top of the seam, 4) concentration at one or more locations within the central portion of the seam, and 5) irregular distribution.

Figure 1 illustrates examples of the distribution patterns for the Beulah-Zap bed. Examples of patterns for the Kinneman Creek bed are given in Karner and others (1). The various ways in which inorganic constituents accumulated in the lignite during and after deposition affect the locations of elements within the seam. The detrital constituents carried in by wind and water will most likely be enriched at the margins of the coal seam and in partings. Included in this group of inorganic constituents are silt-size quartz, feldspar and mica, clay minerals and volcanic ash.

Authigenic minerals are formed in place, primarily by precipitation from aqueous solutions. They may form early in the depositional history under swamp conditions or at any later time as a result of groundwater movement. Similarly, ion exchange with minerals or organic components may also occur. Distribution patterns resulting from the influence of aqueous solutions might be produced by changing water chemistry during the history of the swamp causing concentrations of inorganic elements at one or both margins or within the central portion of the seam. Subsequent groundwater processes, depending on flow directions and differential permeability within the seam, might also lead to varied distribution patterns.

Inorganic elements are also present in plant material and may be distributed in vertical patterns related to the depositional history of the swamp.

Overall, more even distribution patterns of inorganic elements may be characteristic of elements associated with organic components and more pronounced or irregular patterns with elements related to concentrations of detrital and authigenic minerals. Distribution patterns are listed in Table III for the elements analyzed in this study. The distribution of elements in the seams may show characteristics of more than one pattern and are noted accordingly in Table III. Zubovic and others (10) described distribution patterns similar to ours for Ti, V, Cr, Co, Cu, Y and La in several North Dakota lignites.

**Chemical Fractionation.** The bulk coal samples were subjected to chemical fractionation analysis (11) which can be used to categorize how a particular element is bonded in the coal. The elements were divided into three categories: 1) ion-exchangeable, 2) acid-soluble, and 3) residual (Table III). Organically associated elements tend to fall into the ion-exchangeable and acid soluble categories while elements associated with detrital and authigenic minerals may be in any of the three categories.

**Electron Microprobe Analysis.** Direct analysis of inorganic elements associated with organic components can be made by microprobe techniques. An initial study (3) showed that elements present in vitrain, fusain and durain/atritus in the Beulah-Zap bed include Na, Mg, Al, Si, S, K, Ca, Fe Sr and Ba. Further observations were made on lithotypes and macerals for samples from

Table II. Elemental Analysis of a Stratigraphic Sequence Containing Lignite from the Orange Pit of the Beulah Mine, North Dakota. Results in parts per million on a dry coal basis determined by neutron activation analysis unless indicated otherwise.

Height, m†	Lithology	Ash**									
		%	Na	Mg	Al	Si**	S**	K	Ca		
-0.5	Lignite	7.1	7041	1041	2824	767	4678	<500	7317		
0.00	Lignite	6.8	5178	1004	3107	881	3144	<500	9072		
0.50	Lignite	6.7	5833	1150	3472	532	3352	<500	8891		
1.00	Lignite	6.8	6018	1043	2675	1140	3504	<500	7803		
1.50	Lignite	13.0	5826	3526	6710	1635	8471	<500	8016		
2.00	Lignite	6.9	5313	1238	2793	2756	4123	<500	7828		
2.50	Lignite	8.5	6169	1292	4348	7905	5460	<500	11998		
3.00	Lignite	15.7	6278	1449	5869	7122	10243	<500	10872		
3.50	Lignite	10.4	5096	1483	7929	10889	58729	<500	11876		
3.60	Overburden	--	2246	15718	91958	275900	3130	9724	7094		
4.14	Overburden	--	2773	13226	89901	259700	1100	14994	6673		
4.80	Overburden	--	3098	15480	97158	281400	497	8653	7342		
5.10	Overburden	--	2619	15475	84493	288900	1480	10800	6197		
6.10	Overburden	--	2389	16774	88663	294000	1350	14971	9553		
6.70	Overburden	--	2082	9982	51610	187700	3220	14971	9465		
7.30	Overburden	--	2842	12634	66743	277400	12710	6441	12042		
7.35	Overburden	--	2900	14339	78427	284900	840	7988	12401		
8.90	Overburden	--	3028	12471	75153	286200	1070	8994	13916		
9.20	Overburden	--	2863	12793	78030	290700	<100	10006	14862		



Height, m <sup>+</sup>	Sc	Ti	V	Cr	Mn	Fe	Co	Cu**	Zn
-0.5	2.16	132	3.02	2.24	22.4	5147	1.68	3.8	12.6
0.00	0.64	123	2.84	1.62	28.3	3261	0.75	2.2	5.48
0.50	0.57	138	2.73	1.41	29.0	3462	0.70	3.6	6.08
1.00	0.57	144	2.22	1.37	28.0	3289	0.39	3.9	4.78
1.50	0.38	326	5.84	2.08	136	22202	0.37	3.0	<25.0
2.00	0.36	150	2.20	1.89	37.6	3308	0.80	4.4	<25.0
2.50	0.43	162	2.50	2.30	33.3	1706	0.59	5.0	3.46
3.00	0.48	167	2.12	2.60	48.0	30530	0.69	4.8	<25.0
3.50	1.05	226	4.85	3.51	47.0	2897	0.70	6.4	8.57
3.60	15	2890	136	86.3	611	36878	14.0	86	<30.0
4.14	18	4256	165	93.2	2092	50756	13.6	73	<30.0
4.80	16	3880	158	92.4	467	30865	10.9	87	<30.0
5.10	5.1	3674	134	32.4	979	14308	3.99	81	<25.0
6.10	15.8	4557	142	88.0	885	39106	13.8	84	<30.0
6.70	18.7	2760	119	72.3	3542	147377	11.3	46	<30.0
7.30	8.97	3796	80.1	62.9	308	36902	10.1	64	<30.0
7.35	12.9	4131	117	78.7	424	26437	9.95	71	<30.0
8.90	14.0	4360	117	90.8	670	31472	11.3	80	<30.0
9.20	14.0	3541	117	90.8	435	28566	11.4	73	<30.0

Continued on next page

Table II. Continued

Height, m <sup>†</sup>	As	Se	Br	Sr**	Y**	Zr**	Rb	Ag	Cd	Sb
-0.5	10.7	<0.05	1.62	366	6	8	<2.00	<0.15	<5.00	<0.01
0.00	3.90	0.40	1.40	445	5	11	1.37	<0.53	<5.00	0.04
0.50	3.52	0.39	1.49	480	4	13	<2.00	<0.48	<5.00	0.10
1.00	3.34	0.50	1.04	411	2	9	<2.00	<0.79	0.34	0.10
1.50	27.2	0.91	0.84	322	2	ND	<2.00	<0.05	1.10	0.07
2.00	5.24	0.54	0.99	357	2	8	<2.00	<0.53	0.19	<0.01
2.50	3.55	0.44	0.55	518	<1	15	<2.00	<0.75	<5.00	0.06
3.00	39.2	0.79	0.81	334	<1	10	<2.00	<0.37	1.87	0.04
3.50	7.85	0.36	0.92	502	6	16	<2.00	<0.15	<5.00	0.22
3.60	12.66	1.56	0.92	262	26	112	114	<0.08	<2.50	0.44
4.14	<2.50	0.57	1.05	223	28	94	131	<0.08	<2.50	0.50
4.80	5.25	1.40	0.27	239	26	109	164	<0.08	<2.50	0.49
5.10	6.23	0.42	0.55	234	31	126	25.9	<0.49	<5.00	0.51
6.10	3.52	1.25	0.92	230	25	108	127	<0.08	<2.50	0.38
6.70	<2.50	<0.20	1.07	104	18	66	77.8	<0.08	<2.50	0.69
7.30	27.2	1.01	1.41	255	22	169	72.2	<0.08	<2.50	0.40
7.35	4.11	0.84	1.32	274	28	165	108.8	<0.08	<2.50	0.41
8.90	5.01	0.53	1.46	285	25	131	191.8	<0.08	<2.50	0.38
9.20	3.34	1.08	1.08	265	27	164	94.8	<0.08	<2.50	0.30

Height, m <sup>†</sup>	Cs	Ba	La	Ce	Sm	Eu	Yb	Th	U
-0.5	<0.01	714	7.84	8.30	0.53	0.11	0.36	0.57	0.40
0.00	0.04	917	3.30	5.61	0.49	0.09	0.28	0.75	0.24
0.50	<0.48	943	3.62	6.39	0.43	0.06	0.24	0.81	0.23
1.00	0.03	844	3.24	4.92	0.24	0.05	0.09	0.83	0.75
1.50	<0.01	930	12.8	13.1	0.34	0.03	<0.01	0.78	0.40
2.00	0.03	704	0.98	2.42	0.26	0.01	0.06	0.49	0.31
2.50	0.03	1138	1.52	3.18	0.31	0.05	0.09	1.01	0.56
3.00	0.05	1242	2.20	9.98	0.28	0.07	0.08	1.12	1.26
3.50	0.08	720	2.38	4.97	0.55	0.12	0.38	1.75	0.99
3.60	6.57	1075	12.2	63.5	1.17	1.30	1.07	10.4	1.51
4.14	7.56	631	14.6	67.3	1.23	1.29	1.77	10.1	1.03
4.80	7.53	685	13.8	61.2	1.25	1.12	1.33	9.50	0.80
5.10	0.79	285	12.7	18.5	1.26	0.31	0.73	3.26	0.76
6.10	6.38	567	12.3	61.7	1.12	1.33	1.59	9.39	1.09
6.70	4.50	400	16.9	82.9	1.59	1.37	1.46	7.02	2.99
7.30	3.39	444	12.4	69.6	1.15	1.26	1.15	7.85	1.12
7.35	4.53	619	14.6	71.6	1.28	1.35	1.50	9.35	0.80
8.90	5.10	567	14.0	63.0	1.35	1.43	1.52	9.45	1.27
9.20	4.69	511	13.6	64.5	1.22	1.46	1.71	10.2	1.13

+Height from base of first seam.

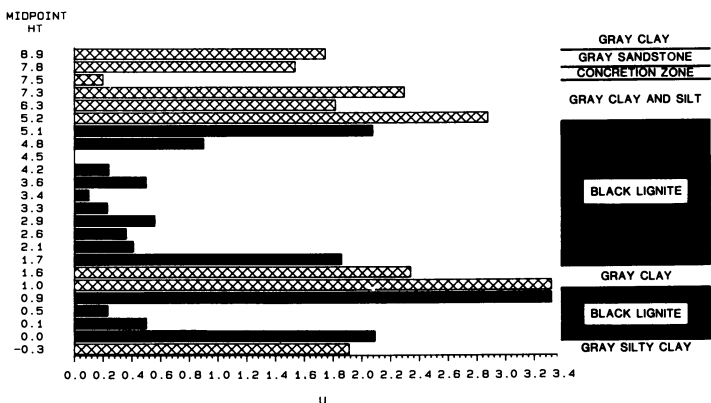
++Ash on a moisture-free basis.

\*XRF of bulk samples.

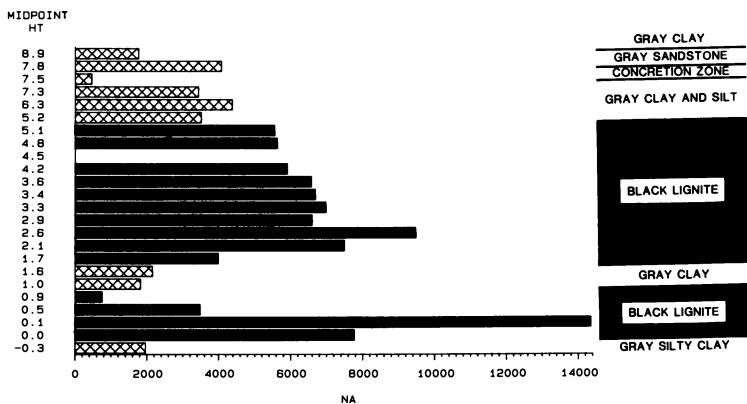
\*\*XRF on ashed lignite and XRF of bulk non-lignite samples.

ND-Not detected.

U DISTRIBUTION IN BEULAH 79 SEAM



NA DISTRIBUTION IN BEULAH 79 SEAM



CA DISTRIBUTION IN BEULAH 79 SEAM

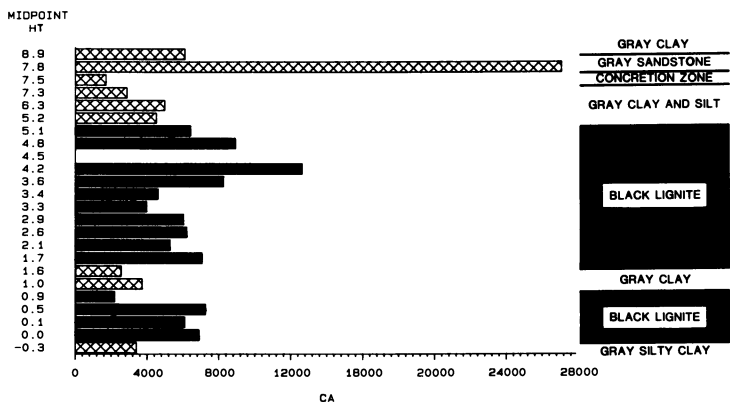


Figure 1. Vertical distribution of U, Na and Ca in parts per million in the Beulah-Zap seam and related sediments. Concentrations of U is at the margins of seams and Na and Ca within the central part of seams.

three locations at lower, middle, and upper locations in the seam. Energy dispersive x-ray spectra in Figure 2 illustrate the following initial results:

1. There is a clear association of elements with the organic components.
2. S and Ca are major components. Na, Mg, and Al are represented by smaller but distinct peaks. Si and Sr peaks strongly overlap. K, Fe, Ba, and some other elements are represented by very low peaks.
3. Vitrain in the samples from a middle location in the seam can be classified into two types exemplified by the spectra for 7-5 and 7-2. Vitrain 7-5 is typical of grains characterized by relatively high S:Ca peak ratios and low Mg:Al ratios while vitrain 7-2 exemplifies grains with low S:Ca and high Mg:Al.
4. Ulminite 1-1 is typical of analyzed grains from the upper part of the seam and falls into the high S:Ca and low Mg:Al category. However, it is much more enriched in S and depleted in Mg than vitrain 7-5.

The elements represent, at least in part, the easily exchangeable, organically bound, inorganic components associated with carboxyl groups in the lignite. In part, the elements may also represent fine-grained authigenic minerals such as Si and Al in kaolinite or amorphous phases. Original plant constituents may also be present.

**Correlation with Ash Content.** The organic and inorganic affinities of elemental constituents have been determined by a number of investigators (4-5). The relationship between the concentration of an element in moisture-free coal and the ash content can be used as a guide to the affinity of that element for, or incorporation in, the mineral matter or the carbonaceous material. If the concentration of an element increases with increasing ash content that element may be characterized as being associated with the inorganic species that form ash, or in other words may be said to have an inorganic affinity. If the concentration shows no correlation with ash content, that element may be said to have an organic affinity. Linear least squares correlation coefficients were calculated for the concentrations of the elements versus the ash content. For example, organic and inorganic affinities for elements from the Center mine indicate the following affinities: seven elements - Na, Ca, Mn, Br, Sr, Y, and Ba - had correlation coefficients below 0.200 and thus show organic affinity in this suite of samples. An additional seven elements - Mg, K, Cu, As, Rb, Ce, and Eu - had correlation coefficients ranging from 0.201 to 0.600 and may be associated with both the carbonaceous and mineral portions of the coal. The remaining 24 elements show inorganic affinity. For a subset of minor elements Ti, V, Cr, Co, Zn, and La, the inorganic affinity correlates with the ionic potential (Spearman rank correlation coefficient  $r_s = .77$ ). This finding is contrary to results reported previously by Zubovic (12) for higher rank coals.

TABLE III. Qualitative Geochemical Relationships Between Geochemical

Distribution Within Lignite Seams at the Beulah Mine					
Beulah Orange Pit	Beulah		Chemical Fractionation Behavior	Affinity By Correlation With Ash Content	
	Upper Seam	Lower Seam			
Na	LM-IR	CE	CE	IE	OR
Mg	CE-UM	UM-IR	UM	IE	IN/OR
Al	UM-IR	MS-IR	MS	AS, RS	IN
Si	UM	MS-IR	MS	RS	IN
P	ND	IR	LM	ND	IN
S	UM-IR	UM	MS	RS, IE	OR
K	ND	ND	UM	RS, AS	IN
Ca	UM-IR	IR	LM-IR	IE, AS	IN/OR
Sc	MS	MS	MS	RS, AS	IN/OR
Ti	UM-IR	MS	MS	RS	IN
V	MS-IR	MS	MS	AS	IN/OR
Cr	MS-IR	MS	MS	RS	IN
Mn	UM-IR	UM	UM	AS, IE	IN/OR
Fe	IR	MS-IR	MS	RS, AS	IN
Co	LM	MS-IR	UM	AS, RS	IN
Cu	UM	LM-IR	LM	ND	IN
Zn	IR	UM	UM	RS	IN
Ge	ND	ND	ND	ND	ND
As	MS-IR	CE-IR	UM	RS	IN
Se	IR	CE-IR	MS	RS	IN
Br	LM	MS	UM-IR	ND	IN/OR
Rb	ND	MS	MS	ND	ND
Sr	CE-IR	ND	ND	IE	OR
Y	MS	ND	ND	ND	ND
Zr	UM-IR	ND	ND	RS	ND
Cd	ND	ND	ND	RS	IN/OR
Sb	UM	MS	MS	RS	IN
Cs	IR	MS	MS	RS	IN
Ba	IR	IR	IR	IE, AS	IN/OR
La	LM-IR	IR	MS	AS, RS	IN
Ce	IR	IR	UM	AS, RS	IN
Sm	MS	MS	UM	AS, RS	IN
Eu	MS	MS-IR	MS	AS, RS	IN
Yb	MS	MS	LM	AS, RS	IN/OR
Th	UM	ND	ND	RS	IN
U	UM	MS	MS	AS, RS	IN

Patterns of Distribution

MS - Enrichment at both margins  
 UM - Enrichment at upper margin  
 LM - Enrichment at lower margin  
 CE - Enrichment at the center of the seam  
 IR - Irregular  
 ND - Not determined

Chemical Fractionation Behavior

IE - Ion-exchangeable  
 AS - Acid soluble  
 RS - Remains in the residue  
 ND - Not determined

## Properties and Elemental Distribution Within Seams

Distribution Within Lignite Seam at the Center Mine			
Center	Chemical Fractionation Behavior	Affinity By Correlation With Ash Content	Ionic Potential Z/r
LM-IR	IE	OR	1.0
CE-IR	IE>>AS	IN/OR	3.0
MS-IR	AS, RS	IN	5.9
MS	RS	IN	9.5
MS-IR	ND	IN	14.3
MS	RS, IE	OR	17.1
LM,	IE, AS, RS	IN	0.13
UM-IR	IE, AS	IN/OR	2.0
MS	AS, RS	IN	3.7
LM-IR	RS	IN	5.9
LM	AS, RS	IN	4.0
LM	RS	IN	4.8
CE	AS, IE	IN/OR	2.5/6.7
MS-IR	AS	IN	2.7/4.7
UM-IR	AS, RS	IN	2.8
LM-IR	RS	IN	1.0/2.8
ND	ND	IN	.88/2.7
LM	ND	ND	2.7/7.5
MS	RS	IN/OR	10.8
LM	RS, IE	IN	14.3
CE-UM	ND	OR	
MS	RS, AS	ND	0.68
CE-IR	IE	OR	1.8
MS	ND	ND	3.4
MS	ND	IN	5.1
MS-IR	ND	IN	.87/2.1
LM-IR	AS, RS	IN	4.0
MS	RS	IN	0.6
MS	IE, AS	IN/OR	1.5
IR	AS, RS	IN	2.6
LM	AS, RS	IN/OR	2.9
MS	AS	IN	3.1
MS	AS	IN/OR	3.2
MS		IN	
MS	RS	IN	3.9
MS	AS, RS	IN	4.2

Affinity By Correlation With Ash Content

IN - Inorganic-high correlation  
OR - Organic-low correlation  
IN/OR - Intermediate correlation  
ND - Not determined

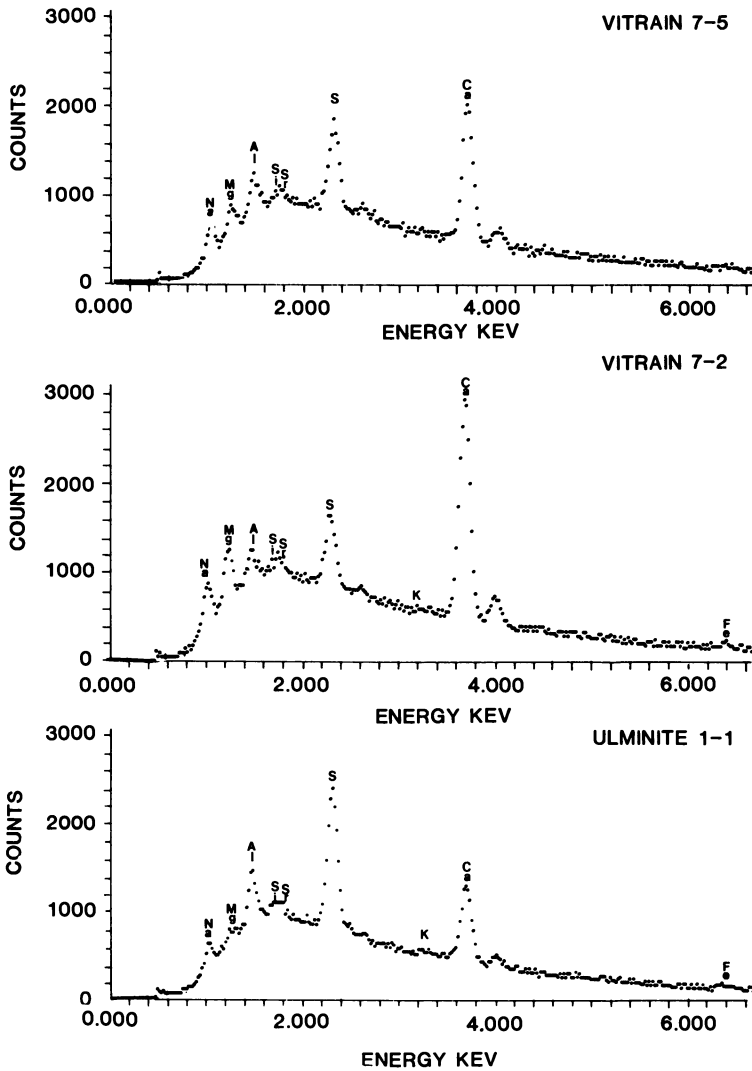


Figure 2. Electron microprobe energy dispersive x-ray spectra of two vitrain grains from the middle part of the Beulah Zap bed and an ulminite grain from the upper part of the seam. Analyses were accumulated for 400 seconds with a current of 1000 picoamps with the beam scanning areas of 10-100 square microns.



**Correlation with Ionic Potential.** The ionic potentials of the elements,  $Z/r$ , where  $Z$  is the ionic charge and  $r$  is the ionic radius, are summarized in Table III. The ionic potentials of elements have a large effect on the association of the element in mineral-forming processes (13). Elements having low ionic potential ( $Z/r < 3$ ), such as Na, Mg, and Ca, associate as hydrated cations. Insoluble hydrolysates have ionic potential of  $3 < Z/r < 12$ , and include, for example, the elements Al, Si, and Ti.

### **Elemental Associations**

Most of the elements that have been considered in this study may be assigned to one or both of two major associations, inorganic and organic, each with characteristic distribution patterns, chemical fractionation behavior, occurrence with organic components, affinity determined by ash correlation and ionic potential category.

**Inorganic Association.** Elements with inorganic association are generally typified by:

1. Distribution patterns with concentration at one or both margins or irregular distribution.
2. Chemical fractionation behavior of elements which are insoluble and remain in the residue.
3. Inorganic affinity by strong positive correlation with ash content.
4. Ionic potential  $3 < Z/r < 12$ .

These elements usually occur in detrital or authigenic mineral grains and include Si, Sc, Ti, V, Cr, Co, Br, Y, Zr, Sb, Cs, La, Ce, Sm, Eu, Yb, Th and U. Common examples are angular, silt-size quartz and feldspar grains which are most abundant in the upper and lower margins of the coal seams and are interpreted to be detrital in origin.

**Organic Association.** Elements with organic association are generally typified by:

1. Distribution patterns with concentration within the central portion of the seam or irregular distribution.
2. Chemical fractionation behavior in which the elements are highly ion-exchangeable or partly ion-exchangeable and partly acid soluble.
3. Direct evidence of presence in organic components by microprobe analysis. Elements appear disseminated throughout the organic component with no evidence of occurrence as discrete mineral grains.
4. Organic affinity by weak or no correlation with ash content.
5. Ionic potential  $Z/r < 3$ .

These elements are usually bonded to organic components and include Na, Mg, Ca, Sr, and Ba.

**Inorganic and Organic Association.** Elements with both inorganic and organic association are generally typified by:

1. Distribution patterns of more than one type commonly including irregular patterns.
2. Chemical fractionation behavior in which the elements belong to two or three of the categories ion-exchangeable, acid soluble, or insoluble.
3. Direct evidence of presence in organic components by microprobe analysis unless present in trace amounts.
4. Intermediate or varied correlation with ash content.
5. No observed pattern of ionic potentials.

These elements are interpreted to occur both in mineral phases and bonded to organic components and include Al, S, K, Mn, Fe, Cu, Zn, As, and Se.

**Unclassified Elements.** Elements with unclear association based on the results of this study include P, Ge, and Cd.

## **Discussion**

**Distribution of Inorganics in Low-Rank Coals.** There are two major aspects to the distribution of inorganics in coals, each of which is important for characterizing the coal, interpreting its geochemical history, and predicting its behavior in utilization processes. For a specific coal sample, the distribution of a given element refers to its association among several possible modes of occurrence including ion exchange sites, coordination sites, and a variety of mineral phases. In addition, in the context of discussing a particular coal deposit, the distribution of a given element refers to the vertical and horizontal variability of that element's concentration in the coal.

The distribution of an element is a result of its geochemical properties -- for example, its likelihood of occurring as a soluble cation, an insoluble hydrolysate, or a chalcophile--and on the properties of the coal, such as the total availability of ion-exchange sites. The variability within a seam reflects both the extent of authigenic mineralization as well as the influence of post-depositional processes. Taken together, the multiplicity of modes of occurrence and the within-seam variability result in the inorganic geochemistry of low-rank coals being extremely complex. Nevertheless, we take as an initial postulate that, regardless of its apparent complexity, the inorganic geochemistry of low-rank coals must be explicable in terms of the fundamental chemical properties of the elements and known geological processes.

**Future Directions.** In future work directed toward the understanding of elemental distributions in low-rank coals and their associations with coal components there are two types of research that we wish to emphasize.

The first type of research emphasizes the direct determination of the chemistry of coal components. This work has been initiated and is partly reported in this paper for the major "inorganic" element chemistry of organic components determined by microprobe techniques. Quantitative analysis in this instance is difficult but necessary. Figure 2 shows that energy dispersive spectra contain information on a number of major and minor elements clearly detectable in lithotypes and macerals. Numerous analyses of components shows consistency of results and interesting patterns of variation as illustrated in Figure 3. Ratios of peak intensities are used in this figure to illustrate patterns of the data while approaches to determine absolute element percentages are being developed. Since intensities are proportional to abundance and have been shown to be reproducible, ratios may be used to infer elemental variation in the components. Figure 3 shows that grains of vitrain from a specific massive coal layer near the center of the seam, by virtue of a group closely spaced points, have a fixed relationship of Mg, Al, S and Ca contents. In contrast, vitrain, hand-picked from a fusain layer, shows a clear range of ratio plots primarily showing a large change in Mg:Al ratio. Average Na/Ca ratios also are shown. These results suggest that vitrain in the Beulah coal has constancy of composition in part, and systematically variable composition in part. One obvious explanation for the variation in the fusain layer would involve hydrogeochemical processes in this apparently more permeable unit. Continued work of this type will be emphasized as well as analysis of inorganic phases and survey of trace elements in specific coal components.

The second type of research emphasizes the correlation of lithologic layering in the coal to the vertical distribution of elements. Current work is being done on the Beulah-Zap bed at the Freedom Mine, site of the Northern Great Plains Gasification Plant. The potential control of vertical element variation with respect to admixed detrital material in the upper and lower margins of the seam and in clay-rich partings is obvious, as is the potential role of even slight concentration of sulfide minerals and various concretionary masses in different parts of the seam. The correlation of chemical variation with layers of different types of lignite is almost unknown. Initial study (Karner and others, in preparation) shows some correlation of chemical variation with layering in the Beulah-Zap bed. This work has promise for interpreting the complexity of vertical distribution patterns of elements reported in this paper.

### **Acknowledgments**

The authors would like to thank Douglas C. Beckwith and Robin G. Roaldson for their assistance in sample preparation and data handling.

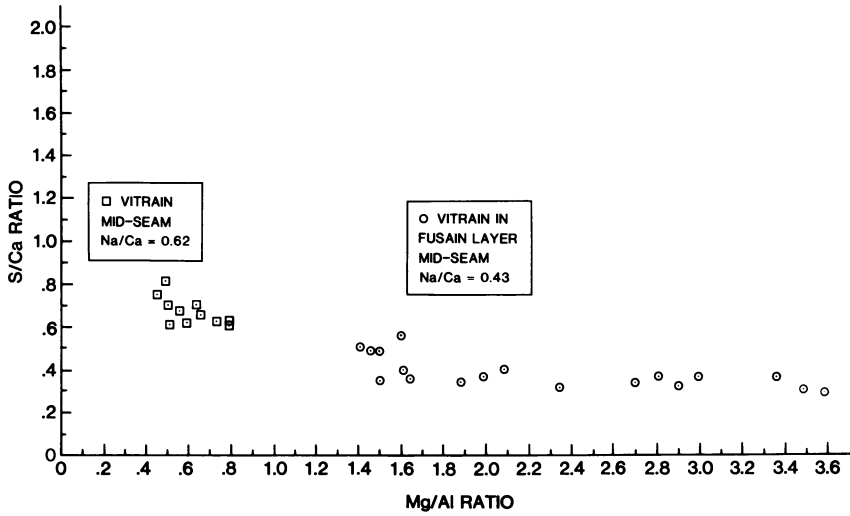


Figure 3. Plot of S/Ca and Mg/Al ratios of vitrain compositions for two locations in the Beulah-Zap seam, North Dakota. Average Na/Ca ratios are given for each location.

**Literature Cited**

1. Karner, F.R.; Benson, S.A.; Schobert, H.H.; and Roaldson, R. In "The Chemistry of Low-Rank Coals"; Schobert, H.H., ACS Symposium Series No. 264, American Chemical Society: Washington, D.C., 1984; pp. 175-193.
2. Benson, S.A. and Holm, P.L. ACS Division of Fuel Chemistry Preprints. 1983, Vol. 28, No. 2, pp. 234-239.
3. Karner, F.R.; Kleesattel, D.R.; Benson, S.A.; and Schobert, H.H. Geological Society of America Abstracts with Programs. 1984, Vol. 16, p. 555.
4. Gluskoter, H.J.; Ruch, R.R.; Miller, W.G.; Cahill, R.A.; Dreker, G.B.; and Kuhn, J.K. Illinois State Geological Survey Circular 499. 1977, p. 109.
5. Nicholls, G.D. In "Coal and Coal-Bearing Strata"; Murchison, D.; and Westoll, T.S., Ed.; American Elsevier: New York, 1968; pp. 269-307.
6. Karner, F.R.; White, S.F.; Brekke, D.W.; and Schobert, H.H. (in preparation).
7. Benson, S.A.; Kleesattel, D.; and Schobert, H.H. ACS Division of Fuel Chemistry Preprints. 1984, Vol. 29, No. 1, pp. 108-113.
8. Weaver, J.N. In "Analytical Methods for Coal and Coal Products"; Karr, C., Jr., Ed.; Academic Press, Inc.: New York, 1978; Vol. 1, pp. 377-401.
9. Benson, S.A. Proc. North Dakota Academy of Science. 1980, Vol. 34, p.10.
10. Zubovic, P.; Stadnichenko, T.; and Sheppey, N.B. In "Geochemistry of Minor Elements in Coals of the Northern Great Plains Coal Province". U.S. Geol. Survey Bull. 1117-A: Washington, D.C., 1961, p. 57.
11. Hurley, J.P. and Benson, S.A. ACS Division Fuel Chemistry Preprints. 1984, Vol. 29, No. 6, pp. 210-216.
12. Zubovic, P., In "Coal Science"; Given, P.H., Ed.; American Chemical Society: Washington, D.C., 1966; Chapter 14.
13. Mason, B. In "Principles of Geochemistry"; John Wiley and Sons Inc.: New York, 2nd Ed., 1964; pp. 155-157.

RECEIVED October 24, 1985

## Volcanic Ash Layers in Coal: Origin, Distribution, Composition, and Significance

Don Triplehorn<sup>1,2</sup> and Bruce Bohor<sup>2</sup>

<sup>1</sup>Department of Geology and Geophysics, University of Alaska, Fairbanks, AK 99701

<sup>2</sup>U.S. Geological Survey, Federal Center, Denver, CO 80225

Volcanic ash that falls into a coal-forming environment stands a good chance of being preserved and contributing to the mineral matter in coal. Such layers are relatively common in some coals although they are commonly not recognized as volcanic in origin even by geologists. The original material usually consists of fine-grained glass, crystals, and rock fragments, but there is a great variety in texture and composition. After burial the glass, in particular, is readily altered so that with increasing geologic age secondary clay minerals become abundant and evidence of the volcanic origin becomes less obvious. Kaolinite is most abundant, but smectite is not uncommon; occasionally unusual minerals occur, such as aluminum phosphates with notable amounts of Sr and rare earths. In North America, volcanic ash layers are most important in western coals of Tertiary and Cretaceous ages; they are generally uncommon in eastern coals or those of greater age.

The main purpose of this paper is to call attention to volcanic eruptions as a source of mineral matter in coal. Volcanic material is apt to have mineral and chemical compositions, as well as patterns of distribution, different from the more usual types of mineral matter in coal. Recognition of volcanic material requires some understanding of the process of origin, an awareness of the considerable variety of materials involved, and an appreciation of the tendency of volcanic materials to undergo substantial alteration so that their genesis is obscured.

Mineral matter in coal most commonly consists of mud carried into the coal-forming environments by streams as overbank deposits during times of flood. The minerals are mainly quartz, feldspars and clay minerals, and these are deposited as shaly partings that become thinner and finer-grained away from the stream channels. By contrast, the volcanic ashes that occur in coals tend to be of the highly siliceous variety associated with explosive eruptions, during which ash is carried high into the atmosphere and transported far downwind. These form thin, uniform, widespread partings in coals,

commonly on the order of an inch thick and displaying little lateral change in thickness or composition. Such silicic (70%  $\text{SiO}_2$ ) volcanic ashes tend to be mostly composed of dust-sized particles of glass, with less than a few percent of mineral grains such as quartz, various feldspars, biotite, zircon, and hornblende. Glass is highly unstable in geologic terms, and alters rapidly to clay; thus the original volcanic ash texture and composition are not evident in the final product.

Some comments on terminology are necessary. "Volcanic ash partings" here refers to sedimentary units bounded by organic-rich material (coal, lignite, or organic shale) and which were deposited as air-fall volcanic ash with essentially no subsequent transport and mixing with terrigenous detrital silicates (clay, mud and sand). No specific grain size or composition is implied. The term "tephra" is now commonly used for modern, unaltered, uncompacted material, while the term "tuff" is used for the compacted (rock) equivalent.

A volcanic origin is obvious where there is glass, volcanic phenocrysts, a limited mineral suite characteristic of volcanic rocks, or absence of terrigenous detritus and lack of sedimentary structures formed by moving water. With increasing age, however, there is progressive alteration and loss of recognizable volcanic features; the product is generally some kind of clay unit. As a general term they might be called altered tuffs. If mainly composed on montmorillonitic (smectitic) clay that is light-colored and sticky when wet, these are commonly called bentonites and mainly occur in marine shales. In older coals they are usually kaolinitic, occur as firm rocks rather than soft clay, and weather to lighter colors than the enclosing coal. These are commonly called "tonsteins", and old term for such fine-grained, hard clay partings that are relatively abundant in European Carboniferous coals. Tonstein was originally applied as a purely descriptive term ("clayrock") but in recent years an origin as an air-fall volcanic ash has become increasingly accepted. We prefer the general term "altered volcanic ash" because there is considerable range in physical appearance, original and secondary mineralogy, as well as in the type of enclosing sediment.

#### ORIGIN

The environment of coal deposition provides one of the best places for deposition and preservation of volcanic ash. The recent eruption of Mt. St. Helens, for example, spread volcanic ash across several western states. On land, almost all of the volcanic ash will be eroded by wind and water, mixed with terrigenous sand and clay, and ultimately dispersed into lakes or the ocean. In marshes or swamps, the general setting in which plant material accumulates to eventually become coal, an ash fall has a good chance of remaining undisturbed because of the shallow water, low stream gradients, and lack of relief. The sediment-baffling effects of vegetation minimizes processes that could cause reworking of the volcanic ash. Portions of such swamps may be so distant from major streams that they receive little or no mud from overbank floods. Thus it is likely that most ash falls in swamps would be buried in organic debris (coal) and remain free of non-volcanic material from fluvial sources.

Only volcanoes characterized by particularly violent eruptive styles are likely to be important in producing the thin, widespread

units of ash most commonly preserved in the geologic record. The explosiveness of eruption is related to several factors, including gas content and geometry of the vent. Of most importance here, however, is the silica content: silica increases the viscosity of magma and the tendency toward explosive eruptions rather than quiet flows. Thus volcanic ash partings in coals are primarily the product of such silica-rich eruptions; this has important consequences in terms of the composition of the altered ash, as will be discussed later.

#### FIELD APPEARANCE OF VOLCANIC ASH PARTINGS IN COALS

Most volcanic ash partings in coal are thin, ranging from 1 mm to a few cm. A few, however, attain thicknesses of more than 1 m. Many are uniform in thickness and have either sharp or gradational boundaries with the enclosing coal. Some, however, pinch and swell rapidly and may consist of a series of lenses rather than a continuous bed, a feature they share with some Carboniferous tonsteins (Williamson, 1970). Light shades of gray, brown, or yellow are most common, reflecting a lower organic content than the adjacent coal. Black and dark brown partings also occur, and sometimes these become obvious only after weathering; the oxidation of organic matter then results in a light-colored surface layer of siliceous material. Figure 1 shows the most common field appearance; in this case for a Cretaceous example from southern Alaska.

To a large extent the grain size and degree of induration of these partings depends upon the amount of post-depositional alteration; this in turn is largely a function of age and depth of burial. For example, lignites 4-5 m.y. old in southern Alaska contain partings that are loose and sandy; in fact, they are clearly recognizable as volcanic ash consisting mostly of glass shards. In contrast, partings in 100 m.y. Kentucky bituminous coal are hard and very fine grained (Seiders, 1965; Bohor and Triplehorn, 1982). The latter probably was similar to the Alaskan example at first, but has completely altered to a compact variety of kaolin known as flint clay.

#### COMPOSITION

Composition of the partings is a function of both the original materials and conditions, and the kind and extent of post-depositional modification. Therefore it is necessary to consider the primary composition (original) separately from the secondary composition (altered).

##### Primary Composition

The solid products of explosive volcanism include individual glass fragments, individual mineral crystals (phenocrysts), and aggregates of these known as rock fragments. Glass is perhaps the most abundant component but there is a great variety in the solid components ejected from modern volcanoes. A given volcano may eject different material over its eruptive lifespan. Even a single eruption, lasting perhaps only a few days, may involve changes in ash composition.

Volcanic ashes are characterized by a limited suite of mineral components. By far the most abundant are quartz, sanidine and



plagioclase feldspars, certain pyroxenes and amphiboles, magnetite, apatite, biotite, and zircon. The presence of these minerals and the absence of others constitute evidence of a volcanic origin. Certain mineral crystal forms, such as the beta form of quartz and hexagonal prisms of biotite, are particularly useful indicators of volcanic origin. Similarly, the presence of sanidine, the high-temperature form of potassium feldspar, suggests a volcanic origin. On the other hand, the presence of non-volcanic minerals such as muscovite, epidote and garnet indicates a non-volcanic origin, or at least some admixture of non-volcanic (probably fluvial) material.

Original grain size of an ash parting reflects the texture of the material produced by a given volcano plus the progressive loss of coarser and denser components as an ash cloud moves downwind. In other words, texture is in part a function of distance from the source volcano. As noted earlier, the most common ash partings in coal are thin, uniform and widespread. These probably were derived from distant volcanoes and consisted originally of silt- and clay-sized particles carried by high-altitude winds. Conversely, where ash partings are coarse-grained, thick, and abundant, the volcanic source is assumed to have been relatively close.

#### Secondary Composition

The primary composition discussed above is important in that it determines in part the final products of alteration. It should be noted, however, that the factors controlling the degree and direction of alteration have not been thoroughly studied. Chemical alteration in the environment of deposition and the length of time involved may be as important as original composition in determining the final product. For example, both kaolinitic and smectitic partings occur in Tertiary coals near Centralia, Washington (Reinink-Smith, 1982) and it is not known if this reflects the differences in original ash composition or some differences within the coal-forming environment that resulted in the formation of different clay minerals from the same ash parent. Triplehorn and Bohor (1981) related differences in the mineralogy of altered volcanic ash partings, in a coal bed in Utah, at least in part, to differences in thickness of the original ash partings which affected the efficiency of leaching.

The main secondary products are clay minerals, either smectite or kaolinite. These clay minerals are derived mainly and most readily from glass, but feldspars, amphiboles, pyroxenes, and biotite also alter in part to clay minerals. The alteration of volcanic ash to kaolinite involves removal of Na, Ca, Mg, K and Fe as well as considerable silica. Pure kaolinite corresponds to a mixture of subequal amounts of silica and alumina plus a small amount of water and virtually nothing else--this is thus the product of very intensive leaching. Smectite on the other hand requires some Mg and more silica than kaolinite. It is thus the product of less intensive leaching than that which produces kaolinite.

It appears that volcanic ash can sometimes alter directly to kaolinite; in other cases a smectitic intermediate stage may be involved. Where alteration has gone to completion, that is, no glass remains and only kaolinite is present, it may be impossible to

determine details of early stages of the alteration process. Even though the process of alteration of the bulk of a parting (presumably glass) may not be clear, individual minerals such as feldspars and biotite can be observed altering directly to kaolinite without any smectite intermediary. Whatever the details, it is clear that a major amount of silicon somehow must be removed in solution (along with lesser amounts of such soluble elements as Na, K, Mg, Ca, and Fe). Because silica, and most of the other components cited, do not appear as secondary minerals in adjacent rock units, they apparently were carried out of the system in solution by passage of groundwater. This is in contrast to some marine bentonites, where silica produced by alteration of volcanic ash often appears nearby as silica cement in significant quantities.

A variety of secondary minerals in addition to clay minerals may occur in altered volcanic ash partings. Some of these may be related to modification of the primary constituents, but others are more likely introduced by ground water taking advantage of the higher permeabilities of volcanic ash layers relative to the adjacent organic material (now coal). Carbonate minerals in quantities too large to have been derived entirely from the primary volcanic material are not uncommon. Siderite is most abundant, although dolomite sometimes is present. Abundant secondary carbonate may obscure the volcanic origin of the original layer because such well-cemented partings are similar in appearance to the purely sedimentary carbonate layers that are very commonly associated with coals.

Recently occurrences of unusual aluminum phosphate minerals have been found with ash partings in coals (Triplehorn and Bohor, 1983). Since that report we have found a number of additional occurrences in Alaska and one in the appalachian area. These minerals were grouped by Palache (*et. al.*, 1951) as the plumbogummite series, with the general formula  $X Al_3(PO_4)_2(OH)_5H_2O$ . End members of interest here include goyazite (where  $X = Sr$ ), gorceixite (Ba), crandallite (Ca), and florencite (Ce, U, and other rare earths). Some of these layers in Alaska are sufficiently radioactive to give a distinct reading on hand-held radiation detectors in the field.

## DISTRIBUTION

Because many geologists are not aware that volcanic ash partings occur in coals, it is difficult to interpret the absence of published reports regarding their occurrences. The abundance of such partings is probably much greater than presently recognized. The following generalities regarding their distribution are mainly limited to North America and are based primarily on our own observations, discussions with others, and interpretation of published reports. Specific references to recognized volcanic ash partings in coals are relatively few and restricted mostly to the past few years.

In simple terms ash partings are relatively abundant in Cretaceous and Tertiary coals of the West and rare in Carboniferous coals of the East. We are less certain of the Gulf Coast Tertiary lignites but they appear to have at least a moderate abundance of

such partings. To a degree this apparent distribution is related to the fact that the volcanic origin of the younger ash beds is more apparent, while older partings commonly appear as kaolinitic clay beds with little evidence of their volcanic heritage (see Triplehorn, 1976; Bohor and Triplehorn, 1981). Even so, there is no question that the absolute frequency is higher in the West.

Locally the abundance of partings can be highly variable. Where many coals are present, ash partings may be distributed sparsely but uniformly or concentrated in just a few coals. Figure 2 shows an example in southwestern Washington, in this case including both kaolinitic and smectitic partings (Reinink-Smith, 1982). In the West, where most of our work has been done, volcanic ash partings are known from numerous coals in Utah, New Mexico, Colorado, Wyoming, Montana and Washington (Bohor, *et. al.*, 1978; Triplehorn and Bohor, 1981). Again, the frequency of partings is highly variable. Individual coals in Montana and Colorado contain up to twenty or more ash partings, while the unusually thick Paleocene coals of the Powder River Basin contain almost none. In Alaska, volcanic ash partings are present in all of the Cretaceous and Tertiary coals we have examined, but appear to be particularly abundant in the Cook Inlet area.

In the Appalachian coal basin and the Eastern Interior Basin, where we have less experience, ash partings appear to be rare (Bohor and Triplehorn, 1982). The lack of ash partings in Carboniferous coals of eastern North America contrasts with their abundance in European coals of the same age. The latter have been studied for over a century, although their volcanic origin was not generally accepted until the last few decades. Bouroz, *et. al.* (1983) provides a good recent summary of some of this work in English.

#### SIGNIFICANCE

The geologic importance of volcanic ash partings in coals has been summarized previously by Triplehorn (1976). Of greatest importance is their use in correlation, the process of determining the time relationships among rocks exposed at different localities. The simplest use is as marker beds, where individual ash falls can be recognized and distinguished from others on the basis of some textural or compositional aspect. Beds containing the same ash layer (whether in coal or any other rock type) are the same age, although the absolute age (in years) is not indicated. The absolute age can sometimes be determined by radiometric age dating of certain minerals in the ashes. Potassium-argon dating is used for such minerals as feldspar and hornblende, while fission-track dating may be used for zircon and apatite (Triplehorn *et. al.*, 1977; Turner *et. al.*, 1980).

It may be of interest here to note that Williamson (1970) mentioned the high radioactivity of certain ash partings (he called them tonsteins) that made them useful in bore-hole studies because they appeared as sharp maxima on gamma-ray logs of coal beds. Such maxima are conspicuous because coals are generally known for their absence of radioactivity. He ascribed the high radioactivity of these partings to an unusual abundance of zircons. We have no specific knowledge of these occurrences, but suggest that the high



Figure 1. Light weathering kaolinite volcanic ash in coal, southern Alaska.

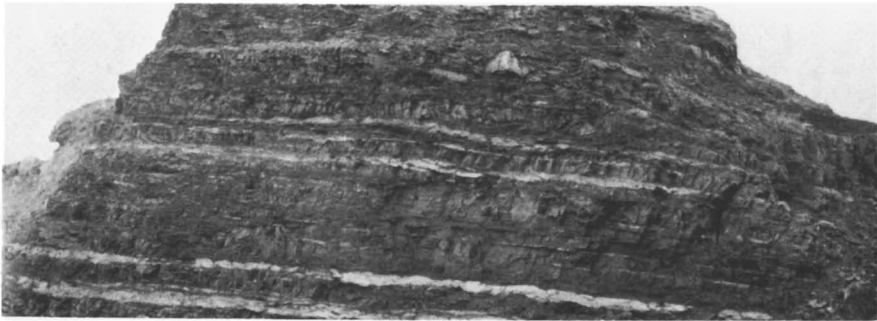


Figure 2. Multiple smectitic and kaolinitic ash partings in the Big Seam, southeastern Washington.

radioactivity might instead be related to uranium-bearing phosphate minerals.

Thus far geologists have paid little attention to the significance of ash partings as indicators of processes and conditions in the coal-forming environment. For example, thin widespread partings lacking penetrating plant material suggest that these originated as ashes that fell into shallow standing water. Thick ashes should have affected the kind and amount of vegetation, and indirectly the nature of the coal immediately overlying thick ash beds. As yet there is little data in these aspects because geologists have not recognized the potential value of such studies.

For those interested in mineral matter in coal, an awareness that some partings may be of volcanic origin may be useful in explaining the distribution of some of these layers and the occurrences of some unusual components, such as strontium, phosphate, or uranium. Volcanic ash partings are likely to be more widespread and uniform in texture, composition and thickness than the more common partings of fluvial origin. They are also more likely to show marked differences from layer to layer, and to contain exotic mineral or chemical components.

#### REFERENCES

- Bohor, B.F., R.M. Pollastro, and R.E. Phillips, 1978, Mineralogical evidence for the volcanic origin of kaolinite partings (tonstein) in Upper Cretaceous and Tertiary coals of the Rocky Mountain region (abstr.): The Clay Mineral Soc., 15th Ann. Mtng., 27th Ann. Clay Mineral Conf. Bloomington, Indiana, Program and Abstracts, p. 47.
- Bohor, B.F., and Triplehorn, D.M., 1981, Volcanic origin of the Flint Clay parting in the Hazard No. 4 (Fire Clay) coal bed of the Breathitt Formation in Eastern Kentucky: Guidebook, Geol. Soc. Am. Annual Meeting, Coal Div. Field trip, Coal and Coal-Bearing Rocks of Eastern Kentucky, Kentucky Geol. Survey, p. 49-54.
- Bouroz, A., D.A. Spears, and F. Arbey, 1983, Review of the formation and evolution of petrographic markers in coal basins: Societe Geologique du Nord, Memoires Tome XVI, 115 pp.
- Palache, C., H. Berman, and C. Frondel, 1951, Dana's System of Mineralogy, 7th ed.: Wiley, New York, 1124 pp.
- Reinink-Smith, L., 1982, The Mineralogy, Geochemistry and Origin of Bentonite Partings in the Eocene Skookumchuck Formation, Centralia Mine, S.W. Washington. Unpublished M.S. Thesis, W. Washington Univ., 1/9 pp.
- Seiders, V.M., 1965, Volcanic origin of flint clay in the Fire Clay coal bed, Breathitt Formation, Eastern Kentucky; in Geological Survey Research, Chapter D: U.S. Geological Survey Professional Paper 525-D, p. D52-D54.

- Triplehorn, D.M., 1976, Volcanic ash partings in coals: characteristics and stratigraphic significance, The Neogene Society, Spring, 1976, Pacific Section, Society of Economic Paleontologists and Mineralogists, p. 9-12.
- Triplehorn, D.M., and B.F. Bohor, 1981, Altered volcanic ash partings in the C-coal, Ferron Sandstone member of the Mancos Shale, Emery County, Utah, U.S. Geol. Surv. Open File Report 81-775, 49 pp.
- Triplehorn, D.M., and B.F. Bohor, 1983, Goyazite in kaolinitic altered tuff beds of Cretaceous age near Denver, Colorado: Clays and Clay Minerals, 31//4, p. 299-304.
- Triplehorn, D.M., D.L. Turner, and C.W. Naeser, 1977, K-Ar and fission-track dating of ash partings in Tertiary coals from the Kenai Peninsula, Alaska. A radiometric age for the Homerian-Clamgulchian stage boundary: Geological Society of Am. Bull., 88, pp. 1156-1160.
- Turner, D.L., D.M. Triplehorn, C.W. Naeser, and V.A. Wolfe, 1980, Radiometric dating of ash partings in Alaskan coal beds and upper Tertiary paleobotanical stages: Geology, 8, p. 92-96.
- Williamson, I.A., 1970, Tonsteins--their nature, origin, and uses: The Mining Magazine, 112, p. 119-125, 200-209.

RECEIVED August 26, 1985

## Reactions and Transformations of Coal Mineral Matter at Elevated Temperatures

G. P. Huffman and F. E. Huggins

Technical Center, U.S. Steel Corporation, Monroeville, PA 15146

An overview is presented of the reactions and transformations of the inorganic constituents of coal at elevated temperatures. Following a brief review of the types of inorganic matter in Eastern and Western coals, reactions and transformations of mineral matter that are of importance in coal combustion are discussed. The importance of ash melting and the utilization of phase diagrams are emphasized in the discussion of slagging behavior and slag deposition. In the section on fouling deposits, emphasis is placed on the reactions of volatile alkalis that give rise to molten phases (alkali sulfates and alkali silicates). Finally, a very brief discussion of the role of mineral matter in other coal conversion processes (liquefaction, carbonization, gasification) is given. Throughout the chapter, the importance of modern analytical techniques (Mössbauer spectroscopy, X-ray absorption spectroscopy, computer-controlled scanning electron microscopy) in the analysis of complex assemblages of minerals and mineral derivatives is stressed.

Coal contains a variety of inorganic constituents that exhibit deleterious behavior in most processes that attempt to convert the energy in coal to a useful form. As coal is heated, the inorganic phases undergo transformations and reactions that yield a complex mixture of solid, molten, and volatile species. These species give rise to slagging and fouling deposits, corrosion, pollution, and other problems. Although such problems are usually associated with the combustion of coal to produce electrical power, they are also common in coal gasification and liquefaction, cokemaking, and iron production. Conversely, certain inorganic constituents (alkalies, calcium, and iron-bearing phases) can have significant and valuable catalytic activity in coal gasification and liquefaction.

The current chapter will briefly review research on this topic.

Nature of the Inorganic Constituents of Coal

It is common practice to make a distinction between the inorganic constituents of so-called "Eastern" and "Western" coals. By definition, Western coals are those for which the CaO+MgO content exceeds the Fe<sub>2</sub>O<sub>3</sub> content of the ash, while the reverse is true for Eastern coals [1]. The inorganic constituents in Eastern coals, which are principally bituminous in rank, are predominantly in the form of discrete mineral particles. Clay minerals (kaolinite, illite) are usually dominant, followed by quartz and pyrite. The range and typical values of the mineral distribution and ash chemistry of Eastern coals are shown in Table I. These data were determined from computer-controlled scanning electron microscopy (CCSEM), Mössbauer spectroscopy, and other measurements on over a hundred coals.

Table I. Inorganic Constituents of Eastern Coals

Mineral Distribution			Typical Ash Chemistry	
Mineral	Range	Typical	Species	Weight %
Quartz	5-44	18	SiO <sub>2</sub>	54
Kaolinite	9-60	32	Al <sub>2</sub> O <sub>3</sub>	29
Illite	2-29	14	Fe <sub>2</sub> O <sub>3</sub>	8
Chlorite	0-15	2	CaO	2
Mixed Silicates	5-31	17	MgO	1
Pyrite	1-27	8	K <sub>2</sub> O	2
Calcite	0-14	3	Na <sub>2</sub> O	1
Siderite/Ankerite	0-11	2	TiO <sub>2</sub>	1
Other Minerals	0-12	4	P <sub>2</sub> O <sub>5</sub>	0.2
			SO <sub>3</sub>	2

Western coals are usually lignites or subbituminous coals. The range and typical values of the inorganic phase distribution and ash chemistry of approximately 20 Western coals examined in this laboratory are shown in Table II. In a recent paper, we discussed the differences between the inorganic constituents of low-rank coals and those of bituminous coals [2]. These differences occur in the calcium-, iron-, and alkali-containing phases. In bituminous coals, the calcium content is typically low (CaO <5% of ash) and all calcium is contained in the mineral calcite. The calcium content of lignites is high (CaO ~10 to 30% of ash) and the calcium is molecularly dispersed throughout the coal macerals as salts of carboxylic acids. The latter point has been directly confirmed by EXAFS (extended X-ray absorption fine structure) spectroscopy [2,3]. Similar differences occur for the alkali elements. Minerals such as illite, which accounts for most of the potassium in bituminous coal, are found in only small amounts in lignite and subbituminous coal (see Tables I and II). In lignites, sodium and potassium are believed to occur as salts of humic or carboxylic acids. Montmorillonite and halite (NaCl) are the dominant Na-containing minerals, and they



occur in both bituminous and lower rank coal. The iron-bearing minerals in unoxidized bituminous coals include pyrite, ferrous iron-bearing clays (illite, chlorite), and carbonates (siderite, ankerite) [4]. In lignites, only pyrite and its weathering products (iron sulfates and oxyhydroxides) are normally observed [2].

Table II. Inorganic Constituents of Western Coals

Mineral Distribution			Typical Ash Chemistry	
Mineral	Range	Typical	Species	Weight %
Quartz	7-22	15	SiO <sub>2</sub>	30
Kaolinite	13-45	30	Al <sub>2</sub> O <sub>3</sub>	15
Illite	0-12	2	Fe <sub>2</sub> O <sub>3</sub>	10
Mixed Silicates	0-22	8	CaO	20
Pyrite	1-26	7	MgO	8
Fe Sulfates	0-5	1	K <sub>2</sub> O	0.7
Fe-rich*	0-14	2	NaO	0.6
Ca-rich**	7-49	25	TiO <sub>2</sub>	0.7
Other minerals***	1-10	7	P <sub>2</sub> O <sub>5</sub>	0.4
			SO <sub>3</sub>	15

\*Principally iron oxyhydroxide.

\*\*Principally calcium bonded to carboxyl groups in the macerals.

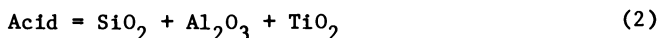
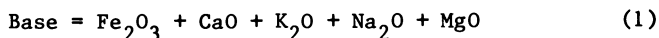
\*\*\*Barite, apatite, montmorillonite, and others

The diversity of transformations and reactions that such complex assemblages of inorganic matter can undergo when coal is combusted or otherwise converted to a more useful form of energy is too complex to be discussed in any detail in a short chapter. Our intention, therefore, is simply to outline some of the major phenomena and to provide the reader with useful references. Most of the chapter will deal with reactions and transformations related to coal combustion, with a short section devoted to other conversion processes.

#### Slagging Behavior; Ash Melting

During pulverized-coal combustion, atmospheric conditions within the coal flame are considered to be reducing in the sense that the stable ionic form of iron is ferrous. After ash particles have left the flame region, they encounter a more oxidizing environment, yielding deposits and fly ash in which the iron may be predominantly ferric or a mixture of ferrous and ferric, dependent on the air-to-fuel ratio. Consequently, it is important to understand the high temperature reactions of ash constituents in both types of environment. This point is recognized in the ASTM ash-fusion test [5] which specifies measurement of the fusion temperatures of ash cones in both a reducing (60% CO, 40% CO<sub>2</sub>) and an oxidizing (air) atmosphere. Numerous empirical formulae have been developed to predict

ash-fusion temperatures (AFTs) and the viscosities of molten coal-ash slags at higher temperatures from ash composition. Detailed discussions of these formulae and their physical basis have been given by Winegartner and his associates [1,6,7], by Watt and Fereday [8,9], and in a recent review article by Reid [10]. The dominant parameter in these relationships is usually the base-to-acid ratio, where "base" and "acid" are simply the sums of the weight percentages of the basic and acidic oxides:



Recently, we examined the behavior of AFTs in the context of ternary phase diagrams [11]. Significant similarities were observed between the dependence of the AFTs on chemical composition and the liquidus curves in appropriate regions of the FeO-SiO<sub>2</sub>-Al<sub>2</sub>O<sub>3</sub>, CaO-SiO<sub>2</sub>-Al<sub>2</sub>O<sub>3</sub>, and K<sub>2</sub>O-SiO<sub>2</sub>-Al<sub>2</sub>O<sub>3</sub> phase diagrams. The development of the Base-SiO<sub>2</sub>-Al<sub>2</sub>O<sub>3</sub> phase diagrams for the prediction of ash behavior appears to be a fruitful area for future research. An example of such a phase diagram is shown in Figure 1 where ash-softening temperatures (ST, reducing) are plotted in what is effectively the "mullite" region of a Base-SiO<sub>2</sub>-Al<sub>2</sub>O<sub>3</sub> phase diagram. The curves of equal ST exhibit great similarity to the liquidus isotherms in true ternary diagrams [12].

The arrow in Figure 1 illustrates the use of the phase diagram to predict STs. In this instance, a bituminous coal with a low ST was blended with two other coals to yield a product with a much higher ST. The blend was chosen with the aim of moving the composition of ash in a direction approximately normal to the equal ST curves. The predicted and observed STs of the original coal and the blend are shown in the inset of Figure 1. The predicted values are probably not as accurate as could be obtained with existing empirical formulae [6], but they are nevertheless quite reasonable.

Ternary and more complex phase diagrams can also contribute to interpretation of the reactions that lead to ash melting. In a reducing environment (60%CO-40%CO<sub>2</sub>), the important reactions for Eastern coals occur primarily within the FeO-SiO<sub>2</sub>-Al<sub>2</sub>O<sub>3</sub> phase diagram [13,14]. Using a variety of techniques (Mössbauer spectroscopy, CCSEM, X-ray diffraction) to investigate quenched ash samples heat treated under conditions similar to the ASTM ash-fusion test, it was established that most Eastern coal ashes exhibit behavior similar to that shown in the schematic diagram of Figure 2. Here, phases that are molten at elevated temperatures appear as glass phases in the quenched specimens. The potassium-containing clay mineral, illite, appears to be the first phase converted to a partially molten form; presumably this is because of the numerous low-temperature eutectic points in the K<sub>2</sub>O-SiO<sub>2</sub>-Al<sub>2</sub>O<sub>3</sub> phase diagram [12]. At approximately 900°C, wustite, derived from pyrite and other iron-rich minerals, begins to react with quartz and aluminosilicates derived from clay minerals to produce a mixture of wustite, fayalite (Fe<sub>2</sub>SiO<sub>4</sub>), and molten ferrous-aluminosilicate phase. At somewhat higher temperatures (~1050°C), fayalite has been largely incorporated into the melt phase, and ferrous iron may react with

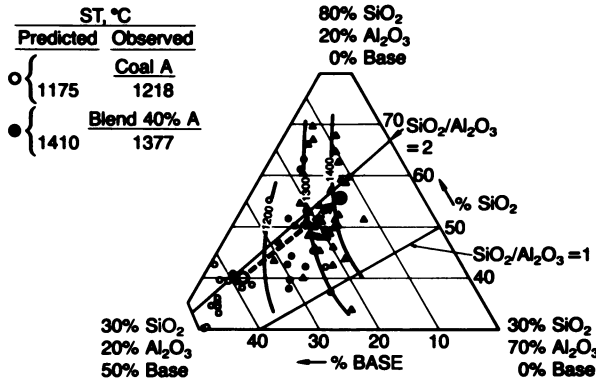


Figure 1 Pseudoternary phase diagram (Base - Al<sub>2</sub>O<sub>3</sub>- SiO<sub>2</sub>) showing spherical temperature (ST) contours. See text for discussion of points connected by arrow and inset.

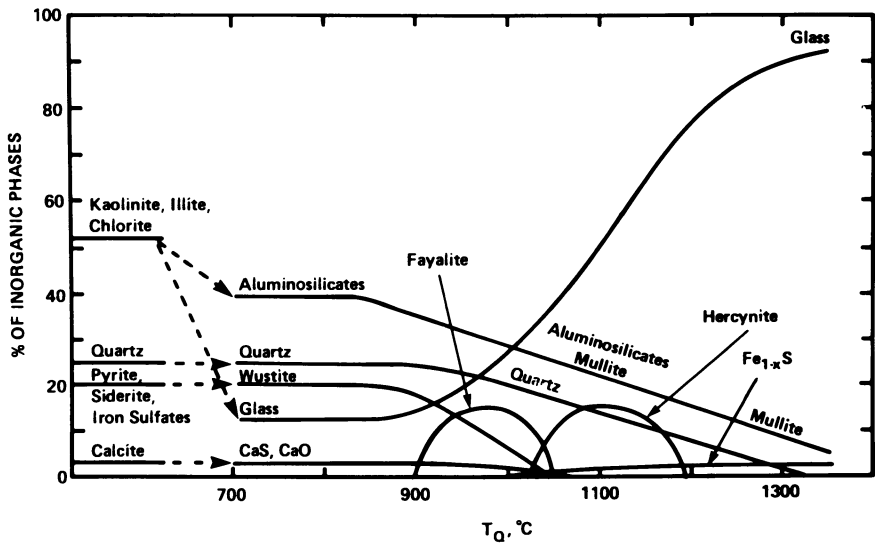


Figure 2 Schematic diagram illustrating high-temperature reactions for minerals in an Eastern-type coal under reducing conditions. Reproduced with permission from reference 14. Copyright 1983 Engineering Foundation.

aluminosilicates to form hercynite ( $\text{FeAl}_2\text{O}_4$ ). This reaction retards melting somewhat and its importance is related to the  $\text{Al}_2\text{O}_3$  content of the ash. Essentially all of the iron is contained in the melt phase for samples quenched from above  $1200^\circ\text{C}$ , as shown in Figure 3. Above  $1200^\circ\text{C}$ , reducing, most Eastern ashes are a mixture of molten aluminosilicates, mullite, quartz, and minor constituents such as iron sulfide, which is also molten, but is immiscible with the viscous silicate melt.

Similar, but less extensive, experiments have also been performed on ash samples quenched from high temperatures in air [13]. Below approximately  $1200^\circ\text{C}$ , essentially all of the glass observed in the samples is derived from the potassium-bearing clay mineral illite. Melting accelerates above approximately  $1300^\circ\text{C}$  and approaches completion for most Eastern ashes at temperatures of the order of  $1500^\circ\text{C}$ . As illustrated by the Mössbauer spectra in Figure 3, higher temperatures are required to produce significant partial melting in an oxidizing environment than in a reducing environment. All of the iron in the specimen quenched from  $1230^\circ\text{C}$  in a reducing atmosphere is contained in ferrous aluminosilicate glass, while only about 30 percent of the iron in the sample quenched from  $1300^\circ\text{C}$  in air has entered a ferric glass phase. This result is typical of Eastern ashes and is not too surprising, as it is well known that ferrous iron is a more effective flux than ferric iron. Moreover, calcium appears to be a more effective flux than ferric iron in an oxidizing environment.

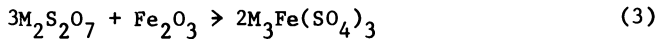
In both reducing and oxidizing atmospheres, significant partial melting of ash occurs at temperatures well below the initial deformation temperature (IDT). It is not uncommon to observe up to 50 percent of the ash in the form of glass at quenching temperatures as low as 200 to  $400^\circ\text{C}$  below the IDT. Such partial melting is important in deposit formation. Not surprisingly, the amount of glass observed at a given temperature in an oxidizing atmosphere is significantly less than that in a reducing atmosphere [13,14].

### Fouling; Volatile Species

Fouling generally refers to the formation of deposits on convective heat-transfer surfaces at relatively low temperatures ( $600$  to  $1000^\circ\text{C}$ ). Excellent discussions of this problem have recently been given by Wibberly and Wall (15) and in the general review article by Reid [10]. Alkali elements (Na, K) are the principal culprits in the formation of such deposits. Within the flame, these elements become volatilized. The ease of volatilization is related to the form in which the alkalis are present in the coal. Organically bound alkalis would be expected to be easily volatilized at typical flame temperatures ( $1400$ – $1500^\circ\text{C}$ ), as would NaCl, the most common form of sodium in bituminous coal. Potassium contained in illite would not be expected to volatilize as readily; illite should rapidly convert to a molten slag at these temperatures. For this reason, the water-soluble alkali content of coal [1] is considered to be a more reliable indicator of fouling than the total alkali content, at least for Eastern coals. Wibberly and Wall [15] list Na, NaOH, and NaCl as likely gaseous species, dependent on chlorine content of the coal, flame temperature, and oxygen potential.

Nonchloride species are probably rapidly converted to oxides ( $\text{Na}_2\text{O}$ ,  $\text{K}_2\text{O}$ ) on leaving the flame front. The volatile alkalis may condense on the surfaces of fly-ash particles carried by the flue gas or on cooler boiler surfaces. Wibberly and Wall [15] performed drop-tube experiments in which silica particles were exposed to synthetic combustion gases containing sodium at temperatures of 1200 to 1600°C. Sodium silicate layers ranging in thickness from 0.03 to 0.3  $\mu\text{m}$  were observed on the particle surfaces, and sintered deposits formed rapidly on stainless steel probes inserted into the lower part of the furnace. Such alkali-silicate layers are molten at the temperatures of interest. The thickness of the sodium silicate layers was decreased by a factor of three when the sodium was introduced in the form of NaCl, rather than in chlorine-free forms.

An excellent review of the role of alkali sulfates is given by Reid [10]. Below 1100°C, alkali oxides and chlorides react rapidly with  $\text{SO}_2$  and  $\text{O}_2$  or  $\text{SO}_3$  to form condensed sulfates on fly-ash particles and metal surfaces. Because of their low melting points, alkali sulfates are very corrosive, and form strongly bonded deposits. The melting points of the most easily formed sulfates,  $\text{Na}_2\text{SO}_4$  and  $\text{K}_2\text{SO}_4$ , are 882°C and 1075°C, respectively, and the minimum melting point of  $\text{Na}_2\text{SO}_4$ - $\text{K}_2\text{SO}_4$  mixtures is 833°C.  $\text{K}_2\text{SO}_4$ - $\text{CaSO}_4$  and  $\text{Na}_2\text{SO}_4$ - $\text{CaSO}_4$  are also commonly observed mixtures, which exhibit melting points in the range from 870 to 970°C. If the  $\text{SO}_3$  content of the atmosphere is sufficiently high, the pyrosulfates,  $\text{K}_2\text{S}_2\text{O}_7$  and  $\text{Na}_2\text{S}_2\text{O}_7$ , may be formed from  $\text{K}_2\text{SO}_4$  and  $\text{Na}_2\text{SO}_4$ . These phases melt at very low temperatures: 400°C for  $\text{Na}_2\text{S}_2\text{O}_7$  and 300°C for  $\text{K}_2\text{S}_2\text{O}_7$ . Crossley [16] has suggested that rapid metal wastage is caused by the reaction of the pyrosulfates with  $\text{Fe}_2\text{O}_3$  to form low-melting point (<600°C) alkali-iron trisulfates:



where M = Na or K. This point of view is supported by the work of Coats et al. [17] which established that liquid melts containing up to 90 percent pyrosulfate can be formed from  $\text{Na}_2\text{SO}_4$ - $\text{K}_2\text{SO}_4$  mixtures in  $\text{SO}_3$  pressures of 100 to 300 ppm at temperatures down to 335°C. Such  $\text{SO}_3$  levels can be readily reached via catalytic oxidation of  $\text{SO}_2$  in the presence of  $\text{Fe}_2\text{O}_3$  [10].

CCSEM analyses of fouling deposits from a boiler furnace in which a North Dakota lignite had been fired are given in Table III. Although the deposits consisted principally of calcium-enriched aluminosilicates, they also contained small but significant amounts of alkali sulfates, intermixed with calcium sulfate. Recently, we conducted potassium K-edge X-ray absorption spectroscopy (XAS) measurements on these and related samples at the Stanford Synchrotron Radiation Laboratory. The X-ray absorption near-edge structures, or XANES, were found to exhibit characteristic forms that could be used to identify the sulfates present. Figure 4 shows the XANES spectra obtained from the secondary superheater deposit (top) and from a deposit collected in a combustion rig (bottom) that was firing a North Dakota lignite. The XANES of the superheater deposit was found to be very similar to that of potassium bisulfate,  $\text{KHSO}_4$ .  $\text{KHSO}_4$  melts at 212°C, and converts rapidly to  $\text{K}_2\text{S}_2\text{O}_7$  above 350°C. The XANES spectrum of the combustion rig deposit, collected at a temperature

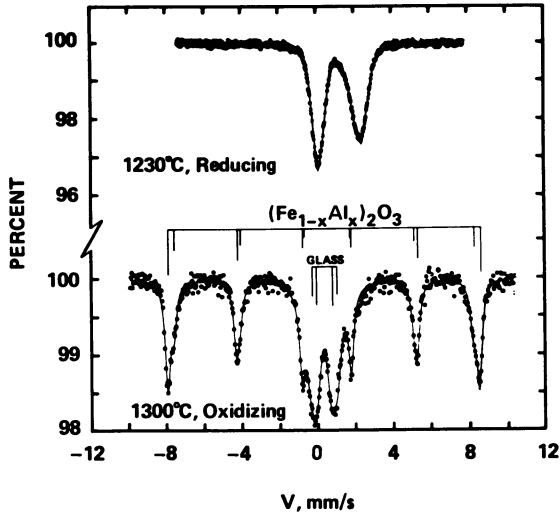


Figure 3 Comparison of typical Mössbauer spectra obtained from Eastern ashes quenched from high temperatures in reducing (top) and oxidizing (bottom) atmospheres.

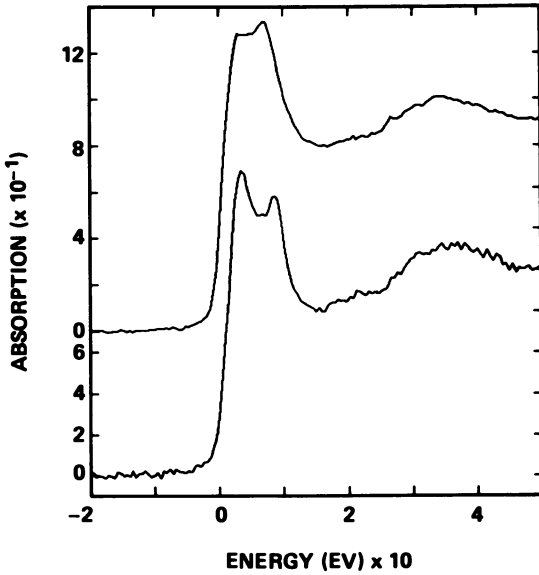


Figure 4 Potassium K-edge XANES spectra obtained from fouling deposits resulting from lignite combustion.

Table III. CCSEM Analyses of Fouling Deposits

CCSEM Category	Sec. Superheater, 990-1050°C	Preheater 750°C
Ca-rich aluminosilicate*	55	63
Ca- and Fe-rich aluminosilicate**	7	6
Alkali sulfate***	2	2
Calcium sulfate + alkali sulfate	4	6
SiO <sub>2</sub>	3	2
Ca-rich	10	6
Hematite	2	1
Ca-Fe ferrite	2	1
Ca-Mg sulfate	3	2
Al-Si rich	5	2
Unidentified, mixed phases	7	5

\*Approximate average composition (mole %) determined from CCSEM energy dispersive X-ray fluorescence spectra was 37% Ca, 8% Mg, 4% Fe, 41% Si, 10% Al (elements with  $Z > 12$ , only).

\*\*Average composition - 31% Ca, 7% Mg, 21% Fe, 32% Si, 9% Al.

\*\*\*Average composition - Na<sub>33</sub>Ca<sub>16</sub>K<sub>3</sub>S<sub>48</sub>.

of 1090°C, could be simulated rather well by weighted addition of the XANES spectra from K<sub>2</sub>SO<sub>4</sub> (60% weight) and K-aluminosilicate glass (40% weight). A more detailed discussion will be given elsewhere [18]. Spiro et al. [19] have used potassium K-edge XAS to investigate combustion products and cyclone deposits from a fluidized bed combustor firing an Eastern coal (Pittsburgh #8). They observed only K-aluminosilicate glass with no evidence of any significant potassium sulfate content. These initial results indicate that XAS will be a very useful method of investigating the structure of individual elements in complex deposits.

#### Reactions and Transformations of Interest for Other Coal Conversion Processes

In this section, examples of the high-temperature behavior of inorganic phases in other conversion processes will be given.

**Liquefaction.** Montano et al. [20] have investigated the transformation of pyrite to pyrrhotite in coal liquefaction environments. They conducted in situ Mossbauer spectroscopy measurements on coals maintained at 1.24 MPa nitrogen pressure and observed changes in the isomer shift at approximately 300°C that signalled the beginning of the transformation of pyrite to pyrrhotite. The transformation accelerated between 300 and 400°C, and from 20 to 80 percent of the pyrite in four different coals was transformed after one hour at 440°C. From examination of both the in situ spectra and the spectra of cooled residues, they concluded that the pyrrhotite underwent covalent bonding to the coal molecules, causing a catalytic effect on coal liquefaction.

**Carbonization.** When coal is heated to temperatures  $\sim 900$  to  $1200^{\circ}\text{C}$  in the absence of air, most of the volatile matter is driven off, leaving a char, or, in the case of metallurgical bituminous coal, a coke. The atmosphere in a coke oven consists principally of hydrogen and methane. Consequently, pyrite is reduced to a mixture of iron sulfide (troilite and pyrrhotite) and iron metal [21]. The amount of iron metal formed depends on both the temperature and the composition of the coke-oven gas. The reduction of iron sulfide to iron metal is desirable since blast furnace operation is more efficient with low sulfur coke. Calcite reacts with the liberated sulfur to form calcium sulfate, thus retaining sulfur in the coke. Calcium XANES spectra of coke produced from Pittsburgh seam coal in which all calcium is initially present as calcite indicate that approximately 70 percent of the calcite is converted to calcium sulfate during coking.

XAS and electron microscopy measurements establish that potassium in coke is present primarily in the form of K-aluminosilicate glass derived from illite. Potassium in coke is of great concern because of its behavior in a blast furnace during ironmaking. In the combustion or "raceway" zone of the blast furnace, potassium can become volatilized. The volatile potassium species condense on coke, brickwork, and metal surfaces in the cooler upper regions of the blast furnace causing several adverse effects, including excessive coke reactivity, alkali attack on brickwork, and alkali-initiated deposits and corrosion. As discussed elsewhere [22,23], XAS measurements can provide insight into the reaction mechanisms of potassium in a blast furnace. For example, the XAS data obtained from a brick that was severely damaged by alkali attack in a blast furnace are shown in Figure 5. The XANES spectrum from the brick is compared to a simulated spectrum obtained by weighted addition of the XANES of KCl (50% weight) and  $\text{K}_2\text{SiO}_3$  (50% weight) in Figure 5a, while the radial structure function derived from the EXAFS (extended X-ray absorption fine structure) of the potassium atoms in the brick appears in Figure 5b. Peaks due to the Cl and K neighbor shells in KCl and to the O and Si neighbor shells in K-aluminosilicate are labeled. From these results, it appears that the mechanism of alkali attack involved vapor-deposition of KCl followed by K-fluxing of the aluminosilicate brick. The results of an investigation of the reaction of potassium with coke using XAS and electron microscopy will be given elsewhere [23].

**Gasification.** Iron exhibits a great diversity of reactions at elevated temperatures when the reaction environment encompasses both reducing and oxidizing conditions at different stages of the process. For example, it is not unusual to observe five or six different iron-bearing compounds in three different oxidation states in char and ash samples obtained from coal-gasification systems. In Figure 6, the Mossbauer spectrum of a char residue from a bench-scale gasification system at the Institute of Gas Technology is shown. The input atmosphere to the gasifier was approximately 5.2%  $\text{O}_2$ , 21.2%  $\text{H}_2\text{O}$ , and the remainder  $\text{N}_2$ , and the average temperature was  $1800^{\circ}\text{F}$ . As indicated in Figure 6, six iron-bearing phases exhibiting three different oxidation states are observed: iron metal, iron sulfide (principally FeS), fayalite ( $\text{Fe}_2\text{SiO}_4$ ), magnetite ( $\text{Fe}_3\text{O}_4$ ), hematite ( $\text{Fe}_2\text{O}_3$ ), glass, wustite, and possibly other minor phases.



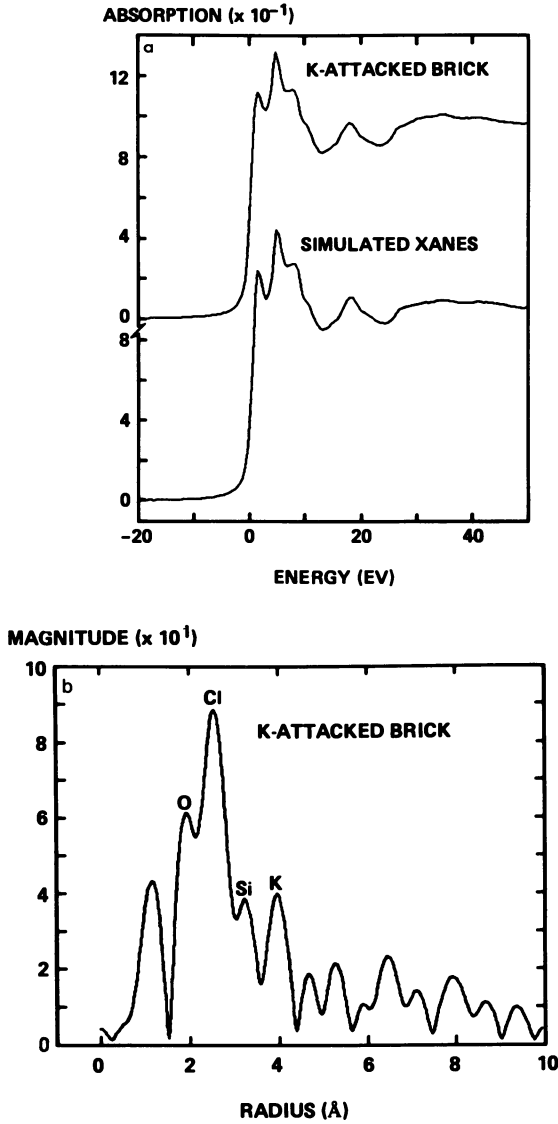


Figure 5 (a) Comparison of the potassium K-edge XANES spectrum of a blast furnace brick to a simulated XANES spectrum (50% KCl + 50%  $\text{K}_2\text{SiO}_3$ ). (b) Radial structure function of potassium derived by Fourier transforming the EXAFS of the K-attacked brick.

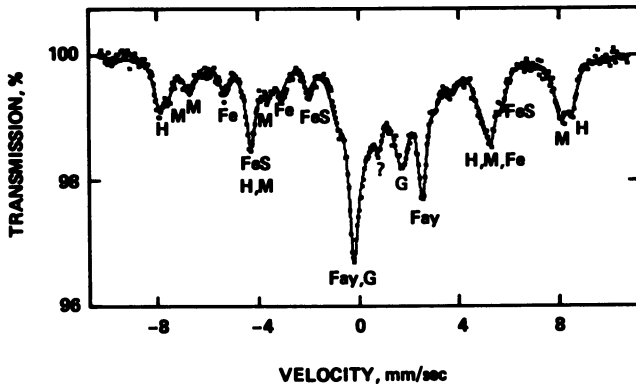


Figure 6  $^{57}\text{Fe}$  Mössbauer spectra of gasification char residue showing peaks from hematite (H), magnetite (M), iron metal (Fe), iron sulfides (FeS), fayalite (Fay), glass + wustite (G), and an unknown phase (?).

A more detailed discussion of this work has been given by Mason et al. [24].

Alkalies and alkaline earths serve as effective catalysts in coal gasification processes [25]. In low rank coals, calcium bound to oxygen anions in carboxyl groups is molecularly dispersed throughout the macerals [2,3]. Similarly, in K-enriched cokes treated at high temperatures, a more or less uniformly dispersed K-C phase is observed [22,23]. Such uniform dispersions greatly increase the activity of the catalytic species.

### Conclusions

Even from this brief overview, it is clear that much remains to be done in the area of understanding mineral-matter behavior in coal combustion and other conversion technologies and even more in combating the sticky problems arising from this component in coal. In particular, there is great need for more detailed investigations of full-scale technological processes, especially now that a number of relatively new and sophisticated techniques are available that can be used to characterize mineral-matter related phenomena in ways that were not possible a few years ago. Such techniques include Mössbauer and EXAFS spectroscopies, which we have highlighted in this article, that have the ability to focus on specific critical elements (Fe, K, S, etc.), and reveal very detailed information about the behavior of that element. However, the observed phenomena in full-scale processes will also need to be interpreted in terms of both kinetic (e.g., drop-tube experiments [15]) and thermodynamic (e.g., phase diagram analysis [11]) approaches, as well as to take into account the form of the mineral matter and its distribution in the original coal. These should be important areas for research on mineral-matter related problems in the future.

### Acknowledgments

We are grateful to a number of colleagues for providing many of the samples discussed in this paper. These colleagues include Ken Ho of the Babcock and Wilcox Company; Dave Mason of the Institute of Gas Technology; Steve Benson, Mike Jones, and Harold Schobert of the University of North Dakota Energy Research Center; and Mike Militzer of U. S. Steel Corporation. We would also like to acknowledge the Stanford Synchrotron Radiation Laboratory (SSRL) for providing beam-time for the XAS experiments and our collaborators in those experiments, F. W. Lytle and R. B. Gregor of the Boeing Company. SSRL is supported by DOE, NSF, and NIH.

The material in this paper is intended for general information only. Any use of this material in relation to any specific application should be based on independent examination and verification of its unrestricted availability for such use, and a determination of suitability for the application by professionally qualified personnel. No license under any United States Steel Corporation patents or other proprietary interest is implied by the publication of this paper. Those making use of or relying upon the material assume all risks and liability arising from such use or reliance.

Literature Cited

1. Winegartner, E. C., Coal Fouling and Slagging Parameters, ASME Special Publication, 1974.
2. Huffman, G. P.; Huggins, F. E. "Analysis of the Inorganic Constituents in Low-Rank Coals," in Chemistry of Low-Rank Coal," Schobert, H. H., Ed., ACS Symposium Series, No. 264, 1984; pp. 159-174.
3. Huggins, F. E.; Huffman, G. P.; Lytle, F. W.; Greeger, R. B. Proceedings of the International Conference on Coal Science, International Energy Agency, NY, 1983, 679-682.
4. Huffman, G. P.; Huggins, F. E. Fuel, 1978, 57, 592-604.
5. 1976 Annual Book of ASTM Standards, Pt. 26, American Society for Testing and Materials, Philadelphia, PA, 263-268.
6. Winegartner, E. C.; Rhodes, B. T. Trans. ASME, J. Eng. for Power, (Series A) 1975, 97, 395-406.
7. Winegartner, E. C.; Ubbens, A. A. Trans. AIME 1976, 260, 67-70.
8. Watt, J. D.; Fereday, F. J. Inst. Fuel 1969, 42, 99-103.
9. Watt, J. D. J. Inst. Fuel 1969, 42, 131-134.
10. Reid, W. T. "Coal Ash--Its Effect on Combustion Systems," Chap. 21, 1389-1446 in Chemistry of Coal Utilization, M. A. Elliott, Ed., J. Wiley, NY, 1981.
11. Huggins, F. E.; Kosmack, D. A.; Huffman, G. P. Fuel 1981, 60, 577-584.
12. Levin, E. M.; McMurdie, H. F.; Hall, H. P. Phase Diagrams for Ceramists, Amer. Ceramic Soc., Inc., Columbus, Ohio, 1964.
13. Huffman, G. P.; Huggins, F. E.; Dunmyre, G. R. Fuel 1981, 60, 585-597.
14. Huffman, G. P.; Huggins, F. E. Fouling and Slagging Resulting from Impurities in Combustion Gases, Bryers, R. W., Ed., Engineering Foundation, New York, NY, 1983; pp. 259-280.
15. Wibberly, L. J.; Wall, T. F. Fouling and Slagging Resulting from Impurities in Combustion Gases, Bryers, R. W., Ed., Engineering Foundation, New York, NY, 1983; pp. 493-513.
16. Crossley, H. E. J. Inst. of Fuel 1967, 40, 342-347.
17. Coats, A. W.; Dear, D. J. A.; Penfold, D. J. Inst. of Fuel 1968, 41, 129-132.
18. Huffman, G. P.; Huggins, F. E.; Greeger, R. B.; Lytle, F. W. submitted to Fuel.
19. Spiro, C. L.; Wong, J.; Lytle, F. W.; Greeger, R. B.; Maylotte, D. H.; Lamson, D. H. Preprint of a paper intended for Fuel.
20. Bommanavar, A. S.; Montano, P. A. Fuel, 1982, 61 523-528.
21. Huffman, G. P.; Huggins, F. E. Chapter 12 in Mössbauer Spectroscopy and Its Chemical Applications, Stevens, J. G.; Shenoy, G. K., Eds., ACS Adv. in Chem. Series 194, 1981; pp. 265-301.
22. Huffman, G. P.; Huggins, F. E.; Greeger, R. B.; Lytle, F. W. SSRL Activity Report 84/01, IX-31, 1984.
23. Huffman, G. P.; Huggins, F. E.; Shoenberger, J. S.; Walker, Lytle, F. W.; Greeger, R. B. Submitted to Fuel.
24. Coal Gasification Research Studies, Proj. 61063, Quart. Report for Aug. 1983 through Nov. 1983, DOE/MC/19301-5.
25. Walker, P. L; Matsumoto, J.; Hanzawa, T; Muira, T; Ismail, I. M. K. Fuel 1983, 62, 140-149.

RECEIVED June 21, 1985

## Mineral Transformations during Ashing of Selected Low-Rank Coals

S. K. Falcone and H. H. Schobert

Energy Research Center, University of North Dakota, University Station, Grand Forks, ND 58202

Inorganic species are present within low-rank coals as ion-exchangeable cations, as coordination complexes, and as discrete minerals. Variations in the inorganic associations of cations affects their relative reactivity and the processes associated with their formation of high temperature minerals. Twelve coals representing the Northern Great Plains and Gulf Coast were ashed 125°C, 750°C, and 1000°C in an oxidizing atmosphere. Each sample was then analyzed for its mineral composition by x-ray diffraction. In addition, model mixtures simulating raw coal mineralogies and organically-bound calcium and sodium were heated to 750°C and 1000°C for comparison to actual coal ashes. The processes responsible for most of the reactions identified were oxidation, dehydration, sulfur fixation, solid-state interactions and vaporization. In addition, it was determined that organically-bound cations, specifically calcium and sodium, were more reactive than cations bound in mineral form in producing new mineral species with pre-existing minerals.

Inorganic species are incorporated in low-rank coals in many ways: as ion-exchangeable cations, as coordination complexes, and as a diverse array of discrete minerals. In some cases an element will be present in more than one form; potassium, for example, occurs both as an exchangeable cation and in association with clay minerals. The variation in association of inorganics among the multiple modes of occurrence results in a very complex series of reactions and mineral transformations when low-rank coals are ashed. In low-rank coal utilization processes the behavior of the inorganic components can be at least as important to effective

operation as the behavior of the carbonaceous portion of the coal. The determination of the extent of the changes in bulk composition and in mineral phases during controlled laboratory ashing is very important in developing an understanding of ash behavior during coal processing and how such changes are related to process conditions.

In the past, mineralogical determinations using ash formed at the standard temperature of 750°C identified minerals which were not originally present in the raw coal but which were artifacts of the ashing procedure. This was due to the alteration of minerals by oxidation, dehydration and other processes at high temperatures. Recent studies by Miller et al (1), Frazer and Belcher (2), and O'Gorman and Walker (3) have concentrated on relating raw coal mineralogy to ash mineralogy of ash generated at low temperatures. Low-temperature ashing (LTA) theoretically would enable one to obtain the true mineralogical composition of a coal since little mineral alteration occurs at typical LTA temperatures of 125°C. Mitchell and Gluskoter (4) expanded this concept to study low to high temperature mineral transformations in ash of subbituminous and bituminous coals. With few exceptions, the application of LTA in ash mineralogy studies has been primarily associated with subbituminous and bituminous coals (5). In fact, Miller et al (1) and Frazer and Belcher (2) state that LTA may be unsuitable for obtaining the original mineralogy in lignites without appropriate pretreatment. This problem is due to the high organic oxygen content with associated inorganic exchangeable cations characteristic of lignites. The presence of organically-bonded inorganics drastically increases the ashing time, thereby increasing the chances of mineral alteration by oxidation. In addition, the release of organically-bound cations and organic sulfur in contact with mineral matter can alter the original coal mineralogy with an extended period of low-temperature ashing.

The purpose of this study was to identify mineral transformations occurring during low and high temperature ashing (125°, 750°, and 1000°C) of low-rank coals and to examine the processes responsible for the mineral transformations. Twelve low-rank coals were selected from the northern Great Plains and Gulf Coast. Nine North Dakota lignites, two Gulf Coast (Texas and Alabama) lignites, and one subbituminous coal from Montana were studied (Table I).

In addition, model mixtures of inorganic compounds simulating those inorganics characteristically found in low-rank coals were also heated to 750° and 1000°C. Minerals used in the model mixture studies included calcite, kaolinite, quartz and pyrite. Calcium and sodium acetates were used to simulate organically-bound calcium and sodium. Sodium sulfate was also used as a sodium and sulfur source. Two-, three- and four-component systems were examined varying the molar ratios of the constituents. In this manner the interaction of minerals and organically-bound inorganics can be traced during the heating process. Of particular interest was the simulation of high temperature processes responsible for forming feldspathic aluminosilicates characteristic of minerals formed when ashing low-rank coals. The model systems discussed are presented in Table II.

Table I. Inorganic Analyses of Raw Coals

Coal Name <sup>++</sup>	Locality	Si	Al	Fe	Mg*	Ca	Na*	S	K	Ti	Ba*
Absaloka <sup>+++</sup>	Big Horn Co., Montana	3.5	1.61	2.58	0.08	0.37	0.33	3.92	0.12	0.06	0.03
Beulah Low Sodium	Mercer Co., North Dakota	0.90	0.54	1.02	1.18	1.57	0.14	2.01	0.09	0.05	0.02
Beulah High Sodium	Mercer Co., North Dakota	0.35	0.29	0.52	0.67	1.81	0.46	0.75	ND	0.06	0.04
Center	Oliver Co., North Dakota	0.66	0.44	0.89	0.94	1.70	0.40	0.65	0.08	0.32	0.04
Choctaw	Choctaw, Alabama	1.06	0.49	1.87	0.56	0.84	0.09	2.50	0.10	0.04	ND
Falkirk	McLean Co., North Dakota	0.86	0.50	0.48	0.91	2.60	0.01	0.55	0.15	0.04	0.02
Gascoyne Blue	Bowman Co., North Dakota	1.09	0.73	0.25	0.38	2.28	0.27	0.93	0.14	0.05	0.13
Gascoyne Red	Bowman Co., North Dakota	2.86	0.87	0.39	0.59	1.74	0.13	1.12	0.13	0.12	0.06
Indian Head	Mercer Co., North Dakota	0.71	0.49	0.68	0.97	1.56	0.62	0.44	0.12	0.04	0.05
Pike	Pike County, Alabama	1.11	0.66	0.36	0.11	1.77	NA	2.28	0.10	0.65	NA
San Miguel	Atascosa Co., Texas	3.58	1.06	0.47	ND	1.20	0.60	1.88	0.35	0.08	NA
Velva	McHenry Co., North Dakota	0.56	0.33	0.26	0.11	0.98	0.09	NA	0.05	0.02	0.03

<sup>†</sup>Concentrations measured by x-ray fluorescence (XRF) unless otherwise specified.

<sup>++</sup>All coals are lignites except for Absaloka subbituminous.

<sup>+++</sup>Absaloka coal analysis completely by NAA.

\*Concentrations measured by neutron activation analyses (NAA).

NA (Not Available) ND (Not Detected)

## Experimental

The mineral matter composition of each coal sample was determined directly by X-ray diffraction (XRD) of low temperature ash (LTA). A LFE Model 504 four-chamber oxygen plasma low temperature asher was used. The ashing procedures used were modified from Miller and Givens' technique (6) for low temperature ashing of subbituminous and bituminous coals. One set of samples was ion-exchanged in 1M ammonium acetate at 70°C for 24 hours and freeze-dried prior to low temperature ashing. This procedure was repeated twice to ensure removal of ion-exchangeable cations. Another, but untreated, sample set was also ashed. Preliminary comparison of sample sets showed the exchanged samples to have lower ashing time and identical mineralogy except for the presence of bassanite in non-exchanged samples. This difference will be discussed later.

The LTA operating procedures used were as follows: a radio frequency power of approximately 150W and an oxygen flow of 100cc/min at 2 psi were maintained along with a chamber pressure of 1mm Hg. Samples were stirred once every two hours during the first eight hours and every eight hours during the remaining ashing time.

Samples were also ashed at 750°C in accordance with ASTM procedure D3174-73 (7) and will be referred to as ASTM samples. Samples were then ashed at 1000°C following the same procedure for 750°C coal ashing and will be referred to as HTA (high temperature ash) samples.

Minerals and other inorganics used in model systems A through J were ground to -60 mesh to match the particle size of the coals used for ashing. Samples were rapidly heated to 750°C and held for two hours at temperature. Half of the sample was removed and air quenched. The remaining portion of the sample was returned to the furnace and heated to 1000°C, held for two hours, and then air quenched.

Mineralogical composition of ash samples and model systems was determined by XRD. X-ray fluorescence (XRF) analysis was also used for bulk elemental analysis of the ash. Raw coal analysis was performed by XRF and neutron activation (NAA). XRF elemental analyses of raw coal samples are listed in Table I. The neutron activation analyses were performed at North Carolina State University.

## Results and Discussion

Mineralogical phases formed at different temperatures for each coal sample are summarized in Table III. The major mineral phases detected by XRD in LTA samples are quartz, pyrite, bassanite, kaolinite and plagioclase. The processes responsible for subsequent mineral transformations include oxidation, vaporization, sulfur fixation, dehydration and solid-state interactions. The temperatures at which specific transformations occur are assigned on the basis of previous experimental work by Mitchell and Gluskoter (4) and published chemical data in the Handbook of Chemistry and Physics (8). In addition to mineral-mineral interactions it is believed that reactions between minerals and exchangeable cations occur (9).



Table II. Synthetic Compound Mixtures and Transformations That Occur During Heating

Compound Mixtures	Molar Ratios	Temp. °C	Analyzed Minerals	Processes
A. Ca (C <sub>2</sub> H <sub>3</sub> O <sub>2</sub> ) <sub>2</sub> + Pyrite (FeS <sub>2</sub> )	2:1	750	Anhydrite (CaSO <sub>4</sub> ) + Magnetite (Fe <sub>3</sub> O <sub>4</sub> )	Oxidation; Pyritic sulfur fixation
		1000	Anhydrite (CaSO <sub>4</sub> ) + Magnetite (Fe <sub>3</sub> O <sub>4</sub> ) + Hematite (Fe <sub>2</sub> O <sub>3</sub> )	Oxidation
B. Calcite (CaCO <sub>3</sub> ) + Pyrite (FeS <sub>2</sub> )	1:2	750	Anhydrite (CaSO <sub>4</sub> ) + Calcite (CaCO <sub>3</sub> ) + Hematite (Fe <sub>2</sub> O <sub>3</sub> )	Oxidation; Pyritic sulfur fixation
		1000	Anhydrite (CaSO <sub>4</sub> ) + Hematite (Fe <sub>2</sub> O <sub>3</sub> ) + Magnetite (Fe <sub>3</sub> O <sub>4</sub> ) + CaO	Oxidation; Decomposition fo CaCO <sub>3</sub>
C. Ca (C <sub>2</sub> H <sub>3</sub> O <sub>2</sub> ) <sub>2</sub> + Kaolinite (Al <sub>2</sub> Si <sub>2</sub> O <sub>5</sub> (OH) <sub>4</sub> )	1:1	750	Amorphous + CaO	Dehydration, oxidation
		1000	Gehlenite (Ca <sub>2</sub> Al <sub>2</sub> SiO <sub>7</sub> )	Interstitial infilling in reordered kaolinite structure
D. NaC <sub>2</sub> H <sub>3</sub> O <sub>2</sub> + Kaolinite (Al <sub>2</sub> Si <sub>2</sub> O <sub>5</sub> (OH) <sub>4</sub> )	1:1	750	Amorphous + Carnegieite (NaAlSiO <sub>4</sub> )	Dehydration; Interstitial infilling in reordered kaolinite structure
		1000	Nepheline (NaAlSiO <sub>4</sub> )	
E. Ca(C <sub>2</sub> H <sub>3</sub> O <sub>2</sub> ) <sub>2</sub> + NaC <sub>2</sub> H <sub>3</sub> O <sub>2</sub> + Kaolinite (Al <sub>2</sub> Si <sub>2</sub> O <sub>5</sub> (OH) <sub>4</sub> )	1:1:1	750	Carnegieite (NaAlSiO <sub>4</sub> )	Dehydration; Interstitial infilling in reordered kaolinite structure
		1000	Nepheline (NaAlSiO <sub>4</sub> ) + Gehlenite (Ca <sub>2</sub> Al <sub>2</sub> SiO <sub>7</sub> )	Interstitial infilling of Ca in reordered clay structure; structural transformation of sodium aluminosilicate

F.	Calcite (CaCO <sub>3</sub> ) + kaolinite (Al <sub>2</sub> Si <sub>2</sub> O <sub>5</sub> (OH) <sub>4</sub> )	2.5:1	750	Calcite (CaCO <sub>3</sub> ) + Amorphous Phase	Dehydration and collapse of kaolinite structure
			1000	Gehlenite (Ca <sub>2</sub> Al <sub>2</sub> SiO <sub>7</sub> ) + CaO + Mullite	Interstitial infilling in reordered kaolinite structure
G.	Na <sub>2</sub> SO <sub>4</sub> + kaolinite (Al <sub>2</sub> Si <sub>2</sub> O <sub>5</sub> (OH) <sub>4</sub> )	1:1	750	NaSO <sub>4</sub> + Amorphous	Dehydration
			1000	Nepheline (NaAlSi <sub>3</sub> O <sub>8</sub> )	Interstitial infilling
H.	Kaolinite (Al <sub>2</sub> Si <sub>2</sub> O <sub>5</sub> (OH) <sub>4</sub> ) + Na <sub>2</sub> SO <sub>4</sub> + Ca(C <sub>2</sub> H <sub>3</sub> O <sub>2</sub> ) <sub>2</sub>	1:1:1	750	Na <sub>2</sub> SO <sub>4</sub> + Amorphous	Dehydration
			1000	Gehlenite (Ca <sub>2</sub> Al <sub>2</sub> SiO <sub>7</sub> ) + Nepheline (NaAlSi <sub>3</sub> O <sub>8</sub> ) + Hauyne (Na,Ca) <sub>6-8</sub> (AlSiO <sub>4</sub> ) (SO <sub>4</sub> ) <sub>1-2</sub>	Interstitial infilling
I.	Kaolinite (Al <sub>2</sub> Si <sub>2</sub> O <sub>5</sub> (OH) <sub>4</sub> ) + NaC <sub>2</sub> H <sub>3</sub> O <sub>2</sub> + Ca(C <sub>2</sub> H <sub>3</sub> O <sub>2</sub> ) <sub>2</sub> + Pyrite (FeS <sub>2</sub> )	1:1:1:1	750	Magnetite (Fe <sub>2</sub> O <sub>3</sub> ) + Anhydrite (CaSO <sub>4</sub> )	Dehydration; Oxidation, Pyritic sulfur fixation
			1000	Hauyne (Na,Ca) <sub>6-8</sub> (AlSiO <sub>4</sub> ) (SO <sub>4</sub> ) <sub>1-2</sub> + Magnetite (Fe <sub>2</sub> O <sub>3</sub> ) + Magnetite (Fe <sub>3</sub> O <sub>4</sub> ) + Anhydrite (CaSO <sub>4</sub> ) + Gehlenite (Ca <sub>2</sub> Al <sub>2</sub> SiO <sub>7</sub> )	Interstitial infilling in reordered kaolinite structure; Oxidation
J.	Kaolinite (Al <sub>2</sub> Si <sub>2</sub> O <sub>5</sub> (OH) <sub>4</sub> ) + Quartz (SiO <sub>2</sub> ) + Na C <sub>2</sub> H <sub>3</sub> O <sub>2</sub> + Ca (C <sub>2</sub> H <sub>3</sub> O <sub>2</sub> ) <sub>2</sub> + Pyrite (FeS <sub>2</sub> )	1:2:1:1:1	750	Quartz (SiO <sub>2</sub> ) + Anhydrite (CaSO <sub>4</sub> ) + Hematite (Fe <sub>2</sub> O <sub>3</sub> )	Dehydration; oxidation, sulfur fixation
			1000	Quartz (SiO <sub>2</sub> ) + Anhydrite (CaSO <sub>4</sub> ) + Hauyne (Na,Ca) <sub>6-8</sub> (AlSiO <sub>4</sub> ) (SO <sub>4</sub> ) <sub>1-2</sub> + Hematite (Fe <sub>2</sub> O <sub>3</sub> ) + Magnetite (Fe <sub>3</sub> O <sub>4</sub> )	Interstitial substitution Oxidation

Table III. Mineralogical Composition

Sample	LTA (125°C) <sup>+</sup>	ASTM (750°C)	HTA (1000°C)
Absaloka	Quartz Pyrite Kaolinite Plagioclase Bassanite	Quartz Anhydrite Hematite	Anhydrite Magnetite Hematite Quartz Melilite Plagioclase Nepheline
Beulah-Low Sodium	Quartz Pyrite Kaolinite Bassanite	Quartz Hematite Magnetite Anhydrite	Anhydrite Pyroxene Magnetite Hauyne Hematite Quartz
Beulah-High Sodium	Quartz Bassanite Kaolinite Pyrite	Anhydrite Hematite Magnetite Quartz Melilite Hauyne	Anhydrite Melilite Magnetite Hematite Hauyne Quartz Corundum
Center	Quartz Bassanite Pyrite Kaolinite	Anhydrite Hematite Quartz	Anhydrite Hauyne Pyroxene Melilite Hematite Quartz
Choctaw	Quartz Pyrite Kaolinite Bassanite Plagioclase	Anhydrite Quartz Hematite Magnetite Plagioclase Pyroxene	Anhydrite Hematite Quartz Magnetite Plagioclase
Falkirk	Quartz Kaolinite Pyrite	Anhydrite Quartz Hematite Magnetite Melilite (trace)	Anhydrite Quartz Melilite Hematite Magnetite Hauyne
Gascoyne Blue- High Sodium	Quartz Kaolinite Pyrite Calcite Sodium Sulfate (trace)	Anhydrite Quartz Hematite Magnetite Nosean Melilite	Anhydrite Melilite Hauyne Quartz

\*Minerals listed in decreasing order of peak intensities and

## of Ash Samples Determined by XRD\*

Sample	LTA ( 125°C)	ASTM (750°C)	HTA (1000°C)
Gascoyne Red- Low Sodium	Quartz Kaolinite Pyrite	Quartz Anhydrite Hematite Magnetite	Quartz Anhydrite Pyroxene Hematite Hauyne
Indian Head- High Sodium	Quartz Pyrite Kaolinite Bassanite	Anhydrite Quartz Hematite Nosean Melilite Hauyne Sodium Sulfate**	Melilite Hematite Anhydrite Hauyne Magnetite Pyroxene
Pike	Quartz Pyrite Kaolinite	Anhydrite Quartz Pyrite	Anhydrite Hematite Melilite Anorthite Quartz
San Miguel	Zeolite (Heulandite) Quartz Kaolinite Pyrite Bassanite Plagioclase	Zeolite Anhydrite Hematite Quartz Plagioclase (Anorthite) Melilite	Plagioclase (Anorthite) Hematite Quartz Magnetite Anhydrite
Velva	Quartz Kaolinite Pyrite Bassanite	Anhydrite Quartz CaO**	Anhydrite Gehlenite Quartz MgO Hauyne**

---

occurrence. \*\*Peak identification not conclusive.

Pyrite ( $\text{FeS}_2$ ) is present in all LTA samples. While Miller et al (1) stated that pyrite may be oxidized with increased low temperature ashing time in lignites no evidence of oxidized forms of iron was seen by XRD. This may be attributed to the pretreatment of samples with ammonium acetate, thereby reducing ashing times as much as 50%. In ASTM samples pyrite is oxidized to hematite ( $\text{Fe}_2\text{O}_3$ ) and magnetite ( $\text{Fe}_3\text{O}_4$ ). According to Miller and Gluskoter (4), pyrite oxidizes at  $500^\circ\text{C}$ . With the oxidation of pyrite to iron oxide rather than iron sulfate, pyritic sulfur is released. The formation of sodium and calcium sulfates detected in ASTM ash can be associated with the release of this pyritic sulfur or organic sulfur and their interaction with carbonates as well as with organically-bound calcium and sodium.

In the model mixture studies calcium acetate was observed to react with pyrite at  $750^\circ$  and  $1000^\circ\text{C}$  to generate anhydrite XRD peaks of greater intensity than those observed for the system of calcite reacting with pyrite (Table II, Systems A and B). Sulfur fixation by calcium released from calcium acetate by pyritic sulfur was greater than in the calcite case probably due to the similar temperatures at which calcium acetate decomposes and pyrite oxidizes ( $400^\circ$  to  $500^\circ\text{C}$ ). Calcite, on the other hand, does not decompose until higher temperatures ( $900^\circ\text{C}$ ); therefore the calcium necessary to form anhydrite is not as readily available. Most of the  $\text{SO}_2$  formed by oxidation of pyrite would be lost to the atmosphere by the time calcite decomposes.

Bassanite ( $\text{CaSO}_4 \cdot 1/2\text{H}_2\text{O}$ ) is present in some of the sample LTAs. While bassanite may form from the dehydration of gypsum ( $\text{CaSO}_4 \cdot 2\text{H}_2\text{O}$ ) during the LTA procedure no significant gypsum was detected in the original coal mineralogy of the samples studied. Therefore, hemihydrated calcium sulfate (bassanite) formed at low temperature may be due to the fixation of organic sulfur by organically-bound calcium cations not completely removed by the ion-exchange procedure (9, 10). In this case, bassanite is simply an artifact of the low temperature ashing procedure. This phenomenon is typical of coals having abundant alkali cations associated with carboxyl groups (6). At such low temperatures it is unlikely that calcite would react with organic sulfur to form  $\text{CaSO}_4 \cdot 1/2 \text{H}_2\text{O}$ . Continued increases in ashing temperature results in complete dehydration of bassanite to anhydrite ( $\text{CaSO}_4$ ) at  $400^\circ\text{C}$ . Anhydrite is a major mineral phase in ASTM and HTA samples.

Kaolinite ( $\text{Al}_2\text{Si}_2\text{O}_5(\text{OH})_4$ ) is present only in LTA samples. Kaolinite dehydration occurs approximately from  $400^\circ$  to  $525^\circ\text{C}$  (4). With removal of water by dehydration, the kaolinite structure collapses, retaining some degree of order and forming metakaolin. No metakaolin was detected by XRD in ASTM samples, perhaps due to its poorly defined crystalline structure. However, it is believed that the basic kaolinite components are present in an amorphous form in ASTM ash. With increasing temperature the collapsed kaolinite structure forms corundum ( $\gamma\text{-Al}_2\text{O}_3$ ). While mullite ( $3\text{Al}_2\text{O}_3 \cdot 2\text{SiO}_2$ ) and cristobalite ( $\text{SiO}_2$ ) have been reported to form from well-ordered kaolinites in bituminous coals at  $1000^\circ\text{C}$  (4) neither were observed in HTA samples. According to Grim (11), the absence of mullite suggests that the original kaolinitic structure was poorly defined. It has also been suggested by Grim (11) that the presence

of impurities in the form of alkali ions, such as in lignites, retards the development of mullites and cristobalite. The mechanism for this is not fully understood.

The collapsed kaolinitic structure acts as a source or framework for several different aluminosilicate complexes formed in HTA ash samples. Common minerals found are as follows: anorthite ( $\text{CaAl}_2\text{Si}_2\text{O}_8$ ), pyroxenes  $(\text{Ca,Na})(\text{Mg,Fe,Al})(\text{Si,Al})_2\text{O}_6$ , melilites  $(\text{Na,Ca})_2(\text{Mg,Fe,Al})(\text{Si,Al})_2\text{O}_7$ , hauyne  $(\text{Na,Ca})_{6-8}(\text{AlSiO}_4)(\text{SO}_4)_{1-2}$ , nosean  $(\text{Na}_8\text{Al}_6\text{Si}_6\text{O}_{24}\text{SO}_4)$  and nepheline  $(\text{Na,K})\text{AlSiO}_4$ . At  $1000^\circ\text{C}$  aluminosilicate minerals form from solid-state reactions of kaolinitic material with cations derived from carbonates, oxides, or sulfates. Interstitial in-filling of alkali cations occurs within the dehydrated kaolinite structure with increasing temperature due to thermal expansion and reordering of the collapsed clay structure. In some coals, particularly those high in sodium, these aluminosilicates are also seen in ASTM samples.

In the model systems C through I (Table II) different sources of calcium and sodium were mixed with clay (kaolinite) and heated to observe their role in forming the aluminosilicates typical of ash fouling deposits. In systems C and D calcium acetate and sodium acetate were mixed with kaolinite in equal molar ratios. X-ray diffractometer patterns showed that both systems were, for the most part, amorphous at  $750^\circ\text{C}$ . However, in system E where sodium and calcium acetate were present in equal molar ratios carnegietite was formed at  $750^\circ\text{C}$ . Carnegietite is a polymorph of nepheline. In carnegietite the sodium cation is tetrahedrally coordinated whereas in nepheline the sodium cation is octahedrally coordinated.

At temperatures greater than  $900^\circ\text{C}$  the formation of new aluminosilicates would be anticipated with the reordering of collapsed clay structures and infilling of interstitial void spaces by cations. In systems C and D nepheline and gehlenite were formed respectively at  $1000^\circ\text{C}$ . In system E both nepheline and gehlenite were formed at  $1000^\circ\text{C}$  showing no detectable mutual interstitial void filling of calcium and sodium within the same aluminosilicate structures. To establish that the results observed with the 1:1 calcium:sodium ratios were not artifacts of a stoichiometric limitation of reactants the molar ratios of calcium to sodium were varied from 1:4 to 4:1 in an attempt to saturate the system with respect to calcium or sodium. X-ray diffractometer patterns of various ratio combinations showed that sodium and calcium continued to fill voids in the same manner as with a 1:1 ratio. The fact that sodium and calcium do not mutually infill void of specific minerals reflects the preferred oxide coordination behavior of the two cations, which in turn is determined by their respective ionic charges and radii. Calcium prefers tetrahedral coordination, so that in general the reaction of calcium ions with kaolinite would result in a gehlenite structure, in which the calcium is tetrahedrally coordinated. On the other hand, sodium favors octahedral coordination, thus forming nepheline structures with sodium in octahedral site.

In system F calcite was used as a calcium source for the formation of gehlenite. The reaction did not proceed as completely as with calcium acetate, as inferred from two observations: 1) some of the calcium remained as calcium oxide upon decomposition of

calcite at 900°C, and 2) mullite, a poorly crystalline form of dehydrated reordered kaolinite, was still present at 1000°C in the presence of calcium oxide.

In systems G and H, sodium sulfate was used as a sodium source mixed with kaolinite and calcium acetate. Sodium sulfate melts at approximately 884°C. Therefore, at 750°C no interaction between kaolinite and sodium sulfate was seen (systems G and H). In system G nepheline was formed at 1000°C, with none of the sulfur released from the sodium sulfate involved in the formation of any new high temperature minerals. However, in system H additional feldspathoids (i.e., gehlenite and hauyne) other than nepheline were formed. In this case, sulfur was involved in forming new high temperature minerals.

System I was comprised of calcium and sodium acetates, kaolinite, and pyrite to see if sulfur-containing aluminosilicates would be formed. As expected, anhydrite ( $\text{CaSO}_4$ ) was formed by pyritic sulfur fixation by calcium. At 1000°C not only did the anhydrite persist but a sulfur containing aluminosilicate, hauyne, was formed in addition to gehlenite.

In systems A through I the major aluminosilicate minerals produced were silica-deficient. However, in systems J where silica was provided in excess in the form of quartz the system still produced only feldspathoids containing only two-thirds as much silica as their silica-rich counterparts (i.e. alkali feldspars). In addition, the quartz peaks in system J were not substantially reduced at higher temperatures. These two facts suggest that  $\text{SiO}_2$  in the form of quartz is inactive up to and at 1000°C. This idea is supported by the fact that quartz peaks are also quite evident in diffractometer patterns of ash samples generated between 750°C and 1000°C. It appears that temperatures in excess of 1000°C are required for quartz to contribute to the formation of silica-rich minerals.

XRD failed to detect calcite in LTA samples possibly due to its extraction by ammonium acetate solution or because the amounts of calcite were below detection limits (~5%). For the most part, calcium is supplied to the system by gypsum and organically-bound calcium. Calcium, whether in the form of bassanite, calcite, or cations in LTA samples, forms anhydrite in ASTM samples. In HTA samples calcium reacts primarily with dehydrated kaolinite forming aluminosilicates.

Figure 1 displays a typical X-ray diffractometer pattern sequence from LTA, ASTM, and HTA samples of the Beulah High Sodium lignite. Major peaks are identified according to the mineral phases present. Mineral transformations at higher temperatures are characterized by the formation of numerous feldspathoids. When comparing several of these diffractometer patterns there is little difference among LTA samples from different coals; on the other hand, the various ASTM and HTA ash samples are quite different. By comparing the mineralogical differences in the ashes to the raw coal elemental compositions, it can be seen that samples containing higher amounts of sodium tend to form alumino-silicates at lower temperatures (750°C) than samples high in calcium. High-sodium coals such as Beulah High Sodium and Gascoyne Blue develop complex silicates in ASTM samples and are prone to forming ash fouling

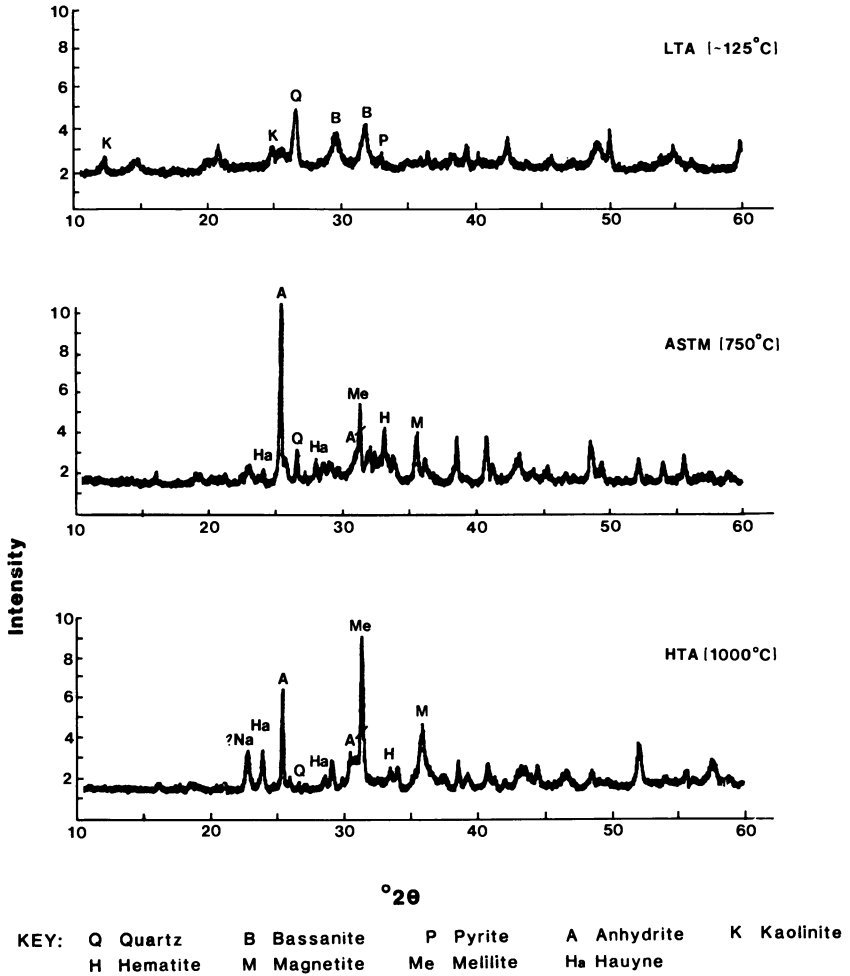


Figure 1. X-ray diffractograms of LTA, ASTM and HTA samples of Beulah high sodium coal.



deposits. Melilites, hauyne, nepheline, nosean and pyroxenes are typical of such aluminosilicates in the ASTM and HTA ash samples. These are minerals commonly found in the fouling deposits of most lignites.

### **Concluding Remarks**

The observations presented in this study reflect the preliminary results of an investigation of the mineral transformations seen in the high temperature combustion of low-rank coals. The mineralogies of the raw coals studied do not vary a great deal. Quartz, kaolinite, pyrite, and bassanite are found in abundance in each LTA sample. Greater differences between samples are apparent at higher temperatures, where complex aluminosilicates predominate. This is a reflection of differences not so much in original mineral matter but in the total inorganic composition of the coal. Specifically, the presence of exchangeable alkali cations accounts for differences in ashing behavior between coal samples (9). Both the type of the cations (specifically, sodium or calcium) and the amounts of each type incorporated in the coal are important in determining the mineral phases formed in the HTA ash.

The processes responsible for most of the reactions identified are oxidation, dehydration, sulfur fixation, solid-state interactions and vaporization. Isolating specific reactions occurring in a multi-component system is difficult; the use of model systems was helpful in tracing mineral transformations. Additional work planned in this area includes research on non-equilibrium systems and experiments in reducing atmospheres.

### **Acknowledgments**

The authors wish to thank Diane Rindt for her help in x-ray diffraction analysis and Steve Braun for his assistance in preparing HTA ash samples. This work was performed under a U.S. Department of Energy Cooperative DOE support Agreement No. DE-FC21-83FE60181.

### **Literature Cited**

1. Miller, R.N.; Yarzab, R.F.: and Given, Peter. Fuel 1979, 58, 4.
2. Frazer, F.W.; and Belcher, C.B. Fuel 1973, 52,41.
3. O'Gorman, J.V.: and Walker, P.L. Fuel 1973, 52,71.
4. Mitchell, R.S.; and Gluskoter, H.J. Fuel 1976, 55,90.
5. Gluskoter, J.J. Fuel 1965, 44, 285.
6. Miller, R.N.; and Given, Peter. 'A Geochemical Study of the Inorganic Constituents in Some Low-Rank Coals' Technical Report, Pennsylvania State University to the U.S. Department of Energy, Rep. FE-2494-TR-1, 1978.
7. Annual Book of American Society of Testing Materials Standards 1979, Part 26: Gaseous Fuels; Coal and Coke; Atmospheric Analysis.
8. Handbook of Chemistry and Physics 54th edition, Chemical Rubber Company, 1973.

9. Morgan, M.E.; Jenkins, R.G.; and Walker, P.L. Jr. Fuel 1981, 60, 189.
10. Painter, P.C.; Coleman, M.M.; Jenkins, R.G.; and Walker, P.L. Jr. Fuel 1978, 57, 125.
11. Grim, R.E. Clay Mineralogy, McGraw-Hill, New York, 1968, Chapter 9.

RECEIVED June 13, 1985

## High-Temperature Interactions among Minerals Occurring in Coal

Donald L. Biggs and Curtis G. Lindsay<sup>1</sup>

Ames Laboratory, Iowa State Mining and Mineral Resources Research Institute, and  
Department of Earth Sciences, Iowa State University, Ames, IA 50011

Minerals known to be present in the low temperature ash extracted from coals were heated in a microscope heating stage from 25° to about 1400°C. Mineral types were arranged in homogeneous fields where two fields shared a linear boundary or three fields were in contact at a point. Because of the known reactivity of calcite and pyrite, all specimens contained this pair. Clay minerals, kaolinite, illite and montmorillonite were used as the third component. Reaction temperature between calcite and pyrite is lowered by the presence of clays. Iron was observed to migrate into the clay domain after the formation of pyrrhotite from pyrite and oldhamite was observed forming between the domain of lime formed from calcite and the pyrrhotite.

Mineral impurities in coal are known to be primary contributors to the slagging and fouling of utility boilers, fly ash and bottom ash production as well as atmospheric pollution. They also produce undesirable effects in some parts of hydrogenation processes such as liquifaction and gasification (1,2,3). Despite a long history of investigation prompted by these observations, many questions remain unanswered.

Simple empirical relationships between fusion temperature of the furnace deposits and the mineralogy of coals have been proposed (4,5,6). More recently attempts have concentrated on a physico-chemical view of the problem comparing ash fusion temperatures with phase relations in three-component chemical systems (7,8). This method of attack has yielded some significant results, but at least some researchers (8) have questioned this approach, which is based

<sup>1</sup>Current address: Department of Geologic Sciences, Virginia Polytechnic Institute, Blacksburg, VA 24061.

on the assumption that these processes occur under conditions of equilibrium.

The aim of the research described here is to observe interactions between minerals known to occur in coals in the most direct fashion possible and in the simplest conditions consistent with causing the reactions to occur. It is considered that observation of simple mixtures of minerals observed to enter into reaction may make possible a better accounting of the processes by which slag and fouling deposits form in furnaces.

### Experimental Methods

Isolation and Identification of Coal Minerals. Two coal samples, collected from different coal basins in the United States (see Table I), were subjected to low-temperature ashing as described by Gluskoter (9). This process avoids destruction of the minerals while oxidizing the organic portion of the coal. This ashing procedure occurs at a much lower temperature than that of the American Society for Testing and Materials (ASTM) method it is given the name of "low-temperature ashing" and generally abbreviated LTA. In formation of a mineral concentrate by LTA, a few changes are anticipated; some clays are reversibly dehydrated, and hydrated surfaces are reduced to the hemihydrate form (for instance gypsum is converted to bassanite). Because these changes are known in advance, due allowance can be made for them.

Table I. Coal Samples, Localities of Origin, and Analyses  
(all samples run-of-mine)

<u>Seam:</u>	Illinois #6		
<u>Locality:</u>	St. Clair County, Illinois		
<u>Analysis:</u>	9 mesh x 0	9 x 32 mesh	9 x 32 mesh
	Raw	Float	Sink
Moisture (%):	5.31	5.44	2.55
Ash, ASTM (%):	32.86	7.10	68.05
Pyritic Sulfur (%):	2.46	0.76	5.08
Total Sulfur (%):	4.57	4.57	5.94
Heating Value (BTU/lb.):	9,039	13,248	3,574
<u>Seam:</u>	Upper Freeport		
<u>Locality:</u>	Grant County, West Virginia		
<u>Analysis:</u>	9 mesh x 0	9 x 32 mesh	9 x 32 mesh
	Raw	Float	Sink
Moisture (%):	0.30	0.68	0.93
Ash, ASTM (%):	35.90	7.26	72.10
Pyritic Sulfur (%):	1.58	0.27	2.62
Total Sulfur (%):	2.18	1.06	3.00
Heating Value (BTU/lb.):	9,695	13,365	3,086

Mineral constituents of the LTA concentrates were identified by x-ray diffraction techniques. Illite, kaolinite, quartz and pyrite are ubiquitous in the mineral suites; calcite occurs in most concentrates. Many other minerals have been identified in coals but were not observed in these specimens.

Heating-Stage Microscopic Observations. Following the characterization of the mineral suites by x-ray diffraction techniques, each LTA concentrate was heated in a heating stage mounted on a microscope fitted for observation in vertically incident light. Concentrates examined in this way and the product phases are found in Table II.

Table II. LTA Samples and Heating Products

LTA Sample	T <sub>max</sub> (°C)	Phases Identified
Upper Freeport raw	560	quartz, illite, pyrrhotite
	1410	quartz, mullite <sup>a</sup>
Upper Freeport 1.40 float	1031	quartz <sup>b</sup>
	1250	quartz <sup>b</sup>
Upper Freeport 1.40 sink	635	quartz, illite, pyrrhotite
	1150	quartz, pyrrhotite, illite <sup>c</sup>
Illinois #6 raw	880 <sup>d</sup>	quartz, illite, pyrrhotite, oldhamite(?)
Illinois #6 1.40 float	625	quartz, illite, pyrrhotite, troilite(?)
	1370	quartz, pyrrhotite
Illinois #6 1.40 sink	920	quartz, illite, pyrrhotite, oldhamite
	1334	quartz, pyrrhotite, oldhamite

<sup>a</sup> XRD peaks occurred at the correct diffraction angles for mullite but were too weak to permit accurate intensity comparisons.

<sup>b</sup> The overall pattern was similar to the one for the illite-kaolinite pair heated to 1410°C, except that stronger peaks for quartz were found in the LTA XRD pattern.

<sup>c</sup> Peaks were detected at some of the diffraction angles for illite, but the intensities were not comparable with standard patterns; it is possible that these were relict peaks of illite as it began to alter.

<sup>d</sup> Another sample of Illinois #6 raw LTA was heated to 1421°C; it formed a hard, dark-colored glass at about 1400°C; this material could not be removed from the heating-stage crucible.

The heating stage is limited to inert atmosphere or vacuum operation. Therefore, reactions sensitive to atmospheric conditions, such as partial pressure of oxygen, cannot be studied. Furthermore, the extremely small particle size of the sample resulted in inability to observe changes occurring below the mount surface and to resolve the specific minerals entering into a reaction at any point in the run.

These difficulties were addressed by obtaining samples of the minerals identified in the LTA concentrate before heating, grinding them to approximately the same size consist as the concentrate, and mounting them in separate domains in the heating stage crucible. The geometry of these mounts is shown in Fig. 1.

### Experiments with Known Minerals

Experiments with Individual Minerals. Single mineral mounts in the heating-stage crucible yielded the expected products, that is, pyrite yielded pyrrhotite and troilite, calcite gave lime and carbon dioxide, and clays reacted under high temperature conditions to yield a silicate glass.

Experiments with Pairs and Triplets of Known Minerals. In these experiments, known minerals were ground and placed in the heating-stage crucible in separate domains as pairs or triplets of minerals. The pairs and triplets were heated and the behavior at their boundaries observed. Table III lists the minerals used in pair mounts and the reaction products obtained by heating.

Because the most reactive phases found in the experiments with pairs of minerals were clays, calcite, and pyrite, these were prepared in triplet mounts. In trials using either montmorillonite or illite with calcite and pyrite, a liquid formed at the mutual boundary of the latter pair at 600-650°C. Pyrite and calcite had, of course, previously reacted and this liquid therefore occurred between the product phases pyrrhotite and lime. Subsequent x-ray analysis showed the presence of pyrrhotite, lime, and oldhamite. In both instances, the temperature of this reaction was lower than that obtained in the pair mount of calcite and pyrite, 1140°C. When kaolinite was in the mount with calcite and pyrite, the same reaction occurred at 750-760°C. Though the mechanism by which the clays reduce the reaction temperature is not yet understood, the differences in reaction temperature with and without clay is considered significant.

The most obvious change in the clays themselves during these experiments was a darkening beginning with pyrite decomposition. This was more marked in the case of illite and montmorillonite. It is considered that in all these cases, the clay mineral structure was destroyed and possibly formed a silicate glass, much like those found in furnace slags but having, perhaps, less oxygen.

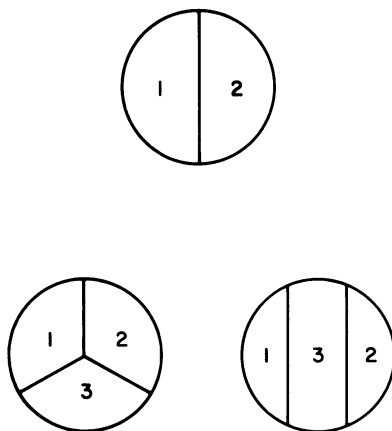


Figure 1. Geometric arrangement of mineral pairs and triplets used in the heating stage experiments and supporting experiments. In all triplet mounts, position 3 was occupied by a clay mineral.

Table III. Mineral Pairs and Heating Products

Mineral Pair	T <sub>max</sub> (°C)	Products Identified <sup>a</sup>
Calcite-illite	1310	lime (CaO)
Calcite-kaolinite	1322	lime (CaO)
Calcite-montmorillonite	1285	(indeterminate) <sup>b</sup>
Calcite-pyrite	1253	lime, pyrrhotite (Fe <sub>1-x</sub> S), oldhamite (CaS)
Calcite-quartz	1467	quartz (SiO <sub>2</sub> ), lime (CaO)
Illite-kaolinite	1410	mullite (Al <sub>2</sub> Si <sub>2</sub> O <sub>13</sub> )
Illite-montmorillonite	662	(indeterminate) <sup>b</sup>
Illite-montmorillonite	1212	(indeterminate) <sup>b</sup>
Illite-pyrite	1519	pyrrhotite, troilite (FeS)
Illite-quartz	1450	quartz
Kaolinite-montmorillonite	1403	mullite (poorly-crystalline) <sup>c</sup>
Kaolinite-pyrite	1445	mullite
Kaolinite-quartz	1220	quartz
Montmorillonite-pyrite	1053	(indeterminate) <sup>b</sup>
Montmorillonite-quartz	1492	quartz
Pyrite-quartz	1571	quartz

<sup>a</sup> Only those products are listed which could be positively identified by XRD; no attempt is made here to deduce the composition of amorphous products.

<sup>b</sup> XRD patterns for these heating products did not match any standard pattern closely; attempts to match with computer routines produced results of low reliability.

<sup>c</sup> "Poorly crystalline" means that diffraction maxima were found corresponding to the indicated phase, but peaks were not sharp and did not have the correct relative intensities in all cases.

**Supporting Experiments.** To examine the effect of oxidizing and reducing atmosphere on these materials, graphite crucibles 10mm in diameter and 2mm deep were packed in the manner described above and heated in a furnace fitted to permit introduction of specified gases during heating. After heating, the samples were examined by scanning electron microscopy and energy dispersive x-ray spectroscopy (SEM/EDS) (Figure 2). Samples treated in this way are listed in Table IV.

In all these cases where pyrite was used with a clay, iron was found to have migrated from the iron sulfide into region that was originally clay. Elemental mapping showed the presence of iron to have completely pervaded the region formerly occupied by clay. In all mounts containing calcite and pyrite, the calcium and sulfur peaks were present in the region originally occupied by calcite and sometimes found in the region that had been pyrite-filled.



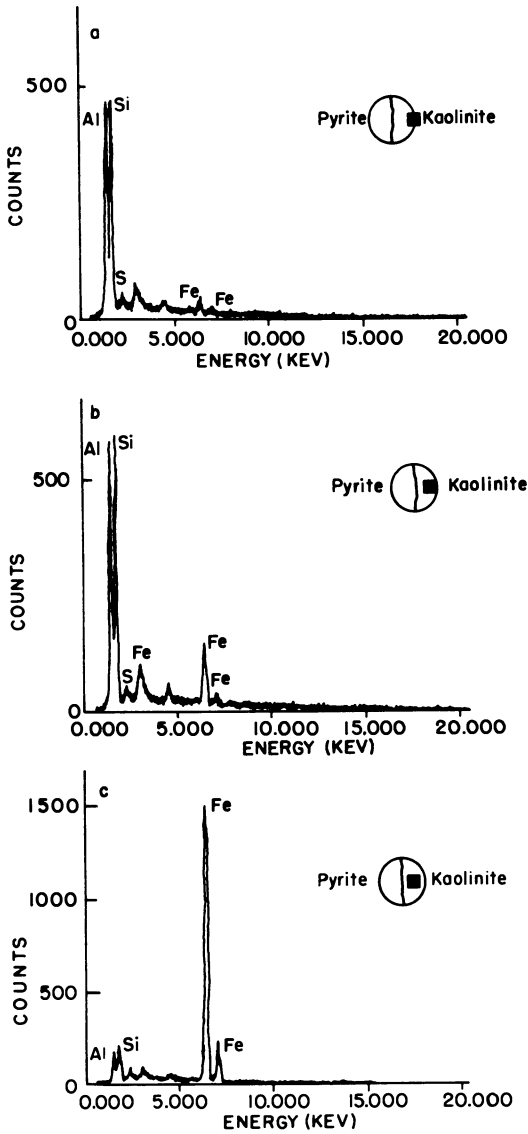


Figure 2. Energy-dispersive spectra from a pyrite-kaolinite mount heated to 1200°C. Locations of the spectra with respect to the sample are indicated by the small squares in the circles.

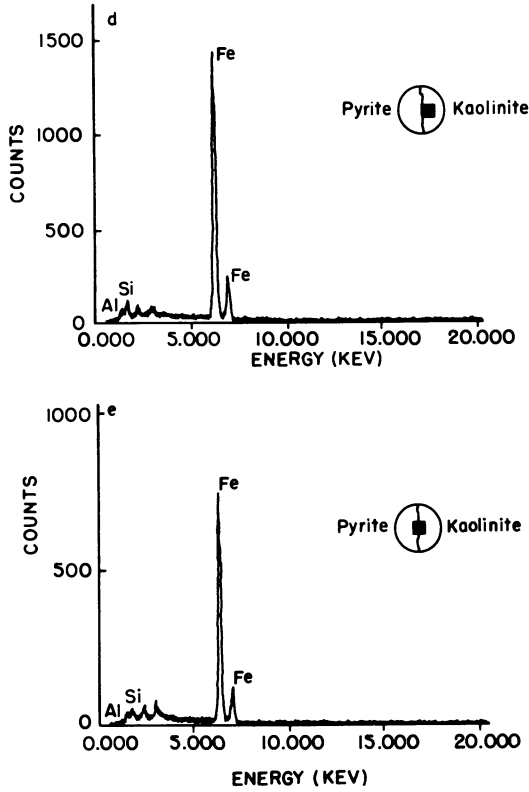


Figure 2. Continued.

Table IV. Subjects of Supporting Experiments

Assemblage	Atmosphere	T (°C)	Duration (min)
Calcite-kaolinite	inert	1400	60
Calcite-quartz	inert	1400	60
Pyrite-quartz	oxidizing	1200	30
Pyrite-quartz	reducing	1200	30
Pyrite-calcite	reducing	1200	30
Pyrite-kaolinite	oxidizing	1200	30
Pyrite-kaolinite	reducing	1200	30
Pyrite-montmorillonite	inert	800	15
Pyrite-montmorillonite	reducing	800	15
Py.-calc.-kao.	reducing	1200	30
Py.-calc.-mont.	inert	800	15
Py.-calc.-mont.	reducing	800	15

Note: The indicated temperature was the steady-state temperature for the trial. The indicated duration was the period of time for which that steady-state temperature was maintained.

### Discussion and Conclusions

It is apparent that the phenomena described here are not complete processes terminating in equilibrium assemblages. The times of reaction are too short for many of the products of silicates such as clays and quartz to come to thermodynamic equilibrium at the new temperature. That this is indeed the case in operation of power-plant boilers is obvious from the consideration of the amount of glass found in furnace slags and fly-ash.

Illite and montmorillonite are similar in structure and differ slightly from kaolinite in this regard. The first two are composed of two silicon-oxygen layers per octahedral layer containing iron, magnesium and aluminum and in kaolinite the ratio of tetrahedral and octahedral layers is 1. In clays thermal modification occurs at lower temperature than silica because the bonds formed between the Al, Fe, and Mg atoms and oxygen are weaker than the Si-O bonds. Clays, therefore, are expected to be more reactive than the silica crystals. There is evidence of drastic structural modifications, if not vitrification, in the clay mineral domains during thermal treatment and that iron enters the region. Further inquiries are in progress to answer these questions.

Calcite appears largely inert at temperatures approaching 600°C in the presence of some of the clay minerals and inert until about 900°C in their absence. The cause of this fluxing is not well understood at this time, but investigations are planned to explain this behavior. At whatever temperature, the reaction observed is the decomposition of calcite to lime (CaO) and carbon dioxide. The extent to which carbon dioxide influences further reaction is not known but must be considered as an important step in a complete explanation.

Like calcite, pyrite is quite reactive and its thermal behavior is influenced by the presence of clay minerals. The initial reaction temperature of pyrite alone or in the presence of calcite alone is to

produce pyrrhotite, ( $\text{Fe}_{1-x}\text{S}$ ) and troilite ( $\text{FeS}$ ). The loss of sulfur is obvious and continues over an appreciable temperature range.

The most important reaction products are those of the iron enrichment of the clay mineral residues, probably a precursor of the iron oxide and glass mixtures commonly observed in slags and fly-ashes, and the formation of the sulfide of calcium, oldhamite. Oldhamite is observed in all experiments where calcite and pyrite interact, whereas anhydrite is observed only where they have reacted in the presence of an oxygen-rich atmosphere. This behavior suggests that oldhamite, formed in the reducing part of a flame, is a necessary precursor to the formation of anhydrite.

#### Acknowledgments

This material is based, in part, on work supported by the U.S. Bureau of Mines, Department of the Interior, under Grant No. G1106002. Any opinions, findings, and conclusions or recommendations expressed in this publication are those of the authors and do not necessarily reflect the views of the U.S. Bureau of Mines, Department of the Interior.

Work on other parts of this publication was performed in Ames Laboratory and was supported by the Assistant Secretary of Fossil Energy, Division of Coal Utilization through the Pittsburgh Energy Technology Center, Coal Preparation Branch. Ames Laboratory is operated for the U.S. Department of Energy by Iowa State University under Contract W-7405-Eng-82.

#### Literature Cited

1. Mukkherjee, D. K.; Chowdhury, B. Fuel 1976, 55, 4-8.
2. Wakely, L. D.; Davis, A.; Jenkins, R. G.; Mitchell, G. D.; Walker, P. L., Jr. Fuel 1979, 58, 379-385.
3. Gray, D. Fuel 1978, 57, 213-216.
4. Moody, A. H.; Langan, D. D. Combustion 1935, 6, 13-20.
5. Gauger, A. W. Procedures of the American Society of Testing Materials 1937, Part I, 376-401.
6. Palmenburg, O. W. Industrial and Engineering Chemistry 1939, 31, 1058-1059.
7. Electric Power Research Institute (EPRI) Report CS-1418, Research Project 736; prepared by Battelle, Columbus Laboratories, 1980.
8. Huggins, F. E.; Kosmack, D. A.; Huffman, G. P. Fuel 1981, 60, 577-584.
9. Gluskoter, H. J. Fuel 1965, 44, 285-291.

RECEIVED June 13, 1985

## Flame Vitrification and Sintering Characteristics of Silicate Ash

Erich Raask

Technical Planning and Research Division, Central Electricity Generating Board,  
Leatherhead, Surrey, United Kingdom

Silicate species constitute the bulk of the mineral matter in most coals, and the formation of boiler deposits depends largely on the physical and pyrochemical changes of the ash residue constituents. In this work the mode of occurrence of coal silicate minerals, and the flame induced vitrification and sodium initiated sintering mechanisms have been studied. The pulverized coal flame temperature is sufficiently high to vitrify the quartz particles. On cooling some devitrification occurs and the rate of sintering depends largely on the ratio of glassy phase to crystalline species in the ash. The flame volatile sodium captured by the vitrified silicate particles can initiate the coalescence of deposited ash by viscous flow and the rate of sintering is markedly increased by the alkali-metal dissolved in the glassy phase.

The flame imprinted characteristics of pulverized coal ash relevant to boiler slagging, corrosion and erosion have been discussed previously (1,2). Silicate minerals constitute between 60 and 90 per cent of ash in most coals and boiler deposits are largely made up from the silicious impurity constituents. This work sets out first to examine the mode of occurrence of the silicate mineral species in coal followed by a characterization assessment of the flame vitrified and sodium enriched silicate ash particles. The ash sintering studies are limited to investigations of the role of sodium in initiating and sustaining the bond forming reactions to the formation of boiler deposits.

### Silica (Quartz) and Silicate Mineral Species in Coal

The quartz and aluminosilicate species found in most coals constitute the bulk of the combustion ash residue. The aluminosilicates include muscovite and illite which contain potassium, and kaolinite species (3-6). The silica ( $\text{SiO}_2$ ) and alumina ( $\text{Al}_2\text{O}_3$ ) as determined by chemical analysis are present in aluminosilicates on an average

weight ratio of 1.5 to 1 as reported by Dixon et al. (6). The excess of silica represents the amount of quartz in coal mineral matter:

$$(\text{SiO}_2)_q = (\text{SiO}_2)_t - 1.5(\text{Al}_2\text{O}_3) \tag{1}$$

Where  $(\text{SiO}_2)_q$ ,  $(\text{SiO}_2)_t$  and  $(\text{Al}_2\text{O}_3)$  denote respectively the quartz, total silica and alumina contents of ash.

An approximate amount of potassium alumino-silicates in coal mineral matter can be obtained from the potassium oxide ( $\text{K}_2\text{O}$ ) content of ash. The amount of non-silicate potassium species is small in most coals and the silicate minerals contain on average 11 per cent  $\text{K}_2\text{O}$  by weight (6). Thus the potassium alumino-silicate content of coal mineral matter ( $\text{K}_{\text{AL-SIL}}$ ) by weight per cent is:

$$\text{K}_{\text{AL-SIL}} = \frac{\text{K}_2\text{O}}{0.11} = 9.1 \text{ K}_2\text{O} \tag{2}$$

where  $\text{K}_2\text{O}$  denotes the potassium oxide content of ash.

The total amount of silicate minerals equals approximately the sum of  $\text{SiO}_2$ ,  $\text{Al}_2\text{O}_3$  and  $\text{K}_2\text{O}$  in ash, and an estimate of kaolinite species is thus given by:

$$\text{Kaolinite} = (\text{SiO}_2 + \text{Al}_2\text{O}_3 + \text{K}_2\text{O}) - (\text{Quartz} + \text{Pot. Silicates}) \tag{3}$$

Table I gives the  $\text{SiO}_2$ ,  $\text{Al}_2\text{O}_3$  and  $\text{K}_2\text{O}$  contents of some US and British bituminous coal ashes (4,7) which were used to calculate the approximate amounts of quartz, potassium alumino-silicate and kaolinite species in the mineral matter.

Table I. Estimated Amounts of Silicate Species in Bituminous Coal Mineral Matter

Type of coal		Ash constituents (weight per cent of ash)			Mineral species (weight per cent)		
		$\text{SiO}_2$	$\text{Al}_2\text{O}_3$	$\text{K}_2\text{O}$	Quartz	Pot. alum. silicates	Kaolinite
Low silica	British	31.1	18.1	1.2	3.9	10.9	26.2
	U.S.	29.2	14.2	1.5	7.9	13.6	23.6
Medium silica	British	46.5	22.8	2.8	12.3	25.5	34.3
	U.S.	46.6	27.8	1.1	4.9	10.0	60.6
High silica	British	55.5	30.0	2.7	10.5	24.5	53.2
	U.S.	56.5	32.2	2.6	8.0	23.6	59.7

Table I shows that the kaolinite species constitute up to 60 per cent of the coal mineral matter. The amount of potassium alumino-silicates, chiefly muscovite and illite is between 10 and 25 per cent, and the quartz content is usually below 12 per cent. The alumino-silicate minerals contain frequently iron, calcium, magnesium and sodium as part replacement for potassium and partly

incorporated in the kaolinite structure. Also, the silicate minerals occur as hydrated species with the inherent water content of between 2 to 5 per cent, thus the silicious mineral contents are likely to be about 5 per cent higher than those given in Table I. The silica and alumina contents of the first two samples are exceptionally low for bituminous coal ashes. The usual concentration range of silica is 35 to 55 per cent and that of alumina is 20 to 30 per cent, thus the aluminosilicate species together with quartz constitute between 60 to 90 per cent of bituminous coal mineral matter.

The silicate species occur in coal chiefly as separate strata and large particle inclusions, and this mode of occurrence is termed the "adventitious" mineral matter. Figure 1a shows a typical sample of the adventitious silicate mineral particles, density separated from pulverized coal. The density separation technique does not remove the small silicate particles, chiefly aluminosilicate species, the "inherent" mineral matter, in the coal substance (Figure 1b). The ash content of bituminous coals delivered to utility power station is usually between 10 and 25 per cent (4,8). About 25 per cent of the ash is present in the form of inherent mineral matter of dispersed small particles and also as mineral elements reacted with the coal substance.

The mineral elements can be held in the coal substance as organo-metallic salts, and also as a result of molecular adsorption and co-valent bonding. The mineral species dissolved in coal pore water, chiefly chlorides can also be considered as part of the inherent matter. The lignites and sub-bituminous coals can have a high fraction of the mineral elements, chiefly sodium, calcium and also aluminium and iron chemically combined in the fuel substance (9,10). The chemical reactivity and porosity of the fuel matrix decrease with the increase of coal age from lignite to bituminous rank. The loss of carboxyl, hydroxyl and quinone bonding sites in the fuel matrix results in a low "chemical" mineral matter content of bituminous coals.

#### Chloride in Coal Pore and Seam Water

Chloride minerals are rarely found in coal in the form of solid species because of high solubility of sodium, calcium and trace metal chlorides in coal strata waters. The "inherent" water content of coal is related to its porosity and thus the moisture content of lignite deposits can exceed 40 per cent decreasing to below 5 per cent in fully bituminous coals (11). Chlorides, chiefly associated with sodium and calcium constitute the bulk of water-soluble matter in British bituminous coals (12). Skipsey (13) has found that the distribution of chlorine coals was closely related to the salinity of mine waters. Hypersaline brines with concentrations of dissolved solids up to 200 kg m<sup>-3</sup> occur in several of the British Coalfields.

The mode of formation of hypersaline brines has been discussed by the osmotic filtration through clay and shale deposits. The salinity of the brine ground waters increases with depth and when they are in contact with fuel bearing strata, correspondingly more chloride is taken up by the fuel. However, according to Skipsey (13) the high rank bituminous coals because of their low porosity are unable to take up large amounts of the chloride and associated cations, and the chlorine content rarely exceeds 0.2 per cent. The

chlorine content of low rank bituminous coals can reach one per cent and correspondingly the sodium fraction associated with chlorine will amount up to 0.4 per cent of coal. That is, the ash from a high chlorine coal can contain up to 3 per cent of flame volatile sodium. The chlorine content of lignites and sub-bituminous coals is usually low, below 0.1 per cent, and sodium is held chiefly in the fuel substance in the form of organo-metal components (9,10).

All coals contain some sodium combined in the aluminosilicate species which will remain largely involatile in the flame. The ratio of the silicate sodium to non-silicate sodium varies over a wide range. The alkali-metal is present chiefly in the silicates in low chlorine bituminous coals. In the high chlorine bituminous coals and in many lignites and sub-bituminous coals it is present mainly in a flame volatile form.

Flame Vitrification of Silica Minerals

A characteristic feature of flame heated ash is that the particles are spherical in shape as shown in Figure 2. The transformation of the angular silicate mineral particles in pulverized coal to spherical particle ash is a result of the surface tension force acting on the vitrified species. The stress (f) on a non-spherical surface section of the particle is:

$$f = 2\gamma/\rho \tag{4}$$

where  $\gamma$  is the surface tension of glassy silicate and  $\rho$  is the radius of curvature. It is evident from Equation (4) that the stress is inversely proportional to the radius of curvature and thus the small sharp-edged particles are first to take a spherical form.

Frenkel (15) has shown that time (t) required to transform an angular particle to sphere is given to first approximation by:

$$r = r_0^{-t/z} \tag{5}$$

where

$$z = 4\pi\eta r_0/\gamma \tag{6}$$

and r is the distance of a point on the original surface from the center of a sphere of equivalent volume having radius  $r_0$ ,  $\eta$  is the viscosity and  $\gamma$  is the surface tension.

Equation (5) can be used to calculate the approximate time required for a particle to assume a spherical shape when the surface tension, viscosity, size and initial shape of particle are known. Alternatively, an estimate of the viscosity for the change to take place, can be made when the residence time of particles at a given temperature is known. Table I gives the calculated values of viscosity when the time for the change is one second. It was assumed that the thickness of moving surface layer was about ten per cent of the radius, and the surface tension of fused ash was taken to be  $0.32 \text{ N m}^{-1}$  as measured previously (16).



Table II. Calculated Viscosities for Spheridization of Different Size Silicate Particles

Particle radius ( $\mu\text{m}$ )	0.01	0.1	1	10	100
Viscosity ( $\text{N s m}^{-2}$ )	$2.5 \times 10^7$	$2.5 \times 10^6$	$2.5 \times 10^5$	$2.5 \times 10^4$	$2.3 \times 10^3$

Table II shows that the small irregularly shaped particles transform to spheres in coal flame when the viscosity of the material is several orders higher than that required for bulk flow under gravity, which is about  $25 \text{ N s m}^{-2}$ . A laboratory technique was used to determine the minimum temperature at which coal mineral species are transformed to spherical shapes (17). Particles of 10 to  $200 \mu\text{m}$  in diameter were introduced into a gas stream and then passed through a vertical furnace. The temperature of the furnace was varied from 1175 to 2025 K and was measured by a radiation pyrometer and by thermocouples placed in the furnace. The residence time of particles in the furnace was between 0.2 and 0.5 sec. depending on the particle size.

Figure 3a shows a surface-fused silicate particle heated to a temperature some 25 K lower than that required for its spheridization. Figure 3b shows a spheridized particle heated in the laboratory furnace. Figure 4 shows the temperature range at which the shape change of different coal mineral particles occurred. The chlorite mineral contains some quartz and the two species spheridized at markedly different temperatures as shown by curves  $D_1$  and  $D_2$ . The temperature of mineral particles in the pulverized coal flame exceeds 1800 K (Figure 5), and it is therefore to be expected that all particles with the exception of large size quartz will vitrify and change to spherical shapes. Figure 6a shows a surface-fused but non-spherical quartz particle found in a sample of fly ash captured in the electrostatic precipitator. Occasionally elongated ellipsoidal particles of aluminosilicates (Figure 6b) can be found in the ash indicating that the high temperature residence time was too short for complete spheridization. However, the majority of the ash particles appear to be spherical as shown in Figure 2.

The spherical silicate ash particles, when viewed at close-up range appear to host a large number of sub-micron particles at the surface (Figure 6c). The microvoids could be silicate crystalloids precipitated from the vitrified phase or sulphate fume particles formed from the non-silicate coal minerals (18). The latter are soluble in a dilute acid (HCl) solution and Figure 6d shows the acid etched particles. Clearly, most of the microvoid particles were dissolved and the leach solution contained sodium and potassium sulphates.

Another diagnostic test for silicate ash is to treat the particles with hydrofluoric (HF) acid solution (18-20). The acid will dissolve the glassy phase revealing skeletons of crystalline species which may be in the form of mullite needles (Figure 6e) or quartz crystalloids (Figure 6f). The ratio of the glassy phase to crystalline species varies from particle to particle depending on

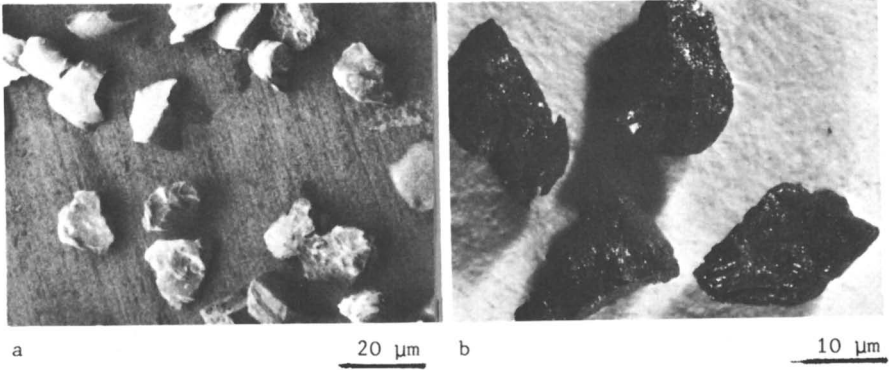


Figure 1. Mineral matter in coal. (a) Adventitious; (b) inherent white particles.

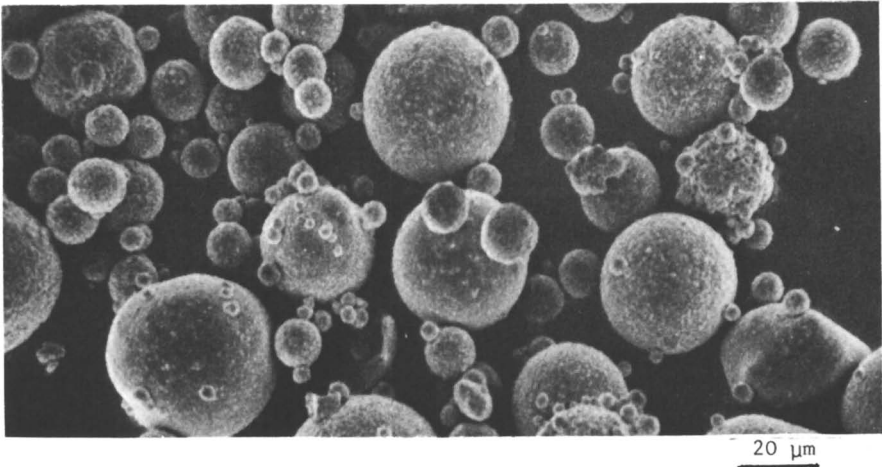


Figure 2. Pulverized fuel ash.

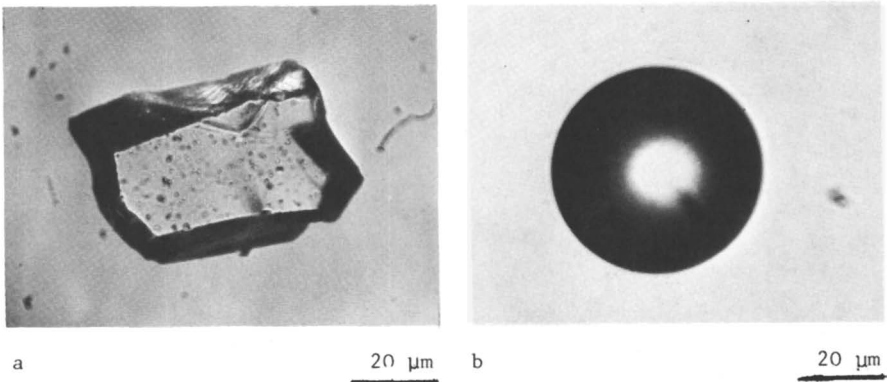


Figure 3. Surface fused (a) and spheroidized (b) silicate particles.

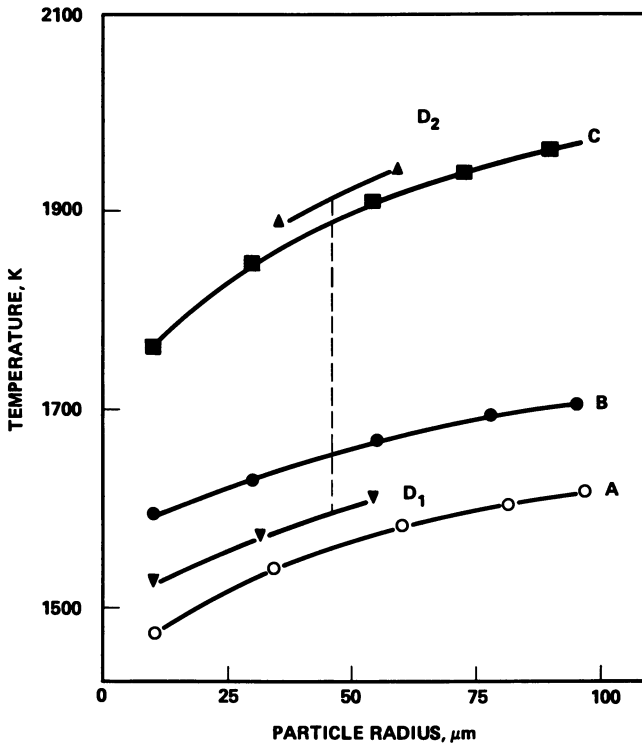


Figure 4. Spherical shape transformation of granular minerals in hot gas streams: A, illite; B, muscovite; C, native quartz; D, chlorite. Reproduced with permission from reference 2. Copyright 1985 Itemisphere Publishing Corp.

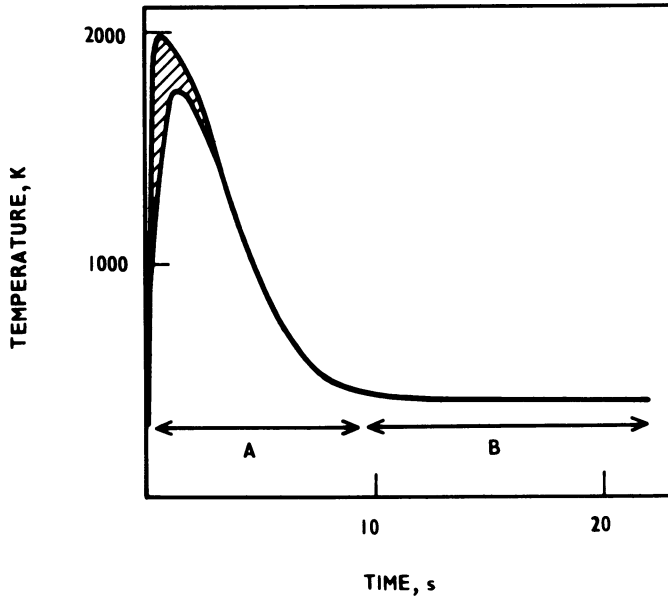


Figure 5. Temperature/time plot for ash particles in a 500 MW pulverized coal fired boiler: 0.1  $\mu\text{m}$  (top curve) to 100  $\mu\text{m}$  (lower curve) sizes. A, combustion and heat exchange chambers; B, electrostatic precipitators and chimney. Reproduced with permission from reference 2. Copyright 1985 Hemisphere Publishing Corp.

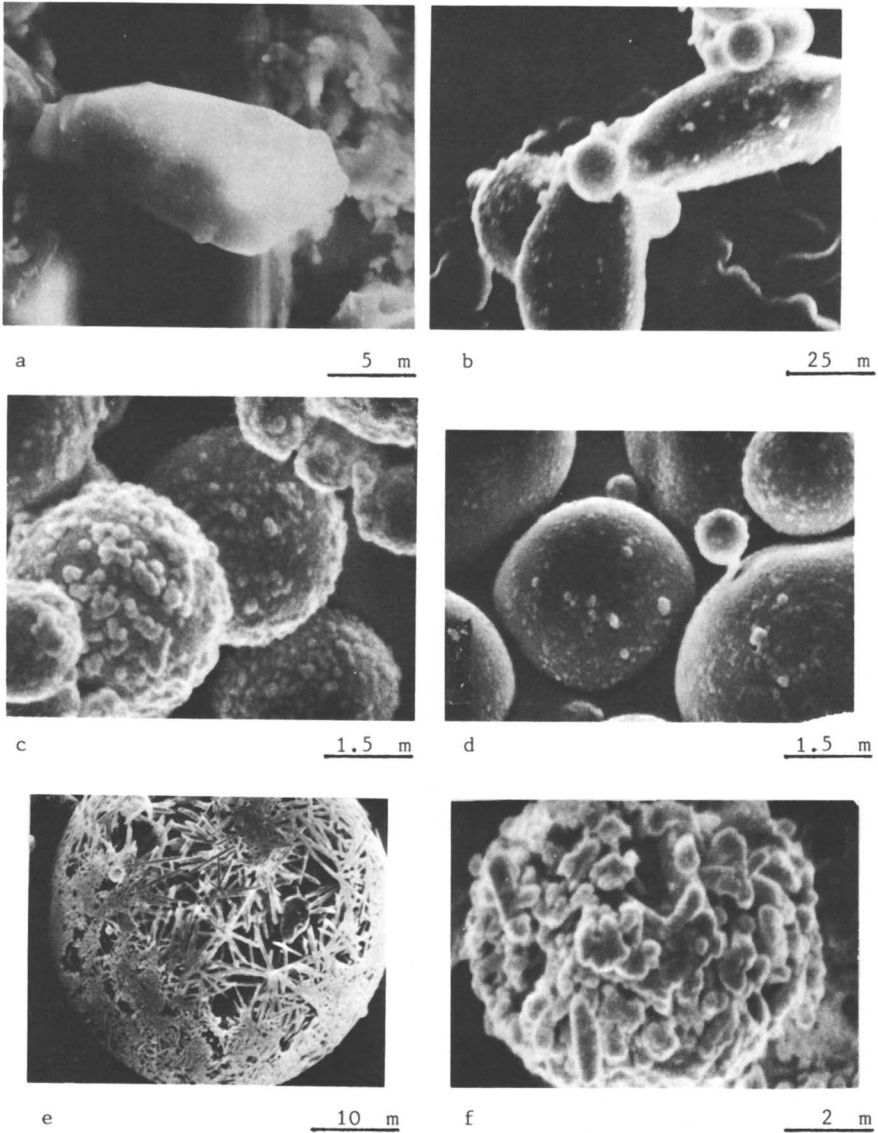


Figure 6. Diagnostic features of flame heated ash. a, unfused quartz particle; b, elongated silicate particles; c, microvoids on ash; d, acid cleaned ash; e, mullite needles in ash; and f, quartz crystalloids.

the original composition of the silicate minerals, the capture of volatile sodium and the rate of cooling of flue gas borne ash. The flame imprinted characteristics of silicate mineral species from the point of view of subsequent sintering are summarized in Table III.

Table III. Vitrification and Recrystallization of Silicates

Constituent species	Particle vitrification		Recrystallization tendency	Glass content
	Temperature range (K)	Extent		
Quartz	1700 to 1900	Medium	Low	Medium
Kaolinite	1600 to 1700	High	High	Medium
Potassium aluminosilicates	1400 to 1600	High	Low	High

The relative amount of coal mineral quartz surviving in the pulverized fuel flame depends on the particle size and temperature. In the intense combustion of cyclone fired boilers the flame temperature exceeds 2000 K and the quartz particles of all sizes will vitrify. Some quartz particles in the crystalline form will survive the flame treatment in pulverized coal fired boilers and the ash may contain 25 per cent of the original coal quartz in the crystalline form (21).

The kaolinite mineral species in coal contain some sodium, calcium and iron in the crystalline structure (6) and the presence of fluxing metals enhances vitrification of the flame heated particles. The high temperature crystalline form of kaolinite species is mullite and the characteristic needle shapes of mullite (Figure 6e) are frequently found in large, above 5  $\mu\text{m}$  diameter particles. The mullite needle crystals in ash are always embedded in a glassy phase of the large particles and it appears that the small, below 5  $\mu\text{m}$  diameter particles of the flame heated kaolinite species are not extensively recrystallized on cooling. The crystalline species of illite and muscovite are not found in the flame heated ash and thus it is likely that the potassium aluminosilicates remain on cooling largely in the form of glassy particles.

The inherent silicate ash (Figure 1b) will coalesce on combustion first to a sintered matrix inside the burning coal particle and also to small slag globules at the surface of coke residue. Figure 7a shows the slag globules on a coke particle separated from pulverized coal ash and Figure 7b shows a lace skeleton of sintered ash in another coke particle revealed after combustion at 900 K.

During combustion of the mineral rich coal particles in the pulverized fuel flame, ash envelopes may be created which can take the form of cenospheres as shown in Figure 7c and d. The gas bubble evolution leading to cenosphere formation (16,22) and fly ash usually contains between 0.1 and 2 per cent by weight of the lightweight ash. The mineral rich coal particles may leave the combustion ash residue also in the form of plerosphere (spheres-

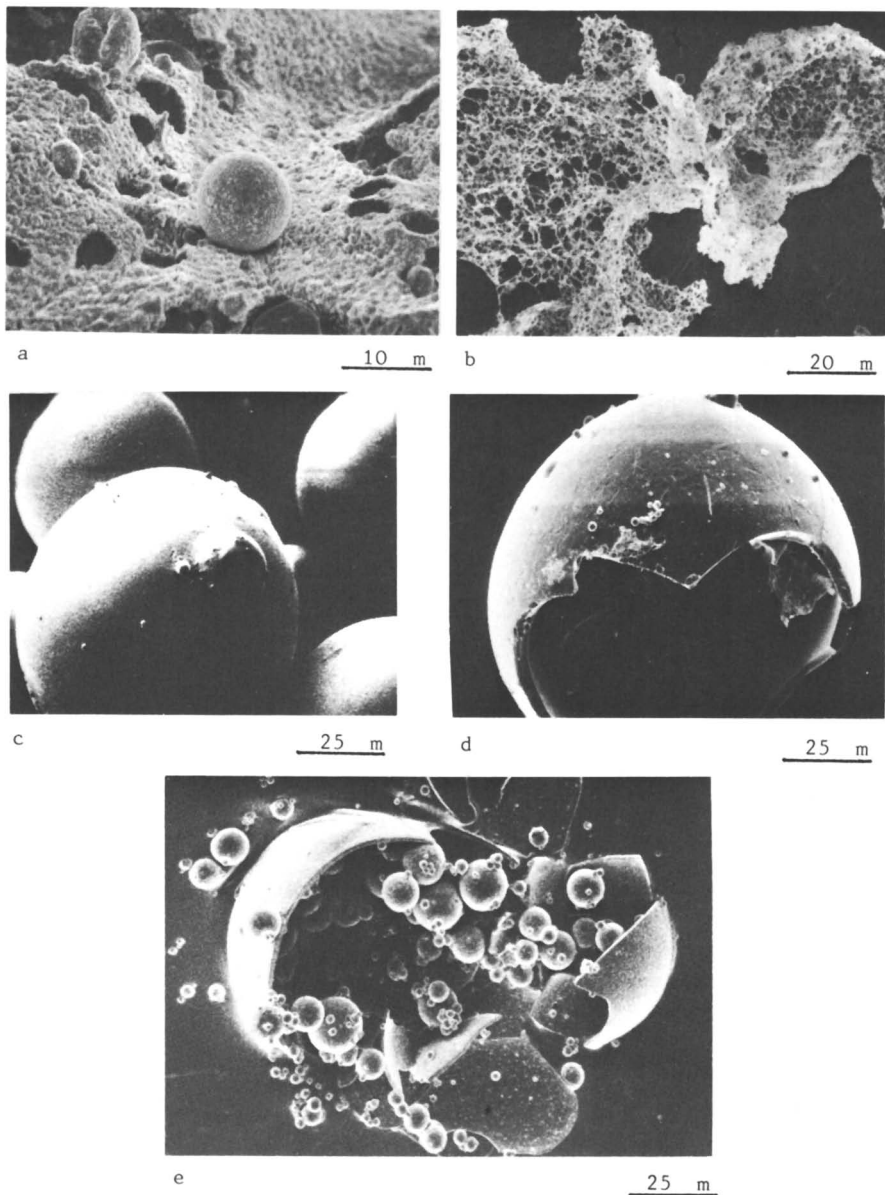


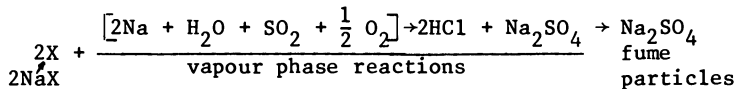
Figure 7. Coalescence products of inherent ash in flame. a, ash particles on coke; b, ash skeleton in coke; c, cenospheres; d, fractures cenosphere; and e, plerosphere.

inside-sphere) as shown in Figure 7e. The above examples show that the inherent silica ash particles undergo extensive coalescence by sintering and slagging during combustion of the host coal particles. However, the adventitious ash retain the particle identity in the flame and the processes of sintering and slagging take place after deposition on boiler tubes.

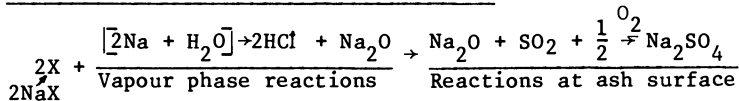
#### Transfer of Flame Volatile Sodium to Silicates

The coal sodium originally present as chloride and organo-metallic compounds is rapidly volatilized in the pulverized coal flame (23). Subsequently the volatile species are partly dissolved in the surface layer of flame heated silicate particles and partly sulphated in the flue gas (8). The formation of sodium sulphate can proceed via two routes:

##### Route 1 - In the Flue Gas



##### Route 2 - At the Surface Ash Particles



Route 1 for genesis of sodium sulphate fume can be described as the non-captive formation and route 2 as the captive formation.

Some potassium sulphate can also be formed via the two routes. Potassium is present in coal chiefly in the form of potassium aluminosilicates (Table I) and a large part of the alkali-metal will remain involatile in the flame heated silicate particles. Some 5 to 20 per cent of the potassium is released for sulphation (24) which takes place partly at the surface of the parent particles (25) and partly via the volatilization routes as described above. However, sodium sulphate content of fly ash heated in pulverized coal flame, and chimney solids is always higher than that of potassium sulphate.

The distribution of the flame volatile sodium between the ash silicate and sulphate phases is markedly influenced by the temperature and residence time of the ash particles in the flame. The high temperature of large boiler flame reduces the viscosity of vitrified silicate particles and as a result a large fraction of the volatile sodium is dissolved in the silicate phase. On average 60 per cent of the sodium is dissolved in the silicate ash particles, the remainder being present as sulphate fume particles in the flue gas (8).

#### The Mechanism and Measurements of Sodium Enhanced Sintering

The formation of sintered ash deposits on boiler tubes requires first a close, molecular distance contact between the particles followed by a growth of particle-to-particle bridges chiefly by viscous flow. Sodium sulphate phase together with some potassium sulphate may play



a significant role in the initial stage of sintering by bringing the silicate particles together as a result of surface tension. Sodium sulphate melts at 1157 K but mixed alkali-metal sulphates can form a molten phase at lower temperatures (26).

Once the close contact between the silicate particles has been established a viscous flow of the particle surface layer can commence and the sinter bonds are established according to Equation 7, as discussed by Frenkel (15):

$$\frac{x^2}{r^2} = \frac{3\gamma t}{2\eta r} \tag{7}$$

where x is the radius of neck growth between the spherical particles of radius r,  $\gamma$  is the surface tension,  $\eta$  is the viscosity of fused ash, and t is the time. The  $(x/r)^2$  ratio can be taken as a criterion of the degree of sintering, i.e. the strength of boiler deposit (s) developed in time t, that is:

$$s = k \left( \frac{x}{r} \right)^2 \tag{8}$$

and the rate of deposit strength development is:

$$\frac{ds}{dt} = \frac{3k\gamma}{2\eta r} \tag{9}$$

where k is a constant.

Equation (9) shows that the rate of ash sintering, i.e. the development of cohesive strength of a deposit matrix is proportional to the surface tension and inversely proportional to the viscosity. The surface tension and particle size are not markedly changed by dissolution of sodium, iron or calcium oxides in the glassy phase of silicate ash. However, the viscosity is markedly changed by the oxides. In particular, an enrichment of sodium in the surface layer of the silicate ash particles can lead to a high rate of sintering.

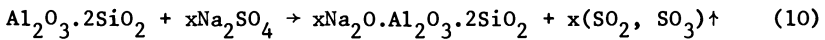
Some of the flame volatile sodium is dissolved in the vitrified silicate ash particles before deposition and an additional amount of sodium is transferred from the sulphate to silicate phases during sintering. The reaction between sodium sulphate and silicates at ash sintering temperatures has been monitored by thermo-gravimetric measurements. Some of the results are given in Table IV.

Table IV. Weight Loss of Sulphate and Sulphate/Silicate Mixtures

Sample	$\text{Na}_2\text{SO}_4$	$\frac{\text{Na}_2\text{SO}_4}{\text{Kaolin}}$	$\frac{\text{Na}_2\text{SO}_4}{\text{Ash}}$	$\text{CaSO}_4$	$\frac{\text{CaSO}_4}{\text{Kaolin}}$	$\frac{\text{CaSO}_4}{\text{Ash}}$
Loss initiation temperature (K)	1425	1085	1175	>1525	1275	1275

Anhydrous sulphate samples and the sulphate/silicate mixtures (50 per cent by weight sulphate) were heated in air at the rate of 6 K per minute.

The results in Table IV show the reaction between sodium sulphate and kaolin commenced at 1085 K as indicated by the weight loss due to release of SO<sub>2</sub> and SO<sub>3</sub>:



A typical bituminous coal ash required a higher temperature of 1175 K for the sulphate decomposition reaction, indicating that the ash silicate species were less reactive than kaolin mineral of small (<5 μm diameter) particle size. Transfer of sodium from the sulphate of silicate phase will reduce the viscosity of the glassy material resulting in an enhanced rate of sintering. At higher temperatures, above 1275 K, calcium sulphate starts to dissociate in the presence of kaolin and thus calcium oxide will be available for the sintering reactions. The specific roles of coal calcium and also the iron mineral species in ash sintering and slag formation have been discussed previously (2).

The sintering rates of bituminous, sub-bituminous and lignite coal ashes of different sodium contents can be determined by the electrical conductance measurements. In this method the conductance across an ash compact is measured and it is an indication of the degree of sintering (27). The sodium ions in the low viscosity glass and molten sulphate are the conductive species and the conductance continuity is provided by the sinter bridges between the particles. Figure 8 (curve B) shows that sub-bituminous coal ash of high (6.3 per cent) sodium oxide content commenced sintering at 1100K as determined by the conductance measurements. The results (27) suggest that the amount of sodium in some ashes are sufficiently high both to initiate and sustain a rapid rate of sintering below 1200 K. In contrast, with low sodium coals the rate of ash sintering and the formation of boiler deposits are related to the calcium and iron contents of coal mineral matter. Several empirical formulae have been proposed for predicting the deposit forming propensity of the lignitic and bituminous coal type ashes based on the sodium content (28). These formulae indicate that a rapid build-up of boiler deposit is to be expected when sodium (Na<sub>2</sub>O) content of bituminous coal exceeds 2.5 per cent, and that of lignite and sub-bituminous coal ashes is above 4 per cent.

The lignite type ashes have comparatively low fouling propensity when the sodium content is below 4 per cent because of the limited amount of clay minerals available for sintering reaction. That is, in some lignite and sub-bituminous coals there is an excess of sodium and calcium available for the high temperature reactions, and the rate of deposit formation depends on the silicate content of ash (2,29). The bituminous coal type ash has an excess of silicates, i.e. the ash is pyrochemically acidic and the rate of sintering depends on the availability of sodium, calcium and iron species in the flame heated deposit material.

The formation of sintered ash deposits is governed chiefly by viscous flow, and the rate of sintering (S<sub>r</sub>) can be expressed in terms of the ratio of glassy material to crystalline species of silicate ash (R<sub>g/c</sub>) and the viscosity of the glassy phase (η), as discussed previously (2):

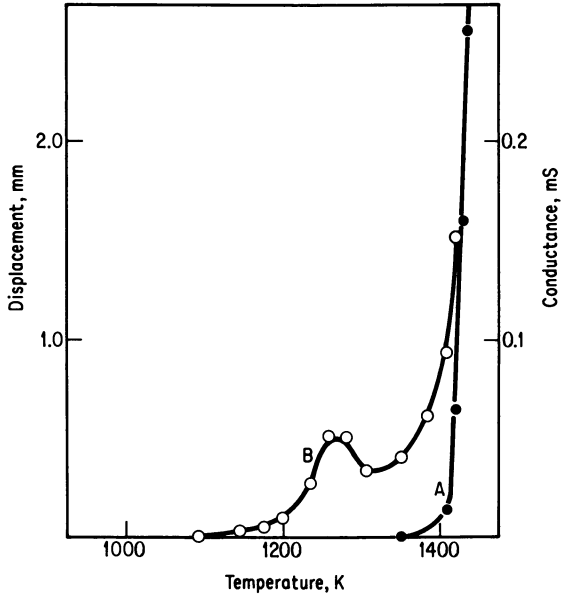


Figure 8. Simultaneous shrinkage and conductance measurements with Leigh Creek (Australian) coal ash. A, shrinkage; and B, conductance. Reproduced with permission from reference 2. Copyright 1985 Hemisphere Publishing Corp.

$$S_r = k_1 (R_{g/c}) \frac{1}{\eta} \quad (11)$$

where  $k_1$  is a constant. The characteristics of flame heated silicate particles, (Figure 4 and Table 3) suggest that the vitrified potassium aluminosilicate particles and the below 5  $\mu\text{m}$  diameter kaolin particles are first to sinter after deposition. The flame vitrified particles have a high glass content and their small size enhances sintering, as evident from Equation (7). It is therefore to be expected that the inherent, small-particle mineral matter (Figure 1b) will enhance sintering.

### Conclusions

Silicate Minerals in Coal. The silicate minerals, kaolinite and potassium aluminosilicate species together with quartz constitute the bulk of mineral matter in most coals. The approximate amounts of different silicate species of the bituminous coal mineral matter can be estimated from ash analysis.

Flame Volatile and Silicate Sodium in Coal. Sodium is rapidly volatilized in the flame when it occurs in a non-silicate compound form, chiefly associated with chlorine in bituminous coals and combined with organic compounds in the lignite and sub-bituminous fuels. The fraction of sodium combined with coal silicates remains largely involatile in the pulverized fuel flame.

Flame Vitrification and Spheridization of Silicate Particles. The aluminosilicate particles vitrify and take a spherical shape in the flame and are partially recrystallized on cooling. Micro-needles of mullite up to 10  $\mu\text{m}$  long and crystalloids of quartz are the principal devitrification products enveloped in a glassy material matrix. Large quartz particles originally present in coal are only surface vitrified and do not spheridize in the flame. The coalescence by sintering and fusion of the small aluminosilicate particles dispersed in the fuel substance occurs when the host coal particles burn in the flame. The products are sintered ash skeletons, cenospheres and plerospheres up to 250  $\mu\text{m}$  in diameter.

Sodium Transfer to Silicate and Sulphate Phases. The flame volatile sodium is partly dissolved in the surface layer of vitrified silicate ash particles and partly sulphated. The sulphate particles, 0.1 to 2  $\mu\text{m}$  in diameter can form on the surface of ash particles or in the flue gas via vapour phase reactions followed by sublimation on cooling. Some potassium sulphate is also formed from a fraction of the alkali-metal released on vitrification of potassium aluminosilicates in the flame.

Initial Stage in Ash Sintering. The sulphate phase can initiate ash sintering by bringing the silicate particles to close contact as a result of the surface tension force. Subsequent sintering proceeds by viscous flow and the rate of sinter bond growth is proportional to the surface tension of silicate glassy phase and inversely proportional to the particle size and the viscosity. The latter

changes exponentially with temperature and thus the viscosity of silicate ash particles governs the rate of sintering at different temperatures.

Decomposition of Sulphate on Silicate Ash Sintering. Sodium sulphates in the initial material deposited on boiler tubes will be decomposed by the pyrochemically acidic silicates in ash when the deposit temperature exceeds 1085 K. The transfer of sodium from the sulphate to silicate phase reduces the viscosity of the glassy material of silicate ash thus increasing the rate of sintering.

Sintering of High Sodium Coal Ashes. Some lignite and sub-bituminous coal ash contains sufficiently high quantities of the flame volatile sodium to initiate and subsequently to sustain a high rate of ash sintering leading to a rapid build-up of boiler deposit. With most bituminous coal ashes the volatile sodium plays a role in initiating sintering but the subsequent deposit and slag formation depends largely on the presence of calcium and iron flux oxides. In general terms, the rate of ash sintering is governed by the ratio of glassy material to crystalline species and the viscosity of the glassy phase.

#### Acknowledgement

The work was carried out at the Central Electricity Research Laboratories and the paper is published by permission of the Central Electricity Generating Board.

#### Literature Cited

1. Raask, E. *J. Eng. Power.* 1982, 104, 858.
2. Raask, E. "Mineral Impurities in Coal Combustion - The Behaviour, Problems and Remedial Measures"; Hemisphere: New York, 1985.
3. Gumz, W.; Kirsch, H.; Mackowsky, M-T. "Slagging Studies: Investigations of Minerals in Fuel and Their Role in Boiler Operation"; Springer-Verlag: Berlin, 1958.
4. O'Gorman, J.W.; Walker, P.L. "Mineral Matter and Trace Elements in U.S. Coals": Dept. Inter. Office of Coal Res. and Dev. Rep. No. 61, Washington, 1972.
5. Rao, C.P.; Gluskoter, J.H. "Occurrence and Distribution of Minerals in Illinois Coals"; III. State Geol. Survey, Circ. No. 476, Urbana, 1973.
6. Dixon, K.; Skipsey, E.; Watts, J.T. *J. Inst. Fuel.* 1970, 43, 124.
7. BCURA. "The Chemical Composition and the Viscometric Properties of the Slags Formed from Ashes of British Coals"; British Coal Utilization Research Association: Report; Leatherhead, U.K., 1963.
8. Raask, E. *Prog. Energy Combust. Sci.* 1982, 8, 261.
9. Sondreal, E.A.; Kube, W.R.; Elder, J.L. "Analysis of the Northern Great Prvince Lignites and Their Ash: A Study of Variability"; U.S. Bureau of Mines: Rep. No. 7158, Washington, 1968.

10. Kiss, L.T. Proc. Coal Science Conf., Dusseldorf, Germany; 1981, p. 773.
11. Francis, W. "Coal, its Formation and Deposition"; Arnold: London, U.K., 1961.
12. Daybell, G.N. J. Inst. Fuel. 1967, 40, 3.
13. Skipsey, E. Fuel. 1975, 54, 121.
14. Dunham, K.C. Trans. Inst. Min. Metal. 1970, 79, B127.
15. Frenkel, J.S. J. Phys. (Moscow). 1945, 9, 385.
16. Raask, E. ASME J. Eng. Power, 1966, Jan., p. 40.
17. Raask, E. Fuel. 1969, 48, 366.
18. Raask, E.; Goetz, L. J. Inst. Energy. 1981, 54, 163.
19. Raask, E.; Bhaskar, M.C. Concrete Res. 1975, 5, 363.
20. Raask, E. Power Ind. Res. 1981, 1, 233.
21. Raask, E. J. Inst. Energy. 1980, 53, 70.
22. Raask, E. J. Inst. Fuel. 1968, 43, 339.
23. Halstead, W.D.; Raask, E. J. Inst. Fuel. 1969, 42, 344.
24. Raask, E. VGB Mitteilungen. 1968, 48, 348.
25. Stinespring, C.D.; Stewart, G.W. Atm. Envir. 1981, 15, 307.
26. Adams, A.M.; Raask, E. "Mechanism of Corrosion by Fuel Impurities"; Marchwood U.K.; Butterworths: London, 1963, p. 196
27. Raask, E. J. Therm. Anal. 1979, 16, 91.
28. Winegartner, E.C. "Coal Fouling and Slagging Parameters"; ASME Commit. on Corrosion and Deposits from Combustion Gases Rep.; New York, 1974.
29. Sondreal, E.A.; Gronhovd, G.H.; Tufte, P.H.; Beckering, W. "Ash Deposition and Corrosion due to Impurities in Combustion Gases"; Hemisphere: Washington, 1978, p. 85.

RECEIVED October 15, 1985

## Viscosity of Synthetic Coal Ash Slags

Karl S. Vorres<sup>1</sup>, Sherman Greenberg<sup>2</sup>, and Roger Poeppel<sup>2</sup>

<sup>1</sup>Chemistry Division, Argonne National Laboratory, Argonne, IL 60439

<sup>2</sup>Materials Science and Technology Division, Argonne National Laboratory, Argonne, IL 60439

Twenty one compositions including SiO<sub>2</sub>, Al<sub>2</sub>O<sub>3</sub>, CaO, MgO and FeO were selected to represent a range of U.S. coal ashes. The viscosities of molten slags were measured over the temperature range 1300-1550°C. The data were plotted as log reciprocal viscosities (fluidities) versus reciprocal absolute temperatures. One or two straight line segments were observed for each composition. At higher temperatures the activation energies are less than 100 Kcal/mole, while the values exceed 100 Kcal/mole in the lower temperature regime. The transition temperatures for the plots with two segments were about 1300-1400°C. The transition is thought to involve the appearance of a significant amount of solid material in the melt. Examination of related ternary equilibrium phase diagrams indicated that the transitions occurred in the temperature regime associated with the disappearance of the liquid phase.

Coal used for energy conversion contains a considerable amount of mineral matter. During the conversion process the mineral matter is heated, and in the higher temperature reactors is converted to a molten material which flows from the reactor at a rate dependent on the viscosity of the slag. In studies of coal slags obtained from electric utility boilers (1,2,3) this behavior has been studied and correlations have been determined between the viscosity of the slag and the chemical composition. These studies have been carried out in a range of gaseous environments typical of the combustion furnace with a range of oxygen concentrations from almost zero to 15%.

The purposes of this study included a determination of the viscosity behavior of synthetic slags over a range of compositions and temperatures characteristic of slagging gasifier operation. The compositions were chosen to be broadly representative of a range of coals from both the eastern and western U.S. The temperatures were chosen to be in the range of satisfactory gasifier operation, and within the limits of the experimental equipment.

The gaseous environments were selected to have the low oxygen partial pressure (about  $10^{-8}$  to  $10^{-9}$  atm) typical of the slagging gasifier.

The viscosity data were to be used as input for a program to investigate corrosion of refractories by slags. Accordingly, the data obtained for the first few slags were compared with correlations developed by Watt and Fereday (1,2) based on chemical composition and by Hoy, Roberts and Williams (3), using a modified version of the silica ratio. In order to simplify the systems for study, the synthetic slags were limited to the five components:  $\text{SiO}_2$ ,  $\text{Al}_2\text{O}_3$ ,  $\text{FeO}$ ,  $\text{CaO}$  and  $\text{MgO}$ . Since they contained no  $\text{Na}_2\text{O}$  or  $\text{K}_2\text{O}$ , the slag compositions were outside the range of the earlier correlations. If this difference was neglected, then the composition four of the 21 synthetic slags used in this program fell inside the range of the compositions for which the correlations were developed. Those outside the range had 10%  $\text{Al}_2\text{O}_3$  or 0%  $\text{MgO}$  or a low silica ratio or a high  $\text{SiO}_2/\text{Al}_2\text{O}_3$  ratio. The earlier correlations, in general, were for only a part of the composition range used for the synthetic slags.

There is an added interest in developing the understanding of the behavior of molten coal ash systems beyond somewhat empirical correlations of chemical compositions expressed in terms of a variety of ratios. It would be desirable to describe the flow behavior in terms of the interactions between the individual constituents, and to understand the nature of the acids and bases, such that the reason for the partial success of empirical correlations using these concepts can be understood.

### Experimental

Slag. The viscosities of 21 synthetic slags, covering the range of compositions expected in slags derived from American coals, were determined in this study. The synthetic slags were prepared from reagent grade chemicals. Calcium carbonate, magnesium oxide and magnetite, ( $\text{Fe}_3\text{O}_4$ ), silica and alumina were used. The components were mixed with water and pressed into pellets using a pressure of 15,000 psig. The pellets were partially dried and inserted in  $\text{Al}_2\text{O}_3$  crucibles about 63 mm high and 32 mm internal diameter for the viscosity measurements. Approximately 65 grams of slag were used and the melt reached a depth of about 35 mm with the measuring "bob" inserted. Although alumina is not a suitable material for long-term containment of these slags at elevated temperatures, the amount of dissolution was insignificant for the 24 hour exposure time without slag motion with respect to the crucible. The composition of the slags is given in Table I.

Viscometer. The apparatus and technique have been described in detail (4). Essentially a Brookfield Rheolog was used to replace the sample head in the rotating cylinder slag corrosion apparatus used in slag/refractory corrosion studies at Argonne National Laboratory (ANL) (5). Appropriate seals and ceramic structural components permit maintenance of the desired low oxygen activity within the measuring chamber. The viscosity measuring bob was a



cylinder 12.8 mm diameter and 11.1 mm high. For measurement at the lower oxygen partial pressures discussed in this paper, the bob and connecting shaft were fabricated of molybdenum. The slag was contained in  $Al_2O_3$  crucibles. The bob and measuring system were calibrated at room temperature using a series of NBS oils ranging from 10 to 600 poise. The voltage-viscosity relationship was linear over the range of rotational speeds used in the calibration runs (0.5-100 rpm). For slag viscosity measurements only one rotational speed, 20 rpm, was used.

Table I. Slag Compositions (weight %).

Composition	Slag Number							
	1	2	3	4	5	6	7	
$SiO_2$	50	50	50	50	50	50	50	
CaO	5	5	5	5	5	5	5	
$Al_2O_3$	10	10	20	20	20	30	30	
FeO	15	25	25	15	5	15	5	
MgO	20	10	0	10	20	0	10	
	8	9	10	11	12	13	14	
$SiO_2$	40	40	40	40	40	40	40	
CaO	15	15	15	15	15	15	15	
$Al_2O_3$	10	10	20	20	20	30	30	
FeO	15	25	25	15	5	15	5	
MgO	20	10	0	10	20	0	10	
	15	16	17	18	19	20	21	
$SiO_2$	30	30	30	30	30	30	30	
CaO	25	25	25	25	25	25	25	
$Al_2O_3$	10	10	20	20	20	30	30	
FeO	15	25	25	15	5	15	5	
MgO	20	10	0	10	20	0	10	

**Procedure.** Viscosity measurements were usually made in a decreasing temperature mode at 50°C intervals after the slag sample had been heated to the desired maximum temperature, typically about 1400-1550°C. The maximum temperature corresponded to the maximum operating temperature expected in commercial coal gasifiers and was also the temperature at which very low (a few centipoise) viscosities were observed. The maximum temperatures were reached in a controlled manner to avoid apparatus problems. The slag was heated from room temperature to 100°C in one hour and held for 1/2 hour. From 100°C to the maximum temperature, the heating rate was 175°C/hour. For viscosity measurements, the slag was kept at each temperature long enough to demonstrate constant viscosity (about

30-60 minutes). In the case of one slag, 12, measurements were also made in an increasing temperature mode to determine if there were hysteresis effects. None were observed for this slag and other work with natural slags confirmed this (4). Measurements made in other laboratories with other slags have shown apparent hysteresis (6). The desired oxygen partial pressure was maintained by flowing H<sub>2</sub>-CO<sub>2</sub>-N<sub>2</sub> (or argon) mixtures of the required composition through the interior of the measuring chamber throughout the experiment. The variation of oxygen partial pressure with gas composition and temperature was calculated using a NASA-developed code (4). At the oxygen partial pressures used, the iron was maintained in the ferrous state.

### Results and Discussion

The data obtained were plotted as viscosity versus temperature for the different materials and displayed the expected exponential increase in viscosity as the temperature decreased. For most of the slags a characteristic sudden increase in viscosity was noted, as in some related studies (1,3). Some typical results are shown and compared with the Watt-Fereday and modified silica ratio projections, assuming only a liquid phase exists, in Figures 1 and 2 (slags 1 & 12).

To further investigate the characteristics of the slags, plots of the logarithm of viscosity versus temperature were made. These indicated straight lines or two line segments. For slags with a sudden increase in viscosity at lower temperatures, two segments were observed. Shear rates were not varied and the various types of non-Newtonian behavior were not explored. A related study indicated pseudoplastic behavior for this type of material (9).

Arrhenius plots were then made. These plots typically involve the logarithm of a rate constant and the reciprocal of the absolute temperature. Viscosity is not a rate parameter, but is defined as the shear stress divided by the shear rate. The reciprocal of the viscosity is the shear rate per unit shear stress and was used in the plots. A typical example is shown in Figure 3. Slag 1 shows a typical high-temperature, low activation energy regime with a transition to a high activation energy, low temperature regime. This behavior was noted for most of the compositions. The other behavior was, as in the case of slag 12, a single straight line covering the range of the data. The slopes and activation energies for slags without the transition tended to be intermediate in the range of the values for runs with the transition.

In order to compare the viscosity behavior of the different compositions for the higher temperature regime and the slags with no transitions, separate plots superimposing the sample series with a constant wt% SiO<sub>2</sub> were made and are shown in Figures 4, 5 and 6. Note the vertical change in scale in Figure 6. The solid portion of the lines represents the actual range of data. The dashed part of the lines was added to facilitate visual comparison. Examination of the plots shows two general tendencies. The reciprocal viscosities or fluidities tend to increase in a series as the amounts of SiO<sub>2</sub> decreases. Additionally, for a given series with a

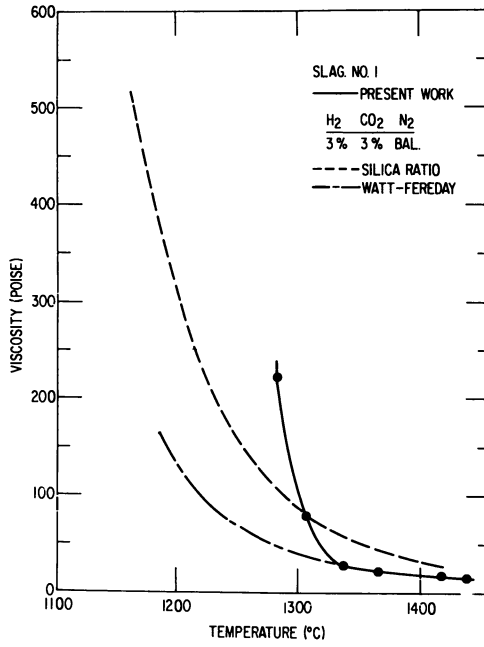


Figure 1. Viscosity of Slag 1.

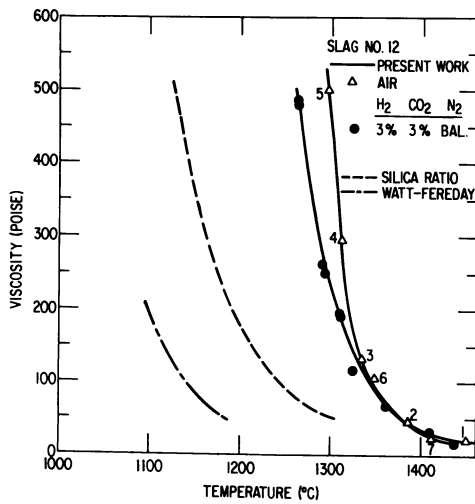


Figure 2. Viscosity of Slag 12.

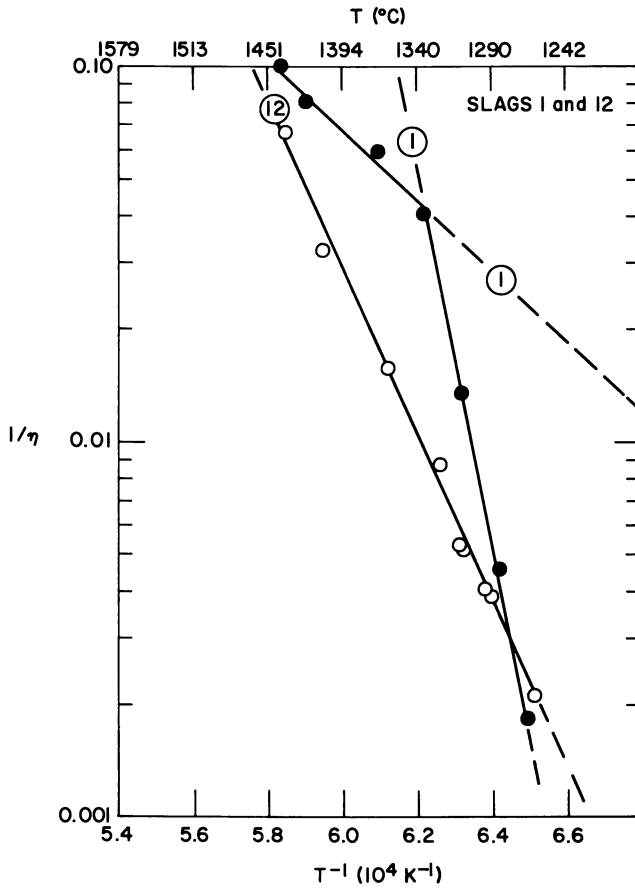


Figure 3. Typical Arrhenius Plots.

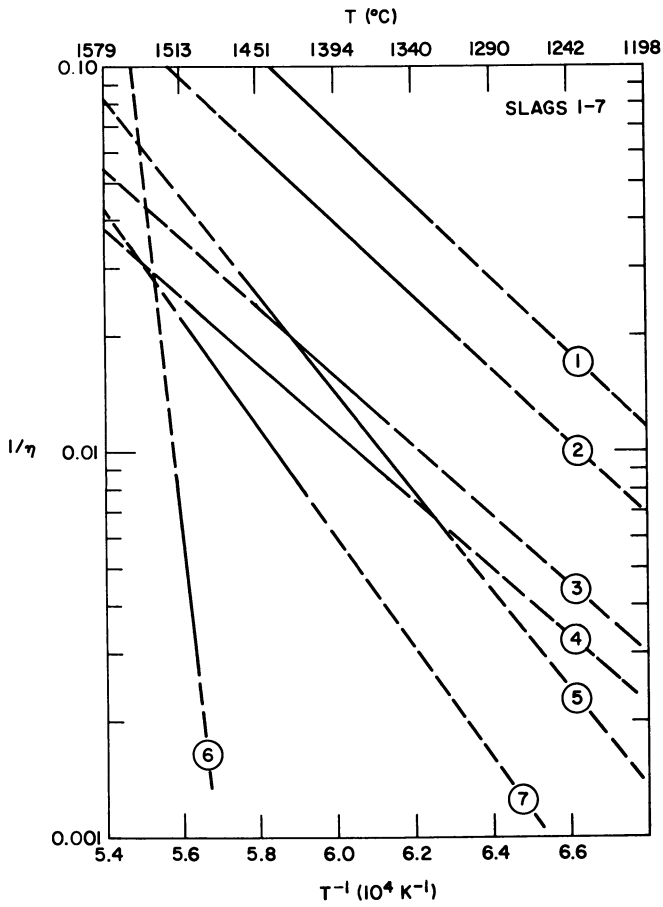


Figure 4. Arrhenius Plots for Slags 1-7.

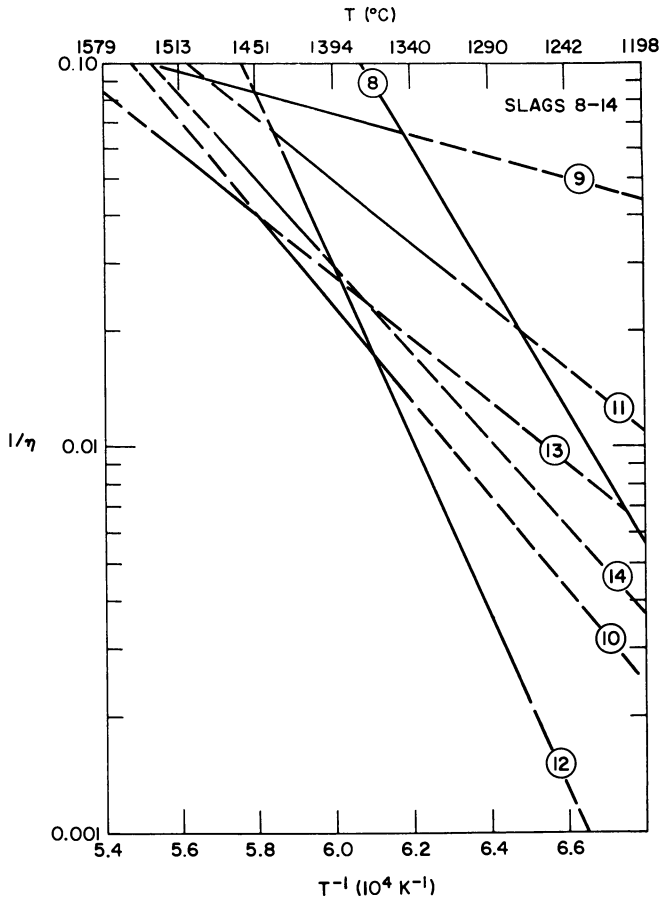


Figure 5. Arrhenius Plots for Slags 8-14, Log of Reciprocal Viscosity vs. Reciprocal Temperature.

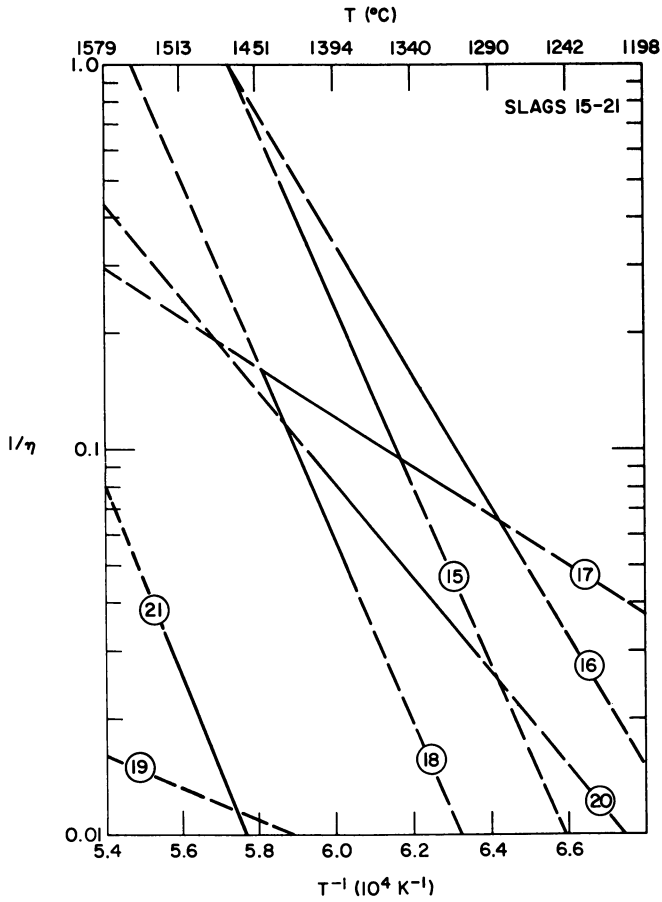


Figure 6. Arrhenius Plots for Slags 15-21, Log of Reciprocal Viscosity vs. Reciprocal Temperature.

fixed wt% SiO<sub>2</sub>, the fluidities are greater for the lower amounts of Al<sub>2</sub>O<sub>3</sub>.

Earlier work (7,10,11) described the chemical behavior of the slag constituents in terms of acids and bases. Vorres (7) used the concept of ionic potential (ratio of ionic charge to crystallographic radius) to differentiate slag constituents on the basis of their ability to attract a common anion (oxide ions in these systems). The strongest acids attract anions most strongly or are most able to effectively compete for anions to complete a regular close packed coordination. The bases are not able to compete for anions, and serve primarily as oxide ion donors.

This type of system involves the formation of large polymers by the acids, and polymer breaking by the bases. In the presence of a large amount of a very strong acid, SiO<sub>2</sub>, some acidic constituents such as Al<sub>2</sub>O<sub>3</sub> and Fe<sub>2</sub>O<sub>3</sub>, behave with an amphoteric character. Iron is quite interesting since it is such a common constituent in coal ash, especially in eastern U.S. coals, and does have two common valence states. Ferric iron behaves as a weak acid while ferrous is classified as a weak base. Thus in the more oxidizing environment of a boiler, coal slags have a more acidic or highly polymerized character than in the less oxidizing environment of the slagging gasifier or cyclone combustor. For the measurements discussed in this chapter, all iron species are believed to exist in the ferrous state.

In a general way, the larger the amount of SiO<sub>2</sub> and total acid constituents, the larger the size of hypothetical average silica polymer species in the melt. Gaskell has described a relationship between silica species and the basic composition (8).

The correlations developed by Watt and Fereday were intended for application to a liquid system. As the temperature varies and increases, the composition of a dynamic system is subject to changes due to preferential volatilization of species with higher vapor pressures. The alkalis typically have the higher vapor pressures in these systems. The acidity can be expected to slightly increase as a result of this volatilization.

As the temperatures are reduced, solid phases will crystallize from the melt. The Watt and Fereday correlations do not apply to this region. The studies reported here include the temperature region in which crystals can be expected to form. The authors did not find literature references to phase equilibria studies for the SiO<sub>2</sub>-Al<sub>2</sub>O<sub>3</sub>-CaO-MgO-FeO or SiO<sub>2</sub>-Al<sub>2</sub>O<sub>3</sub>-CaO-MgO systems in the composition region of interest. As a result some speculation on behavior is involved in any extensive interpretation of the data.

Activation energies and the temperature ranges of data are given in Table II. Initial statistical analyses have not shown a strong correlation of activation energies with any of the slag constituents.

A wide range of activation energies with very high values was obtained for the lower temperature regime. In a number of cases both the temperature range and the number of points were small, such that the relative error in these values can be large. When the data cover the range from 1300-1400°C the transition from the lower to the higher activation energies generally occurred in this range. One reason for the observed results is that the



Table II. Activation Energies, Range of Temperatures and Mole Fractions.

Slag #	High Temperature		Low Temperature		Mole Fractions					Sum Base	B/A
	Ea	Range	Ea	Range	SiO <sub>2</sub>	Al <sub>2</sub> O <sub>3</sub>	CaO	FeO	MgO		
1	38.8	1440-1340	374	1340-1268	.483	.057	.052	.121	.288	.461	0.85
2	44.6	1460-1315	148	1315-1244	.515	.061	.055	.215	.154	.424	0.74
3	51.0	1456-1344			.568	.134	.061	.237	.000	.298	0.42
4	37.9	1513-1335	960	1335-1299	.529	.125	.057	.133	.158	.348	0.53
5	59.3	1462-1312	106	1312-1273	.495	.117	.053	.041	.295	.389	0.64
6	106	1550-1520	363	1520-1500	.584	.209	.063	.147	.000	.210	0.26
7	70.1	1515-1415			.543	.192	.058	.045	.162	.265	0.36
8	83.4	1353-1192			.384	.056	.154	.120	.286	.560	1.27
9	14.0	1455-1295	85.6	1295-1170	.409	.060	.164	.214	.152	.530	1.11
10	52.0	1454-1330	288	1330-1314	.451	.133	.181	.235	.000	.416	0.71
11	39.0	1439-1300	261	1300-1265	.420	.124	.169	.132	.156	.457	0.84
12	101	1436-1262			.393	.116	.158	.041	.293	.492	0.97
13	35.5	1535-1460	90.0	1460-1420	.464	.205	.186	.145	.000	.331	0.49
14	50.8	1484-1400	469	1400-1380	.431	.190	.173	.045	.161	.378	0.61
15	107	1434-1339			.286	.056	.255	.119	.284	.658	1.92
16	86.0	1390-1231			.272	.060	.272	.212	.151	.635	1.74
17	40.3	1414-1315	240	1315-1246	.335	.132	.299	.234	.000	.533	1.14
18	66.8	1448-1202			.313	.123	.279	.131	.155	.565	1.30
19	20.1	1459-1351	297	1351-1328	.293	.115	.261	.041	.291	.593	1.46
20	56.5	1402-1294			.345	.203	.308	.144	.000	.452	0.82
21	111	1532-1415			.321	.189	.286	.045	.159	.490	0.96

Sum Base = sum of mole fractions of CaO, MgO, FeO.  
 B/A = sum base/mole fractions of SiO<sub>2</sub> + Al<sub>2</sub>O<sub>3</sub>.

concentration of crystallites increased sufficiently to interact with one another, hindering rotation of the bob.

In order to interpret the data the ternary equilibrium phase diagrams for the systems  $\text{SiO}_2\text{-Al}_2\text{O}_3\text{-MO}$  were examined where MO is either CaO, FeO, or MgO. The mole fractions of each of the constituents were calculated as also shown in Table II, and the ternary diagram corresponding to the major base in the group CaO, FeO or MgO was selected. Usually a ternary eutectic was found in the temperature region which would be expected for a system most closely corresponding to the sample composition. This eutectic temperature was close to the observed transition temperatures in the viscosity data.

Many of the highest temperatures used were significantly below those associated with the appearance of one or more solid phases from the melt. These solid phases could have been present through the entire series of measurements on the slag. The silica rich systems are known to be slow to initiate formation of solid phases. Kalmanovitch has shown that the observed phases are not always those which are expected on the basis of the corresponding normalized phase equilibrium diagrams (12). It is thought that the transition is due to a change from a system which has a significant amount of liquid phase to one in which the system is predominantly solid phases, and the measured apparent viscosity reflects the large energy requirement for two solid surfaces or particles to move past one another through some shearing action.

The transitions have also been observed in studies of natural coal ashes which have had increasing amounts of calcium oxide added. The data were interpreted in terms of a saturation and the authors felt that the base then served as an further polymerizer in the network (13).

There is a continuing interest in establishing a relationship between the composition of a molten oxide system containing silica and the viscosity of the system over a range of temperatures. Systems of this type are of interest, for example, in the study of magmas (9), fluxes for casting steel (14) and in metallurgy. Correlations have been developed by Bottinga and Weil for magma systems (15). Urbain has described correlations for silicate materials (16).

The interpretation of the viscosity-temperature behavior of these complex systems is difficult since many aspects of the melt conditions must be simultaneously considered. These include: the chemical composition of the melt to establish the nature of the polymeric network including the amphoteric behavior of species like  $\text{Al}_2\text{O}_3$  and  $\text{Fe}_2\text{O}_3$ , as well as the acid/base behavior of mixed valence constituents such as iron oxides, and the formation of immiscible liquid phases sometimes associated with the existence of several types of stable anions of significantly different size or charge in the system; the nature of the container since some of it may dissolve and affect the composition of the melt; the existence of a solid phase to establish the effect on the composition of the residual liquid phase (the solid phase may not be the one expected from related phase equilibrium studies); the relative amount of the liquid and solid phases to establish the composition of the liquid phase (this composition changes as the solid crystallizes out of

the melt); the thermal history of the sample since the reactions in viscous media tend to be sluggish, such that crystalline phases may be slow to form and changes in the polymeric equilibrium size may not have been achieved. In addition the loss of volatile species and the resultant change in the composition of the residual liquid must be considered. In practice, many investigators consider a number of these factors. Future work will be improved to the extent that more of them are included in the reports of research in this field.

### Conclusions

A series of 21 synthetic coal ash slags were studied. It was observed that:

- (1) Plots of the logarithm of viscosity versus temperature showed one or two straight line segments, consistent with other observations on similar systems in the temperature range studied.
- (2) Plots of the logarithm of the reciprocal of viscosity versus reciprocal of absolute temperature also showed one or two straight line segments, indicating one or two mechanisms were operative over the temperature range.
- (3) For three series, varying in SiO<sub>2</sub> content, those with the greatest SiO<sub>2</sub> content had the highest viscosities.
- (4) Within a series of given SiO<sub>2</sub> content, those members with the highest Al<sub>2</sub>O<sub>3</sub> content had the highest viscosity.
- (5) For slags exhibiting a transition in behavior, the transition temperature could usually be associated with a ternary eutectic temperature in the phase equilibrium diagram for the most closely related ternary system.
- (6) Many of the slags probably had a solid phase precipitating from the liquid phase during the cooling period before the transition temperature.

### Acknowledgments

The authors gratefully acknowledge the support from the Chemical Sciences Division of the Office of Basic Energy Sciences and from the Surface Gasification Materials Program of the U.S. Department of Energy, under contract number W-31-109-ENG-38.

### Literature Cited

1. Watt, J. D.; Fereday, F. J. Inst. Fuel 1969, 42, 101.
2. Watt, J. D. J. Inst. Fuel 1969, 42, 131.

3. Hoy, H. R.; Roberts, A. G.; Williams, D. M. IGE Journal 1965, 5, 444.
4. Chen, J.; Greenberg, S.; Poeppel, R. "The Viscosity of Coal Slags as a Function of Composition, Temperature and Oxygen Partial Pressure", U. S. Department of Energy ANL/FE-83-30 (March, 1984).
5. Greenberg, S.; R. Poeppel, R.; et al., "The Corrosion of Ceramic Refractories Exposed to Synthetic Coal Slags By Means of the Rotating-Cylinder Technique: An Interim Report", U. S. Department of Energy ANL/FE-83-31, (September, 1984).
6. Streeter, R. C.; Diehl, E. K.; Schobert, H. H. Preprints Am. Chem. Soc. Div. Fuel Chem. 1983, 28(4), 174.
7. Vorres, K. S. Preprints Am. Chem. Soc. Div. Fuel Chem. 1977, 22(4), 118.
8. Gaskell, D. R. Metallurgical Treatises, Metallurgical Society of AIME, 1982, 59.
9. Weed, H. C.; Ryerson, F. J.; Piwinski, A. J. Preprints Am. Chem. Soc. Div. Fuel Chem. 1984, 29(4), 157 and subsequent chapter in this volume.
10. Sage, W. L.; McIlroy, J. B. Trans. ASME, J. Eng. Power, Ser. A, 1960, 82, 145.
11. Reid, W. T. in "Chemistry of Coal Utilization", Second Supplementary Vol., Elliott, M. A., Ed.; Wiley-Interscience, New York, 1981; p. 1389.
12. Kalmanovitch, D. P.; and J. Williamson, J. Preprints, Am. Chem. Soc. Div. Fuel Chem. Div. 1984, 29(4), 162 and subsequent chapter in this volume.
13. Wang, C-s; Wang, C-y "The Relationship between Viscosity and Mole Composition of Coal Ash with Addition of Calcia", (Chinese) J. Coal Science, 1984, 1, 39-45.
14. McCauley, W. L.; Apelian, D. Preprints Am. Chem. Soc. Div. Fuel Chem. 1984, 29(4), 151 and this volume.
15. Bottinga, Y.; Weil, D. F. Am. J. Science 1972, 272, 438-75.
16. Urbain, G.; Cambier, F.; Deletter, M.; Anseau, M. R. Trans. Brit. Ceram. Soc. 1981, 80, 139-41.

RECEIVED October 24, 1985

## Sulfur Solubility in Slags for Cyclone Coal Combustors

David H. DeYoung

Smelting Process Development Division, Alcoa Laboratories, New Kensington, PA 15068

The absorption of sulfur by coal slags has been investigated to evaluate in-situ desulfurization of gases in coal combustors. Slag compositions which consisted of coal ash and inorganic additives, and which had low fusion temperatures and high capacities for sulfur, were identified. The sulfide capacities  $[(\% S)_{\text{slag}} (P_{\text{O}_2}/P_{\text{S}_2})^{1/2}]$  of these slags were measured at 1000 to 1300°C, and at oxygen potentials ranging from  $10^{-13}$  to  $10^{-11}$  atm, respectively. Results for slags based on the FeO-Al<sub>2</sub>O<sub>3</sub>-SiO<sub>2</sub>, CaO-Al<sub>2</sub>O<sub>3</sub>-SiO<sub>2</sub>, and Na<sub>2</sub>O-Al<sub>2</sub>O<sub>3</sub>-SiO<sub>2</sub> systems showed that at a given basicity the sulfide capacities were ranked in the order FeO > CaO > Na<sub>2</sub>O. These results were used to quantitatively evaluate desulfurization in a staged, slagging, cyclone combustor.

This study was conducted to select potential slag compositions for use in a slagging, staged, cyclone coal combustor, and to obtain the necessary data to evaluate the desulfurizing ability of the combustor. The first stage of such a combustor would be operated quite reducing to facilitate sulfur removal by a slag formed from the coal ash and inorganic additives (e.g., lime). A tangential motion imparted to the gas would throw ash, coal, and additives to the combustor wall where they would combine to form a molten slag. This slag, containing some dissolved sulfur, would continually drain out of a taphole at the exit end of the horizontally-placed cylindrical combustor. Advantages of this type of combustor are removal of some sulfur, low particulate emissions, and low NO<sub>x</sub> emissions.

This paper will be divided into three parts. First, the selection of slag compositions will be outlined. Second, sulfide capacity measurements of these slags will be discussed. Third, the desulfurizing potential of a slagging, cyclone combustor will be evaluated using these measurements.

### Slag Composition Selection

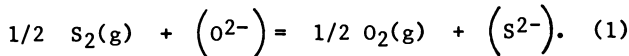
The strategy was first to select possible additives, then locate phase diagrams for systems of major ash components plus additives, and finally, select low-melting eutectic compositions as candidate slags. Additives were chosen for their known ability to form low-melting silicates (e.g., the alkalis) or for their known ability for desulfurization (e.g., the alkaline earth elements). An eastern coal was used for tests of a pilot combustor. Its ash composition, used to calculate additive compositions, is given in Table I. Major components,  $\text{SiO}_2$ ,  $\text{Al}_2\text{O}_3$ , and  $\text{Fe}_2\text{O}_3$ , account for approximately 80% of the ash.

Ternary phase diagrams for the  $\text{SiO}_2$ - $\text{Al}_2\text{O}_3$ -additive and  $\text{SiO}_2$ - $\text{FeO}$ -additive systems were investigated for possible slag compositions. Unless otherwise noted, all phase diagrams were taken from Levin, et al (1-3) or Roth, et al (4). The selected compositions which were tested are given in Table II, as are estimated liquidus temperatures. Obviously, the liquidus temperature of the slag consisting of coal ash and the additive will be different from those given by the phase diagrams because of the minor components of the ash. However, the phase diagrams provide reasonable initial selections. Additive compositions and quantities are given in Table III.

### Sulfide Capacity Measurements

Sulfide capacities of the selected slag compositions were measured to rate the slags and to provide data for evaluation of the operation of a combustor with these slags.

Chemistry of Sulfur in Slags. There has been considerable research on the chemistry of sulfur in slags reported in the literature. Most was aimed toward understanding and improving the desulfurization of iron and steel. These studies (5-7) have shown that at high oxygen potentials sulfur dissolves in slags as a sulfate, and at low oxygen potentials, the condition relevant to the two-stage combustor, sulfur dissolves as a sulfide. This can be represented by the reaction,



A quantity called the sulfide capacity (6) can be defined as:

$$C_S \equiv (\text{wt } \% \text{ S}) \left[ \frac{P_{\text{O}_2}}{P_{\text{S}_2}} \right]^{1/2} \quad (2)$$

where wt % S refers to sulfur dissolved in the slag, and  $P_{\text{O}_2}$  and  $P_{\text{S}_2}$  are the partial pressures of oxygen and sulfur in the atmosphere with which the slag is equilibrated. The sulfide capacity for many slags has been found (5,6) to be independent of sulfur and oxygen potentials for wide ranges, and therefore is a useful quantity for rating slags. One exception relevant to

Table I. Ash From Loveridge Seam (West Virginia) Coal

Component	Wt Pct.	Ash Analysis
		Normalized (excluding sulfur and taking iron as FeO)
Al <sub>2</sub> O <sub>3</sub>	18.4	24.1
SiO <sub>2</sub>	44.5	47.8
Fe <sub>2</sub> O <sub>3</sub>	15.9	17.4 (FeO)
CaO	4.56	4.9
MgO	1.08	1.2
Na <sub>2</sub> O	1.10	1.5
K <sub>2</sub> O	1.11	1.3
TiO <sub>2</sub>	1.20	1.1
SO <sub>3</sub>	9.02	--
P <sub>2</sub> O <sub>5</sub>	0.33	0.5

Table II. Normalized Compositions of Candidate Slags - Major Components Only

Slag No.	Composition, Wt. Pct.					Liquidus Temperature (°C) (Major Components Only)
	SiO <sub>2</sub>	Al <sub>2</sub> O <sub>3</sub>	FeO	Na <sub>2</sub> O	CaO	
2-A-1	46.0	19.9	34.1			1205
2-A-2	40.0	12.0	48.0			1083
2-A-3	18.1	5.9	76.0			1148
2-A-7	43.3	19.8	36.9			1220
2-A-8	35.3	14.1	50.6			1200
2-A-9	27.0	8.3	64.4			1150
2-A-10	23.6	5.9	70.4			1155
2-B-1	39.3		48.0	12.7		1000
2-B-2	56.4		21.8	21.8		?
2-B-3	33.2		26.2	40.6		1050
DSE-1	42.5		28.9	28.6		900
DSE-2	37.0		26.0	37.0		
2-C-1	37.7		46.4		15.7	1093
2-D-1	43.8	18.2		37.9		915
2-D-2	62.7	23.2		14.0		1063
2-D-3	61.6	12.2		26.2		732
2-E-1	42.1	20.1			37.8	1265
2-I-1	55.3	21.5	10.0	13.1		990

Table III. Additive Compositions For Candidate Slags

Slag No.	Additive Mass g/g Ash	Additive Composition, Wt. Pct.						Other
		SiO <sub>2</sub>	Al <sub>2</sub> O <sub>3</sub>	Fe <sub>2</sub> O <sub>3</sub>	Na <sub>2</sub> CO <sub>3</sub>	CaO		
2-A-1	0.34	22.9		77.1				
2-A-2	1.20	27.0		73.0				
2-A-3	3.52	7.4		92.6				
2-A-4	3.74	7.0		87.2				5.8 % CaF <sub>2</sub>
2-A-5	3.52	1.6		92.6				5.8 % B <sub>2</sub> O <sub>3</sub>
2-A-6	3.52	1.6		92.6				5.8 % P <sub>2</sub> O <sub>5</sub>
2-A-7	0.36	13.9		86.1				
2-A-8	0.89	13.9		86.1				
2-A-9	2.19	13.9		86.1				
2-A-10	3.47	13.9		86.1				
2-A-10b	4.07	11.8		73.5				14.7 % MgO
2-A-11	3.49	7.5		86.7	2.5			3.4 % CaF <sub>2</sub>
2-A-12	4.99	13.9		86.1				
2-B-1	0.69			65.7		34.2		
2-B-2	0.30			3.9		96.1		
2-B-3	1.20			18.9		81.1		
DSE-1	0.69			24.2		75.8		
DSE-2	0.97			18.5		81.5		
2-C-1	0.61			75.5			24.5	
2-D-1	0.93	10.9				89.1		
2-D-2	0.40	43.8				56.2		
2-D-3	1.60	46.3				53.7		
2-E-1	0.43	6.3					93.7	
2-I-1	0.99	49.1	13.5			37.4		



this study is that, for slags containing  $\text{FeO}$ ,  $C_s$  is expected to change with oxygen potential as the ratio of ferrous to ferric ions in the slag changes.

A review of the literature (5-22) showed that virtually all work on sulfur in slags was on systems relevant to the desulfurization of iron and steel and at temperatures ranging from 1400-1600°C. No data were found for low-melting slags (liquidus temperatures, approximately 1000-1100°C), and particularly for the iron-alkali-aluminosilicates from which many of the proposed compositions are composed. Therefore, experimental measurements were necessary to obtain the data needed for selection of slags.

**Experimental Method.** An equilibration technique was chosen to measure the sulfide capacities of the candidate slags. Slag samples were equilibrated with a  $\text{CO-CO}_2\text{-SO}_2$  gas mixture having fixed oxygen and sulfur potentials, quenched to room temperature, and analyzed for sulfur. Sulfide capacities were then calculated from the sulfur concentrations using Equation 2. This technique was chosen because it is a direct method, and because the oxygen and sulfur potentials could be accurately controlled, and, if necessary, these could be set to match the activities for oxygen and sulfur which were anticipated in the actual coal combustor. The apparatus used for sulfide capacity measurements is shown schematically in Figure 1.

Slags were prepared by mixing preweighed amounts of additives and coal ash. The coal ash was obtained from Bituminous Coal Research, Inc. It was prepared by ashing Loveridge Seam, West Virginia coal in air at 750°C, followed by a reduction in a 60% $\text{CO}$ -40% $\text{CO}_2$  gas at 1000°C, then cooled under nitrogen.

The gas compositions for each experiment were chosen to obtain as low an oxygen potential as possible, without reducing  $\text{FeO}$  to  $\text{Fe}$  metal. They were also chosen to obtain as low a sulfur potential as possible to match anticipated conditions in the actual combustor, yet large enough so that they could be prepared by mixing gases. The equilibration time for slag samples was determined by periodic analyses of the gas exiting the reactor. Quenched slag samples were analyzed for sulfur using a Leco titrator, and were analyzed for Si, Al, Fe, Na, K, Ca, Mg, Ti, and P by atomic absorption.

**Results.** Table IV gives the results for all sulfide capacity measurements. Figures 2 and 3 show ternary phase diagrams for selected systems on which the results are shown. Compositions shown were obtained by taking the three major components from the slag analyses and normalizing to 100%. The sulfide capacities are shown as a function of basicity in Figure 4, which summarizes all results of this study. Molar basicities ( $\Sigma$ mole fraction bases/ $\Sigma$ mole fraction acids) were calculated from the slag analyses.

It was found that after equilibration with the sulfurizing gas, certain slags in the  $\text{FeO-Al}_2\text{O}_3\text{-SiO}_2$  system consisted of two immiscible liquids at 1100°C. One phase was a

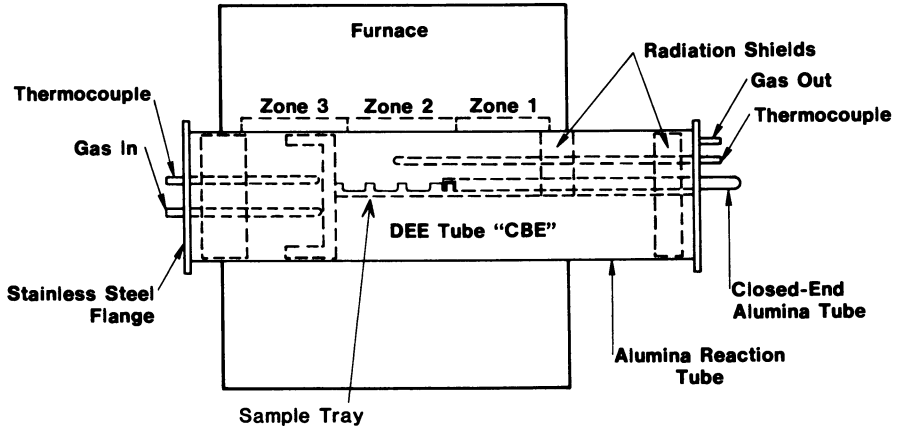


Figure 1. Reactor used for sulfide capacity measurements.

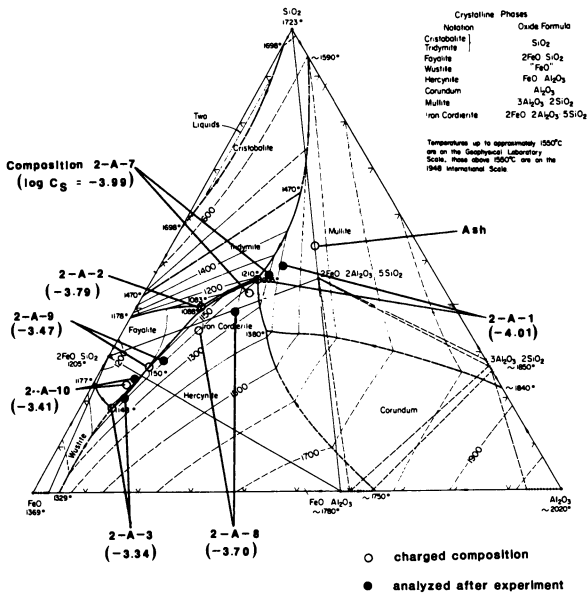


Figure 2. The FeO-Al<sub>2</sub>O<sub>3</sub>-SiO<sub>2</sub> phase diagram (1) with measured sulfide capacities indicated. Oxide phases in equilibrium with metallic iron. Reproduced with permission from reference 1. Copyright 1964 American Ceramic Society.

Table IV. Sulfide Capacity Measurements

Exp't. No.	T (°C)	Run Time (h)	Slag Composition	Wt % S	Log C <sub>S</sub>
2 <sup>a</sup>	1100	24	DSE-1	4.22	-4.31
			"	5.34	-4.21
			2-B-1	6.05	-4.16
			2-B-2	0.26	-5.52
			2-D-1	0.96	-4.96
			2-D-2 <sup>d</sup>	0.87	-5.00
4 <sup>c</sup>	1100	115	DSE-1	4.31	-4.06
			2-A-1	4.80	-4.01
			2-A-2 <sup>d</sup>		
			2-A-3 <sup>e</sup>	22.5	-3.34
			2-A-4 <sup>e</sup>	23.5	-3.32
			2-C-1	7.91	-3.79
5 <sup>c</sup>	1100	144.6	2-A-5 <sup>e</sup>	20.2	-3.38
			2-A-6 <sup>e</sup>	13.4	-3.56
			2-A-7	5.06	-3.99
			2-A-8	9.81	-3.70
			2-A-9 <sup>e</sup>	16.6	-3.47
			2-A-10 <sup>e</sup>	19.1	-3.41
			2-A-11 <sup>d</sup>		
7 <sup>f</sup>	1000	168.75	2-A-3 <sup>b</sup>	25.4	
			2-A-4 <sup>b</sup>	25.1	
			2-A-5 <sup>b</sup>	25.5	
			2-A-6 <sup>b</sup>	24.1	
			2-A-10 <sup>b</sup>	23.6	
			2-A-11 <sup>b</sup>	24.2	
			2-A-12 <sup>b</sup>	25.8	
			2-A-3a <sup>b</sup>	26.3	
			2-I-1	0.44	-5.04
			11 <sup>g</sup>	1300	70.0
2-A-10	1.97	-3.00			
2-A-10b	3.10	-2.80			

<sup>a</sup>Gas composition: 70% CO-29.5% CO<sub>2</sub>-0.5% SO<sub>2</sub>. X<sub>O<sub>2</sub></sub> = 7.2 x 10<sup>-14</sup>;

X<sub>S<sub>2</sub></sub> = 5.4 x 10<sup>-4</sup>. <sup>b</sup>Did not melt. <sup>c</sup>Gas composition: 70.2% CO-29.6% CO<sub>2</sub>-0.25% SO<sub>2</sub>. X<sub>O<sub>2</sub></sub> = 6.8 x 10<sup>-14</sup>; X<sub>S<sub>2</sub></sub> = 1.6 x 10<sup>-4</sup>.

<sup>d</sup>Sample crept out. <sup>e</sup>Two phases. <sup>f</sup>Gas composition: 74.5% CO-25.3% CO<sub>2</sub>-0.18% SO<sub>2</sub>. X<sub>O<sub>2</sub></sub> = 6.8 x 10<sup>-14</sup>; X<sub>S<sub>2</sub></sub> = 1.6 x 10<sup>-4</sup>.

<sup>g</sup>Gas composition: 66.3% CO-33.6% CO<sub>2</sub>-0.14% SO<sub>2</sub>. X<sub>O<sub>2</sub></sub> = 4.9 x 10<sup>-11</sup>; X<sub>S<sub>2</sub></sub> = 1.9 x 10<sup>-4</sup>.

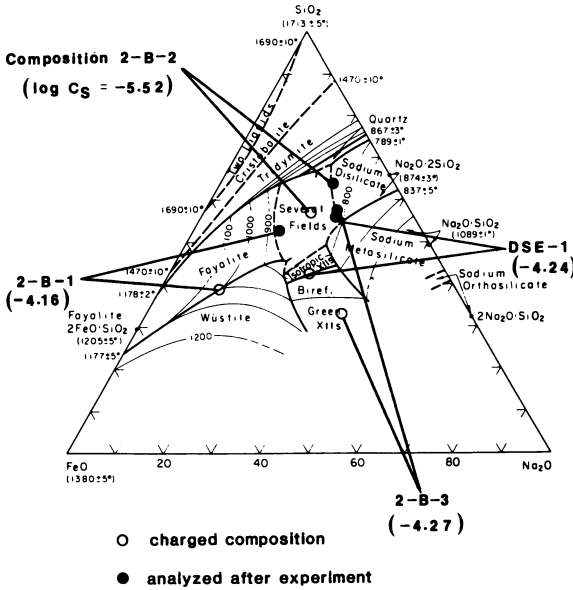


Figure 3. The FeO-Na<sub>2</sub>O-SiO<sub>2</sub> phase diagram (2) with measured sulfide capacities indicated. Oxide phases in equilibrium with metallic iron. Reproduced with permission from reference 2. Copyright 1969 American Ceramic Society.

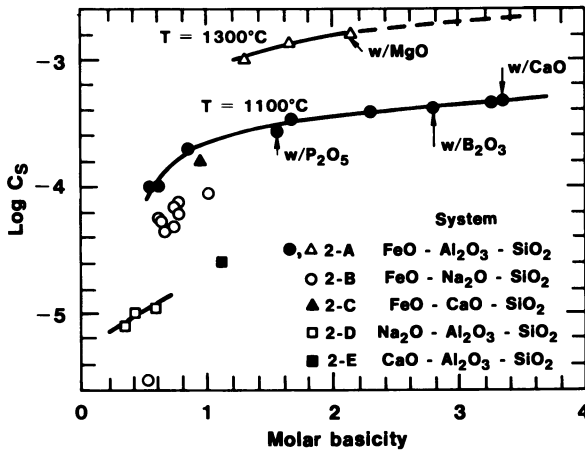


Figure 4. Measured sulfide capacities of candidate slags. Basicity calculated from chemical analyses. Points denoted by w/P<sub>2</sub>O<sub>5</sub> and w/B<sub>2</sub>O<sub>3</sub>, represent slags in which 5% SiO<sub>2</sub> was replaced by 5% of these oxides. Point denoted by w/CaO is for slag to which 5% CaF<sub>2</sub> was added, but all fluorine was lost during experiment. Point denoted by w/MgO for slag to which 12% MgO was added.

glass. The other phase had a metallic appearance and will be referred to as the "matte phase". The sulfide capacities for these slags should be considered as "apparent" because the sulfide capacity is defined for a single liquid phase. The matte phase in all of these double-phased slags contained 27-31% S, while the glass phase contained from 0.2 to 13% S. X-ray diffraction analyses showed the glass phase to be amorphous and the matte phase to contain FeS and FeS<sub>2</sub>.

Discussion. Slag compositions 2-A-1, 2-A-7, 2-B-2, 2-C-1, 2-D-2, and 2-E-1 were closest to the coal ash composition given in Table I, containing 25-38% additive. As seen from Table IV, log C<sub>S</sub> ranged from approximately -3.8 to -5.5 at 1100°C. Using the basicity of the ash calculated from Table I and the data shown in Figure 4, the sulfide capacity for pure ash is estimated to be approximately log C<sub>S</sub> = -5.2. This is quite low as compared to results obtained for slags containing significant quantities of additives. As will be demonstrated later in the report, sulfur captured by coal ash slag with this sulfide capacity would be insignificant even at very favorable conditions - very low oxygen potential and low temperature.

There is a general correlation between sulfide capacity and basicity for a given system, as shown in Figure 4. There is a sharp drop in sulfide capacity between basicities of 1.0 to 0.5, which corresponds to the metasilicate to disilicate compositions in a binary silicate. For a given basicity, systems 2-A (FeO) and 2-C (FeO, CaO) have significantly higher sulfide capacities than systems 2-D (Na<sub>2</sub>O) and 2-E (CaO), so that for a given basicity, FeO is superior to CaO and Na<sub>2</sub>O as an additive. This is not what would be expected considering the standard free energies of formation of the sulfides and oxides of Fe, Ca, and Na.

Considering standard free energies for the formation of metal sulfides from metal oxides, FeO and CaO should be approximately equivalent desulfurizers and Na<sub>2</sub>O should be superior. However, slags are far from ideal solutions because of the strong interactions among species -- particularly with SiO<sub>2</sub>. This is why experimental measurements of sulfide capacities were needed. Free energy of mixing data (24) for Na<sub>2</sub>O, CaO, and FeO binary silicates show that the chemical interaction with silica decreases in the order Na<sub>2</sub>O, CaO, FeO, and for a given basicity, the activity of the basic oxide in the silicates increase in the order Na<sub>2</sub>O, CaO, and FeO. On this basis, FeO should be a better desulfurizer than CaO or Na<sub>2</sub>O. This is consistent with the present results. Not surprisingly, the metal oxide-silica interaction is a major factor in the desulfurization ability of the slag.

Several modifications of slags based on the FeO-Al<sub>2</sub>O<sub>3</sub>-SiO<sub>2</sub> system were tested to determine if a less expensive additive could be substituted for some of the iron or if additives could be used to reduce liquidus temperatures. Figure 4 shows that replacing a portion of the iron oxide in slags of the FeO-Al<sub>2</sub>O<sub>3</sub>-SiO<sub>2</sub> system with CaO (5 wt %) or MgO (12 wt %) had no effect on the sulfide capacities. Results for composition 2-C-1 also support this conclusion, because for

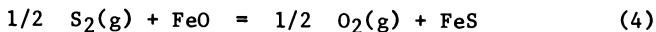
this composition approximately 14% of the FeO of an equivalent composition in the FeO-Al<sub>2</sub>O<sub>3</sub>-SiO<sub>2</sub> system was replaced by CaO, with only a slight decrease in sulfide capacity.

Replacement of portions of the SiO<sub>2</sub> in FeO-Al<sub>2</sub>O<sub>3</sub>-SiO<sub>2</sub> slags by B<sub>2</sub>O<sub>3</sub> or P<sub>2</sub>O<sub>5</sub> has no effect on sulfide capacities; therefore, these additives are potentially useful for reducing slag liquidus temperatures.

Figure 5 compares some results of this study to those found in the literature for similar slags at higher temperatures. These literature data were adjusted to a basicity of 1.65 using data given in Figure 4. The data from this study are quite consistent with the literature data. The linearity of the sulfide capacity with inverse temperature is consistent with the theoretical relationship,

$$\frac{d \ln C_S}{d(1/T)} = -\Delta H^\circ / R + H_{FeO}^M / R - H_{FeS}^M / R \quad (3)$$

where  $\Delta H^\circ$  is the standard enthalpy change for the reaction,



and  $H_{FeO}^M$  and  $H_{FeS}^M$

are the partial molar enthalpies of mixing of FeO and FeS in the slag. This relationship can be derived from Equation 2, the equilibrium constant for Equation 4, and the Gibbs-Helmholtz equation.

Most of the slags tested were found to have been partially or completely melted at 1100°C. However, at 1000°C, all slags from the FeO-Al<sub>2</sub>O<sub>3</sub>-SiO<sub>2</sub> system were not molten. It is thought that for these compositions the entire additive reacted with sulfur species in the atmosphere while none reacted with the SiO<sub>2</sub> or with other components in the ash. Hence, sulfide capacities measured from this experiment are not true sulfide capacities of the slags. Another point which supports this is that the "measured" sulfide capacities at 1000°C are greater than those at 1100°C, while Figure 5 shows the opposite trend for results for molten slags. Also, other literature data show that sulfide capacities generally increase with temperature.

This points out an inherent disadvantage in using a coal ash slag for desulfurization. When silica reacts with the desulfurizing agent, e.g., lime, the effectiveness of the desulfurizing compound is greatly reduced. Hence, it is desirable to design a desulfurizing combustor in which the ash does not react with the desulfurizing material.

#### Evaluation Of A Pilot Combustor

Calculations. The measured sulfide capacities were used to estimate sulfur emissions from a staged, slagging, cyclone combustor operating close to equilibrium, and to determine the

effects of various operating variables on the sulfur removal. To calculate sulfur emissions, an equation for gas-slag chemical equilibrium for sulfur (Equation 2) and a mass balance for sulfur are solved simultaneously. First, the equilibrium gas compositions were calculated for the combustion of coal with air for a range of sulfur concentrations in the coal. This was done using Alcoa's Chemical Equilibrium Computer Program (23). Next, the concentrations of sulfur in the slags for equilibrium with the combustion gases were calculated. Finally, the quantity of additives needed to obtain these compositions were calculated from sulfur mass balances.

**Results.** Figure 6 shows an example of the results for these calculations, for combustion with 55% of stoichiometric air (stage 1) at 1100°C. This is an isothermal calculation, i.e., both slag and gas temperatures are assumed to be 1100°C. Obviously, this cannot occur in practice, but the results of the calculation should provide an upper bound for sulfur removal. A reasonable goal for the sulfur capture, considering projections of future EPA regulations, is 70%. The slag mass can vary between 85 and 350 g/kg coal (the upper limit was established from a heat balance for Alcoa's pilot combustor), so the necessary log  $C_S$  for a 70% sulfur removal is between -2.75 and -3.3. A sulfide capacity of log  $C_S = -3.3$  at 1100°C was obtained for certain slags based on the FeO-Al<sub>2</sub>O<sub>3</sub>-SiO<sub>2</sub> system, e.g., compositions 2-A-3 or 2-A-10. This shows that 70% sulfur removal is thermodynamically possible.

As the combustion stoichiometry is decreased, the curves in Figures 6 are rotated counterclockwise about the origin, i.e., the sulfur removal is increased. An increase in temperature will have the opposite effect. The curves are rotated clockwise about the origin. However, for a particular slag composition the sulfide capacity increases with temperature, as shown in Figure 5. The net result of the two opposing effects (using the temperature behavior shown in Figure 5) is that the sulfur removal decreases with increasing temperature. In the range of coal-sulfur contents investigated, 2-6%, the fraction of sulfur removed by slag does not change with sulfur content in the coal. The total sulfur emitted increases with increasing sulfur concentration in the coal, but the sulfur removal by the slag also increases.

A final point to note regarding sulfur removal is that as the concentration of hydrogen in the combustion gases is decreased, the sulfur removal by the slag will increase. This is due to the high stability of the hydrogen-sulfur species, such as H<sub>2</sub>S(g), as compared to the carbon-sulfur species, such as COS. Thus, drying and charring of coal would significantly increase the theoretical removal of sulfur by the slag.

These calculations assume gas-slag equilibrium with respect to sulfur. This is probably only approached at the gas-slag surface near the exit of the first stage. At the entrance end of the combustor, the conditions would probably be more oxidizing than conditions calculated from the overall combustion stoichiometry,  $\phi$ , and thus sulfur solubility in the slag would

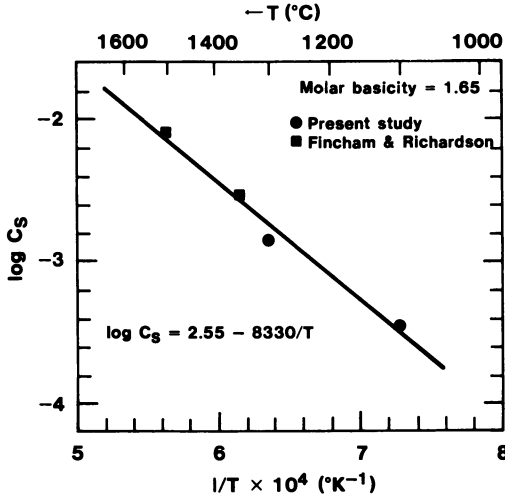


Figure 5. Comparison of results from this study to those of Fincham and Richardson (6) for an iron silicate with molar basicity of 1.65. Data from Fincham and Richardson were for pure iron silicates while these from the present study contained some coal ash.

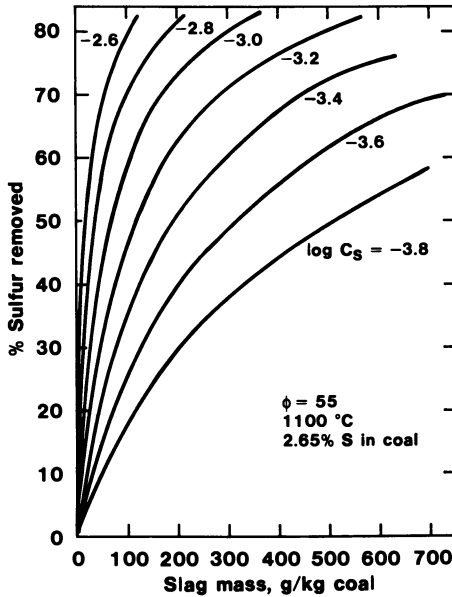


Figure 6. Equilibrium sulfur removal by slag for a combustor operating with Loveridge Seam (West Virginia) coal.



be less than that calculated. At some depth below the slag surface near this entrance end of the first stage, the conditions would be more reducing than those calculated from the overall combustion stoichiometry. This would result in increased sulfur solubility. The actual combustion process and sulfur removal processes are quite complex, and the extent of sulfur removal will depend on the combustion kinetics. For example, consider two extreme situations. In one, where most coal is combusted after it hits the slagged wall, sulfur removal should be relatively good. In the other extreme, where all the coal is combusted before it reaches the slagged wall, sulfur removal would be relatively poor because it would be dependent on mass transport through the gas phase, and the gas has a relatively short residence time.

In summary, the kinetics of the combustion process is important with regard to sulfur removal. The kinetics must be considered either by modelling or experimentation before a final judgment on desulfurization in a slagging, cyclone combustor can be made. The results of this study show that it is theoretically possible.

### Conclusions

Sulfide capacity measurements of relatively low melting (approximately 1100°C in most cases) slags based on the FeO-Al<sub>2</sub>O<sub>3</sub>-SiO<sub>2</sub>, FeO-Na<sub>2</sub>O-SiO<sub>2</sub>, FeO-CaO-SiO<sub>2</sub>, Na<sub>2</sub>O-Al<sub>2</sub>O<sub>3</sub>-SiO<sub>2</sub>, and CaO-Al<sub>2</sub>O<sub>3</sub>-SiO<sub>2</sub> systems but composed of coal ash + additives, have shown that the FeO-Al<sub>2</sub>O<sub>3</sub>-SiO<sub>2</sub>-based slags had the highest sulfide capacities. For a given basicity, the sulfide capacities could be ranked in the following order: FeO-Al<sub>2</sub>O<sub>3</sub>-SiO<sub>2</sub> > FeO-CaO-SiO<sub>2</sub> > FeO-Na<sub>2</sub>O-SiO<sub>2</sub> > CaO-Al<sub>2</sub>O<sub>3</sub>-SiO<sub>2</sub> > Na<sub>2</sub>O-Al<sub>2</sub>O<sub>3</sub>-SiO<sub>2</sub>. The chemical interaction of the basic oxides with silica appears to be a dominant factor controlling the sulfide capacity. There was good correlation between sulfide capacity and slag basicity, and sulfide capacities increased with temperature.

Calculations of the equilibrium sulfur removal for a commercial combustor using the measured sulfide capacities, showed that it was theoretically possible to remove 70% or more of the sulfur in coal. The sulfur removal increases with decreasing temperature, decreasing combustion stoichiometry in the first stage of the burner, increasing slag flow, and decreasing content of hydrogen in the fuel. This work showed that a slagging, cyclone combustor can remove sulfur into the slag, but kinetic modelling and/or experimentation is needed to prove whether or not the concept will work.

### Acknowledgment

This work was sponsored by the U.S. Department of Energy under Contract No. DE-AC07-78CS40037, "Pulverized Coal Firing of Aluminum Melting Furnaces."

Literature Cited

1. E. M. Levin, C. R. Robbins, and H. F. McMurdie: Phase Diagrams for Ceramists, American Ceramic Society, Columbus, OH (1964).
2. E. M. Levin, C. R. Robbins, and H. F. McMurdie: Phase Diagrams for Ceramists, 1969 Supplement, American Ceramic Society, Columbus, OH (1969).
3. E. M. Levin and H. F. McMurdie: Phase Diagram for Ceramists, 1975 Supplement, American Ceramic Society, Columbus, OH (1975).
4. R. S. Roth, T. Negas, and L. P. Cook: Phase Diagrams for Ceramists, Volume IV, American Ceramic Society, Columbus, OH (1981).
5. G. R. St. Pierre and J. Chipman: Trans. AIME, v. 206, pp. 1474-1483 (1956).
6. C.J.B. Fincham and F. D. Richardson: Proc. R. Soc. Series A223, 40 (1954) and J. Iron Steel Inst., 178, 4 (1954).
7. F. D. Richardson: Physical Chemistry of Melts in Metallurgy, v. 2, pp. 291-304, Academic Press, London (1974).
8. P. T. Carter and T. G. McFarlane: J. Iron Steel Inst., 185, 54 (1957).
9. K. P. Abraham, M. W. Davies, and F. D. Richardson: J. Iron Steel Inst., v. 196, pp. 309-312 (1960).
10. K. P. Abraham and F. D. Richardson: J. Iron Steel Inst., v. 196, pp. 313-317 (1960).
11. E. W. Dewing and F. D. Richardson: J. Iron Steel Inst., v. 194, 194, pp. 446-450 (1960).
12. R. A. Sharma and F. D. Richardson: J. Iron Steel Inst., v. 198, pp. 386-390 (1961).
13. R. A. Sharma and F. D. Richardson: J. Iron Steel Inst., v. 200, pp. 373-379 (1962).
14. G.J.W. Kor and F. D. Richardson: J. Iron Steel Inst. v. 206, pp. 700-704 (1968).
15. G.J.W. Kor and F. D. Richardson: Trans. AIME, v. 245, pp. 319-327 (1969).
16. R. J. Hawkins, S. G. Meherali, and M. W. Davis: J. Iron Steel Inst., v. 209, pp. 646-657 (1971).
17. A. Bronson and G. R. St. Pierre, Met. Trans. B, v. 10B, pp. 375-380 (1979).
18. A. Bronson and G.R. St. Pierre: Met. Trans. B, v. 12B, pp. 729-731 (1981).
19. H. B. Bell: Can. Met. Quart., v. 20 (2), pp. 169-179 (1981).
20. J. D. Shim and S. Ban-ya: Tetsu-to-Hagane, v. 68, pp. 251-60 (1982).
21. S. D. Brown, R. J. Roxburgh, I. Ghita, and H. B. Bell: Ironmaking and Steelmaking, v. 9, pp. 163-67 (1982).
22. I. Ghita and H. B. Bell: Ironmaking and Steelmaking, v. 9, pp. 239-43 (1982).
23. W. E. Wahnsiedler: "Chemical Equilibrium Package Users Manual," Alcoa Laboratories Report No. 7-78-25.
24. D. R. Gaskell: Metallurgical Treatises, J. K. Tien and J. F. Elliott, ed., p. 60, TMS-AIME, Warrendale, PA (1981).

RECEIVED July 23, 1985

## Analyses of Thermodynamic Properties of Molten Slags

Milton Blander<sup>1</sup> and Arthur D. Pelton<sup>2</sup>

<sup>1</sup>Argonne National Laboratory, Argonne, IL 60439

<sup>2</sup>Ecole Polytechnique, Université de Montreal, Montreal, PQ H3C 3A7, Canada

A novel technique has been developed for the simultaneous analysis of all thermodynamic data (including liquidus phase diagrams, activities of components, free energies of formation of compounds, volatilities, miscibility gaps, etc.) on highly ordered binary solutions such as silicates. The results for a number of silicate and aluminate solutions lead to an accurate description of all reliable solution data on a given binary and, because of the nature of the equations used for the analysis, they also provide a reliable means for interpolating or extrapolating outside the range of the data. When silica is the only acid component, a simple combining rule appears to lead to good predictions of the properties of multicomponent systems based solely on data for the binary systems. Concepts developed for molten salts lead to correlations of our results with fundamental physical properties and interactions of ions in terms of ionic radii, charge, polarizabilities, dispersion interactions, and ligand field effects.

Silica based slag systems are highly ordered liquids which have been a difficult class of materials on which to perform thermodynamic analyses. (1-5) To our knowledge, no satisfactory, self-consistent prior method of analysis has been developed for systems as ordered and complex as silicates which incorporates all known data in a meaningful way. In this paper, we discuss the results of a method of analysis which permits one to simultaneously analyze a large amount of different types of data on binary systems. The calculations lead to a small set of parameters which permit one to calculate the thermodynamic properties of slag solutions as a function of temperature and composition. The thermodynamic self-consistency and the form of the equations used provide some confidence in the use of the results for interpolations and extrapolations outside the range of data. In addition, for systems in which silica is the only acid constituent, we propose a theoretically justified combining rule to calculate the properties of ternary systems based solely on data for the three subsidiary binaries. The results are in good agreement with available data.

The ionic nature of molten silicates suggests that many of the theories and correlations developed for molten salts (6) can be applied to the development of correlations

between the relative magnitudes of the deviations from ideal solution behavior in terms of ionic radii, charges, polarizabilities, dispersion interactions and ligand field effects.

#### Calculational Method (7)

The molar free energy of mixing,  $\Delta G_m$  of a silicate is represented by the expression

$$\Delta G_m = \sum_i RTX_i \ln X_i + \sum_i RTX_i \ln \gamma_i = \Delta G_m^{ideal} + G^E \quad (1)$$

where  $X_i$  is the mole fraction of component  $i$ ,  $\gamma_i$ , the activity coefficient, represents deviations from ideal solution behavior of component  $i$ ,  $\Delta G_m^{ideal}$  is the molar free energy of mixing of a hypothetical ideal solution and  $G^E$  is the molar excess free energy of mixing which represents the deviations from ideality of the molar free energy of solution. The conventional representation of  $\ln \gamma_i$  and  $G^E$  is a power series in mole fractions. The complexity of ordered solutions would require a very long power series in order to obtain a reasonable representation of their properties. This arises from the tendency of such solutions to have a "V" shaped dependence of the enthalpy of mixing and an "m" shaped dependence of the entropy of mixing on concentration. (1) The fitting of data using a long polynomial will generally be poor and ambiguous in such systems. In order to obtain reasonable fits, one must use equations which inherently have the concentration and temperature dependence of ordered solutions built in.

We have deduced a set of equations with such properties based on empirical modifications of the quasi-chemical theory. (7-8) For binary systems the excess free energy of mixing is given by the expression

$$G^E = (aX_1 + bX_2) \left[ y_1 \ln \frac{K-1+2y_1}{y_1(K+1)} + y_2 \ln \frac{K-1+2y_2}{y_2(K+1)} \right] \quad (2)$$

where  $X_i$  is the mole fraction of component  $i$ , and the values of  $a$  and  $b$  are equal to 0.34435 times the cationic charge of components 1 and 2, respectively. The quantities  $y_i$  are equivalent fractions which for component 2 is given by the expression  $y_2 = bX_2/(aX_1 + bX_2)$  and  $K$  is given by the equation

$$K = 1 + 4y_1y_2[\exp(W_{12}/RT) - 1]^{1/2} \quad (3)$$

where  $W_{12}$  is an energy which is taken to be dependent on temperature and is written as a polynomial in concentration

$$W_{12} = \sum_{k=0} (h_k - Ts_k)y_2^k \quad (4)$$

where no more than four values of  $k$  chosen between 1 and 7 were found to be needed and where we generally take the component 2 to be more acid than component 1.

All these quantities define the number of the 1-1, 2-2, and 1-2 bonds in the quasi-chemical model,  $n_{11}$ ,  $n_{22}$ , and  $n_{12}$ . The total number of bonds to each component 1 cation is  $2a$  and to component 2,  $2b$  so that if  $n_i$  is the number of moles of component  $i$ , then

$$an_1 = n_{11} + n_{12}/2 \quad (5)$$

$$bn_2 = n_{22} + n_{12}/2$$

and if the fraction of  $ij$  bonds,  $X_{ij} = n_{ij}/\sum n_{ij}$ , then

$$\begin{aligned} X_{11} &= y_1 - X_{12}/2 \\ X_{22} &= y_2 - X_{12}/2 \end{aligned} \quad (6)$$

and the distribution of bonds is governed by the equation

$$(X_{12}^2/X_{11}X_{22}) = 4\exp(-W_{12}/RT) = \alpha_{12}^2 \quad (7)$$

The solutions to Eqs. (6) and (7) can be used to calculate the molar excess free energy from the equation

$$\frac{G^E}{RT} = aX_1\ell n\frac{X_{11}}{y_1^2} + bX_2\ell n\frac{X_{22}}{y_2^2} \quad (8)$$

which is equivalent to Eq. (2). The equations are somewhat more complex for ternary systems with the two equations of Eq. (6) replaced by the three equations

$$\begin{aligned} X_{11} &= y_1 - X_{12}/2 - X_{13}/2 \\ X_{22} &= y_2 - X_{12}/2 - X_{23}/2 \\ X_{33} &= y_3 - X_{13}/2 - X_{23}/2 \end{aligned} \quad (9)$$

where now, for example,  $y_3 = cX_3/(aX_1 + bX_2 + cX_3)$ . In addition there are three equations replacing Eq. (7) of the form

$$(X_{ij}^2/X_{ii}X_{jj}) = \alpha_{ij}^2 = 4\exp(-W_{ij}/RT) \quad (10)$$

By substituting Eq. (9) into Eq. (10), one obtains three simultaneous equations with three unknowns which can be solved numerically. The power series representation of the three values of  $W_{ij}$  can be approximated in several ways. For systems with only one acid component (*e.g.*, silica) and with the remaining components being basic, a logical representation is the "asymmetric approximation." If we choose  $\text{SiO}_2$  to be component 1, then we set

$$\begin{aligned} W_{12} &= c_0 + c_1y_1 + c_2y_1^2 + \dots \\ W_{13} &= c'_0 + c'_1y_1 + c'_2y_1^2 + \dots \end{aligned} \quad (11)$$

and

$$W_{23} = c''_0 + c''_1t_{23} + c''_2t_{23}^2 + \dots$$

where  $t_{ij} = y_j/(y_i + y_j)$ . The coefficients  $c_i$  contain a constant and a temperature dependent term.

The molar excess free energy of the ternary system is given by the expression

$$\frac{G^E}{RT} = aX_1 \ln \frac{X_{11}}{y_1^2} + bX_2 \ln \frac{X_{22}}{y_2^2} + cX_3 \ln \frac{X_{33}}{y_3^2} \quad (12)$$

With the equations we have given, one can calculate the properties of a ternary system based on the properties of the three subsidiary binaries. This approximation leads to very good representations of ternary data. (8)

For binary systems, the parameters  $h_j$  and  $s_j$  are deduced from a complex optimization procedure which performs a global and simultaneous analysis of all thermodynamic data on a system. This includes liquidus phase diagrams, activity data, data on miscibility gaps, enthalpies of fusion, free energies of formation of compounds, etc. The small set of resultant parameters (seven at most in the systems considered including temperature coefficients) are then used to recalculate the input data to double check the accuracy of the curve fitting procedure as well as the efficacy of the use of the equations for representing the data. The results were generally very good. For multicomponent systems, we used the asymmetric approximation given in Eq.(11). When silica is the only acid component, the predictions based on this approximation were in very good agreement with measured data. (8) A partial theoretical justification for such a method can be based on theories for ternary systems. (8-9)

#### Results of Thermodynamic Analyses

We have performed analyses of ten of the fifteen binary systems and six of the twenty ternary systems containing the components MgO, FeO, CaO, Na<sub>2</sub>O, Al<sub>2</sub>O<sub>3</sub>, and SiO<sub>2</sub>. (7-8) (Table I)

Table I  
Systems Which Have Been Analyzed

Binary Systems		Ternary Systems
CaO-SiO <sub>2</sub>	CaO-AlO <sub>1.5</sub>	CaO-AlO <sub>1.5</sub> -SiO <sub>2</sub>
FeO-SiO <sub>2</sub>	NaO <sub>0.5</sub> -AlO <sub>1.5</sub>	NaO <sub>0.5</sub> -CaO-SiO <sub>2</sub>
MgO-SiO <sub>2</sub>	MgO-FeO	NaO <sub>0.5</sub> -AlO <sub>1.5</sub> -SiO <sub>2</sub>
NaO <sub>0.5</sub> -SiO <sub>2</sub>	MgO-CaO	CaO-FeO-SiO <sub>2</sub>
AlO <sub>0.5</sub> -SiO <sub>2</sub>	CaO-FeO	CaO-MgO-SiO <sub>2</sub>
		MgO-FeO-SiO <sub>2</sub>

We illustrate our calculations for one ternary system below. The analysis of the three binary subsystems and the ternary system CaO-FeO-SiO<sub>2</sub> was performed using as input the liquidus phase diagram, (10) activities of CaO, (11) and SiO<sub>2</sub> (12), the free energies of formation of CaSiO<sub>3</sub> and Ca<sub>2</sub>SiO<sub>4</sub>, (13) and the miscibility gap (14) in the CaO-SiO<sub>2</sub> system, measured activities of FeO in the CaO-FeO system, (15) and the activities of FeO, (16-18) the phase diagram (19) and the free energy of formation of Fe<sub>2</sub>SiO<sub>4</sub> (13) in the FeO-SiO<sub>2</sub> system. To illustrate some of the results, we exhibit (1) the calculated phase diagram of the FeO-SiO<sub>2</sub> system in Fig. 1 along with measured values of the invariant points and (2) a comparison of activities of "FeO" measured in the iron saturated molten FeO-SiO<sub>2</sub> system with calculated values in Fig. 2.

Using our asymmetric combining rules, the data for the binary systems were combined and led to the results for ternary systems given in Fig. 3; this figure illustrates

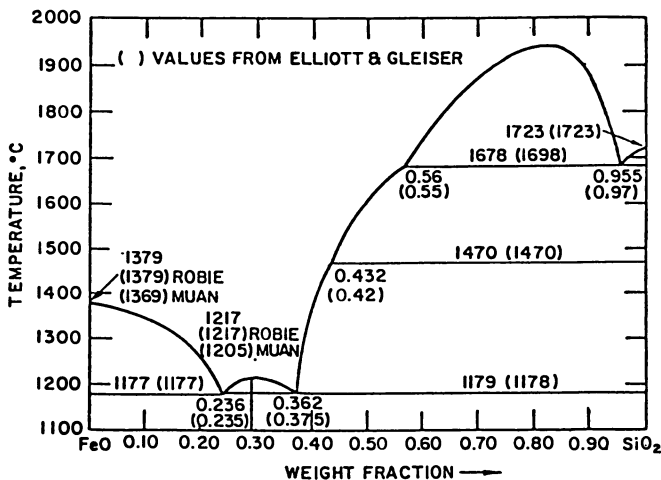


Figure 1. Calculated phase diagram of the FeO-SiO<sub>2</sub> system. Numbers in parentheses are measured values from Muan and Osborne (10) and Robie, et al. (13)

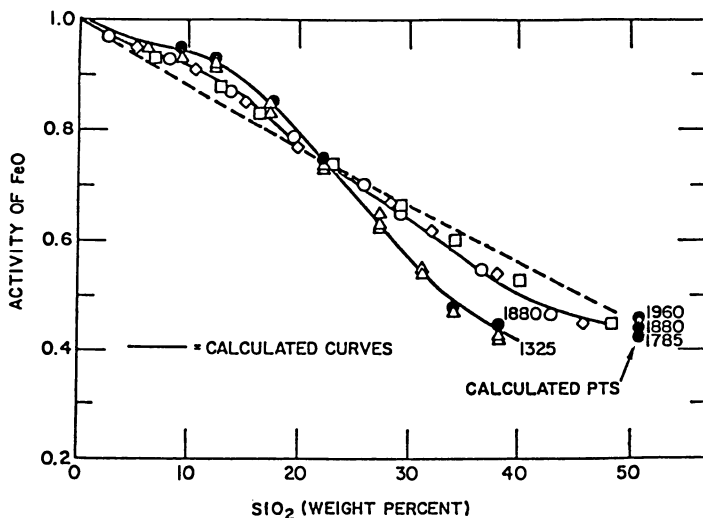
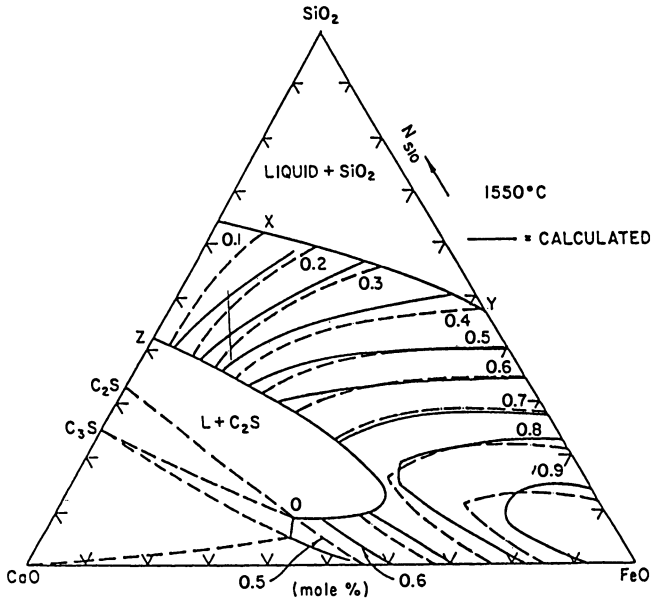


Figure 2. Activities of "FeO" measured in iron saturated molten FeO-SiO<sub>2</sub> at 1325°C ( $\Delta$ ) (17), 1785°C (O) (16), 1880°C ( $\diamond$ ) (16), and 1960°C ( $\square$ ) (16). The two solid lines represent calculated points at 1325°C and 1880°C. The filled circles along one solid line represent individual calculated points and the three filled circles labeled 1960, 1880, and 1785 represent calculated points at three temperatures and fixed composition which illustrate the calculated temperature dependence.



**Figure 3.** Activities of FeO in iron saturated CaO-FeO-SiO<sub>2</sub> at 1550°C. Dashed lines are from Timucin and Morris (20) and the solid lines represent our calculations.

Publication Date: April 2, 1986 | doi: 10.1021/bk-1986-0301.ch014



the correspondence between calculated and measured values (20) of the activities of FeO in the CaO-FeO-SiO<sub>2</sub> system. The differences are well within the uncertainties in the measurements. We find that this method essentially permits us to make predictions in ternary systems based solely on data for the three subsidiary binary systems for cases in which silica is the only acid component. When alumina and silica were both present, a more complex representation was necessary.

The good correspondence of calculations with the complex concentration dependence of activities in the CaO-FeO-SiO<sub>2</sub> system illustrates the fact that our equations properly take into account the kinds of ternary interaction terms known to exist in such systems. (8,9,21) This feature lends confidence in the use of our equations for predictions in multicomponent systems (containing only silica as an acid component) based solely upon the subsidiary binaries. If, as it appears, this is generally true, our method provides an important predictive capability.

### Correlations of Properties

Theories and concepts which have been developed for molten salt solutions can be used to correlate the thermodynamic properties of silicates. (8) Coulomb interactions lead to a dependence of thermodynamic functions on the inverse of the cation-anion interatomic distance. Thus, by analogy with molten salts, one would expect a linear dependence of the magnitudes of free energies of mixing on this parameter which is in a direction such that negative deviations from ideality increase in the order Li<sup>+</sup>, Na<sup>+</sup>, K<sup>+</sup>, Rb<sup>+</sup>, Cs<sup>+</sup>, and Mg<sup>++</sup>, Ca<sup>++</sup>, Sr<sup>++</sup>, and Ba<sup>++</sup>. In addition, solutions with monovalent alkali oxides should exhibit more negative deviations from ideality than those with divalent alkaline earth oxides. The polarizability of oxide anions leads to an additional contribution with a similar dependence on cations. The magnitude of cation-cation dispersion interactions are related to the polarizabilities, ionization potentials and interaction distances. Thus, the dissolution of oxides of cations with large dispersion interactions leads to a loss of this negative energy and hence to a positive contribution to deviations from ideality. In addition ligand field effects for divalent transition metals tend to contribute to negative deviations from ideal solution behavior in molten salts with monovalent cations. The effective charge of Si is greater than two and one would thus expect a positive contribution to deviations from ideal solution behavior from this source. The effect for Mn<sup>2+</sup> which has a half filled shell for example, should be much less positive than for Fe<sup>2+</sup>.

The data for testing these influences on solution behavior are too sparse to reach quantitative conclusions. However, the general trends are in the right direction. Measured deviations from ideality of silicates with divalent oxides become more negative (or less positive) in the order Fe<sup>+2</sup>, Mn<sup>2+</sup>, Pb<sup>2+</sup>, Mg<sup>2+</sup>, Ca<sup>2+</sup>. (1,7,9,22) In this view, ligand field effects lead to Fe<sup>2+</sup> preceding Mn<sup>2+</sup> and Mn<sup>2+</sup> preceding even Mg<sup>2+</sup> which has a smaller radius; dispersion interactions lead to Pb<sup>2+</sup> preceding even Mg<sup>2+</sup> even though its radius is even larger than Ca<sup>2+</sup> and Sr<sup>2+</sup>; finally, coulomb and polarization interactions lead to Mg<sup>2+</sup> preceding Ca<sup>2+</sup>. With careful measurements of a larger number of binary silicate systems, it should be possible to develop useful correlations and a means of making reasonable predictions of the magnitudes of thermodynamic properties of silicates.

### Conclusions

There are several significant conclusions which can be reached.

1. We have performed analyses of thermodynamic data on binary silicate systems

- which lead to a unique and accurate mathematical representation of their known properties.
2. Our use of equations which have the properties of ordered liquids built in appears to have the innate capability for representing a mass of different types of data on binary systems measured in various ranges of temperature and composition. This result lends confidence in the use of our analyses for interpolations and extrapolations outside the range of measurements to calculate thermodynamic properties at unmeasured temperatures and compositions.
  3. We can theoretically justify an "asymmetric" combining rule which, for cases in which silica is the only acid component, leads to a *priori* predictions for ternary systems based on data for the three subsidiary binaries. It appears likely that such predictions would be valid for multicomponent systems.
  4. A preliminary examination of thermodynamic data on silicates indicates that correlations developed for molten salts may be useful in understanding and ultimately in predicting magnitudes of the thermodynamic solution properties of silicates.

#### Acknowledgments

Work performed under the auspices the Morgantown Energy Technology Center of the U. S. Department of Energy.

#### References

1. Lin, P.L.; Pelton, A. D. Metall. Trans. 1979, 10B, 667-676.
2. Masson, C. R.; Smith, I. B.; Whiteway, S. G. Can. J. Chem. 1977, 48, 1456-1464; Proc. 11th International Congress on Glass, J. Gotz, Ed., Prague, 1977, Vol. 1, pp. 3-41.
3. Gaskell, D. R. Metall. Trans. 1977, 8B, 131-145.
4. Fincham, C. J. B.; Richardson, F. D. Proc. Roy. Soc. 1954, 223, 40.
5. Toop, G. W.; Samis, C. S. Trans. TMS-AIME 1962, 224, 878-887.
6. Blander, M. "Thermodynamic Properties of Molten Salt Solutions," Molten Salt Chemistry, Blander, M., Ed., Interscience, N.Y., 1964, pp. 127-237.
7. Blander, M.; Pelton, A. D. "Computer Assisted Analyses of the Thermodynamic Properties of Slags in Coal Combustion Systems," ANL/FE-83-19, Argonne National Laboratory, Argonne, IL, 1983 Available from NTIS, U.S. Dept. of Commerce, Washington, D.C.
8. Pelton, A. D.; Blander, M. "Computer Assisted Analysis of the Thermodynamic Properties and Phase Diagrams of Slags" in Proc. Second Int'l. Symp. on Metallurgical Slags and Fluxes, Fine, H. A.; Gaskell, D. R., eds., TMS-AIME, Warrendale PA, 1984, pps 281-294; Blander, M.; Pelton, A. D. "Analyses and Predictions of the Thermodynamic Properties of Multicomponent Silicates", *ibid*, pps 295-304
9. Saboungi, M.-L.; Blander, M. J. Chem. Phys. 1975, 63, 212-220; J. Amer. Ceram. Soc. 1975, 58, 1-7.
10. Muan, A; Osborne, E. F. "Phase Equilibria Among Oxides in Steelmaking," Addison-Wesley Publishing Co., Reading, Mass. 1965.

11. Sharma, R. A.; Richardson, F. D. J. Iron Steel Inst. 1962, 200, 373; 1961, 198, 308.
12. Rein, R. H.; Chipman, J., Trans. AIME 1965, 233, 415-425.
13. Robie, R. A.; Hemingway, B. S.; Fisher, J. R. "Thermodynamic Properties of Minerals and Related Substances at 298.15 K and 1 Bar Pressure and at Higher Temperatures," Geologic Survey Bulletin 1452, U.S. Govt. Printing Office, Washington, D.C. 1978.
14. Ol'shanskii, Ya. I., Dokl. Akad. Nauk SSSR 1951, 76, 94; Tewhey, J. D.; Hess, P. C. Phys. Chem. Glasses 1979, 20, 41-53.
15. Elliott, J. F. Trans. AIME 1955, 203, 485.
16. Distin, P. A.; Whiteway, S. G.; Masson, C. R. Can. Met. quart. 1971, 10, 73.
17. Schuhmann, R; Ensio, P. J. Metals 1951, 3, 401.
18. Bodsworth, C. J. Iron and Steel Inst., London 1959, 193, 13.
19. Levin, E. M.; Robbins, C. R.; McMurdie, H. F. "Phase Diagrams for Ceramists," Am. Ceram. Soc., Columbus, Ohio 1964; Supplement, 1969; E. M. Levin and H. F. McMurdie, Supplement 1975.
20. Timucin, M.; Morris, A. E. Met. Trans. 1970, 1, 19.
21. Blander, M., "Some Fundamental Concepts in the Chemistry of Molten Salts" in Molten Salts, G. Mamantov, ed., Marcel Dekker, New York 1969.
22. Gaye, H.; Riboud, P. "Données Experimentales sur les Activités des Constituants de Laitiers," IRSID PCM-RE 337, St. Germain-en-Laye, France 1976.

RECEIVED January 24, 1986

## Estimation of Physicochemical Properties of Coal Slags and Ashes

K. C. Mills

National Physical Laboratory, Teddington, Middlesex TW11 0LW, United Kingdom

The various methods available for estimating the melting range, viscosity, density, surface tension, heat capacity, enthalpy, thermal conductivity, absorption coefficient and emissivity of coal slags and ashes are reviewed and evaluated. New routines for estimating the density, surface tension, heat capacity and enthalpy of coal slags from their chemical composition are presented and assessed. It was concluded that the distribution of iron in the slag between free Fe, FeO and Fe<sub>2</sub>O<sub>3</sub> was very important as virtually every physical property of the slag was greatly influenced by this factor.

Slags formed during the gasification of coal usually contain SiO<sub>2</sub>, Al<sub>2</sub>O<sub>3</sub>, iron oxides, CaO, Na<sub>2</sub>O and K<sub>2</sub>O with minor amounts of various other oxides. A knowledge of the physico-chemical properties of these slags can improve the control of the process eg. the amount of flux required to bring the slag viscosity to a level suitable for tapping can be calculated from viscosity-composition relations. Physical property data for the coal slags can also improve process design by providing input values for mathematical models of the process eg. thermal properties of the slags are needed for heat balance calculations. There is an appreciable variation in the composition of slags formed from various coals and even from different batches of the same stock on occasions and these compositional variations can give rise to considerable differences in the physical properties. As the chemical analysis is frequently available on a routine basis it would be particularly desirable to have reliable models for the prediction of physico-chemical properties from their chemical composition. Furthermore such models would have the further advantage that the need for arduous interpolations on pseudo-ternary plots for slags, which are really multicomponent and interactive systems, would be eliminated.

This chapter not subject to U.S. copyright.  
Published 1986, American Chemical Society

The properties of slags are dependent not only upon chemical composition, but upon other factors also. The most pronounced deviations from additivity rules based on composition arise in the estimation of those properties which involve ionic transport eg. electrical conductivity. However surface tension values estimated from additivity rules are frequently in error as bulk thermodynamic properties do not apply at surfaces. Furthermore, virtually all the physical properties of slags are, to some extent, dependent upon the structure of the slag (viz. the length of silicate chains, degree of crystallinity etc.) thus estimation procedures have to accommodate these structural factors, where possible.

There is only a limited amount of physical property data available for coal slags and consequently it has been necessary to examine a much broader range of silicates including magmatic liquids and those slags encountered in steelmaking, glassmaking and non-ferrous processes. Thus the models described here should have a much wider range of applicability.

A critical evaluation of the extant physical property data has shown that virtually every physical property is markedly dependent upon the distribution of iron in the slag between  $\text{FeO}$ ,  $\text{Fe}_2\text{O}_3$  and free iron. Frequently these distributions are not reported and appropriate values cannot readily be predicted since the oxidation state depends upon (i) the partial pressure of oxygen,  $p_{\text{O}_2}$  (1) (ii) temperature (1),  $T$  and (iii) the nature of the other oxides present, thus  $\text{CaO}$ ,  $\text{Na}_2\text{O}$  and  $\text{K}_2\text{O}$  (1) (2) (3) increase the amount of  $\text{Fe}_2\text{O}_3$  while  $\text{SiO}_2$  increases the amount of  $\text{FeO}$ . Even when the iron distributions are given the values are vulnerable to error owing to difficulties in chemical analysis and the possibility of some redistribution of the  $\text{Fe}/\text{Fe}^{2+}/\text{Fe}^{3+}$  ratios during the quench. Nevertheless it is strongly recommended that all future physical property determinations on coal slags should be accompanied by chemical analysis for  $\text{Fe}(\text{free})$ ,  $\text{FeO}$  and  $\text{Fe}_2\text{O}_3$  on the quenched specimen.

### Models for Estimating Physico-Chemical Properties.

#### Melting Range

Empirical rules have been formulated (4-6) for the estimation of melting range on the basis of the basicity of the slag or ash. However the various constants used in the calculations are applicable to very narrow compositional ranges and thus a large number of constants are required to represent the slags formed from different coals.

A more universal approach has been adopted by Gaye (7) (8) who expressed, the dependency of liquidus temperature,  $T_{\text{liq}}$ , upon chemical composition as polynomials for each of the phases (or compounds) formed by the slag. The maximum calculated value of  $T_{\text{liq}}$  for the various phases is the  $T_{\text{liq}}$  value. Good agreement was obtained between the calculated and experimental values for  $T_{\text{liq}}$  for the systems,  $\text{SiO}_2 + \text{Al}_2\text{O}_3 + \text{MgO} + \text{FeO}$  and  $\text{SiO}_2 + \text{Al}_2\text{O}_3 + \text{MgO} + \text{CaO}$ . However development of this model to cover the multicomponent coal slags could prove difficult.

A second model due to Gaye (9) would appear to offer more promise; it is based on the Kapoor-Frohberg model for the estimation of activities and assumes that both acidic and basic oxides are made up of symmetrical cells and these interact to form asymmetrical cells. The activities of the various oxides calculated for quaternary slags with this model are in excellent agreement with those determined experimentally. Values of  $T_{liq}$  for a given composition can be derived by determining the temperature at which the solid phase formed has an activity of one. The model has been developed for systems based on seven components,  $SiO_2$ ,  $Al_2O_3$ ,  $CaO$ ,  $MgO$ ,  $FeO$ ,  $Fe_2O_3$  and  $MnO$ . The model will have to be enlarged to include  $Na_2O$  etc before it can be used for the reliable estimation of  $T_{liq}$  of coal slags but it would seem to have considerable promise and has the decided advantage that activity data for the various component oxides are also produced.

Viscosity ( $\eta$ ). Several models have been reported for the estimation of viscosities ( $\eta$ ) of silicate melts to cover the compositional ranges of glasses (10,11) steelmaking slags (12,14), magmas (15-18) and coal slags and ashes (19-24). The temperature (T) dependence of the viscosity is expressed in the form of the Arrhenius relationship (equation 1) or the Frenkel relationship (equation 2 which is sometimes known as the Weymann equation) where A and B are constants, E is the activation energy and R is the Gas Constant.

$$\eta = A \exp (E/RT) \quad (1)$$

$$\eta = AT \exp (B/RT) \quad (2)$$

Estimated viscosities have been calculated using these various models and the closest agreement with experimental values was obtained with the models due to Riboud *et al* (13) and Urbain *et al* (17)(18). These estimation procedures use the Frenkel relationship and thus their superiority may be largely due to the use of equation (2). The model due to Schobert which involves petrographic classification has not been assessed and this procedure may provide reliable estimates of viscosity for coal slags but could not be applied to slags covering a wide range of composition. Thus effort in the present study was focussed predominantly on the Riboud and Urbain models.

Model due to Riboud *et al* (13). The slag constituents are classified in five different categories in this model. The mole fractions (x) for those categories being given by

$$(i) \quad x("SiO_2") = x(SiO_2) + X(PO_{2.5}) + x(TiO_2) + x(ZrO_2)$$

$$(ii) \quad x("CaO") = x(CaO) + x(MgO) + x(FeO) + x(FeO_{1.5})$$

$$(iii) \quad x(Al_2O_3)$$

$$(iv) \quad x(CaF_2) \text{ and}$$

$$(v) \quad x("Na_2O") = x(Na_2O) + x(K_2O).$$

The parameters A and B of equation (2) are calculated from the mole fraction of the five categories by using equations (3) and (4) and the

$$A = \exp(-19.81+1.73x("CaO")+5.82x(CaF_2)+7.02x(Na_2O)-33.76x(Al_2O_3)) \quad (3)$$

$$B = +31140-23896x("CaO")-46356x(CaF_2)-39159x("Na_2O")+68833x(Al_2O_3) \quad (4)$$

viscosity for the temperatures in question by use of equation 2.

Model due to Urbain et al<sup>(18)</sup>. In this model the parameters A and B are calculated by dividing the slag constituents into three categories (i) "glass formers",  $x_G = x(\text{SiO}_2) + x(\text{P}_2\text{O}_5)$  (ii) "modifiers",  $x_M = x(\text{CaO}) + x(\text{MgO}) + x(\text{Na}_2\text{O}) + x(\text{K}_2\text{O}) + 3x(\text{CaF}_2) + x(\text{FeO}) + x(\text{MnO}) + 2x(\text{TiO}_2) + 2x(\text{ZrO}_2)$  and (iii) "amphoterics",  $x_A = x(\text{Al}_2\text{O}_3) + x(\text{Fe}_2\text{O}_3) + x(\text{B}_2\text{O}_3)$ .

However we consider that  $\text{Fe}_2\text{O}_3$  behaves more like a modifier than an amphoteric and in our revised programme  $1.5 x(\text{FeO}_{1.5})$  has been added to  $x_M$  and  $x(\text{Fe}_2\text{O}_3)$  removed from  $x_A$ . "Normalized" values  $x_G^*$  and  $x_M^*$  and  $x_A^*$  are obtained by dividing the mole fractions,  $x_G$ ,  $x_M$  and  $x_A$  by the term  $(1 + 2x(\text{CaF}_2) + 0.5 x(\text{FeO}_{1.5}) + x(\text{TiO}_2) + x(\text{ZrO}_2))$ . Urbain proposed that the parameter B was influenced both by the ratio,  $\beta = x_M^*/(x_M^* + x_A^*)$  and by  $x_G^*$ . The parameter B can be expressed in the form of equation (5) where  $B_1$ ,  $B_2$  and  $B_3$  can be obtained by equation (6).

$$B = B_0 + B_1 x_G^* + B_2 (x_G^*)^2 + B_3 (x_G^*)^3 \quad (5)$$

$$B_i = a_i + b_i \beta + c_i \beta^2 \quad (6)$$

$B_0$ ,  $B_1$ ,  $B_2$  and  $B_3$  can be calculated from the equations listed in Table I and these parameters are then introduced into equation (5) to calculate B. The parameter A can be calculated from B by equation (7) and the viscosity of the slag (in PaS) can then be determined using equation(8).

$$- \ln A = 0.2693 B + 11.6725 \quad (7)$$

$$\eta = 0.1 \text{ AT exp } (10^3 B/T) \quad (8)$$

Table I. The relationship of  $B_0$ ,  $B_1$ ,  $B_2$  and  $B_3$  with the function  $\beta$

$B_0$	= 13.8	+ 39.9355 $\beta$	- 44.049 $\beta^2$
$B_1$	= 30.481	- 117.1505 $\beta$	+ 129.9978 $\beta^2$
$B_2$	= -40.9429	+ 234.0486 $\beta$	- 300.04 $\beta^2$
$B_3$	= 60.7619	- 153.9276 $\beta$	+ 211.1616 $\beta^2$

Modifications to the Urbain Model. Urbain<sup>(18)</sup> has recently modified the model to calculate separate B values for different individual modifiers, CaO, MgO and MnO. The global B value for a slag containing all three oxides can be derived using equation (9)

$$B(\text{global}) = \frac{x(\text{CaO})B(\text{CaO}) + x(\text{MgO})B(\text{MgO}) + x(\text{MnO})B(\text{MnO})}{x(\text{CaO}) + x(\text{MgO}) + x(\text{MnO})} \quad (9)$$

Assessment of the Viscosity Models. These two models have<sup>(13,18)</sup> been used to calculate the viscosities of slags with widely-varying compositions and it has been found that both give values which agree well with experiment. The model of Urbain gives a slightly better fit than the Riboud model. The discrepancies between the experimental values and the predicted values are of the order of  $\pm 30\%$  which are of similar magnitude to the experimental uncertainties for viscosity measurements.

### Density ( $\rho$ )

Recently Keene<sup>(25)</sup> has reported that the density at 1673K of molten slags can be obtained within  $\pm 5\%$  using the equation(10)

$$\frac{\rho}{\text{gcm}^{-3}} = 2.49 + 0.012 (\% \text{FeO} + \% \text{Fe}_2\text{O}_3 + \% \text{MnO} + \% \text{NiO}) \quad (10)$$

An additive method for the estimation of densities ( $\rho$ ) in slags has been widely used for some time<sup>(26,27)</sup>. In this method, the molar volume,  $V$ , can be obtained from equations (11) and (12) below where  $M$ ,  $x$  and  $\bar{V}$  are the molecular weight, mole fraction and the partial molar volume, respectively, and 1, 2 and 3 denote the various oxide constituents of the slag.

$$V = M_1x_1 + M_2x_2 + M_3x_3 / \rho \quad (11)$$

$$V = x_1\bar{V}_1 + x_2\bar{V}_2 + x_3\bar{V}_3 \quad (12)$$

The partial molar volume is usually assumed to be equal to the molar volume of the pure component ( $V^0$ ). Bottinga and Weill<sup>(28)</sup> produced a series of values of  $\bar{V}$  for various oxides assuming a constant value for  $\bar{V}(\text{SiO}_2)$  and it was claimed that good estimations of the density could be obtained for compositions containing between 40 and 80%  $\text{SiO}_2$ . Two more recent studies<sup>(29)(30)</sup> also concluded that  $\bar{V}(\text{SiO}_2)$  was independent of composition and have revised the  $\bar{V}$  values for the various oxides. However it has been pointed out<sup>(31,32)</sup> that the density of the slag is also related to its structure. Silicate slags contain a mixture of chains, rings and basic silicate units, which are dependent upon the silica concentration and upon the nature of the cations present. Thus the densities of silicate slags estimated using a constant value for  $\bar{V}(\text{SiO}_2)$  will be subject to error as the arrangement of these silicate chains varies with silica concentration.

Furthermore Grau and Masson<sup>(31)</sup> pointed out that for the series,  $\text{MO}$ ,  $\text{M}_2\text{SiO}_4$ ,  $\text{M}_3\text{Si}_2\text{O}_7$ , the partial molar volume of  $\text{SiO}_2$  is not constant. They calculated a  $\Delta\bar{V}$  term for the differences between any two members of the series and in this way, calculated values were derived for the systems  $\text{FeO} + \text{SiO}_2$ ,  $\text{PbO} + \text{SiO}_2$ ,  $\text{FeO} + \text{MnO} + \text{SiO}_2$  and  $\text{FeO} + \text{CaO} + \text{SiO}_2$ , for compositions in the range  $x_{\text{SiO}_2} = 0.5$  to 1.0. However this method is not suitable for calculating densities of multicomponent systems.

Very recently, Bottinga *et al.*<sup>(33)</sup> have presented a model in which the partial molar volumes of alumina-silicate liquids were considered to be composition-dependent.



New Model for Calculating the Densities of Slags. Slags containing  $\text{SiO}_2$ ,  $\text{Al}_2\text{O}_3$  and  $\text{P}_2\text{O}_5$  consist of chains, rings and complexes which are dependent upon the amount and nature of the cations present. Thus it is necessary to make the partial molar volumes dependent upon composition for oxides of this type. If in a binary system, equation (12) were applicable and if  $\bar{V}_i = V_1^0$  i.e.  $\bar{V}$  is independent of composition, then the curve of  $V$  as a function of composition will be that shown by the solid line in Figure 1a and the two  $x_i\bar{V}_i$  contributions by the dotted lines. If we now consider a binary silicate system the molar volume ( $V$ ) would have the form shown as a solid line in Figure 1b. It is reasonable to assume that  $V(M_yO)$  is independent of composition and would have the form of  $x_1\bar{V}_1$  in Figure 1b. The parameter  $x_2\bar{V}_2$  can be derived for  $\text{SiO}_2$  by use of equation (13) below.

$$x_2\bar{V}_2 = V - x_1\bar{V}_1 \quad (13)$$

Thus  $x_2\bar{V}_2$  will have the form of the curve shown in Figure 1b.

It is possible to derive  $x\bar{V}$  for  $\text{SiO}_2$  in ternary and quaternary slags by using equation (14). Values for  $x\bar{V}$  ( $\text{SiO}_2$ ) have been derived using experimental density data for the systems,  $\text{FeO} + \text{SiO}_2$ ,  $\text{CaO} + \text{SiO}_2$ ,  $\text{MnO} + \text{SiO}_2$ ,  $\text{Na}_2\text{O} + \text{SiO}_2$ ,  $\text{K}_2\text{O} + \text{SiO}_2$  and  $\text{CaO} + \text{FeO} + \text{SiO}_2$  and are plotted against  $x(\text{SiO}_2)$  in Figure 2. It can be seen from this figure that there is excellent agreement between the  $x\bar{V}(\text{SiO}_2)$  calculated from different sources, with the exception of that for the  $\text{MnO} + \text{SiO}_2$  system. However the reliability of the experimental data for this system, have been questioned previously. From this curve for  $x\bar{V}(\text{SiO}_2)$  we can derive the relationship,  $\bar{V}(\text{SiO}_2) = 19.55 + 7.966.x(\text{SiO}_2)$ . The recommended values for  $\bar{V}$  for the various oxides at 1500 °C are given in Table II.

$$x\bar{V}(\text{SiO}_2) = V - x_1\bar{V}_1 - x_2\bar{V}_2 - x_3\bar{V}_3 \quad (14)$$

Values for  $x\bar{V}$  ( $\text{Al}_2\text{O}_3$ ) were determined in a similar manner by using experimental density data for the systems,  $\text{CaO} + \text{Al}_2\text{O}_3$ ,  $\text{CaF}_2 + \text{Al}_2\text{O}_3$ ,  $\text{SiO}_2 + \text{Al}_2\text{O}_3$ ,  $\text{MgO} + \text{CaO} + \text{Al}_2\text{O}_3$  and  $\text{MnO} + \text{SiO}_2 + \text{Al}_2\text{O}_3$ . The  $x\bar{V}$  ( $\text{Al}_2\text{O}_3$ ) results are plotted in Figure 3 and the relationship  $\bar{V}(\text{Al}_2\text{O}_3) = 28.31 + 32 x(\text{Al}_2\text{O}_3) - 31.45 x^2(\text{Al}_2\text{O}_3)$  was derived from this curve.

There are few experimental data for the density of phosphate slags but  $x\bar{V}(\text{P}_2\text{O}_5)$  values were derived from data for the systems  $\text{CaO} + \text{FeO} + \text{P}_2\text{O}_5$  and  $\text{Na}_2\text{O} + \text{P}_2\text{O}_5$ . A constant value of  $\bar{V} = 65.7 \text{ cm}^3 \text{ mol}^{-1}$  was obtained from the selected linear relationship.

In order to provide a temperature coefficient, the temperature dependencies of the molar volumes ( $dV/dT$ ) of many slag systems were examined and a mean value of  $0.01\% \text{ K}^{-1}$  was adopted.

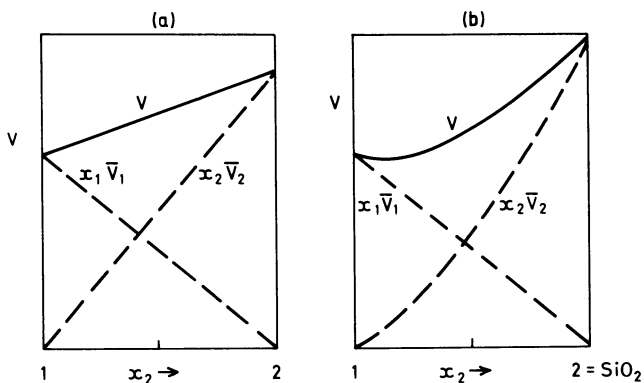


Figure 1 The molar volume of binary slag systems as a function of composition showing the individual  $x_i \bar{V}_i$  contributions.

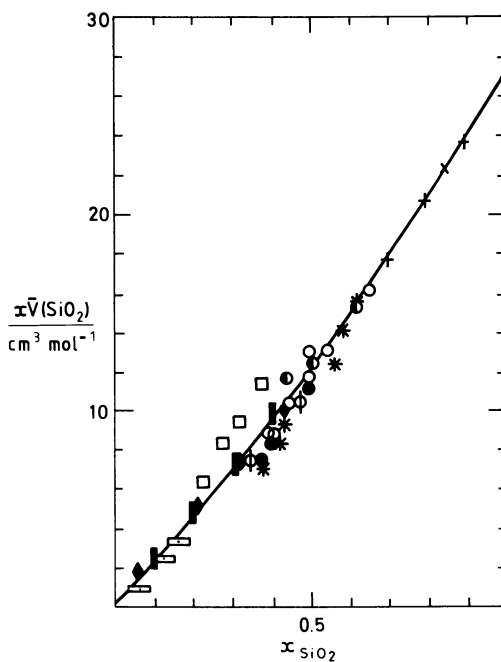


Figure 2  $x\bar{V}(\text{SiO}_2)$  as a function of  $x(\text{SiO}_2)$

Table II. Recommended values for the partial molar volumes,  $\bar{V}$ , of various slag constituents at 1500 °C

SiO <sub>2</sub>	19.55 + 7.966 x(SiO <sub>2</sub> )	FeO	15.8		
Al <sub>2</sub> O <sub>3</sub>	28.31 + 32 x(Al <sub>2</sub> O <sub>3</sub> )-31.45 x <sup>2</sup> (Al <sub>2</sub> O <sub>3</sub> )	Fe <sub>2</sub> O <sub>3</sub>	38.4	CaF <sub>2</sub>	31.3
CaO	20.7	MnO	15.6	P <sub>2</sub> O <sub>5</sub>	65.7
MgO	16.1	Na <sub>2</sub> O	33	TiO <sub>2</sub>	24

Units of  $\bar{V}$  = cm<sup>3</sup> mol<sup>-1</sup> = 10<sup>-6</sup> m<sup>3</sup> mol<sup>-1</sup>

Assessment of density models. An analysis of the uncertainties associated with the estimation of densities with this model has not yet been completed. However on the basis of those values obtained so far the standard deviation of the factor  $(\rho_{est} - \rho_{expt} / \rho_{expt})$  is between 1 and 2% and less than that recorded using the method due to Bottinga et al (33). The experimental uncertainties associated with density measurements for slags are ca.  $\pm$  2%.

### Surface Tension ( $\gamma$ )

Methods for estimating the surface tension of slags based on the addition of the partial molar contributions ( $\bar{\gamma}$ ) of the individual constituents have been reported by Appen (34) by Boni and Derge (35) and by Popel (36). All these methods make use of equation (15) where 1, 2, 3 etc denote the various slag constituents.

$$\gamma = x_1 \bar{\gamma}_1 + x_2 \bar{\gamma}_2 + x_3 \bar{\gamma}_3 + \dots \quad (15)$$

Values of  $\bar{\gamma}_1$  are often taken to be the surface tension of the pure components,  $\bar{\gamma}^\circ$ , and have also been obtained by iterative procedures. Figure 4a shows a typical plot of  $\gamma$  as a function of  $x$  for a binary slag and the individual  $x_1 \bar{\gamma}_1$  contributions have also been included. These methods work well for certain slag mixtures but break down when surface-active constituents, such as P<sub>2</sub>O<sub>5</sub>, are present. These components migrate preferentially to the surface and cause a sharp decrease in the surface tension and consequently only very small concentrations are required to cause an appreciable decrease in  $\gamma$ . Thus some unreported or undetected impurity could have a marked effect on the surface tension of the slag and thereby produce an apparent error in the value estimated by the model. In this respect surface tension differs from all the other physical properties which are essentially bulk properties.

New Model for Calculating the Surface Tension of Slags. Figure 4a shows the surface tension of two slag constituents which are not surface active. For a binary mixture with one surface active component the surface tension-composition relationship will have the form of that shown in Figure 4b where 2 denotes the surface-active constituent. If we assume that  $x\bar{\gamma}$  for component 1 is unaffected, then the term  $\bar{\gamma}_2 x_2$ , the partial molar contribution of the surface

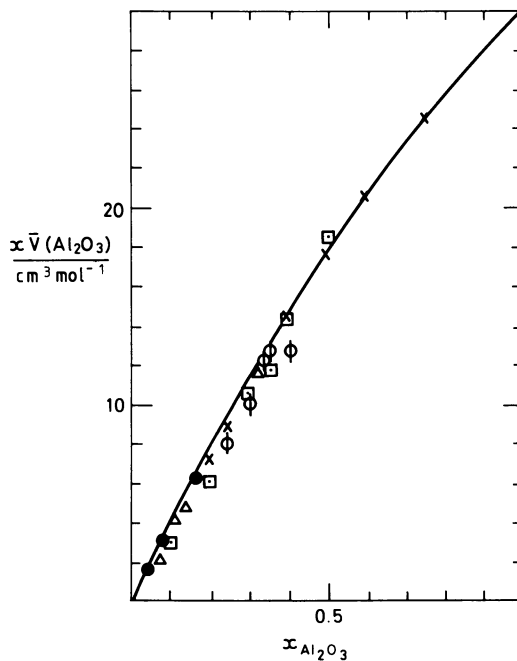


Figure 3  $x\bar{V}(\text{Al}_2\text{O}_3)$  as a function of  $x(\text{Al}_2\text{O}_3)$

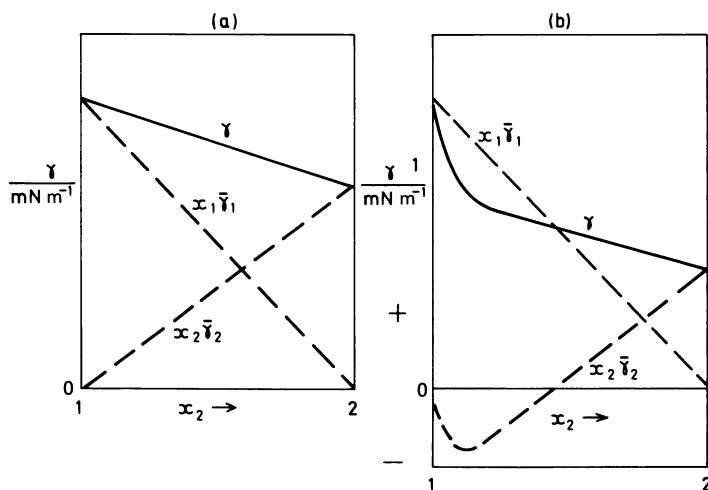


Figure 4 The composition dependence of  $\gamma$ ,  $x_1\bar{V}_1$ , and  $x_2\bar{V}_2$  for binary slag systems with (a) non-surface-active constituents and (b) one surface-active constituent.

active material, can be calculated by equation (16) below. The term  $(x_2\bar{\gamma}_2)$  can similarly be calculated for ternary and quaternary systems providing there is only one surface active component.

$$x_2\bar{\gamma}_2 = \gamma - x_1\bar{\gamma}_1 \tag{16}$$

The compositional dependence of the  $(x_2\bar{\gamma}_2)$  term is shown in Figure 4b and it should be noted that as  $x_2 \rightarrow 1$  then  $x_2\bar{\gamma}_2 \rightarrow \gamma_2^0$ . Values of  $(x\bar{\gamma})$  for various surface active materials derived from experimental surface tension data are shown in Figure 5. It is possible to deal with the compositional dependence of these  $(x\bar{\gamma})$  values by considering two curves viz. one operating up to the point N and the other representing values of x where  $x > N$ . The partial surface tension for non-surface active constituents is shown in Table III and the equations for calculating  $\bar{\gamma}$  for surface active components and values of N are given in Table IV. There is a considerable discrepancy in the relationships between  $x_2\bar{\gamma}_2$  and  $x_2\gamma_2$  for  $B_2O_3$  obtained from experimental data on two different systems, and a mean value has been adopted until further data become available.

Table III. Partial molar surface tension,  $\bar{\gamma}$ , at 1500 °C for different slag constituents

Oxide	SiO <sub>2</sub>	CaO	Al <sub>2</sub> O <sub>3</sub>	MgO	FeO	MnO	TiO <sub>2</sub>
$\bar{\gamma}/mNm^{-1}$	260	625	655	635	645	645	360

Table IV. Values of  $x\bar{\gamma}$  at 1500 °C for surface-active constituents

Slag Constituent	$x_1\bar{\gamma}_1$ for $x < N$	N	$x_1\bar{\gamma}_1$ for $x > N$
Fe <sub>2</sub> O <sub>3</sub>	-3.7 - 2972 x + 14312 x <sup>2</sup>	0.125	-216.2 + 516.2 x
Na <sub>2</sub> O	0.8 - 1388 x - 6723 x <sup>2</sup>	0.115	-115.9 + 412.9 x
K <sub>2</sub> O	0.8 - 1388 x - 6723 x <sup>2</sup>	0.115	- 94.5 + 254.5 x
P <sub>2</sub> O <sub>5</sub>	-5.2 - 3454 x + 22178 x <sup>2</sup>	0.12	-142.5 + 167.5 x
B <sub>2</sub> O <sub>3</sub>	-5.2 - 3454 x + 22178 x <sup>2</sup>	0.10	-155.3 + 265.3 x
Cr <sub>2</sub> O <sub>3</sub>	- 1248 x + 8735 x <sup>2</sup>	0.05	- 84.2 + 884.2 x
CaF <sub>2</sub>	-2 - 934 x + 4769 x <sup>2</sup>	0.13	- 92.5 + 382.5 x
S	-0.8 - 3540 x + 55220 x <sup>2</sup>	0.04	- 70.8 + 420.8 x

The reported values of  $(d\bar{\gamma}/dT)$  for various slag systems were examined and a mean value of  $-0.15 mN m^{-1} K^{-1}$  was applied as a temperature coefficient.

Assessment of the Model. The standard deviation of the factor  $((\bar{\gamma}_{est} - \bar{\gamma}_{expt})/\bar{\gamma}_{expt})$  was ca. + 10%. Undoubtedly, much of the uncertainty arises from experimental errors, where the effect of unreported surface active impurities and the nature of the gaseous atmosphere could have a marked effect on the value of surface tension. Another major source of error is the amount of Fe<sub>2</sub>O<sub>3</sub> present in the slag, and this investigation has shown clearly that Fe<sub>2</sub>O<sub>3</sub> is very surface active. Few investigators report the  $(Fe^{3+}/Fe^{2+})$  ratio which is dependent upon, (i) P<sub>2</sub>O<sub>5</sub>, (ii) T<sub>1</sub> and (iii) the

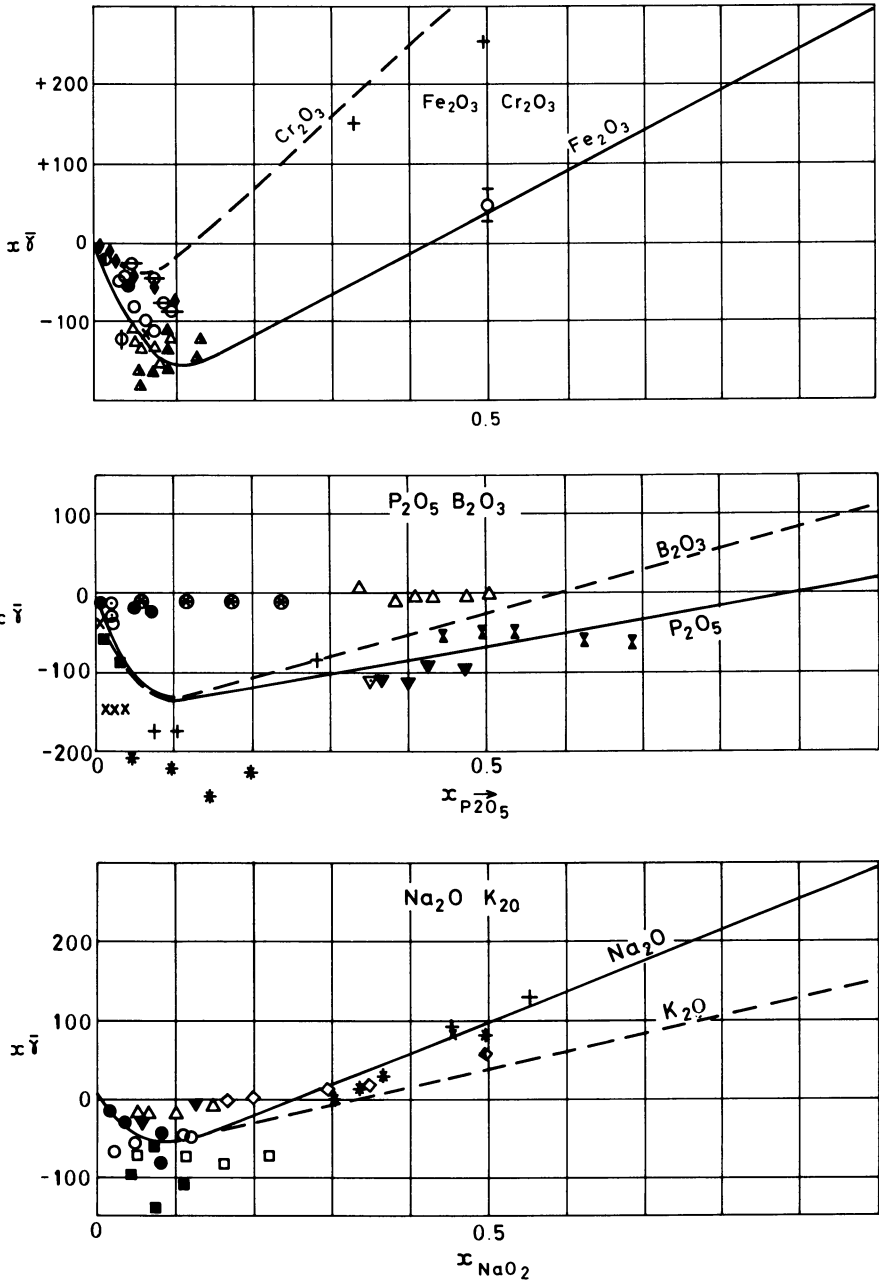


Figure 5 The compositional dependence of  $x_1\bar{\gamma}_1$ , for various surface active constituents.

nature and amount of other oxides present so even, when quoted, the ratio may be in error. Thus, if a decrease in  $\bar{Y}$  is recorded when  $\text{Na}_2\text{O}$  is added to the slag, it is questionable whether this decrease is due to an increase in  $\text{Fe}_2\text{O}_3$  content or to the surface activity of the  $\text{Na}_2\text{O}$ . In this investigation, attempts were made to adjust  $\bar{Y}$  for an increase in  $\text{Fe}_2\text{O}_3$  content but the effect of basic oxides on the ratio is not well documented and some error may result.

A major unresolved problem concerns the situation where the slag contains more than one surface active component. It is possible that there is some competition for sites on the surface and hence the decrease in  $\bar{Y}$  would not be as sharp as that calculated from the summation of  $(x_A \bar{Y}_A + x_B \bar{Y}_B)$  where A and B denote surface active constituents. In this case, the model may overestimate the decrease in  $\bar{Y}$ . There are no extant data to confirm this possibility, and  $(\text{Na}_2\text{O} + \text{K}_2\text{O})$  has been included as a single contribution in the model.

### Thermal Properties

The computations of the thermal losses in the converter by conductive and radiative processes require knowledge of the following thermal properties, heat capacity, enthalpy, thermal conductivity, absorption coefficient and emissivity.

### Heat Capacity $C_p$ and Enthalpy $(H_T - H_{298})$

When a silicate liquid is cooled the structure of the solid formed is dependent upon the cooling rate and the thermal history of the sample. Consider a liquid at a temperature corresponding to the point C in Figure 6, a rapid quench will produce a glass and the enthalpy evolved will follow the path CLGA. By contrast, a very slow cooling rate will result in the formation of a crystalline slag, the enthalpy evolution following the path CL DB. It will be noted from Figure 6 that  $(H_T - H_{298})_{\text{cryst}} = (H_T - H_{298})_{\text{glass}} + \Delta H^{\text{vit}}$ , where  $\Delta H^{\text{vit}}$  is the enthalpy of the endothermic transformation of crystal  $\rightarrow$  glass). The  $C_p$  values for the various phases can be summarized as:

$$C_p(\text{crystal}) = C_p(\text{glass}) < C_p(\text{supercooled liquid}) = C_p(\text{liquid})$$

It can be seen from Figure 6 that at the glass temperature ( $T_{g1}$ ) there is a sudden increase in  $C_p$  ( $\Delta C_p^{gl}$ ) as the glass transforms into a supercooled liquid. Drop calorimetry studies on the glass phase at temperatures between  $T_{g1}$  and  $T_{liq}$  will produce progressively more crystallization as  $T_{liq}$  is approached and consequently the  $(H_T - H_{298}) - T$  relationship will be similar to that depicted by the dots in Figure 6 and not the path, AGLC; the magnitude of the apparent enthalpy of fusion ( $\Delta H^{\text{fus}}$ ) will be dependent upon the fraction of the sample crystallized during annealing at temperatures between  $T_{g1}$  and  $T_{liq}$ . The  $C_p$  values for the liquid and supercooled liquids have been reported to be constant and independent of temperature (37). It follows from the triangle GEL in Figure 6 that  $C_p^{gl}(T_{liq} - T_{g1}) = \Delta H^{\text{fus}}$ . Thus, it is possible to estimate the enthalpy of a slag with a glassy structure from estimates of  $C_p(\text{glass})$ ,  $C_p(\text{liq})$  and  $T_{g1}$ . However the estimation of  $T_{g1}$  is

difficult as it can vary between 700 and 1100 K and the various estimation rules suggested are known to be prone to appreciable errors(38). Inspection of literature data(38,39) indicates that the glass transformation occurs when  $C_p$  attains a value of ca.  $1.1 \text{ J K}^{-1}\text{g}^{-1}$ ; this rule has been used in the development of the following model for the estimation of  $(H_T - H_{298})$  and  $C_p$  of slags with a glassy structure.

The  $C_p$  for glass liquid and supercooled liquid phases can be estimated from the slag composition using partial molar heat capacities ( $\bar{C}_p$ ) as shown in equation (17)

$$C_p = x_1 \bar{C}_{p1} + x_2 \bar{C}_{p2} + x_3 \bar{C}_{p3} + x_4 \bar{C}_{p4} + \dots \quad (17)$$

For most materials the temperature dependence of  $C_p$  is usually expressed in the form given by equation (18) where a, b and c are constants

$$C_p = a + bT - cT^{-2} \quad (18)$$

The enthalpy at T relative to 298K (25 °C) is obtained from equation (19) for the glass phase

$$(H_T - H_{298}) = \int_{298}^T C_p dT = a(T-298) + \frac{b}{2}(T^2-298^2) + \frac{c}{T} - \frac{c}{298} \quad (19)$$

Values of a, b and c for the various slag components are given in Table V and it should be noted that the  $P_2O_5$  and S in the slag were calculated as  $CaP_2O_6$  and  $CaSO_4$ , respectively. The amount of CaO used in the calculation of  $x\bar{C}_p$  (CaO) should be adjusted using the relationship  $x(\text{CaO}) = x(\text{CaO, total}) - x(P_2O_5) - x(S)$  to account for the CaO in  $CaP_2O_6$  and  $CaSO_4$ . The model also takes into account the presence of free iron in the slag.

Carmichael et al. (40) have reported  $\bar{C}_p$  values for liquid slags and these values (given in Table V) have been adopted except in the case of  $Al_2O_3$  and  $Fe_2O_3$  where other values have been preferred. These values for  $C_p$  for the liquid phase have also been extended to the temperature range between  $T_{g1}$  and  $T_{sol}$  where a supercooled liquid could be formed.

Thus  $(H_T - H_{298})$  values for a liquid slag at temperature T can be estimated by determining  $T_{g1}$  (ie temperature at which  $C_p = 1.1 \text{ J K}^{-1} \text{ g}^{-1}$ ) and calculating  $(H_{T_{g1}} - H_{298})$  from equation(19) and  $(H_T - H_{T_{g1}})$  from  $C_p(\text{liq}) \cdot (T - T_{g1})$ .

Values of  $\bar{C}_p(\text{glass})$  obtained with this model lie within 2% of the experimental values and the  $\Delta C_p(\text{liq})$  values also appear to agree with experimental data; values of  $C_p^{gl}$  at  $T_{g1}$  calculated using the model lie within the range of experimental values(38,39) of 0.15 to 0.30  $\text{J K}^{-1} \text{ g}^{-1}$ . One major uncertainty would appear to lie in the calculation of  $T_{g1}$ , however it can be shown that an error in  $T_{g1}$  of 100 K would only produce an error of ca. 1% in the value of



Table V

Slag Compo- nent	M	$C_p(\text{cryst})/\text{calK}^{-1}\text{mol}^{-1} = a+bT -c/T^2$			$\bar{C}_p(\text{liq})$
		a	$b \cdot 10^3$	$c \cdot 10^{-5}$	$\text{cal K}^{-1}\text{mol}^{-1}$
SiO <sub>2</sub>	60.09	13.38	3.68	3.45	20.79
CaO	56.08	11.67	1.08	1.56	19.3
Al <sub>2</sub> O <sub>3</sub>	101.96	27.49	2.82	8.4	35
MgO	40.31	10.18	1.78	1.48	21.6
K <sub>2</sub> O	94.2	15.7	5.4	0	17.7
Na <sub>2</sub> O	61.98	15.7	5.4	0	22
TiO <sub>2</sub>	79.9	17.97	0.28	4.35	26.7
MnO	70.94	11.11	1.94	0.88	19.1
FeO	71.85	11.66	2.0	0.67	18.3
Fe <sub>2</sub> O <sub>3</sub>	159.7	23.49	18.6	3.55	45.7
Fe	55.85	3.04	7.58	-0.6	10.5
P <sub>2</sub> O <sub>5</sub>	141.91	43.63	11.1	10.86	58
CaF <sub>2</sub>	78.08	14.3	7.28	-0.47	23
SO <sub>3</sub>	80.06	16.78	23.6	0	42

1 cal = 4.184 J; T in K

(H<sub>1900</sub> - H<sub>298</sub>) for the slag. The most serious source of error would thus appear to arise through crystallization of the sample during quenching, as few data are available for  $\Delta H_{\text{vit}}$ , the magnitude of errors arising from this source have not been evaluated.

Values of  $C_p$  and enthalpy estimated by this model have been checked recently<sup>(41)</sup> against experimental values for a coal slag and it can be seen from Figure 7 that estimated values lie within 2% of the experimental results and that the enthalpy varies with temperature as predicted in Figure 6. Enthalpies estimated for liquid coal slags and ashes with the aid of this model were always found to lie within 5% of the experimental values. However it should be noted that the experimental enthalpy values obtained in the temperature range between  $T_{\text{gl}}$  and  $T_{\text{sol}}$  have little significance since these refer to samples with different and undefined crystallinities.

### Heat Transfer in Slags

Heat is transferred through slags by a variety of mechanisms which include convection, radiation and various thermal conduction processes, viz. thermal ("phonon") conductivity, ( $k_c$ ), electronic conductivity ( $k_{e1}$ ) and radiation conductivity ( $k_R$ ). Methods for estimating the various physical properties involved in these processes are considered below.

### Thermal Conductivity (k)

Heat is transferred by phonons which are quanta of energy associated with each mode of vibration in the sample. Scattering of the phonons causes a decrease in the thermal conductivity and thus the conductivity ( $k_c$ ) is sensitive to the structure of the slag and

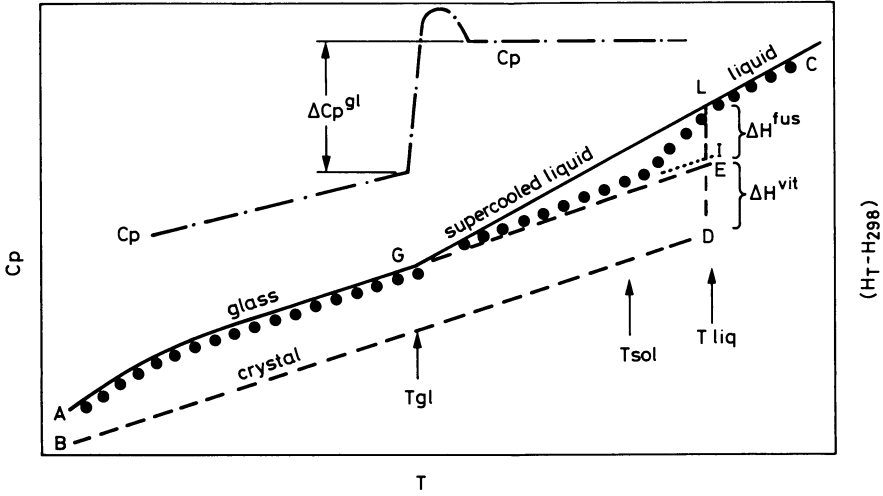


Figure 6  $C_p$  and enthalpy data for glassy and crystalline phases of a slag; ● ● indicates typical drop calorimetry results.

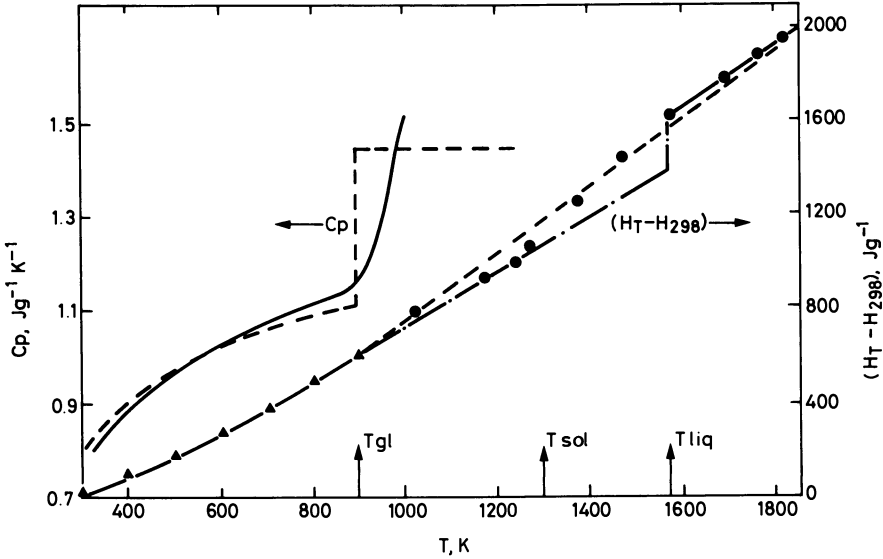


Figure 7  $C_p$  and enthalpy results for a slag; — experimental values; ▲, D.S.C. results; ●, drop calorimetry results; - - -, estimated values; - . . ., values extrapolated from glass phase.

consequently those factors affecting structure such as the basicity. Despite this structure dependence, estimation rules based on the additivity principle (equation (20)) have been proposed<sup>(42,43)</sup>.

$$k = (\%i)k_i + (\%j)k_j + \dots \quad (20)$$

Other models have been developed which relate  $k$  to the volume concentration of the oxides in the glass<sup>(44)</sup> and a third approach<sup>(45)</sup> relates the thermal resistance ( $1/k_c$ ) to  $x_i m_i$  where  $m_i$  is the effectiveness of the modifier of component  $i$  in scattering phonons.

However in coal slags there is frequently an appreciable degree of crystallization and the thermal conductivity value varies with the thermal history of the sample<sup>(41,46)</sup>, so that rules developed for glasses may not be appropriate to coal slags. Recent work carried out on a large number of silicate slags<sup>(47)</sup> indicated that the thermal diffusivity,  $a$ , ( $a = k/C_p \cdot \rho$ ) of various slags was independent of both composition and temperature in the range (500-1300 K) with  $a(\text{glass}) = 4.5(+0.5) \times 10^{-7} \text{ m}^2\text{s}^{-1}$ ;  $a(\text{cryst}) = 6 \times 10^{-7} \text{ m}^2\text{s}^{-1}$  and  $a(\text{liq}) \approx a(\text{glass})$ . These data are consistent with values reported for coal slags<sup>(41,46)</sup> and steelmaking slags<sup>(48)</sup>. However, the values reported by Nauman et al<sup>(49)</sup> indicate that at high FeO contents (>20%) both  $k$  and  $a$  increase with increasing FeO content ( $k = 0.8 + 1.7 \times 10^{-2} (\% \text{ FeO}) \text{ Wm}^{-1}\text{K}^{-1}$ ).

#### Absorption Coefficient ( $\alpha$ )

Radiation conductivity ( $k_R$ ) can be the predominant mode of heat transfer through semi-transport media like glasses and the magnitude of  $k_R$  is determined largely by the optical properties such as the absorption coefficient ( $\alpha$ ) and the refractive index ( $n$ ). The value of  $k_R$  increases as the slag thickness ( $d$ ) is increased until a critical point is attained, above which  $k_R$  remains constant and independent of thickness. The slag is then said to be "optically thick" and this condition applies when  $\alpha d > 3.5$  and values of  $k_R$  can be calculated using equation (21), where  $\sigma$  is the Stefan-Boltzmann constant. In recent years formulae have been

$$k_R = \frac{16 n^2 T^3 \sigma}{3 \alpha} \quad (21)$$

proposed for the calculation of  $k_R$  for optically thin conditions. The absorption coefficient ( $\alpha$ ) is markedly dependent upon the amounts of  $\text{Fe}^{2+}$  and  $\text{Mn}^{2+}$  present in the slags<sup>(50)</sup>; at levels of  $\text{FeO} \leq 5\%$  the following relationship can be supplied,  $\alpha(\text{cm}^{-1}) = 11(\% \text{ FeO})$ . Temperature appears to have little effect on the absorption coefficient of glasses but the absorption of magmas have been reported to increase with increasing temperature<sup>(51,52)</sup>. Crystallization of the slag will result in a large increase in the absorption (or extinction) coefficient which could reduce  $k_R$  to virtually zero.

Emissivity ( $\epsilon$ )

The emissivity ( $\epsilon$ ) of a semi-transparent medium is a bulk property in contrast to  $\epsilon$  (metal) which is solely dependent upon the surface. On the basis of the spectral and total normal emissivity data reported for coal and metallurgical slags, the value  $\epsilon = 0.8 \pm 0.1$  can be adopted for coal slags in the range (1100 - 1900 K).

## CONCLUSIONS

- 1) Estimation procedures based on the chemical composition of the slag have now been developed for the prediction of viscosity, surface tension, density and heat capacity.
- 2) The accuracy of these estimation routines for some physical properties (eg. viscosity, surface tension) can be improved when more reliable experimental data become available.
- 3) The distribution of iron in the slag between Fe, FeO and Fe<sub>2</sub>O<sub>3</sub> has a pronounced effect on virtually all the physical properties and it is recommended that experimental data for the properties of the slag should always be accompanied by values for the distribution of iron.
- 4) The development of models for the prediction of some physical properties (thermal conductivities, absorption coefficient) is restricted by the limited amount of experimental data available.

## REFERENCES

- 1) DARKEN, L. S; and GURRY, R. W. J. Am. Chem. Soc. 1946, 68, 798.
- 2) LARSON, H.; CHIPMAN, J. J. Metals, 1953, Sept., 1089.
- 3) BANYA, S.; SHIM, J. D. Canad. Metall. Q., 1982, 21, 319.
- 4) SONDRAL, E. A.; ELLMAN, R. C. Fusibility of ash from lignite and its correlation with ash composition. US Energy Res. and Develop. Admin. GFERC/RI-75-1, Pittsburgh, 1975.
- 5) WINEGARTNER, E. C.; RHODES, B. T. J. Eng. Power, 1975, 97, 395.
- 6) BRYERS, R. W.; TAYLOR, T. E. J. Eng. Power, 1976, 98, 528.
- 7) STEILER, J. M. Commission of the European Communities Research Contract, 7210 CA/3/3/03. Thermodynamic data for steelmaking. 1981, Eur N7820, BP 1003, Luxembourg 1982.
- 8) GAYE, H. Ironmaking and Steelmaking, 1984, 11, 67.
- 9) GAYE, H. Proc. Metallurgical Conference, Centenary of Teaching of Metallurgy, held at Strathclyde University, 25/26 June 1984.

- 10) OCHOTIN, M. W. Steklo Keram., 1954, 11, 7.
- 11) LYON, K. C. J. Res. Natl. Bur Stand., 1974, 78, 497.
- 12) McCAULEY, W. D. and APELIAN, D. Canad. Metall. Quart., 1981, 20, 247.
- 13) RIBOUD, P. V.; ROUX, Y; LUCAS, L. D.; GAYE, H. Fachber. Huttenpraxis Metalweiterverarb., 1981, 19, 859.
- 14) MAIRY, B. Private communication, Centre Recherches Metallurgique, Liege, Belgium.
- 15) BOTTINGA, Y.; WEILL, D. F. Am. J. Sci., 1972, 272, 438.
- 16) SHAW, H. Am. J. Sci., 1972, 272, 870.
- 17) URBAIN, G.; CAMBIER, F.; DELETTER, M.; ANSEAU, M. R. Trans. J. Brit. Ceram. Soc., 1981, 80, 139.
- 18) URBAIN, G. private communication, CNRS, Laboratoire de Ultras-Refractaires, Odeillo, France, Jan. 1983.
- 19) WATT, J. D.; FEREDAY, D. J. Instr. Fuel, 1969, 338, 99.
- 20) BOKAMP, Inst. of Gas Technol. Preparation of a coal conversion systems Technical data Book. Energy Res. and Dev. Admin. Report Fe-1730-21 (1976).
- 21) CAPPS, W.; KAUFFMAN, D. Natl. Bur. Stand. Quart. Prog. Report. to Office of Coal Res., Dept. Interior, 30/9/74.
- 22) SCHOBERT, H. H. Div. Fuel Chem. Prep., 1977, 22, 143.
- 23) SCHOBERT, H. H.; WITTHOEFFT, C. Fuel Proc. Technol., 1981, 5, 157.
- 24) HENSLEE, S.P.; KELSEY, P. V. Jr. US Dept. of Energy Report, EGG-FM-6049, Sept. 1982.
- 25) KEENE, B. J. National Physical Laboratory Report, DMA(D)75, Feb. 1984.
- 26) MOREY, G. H. "Properties of Glasses", Reinhold, New York, 1954, p 217.
- 27) HUGGINS, M L; SUN, K. H. J. Am. Ceram. Soc. 1948, 26, 4.
- 28) BOTTINGA, H.; WEILL, D. E. Am. J. Sci., 1972, 272, 438.
- 29) NELSON, S. A.; CARMICHAEL, I.S.E. Contrib. Mineral Petrol. 1979, 71, 117.

- 30) MO, Y.; CARMICHAEL, I.S.E.; RIVERS, M.; STEBBINS, J.; Mineralog. Mag., 1982, 45, 237.
- 31) GRAU, A.E.; MASSON, C. R. Canad. Metall. Quart., 1976, 15, 367.
- 32) LEE, Y. E., GASKELL, D. R. Metall. Trans., 1974, 5, 853.
- 33) BOTTINGA, Y.; WEILL, D. E.; RICHEL, P. Geochim Cosmochim. Acta. 1982, 46, 909.
- 34) APPEN, A. A.; SHISHKOV, K. A.; KAYALOVA, S. S. Zhur. Fiz. Khim. 1952, 26, 1131.
- 35) BONI, R. E.; DERGE, G. J. Metals, 1956, 8, 53.
- 36) POPEL, S. E. "Metallurgy of slags and their use in building." 1962, p 67.
- 37) RICHEL, P.; BOTTINGA, Y. Geochim, Cosmochim Acta, 1984, 44, 1533.
- 38) BACON, C. R. Am. J. Sci., 1977, 277, 109.
- 39) MOYNIHAN, C. T.; EASTEAL, S; A. J.; TRAN, D. C.; WILDER, J. A., DONOVAN, E. P. J. Am. Ceram. Soc., 1976, 59, 137.
- 40) CARMICHAEL, I. S. E.; NICHOLLS, J.; SPERA, F. J.; WOOD, B. J.; NELSON, S. A. Phil. Trans. Roy. Soc. (London), 1977, A286, 373.
- 41) RHINES, J. R.; MILLS, K. C.; PUTLAND, F. H. High Temp-High Pressure in press.
- 42) MOREY, G. W. "Properties of Glass," Reinhold, New York, 1954, p 217.
- 43) ABAKOVA, I. G.; SERGEEV, O. A. "Thermophysical properties of glasses." Proc. of Metrological Inst. of USSR, No. 129 (189), Moscow-Leningrad, 1971, p 13.
- 44) MISNAR, A. "Thermal conductivity of solid, gases and composite materials." Leningrad, 1968.
- 45) VAVILOU, Y. V.; KOMAROV, V. E.; TABUNOVA, W. A. Phys. Chem. Glasses, 1982, 8, 472.
- 46) GIBBY, R. L.; BATES, J. L. Proc. 10th Thermal Conductivity Conf. held Newton, Mass. Sept. 1970, p IV-7,8.
- 47) RHINES, J. R.; MILLS, K. C. unpublished work, 1984.
- 48) FINE, H. A.; ENGH, T.; ELLIOTT, J. F. Metal. Trans. B. 1976, 7B, 277.

- 49) NAUMAN, J.; FOO, G.; ELLIOTT, J. F. "Extractive Metallurgy of Copper." Chapter 12, p 237.
- 50) STEELE, F. N.; DOUGLAS, R. W. Phys. Chem. Glasses, 1965, 6, 246.
- 51) FUKAO, Y.; MITZUTANI, H.; UYEDA, S. Phys. Earth Planet Interiors, 168, 1, 57.
- 52) ARONSON, J. R.; BELLOTI, L. H.; ECKROAD, S. W.; EMSLIE, A. G.; McCONNEL, R. K.; THUNA, P. C.; von. J. Geophys. Res., 1970, 75, 3443.

RECEIVED June 17, 1985

## Viscosity of Fluxes for the Continuous Casting of Steel

W. L. McCauley and D. Apelian

Materials Engineering, Drexel University, Philadelphia, PA 19104

The effects of composition and temperature on the viscosity of oxide melts suitable for use as casting fluxes is discussed. A relation to express the temperature dependence of viscosity for oxide melts based on the Clausius-Clapeyron Equation is evaluated, viz.,  $\ln \eta = C_1 + C_2/T + C_3 \ln T$ . This relation produces a better description of the temperature dependence of fused oxides than the more familiar Arrhenius equation.

Mold fluxes are routinely used in both continuous casting and bottom pouring of steel. These fluxes are generally calcium silicate based compositions with alkali oxides [(Li, Na, K)<sub>2</sub>O] and fluorides [CaF<sub>2</sub>, NaF] added as fluidizers. The compositions frequently use fly ash as the base material because it provides a significant concentration of silica in a prefused form easily dissolved as the powder melts on the liquid steel.

A variety of properties of the flux must be controlled, including fusion characteristics (fusion temperature range and sintering characteristics), insulation characteristics, flow properties of the powder, viscosity of the molten flux, and non-metallic absorption ability. The viscosity influences the consumption rate of flux, heat transfer in the mold, and non-metallic dissolution rate, and has been the subject of published and unpublished work over the last ten years.

In this paper, recent work on the viscosity of mold flux compositions is reviewed, and a relation to describe the temperature dependence of viscosity is discussed. This relation is based on the Clausius-Clapeyron Equation and was originally developed by Kirchoff and Rankine to describe the temperature dependence of vapor pressure.

### Previous Work

Several recent publications have discussed the effects of compositional variables on the viscosity of oxide melts for use as mold fluxes. Lanyi (1) measured the viscosity of several continuous casting fluxes and found that the viscosity correlated well with the combined silica and alumina content of the flux. The fluxes



evaluated contained 30 to 55%  $\text{SiO}_2 + \text{Al}_2\text{O}_3$ , 20 to 45%  $\text{CaO} + \text{MgO}$ , 0 to 8%  $\text{FeO}$ , 15 to 35%  $\text{R}_2\text{O} + \text{F}$ , and 0 to 5%  $\text{B}_2\text{O}_3$ . The viscosity at  $1300^\circ\text{C}$  ranged from 0.06 to 3.2 Pa·s. Lanyi was also able to correlate the activation energy for viscous flow in the Arrhenius Equation with the flux basicity ratio and viscosity.

McCauley and Apelian (2) measured the viscosity of mixtures containing only  $\text{SiO}_2$ ,  $\text{Al}_2\text{O}_3$ ,  $\text{CaO}$ ,  $\text{Na}_2\text{O}$ , and  $\text{CaF}_2$ , in an attempt to isolate the effects of glass network modifiers and network breakers in mold flux type compositions. Viscosity at  $1300^\circ\text{C}$  ranged from 0.1 to 2.8 Pa·s. Their results showed that the flux viscosity could be expressed as a quadratic function of the ratio of network forming cations (silicon and aluminum) to anions (oxygen and fluorine).

Riboud, et al. (3) examined a slightly broader range of controlled chemistries than McCauley and Apelian as well as several industrial fluxes similar to those used by Lanyi. Riboud used the Frenkel relation

$$\eta = A T \exp(B/T) \quad (1)$$

to describe both the compositional and temperature effects on viscosity,  $\eta$ . In Equation 1, the viscosity parameters, A and B, are expressed in terms of the compositional values. This relation yields a predicted viscosity within 20% of the measured values over a wide composition range.

Nichols (4) measured the viscosity of several bottom pouring flux compositions. These fluxes contained only 5 to 20% alkali oxides and fluorides and 50 to 70%  $\text{SiO}_2 + \text{Al}_2\text{O}_3$ . Viscosity ranged from 5 to 80 Pa·s at  $1500^\circ\text{C}$ , much higher than continuous casting fluxes. Although the correlation fails for the lower viscosity fluxes, Nichols also showed good correlation for viscosity with the silica content.

The results indicate that, for mold flux oxide compositions, the viscosity is dependent on the quantity of network forming oxides present, principally silica and alumina. This is demonstrated by the results of McCauley (2) in Figure 1. In this case, it is the ratio of network forming ions to total anion concentration. However, as shown in Figure 2, the viscosity/reciprocal temperature relationship is not linear and cannot be adequately represented by the Arrhenius Equation over a wide temperature range.

### Viscosity vs. Temperature

Viscosity can be considered as a measure of the ease of movement of molecules in a liquid undergoing shear. Several factors may influence this ease of movement including molecule size and intermolecular attraction, but a major factor is the amount of space available between the molecules, hence, the variety of models incorporating a free volume term.

The Clausius-Clapeyron equation relates pressure with temperature, enthalpy, and volume, and has been used to develop semi-theoretical expressions of vapor pressure (5). Many properties, including viscosity, can be related to an energy barrier, free volume and temperature. The attempt here is to express viscosity in the form of the Clausius-Clapeyron equation.

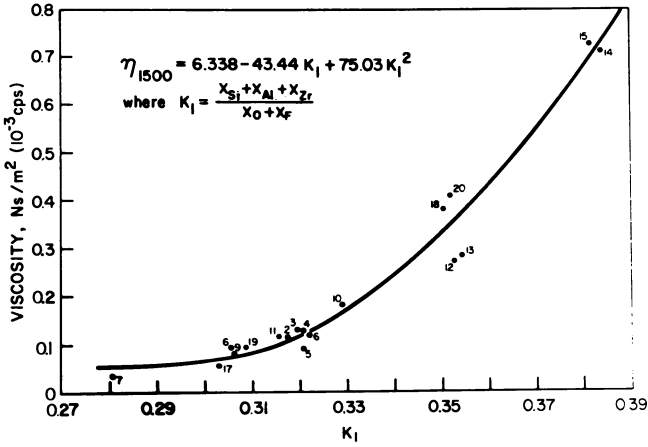


Figure 1. Viscosity at 1500°C as a function of network forming ions for the fluxes in Table I.

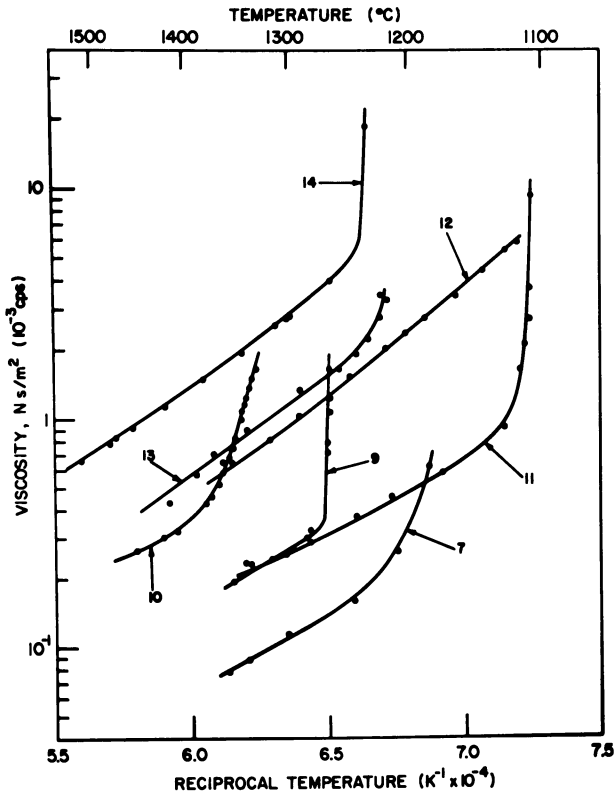


Figure 2. Typical viscosity results vs. reciprocal temperature for some of the fluxes listed in Table I.

The Clausius-Clapeyron equation can be written

$$\frac{dP}{dT} = \frac{\Delta H}{T\Delta V} = \frac{\Delta H}{T(V-V_0)} \quad (2)$$

where P, T, and  $\Delta H$  have their usual meaning. For this discussion,  $\Delta V$  is a measure of free volume or the difference between the volume at temperature and the volume at some standard state, e.g., at absolute zero or solid volume at the melting point.

Equation 2 can be rewritten as

$$\frac{d(\ln P)}{d(1/T)} = \frac{\Delta H}{R\Delta z} \quad (3)$$

where  $\Delta z = PV/RT - PV_0/RT$

Expanding  $\Delta H$  to the series form and integrating with respect to  $1/T$  yields

$$\ln P = \frac{1}{R} \left[ a - \frac{\Delta H_0}{T} + b \ln T + dT + \frac{e}{2}T^2 + \dots \right] \quad (4)$$

If the higher order terms are ignored, the expression reduces to

$$\ln P = A - \frac{B}{T} + C \ln T \quad (5)$$

Such a derivation was originally developed and used by Kirchoff [1858] and Rankine [1849] (5) to express the temperature dependence of vapor pressure. It was also successfully used by Brostow (6) to express the temperature dependence of the isothermal compressibility of a wide variety of organic liquids, some metallic liquids and water. By a similar analogy, we have used it to express the viscosity of liquid mold fluxes.

### Regression Analysis

The viscosity of twenty flux compositions determined earlier (2) were used to evaluate the Kirchoff-Rankine Equation. The compositions of these fluxes are given in Table I with a summary of the viscosities given in Table II. The flux viscosity data was fitted to the Kirchoff-Rankine equation as

$$\eta = \exp\left(C_1 + \frac{C_2}{T} + C_3 \ln T\right) \quad (6)$$

and to the Arrhenius Equation

$$\eta = A \exp(E/RT) \quad (7)$$

using the Marquardt method of non-linear least squares regression in the Statistical Analysis Systems [SAS] program package (7). The results of the regression are given in Table III, with the standard deviation and an average difference between calculated and measured values.

Table I. Experimental Fluxes - Frit Composition, wt%

Flux	SiO <sub>2</sub>	Al <sub>2</sub> O <sub>3</sub>	CaO	Na <sub>2</sub> O	CaF <sub>2</sub>	MgO	ZrO <sub>2</sub>	Total	V-ratio
1	34.8	10.2	32.7	10.7	7.6	0.9	0.6	97.5	0.94
2	34.4	9.8	32.1	10.9	8.4	0.7	0.6	96.9	0.93
3	34.5	10.0	32.7	11.0	7.6	0.7	0.7	97.2	0.95
4	34.6	10.1	32.5	10.8	7.8	0.6	0.6	97.0	0.94
5	34.6	10.3	32.3	10.9	8.0	0.7	0.5	97.3	0.93
6	34.7	10.1	33.0	10.8	7.2	0.6	0.6	97.0	0.95
7	26.7	9.8	31.8	14.4	11.7	0.6	1.9	96.9	1.19
8	30.7	8.9	32.6	12.9	2.3	0.7	8.8	96.9	1.06
9	31.2	10.4	40.3	5.7	7.6	0.8	0.7	96.7	1.29
10	35.2	10.3	40.8	5.7	3.3	0.9	0.8	97.0	1.16
11	33.5	10.4	24.9	15.1	11.5	0.5	0.4	96.3	0.77
12	38.8	10.4	26.2	15.1	3.5	0.7	0.9	95.6	0.67
13	41.9	10.6	29.5	6.8	7.8	0.7	0.9	98.2	0.77
14	48.0	10.6	28.6	6.5	3.3	0.8	1.4	99.2	0.60
15	46.8	10.4	22.2	10.7	5.5	0.6	2.7	98.9	0.47
16	30.6	10.0	36.2	10.3	7.0	1.0	2.1	97.2	1.18
17	30.0	10.2	27.8	18.6	8.2	0.8	1.6	97.2	0.93
18	39.6	10.4	35.7	4.0	4.7	1.0	1.3	96.7	0.90
19	32.4	10.4	30.4	10.8	11.7	0.7	1.1	97.5	0.94
20	39.1	10.4	32.6	11.3	1.7	0.9	1.2	97.2	0.83

Table II. Summary of Flux Viscosities

Flux	Viscosity at 1300°C, Ns m <sup>-2</sup>	Viscosity at 1400°C, Ns m <sup>-2</sup>	Viscosity at 1500°C, Ns m <sup>-2</sup>
1	0.395	0.230	0.135
2	0.310	0.175	0.112
3	0.340	0.205	0.128
4	0.485	0.235	0.125
5	0.290	0.190	0.088
6	0.510	0.230	0.122
7	0.110	0.065	0.035
8	NA*	NA*	NA*
9	0.280	0.160	0.080
10	6.00	0.360	0.180
11	0.270	0.150	0.114
12	0.930	0.460	0.270
13	1.15	0.530	0.280
14	2.80	1.30	0.710
15	2.40	1.30	0.725
16	7.00	0.170	0.090
17	0.160	0.115	0.059
18	1.40	0.670	0.380
19	0.250	0.130	0.094
20	1.40	0.720	0.410

\*Not available

In some cases, viz., Fluxes 5, 6 and 13 in Table III, the signs of the coefficients are reversed, and a concave downward curve is generated. This is most likely caused by the regression being trapped at a local minimum in the data and assuming convergence at that point. It is required for these cases that the size of the regression step should be increased to avoid the local minima, which SAS does not allow. Also, there may not be enough data points to expand the regression step as is probably true for Fluxes 6 and 13.

For the majority of fluxes evaluated, the standard deviation,  $s$ , and the average percent variation,  $\Delta\%$ , is lower for the Kirchoff-Rankine fitted equation vs. the Arrhenius Equation, indicating a better fit of the experimental data. The difference is most pronounced for those fluxes where the nonlinearity of the experimental  $\ln\eta$  vs.  $1/T$  data is greatest.

### Discussion

When the nonlinearity of the log viscosity vs. reciprocal temperature data was first observed, tests were made to insure that the curvature was real and not an artifact of the experimental apparatus. Hysteresis curves and constant temperature for extended time tests showed that the nonlinearity was not caused of devolatilization alkali or fluoride constituents or from thermal deviations in the furnace setup. It was found that the observed curvature of the data was not an artifact and represented the true physical behavior of the materials. The application of the Kirchoff-Rankine equation

Table III. Regression Analysis Results

Flux	Andrade-Arrhenius Equation				Kirchoff-Rankine Equation						+++ n
	A (Pa.s)	E (cal/mole)	s <sup>†</sup>	$\Delta\%^{++}$	C <sub>1</sub>	C <sub>2</sub>	C <sub>3</sub>	s	$\Delta\%$		
1	8.831E-6	33783	7.03E-3	2.40	-184.35	51341	20.502	6.36E-3	1.94	12	
2	2.704E-6	36304	1.99E-2	7.98	-282.59	68183	32.337	1.27E-2	3.47	6	
3	2.332E-6	30095	8.92E-3	2.08	-184.30	47516	20.792	5.68E-3	1.42	6	
4	8.016E-7	41748	1.82E-2	2.73	-278.11	71633	31.502	1.67E-2	3.20	6	
5	2.528E-5	29493	2.15E-2	4.14	132.94	-10764	-17.290	2.10E-2	3.91	14	
6	8.079E-7	41814	2.33E-2	5.41	123.80	-5309	-16.447	2.29E-2	5.68	7	
7	1.963E-7	41439	1.31E-2	7.01	-1511.91	297516	179.394	5.72E-3	3.91	5	
9	1.496E-5	30736	1.22E-2	3.15	-1626.10	321853	192.942	1.11E-2	3.62	6	
10	7.5E-3	36000*	-	-	-8603.16	1735752	1019.0	2.83E-2	3.97	18	
11	7.820E-6	32510	1.43E-2	3.15	-276.14	63473	31.935	5.81E-3	1.52	7	
12	4.828E-7	45110	6.00E-2	2.95	-239.51	62253	27.155	3.35E-2	1.10	12	
13	2.661E-6	40700	5.19E-2	4.69	169.80	-13879	-21.843	5.00E-2	3.89	8	
14	5.488E-8	48579	2.26E-1	13.00	-987.72	212141	116.012	9.85E-2	5.30	11	
15	5.761E-6	40568	1.32E-1	5.57	-233.90	60668	26.660	6.26E-2	3.07	10	
16	2.0E-2	30000*	-	-	-42701.6	8456727	5071.8	8.69E-2	15.8	17	
17	5.469E-6	32981	8.65E-3	5.05	-483.18	105664	56.221	1.60E-3	0.84	5	
18	4.126E-6	39880	2.66E-2	3.01	-200.79	56382	22.457	1.66E-2	1.84	6	
19	7.393E-6	32313	1.48E-2	7.39	-377.12	85334	43.656	8.69E-3	4.89	7	
20	1.493E-7	50240	1.62E-1	16.46	-517.30	116706	60.246	5.32E-2	4.46	8	

\* estimated

+ s =  $\epsilon(\eta_{exp} - \eta_{calc}) / (n-1)$

++  $\frac{\Delta\%}{\Delta\%} = \frac{1}{n} \frac{\eta_{exp} - \eta_{calc}}{\eta_{exp}} \times 100$

+++ n = number of observations

produced a more accurate description of the temperature dependence of viscosity.

Additional work on liquid metals, simple chloride salts and some small molecule organic liquids (8) indicates that the advantage of the Kirchoff-Rankine equation over the Andrade-Arrhenius equation improves as the size of the melt species increases. The improvement in the description of viscosity vs. temperature for metals and simple salts (e.g., NaCl and BiCl<sub>2</sub>) is not great, but for materials with larger melt species (e.g., silicate melts and organic liquids), there is a distinct improvement.

### Summary

The evaluation of the viscosity of mold fluxes has shown that the viscosity is primarily controlled by the concentration of network forming oxides, particularly the silica content. It has also been demonstrated that the temperature dependence of viscosity can be expressed by the relation,  $\ln\eta = C_1 + C_2/T + C_3\ln T$ , derived from the Clausius-Clapeyron Equation. This relation produces a better description of viscosity vs. temperature than the more familiar Arrhenius Equation.

### Literature Cited

1. Lanyi, M. D. M.S. Thesis, University of Cincinnati, 1980.
2. McCauley, W. L.; Apelian, D. Canadian Metallurgical Quarterly, 1984, 20, 247-262.
3. Riboud, P. V.; Roux, Y.; Lucas, L. D.; Gaye, H. Fach. Huttenpraxis Metalveiterverarbeitung 1981, 19, 1-8.
4. Nichols, M. W.; Lingras, A. P.; Apelian, D. 2nd Int. Sym. on Metallurgical Slags and Fluxes, Fine, H. A.; Gaskell, D. R.; Eds.; TMS-AIME, 1984, pp. 235-251.
5. G. W. Thomson, Chemical Review, 1946, 38, 1-39.
6. W. Brostow and P. Maynadier, High Temperature Science, 1979, 11, 7-21.
7. SAS User's Guide, SAS Institute, Inc., Cary, North Carolina, 1979.
8. McCauley, W. L.; Apelian, D. 2nd Int. Sym. on Metallurgical Slags and Fluxes, Fine, H. A.; Gaskell, D. R.; Eds.; TMS-AIME, 1984, pp. 925-947.

RECEIVED August 5, 1985

## Rheological Properties of Molten Kilauea Iki Basalt Containing Suspended Crystals

H. C. Weed, F. J. Ryerson, and A. J. Piwinski

University of California, Lawrence Livermore National Laboratory, Livermore, CA 94550

In order to model the flow behavior of molten silicate suspensions such as magmas and slags, the rheological behavior must be known as a function of the concentration of suspended crystals, melt composition, and external conditions. We have determined the viscosity and crystallization sequence for a Kilauea Iki basalt between 1250°C and 1149°C at 100 kPa total pressure and fO<sub>2</sub> corresponding to the quartz-fayalite-magnetite buffer in an iron-saturated Pt30Rh rotating cup, viscometer of the Couette type. The apparent viscosity varies from 9 to 879 Pa.s. The concentration of suspended crystals varies from 18 volume percent at 1250°C to 59 volume percent at 1149°C. The molten silicate suspension shows power-law behavior:

$$\log |\tau_{yx}| = A_0 + A_1 \log |du/dx|,$$

where  $\tau_{yx}$  is the shear stress and  $(du/dx)$  the shear rate. Since  $A_1 \leq 1$ , the apparent viscosity decreases with increasing shear rate and the system is pseudoplastic.

In order to understand the flow behavior of molten silicates containing suspended crystals, we need to know the rheological properties of the system as a function of volume fraction of the suspended crystalline phases at appropriate temperatures, oxygen fugacities and melt compositions. Because of the widespread occurrence of silicates, this approach can be applied to magma transport during volcanic eruptions, large scale convective and mixing processes in magmatic systems, and fouling of internal boiler surfaces by coal ash slags in plants burning pulverized coal. The first system we have studied is a basaltic lava from Kilauea Iki, Hawaii, for which we have determined the crystallization sequence and the dynamic viscosity.



### Experimental Methods

**Starting Material.** The starting material for these experiments is Kilauea Iki basalt fragments which have been ground in a tungsten carbide shatterbox to -100 mesh and homogenized by mixing with a paddle and then tumbling for 1.5 hours. This material was then fused in air at 1400°C for about 3.3 hours, quenched in deionized water, rinsed with acetone, and dried under vacuum (15  $\mu\text{m}$ ) at 110°C for 70 hours. The dried material was ground in a boron carbide mortar and pestle and stored in a screw cap glass bottle before use. Light microscopic examination shows that it is clear, free of opaque inclusions, and isotropic under crossed nicols; it is therefore presumed to be glass.

**Crystallization Sequence Determination.** The starting material for the determination of the crystallization sequence was the homogenized -100 mesh rock powder before fusion. Samples were in the form of spherical beads suspended by surface tension in platinum loops as described by Grove *et al.* (1). They were prepared by pressing about 190 mg of powder into a cylindrical pellet with two or three drops of ethanol as a binder. The diameter of the platinum wire was 0.25 mm and the diameter of the loop about 3 mm. The pellet was fused to the loop by resistive heating of the platinum and then suspended from a platinum bridgewire by an  $\text{Al}_2\text{O}_3$  connector which insulated it electrically from the bridgewire. The bridgewire was connected across two platinum leads which suspended the entire assembly from the top end fitting of the vertical furnace tube. Oxygen fugacity ( $f_{\text{O}_2}$ ) was controlled by adjusting the mixing ratio of a  $\text{CO}/\text{CO}_2$  gas mixture flowing through the furnace tube; it was maintained at the quartz-fayalite-magnetite (QFM) buffer (2, 3) and was monitored by recording the EMF from a solid state  $\text{O}_2$  sensor in the form of a CaO-stabilized  $\text{ZrO}_2$  tube which extended from the lower end of the furnace tube into the hot zone next to the sample (4). Pure  $\text{O}_2$  at 110 kPa (1 atm) was circulated inside the  $\text{ZrO}_2$  tube as the reference gas. The CO was Matheson C. P. grade or equivalent; the  $\text{CO}_2$  was Matheson Coleman Instrument grade or equivalent. Sample temperatures were measured by a Pt/10Rh thermocouple in the hot zone; the thermocouple had been calibrated at the gold point (1063°C). Run times varied from 77 hours at 1270°C to 738 hours at 1130°C. The sample was quenched in deionized water by electrically fusing the bridgewire, which dropped the sample out of the furnace tube. The quenched sample was mounted and polished for analysis. The elemental composition and the phases present were determined by wavelength dispersive X-ray analysis with a fully automated JEOL 733 Superprobe. The weight percentages of the phases present were determined from constrained least squares analysis of the bulk composition and the compositions of the individual phases in each experiment. Weight percentages were converted to volume percentages using estimated densities for the melt and crystalline phases. The calculated volume percentages were compared with those determined by reflected light point counts (1000 pts) of selected experiments. The results of the two methods are in good agreement (Figure 1). The size distribution was not determined.

**Viscometry.** The starting material for the viscosity determinations was the fused and re-ground glass described above. The viscometer was of the rotating cup Couette type in which the torque and temperature were measured at the bob (5). The cup was cylindrical in shape with a radius of 10.0 mm and a hemispherical bottom. The length of the cylindrical portion was 32.5 mm. The bob was the same shape, with a radius of 8.25 mm and an overall length of 88.1 mm. They were aligned with the hemispheres concentric by means of x-y-z micrometer adjusting screws on the framework which supported the bob. They were fabricated from Pt/30Rh alloy, with an Fe-rich surface produced by heating with a melt (25 weight percent  $\text{Fe}_3\text{O}_4$ , 75 weight percent  $\text{Na}_2\text{SiO}_3$ ) under  $\text{fO}_2$  corresponding to the iron-wüstite buffer (3). This is intended to minimize Fe transport from the Kilauea Iki melt to the bob and cup (6). Oxygen fugacity was controlled by passing  $\text{CO}/\text{CO}_2$  gas mixtures through the inner sample tube, which was isolated from the rest of the furnace by water-cooled rotatable mercury seals at the inlet and outlet ends. Flow rates were controlled by vernier throttle valves and ball-type flowmeters; the meter settings were calculated from the manufacturer's published curves (7). The  $\text{CO}/\text{CO}_2$  ratio was adjusted to give an  $\text{fO}_2$  corresponding to an extrapolation of the quartz-fayalite-magnetite (QFM) buffer (2,3). The total flow rate was  $581 \text{ cm}^3/\text{min}$  corresponding to a linear velocity of  $0.9 \text{ cm}/\text{sec}$  at room temperature and pressure; this had been shown to be large enough to avoid unmixing of the gases due to thermal diffusion effects (8). The CO was Matheson C. P. grade or equivalent; the  $\text{CO}_2$  was Matheson Coleman Instrument grade or equivalent. Temperature was measured by a Pt6Rh/Pt30Rh thermocouple which had been calibrated against a pyrometer and standard lamp, with appropriate corrections for intensity losses due to windows and a reflecting prism in the optical train. The accuracy of the temperature measurement was estimated to be  $\pm 2^\circ\text{C}$  (9). Torque was measured by a calibrated torsion bar in which the angular deflection and torque were read from four strain gauges mounted on the faces of the bar and connected as a Wheatstone bridge. The unit used in these measurements had a range of  $\pm 0.353 \text{ N}\cdot\text{m}$  ( $\pm 50 \text{ oz}\cdot\text{in}$ ) and digital readout to  $7.1 \times 10^{-4} \text{ N}\cdot\text{m}$  ( $0.1 \text{ oz}\cdot\text{in}$ ). The tachometer was a toothed wheel and magnetic pickup with a range of  $\pm 999 \text{ rev}/\text{min}$ , readable to  $1 \text{ rev}/\text{min}$ .

Three types of viscometry experiments were performed: calibration measurements on a standard oil to determine the effective length of the cylindrical column of liquid, isothermal runs on the basalt melts, and polythermal exploratory runs on the basalt melts. Calibration measurements were performed on Brookfield oil ( $\mu_0=105 \text{ Pa}\cdot\text{s}$ ) at room temperature and under laboratory atmosphere. The effective length was determined over a range which included the length of the melt samples. Rotation speed was varied from 0 to  $\pm 220 \text{ rev}/\text{min}$  in  $40 \text{ rev}/\text{min}$  steps, with increasing speed values at even multiples of  $20 \text{ rev}/\text{min}$  and decreasing speed values at odd multiples of  $20 \text{ rev}/\text{min}$ . The positive rotational direction was selected first. At least two torque readings were taken at each value of the rotational speed. The same procedure was followed during isothermal runs on the basalt melts, except that the temperature was noted for each torque

measurement at constant rotational speed in order to monitor the temperature increase due to viscous energy dissipation. The melt sample weight was about 6.65 g, which with an assumed density of 2.78 g/cm<sup>3</sup> corresponded to a geometrical length of 14.7 mm for the cylindrical part of the sample. The temperature settings were approached from above by going from room temperature to 1260°C or 1270°C at 100°C/hr to 150°C/hr, then cooling the system at about 1°C/min until the desired temperature was reached. The effect of changing the heating and cooling rates on the viscosity was not explored. Polythermal runs were made at a constant rotational speed, usually 90 to 100 rev/min, and were used to explore the temperature range over which suitable torque readings could be obtained.

### Results and Discussion

Crystallization Sequence. Table I shows the major element bulk composition of the starting materials used in our experiments and those of Shaw *et al.* (10). Kilauea Iki basalt contains less Al<sub>2</sub>O<sub>3</sub> and CaO than their material, and much more MgO. Both are within the normal range for basaltic lavas.

Table I. Analyses of Starting Material

Oxide, Wt.%	Kilauea Iki	Shaw <i>et al.</i> (10)
SiO <sub>2</sub>	46.29	50.14
Al <sub>2</sub> O <sub>3</sub>	10.44	13.37
MgO	17.90	8.20
FeO	11.34*	10.13
Fe <sub>2</sub> O <sub>3</sub>	-	1.21
CaO	8.49	10.80
Na <sub>2</sub> O	1.84	2.32
P <sub>2</sub> O <sub>5</sub>	0.22	0.27
K <sub>2</sub> O	0.40	0.53
TiO <sub>2</sub>	1.89	2.63
MnO	0.19	0.17
TOTAL	99.90	99.77

\*All iron as FeO

The experimental results obtained at the QFM buffer are listed in Table II. and type formulas for the various mineral series in Table III. Olivine and chrome spinel are the only crystalline phases which occur between 1240°C and 1179°C; clinopyroxene and plagioclase feldspar crystallize at approximately 1170°C. The concentration of crystals increases from about 22 weight percent to about 28 weight percent between 1250°C and 1180°C. The liquid line of descent is characterized by a slight SiO<sub>2</sub>, Al<sub>2</sub>O<sub>3</sub> and alkali enrichment and an FeO and MgO depletion.

The volume percentage of melt as a function of temperature is shown in Figure 1. The break in slope at approximately 1170°C corresponds to the appearance of clinopyroxene and plagioclase feldspar (see Table II.). The volume percentage of melt,  $V_m$ , is given by Equations 1 and 2:

Table II. Results of Selected Kilauea Iki Liquidus Experiments

Exp't No.	Time (Hrs)	Temp (°C)	Experiment Products	Vol % Melt <sup>a</sup>	Wt % Melt <sup>b</sup>
14	93.0	1240	olivine, chrome spinel, glass	71.8	78.1
9	189.5	1230	olivine, chrome spinel, glass	80.2 <sup>c</sup>	76.1
8	24.0	1219	olivine, chrome spinel, glass	77.3	74.8
10	290.0	1209	olivine, chrome spinel, glass	76.2	74.2
12	289.0	1189	olivine, chrome spinel, glass	63.8	72.5
13	364.0	1179	olivine, chrome spinel, glass	71.8	71.5
16	380.0	1170	olivine, chrome spinel, clinopyroxene, plagioclase, glass	69.6	68.5
19	400.0	1160	olivine, chrome spinel, clinopyroxene, plagioclase, glass	54.7	53.5
20	400.0	1149	olivine, chrome spinel, clinopyroxene, plagioclase, glass	40.7	49.8

a) Volume percent of melt was determined by a 1000 point mode on metallograph.

b) Weight percent of melt was determined by constrained least squares analysis of phase compositions.

c) Volume percent glass was determined by an 850 point mode on metallograph.

Table III. Type Formulae for Mineral Series

Name	Type Formula
Olivine	(Mg, Fe) SiO <sub>4</sub>
Chrome Spinel	AB <sub>2</sub> O <sub>4</sub> A = Mg, Fe <sup>2+</sup> , Zn, Mn <sup>2+</sup> , Ni B = Al, Fe <sup>3+</sup> , Mn <sup>3+</sup> , Cr
Clinopyroxene	ABSi <sub>2</sub> O <sub>6</sub> A = Mg, Fe <sup>2+</sup> , Ca, Na B = Mg, Fe <sup>2+</sup> , Al
Plagioclase	Ranges from NaAlSi <sub>3</sub> O <sub>8</sub> to CaAl <sub>2</sub> Si <sub>2</sub> O <sub>8</sub>

$$V_m (O1+Chsp) = 0.157 T(^{\circ}C) - 114.0, \text{ where } T(^{\circ}C) \geq 1170, \quad (1)$$

$$V_m = 1.36 T(^{\circ}C) - 1522.7, \text{ where } T(^{\circ}C) \leq 1170. \quad (2)$$

Extrapolation of Equation 1 to  $V_m=100$  corresponds to  $T=1360^{\circ}C$  for the liquidus. Extrapolation of Equation 3 to  $V_m=0$  yields  $T=1119^{\circ}C$  for the disappearance of liquid, the solidus temperature. This is a complex system for which complete phase diagrams are not available; pseudoternary diagrams such as those presented by Grove *et al.* (1) for similar compositions are generally applicable to this composition.

**Viscometry.** During viscosity measurements sigmoidal torque versus rotation speed curves are obtained at all investigated temperatures. The curves are linear at rotation speeds less than 0.4 revs/sec, with a positive slope. The curves become concave toward the rotation speed axis at higher rotation rates, indicating pseudoplastic behavior (11). This behavior becomes more pronounced at low temperature as the concentration of suspended crystals increases. Also, at a given rotational speed, the observed torque appears to be slightly lower for negative rotation than for positive rotation. This indicates slight thixotropic behavior of the sample, since positive rotation is used first during experiments. At temperatures near  $1149^{\circ}C$ , torque measurements are more erratic than at higher temperatures. This may be due to segregation of crystals which causes the sample to rotate intermittently as a rigid body, or due to localized remelting of crystals by viscous heating which increases at lower temperatures.

We have analyzed the results in terms of the power law indicated by Equation 3:

$$\log |\tau_{yx}| = A_1 + A_2 \log |du/dx| \quad (3)$$

where  $|\tau_{yx}|$  is the absolute value of the shear stress and  $|du/dx|$  the absolute value of the shear rate, calculated by a modification of the method of Krieger and Elrod (12) which applies to non-Newtonian systems. The apparent viscosity,  $\mu$ , is

$$\mu = \tau_{yx}/(du/dx) \quad (4)$$

The flow curve, Fig. 2, is a plot of Equation 3 showing experimental results obtained at the  $1186^{\circ}C$  isotherm. Fig. 3 is a log-log plot of apparent viscosity as a function of shear rate at the same temperature. The apparent viscosity decreases with increasing shear rate, which is characteristic for pseudoplastic systems (11). The logarithm of the viscosity at unit shear rate,  $\log \mu_0$ , is calculated from Equation 3:

$$\log \mu_0 = A_1 \quad (5)$$

Table IV gives  $\mu_0$  as a function of temperature. It varies from 9 Pa.s at  $1249^{\circ}C$  to 879 Pa.s at  $1149^{\circ}C$ . The accuracy is estimated as  $\pm 15\%$  above  $1170^{\circ}C$ ; at  $1149^{\circ}C$ , where the system shows erratic behavior, the accuracy is estimated as  $\pm 50\%$ .

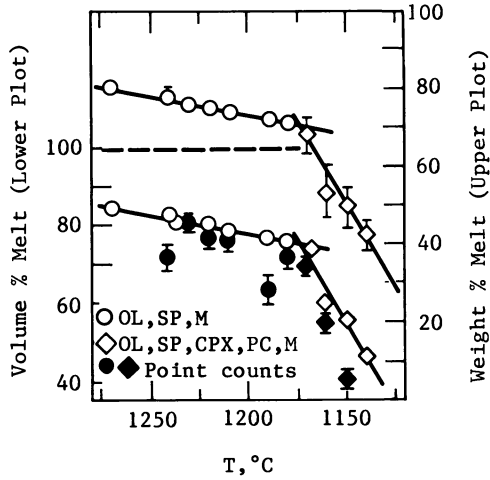


Figure 1. Volume percent and weight percent melt as a function of temperature for Kilauea Iki basalt. Vertical bars indicate two standard deviations.

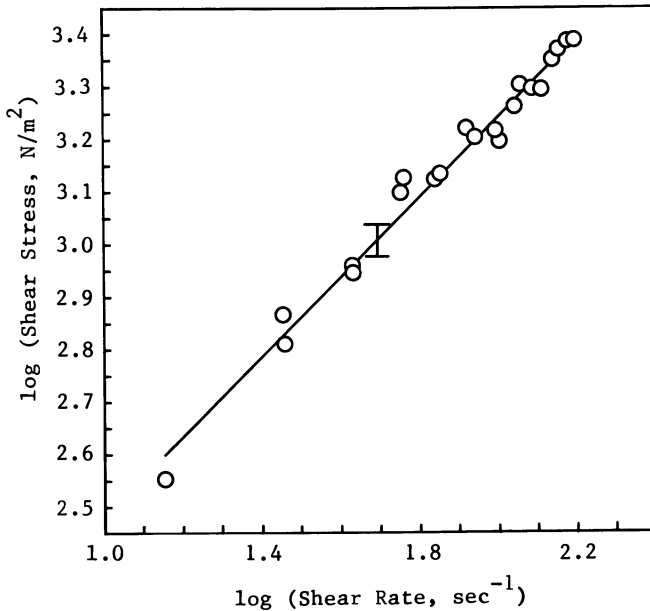


Figure 2. Least squares fit of  $\log$  (Shear Stress) vs.  $\log$  (Shear Rate) for Kilauea Iki basalt at 1186°C. Vertical bar indicates two standard deviations.

Table IV. Apparent Activation Energies from Least Squares Analysis of  $\log \mu_0$  vs.  $1/(T,K)$  for Kilauea Iki Basalt, Halemaumau Basalt, and Coal Slag X

System	T, °C	Apparent Activation Energy Kcal mol <sup>-1</sup>	Standard Deviation Least Squares Fit
Kilauea Iki	1249-1170	123 + 10	.09
	1170-1150	452 + 21	.04
Halemaumau	1300-1158	86 + 9	.12
	1158-1125	635 + 64	.18
Coal Slag X	1482-1330	53 + 1	.013
	1330-1260	424 + 27	.14

The results of least-squares analyses of  $\log \mu_0$  vs.  $(1/T,K)$  are shown in Figure 4 and Table V for this investigation on Kilauea Iki basalt, for the work of Shaw on Halemaumau basalt (10,13) and for Corey's report on Coal Slag X (14). The Kilauea Iki data show a sharp increase in slope at 1170°C as indicated by the limiting straight lines above and below this temperature. Below 1170°C, appreciable crystallization occurs as shown in Table II and Fig. 1, and the system shows strongly pseudoplastic behavior. Shaw's results on Halemaumau basalt (13), which is a Hawaiian basalt quite similar to Kilauea Iki, show a sharp increase in slope at 1158°C. This system shows pseudoplastic behavior at 1125°C and Newtonian behavior at higher temperatures. The results of Corey (14) on Coal Slag X indicate a sharp change in rheological behavior at 1330°C. His original paper gives no details on the calculation of the viscosity results, and no information on the crystallization sequence of the coal slag on which they were obtained. The similarity of the basalt and coal slag data indicates that rheological behavior of the coal slag may be affected by suspended crystalline material at temperatures near 1330°C. A recent study on slagging in large coal-burning furnaces correlates the slagging behavior with ash composition, ash particle morphology, and calculated critical viscosity temperature  $T_{cv}$  (15). The methods of the present investigation can be applied in order to measure the critical viscosity temperatures and compositions directly, which should improve the experimental basis for the correlation.

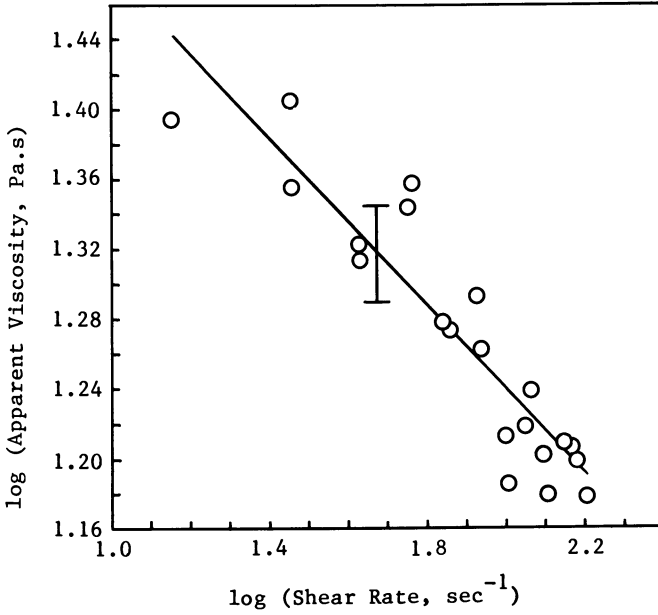


Figure 3. Log (Apparent Viscosity) vs. log (Shear Rate) for Kilauea Iki basalt at 1186°C. Vertical bar indicates two standard deviations.

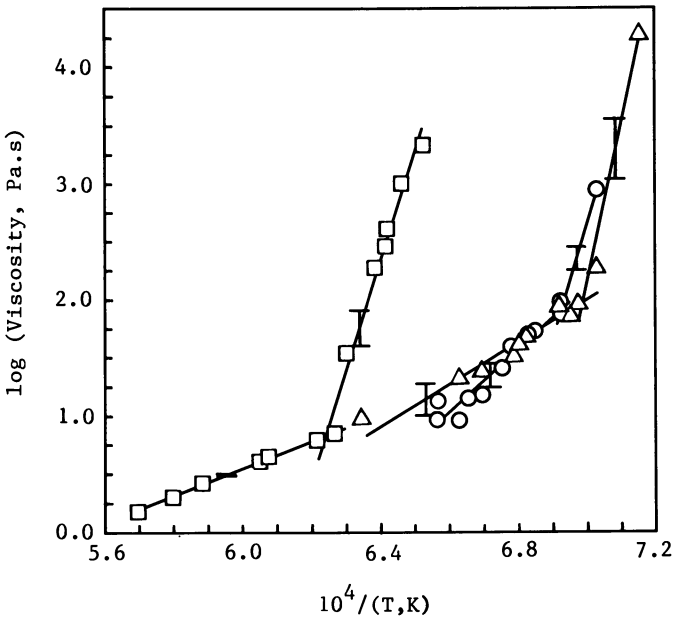


Figure 4. Least squares analysis of log (Viscosity) vs. reciprocal temperature. Present study O; Shaw (13) Δ; Corey (14) □. Vertical bars indicate two standard deviations.



Table V. Apparent Viscosity at Unit Shear Rate ( $\mu_0$ ) vs. Temperature (t, °C) for Kilauea Iki Basaltic Lava

Run No.	T, °C	$\mu$ , Pa.s
57	1249	13
63	1249	9
58	1235	9
64	1229	14
59	1220	15
65	1208	25
60	1201	38
66	1188	51
61	1186	52
62	1171	71
67	1170	94
68	1149	879

In both the studies on basalts, the breaks in the slope of the log  $\mu_0$  vs. (1/T,K) curves occur at 20 to 30 volume percent of suspended crystals. The non-Newtonian behavior of these molten silicate suspensions appears to arise from the increasing concentration of suspended crystals in the melt. This suggests that in modeling fluid flow in silicate systems, power law behavior should be considered when the suspended crystal concentration exceeds 20 volume percent.

#### Acknowledgments

This work was performed under the auspices of the U.S. Department of Energy by the Lawrence Livermore National Laboratory under contract number W-7405-ENG-48.

#### Literature Cited

1. Grove, T. L.; Gerlach, D. C.; Sando, T. W. Contrib. Mineral. Petrol. 1982, 80, 160-182.
2. Deines, P; Nafziger, R. H.; Ulmer, G. C.; Woermann, E. "Temperature-Oxygen Fugacity Tables for Selected Gas Mixtures in the C-H-O System at One Atmosphere Total Pressure"; Bulletin, Earth and Mineral Sciences Experiment Station, No. 88, College of Earth and Mineral Sciences, The Pennsylvania State University, University Park, PA, 1971.
3. Huebner, J. S. In "Research Techniques for High Pressure and High Temperature"; Ulmer, G. C., Ed.; Springer-Verlag, New York, 1971; pp. 123-177.
4. Williams, Richard J.; Mullins, O. "A System Using Solid Ceramic Oxygen Electrolyte Cells to Measure Oxygen Fugacities in Gas-Mixing Systems"; Technical Memorandum TMX-58167, Lyndon B. Johnson Space Center, Houston, TX 77058 1976.
5. Weed, H. C.; Dibley, L.; Piwinski, A. J. "A High-Temperature Viscometer for Use at 100 kPa"; UCRL-52477, Lawrence Livermore National Laboratory, Livermore, CA 94550, 1978.

6. Grove, T. L. Contrib. Mineral. Petrol. 1981, 78, 298-304.
7. "The F and P Tri-flat (Low Flow Rate) Variable Area Flowmeter Handbook; Application, Sizing, and Calibration Prediction Data", Catalog 10A9010, Fischer and Porter Co., Hatboro, Pa, Pub. 13317, September, 1959.
8. Darken, L. S.; Gurry, R. W. J. Am. Chem. Soc., 1945, 67, 1398-1412.
9. Weed, H. C.; Piwinskii, A. J.; Dibley, L. L. "Experimental Study of the Dynamic Viscosity of Some Silicate Melts to 1953K at 150 kPa", UCRL-52757, Lawrence Livermore National Laboratory, Livermore, CA, 94550, 1979, p. 2.
10. Shaw, H. R.; Wright, T. L.; Peck, D. L.; Okamura, R. Amer. Jour. Sci. 1968, 266, 225-64.
11. Skelland, A. H. P. "Non-Newtonian Flow and Heat Transfer"; J. Wiley and Sons, New York, 1967, pp. 5-12.
12. Krieger, I.; Elrod, H. J. Appl. Phys. 1953, 14, 134-6.
13. Shaw, H. R. Jour. Petrology 1969, 10, 510-535.
14. Corey, R. C. "Measurement and Significance of the Flow Properties of Coal-Ash Slag"; Bulletin No. 618, U. S. Bureau of Mines 1964, pp. 1-64.
15. Hazard, H. R. "Influence of Coal Mineral Matter on Slagging of Utility Boilers"; EPRI CS-1418, Project 736, Final Report, Electric Power Research Institute, Palo Alto, CA 94304, 1980.

RECEIVED October 24, 1985

## Crystallization of Coal Ash Melts

D. P. Kalmanovitch<sup>1</sup> and J. Williamson

Department of Metallurgy and Materials Science, Imperial College, London SW7, England

When coal is burnt in pulverized fuel (p. f.) utility boilers the inorganic material inherent to the fuel may form deposits on the heat absorbing surfaces causing significant reduction in thermal efficiency. This study has involved the investigation of the crystallization of coal ash melts and the relationship to the formation and growth of these troublesome deposits.

The crystallization behaviour of compositions in the systems  $\text{CaO-Al}_2\text{O}_3\text{-SiO}_2$ ,  $\text{CaO-MgO-Al}_2\text{O}_3\text{-SiO}_2$  and  $\text{CaO-Al}_2\text{O}_3\text{-SiO}_2$ -iron oxide relevant to coal ash compositions has been studied. The observations have been compared with the devitrification behaviour of both eastern and western type coal ashes determined under laboratory conditions. Results show that the crystallization of ash melts is well represented by the system  $\text{CaO-FeO-Al}_2\text{O}_3\text{-SiO}_2$ . The quaternary system has been constructed from literature data as planes of constant FeO content (5-30 wt% at 5% increments) and used to predict the behaviour of boiler deposits.

The formation of ash deposits within coal-fired boilers may cause serious operating problems and reduction in thermal efficiency. These deposits vary in nature from friable, slightly sintered fouling to dense semi-vitreous slags. Utility boiler designers and operators use a variety of methods (1) to ascertain various design criteria or the likelihood of an ash to form deposits (it's slagging propensity). Chief amongst these methods is the standard ash fusion test (2) in which a coal ash is heated at a given rate in air and a mildly reducing atmosphere while the temperatures at which various

-----

<sup>1</sup>Current address: Energy Research Center, University of North Dakota, Grand Forks, ND 58202.

degrees of deformation of a cone of ash are recorded. This method has been known to give inaccurate indications of slagging propensity due mainly to the subjective nature of the test and the fact that the technique does not duplicate the thermal history experienced by coal mineral matter in a pulverized fuel (p. f.) boiler.

Various laboratory studies, e.g. those of Padia (3) and Raask (4) have shown that significant fusion of coal mineral matter (the precursor to ash) occurs within a very short time-frame at temperatures analogous to those in the combustion zone of a boiler (about 1550-1650 C). This is confirmed by microscopic studies of p. f. fly-ash. The residence times of ash particles in utility boiler systems has been estimated by Raask to be 2 seconds with a temperature gradient ranging from 1650 to 3000 C. The studies show that the characteristic nature of fly ash, that of hollow cenospheres is due to the formation of a significant amount of liquid phase within the 2s time frame. This is further confirmed by mineralogical analysis of the particles which reveals an amorphous phase (glass) and sometimes the presence of a refractory phase which had crystallized from a liquid. Both features are not products of the thermal decomposition of individual coal mineral particles (4,5,6). Raask (4) has shown that the growth of deposits is predominantly via sintering by viscous flow. The rate of increase in strength (s) i.e. growth of the deposit being given by:

$$\frac{ds}{dt} = \frac{3 \gamma k}{2 \eta r}$$

Where  $\gamma$  is the surface tension coefficient,  $k$  a constant,  $r$  the initial radius of the particle and  $\eta$  the viscosity of the liquid phase. It can be seen that the nature of a deposit can be described by the degree of sintering which has taken place. For a given coal ash the parameters  $r$  and  $\gamma$  are effectively constant with respect to the variability of the viscosity. Therefore the factors which affect the rheological behaviour will determine to a great extent the rate of growth by viscous flow. For homogeneous melts the determining factors are temperature and chemical composition. Lauf (6) has observed that the amount of fly ash particles emitted at the outlet of various boilers was inversely proportional to the calculated viscosity (using a method based on chemical composition) at a given temperature. This qualitatively confirms the relation above. A factor which has not received attention in the literature is the crystallization of the ash particles and/or the deposits already present. With devitrification of a phase from a homogeneous melt the composition of the liquid phase will change depending on the precipitating phase and the degree of crystallization. This in turn will directly affect the viscosity and therefore the rate of growth of the deposits.

Thus it will be of great value to be able to predict to some extent the crystallization behaviour of coal ash melts. For simplicity it is necessary to consider that crystallization will be from a homogeneous melt. The data may be applied to the phenomena of boiler slagging by using an accurate model of the viscosity of ash melts based on chemical composition. The main aim of the study has been to obtain relevant crystallization data of coal ashes and

to model the behaviour so as to be able to predict the devitrification of a given ash. Coal ash is usually described as a mixture of up to 11 oxide components and though various investigators (7) have attempted to simplify the system by using certain empirical equivalences the authors chose to use the major three or four components to model the behaviour.

For eastern type coal ashes the major components are silica, alumina, iron oxide and lime, whereas for western type ashes the major components are silica, alumina, lime and iron oxide or magnesia. In both cases these components may comprise 90 wt% or more of the total composition of the ash. Sanyal and Williamson (8) have shown that the initial crystallization of two western type ashes of low iron oxide contents (5% or less) could be described by the normalized composition on the ternary equilibrium diagram of the system  $\text{CaO-Al}_2\text{O}_3\text{-SiO}_2$ . That is, the crystallization behaviour of the ashes was the same as that which would be expected if the remaining components were not present. The study presented here has extended the investigation to the devitrification of an eastern type as well as western type ashes and the crystallization of compositions in the systems  $\text{CaO-Al}_2\text{O}_3\text{-SiO}_2$ ,  $\text{CaO-MgO-Al}_2\text{O}_3\text{-SiO}_2$ , and  $\text{CaO-Al}_2\text{O}_3\text{-SiO}_2\text{-iron oxide}$  relevant to coal ashes. The study of the ternary and quaternary systems was to determine which governed the behaviour of ashes most adequately. The results have been used to look at the behaviour of ash melts in relation to the phenomena of boiler deposits.

### Experimental

**Crystallization of ash melts:** The three ashes studied were supplied by Babcock Power Ltd. (U. K.) and the chemical compositions are listed in Table I. Ashes 1 and 2 were of western type from coals fired at Matla Power Station, South Africa whereas ash 3 was of eastern type from a coal fired at Drax Power Station, U. K.. The roasted ashes (treated at 800 C overnight) were fused at 1500-1550 C for up to 1 hr. in Pt envelopes in an electric muffle furnace. Crystallization of the melts was induced by reducing the temperature of the furnace to a given level and leaving for a given time. The process was repeated over a range of temperatures and times for each of the ashes. The samples were analyzed by petrographic microscopy and powder X-ray diffraction.

Table I. Chemical composition of coal ashes studied

	wt%		
	Ash 1	Ash 2	Ash 3
$\text{SiO}_2$	43.1	51.2	54.5
$\text{Al}_2\text{O}_3$	27.8	29.0	26.4
$\text{Fe}_2\text{O}_3$	5.1	4.8	9.4
$\text{CaO}$	17.3	9.5	1.5
$\text{MgO}$	3.8	2.6	1.6
$\text{Na}_2\text{O}$	0.7	0.6	1.2
$\text{K}_2\text{O}$	0.3	1.0	4.2
$\text{TiO}_2$	1.9	1.3	4.2
	<u>100.0</u>	<u>100.0</u>	<u>100.0</u>

Crystallization of model compositions: A series of five CaO, Al<sub>2</sub>O<sub>3</sub> and SiO<sub>2</sub> compositions were chosen (designated A, B, C, D and E) to be of relevance to coal ashes. Composition A was the normalized composition of ash 1 whereas that of B corresponded to that of an ash studied by Sanyal and Williamson (8). The compositions have been listed in Table II. Homogeneous glasses were prepared for each of the compositions by fusing the correct mixture of components in a Pt crucible at 1550 C. Crystallization of each glass was determined by remelting a small sample in a Pt envelope at 1550 C for 0.5 hr. and reducing the temperature to a given level for a given time. The quenched samples were analyzed using petrographic microscopy and X-ray diffraction.

Table II. Composition of CaO-Al<sub>2</sub>O<sub>3</sub>-SiO<sub>2</sub> glasses.

Glass	Composition wt%		
	SiO <sub>2</sub>	Al <sub>2</sub> O <sub>3</sub>	CaO
A	49.0	31.5	19.5
B	37.0	25.0	38.0
C	41.5	27.0	31.5
D	44.0	28.5	27.5
E	49.0	35.0	16.0

The crystallization of glasses in the system CaO-MgO-Al<sub>2</sub>O<sub>3</sub>-SiO<sub>2</sub> was studied as follows: The five ternary compositions A-E were used as the basis of two series of glasses with 5 and 10 wt% MgO. This covers the usual range of magnesia content in coal ashes. The compositions are listed in Table III. The preparation of the glasses, the determination of the crystallization behaviour and analysis of quenched samples were analogous to the methods used for the ternary compositions.

Table III. Composition of CaO-MgO-Al<sub>2</sub>O<sub>3</sub>-SiO<sub>2</sub> glasses.

Glass	Composition wt%			
	SiO <sub>2</sub>	Al <sub>2</sub> O <sub>3</sub>	CaO	MgO
am5	47.0	30.0	18.0	5.0
bm5	35.0	24.0	36.0	5.0
cm5	39.0	26.0	30.0	5.0
dm5	42.0	27.0	26.0	5.0
em5	47.0	33.0	15.0	5.0
aml0	44.1	28.4	17.5	10.0
bml0	33.3	22.5	34.2	10.0
cm10	37.6	24.3	28.3	10.0
dml0	39.6	25.6	24.8	10.0
em10	44.1	31.5	14.4	10.0

Iron can exist in three oxidation states but in a modern p. f.

boiler only the states of ferrous and ferric are observed. Unlike magnesia, the range of iron oxide content in coal ashes is quite wide; some eastern type ashes may have an iron oxide content of 50% though 15 - 20 % is more common. Therefore the study of the system  $\text{CaO-Al}_2\text{O}_3\text{-SiO}_2$ -iron oxide must take into account both the wide range of iron oxide contents and the variable oxidation states. The five ternary compositions A-E were used as the basis of two series of compositions with 5 and 10 wt% equivalent FeO. A further two series of glasses were prepared based on the compositions A, B and E with 15 and 20 wt% equivalent FeO. The compositions are listed in Table IV.

Glasses were prepared for each composition by mixing the correct proportions (with  $\text{CaCO}_3$  as the source of CaO and iron [II] oxalate,  $\text{FeC}_2\text{O}_4 \cdot 2\text{H}_2\text{O}$  as the source of FeO) and fusing in a Pt crucible at 1500-1550 C in an electric muffle furnace. Crystallization of the homogeneous glasses was performed in a vertical tube furnace with a controlled atmosphere ( $\text{CO}_2/\text{H}_2$  1:1 v/v with a total flow rate of 200 ml per min.). This is the same atmosphere used in the ash fusion test (2). The quenched sample was analyzed by petrographic microscopy, powder X-ray diffraction and chemical analysis (to determine the ferrous/total iron ratio) using the method of Hey (9).

Table IV. Composition of  $\text{CaO-Al}_2\text{O}_3\text{-SiO}_2$ -iron oxide glasses.

Glass	Composition wt%			
	$\text{SiO}_2$	$\text{Al}_2\text{O}_3$	CaO	FeO*
af5	47.0	30.0	18.0	5.0
bf5	35.0	24.0	36.0	5.0
cf5	39.0	26.0	30.0	5.0
df5	42.0	27.0	26.0	5.0
ef5	47.0	33.0	15.0	5.0
af10	44.0	28.4	17.6	10.0
bf10	33.3	22.4	34.3	10.0
cf10	37.4	24.2	28.4	10.0
df10	39.5	25.6	24.8	10.0
ef10	44.0	31.6	14.4	10.0
af15	41.6	26.8	16.6	15.0
bf15	31.5	21.2	32.3	15.0
ef15	41.6	29.8	13.6	15.0
af20	39.2	25.2	15.6	20.0
bf20	29.6	20.0	30.4	20.0
ef20	39.2	28.0	12.8	20.0

\*equivalent FeO

## Results

Crystallization of ash melts: The results of the crystallization of the three ash melts studied are listed in Table V. The only phase observed to precipitate for the western type ashes was anorthite ( $\text{CaO} \cdot \text{Al}_2\text{O}_3 \cdot 2\text{SiO}_2$ ) despite lengthy treatment. The eastern type ash showed different behaviour with mullite ( $3\text{Al}_2\text{O}_3 \cdot 2\text{SiO}_2$ ) as the

primary phase. A secondary phase of hematite ( $\text{Fe}_2\text{O}_3$ ) was detected in a sample treated at 1250 C but optical analysis revealed that this phase was only on the surface (i.e. the air-melt interface). The true secondary phase was observed in samples treated in the temperature range 1200-1100 C and was determined to be a member of the iron spinel solid solution series; magnetite ( $\text{FeO}\cdot\text{Fe}_2\text{O}_3$ )-hercynite ( $\text{FeO}\cdot\text{Al}_2\text{O}_3$ ). Hematite was again observed in samples quenched from temperatures below 1100 C (at the surface of the sample).

Table V. Crystallization behaviour of coal ash melts.

	Crystallization treatment*		Crystalline phases observed.
	Temp./ C	Time/h.	
Ash 1	1390	80	glass
	1150	180	anorthite
	1100	42	anorthite
	1050	22	anorthite
	950	80	anorthite
	900	24	anorthite
Ash 2	1300	1	anorthite
	1200	10	anorthite
	1100	24	anorthite
	1000	15	anorthite
Ash 3	1400	18	mullite
	1350	2	mullite + hematite
	1200	20	mullite + iron spinel
	1200	40	mullite + iron spinel
	1170	4	mullite + iron spinel
	1100	26	mullite + iron spinel
	1050	2	mullite + hematite

\* Crystallization treatment after fusion at 1450 - 1550 C.

Crystallization of ternary compositions: The observed crystallization behaviour of the five ternary glasses studied has been compiled in Table VI. The liquidus temperature included in the Table was obtained from the equilibrium phase diagram of the system for each of the compositions (11). The temperature of appearance of the secondary or tertiary phase is that of the highest treatment temperature at which that phase was observed. Only the glass B was observed to crystallize to the three components expected from the phase diagram, i.e. the primary phase of gehlenite ( $2\text{CaO}\cdot\text{Al}_2\text{O}_3\cdot\text{SiO}_2$ ), followed by anorthite and cyclo wollastonite ( $\text{CaO}\cdot\text{SiO}_2$ ). The remaining glasses only crystallized anorthite despite lengthy treatment at temperatures near their respective eutectics.

Crystallization of  $\text{CaO}\text{-MgO}\text{-Al}_2\text{O}_3\text{-SiO}_2$  glasses: The results of the crystallization studies of the quaternary glasses have been compiled in Table VII. The liquidus temperature was determined experimentally by extensive series of quenching runs. The temperature of appearance of the secondary and tertiary phase is the highest temperature at which the respective phase was observed. The phase melilite is a solid solution series between gehlenite and



Table VI. Crystallization behaviour observed for the  $\text{CaO-Al}_2\text{O}_3\text{-SiO}_2$  glasses.

Glass	Liquidus Temp./C	Primary Phase	Temp. C	Sec.* h.	Secondary Phase	Temp. C	Tert.* h.	Tertiary Phase
A	1520	Anorthite	1100	76	n.o.	-	-	n.o.
B	1450	Gehlenite	1200	60	Anorthite	1200	60	Cyclowoll.
C	1390	Anorthite	1100	72	n.o.	-	-	n.o.
D	1450	Anorthite	1100	105	n.o.	-	-	n.o.
E	1510	Anorthite	1100	72	n.o.	-	-	n.o.

\* Temperature of appearance of subsequent phase after temperature treatment listed.

n.o. - not observed

Anorthite -  $\text{CaO}\cdot\text{Al}_2\text{O}_3\cdot 2\text{SiO}_2$ , Gehlenite -  $2\text{CaO}\cdot\text{Al}_2\text{O}_3\cdot\text{SiO}_2$ ,

Cyclowoll. - cyclowollastonite  $\text{CaO}\cdot\text{SiO}_2$  (high - temperature polymorph)

Table VII. Observed crystallization behaviour of CaO-MgO-Al<sub>2</sub>O<sub>3</sub>-SiO<sub>2</sub> glasses.

Glass	Liquidus Temp/ C	Primary Phase	Temp. Sec. Phase/ C	Secondary Phase	Temp. Tert. Phase/ C	Tertiary Phase
am5	1450	Anorthite	-	n.o.	-	n.o.
bm5	1420	Melilite	1300	Anorthite	1200	Spinel
cm5	1350	Anorthite	1300	Melilite	1200	Spinel
dm5	1410	Anorthite	-	n.o.	-	n.o.
em5	1470	Anorthite	1350	Spinel	1200	Cordierite
amL0	1420	Anorthite	1360	Spinel	1300	Melilite
bmL0	1460	Spinel	1300	Melilite	-	n.o.
cmL0	1450	Spinel	1200	Anorthite	1200	Melilite
dmL0	1440	Spinel	1350	Anorthite	1200	Melilite
emL0	1455	Spinel	1400	Anorthite	-	n.o.

Melilite: Solid solution gehlenite (2CaO.Al<sub>2</sub>O<sub>3</sub>.SiO<sub>2</sub>) - akermanite (2CaO.MgO.2SiO<sub>2</sub>). Cordierite: 2MgO.2Al<sub>2</sub>O<sub>3</sub>.5SiO<sub>2</sub>. Spinel: MgO.Al<sub>2</sub>O<sub>3</sub>. n.o. - not observed

akermanite ( $2\text{CaO}\cdot\text{MgO}\cdot 2\text{SiO}_2$ ). Of the glasses containing 5% MgO only bm5, cm5 and em5 crystallized to three components. Glasses am5 and dm5 only precipitated anorthite. All the glasses containing 10% MgO were observed to have a primary crystalline phase of spinel ( $\text{MgO}\cdot\text{Al}_2\text{O}_3$ ) except am10 where the primary phase was anorthite. The glasses bm10 and am10 only precipitated the primary and secondary phases whereas the remaining glasses crystallized to three components. There was no evidence of a fourth phase in any of the treated samples.

Crystallization of  $\text{CaO}\text{-Al}_2\text{O}_3\text{-SiO}_2$ -iron oxide glasses: The devitrification behaviour of the iron oxide glasses has been compiled in Table VIII. The liquidus temperature indicated is the highest treatment temperature at which a crystalline phase was or was not present (hence the inequality). The temperature of appearance of subsequent phases is analogous to that described above. While only anorthite was observed to crystallize for the glass af5, the other glasses precipitated secondary and tertiary phases and those of cf10 and bf15 crystallized to four components. The calcium silicate phase determined in some of the quenched samples was either cyclo wollastonite or the low temperature polymorph wollastonite depending on the heat treatment. The glass bf20 showed anomalous behaviour: the initial secondary phase observed was iron wollastonite,  $(\text{CaO},\text{FeO})\cdot\text{SiO}_2$  but at lower temperatures, less than 1100 C anorthite and olivine ( $\text{CaO},\text{FeO}\cdot\text{SiO}_2$ ) were present with the primary phase of melilite. A full description of the results may be found elsewhere (10). The results of the analysis of the ferrous/total iron ratio showed wide variation. The value was found to be dependent on the composition of the melt, temperature treatment and crystallization behaviour. Nevertheless there was a significant amount of ferric iron present in most of the samples.

### Discussion

To be able to correlate the crystallization behaviour of the ash melts it is necessary to describe the devitrification of the model compositions. In the case of the ternary glasses the crystallization behaviour can be understood from the equilibrium phase diagram, Figure 1. The compositions have been plotted on the diagram and the initial crystallization paths drawn. The crystallization path is the extrapolation of the line connecting the composition of the primary phase and the composition of the glass to a given point on the diagram within the primary phase field, usually an isotherm. The path indicates the change in composition of the liquid phase as crystallization proceeds and can be used to evaluate the proportion of liquid and solid phases at a given temperature. For more details see Levin et al. (11). As can be seen, the primary phase predicted from the diagram agrees with the observed behaviour of the ternary glasses. The reluctance of the secondary phase to crystallize for glasses A and E can be understood from the crystallization path. As crystallization of anorthite proceeds the residual liquid phase becomes enriched in silica, becoming more viscous and stable towards devitrification. Glasses C and D were expected to crystallize to two or more components. The observed behaviour of only the primary phase precipitating may be because

Table VIII. Observed crystallization behaviour for the  $\text{CaO-Al}_2\text{O}_3\text{-SiO}_2$ -iron oxide glasses.

Class	Liquidus Temp/C	Primary Phase	Temp. Sec. C	Secondary Phase	Temp. Tert. C	Tertiary Phase	Temp. Quat. C	Quaternary Phase
af5	>1480	anorthite	-	n.o.	-	n.o.	-	n.o.
bf5	>1300	mellilite	1200	anorthite	1200	calcium silicate	-	n.o.
cf5	>1450	anorthite	1200	mellilite	1100	calcium silicate	-	n.o.
df5	>1400	anorthite	1200	mellilite	1100	calcium silicate	-	n.o.
ef5	<1500	anorthite	1200	iron spinel	-	n.o.	-	n.o.
af10	<1480	anorthite	1000	fayalite	-	n.o.	-	n.o.
bf10	>1420	mellilite	1200	anorthite	1100	calcium silicate	-	n.o.
cf10	<1420	anorthite	1200	mellilite	1100	iron spinel	1000	olivine
df10	>1420	anorthite	1300	mellilite	1000	olivine	-	n.o.
ef10	>1400	anorthite	1200	iron spinel	1000	fayalite	-	n.o.
af15	>1400	anorthite	1400	fayalite	-	n.o.	-	n.o.
bf15	<1350	mellilite	1300	iron wollast.	900	anorthite	900	iron spinel
ef15	>1350	anorthite	1100	iron spinel	1000	fayalite	-	n.o.
af20	<1350	anorthite	1300	fayalite	-	n.o.	-	n.o.
bf20	>1300	mellilite	1300	iron wollast.	-	n.o.	-	n.o.
ef20	<1450	anorthite	1400	fayalite	1300	iron spinel	-	n.o.

n.o. - not observed; anorthite ( $\text{CaOAl}_2\text{O}_7\cdot 2\text{SiO}_2$ ); mellilite ( $2\text{CaOAl}_2\text{O}_7\cdot \text{SiO}_2$ ) - may take up iron in solid solution; iron spinel - solid solution  $\text{FeOFe}_2\text{O}_3 - \text{FeOAl}_2\text{O}_3$ ; fayalite ( $2\text{FeO}\cdot \text{SiO}_2$ ); iron wollast. [ $(\text{CaO}, \text{FeO})\cdot \text{SiO}_2$ ]; calcium silicate (wollastonite or cyclo-wollastonite); olivine ( $\text{CaO}, \text{FeO}, \text{SiO}_2$ ).

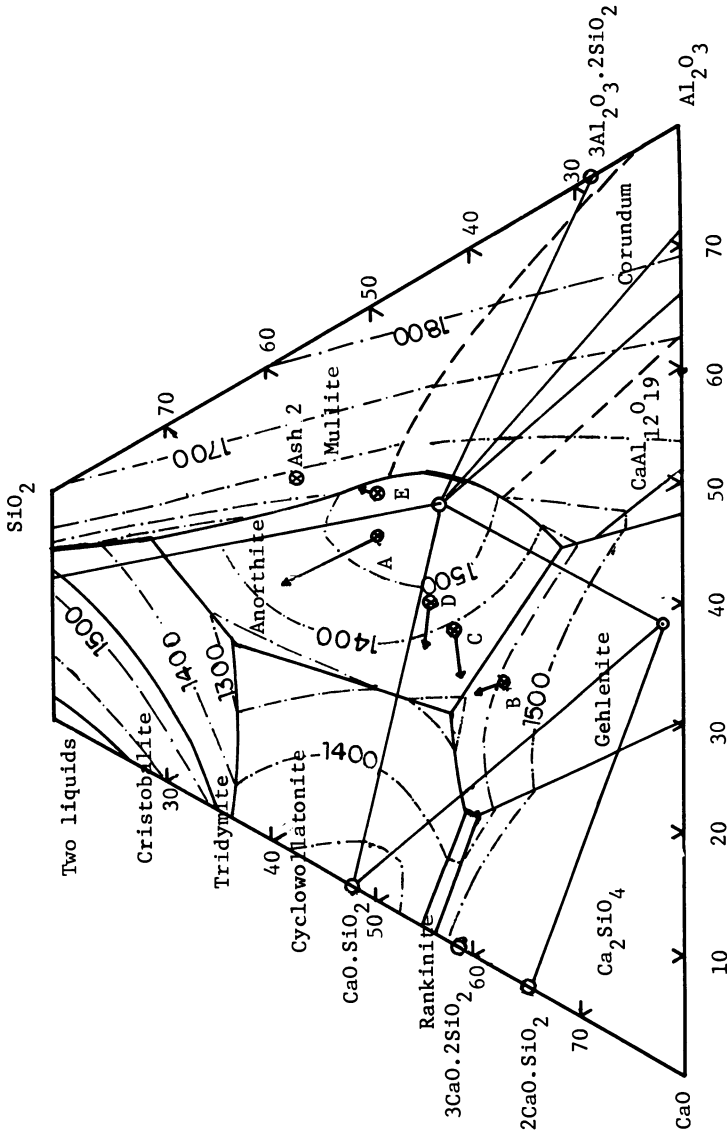


Figure 1. System CaO-Al<sub>2</sub>O<sub>3</sub>-SiO<sub>2</sub>.

insufficient time was allowed for the samples to reach equilibrium. Glass B has a relatively high lime content and although crystallization of gehlenite would produce a liquid phase enriched in silica the liquid would be expected to be relatively fluid compared to those of the other compositions. The close proximity of the composition to the boundary and eutectic would tend to prevent any enrichment of viscous components in the liquid phase from having a profound effect. Therefore the crystallization of glass B to three components would not be unexpected.

The crystallization behaviour of the glasses containing MgO is more difficult to describe. Unlike ternary systems, four component phase diagrams are properly represented by a regular tetrahedron with each apex representing 100% of each component. The crystallization path is therefore in three dimensions which is sometimes difficult to visualize. The method of representation chosen to describe the observed behaviour is as planes of constant MgO content in the regions of interest to this study. Figures 2, 3, and 4 are planes of the quaternary system at 5, 10 and 15 wt% levels respectively and have been compiled from various sources (10,12,13,14). Analysis of the planes indicates the profound effect magnesia has on the primary phase fields. The 5% plane contains magnesia bearing phases such as spinel and pyroxene (a solid solution series between diopside,  $\text{CaO.MgO.2SiO}_2$  and enstatite,  $\text{MgO.SiO}_2$ ). On the 10% MgO plane the spinel field is very dominant and the primary phase fields of the base ternary system (i.e.  $\text{CaO-Al}_2\text{O}_3\text{-SiO}_2$ ) have a very minor presence. The 15% MgO plane, Figure 4 is predominantly composed of magnesia bearing phases with spinel being dominant. The composition of the glasses studied have been plotted on the appropriate plane. The phase diagram not only correctly predicts the primary crystallization observed for the quaternary glasses but also indicates what subsequent devitrification may take place. While it is too complex to discuss here it is possible to calculate the change in composition of the liquid phase with crystallization for multi-component systems. For the purposes of this study it is only necessary to qualitatively indicate the crystallization path. With reference to the 5% MgO plane and compositions falling in the primary field of anorthite it is clear that as the phase precipitates the liquid must become proportionally richer in magnesia. Therefore the crystallization path must be towards the MgO apex of the system. The actual direction of the path will be dependent on the original composition. As the 10% plane comprises mainly MgO containing phases the secondary phase would be expected to be a magnesia bearing phase. The reverse situation is also true, for compositions on the 10% plane and in the primary phase field of spinel the secondary phase would be expected to comprise components of the base ternary systems. This behaviour was observed with the compositions studied in this investigation with the exceptions of those samples which crystallized anorthite only. The behaviour of these glasses can be explained in terms of the viscosity of the melt hindering further crystallization. This generalization of crystallization of quaternary systems must be used with care especially when the precipitating phase may be a solid solution.

Under the laboratory conditions used to study the glasses containing iron oxide both ferric and ferrous iron would be expected

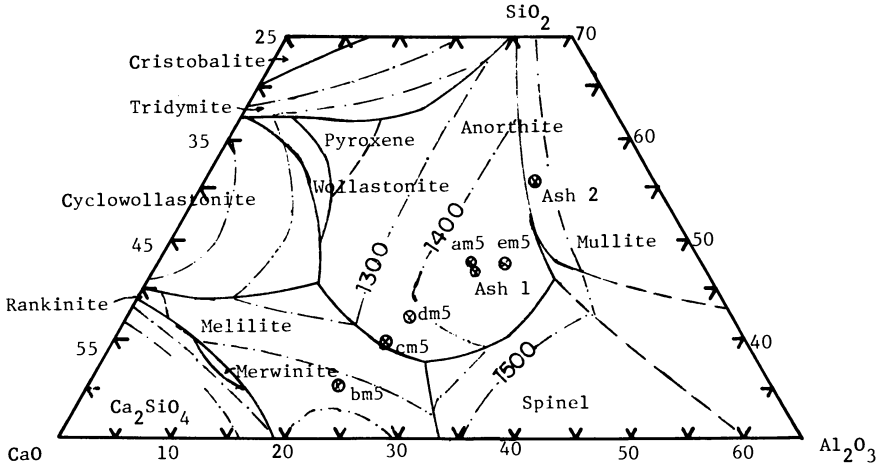


Figure 2. System CaO-MgO-Al<sub>2</sub>O<sub>3</sub>-SiO<sub>2</sub>, 5% MgO plane.

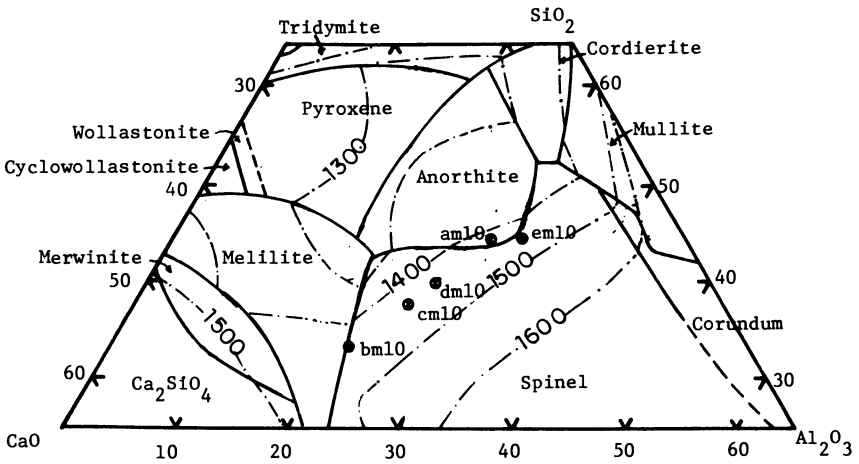


Figure 3. System CaO-MgO-Al<sub>2</sub>O<sub>3</sub>-SiO<sub>2</sub>, 10% MgO plane.

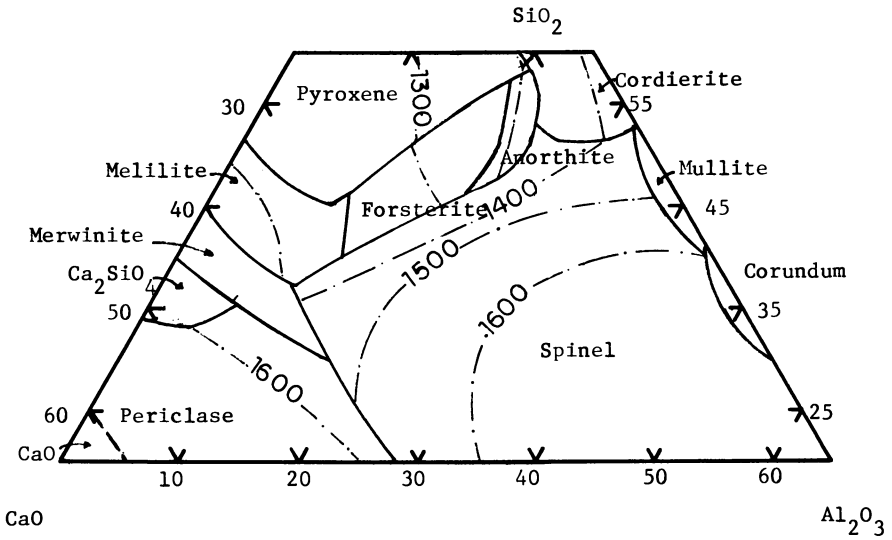


Figure 4. System CaO-MgO-Al<sub>2</sub>O<sub>3</sub>-SiO<sub>2</sub>, 15% MgO plane.



to be present. Therefore the system is a five component or quinary. These systems are extremely difficult to represent and it is therefore necessary to make simplifications to obtain a clearer understanding of the data. With reference to the results obtained, Table VIII, it can be seen that when an iron-bearing phase was observed the form of iron was ferrous, e.g. fayalite,  $2\text{FeO}\cdot\text{SiO}_2$ . (There was some evidence of  $\text{Fe}_2\text{O}_3$  in solid solution with the iron spinel phase.). Therefore as phase diagrams represent the crystalline phases which are in equilibrium with a liquid phase it is possible to describe the system  $\text{CaO-Al}_2\text{O}_3\text{-SiO}_2\text{-iron oxide}$  as a quaternary. It is assumed that all the iron is present as  $\text{FeO}$ . Using this approximation planes of constant  $\text{FeO}$  content were constructed from a number of sources (15, 16) at 5, 10, 15, 20, 25, and 30% levels (Figures 5-10). In comparison to the analogous system containing  $\text{MgO}$  it can be seen that  $\text{FeO}$  does not have such a significant effect on the phase assemblages. Both the 5 and 10% planes are remarkably similar to the base ternary system. There are no significant primary phase fields containing iron oxide until the 15% plane. Even at the 30% level anorthite is still present as a primary phase. To confirm the approximation used in deciding to use the quaternary system it is necessary to check the results of this study. The compositions studied (with the iron oxide taken to be  $\text{FeO}$ ) have been plotted on the appropriate plane. For all the compositions studied the system correctly predicts the primary phase observed. Furthermore, as with the system above the crystallization of subsequent phases can be explained by using the diagrams. There were however some effects due to the presence of ferric iron observed in the study (10).

An important aspect to this study was the determination of the system which most adequately describes the crystallization of the coal ash melts. The compositions of the three ashes studied have been normalized to the required number of components and plotted on the appropriate phase diagram. Normalization must be treated with care because, while only the major three or four components are assumed to be present, minor components may have a disproportionate effect on the crystallization. In the case of the eastern type ash the low  $\text{CaO}$  and  $\text{MgO}$  content reduced the need for plotting on the corresponding diagram.

The observed primary crystalline phase is compared to that predicted for the normalized compositions in Table IX. For ash 1 all the systems correctly predicted the crystallization of anorthite. However for ash 2 only the system  $\text{CaO-FeO-Al}_2\text{O}_3\text{-SiO}_2$  predicted that the observed primary phase would be anorthite. This system also predicted that the primary phase for ash 3 would be mullite. From the results of the crystallization of the model compositions the secondary phase of iron spinel would not be unexpected. The system can also explain in part why only anorthite was observed to crystallize for the western type ashes. For example, for ash 1 the normalized composition lies on the 5%  $\text{FeO}$  plane, with reference to the planes of higher  $\text{FeO}$  content it can be seen that significant crystallization of anorthite must occur before a secondary phase would be expected to precipitate. Therefore the system  $\text{CaO-FeO-Al}_2\text{O}_3\text{-SiO}_2$  appears to govern the crystallization behaviour of ash melts determined under laboratory conditions.

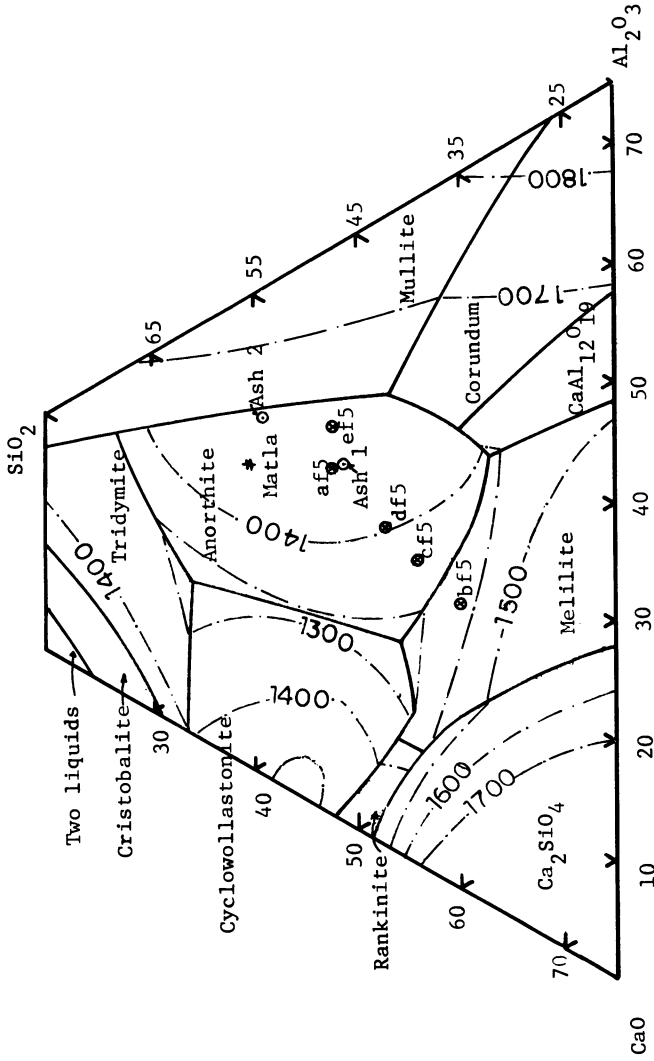


Figure 5. System CaO-FeO-Al<sub>2</sub>O<sub>3</sub>-SiO<sub>2</sub>, 5% FeO plane.

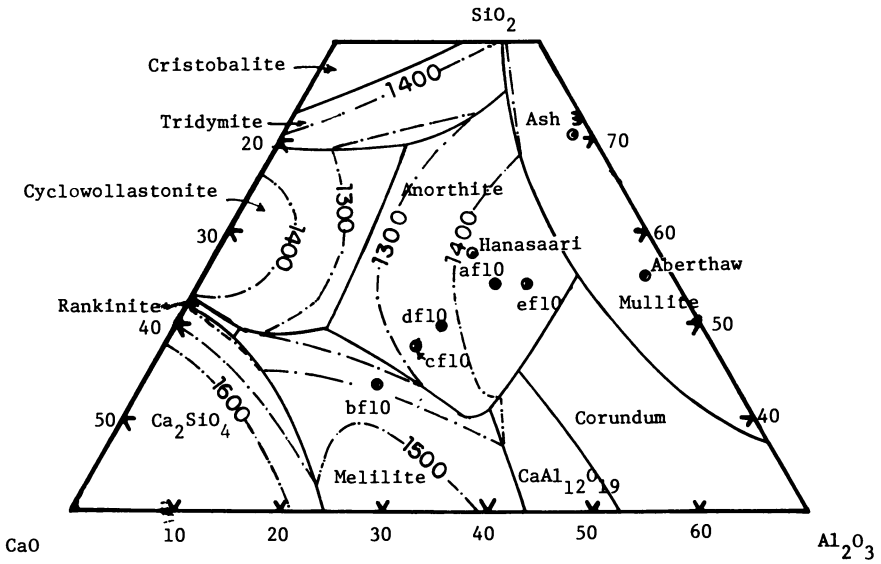


Figure 6. System CaO-FeO-Al<sub>2</sub>O<sub>3</sub>-SiO<sub>2</sub>, 10% FeO plane.

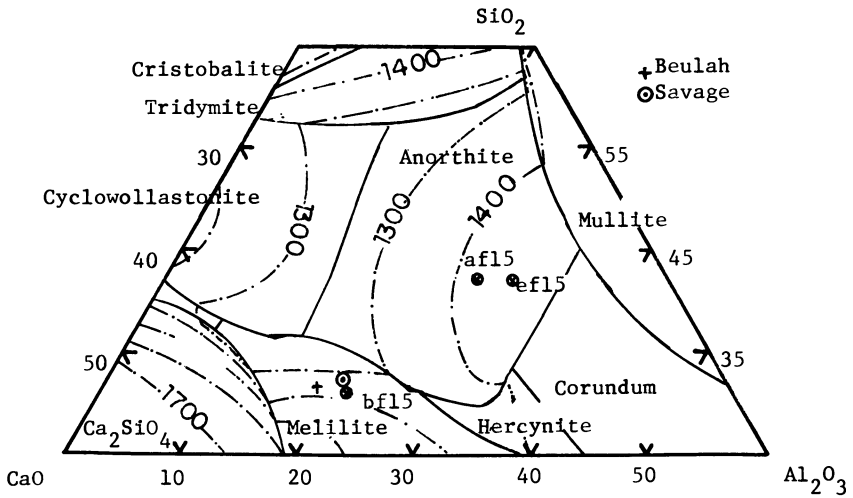


Figure 7. System CaO-FeO-Al<sub>2</sub>O<sub>3</sub>-SiO<sub>2</sub>, 15% FeO plane.

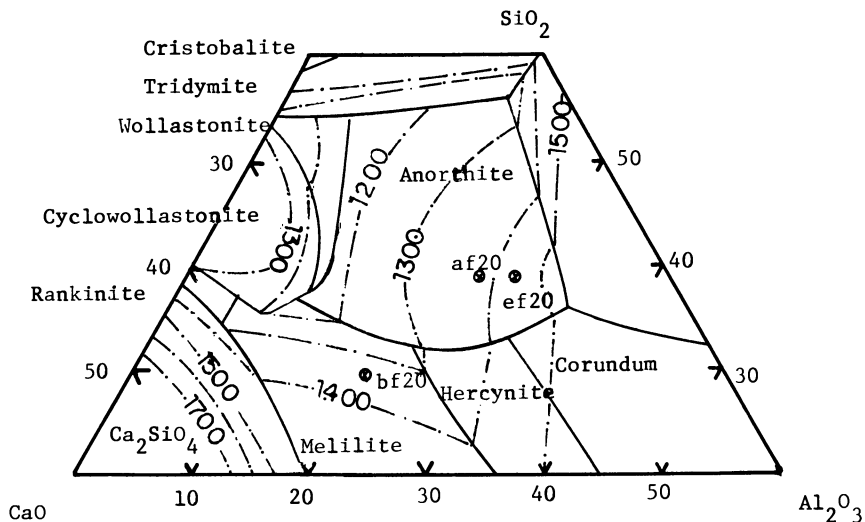


Figure 8. System CaO-FeO-Al<sub>2</sub>O<sub>3</sub>-SiO<sub>2</sub>, 20% FeO plane.

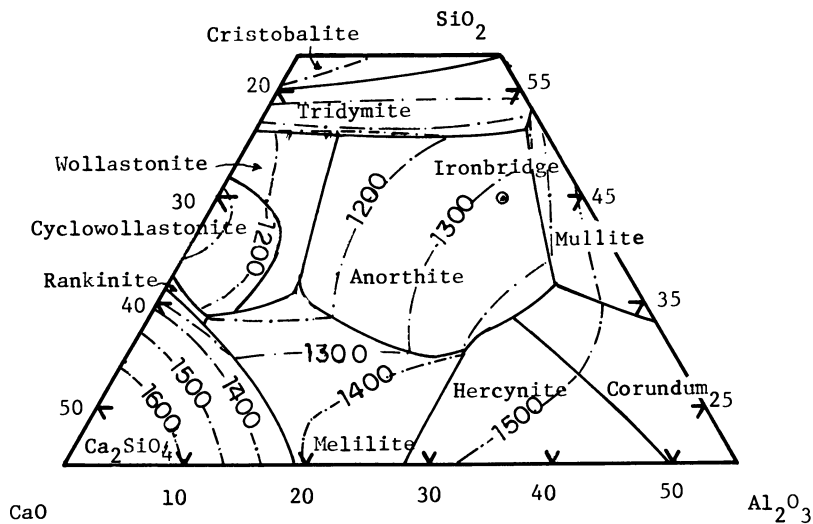


Figure 9. System CaO-FeO-Al<sub>2</sub>O<sub>3</sub>-SiO<sub>2</sub>, 25% FeO plane.

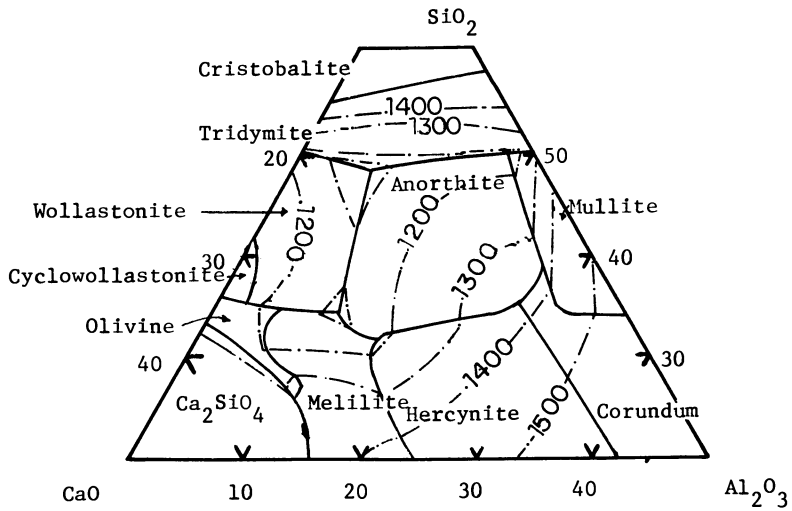


Figure 10. System  $\text{CaO}-\text{FeO}-\text{Al}_2\text{O}_3-\text{SiO}_2$ , 30%  $\text{FeO}$  plane.

Table IX. Comparison of observed crystallization of ash melts with that predicted from relevant phase diagrams.

Ash	Observed primary phase	Predicted primary phase		
		System 1	System 2	System 3
1	Anorthite	Anorthite	Anorthite	Anorthite
2	Anorthite	Mullite	Mullite	Anorthite
3	Mullite	n. d.	n. d.	Mullite

System 1;  $\text{CaO-Al}_2\text{O}_3\text{-SiO}_2$ . System 2;  $\text{CaO-MgO-Al}_2\text{O}_3\text{-SiO}_2$ .

System 3;  $\text{CaO-FeO-Al}_2\text{O}_3\text{-SiO}_2$ .

To be able to relate the results of this study to the phenomena of boiler deposits it is necessary to look at the mineralogy of deposits. Table X is a comparison of the crystalline phases observed in deposits from six utility boilers with the primary phase predicted from the quaternary system. Three deposits are of western type and three are of eastern type. The normalized compositions of the deposits have been included in the Table and plotted on the appropriate plane of the equilibrium system. In the case of the western type deposits the quaternary system correctly predicts the primary phase. This was also the case for the eastern type deposits except for Ironbridge where iron spinel was the primary phase whereas anorthite was predicted. This anomaly may be due to the presence of significant amount of ferric iron and the effect of minor components. Nevertheless the system  $\text{CaO-FeO-Al}_2\text{O}_3\text{-SiO}_2$  appears to govern the crystallization of coal ash deposits to a significant extent.

The ability to predict to some degree the crystallization behaviour of an ash melt may give a valuable insight into the deposition potential of the ash. The growth of deposits has been shown above to be predominantly via a mechanism of viscous flow. For an ash melt crystallizing the composition of the residual liquid phase will change depending on; the original composition, the crystallizing phases and the degree of crystallization. The effect of various components on the rheological behaviour of a melt have not been rigorously determined. However it is known that "acidic" components such as silica and ferric oxide increase viscosity whereas "basic" components e.g. the alkali and alkali earth oxides decrease the viscosity of a melt. Therefore an ash melt which becomes relatively enriched in acid as crystallization proceeds will produce a viscous melt. Conversely if the residual liquid phase becomes enriched in basic oxides the liquid phase will become more fluid. From the model developed by Raask (4) the melt with the viscous liquid phase will produce a weaker deposit than the melt with a fluid residual liquid phase. The strength of the deposit is a measure of the degree of sintering and therefore indicates the rate of growth. Details of the preliminary development of a method to determine the slagging propensity of an ash based on high temperature equilibria and the results of this study may be found elsewhere (17).

Table X. Crystalline phases observed in coal ash deposits compared with that predicted from the system CaO-FeO-Al<sub>2</sub>O<sub>3</sub>-SiO<sub>2</sub>.

Coal /Utility	Composition wt% (normalized)			Crystalline phases observed	Predicted primary Phase	Figure Number
	SiO <sub>2</sub>	Al <sub>2</sub> O <sub>3</sub>	FeO			
Beulah(18) #	31.7	18.4	33.3	Melilite	Melilite	7
Savage(18) #	32.2	20.3	33.9	Melilite	Melilite	7
Matla(10) #	55.7	25.5	14.1	Anorthite	Anorthite	5
Ironbridge(10) *	44.3	23.8	4.8	Iron spinel + anorthite + mullite	Anorthite	9
Hansaari(10) *	56.5	24.1	8.4	Anorthite + iron spinel	Anorthite	6
Aberthaw(10) *	55.6	33.6	2.1	Mullite	Mullite	6

# - western type ash; \* - eastern type ash.

### Conclusions

While coal ash is a complex mixture of mineral components the crystallization behaviour of homogeneous ash melts has been shown to be governed by the major oxide components. The equilibrium system  $\text{CaO-FeO-Al}_2\text{O}_3\text{-SiO}_2$  has been shown to be able to model the initial crystallization behaviour of ash melts. Furthermore the system also appears to govern the crystallization of boiler deposits to a significant extent. The applicability of the use of phase equilibria data to the phenomena of boiler deposits has been indicated.

### Acknowledgments

D. Kalmanovitch gratefully acknowledges the award of a SERC (U. K.) CASE Studentship (1980-1983) and the sponsorship provided by Babcock Power Ltd. U. K.. The facilities and support given by the Combustion and Carbonization Research Laboratory of Energy Mines & Resources Canada through an NSERC Visiting Fellowship (1983-1985) to D. K. is also acknowledged.

### References

1. Winegartner, E.C.; "Coal fouling and slagging parameters". A.S.M.E. Special Publication, 1974.
2. British Standard 1016, Pt. 15, 1970.
3. Padia, A.S.; DSc Thesis, MIT, 1976.
4. Raask, E.; J. Eng. Power; 1982, 104, 856-66
5. Raask, E. and Goetz, L.; J. Inst. Energy, 1981, 54, 163.
6. Lauf, R.J.; Fuel, 1981, 60, 1177-79
7. Barrett, E.P.; "Chemistry of Coal Utilization", Ed. E. Lowry, vol. 1, 1945, Ch. 15.
8. Sanyal, A. and Williamson, J.; J. Inst. Energy, 1981, 54, 158-62
9. Hey, M.H.; Min. Mag., 1941, 26, 116-8.
10. Kalmanovitch, D. P.; Ph. D. Thesis, University of London, 1983.
11. Levin, E.M., Robbins, C.R., McMurdie, H.F., "Phase diagrams for ceramists." Amer. Ceram. Soc., Columbus, 1964, Introductory chapter.
12. Gutt, W. and Russell, A. D.; Jnl. Mat. Sci., 1977, 12, 1869-79.
13. Cavalier, G. and Sandrea-Deudon, M.; Rev. de Metallurgie, 1960, 57, 1143-57.
14. Prince, A. T.; J. Am. Ceram. Soc., 1942, 25, 241-74
15. Schairer, J. F.; J. Am. Ceram. Soc., 1954, 37, 402-9
16. Muan, A. and Osborn, E. F.; "Phase diagrams for ceramists" Ed. Levin, E.M. et al., Amer. Ceram. Soc., Columbus, 1964, 288.
17. Kalmanovitch, D. P. and Williamson, J.; Presented at the 3rd Impurities in Combustion Gases. July 1984, Copper Mountain, Denver.
18. Tufte, P.H. and Beckering, W.A.; A proposed mechanism for ash fouling burning Great Plains lignite, ASME Meeting, Nov. 17 -22, 1974, New York, No. 74-WA/CD-3.

RECEIVED June 21, 1985



## Heat Transfer and Thermal Conductivity of Coal Slags

K. C. Mills

National Physical Laboratory, Teddington, Middlesex TW11 0LW, United Kingdom

The various factors affecting the complex heat transfer processes which occur in semi-transparent media like slags are discussed. This information has been used to evaluate the validity of the various experimental methods available for measuring the thermal conductivity of slags. A critical assessment of published experimental data for slags and magmas covering a wide composition range has been carried out. This review of thermal conductivity data showed that both the ( $\text{Fe}^{2+}/\text{Fe}^{3+}$ ) ratio and the crystallinity of the slag greatly influence the amount of heat transferred through the slag by radiation conduction. The heat transferred across the solid slag formed on the walls of the vessel has been shown to be dependent upon the thermal resistance of the slag/metal interface which, in turn, appears to be dependent upon the mineralogical constitution of the slag.

During the gasification of coal, both molten and solid slags are formed in the converter, and the heat transfer within the gasification chamber is governed to a large extent by the thermal properties of the slag phase. Thus in order to carry out either heat balance or modelling calculations it is necessary to have reliable data for the thermal properties of both solid and liquid coal slags. However, the thermal transfer mechanisms in high temperature processes involving slags are exceedingly complex since heat can be transported by convection, radiation and thermal conduction. In order to simplify the analysis of the combined conductive-radiative thermal flux it is necessary to resort to one of the various heat transfer models available. The most widely-used model is the diffusion approximation in which the thermal flux is used to derive an effective or total thermal conductivity ( $k_{\text{eff}}$ ) which is, in turn, considered to be made up of contributions from (i) the thermal ("phonon") conductivity,  $k_c$ , (ii) radiation conductivity,  $k_R$  and

This chapter not subject to U.S. copyright.  
Published 1986, American Chemical Society

(iii) electronic conductivity,  $k_{el}$ . Heat balance calculations must take account of each of these thermal transport mechanisms and this is particularly important as the boundary conditions in the experimental determination of the thermal conductivity of a slag may vary appreciably from those applying to the slag in the gasifier. Thus it is necessary, where possible, to determine the individual contributions to the total heat flux for each condition. In the present paper the factors affecting the thermal conductivity of slags will be examined and the various methods available for the measurement of thermal conductivities will be assessed. Finally, experimental data for the thermal conductivity of slags, glasses and magmas will be evaluated to provide a reliable data base for the thermal conductivity of slags, and to determine the likely effects of variations in chemical composition upon values for coal slags.

#### Thermal conduction mechanisms

Thermal "phonon" conductivity ( $k_c$ ). Heat is transferred through a medium by phonons, which are quanta of energy associated with each mode of vibration in the sample. This mode of conduction is thus referred to as thermal, phonon or lattice conduction. Scattering of the phonons causes a decrease in the thermal conductivity which is therefore sensitive to the structure of the sample. Scattering of the phonons can occur by collisions of the phonons with one another, or by impact with grain boundaries or crystal imperfections, such as pores. Thus a low-density, highly-porous material will have a low thermal conductivity. In glassy, non-crystalline materials it has been suggested that thermal conductivity decreases as the disordering of the silicate network increases.

#### Radiation conductivity ( $k_R$ )

Measurements of the thermal conductivity of glasses were found to be dependent upon the thickness of the specimens used, and this is shown in Figure 1. This behaviour was ascribed to the contribution from radiation conductivity,  $k_R$ , which can occur in semi-transparent media like slags and glasses. Radiation conductivity occurs by a mechanism involving absorption and emittance of radiant energy by various sections through the medium. Consider a thin section in the slag, radiant energy absorbed by the section will cause it to increase in temperature and consequently radiant heat will be emitted to cooler sections. This process can occur continuously through the medium and it is obvious that the energy transferred in this way will increase with increasing number of sections (ie. increasing thickness) until the point is reached where  $k_R$  attains a constant value. At this point the slag is said to be "optically thick", and this is usually considered to occur when  $\alpha d > 3.5$ , where  $\alpha$  and  $d$  are the absorption coefficient and thickness of the slag, respectively.

At high temperature, radiation conduction can be the predominant mode of heat transfer, eg. in glassmaking more than 90% of the thermal transfer occurs by radiation conduction. The radiation conductivity can be calculated for an optically-thick sample if steady-state conditions apply and if it is assumed that the absorption coefficient of the medium,  $\alpha$ , is independent of

wavelength,  $\lambda$ , ie. grey-body conditions obtain. For these conditions  $k_R$  can be calculated by use of Equation 1, where  $\sigma$  and  $n$  are the Stefan-Boltzmann constant and refractive index, respectively.

$$k_R = \frac{16 \sigma n^2 T^3}{3 \alpha} \quad (1)$$

Values of  $k_R$  cannot easily be calculated for optically-thin samples ( $\alpha d < 3.5$ ) and for some measurement techniques involving non-steady state conditions. Thus it is obvious that reliable values of thermal conductivity can only be obtained when either  $k_R$  is negligible, or where it can be calculated reliably for optically-thick conditions.

Absorption coefficient ( $\alpha$ ). The absorption coefficient is a very important parameter, which determines (i) the magnitude of  $k_R$  (Equation 1) and (ii) the thickness at which a slag becomes optically thick ( $\alpha d > 3.5$ ). Hence increasing  $\alpha$  has the effect of decreasing  $k_R$  and decreasing the depth at which a slag becomes optically thick. If a particular slag sample were optically thin, these two factors would operate in opposition to one another. The absorption coefficient is markedly dependent upon the amounts of FeO and MnO present in the slag<sup>(2)</sup>; although Fe<sub>2</sub>O<sub>3</sub> absorbs infra-red radiation, its effect on  $\alpha$  is much less pronounced than that of FeO. An empirical rule has been derived<sup>(2)</sup> for glasses containing less than 5% FeO, from which the absorption coefficient at room temperature is given by the relationship,  $\alpha = 11. (\% \text{ FeO})$ .

A basic assumption adopted in deriving Equation 1 was that  $\alpha$  was independent of wavelength; however, in practice the spectral absorption coefficient ( $\alpha_\lambda$ ) varies with the wavelength ( $\lambda$ ) as shown in Figure 2 for a glass containing ca. 5% FeO<sup>(2)</sup>. It can be seen from this figure that there is strong absorption by FeO at ca. 1  $\mu\text{m}$  and by SiO<sub>2</sub> at ca. 4.4  $\mu\text{m}$ . At high temperatures this restricts absorption by the slag to a "window", in the wavelength range 1-4.4  $\mu\text{m}$ . However, even within this wavelength band there is some variation in  $\alpha_\lambda$  and the average absorption coefficient,  $\alpha_m$ , is determined by weighting of the  $\alpha_\lambda$  values.

The average absorption coefficient,  $\alpha_m$ , can be affected by temperature in two different ways. Firstly, the absorption spectrum, ie, ( $\alpha_\lambda$ ), can change markedly with temperature and consequently alter the value of  $\alpha_m$ . Secondly, even if the absorption spectrum is unaffected by temperature,  $\alpha_m$  would continue to be a function of temperature because the wavelength distribution used in deriving  $\alpha_m$  is itself a function of temperature. This can be seen in Figure 3 where the fraction of total energy emitted in the "window" 1-4.4  $\mu\text{m}$  constitutes 61.1%, 79.5% and 81.9% of the total energy emitted at 1073 K, 1573 K and 1773 K, respectively. In a similar manner, the various  $\alpha_\lambda$  values of the spectrum will have to be weighted differently in the calculation of  $\alpha_m$  for the three temperatures in question.

It can be seen from Figure 2 that  $\alpha_m$  increases with increasing temperature<sup>(4,5,6)</sup> and similar behaviour has been observed in rocks and minerals<sup>(4,5,6)</sup>. By contrast, the absorption coefficients ( $\alpha$ ) of amber glass have been found to decrease with increasing temperature.

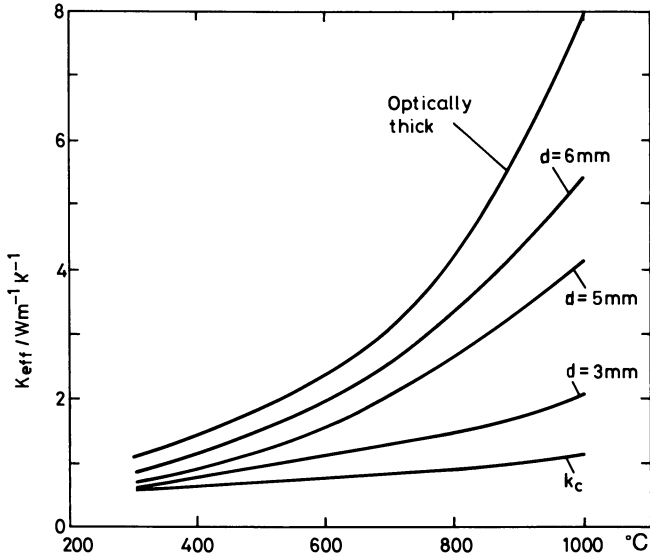


Figure 1. The dependence of  $k_{eff}$  upon the thickness of the sample.

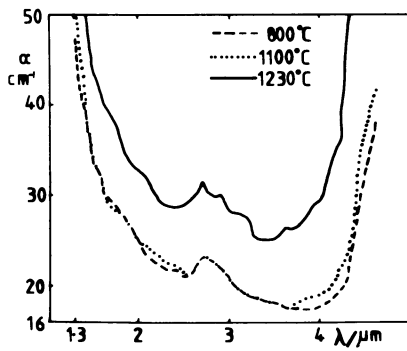


Figure 2. The wavelength dependence of  $\alpha$  of a glass containing 67%  $\text{SiO}_2$  + 16%  $\text{Na}_2\text{O}$  + 9% ( $\text{FeO}$  +  $\text{Fe}_2\text{O}_3$ ).

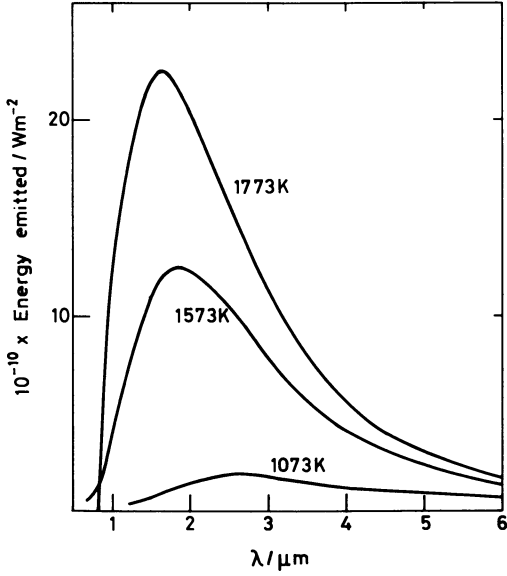


Figure 3. Wavelength distribution of the source energy emission for a black body.

Extinction coefficient (E). In solids, radiant energy can be scattered by grain boundaries, pores and cracks in the material. In these cases, it is necessary to use the extinction coefficient (E) which is given by the relationship  $E = \alpha + s$ , where  $s$  is the scattering coefficient.

Electronic conductivity ( $k_{el}$ ). It has been reported that glasses which contain significant concentrations of  $Fe^{2+}$  ions behave in a similar manner to semi-conductors and hence thermal conduction via conduction electrons, holes, etc could be significant, according to Fine *et al* (7). Little is known of this mechanism in relation to the heat transfer in slags and consequently the contribution of  $k_{el}$  to the measured thermal conductivities has been ignored in this review.

Total thermal conductivity ( $k_{eff}$ ). In practice, the radiation and conduction contributions to the heat flux (Q) are interactive, and the interpretation of the combined conductive-radiative heat transfer is complex. Various models have therefore been proposed to simplify the theory of the heat transfer process. One widely-used model is the diffusion approximation which assumes that the heat flux (Q) is given by Equation 2, where  $k_{eff}$  is the effective thermal conductivity and is defined by Equation 3 where  $x$  is the distance. Gardon (8) has pointed out that this model only applies strictly when (i)  $k_R$  is small and (ii)  $\alpha d > 8$ .

$$Q = -k_{eff} (dT/dx) \quad (2)$$

$$k_{eff} = k_c + k_R \quad (3)$$

#### Experimental Methods for Determining Thermal Conductivity

The experimental methods available for measuring thermal conductivities are summarised below; more detailed reviews of the experimental techniques are available elsewhere (3, 9, 10, 11). The techniques for the determination of thermal conductivity can be divided into three classes: (i) steady-state methods, (ii) non-steady state methods, and (iii) indirect methods. The steady-state methods usually yield  $k_{eff}$  values and the non-steady state techniques usually produce thermal diffusivity ( $a_{eff}$ ) values, which can be converted to thermal conductivity values by use of Equation 4, where  $\rho$  and  $C_p$  are the density and heat capacity respectively of the slag.

$$k = a \cdot C_p \cdot \rho \quad (4)$$

Steady-state methods. These methods all yield  $k_{eff}$  values provided that the specimen is optically thick.

In the linear heat-flow method two disc-shaped specimens are placed on either side of an electrically-heated plate and the temperature profiles across the samples are monitored by thermocouples sited on both faces of the specimens. The apparatus is well insulated to minimise heat losses. In some versions of this method, the total heat flux passing through the samples is determined

by calorimeters in contact with the specimens. When high-temperature measurements are required, this technique is usually operated as a comparative method<sup>(12)</sup>.

In the radial heat-flow method the specimen is in the shape of a hollow cylinder, which is positioned in the annulus between two coaxial cylinders with the internal cylinder acting as a radial heat source<sup>(13)</sup>. The temperature profile across the specimen is determined by thermocouples placed on the inside walls of the two cylinders. This method requires a large isothermal zone in the furnace, which is difficult to achieve at high temperatures. When this technique is used for measurements on liquids, errors can occur from convective heat transfer.

Non-steady state methods. In the radial wave method the slag is placed in a cylindrical crucible situated in the isothermal zone of a furnace, and thermocouples are located on the walls and along the geometric axis of the crucible (the slag). The outside wall of the crucible is then subjected to variation of temperature and the variation in temperature of the central thermocouple is monitored. There is a phase shift between the input and output which is related to the thermal diffusivity of the slag. In the modification of this apparatus used by Elliott and co-workers<sup>(7,14)</sup> the periodic variation in temperature is produced in a wire running along the central axis of the cylindrical crucible, and the phase shift is measured by thermocouples located on the walls of the crucible. The thermal diffusivity values obtained with this method may be vulnerable to errors arising from convective heat transfer.

In the modulated beam method the specimen is in the form of a disc, which is maintained at a constant temperature, whilst the front face is subjected to a laser beam which produces a periodic variation in temperature of constant frequency. The phase shift between this input and the signal from a temperature sensor in contact with the back face is determined. By carrying out measurements at two or more frequencies, Schatz and Simmons<sup>(8)</sup> were able to derive values of both  $a_{\text{eff}}$  and the extinction coefficient. If this method were applied to measurements in liquids, it too would be prone to errors caused by convection.

The laser pulse method<sup>(15,16)</sup> when applied to solids uses a disc-shaped slag specimen coated with metallic films on both planar surfaces. A laser pulse is directed on to the front face of the specimen and the temperature of the back face is monitored continuously. The maximum temperature increase of the back face ( $\Delta T_{\text{max}}$ ) usually occurs after ca. 10 seconds, and  $a_{\text{eff}}$  may be computed from the time taken ( $t_{0.5}$ ) for the back face to attain a temperature rise of  $(0.5 \Delta T_{\text{max}})$ . The method has also been applied to measurements on liquid slags<sup>(15,17)</sup> which were contained in  $\text{Al}_2\text{O}_3$  or BN crucibles. The major advantage of this technique is that the short duration of the experiment minimises the errors due to convection. The major disadvantage is that the maximum specimen thickness is about 0.4 cm, and consequently optically-thick conditions only apply when the extinction coefficient is greater than  $9 \text{ cm}^{-1}$ . A second disadvantage is that the laser pulse method is a transient technique and  $k_p$  cannot be calculated by Equation 1, which is applicable to steady-state conditions; at the present time no formulae exist for the calculation

of  $k_R$  for this method. Thus this technique is most useful when applied to specimens which have (i) very small values of  $\alpha d$  (ie.  $\alpha d \ll 3.5$ ) where  $a_{eff} = a_c$ , or (ii) large extinction coefficients where  $k_R$  is negligible and thus  $a_{eff} = a_c$ .

The line source method is also a transient technique and is the standard method for measuring the thermal conductivities of liquids at lower temperatures. In the high-temperature versions, this method consists of a fine Pt wire (ca. 0.1 mm dia) which is placed centrally in a crucible of molten slag. This wire acts as both heating element and temperature sensor. When an AC or DC current is applied to the wire, the temperature rise of the wire ( $\Delta T$ ) is monitored continuously during the heating period (ca. 1 second). A linear relationship exists between  $\Delta T$  and  $\ln$  (time), the slope of which is proportional to  $(1/k)$ . This method has the advantage that convectional heat transfer is eliminated (if convection does occur it results in a non-linear  $\Delta T$ - $\ln$  (time) plot and can therefore be readily detected). Routines are available for calculating the value of  $k_R$  for optically-thick conditions (18); however, de Castro *et al* (19<sub>R</sub>) have recently proposed that  $k_R$  is negligible in the values of  $k_{eff}$  measured by this technique at ambient temperatures (ie.  $k_R = 0$ ,  $k_{eff} = k_c$ ). There is evidence to support the view that  $k_R = 0$ , as measurements made with this technique at higher temperatures (20, 21, 22) yield much lower values of  $k_{eff}$  for slags than those obtained by steady-state techniques. Furthermore, Powell and Mills (23) have pointed out that the thermal conductivity data for molten salts become more consistent if  $k_R$  is taken to be zero in the various line-source determinations.

Indirect measurements of  $k_R$ . The absorption (or extinction) coefficient can be determined by measurement of the optical transmissivity ( $\tau$ ) of the slag as a function of wavelength; the absorption coefficient ( $\alpha$ ) is given by equation (5), where  $d$  is the thickness of the specimen.

$$\alpha = -\ln(\tau)/d \quad (5)$$

Measurements at high temperatures are carried out using an assembly of mirrors positioned in a tube furnace. The transmitted beam is diverted into an infrared spectrophotometer where the transmissivity is determined. Blazeck and Endrys (2) have reported that  $k_R$  values for glasses calculated from absorption coefficient data are in good agreement with values of  $(k_{eff} - k_c)$  determined experimentally.

Summary of experimental limitations.

- (i) It is important to ensure that the thermal conductivity measurements on semi-transparent media are carried out with optically-thick specimens, as  $k_R$  cannot easily be calculated for optically-thin conditions. It is recommended that absorption coefficient measurements should also be carried out to determine the slag thickness required to produce an optically-thick specimen.
- (ii) The non-transient techniques are prone to errors due to convectional heat transfer.
- (iii) At the present time no reliable routines are available for



calculating the  $k_R$  contribution to the overall thermal conductivity measured in transient techniques; there is some evidence to suggest that  $k_R$  is negligible in measurements obtained by the line source method.

### Review of the Extant Data for Slags

Coal slags vary appreciably in composition and since there is a paucity of data for coal slags; it is necessary to study a range of slag compositions to determine the effects of compositional change on the thermal conductivity. One problem continually encountered is that the distribution of Fe in slags between ( $\text{Fe}^{3+}$ ), ( $\text{Fe}^{2+}$ ) and free iron is not reported, and this can have a marked effect on the absorption coefficient and consequently on  $k_R$ . Furthermore, the ratio of ( $\text{Fe}^{2+}/\text{Fe}^{3+}$ ) is known to vary with (i) temperature, (ii)  $p(\text{O}_2)$  and (iii) the composition of the slag, ( $\text{Fe}^{2+}$ ) increasing with increasing  $\text{SiO}_2$  and  $\text{TiO}_2$  and decreasing CaO and  $\text{Na}_2\text{O}$  contents.

$\text{CaO} + \text{SiO}_2 + \text{FeO}$ . Fine et al (7) determined the absorption spectra at room temperature of three slags containing 0, 7 and 14% FeO (Figure 4). The absorption coefficients of the slags containing 7 and 14% FeO will probably increase with increasing temperature since the ( $\text{Fe}^{2+}/\text{Fe}^{3+}$ ) ratio will increase. An increase in  $\alpha$  with increasing temperature can also be seen in Figure 2. Fine et al (7) used the radial wave method to determine  $a_{\text{eff}}$  of solid and liquid slags containing 0 to 25% FeO; their results are summarised in Equation 6, where B represents the basicity, ie. ( $\text{CaO}/\text{SiO}_2$ ) ratio and T is the temperature in ( $^\circ\text{C}$ ).

$$a_{\text{eff}} = 10^{-7} (1.5 - 0.5 B) + 1.8 \times 10^{-6} \frac{(T/1500)^3}{(\% \text{FeO})^{0.8}} \text{ m}^2 \text{ s}^{-1} \quad (6)$$

This equation indicates that increasing the FeO content results in a reduction of  $a_{\text{eff}}$ ; this behaviour is due presumably to the increase in  $\alpha$  and hence the consequent decrease in  $k_R$  with increasing FeO content. However, Nauman et al (24) using the same experimental technique as Fine et al (7) obtained the  $k_{\text{eff}} - (\% \text{FeO})$  relationship shown in Figure 5 for molten slags with high FeO contents. The density of slags are known to increase with increasing ( $\text{FeO}$ ,  $\text{MnO}$ ) content, thus  $k(\frac{= a \cdot C}{\rho})$  would be expected to increase as the level of FeO increases (25). However, calculations have shown that this increase in  $k$  would be ca. 30%, and this alone would not account for the increase shown in Figure 5. Thus it must be concluded that FeO additions do increase the thermal diffusivity of the system. In these slags with high FeO content, the absorption coefficient must be very high and thus  $k_R$  must be negligible and  $k_{\text{eff}} = k_c$ .

$\text{CaO} + \text{Al}_2\text{O}_3 + \text{SiO}_2$ . Measurements on solid slags have been reported by Kingery (12) (comparative linear heat-flow method), Osinovskikh (22) and Susa et al (21) (line source method), and for the liquid phase by Susa et al (21) and Ogino et al (13) (radial heat-flow); the results are summarised in Figure 6. The data recorded

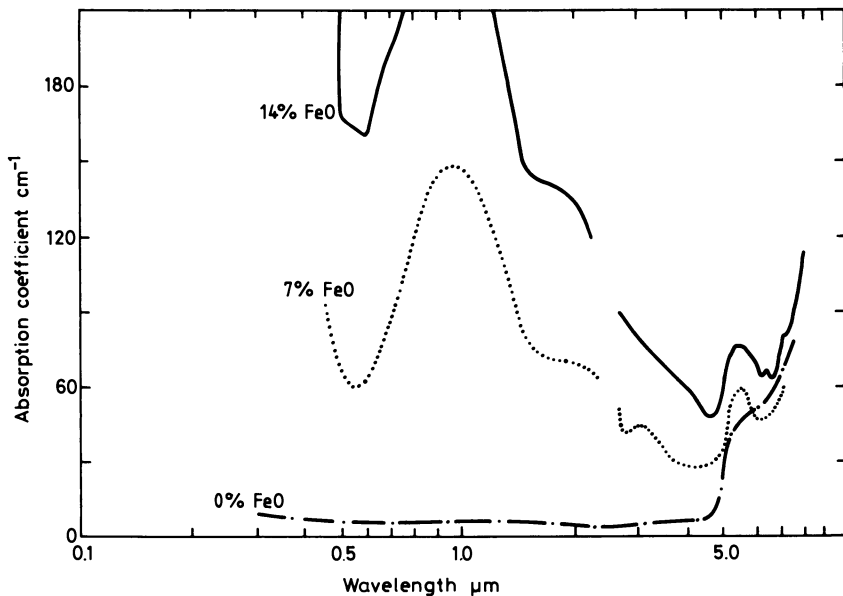


Figure 4. The absorption spectra at room temperature for slags containing FeO<sub>x</sub> + CaO + SiO<sub>2</sub>.

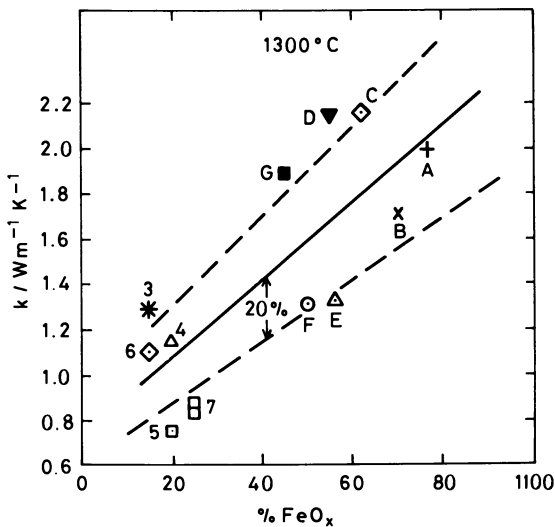


Figure 5. The thermal conductivity of slags of the system FeO<sub>x</sub> + CaO+SiO<sub>2</sub> as a function of the FeO<sub>x</sub> content. The letters and numerals refer to the specimen numbers (14).

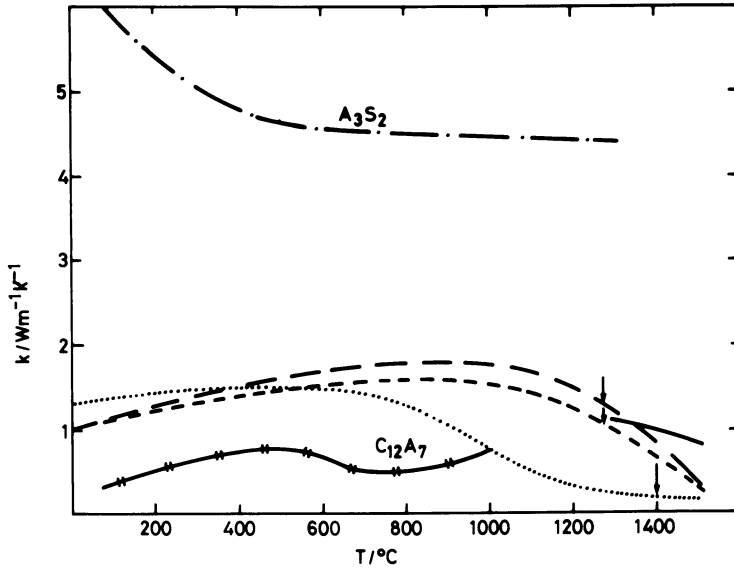


Figure 6. Thermal conductivities of slags from the system,  $\text{CaO} + \text{Al}_2\text{O}_3 + \text{SiO}_2$ ; — · —, Kingery for  $3\text{Al}_2\text{O}_3 \cdot 2\text{SiO}_2$ ; Ogino et al.: —; Susa, ·····, 50%  $\text{CaO} + 50\% \text{Al}_2\text{O}_3$ ; ----, 40%  $\text{CaO} + 40\% \text{SiO}_2 + 20\% \text{Al}_2\text{O}_3$ ; — — —, 25%  $\text{CaO} + 60\% \text{SiO}_2 + 15\% \text{Al}_2\text{O}_3$ ; —, Osinovskikh; ↓,  $T_{\text{liq}}$ .

by Osinovskikh<sup>(25)</sup> appear to be too low, but there is some measure of agreement between the data obtained by other investigators for the liquid near the liquidus temperature ( $T_{liq}$ ). However, the reported, thermal conductivity values diverge as the temperature increases, and this is possibly due to the negligible contribution of  $k_R$  in the line source measurements<sup>(20)</sup> and the effects of  $k_R$  and convective heat transfer on the value due to Ogino<sup>(13)</sup>. The value due to Kingery<sup>(12)</sup> for the compound  $3Al_2O_3 \cdot 2SiO_2$  is appreciably higher than that for the slags of the ternary system.

MgO + Al<sub>2</sub>O<sub>3</sub> + SiO<sub>2</sub>. Values for the various binary compounds occurring in this system have been reported by Rudkin<sup>(26)</sup> and by Kingery<sup>(12)</sup> (comparative linear heat-flow method), and by Schatz and Simmons<sup>(6)</sup> (modulated beam method) for temperatures up to 1300 °C; there is excellent agreement between the values obtained by the latter two groups of workers. Schatz and Simmons<sup>(6)</sup> reported that the extinction coefficient of  $2MgO \cdot SiO_2$  increases from  $5 \text{ cm}^{-1}$  at 270 °C to  $25 \text{ cm}^{-1}$  at 1300 °C.

Na<sub>2</sub>O + SiO<sub>2</sub>. Susa *et al*<sup>(21)</sup> (line source method) reported thermal conductivity data for solid and liquid slags for three compositions; the single value obtained by Ogino *et al*<sup>(13)</sup> (radial heat-flow method) is in reasonable agreement with these data.

Glasses. Blazek and Endrys<sup>(3)</sup> have reviewed the thermal conductivity data for glasses. The lattice thermal conductivity,  $k$ , for glasses is relatively unaffected by composition and was found to increase with temperature from  $1 \text{ Wm}^{-1} \text{ K}^{-1}$  at 25 °C to  $2.7 \text{ Wm}^{-1} \text{ K}^{-1}$  at 1300 °C. However, radiation conduction is frequently the dominant mode of heat conduction in glasses at high temperatures.

CaF<sub>2</sub>-based slags. Extinction coefficients have been reported ( $1.3 \text{ cm}^{-1}$  for 1000-1300 °C) by Keene and Mills<sup>(27)</sup>, and absorption coefficients ( $1.3 \text{ cm}^{-1}$ ) for the liquid state by Mitchell and Wadier<sup>(22)</sup>.

The thermal conductivity values for polycrystalline (optically-thick) CaF<sub>2</sub> obtained by Kingery<sup>(12)</sup> (comparative linear flow method) and by Taylor and Mills<sup>(16)</sup> (laser pulse method) are in reasonable agreement (Figure 7). However, there is an appreciable discrepancy between the values of  $k$  obtained by the line source method<sup>(20-22)</sup> and the single value due to Ogino *et al*<sup>(13)</sup> (radial heat source method).

The reason for the discrepancy probably lies in the magnitude of the  $k_R$  values measured in the two experiments, as  $k_R$  is probably negligible for the line source technique, in contrast to the steady-state method where  $k_R$  would be appreciable despite the fact that the sample was probably optically thin ( $\alpha d \approx 0.8$ ).

TiO<sub>2</sub>-based slags. Values of thermal diffusivity,  $a_{eff}$ , of  $3 \times 10^{-7} \text{ m}^2 \text{ s}^{-1}$  have been reported by Raflovich and Denisova<sup>(28)</sup> for slags based on TiO<sub>2</sub> (>45%) and (<35%) SiO<sub>2</sub> with small amounts of Al<sub>2</sub>O<sub>3</sub> and Fe<sub>2</sub>O<sub>3</sub>. The data reported by Osinovskikh *et al*<sup>(25)</sup> for slags with less than 15% TiO<sub>2</sub> are much lower and this is probably due to the high porosity of the sample used.

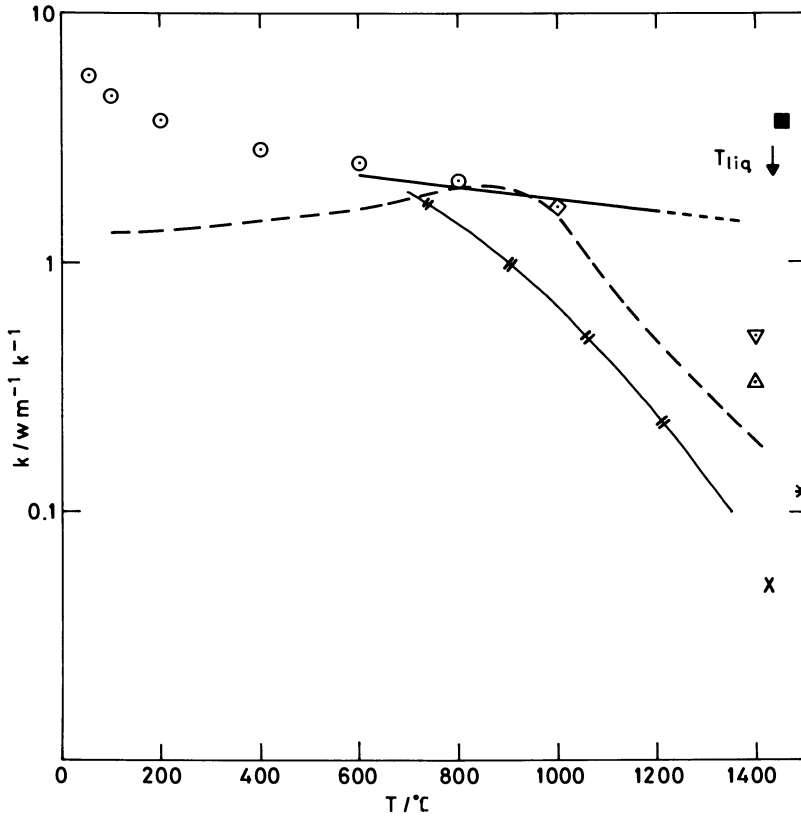


Figure 7. The thermal conductivity of  $\text{CaF}_2$  and  $\text{CaF}_2$ -based slags;  $\text{CaF}_2$ ; \*, Powell; ○, Charvat; — · — · —, Taylor; x, Nagata; ■, Ogino; ▽, Mitchell;  $\text{CaF}_2$ -based slags, — — —, Susa et al; △, Mitchell.

Continuous casting slags. These slags have the approximate composition ( $\text{CaO} = \text{SiO}_2 = 35\%$ ;  $\text{Al}_2\text{O}_3 = 7\%$ ;  $\text{Na}_2\text{O}$  4-15% and  $\text{CaF}_2$  5-8%). Olusanya<sup>(29)</sup> has reported that the absorption coefficients lie in the range ( $0.5 - 5 \text{ cm}^{-1}$ ) and thus  $k_R$  could be appreciable in these slags. Values of  $a_{\text{eff}}$  were obtained for ten glassy-slugs by Taylor and Mills<sup>(30)</sup> (laser pulse method) and were between 4 and  $5 \times 10^{-7} \text{ m}^2 \text{ s}^{-1}$  (Figure 8). These slags were optically thin ( $\alpha d = 0.4$ ) and thus we might expect  $k_R$  to be small and  $k_{\text{eff}} \approx k_c$ . Some crystallisation of the samples occurred at temperatures above the glass temperature in these experiments, and this resulted in an initial decrease in  $a_{\text{eff}}$ , which was subsequently followed by an increase in the thermal diffusivity. Taylor and Mills reported that  $a_{\text{eff}}$  of a crystallised specimen had a value of ca.  $6 \times 10^{-7} \text{ m}^2 \text{ s}^{-1}$ , which is higher than that of the glassy specimens; the crystalline samples would have a higher extinction coefficient and thus  $k_R$  would be low and hence  $a_{\text{eff}} = a_c$ . Thermal conductivity values for the liquid phase have been obtained by Nagata et al<sup>(31)</sup> and by Powell et al<sup>(32)</sup> (line source method), and by Taylor and Edwards<sup>(17)</sup> (laser pulse method) and by Ohmiya et al<sup>(33)</sup> (interpretation of thermal flux data). As can be seen from Figure 8, the results from the line source technique are lower than the other data, and this probably reflects the fact that  $k_R$  is negligible in the line source experiments. The increase in  $k_{\text{eff}}$  observed by Taylor and Edwards<sup>(17)</sup> above the solidus temperature is probably due to the decrease in  $\alpha$  (and increase in  $k_R$ ), as liquid is formed from crystallised slag.

Blast furnace slags. Values of  $k_{\text{eff}}$  have been reported by Ischenko<sup>(34)</sup> and by Vargaftik and Oleschuk<sup>(35)</sup> for temperatures in the range (200-1000 °C). The values given are lower than those reported for other slags, which is presumably due to the high porosity of the samples used by these workers.

Rocks and Minerals. Absorption and extinction coefficients for several rocks and minerals<sup>(4,2,6)</sup> were found to increase appreciably at high temperatures, eg  $\alpha_{\text{OM}}$  (peridot) increases from  $0.5 \text{ cm}^{-1}$  at 25 °C to  $4.3 \text{ cm}^{-1}$  at 1240 °C. Values of  $k_{\text{eff}}$  (or  $a_{\text{eff}}$ ) have been recorded by Kingery<sup>(12)</sup>, by Kawada<sup>(36)</sup> (comparative linear flow method), by Murase and McBirney<sup>(37)</sup> (radial heat flow), and by Schatz and Simmons<sup>(6)</sup> (modulated beam method). The results are given in Figure 9, and Schatz and Simmons<sup>(6)</sup> reported that for forsterite and olivine at 1300 °C, approximately half of the measured  $k_{\text{eff}}$  value was due to the contribution of  $k_R$ . There is good agreement between the results reported by Kingery and by Schatz and Simmons for  $k_{\text{eff}}$  of forsterite. The values of  $k_{\text{eff}}$  reported by Murase and McBirney are appreciably lower than those reported by other investigators, which may indicate systematic errors in the method, or may merely be due to the higher  $\text{SiO}_2$  content of the samples studied by Murase and McBirney. The sharp increase in  $k$  recorded above 1100 °C for some samples probably indicates the onset of melting, which causes the extinction coefficient to decrease and hence  $k_R$  to increase appreciably. It is noticeable that Kawada<sup>(36)</sup> recorded no marked increase in  $k_{\text{eff}}$  for dunite (DU), which has an FeO content of 13% and where  $k_R$  would be negligible.

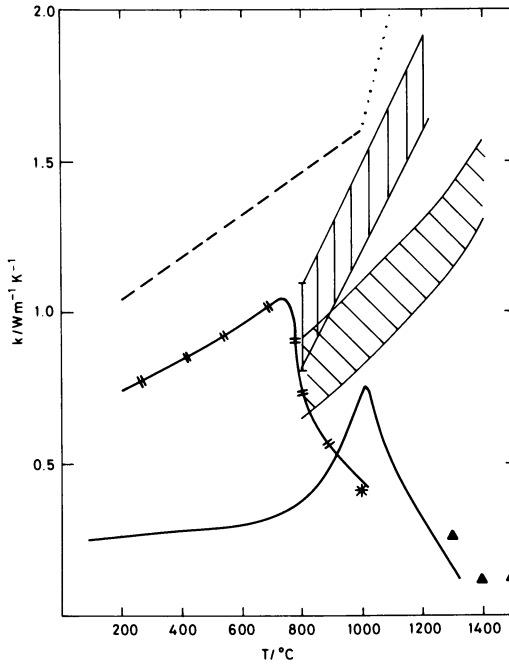


Figure 8. Thermal conductivity of continuous-casting slags; ---, ....., Taylor, and Taylor and Edwards; —, — — —, Nagata; ||||, Ohmiya; \*, average  $k_c$  value, Ohmiya; ▲, Powell.

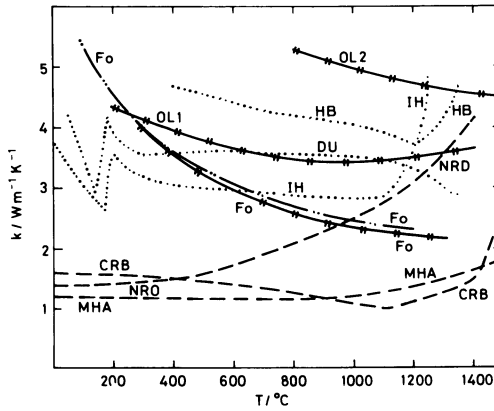


Figure 9. The thermal conductivity of rocks and minerals; ---, Murase; —, Schatz; — · — ·, Kingery; ....., Kawada; the letters refer to samples.

Coal slags. The experimental details of various investigations concerned with these slags are summarised in Table 1. The results are presented in Figure 10; only the upper and lower  $a$ -( $T$ ) curves reported by Gibby and Bates have been plotted.

The absorption coefficients of these slags are probably quite high, as they contain appreciable levels of FeO and free Fe. Thus the radiation contribution,  $k_R$ , will be relatively small. There is good agreement between the results of the investigations when the appreciable differences in the composition of the slags is taken into account. Gibby and Bates<sup>(15)</sup> reported that for solid slags the value of  $a_{\text{eff}}$  varied appreciably from run to run and appeared to be dependent upon the thermal history of the sample. This behaviour was attributed to the crystallinity of the sample and the fact that  $a_{\text{eff}}(\text{crystalline}) > a_{\text{eff}}(\text{glass})$ , which is in agreement with the observations on continuous-casting slags. Gibby and Bates<sup>(15)</sup> also observed that  $K_2O$  additions resulted in a decrease in  $a_{\text{eff}}$  up to 900 °C, and that the  $a_{\text{eff}}$ -( $T$ ) relationship showed a sharp inflection around 950 °C, which was attributed to the crystallisation of the slags.

These workers also reported that  $a_{\text{eff}}$  appeared to decrease with increasing  $SiO_2$  content or with the ratio  $(SiO_2 / (Fe_2O_3 + MgO + CaO))$ . This implies that  $k$  is probably dependent upon the structure of the silicate slag, and thus it should be possible to build up a reliable model for the estimation of  $k$  in due course. However, it is also possible that the decrease in  $a_{\text{eff}}$  with increasing  $SiO_2$  content resulted from the lower fraction of crystalline phase present in the slag.

### Discussion

The thermal conductivity data for slags, magmas and glasses have been collated in Figure 11. It can be seen that  $k_{\text{eff}}$  values for solid coal slags are similar to those for slags from the systems  $CaO + Al_2O_3 + SiO_2$  and  $CaO + SiO_2 + FeO$  and for those used in continuous casting. Thus it would appear that the chemical composition of the slag has little effect on the values of  $k_{\text{eff}}$ ; however, certain oxides (eg  $SiO_2$ ,  $CaO$ ) could exert some influence on the conductivity by altering the crystallinity of the slag. Furthermore, the radiation conduction will also be affected by the crystallinity of the sample as the extinction coefficient will be high for crystalline materials.

It is more difficult to evaluate the thermal conductivity of molten slags, although the data obtained for coal slags<sup>(15)</sup> and for slags of the system  $CaO + FeO + SiO_2$ <sup>(16)</sup><sup>(14)</sup> indicate that  $k_{\text{eff}}$  for the liquid near the melting-point is similar to that for the solid phase. It is noticeable that the  $k_{\text{eff}}$  values obtained for liquid slags by the line source method are considerably lower than the values obtained with other techniques. It is possible that the line source method is prone to systematic errors when applied to molten slags, but a more likely explanation is that the  $k_R$  is negligible in these experiments. As coal slags contain relatively high levels of  $(FeO + Fe_2O_3)$ , it would be expected that the absorption coefficient of the slag would be high and that the  $k_R$  contribution would be



Table 1. Experimental Details

Reference	No	Slag composition					Sample	Method	Temperature Range °C
		%CaO + MgO	%SiO <sub>2</sub>	%FeO	%Fe <sub>2</sub> O <sub>3</sub>	%Al <sub>2</sub> O <sub>3</sub>			
Vargaftik(34)	A	12.8	35.9	29.0	5.3	14.3	Liquid, solidified slag; (10 mm) softening point - ca 1000 °C	Radial heat flow method. Pt and stain-less steel crucibles	25 - 1348
	B	3.8	53.5	14.1	6.0	22.7			
	C	2.2	50.8	21.0	-	13.0			
Gibby and Bates(15)			33-61	6-9	6-36	14-32	6 samples, liquid and solid	Laser pulse method	100 - 1600
		27	34	6.5	4.5%	22			
Taylor(30)					free Fe	+3% Na <sub>2</sub> O	Glass, (1 mm)	Laser pulse method	200 - 950

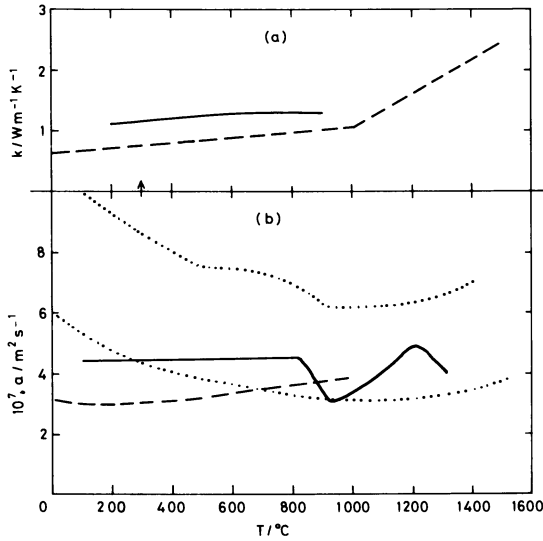


Figure 10. (a) Thermal conductivity (b) thermal diffusivity of coal slags; —, Taylor; — — —, Vargaftik; ..... , upper and lower limits of a values reported by Gibby and Bates.

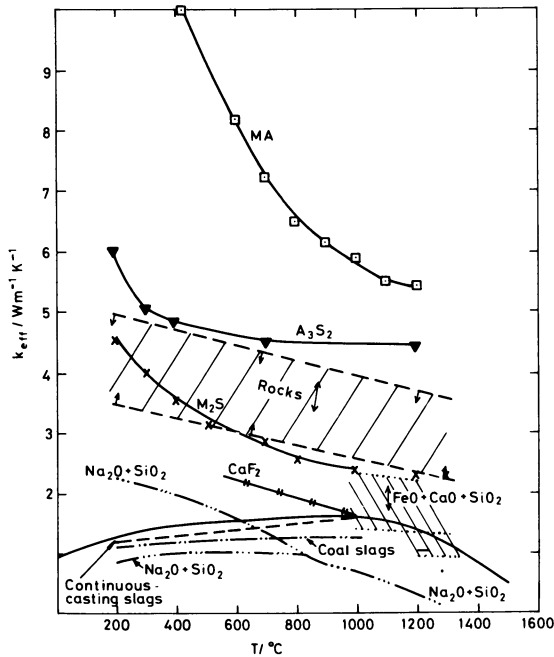


Figure 11. The thermal conductivity of various slags, glasses and minerals:  $\square$ ,  $MgO \cdot Al_2O_3$ ;  $\nabla$ ,  $3Si_2O_3 \cdot 2SiO_2$ ; X,  $2MgO \cdot SiO_2$ ;  $*$ ,  $CaF_2$ -based slags; - - - ,  $Na_2O + SiO_2$ ; ---, continuous-casting slags; and ····, coal slags.

small. However  $k_R$  increases dramatically with temperature and even a slag with a relatively high absorption coefficient of  $100 \text{ cm}^{-1}$  would give rise to a contribution of  $k_R$  of  $0.4 \text{ Wm}^{-1} \text{ K}^{-1}$  at 1800 K.

However as the absorption coefficient is very dependent upon the ( $\text{Fe}^{2+}$ ) concentration the  $k_R$  value will be dependent upon the various factors affecting the ( $\text{Fe}^{2+}/\text{Fe}^{3+}$ ) ratio in the slag viz. the ratio increases with; (i) increasing temperature; (ii) decreasing  $p(\text{O}_2)$ ; (iii) increasing  $\text{SiO}_2$  and  $\text{TiO}_2$  contents and decreasing  $\text{CaO}$ ,  $\text{Na}_2\text{O}$  and  $\text{K}_2\text{O}$  contents in the slag. This review has revealed the urgent need for absorption coefficient data for coal slags at high temperatures and for information relating the absorption coefficient to the  $\text{FeO}$  content of the slag.

The heat transfer process in the coal gasifier can also be affected by the layer of slag which lines the walls of the gasifier. Recently, Grieveson and Bagha<sup>(38)</sup> have developed a simple experiment for measuring the thermal flux ( $Q$ ) in various slags used in the continuous casting of steel. A water-cooled, copper finger is lowered into a crucible containing molten iron covered with a layer of slag and a layer of solidified slag forms around the cold finger. The thermal flux is determined by measuring the temperature rise of the cooling water flowing through the copper finger. It was found that the heat flux was related to; (i) the thickness of the slag layer; and (ii) the thermal resistance of the Cu/slag interface. The thickness of the slag layer is, in turn, dependent upon the viscosity of the slag and upon other factors determining the "melt back" of the slag layer. Grieveson and Bagha<sup>(38)</sup> observed that the thermal resistance of the Cu/slag interface appeared to be related to; (i) the mineralogical constitution of the slag; and (ii) the strength of the adhesive bond between the copper and the slag eg. the heat flux,  $Q$ , recorded with slags from  $\text{CaO.SiO}_2$  phase field, which gives good Cu/slag adhesion, is greater than the  $Q$  recorded for slags from  $\text{CaO.Al}_2\text{O}_3.2\text{SiO}_2$  phase field with poor Cu/slag adhesion. Thus relatively simple experiments like these simulation tests can provide a valuable insight into the factors affecting heat transfer mechanisms occurring in industrial processes.

### Conclusions

- (i) Experimental data for the thermal conductivities of slags must be carefully analysed to establish the boundary conditions of the experiment (eg. optical thickness of the specimen, magnitude of  $k_R$  etc). This evaluation of the data allows one to determine the suitability of a specific thermal conductivity value for subsequent use in heat balance calculations for the gasifier.
- (ii) The thermal conductivities of coal slags are not very dependent upon the chemical composition of the slag.
- (iii) The thermal conductivity of the slag is dependent upon the degree of crystallisation and consequently upon the thermal history of the specimen; the thermal conductivity of the crystalline phase is greater than that of the glassy phase.
- (iv) The radiation conduction,  $k_R$ , is principally determined by the magnitude of the absorption (or extinction) coefficient. As the absorption coefficient of the slag is largely dependent upon the ( $\text{Fe}^{2+}$ ) concentration in the slag, it will also be dependent upon the factors affecting the ( $\text{Fe}^{2+}/\text{Fe}^{3+}$ ) ratio viz.

- temperature,  $p(O_2)$  and the  $SiO_2$ ,  $CaO$  and  $Na_2O$  contents of the slag.
- (v) Experimental data are required for the absorption coefficients of coal slags at high temperatures so that the relationship between  $\alpha$  and the  $FeO$  content can be established.
- (vi) Heat transfer in the coal gasifier will be partially dependent upon the thermal resistance of the slag/wall interface and this, in turn, will be dependent upon the mineralogical constitution of the slag adjacent to the wall.

#### Acknowledgements

Valuable discussions with B. J. Keene, (National Physical Laboratory) Professor P. Grieveson (Imperial College) and Dr. R. Taylor (UMIST) are gratefully acknowledged.

#### References

- (1) Ammar, M.M; Gharib, S; Halawa, M M; El Badry, K; Ghoneim, N A; Batal, N A; E L, Batal, H A. J. Non-Cryst. Solids 1982, 53, 165.
- (2) Steele, F.N; Douglas, R.W. Phys. Chem. Glasses 1965, 6, 246.
- (3) Blazek, A; Endrysz, J. Review of thermal conductivity data in glass, Part II Thermal conductivity at high temperatures published Intl. Commission on Glass, 1983.
- (4) Fukao, Y, Mizutani, H; Uyeda, S. Phys. Earth Planet Interiors 1968, 1, 57.
- (5) Aronson, J.R; Belloti, L.H; Ecroad, S.W; Emslie, A.G; McConnel, R.K; Thuna, P.C von. J. Geophys. Res. 1970, 75, 3443.
- (6) Schatz, J.F; Simmons, G. J. Geophys. Res. 1972, 77, 6966.
- (7) Fine, H.A; Engh, T; Elliott, J.F. Metall. Trans B, 1976, 7B, 277.
- (8) Gardon, R. paper presented at 2nd Intl. Thermal Conductivity Conference, Ottawa, 1962, 167.
- (9) Gardon, R. Review of thermal conductivity data in glass, Part I Thermal conductivity at low and moderate temperatures published Intl. Commission on Glass, 1983.
- (10) Touloukian, Y.S; Powell, R.W; Ho C.Y; Klemens, P.G. "Thermophysical Properties of Matter", volumes 1 (1970) and volume 10 (1973) published by IFI/Plenum, New York.
- (11) Tye, R.P, "Thermal conductivity", volumes 1 and 2, 1969, published by Academic Press, New York.
- (12) Kingery, W.D; Francl, J; Coble, R.L; Vasilos, T. J. Amer. Ceram. Soc., 1954, 37, 107.
- (13) Ogino, K; Nishiwaki, A; Yamamoto, K; Hama, S. Paper presented at Intl. Symp. Phys. Chem. Steelmaking, Toronto, 1982, III-33.
- (14) Nauman, J; Foo, G; Elliott, J F. Extractive Metallurgy of Copper, Chapter 12, 237.
- (15) Gibby, R.L; Bates, J.L. 10th Thermal Conductivity Conference, held Newton, Mass., Sept. 1970, IV-7,8. See also Bates, J.L. Final Report to National Science Foundation, Grant GI-44100 Properties of Molten coal slags relating to open cycle MHD, Dec. 1975.
- (16) Taylor, R; Mills, K.C. Arch. f. Eisenhuttenw., 1982, 53, 55.

- (17) Taylor, R; Edwards, R. cited by Mills, K.C and Grieveson, P, a paper presented at the Centenary Conference 1984, "Perspectives in Metallurgy" Sheffield University, July 1984.
- (18) Saito, A. Bull. Jap. Soc. Mech. Engr., 1980, 23, 1459.
- (19) de Castro, C.A.N; Li, S.F.Y; Maitland, G.C; Wakeham, W.A. in press Intl. J. Thermophys. (1984).
- (20) Mills, K.C; Powell, J.S; Bryant, J.W; Keene, B.J. Canad. Metall. Q., 1981, 20, 93.
- (21) Susa, M; Nagata, K; Goto, K.S. Trans. Iron Steel Inst. Japan, 1982 22, B42.
- (22) Mitchell, A; Wadier, J.F. Canad. Metall. Q, 1981, 20, 373.
- (23) Powell, J.S; Mills, K.C. Paper presented at the Ninth European Conference on Thermophysical Properties held in Manchester, September 1984.
- (24) Mills, K.C. Paper entitled "Estimation of physico-chemical properties of coal slags and ashes" to be presented at this conference.
- (25) Osinovskikh, L.L; Kochetov, N.N; Bratchikov, S.G. Trudy Urals N-I Chern. Met., 1968 (8), 71.
- (26) Rudkin, R.L. Report US AF., ASD-TDR-62-24 II.
- (27) Keene, B.J; Mills, K.C. Arch f Eisenhüttenw. 1981, 52, 311.
- (28) Rafalovich, I.M; Denisova, I.A. Fiz. Khim Rasplav. Schlakov, 1970, 181.
- (29) Olusanya, A. "The Fundamental Properties of Continuous Casting Fluxes" PhD Thesis, Imperial College, London, 1983.
- (30) Mills, K.C; Grieveson, P; Olusanya, A; Bagha, S; Taylor, R. Paper entitled "Thermal and Physico-chemical properties of continuous-casting slags" to be presented at Ninth European Conference on Thermophysical Properties to be held in Manchester, Sept. 1984.
- (31) Nagata, K; Goto, K.S. Private communication, Tokyo Inst. of Technology, 1984.
- (32) Powell, J.S; Mills, K.C. Unpublished thermal conductivity data on casting powders, National Physical Laboratory, 1984.
- (33) Ohmiya, S; Tacke, K.H; Sshwerdtfeger, K. Ironmaking and Steelmaking, 1983, 10, 24.
- (34) Varkaftik, N.B; Oleshchuk, O.N. Teploenergetika, 1955, 4, 13.
- (35) Ischenko, K.D. Met. Kobosokhim, 1970, (21), 82.
- (36) Kawada, K. Bull. Earthquake Res. Inst., 1966, 44, 1071.
- (37) Murase, T; McBirney, A.R. Science, 1970, 170, 16S.
- (38) Grieveson, P; Bagha, S cited by Mills, K.C; Grieveson, P in a paper presented at the Centenary Conference 1984, "Perspectives in Metallurgy", Sheffield University, July 1984.

RECEIVED June 17, 1985

## Solid-Liquid-Vapor Interactions in Alkali-Rich Coal Slags

L. P. Cook and J. W. Hastie

National Bureau of Standards, Gaithersburg, MD 20899

Volcanic ash that falls into a coal-forming environment stands a good chance of being preserved and contributing to the mineral matter in coal. Such layers are relatively common in some coals although they are commonly not recognized as volcanic in origin even by geologists. The original material usually consists of fine-grained glass, crystals, and rock fragments, but there is a great variety in texture and composition. After burial the glass, in particular, is readily altered so that with increasing geologic age secondary clay minerals become abundant and evidence of the volcanic origin becomes less obvious. Kaolinite is most abundant, but smectite is not uncommon; occasionally unusual minerals occur, such as aluminum phosphates with notable amounts of Sr and rare earths. In North America, volcanic ash layers are most important in western coals of Tertiary and Cretaceous ages; they are generally uncommon in eastern coals or those of greater age.

Sodium and potassium are important constituents of the clay minerals found in most coals. As the coal is combusted these metals may be vaporized, transported and reabsorbed by slag in the cooler portions of the system, leading to the production of slags having concentrations of alkalis several times that of the primary mineral matter. Without doubt the most marked concentrations occur in slags from magnetohydrodynamic generators, where potassium salts are deliberately added to the combustion gases to enhance electrical conductivity of the plasma. Slags from MHD generators have  $K_2O$  concentrations approaching 20 wt%.

The corrosive effects of these high alkali slags on ceramic components of combustion systems are well known. Corrosion arises from the fact that such slags are good solvents for a wide range of materials. Furthermore, when many ceramics come into contact with high alkali slags, destructive reactions producing new solids may occur. For example, alumina, a widely used refractory, may react to produce  $NaAlSiO_4$ ,  $KAlSiO_4$  or beta alumina, depending upon the

activities of silica and the alkalis. In most situations, reactions of this type would result in loss of structural integrity of the ceramic.

For these and related reasons, there is need for detailed knowledge of the physical chemistry of high alkali coal ash - derived slags. NBS has an ongoing theoretical and experimental program to systematically determine the nature of solid-liquid-vapor equilibria in high alkali coal slags. Given the wide variability of coal slag, this necessitates a close interaction between theory and experiment, if significant progress is to be made.

Experimentally, three principal methods are being utilized. Application of the high temperature quenching method, with examination of results by x-ray diffraction and electron microprobe methods, is facilitated by the fact that most silicate melts quench readily to glasses, preserving the textural and chemical relationships which prevailed under equilibrium at high temperatures. On the other hand, the relatively slow kinetics makes necessary great care in the determination of alkali vapor pressures by the Knudsen effusion/mass spectrometric method. Nonetheless the technique has been used successfully at NBS in determining vapor pressures by closely correlating effusion experiments with on-going quench experiments. Similarly, the application of the third principal experimental method, high temperature differential thermal-thermogravimetric analysis, requires a degree of caution.

There has long been interest in the development of models for the prediction of coal slag phase equilibria. While silicate phase diagrams of limited compositional range have been successfully modeled, a single model for accurate prediction of slag phase equilibria in general will require that considerably more progress be made not only in our understanding of the structural chemistry of slags but also in the availability of thermochemical data needed for such models. Progress to date is related to the realization that treatment of silicate liquids as polymerized melts may be necessary for very precise prediction of phase relationships. Also important is the discovery that alkali activities can be modeled over a wide range of compositions by treating slags as composed of mixtures of complex mineral melts such as  $\text{CaAl}_2\text{Si}_2\text{O}_8$ ,  $\text{KAlSiO}_4$ ,  $\text{NaAlSi}_3\text{O}_8$ , etc. Thus coal slags, while not chemically ideal mixtures of the oxide components, appear to be much more ideal with respect to a choice of more complex components.

### Phase Equilibria in Coal Slags

Coal Slag as a 7-Component System. The variability of coal ash composition is directly related to variations in the proportions of mineral impurities such as  $\text{SiO}_2$ ,  $\text{CaCO}_3$ ,  $\text{CaMg}(\text{CO}_3)_2$ ,  $\text{CaSO}_4 \cdot 2\text{H}_2\text{O}$ ,  $\text{Fe}_2\text{O}_3$ ,  $\text{FeS}_2$ , and the clay minerals which comprise a complex group of hydrated alkali aluminosilicates. Coal ashes may vary widely in their contents of iron, calcium and magnesium, but do not vary as greatly in the amount of silica and alumina they contain. In fact, of the 323 coal ash analyses reported in U.S. Bureau of Mines Bull. 567 (1), the great majority have a  $\text{SiO}_2/(\text{SiO}_2+\text{Al}_2\text{O}_3)$  mole ratio between .67 and .80, with a well defined maximum near .75 (2). The bulk chemistry of the ash is related to the conditions of formation of the coal. In general lignites and subbituminous coals of the western U.S.A. are high in calcium while bituminous coals of the

eastern U.S.A. contain more iron. Table I gives typical analyses for ashes from these coals, and includes for comparison an analysis of coal slag from a magnetohydrodynamic generator. From this table, it can be seen that, in general, coal slag must be regarded as a seven component substance, if minor constituents such as  $TiO_2$  and  $P_2O_5$  are ignored and if sulfur is assumed to vaporize at high temperature. To account for the fact that  $Fe_2O_3$  reduces partially to  $FeO$  with increasing temperature would require an added component. However the number may be reduced again to seven if the oxygen partial pressure is included as an intensive variable along with temperature and composition. By doing this the need to specify both  $FeO$  and  $Fe_2O_3$  in defining the bulk composition is eliminated; these are replaced by  $FeO_x$ , where  $x$  is determined by the oxygen partial pressure.

Table I. Typical Coal Ash Analyses (wt %).

	Montana Coal <sup>(3)</sup>	Illinois Coal <sup>(3)</sup>	MHD Slag <sup>(4)</sup>
$K_2O$	0.4	1.4	20.2
$Na_2O$	0.4	1.6	0.5
$CaO$	11.9	8.2	3.9
$MgO$	3.9	0.8	1.1
$Al_2O_3$	21.4	16.2	12.4
$Fe_2O_3$	10.0	23.7	14.7
$SiO_2$	42.5	37.5	48.3
$TiO_2$	0.8	0.8	0.5
$P_2O_5$	0.3	0.1	-
$SO_3$	8.1	8.9	0.2

Representation of Solid-Liquid-Vapor Equilibria. Ready visualization of a range of phenomena is one of the attributes making phase diagrams indispensable in understanding the chemistry of heterogeneous systems. However, although advanced multidimensional projective methods have been derived for the representation of  $n$ -component systems <sup>(5)</sup>, these do not in general lead to easily visualized diagrams. Thus for the seven component coal slag system, alternative methods must be used.

It is useful to subdivide the slag system into smaller systems. The system  $Al_2O_3$ - $SiO_2$  is perhaps the most fundamental system for all slags, and to this one may think of adding progressively combinations of the alkalis and  $CaO$ ,  $MgO$  and  $FeO_x$ , until the desired degree of complexity is reached. Constituent systems making up the slag system are summarized in Table II. Data are available for parts of many of these systems <sup>(6-10)</sup>, but as the number of components increases, data become progressively fewer.

At NBS, experimental work is presently concentrating on the system  $K_2O$ - $CaO$ - $Al_2O_3$ - $SiO_2$ . This along with  $K_2O$ - $FeO_x$ - $Al_2O_3$ - $SiO_2$  and  $K_2O$ - $MgO$ - $Al_2O_3$ - $SiO_2$ , forms the basis for modeling potassium-rich slags. The approach has been to establish subsolidus equilibria (Figure 1) and then to combine these data with literature thermochemical data via solid state reactions of the type

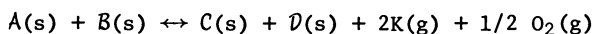




Table II. Breakdown of Lower Order Systems Comprising 7-Component Coal Slag System.

	(+CaO)	(+MgO)	(+FeO <sub>x</sub> )	(+CaO +MgO)
Al <sub>2</sub> O <sub>3</sub> -SiO <sub>2</sub> (BASE SYSTEM)	CaO-AL <sub>2</sub> O <sub>3</sub> -SiO <sub>2</sub>	MgO-AL <sub>2</sub> O <sub>3</sub> -SiO <sub>2</sub>	FeO <sub>x</sub> -AL <sub>2</sub> O <sub>3</sub> -SiO <sub>2</sub>	CaO-MgO-AL <sub>2</sub> O <sub>3</sub> -SiO <sub>2</sub>
(+K <sub>2</sub> O)	K <sub>2</sub> O-CaO-AL <sub>2</sub> O <sub>3</sub> -SiO <sub>2</sub>	K <sub>2</sub> O-MgO-AL <sub>2</sub> O <sub>3</sub> -SiO <sub>2</sub>	K <sub>2</sub> O-FeO <sub>x</sub> -AL <sub>2</sub> O <sub>3</sub> -SiO <sub>2</sub>	K <sub>2</sub> O-CaO-MgO-AL <sub>2</sub> O <sub>3</sub> -SiO <sub>2</sub>
(+Na <sub>2</sub> O)	Na <sub>2</sub> O-CaO-AL <sub>2</sub> O <sub>3</sub> -SiO <sub>2</sub>	Na <sub>2</sub> O-MgO-AL <sub>2</sub> O <sub>3</sub> -SiO <sub>2</sub>	Na <sub>2</sub> O-FeO <sub>x</sub> -AL <sub>2</sub> O <sub>3</sub> -SiO <sub>2</sub>	Na <sub>2</sub> O-CaO-MgO-AL <sub>2</sub> O <sub>3</sub> -SiO <sub>2</sub>
(+K <sub>2</sub> O +Na <sub>2</sub> O)	K <sub>2</sub> O-Na <sub>2</sub> O-AL <sub>2</sub> O <sub>3</sub> -SiO <sub>2</sub>	K <sub>2</sub> O-Na <sub>2</sub> O-MgO-AL <sub>2</sub> O <sub>3</sub> -SiO <sub>2</sub>	K <sub>2</sub> O-Na <sub>2</sub> O-FeO <sub>x</sub> -AL <sub>2</sub> O <sub>3</sub> -SiO <sub>2</sub>	K <sub>2</sub> O-Na <sub>2</sub> O-CaO-MgO-AL <sub>2</sub> O <sub>3</sub> -SiO <sub>2</sub>
	(+CaO +FeO <sub>x</sub> )	(+MgO +FeO <sub>x</sub> )	(+CaO +MgO +FeO <sub>x</sub> )	
	CaO-FeO <sub>x</sub> -AL <sub>2</sub> O <sub>3</sub> -SiO <sub>2</sub>	MgO-FeO <sub>x</sub> -AL <sub>2</sub> O <sub>3</sub> -SiO <sub>2</sub>	CaO-MgO-FeO <sub>x</sub> -AL <sub>2</sub> O <sub>3</sub> -SiO <sub>2</sub>	
(+K <sub>2</sub> O)	K <sub>2</sub> O-CaO-FeO <sub>x</sub> -AL <sub>2</sub> O <sub>3</sub> -SiO <sub>2</sub>	K <sub>2</sub> O-MgO-FeO <sub>x</sub> -AL <sub>2</sub> O <sub>3</sub> -SiO <sub>2</sub>	K <sub>2</sub> O-CaO-MgO-FeO <sub>x</sub> -AL <sub>2</sub> O <sub>3</sub> -SiO <sub>2</sub>	
(+Na <sub>2</sub> O)	Na <sub>2</sub> O-CaO-FeO <sub>x</sub> -AL <sub>2</sub> O <sub>3</sub> -SiO <sub>2</sub>	Na <sub>2</sub> O-MgO-FeO <sub>x</sub> -AL <sub>2</sub> O <sub>3</sub> -SiO <sub>2</sub>	Na <sub>2</sub> O-CaO-MgO-FeO <sub>x</sub> -AL <sub>2</sub> O <sub>3</sub> -SiO <sub>2</sub>	
(+K <sub>2</sub> O +Na <sub>2</sub> O)	K <sub>2</sub> O-Na <sub>2</sub> O-CaO-FeO <sub>x</sub> -AL <sub>2</sub> O <sub>3</sub> -SiO <sub>2</sub>	K <sub>2</sub> O-Na <sub>2</sub> O-MgO-FeO <sub>x</sub> -AL <sub>2</sub> O <sub>3</sub> -SiO <sub>2</sub>	K <sub>2</sub> O-Na <sub>2</sub> O-CaO-MgO-FeO <sub>x</sub> -AL <sub>2</sub> O <sub>3</sub> -SiO <sub>2</sub>	(COAL SLAG SYSTEM)

where A, B, C and D denote crystalline solids. At the temperature of minimum melting, such calculations provide a direct link between the phase diagram and the measurements of potassium vapor pressure which are independent of any solution model (Figure 2). This approach aids greatly in the determination of an internally consistent set of thermochemical data.

As the systems investigated become more complex (more components), other techniques may be used to reduce the number of variables, so that results can be portrayed graphically. For example, in principle phase equilibria at 1 atm in the system  $K_2O-CaO-FeO_x-Al_2O_3-SiO_2$  could be portrayed in three dimensions graphically as a tetrahedral diagram at constant  $\mu_{K_2O}$  or  $P_{K_2O}$ , T and  $P_{O_2}$ . Another way of reducing

the dimensionality of the representational problem is to deal with saturation surfaces - this is actually a form of projection. For example by considering the equilibria in which  $Al_2O_3$  participated as a phase, the need to use  $Al_2O_3$  as a representational component would be eliminated.

Role of Polymerization Theory. One of the major problems in prediction and calculation of phase equilibria is the formulation of accurate expressions for the free energy of mixing of silicate melts. Relatively few calorimetric measurements are available, and hence the importance of sound methods of estimation and prediction of mixing data to within the required degree of accuracy. Polymer theory, extended in the 1960's to include silicate melts by Masson (11) and others holds promise. It is perhaps the only general theory for silicate melts which deals quantitatively with the problem of melt structure. This has been used, with a surprising degree of success, to calculate phase equilibria in binary oxide systems (12,13). Preliminary calculations on multicomponent slags have shown that polymer theory, when treated in a quasichemical fashion, is highly flexible, and can accommodate seven component liquid immiscibility by making relatively few estimates and assumptions (Figure 3). However, attempts to fit liquidus surfaces in the system  $K_2O-CaO-Al_2O_3-SiO_2$  have met with only partial success. Further applications and extensions of polymer theory in this quaternary system are hampered by a lack of experimental data, and an attempt is being made to rectify this situation.

### Solution Model for the Prediction of Alkali Vapor Pressures

Basis of the Model. The model employed for prediction of vapor pressures in multicomponent coal slags has been outlined in (14). Briefly, large negative deviations from ideal thermodynamic activity behavior are attributed to the formation of complex liquids and solids (actual components) such as  $K_2SiO_3$ ,  $KAlSiO_4$ , etc. The free energies of formation ( $\Delta G_f$ ) are either known or can be estimated for these liquids and solids. By minimizing the total system free energy, one can calculate the equilibrium composition with respect to these components. Thus, for instance the mole fraction of  $K_2O$  present ( $X^*_{[K_2O]}$ ) in equilibrium with  $K_2SiO_3$ , and other complex liquids (and solids) containing  $K_2O$ , is known. As has been shown previously for the ternary systems, the component activities can, to

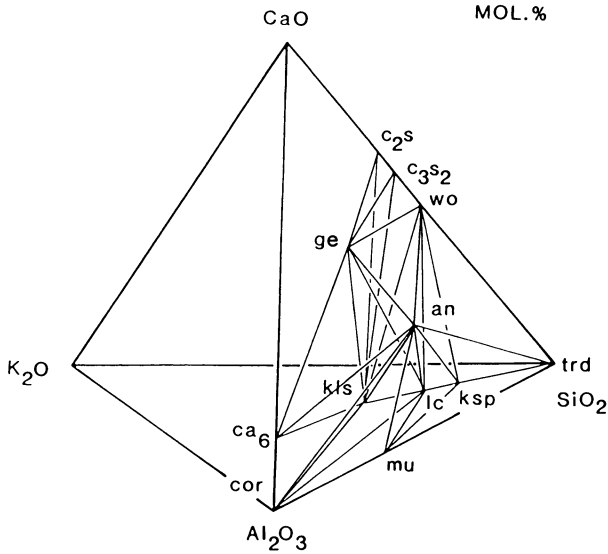


Figure 1. Experimentally determined subsolidus phase relations in the system  $K_2O-CaO-Al_2O_3-SiO_2$ .  $c_2s = Ca_2SiO_4$   $trd = SiO_2$   
 $c_3s_2 = Ca_3Si_2O_7$   $ksp = KAlSi_3O_8$   $wo = CaSiO_3$   $lc = KAlSi_2O_6$   
 $ge = Ca_2Al_2SiO_7$   $kfs = KAlSiO_4$   $an = CaAl_2Si_2O_8$   $mu = 3Al_2O_3 \cdot 2SiO_2$   
 $ca_6 = CaAl_{12}O_{19}$   $cor = Al_2O_3$

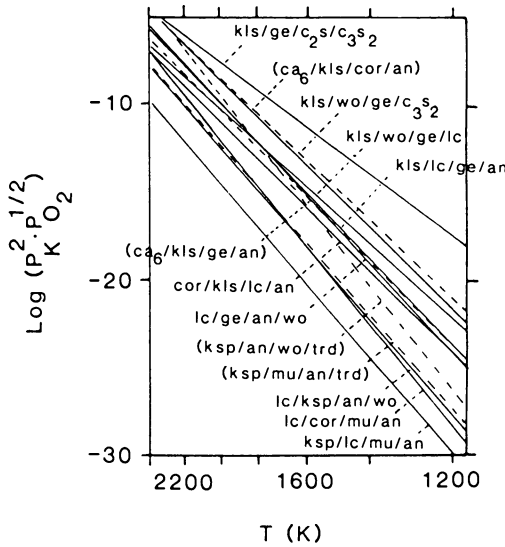


Figure 2. Calculated potassia pressures for solid assemblages in  $K_2O-CaO-Al_2O_3-SiO_2$  (see Figure 1). Thermochemical data used were from (19). Dashed lines with labels in parentheses involve incongruently melting solids. All equilibria are metastable above the minimum melting temperatures.

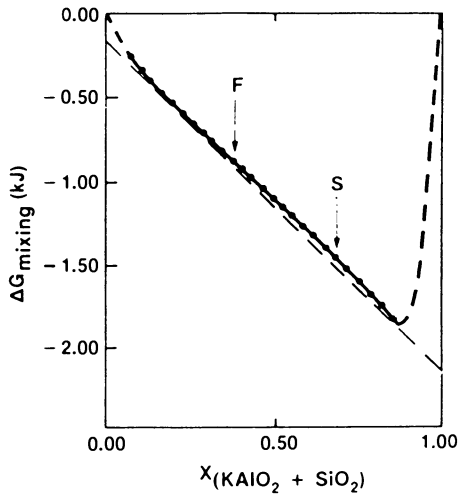


Figure 3. Calculated free energy of mixing along a compositional vector in the system  $\text{K}_2\text{O}-\text{CaO}-\text{MgO}-\text{FeO}-\text{Al}_2\text{O}_3-\text{SiO}_2$  passing through experimentally determined compositions of immiscible melts (F and S). Calculations were made using the quasichemical melt polymerization theory (23). The compositions of predicted and observed immiscible melts can be made to agree reasonably well by adjustments in polymerization equilibrium constants and in the ratio  $(\text{Fe}^{+3}/\text{Fe}^{+3} + \text{Fe}^{+2})$ .

a good approximation, be equated to these mole fraction quantities (15). From this assumption it also follows that potassium partial pressures can be obtained from the relationship

$$P_K = \left\{ 2 \cdot X^* [K_2O]^{K_p} \right\}^{0.4},$$

where  $K_p$  is the stoichiometric dissociation constant for pure  $K_2O$  (liquid or solid) to  $K$  and  $O_2$ . In the following discussion the model is tested by comparing predicted  $P_K$  data determined in this manner with experimental values. Thermodynamic activities and phase compositions were also calculated using this model. The experimental

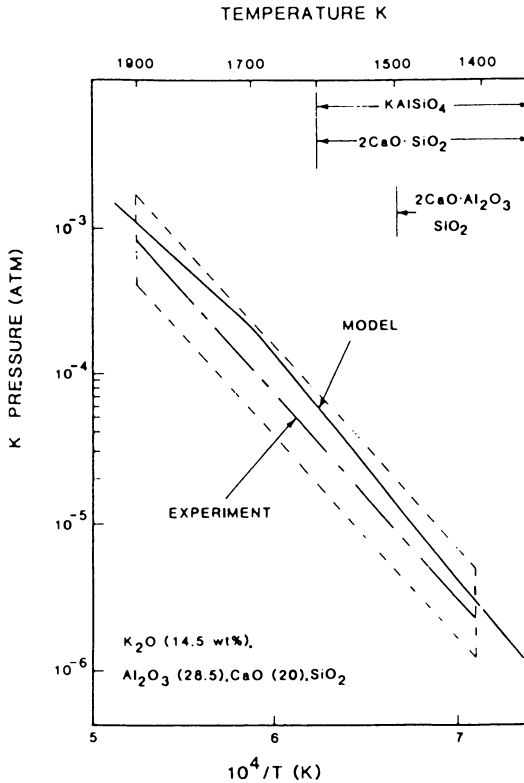


Figure 4. Comparison of ideal mixing of complex components solution model (solid curve) and experimental (broken curve) K-pressure data as a function of reciprocal temperature, for a composition in the  $K_2O$ - $CaO$ - $Al_2O_3$ - $SiO_2$  system. Compounds listed are solid precipitates formed over the temperature interval indicated.

K-pressure data were obtained by Knudsen effusion mass spectrometry as discussed in detail elsewhere (16).

Method of Calculation. The SOLGASMIX computer program (17) used for calculation of the equilibrium composition and hence activities utilizes a data base of the type given in (14). The coefficients to the  $\Delta G_f$  equation were obtained by fitting  $\Delta G_f$  vs T data available in JANAF (18), Robie et al (19), Barin and Knacke (20), Rein and Chipman (21) and Kelley (22). In some cases no literature data were available and we estimated functions in the manner described earlier (16). Many of the compounds used in the calculation are mineral phases such as mullite ( $Al_6Si_2O_{13}$ ), kaliophilite ( $KAlSiO_4$ ), leucite ( $KAlSi_2O_6$ ), feldspar ( $KAlSi_3O_8$ ), and gehlenite ( $Ca_2Al_2SiO_7$ ).

Application to the  $K_2O$ - $CaO$ - $Al_2O_3$ - $SiO_2$  System. Figure 4 shows results of calculations for potassium pressures made using the model. As can be seen these agree with experimental results within limits of experimental error over a wide range of temperature. The calculations also indicate temperatures of precipitation of various solids in the quaternary system. These predictions are being checked by experiment. Other potassium pressure calculations (not shown) show similarly good agreement with experiment in the system  $K_2O$ - $CaO$ - $Al_2O_3$ - $SiO_2$ .

### Summary

An integrated experimental/theoretical approach to the problem of non-condensed (solid-liquid-vapor) phase equilibria in multicomponent coal slags has been outlined, including methods for the presentation of results. This relies upon prediction as an important tool in planning experimental work. Theory in turn benefits from experimental feedback, resulting in a continual evolution of models. Hopefully this will lead to generalized solution models capable of predicting slag phase equilibria with a greater degree of accuracy.

### Literature Cited

1. Selvig, W. A. and Gibson, F. H.: 1956, Bureau of Mines Bull. 567.
2. Cook, L. P.: 1978, Proc. 17th Symposium on Engineering Aspects of Magnetohydrodynamics, Stanford Univ., Stanford, Calif., p. C.1.2-C.1.6.
3. Petrick, M. and Shumyatsky, B. Ya., editors: "Open-Cycle Magnetohydrodynamic Electrical Power Generation" (Argonne, Illinois: Argonne National Lab.), p. 420-421.
4. Long, W.: 1978, Pers. Commun., Univ. Tenn. Space Inst.
5. Palatink, L. S. and Landau, A. I.: 1964, "Phase Equilibria in Multicomponent Systems" (New York: Holt, Rinehart and Winston).
6. Levin, E. M., Robbins, C. R. and McMurdie, H. F.: 1964, "Phase Diagrams for Ceramists" (Columbus: The American Ceramic Society).
7. Levin, E. M., Robbins, C. R. and McMurdie, H. F.: 1969, "Phase Diagrams for Ceramists, 1969 Supplement" (Columbus: The American Ceramic Society).

8. Levin, E. M., Robbins, C. R. and McMurdie, H. F.: 1975, "Phase Diagrams for Ceramists, 1975 Supplement" (Columbus: The American Ceramic Society).
9. Roth, R. S., Negas, T. and Cook, L. P.: 1981, "Phase Diagrams for Ceramists, Volume IV" (Columbus: The American Ceramic Society).
10. Roth, R. S., Negas, T. and Cook, L. P.: 1983, "Phase Diagrams for Ceramists, Volume V" (Columbus: The American Ceramic Society).
11. Masson, C. K., Smith, I. B. and Whiteway, S. G.: 1970, Canad. J. Chem., 48, 1456.
12. Fraser, D. G., editor: 1976, "Thermodynamics in Geology" (Oxford, England: NATO Adv. Study Inst.).
13. Lin, P. L. and Pelton, A. D.: 1979, Metall. Trans. 10B, 667.
14. Hastie, J. W., Bonnell, D. W. and Plante, E. R.: 1983, Proc. Annual Meeting of Electrochem. Society, San Francisco, Calif.
15. Hastie, J. W., Horton, W. S., Plante, E. R., and Bonnell, D. W.: Thermodynamic Models of Alkali Vapor Transport in Silicate Systems, IUPAC Conf., Chemistry of Materials at High Temperatures, Harwell, U.K., August 1981; High Temp. High Press, in press.
16. Hastie, J. W., Plante, E. R. and Bonnell, D. W.: 1982, Alkali Vapor Transport in Coal Conversion and Combustion Systems. ACS Symp. Series, 179, p. 543-600, Gole, J. L., and Stwalley, W. C., eds. Metal Bonding and Interactions in High Temperature Systems with Emphasis on Alkali Metals (see also NBSIR 81-2279).
17. Eriksson, G.: 1975, Chemica Scripta, 8, p. 100.
18. JANAF: 1971, Joint Army, Navy, Air Force Thermochemical Tables, 2nd Ed. NSRDS-NBS 37. See also later supplements for 1971-1981.
19. Robie, R. A., Hemingway, B. S., Fisher, J. R.: 1979, Thermodynamic Properties of Minerals and Related Substances at 298.15 K and 1 Bar ( $10^5$  Pascals) Pressure and at Higher Temperatures, Geol. Survey Bull. 1452 (Washington, D.C.: U.S. Govt. Printing Office).
20. Barin, I. and Knacke, O.: 1973, "Thermochemical Properties of Inorganic Substances" (New York: Springer Verlag).
21. Rein, R. H. and Chipman, J.: 1965, Trans. Metall. Soc. AIME, 233, p. 415.
22. Kelley, K. K.: 1962, U.S. Bur. Mines Rep. Invest., No. 5901.
23. Cook, L. P.: 1980: Proc. Seventh International Conference on MHD Electrical Power Generation, MIT, Cambridge, Mass., p. 212-219.

RECEIVED October 24, 1985

## Coal Ash Deposition in Boilers

R. W. Borio and A. A. Levasseur

Combustion Engineering, Inc., Windsor, CT 06095

There is a need for improved mineral matter behavior predictive techniques for coal fired boilers. This paper presents an assessment of older, traditional methods; it presents some of the newer, improved methods; and it identifies some of the remaining areas of uncertainty. Traditional ASTM techniques do not always provide accurate predictive information on mineral matter behavior. No one test can adequately describe coal ash behavior; a combination of tests, each designed to focus on a particular aspect of ash behavior represents a logical approach. Techniques for assessing potential slagging due to pyrites and fouling due to alkalis are described. The use of SEM as a promising new tool for accurate characterization of mineral matter is suggested. A major area of uncertainty is the location and extent of ash deposition in a commercial boiler as ascertained from bench scale results.

The management of coal ash in utility boilers continues to be one of the most important fuel property considerations in the design and operation of commercial boilers. The behavior of mineral matter in coal can significantly influence furnace sizing, heat transfer surface placement, and convection pass tube spacing. Ironically, many of the more reactive, low rank U. S. coals must have larger furnaces than the less reactive higher rank coals. This is strictly a requirement based on the mineral matter behavior; Figure 1 illustrates this point. Given the same mineral matter behavior the more reactive, lower rank coals would require less residence time and therefore smaller furnace volumes than the less reactive, higher rank coals.

Although pulverized coal has been fired for more than 50 years and much is known about combustion behavior there are still a number of boilers experiencing operational problems from coal ash effects. Ash-related problems are one of the primary causes of unscheduled outages, unit derating and unavailability. Because of variability in a given coal seam and since many boiler operators may experience changes in their coal supply during the life of a boiler, operational problems caused by changes in coal ash properties can significantly affect boiler performance. Not only must the initial boiler design be correctly determined based on the specification coal but reliable judgements must be made regarding the suitability



of other candidate coals and their effect on operation during the lifetime of the boiler.

The increased emphasis on coal usage in this country and, indeed, the significant effort underway to consider coal water mixtures as possible oil substitutes in oil-designed boilers underscores the need to improve the prediction of mineral matter behavior in a boiler environment.

Coal is a very heterogeneous, complex material which produces heterogeneous, complex products during combustion. Since, during combustion of pulverized coal, coal particles of various organic and mineral matter compositions can behave in completely different manners, predictions based upon the overall or average composition may be misleading. Like many of the currently-used ASTM coal analyses, the method for determining ash fusibility temperatures was developed when stoker firing was a predominant coal firing technique; the methodologies and conditions employed during many of the ASTM tests reflect this. It is not surprising that the usefulness of some ASTM test results may be limited when used for a pulverized coal firing application. In recent years researchers have developed methodologies for characterizing coal ash behavior that better reflect the fundamental mechanisms controlling behavior and more closely simulate the conditions that exist in a pulverized coal fired boiler.

Clearly there is a need for improved techniques for predicting the behavior of mineral matter. This paper will provide a statement of the ash deposition problem in pulverized coal fired boilers; it will present an assessment of the older, traditional methods for predicting mineral matter behavior; and it will address some of the newer techniques that have been suggested as better ways of characterizing coal ash behavior. Additionally some areas of uncertainty will be identified which require the development of better predictive techniques.

#### STATEMENT OF THE PROBLEM

The presence of ash deposits and flyash can create the following problems in a boiler:

1. Reduced heat transfer
2. Impedance of gas flow
3. Physical damage to pressure parts
4. Corrosion of pressure parts
5. Erosion of pressure parts

These problems can result in reduced generating capacity, unscheduled outages, reduced availability, and costly modifications.

Ash which deposits on boiler walls in the radiant section of a furnace is generally referred to as slag. Ash deposition on convection tube sections downstream of the furnace radiant zone is

typically referred to as fouling. Ash slagging and fouling can result in problems listed in items 1 through 4. Item 5, erosion, is the result of impingement of abrasive ash on pressure parts. Often coal ash deposit effects are inter-related. For example, slagging will restrict waterwall heat absorption changing the temperature distribution in the boiler which in turn influences the nature and quantity of ash deposition in downstream convective sections. Ash deposits accumulated on convection tubes can reduce the cross-sectional flow area increasing fan requirements and also creating higher local gas velocities which accelerate fly ash erosion. In-situ deposit reactions can produce liquid phase components which are instrumental in tube corrosion.

One of the most common manifestations of a deposition problem is reduced heat transfer in the radiant zone of a furnace. Decreased heat transfer due to a reduction in surface absorptivity is a result of the combination of radiative properties of the deposit (emissivity/absorptivity) and thermal resistance (conductivity) of a deposit. Thermal resistance (thermal conductivity and deposit overall thickness) is usually more significant because of its effect on absorbing surface temperature.

Previous work has indicated that the physical state of the deposit can have a significant effect on the radiative properties, specifically molten deposits show higher emissivities/absorptivities than sintered or powdery deposits (1). Although thin, molten deposits are less troublesome from a heat transfer aspect than thick, sintered deposits, molten deposits are usually more difficult to remove and cause frozen deposits to collect in the lower reaches of the furnace where physical removal then becomes a problem for the wall blowers.

Impedance to gas flow is the result of heavy fouling on tubes in the convective section. Problems of this type are most likely to occur with coals having high sodium contents, such as those found in low rank coal deposits in Western U.S. seams. Hard, bonded deposits can occur which are resistant to removal by the retractable sootblowers.

Physical damage to pressure parts can occur if large deposits accumulate in the upper furnace and become dislodged or blown off and drop onto the slopes of the lower furnace. Such deposits are usually characterized by their relatively high bonding strengths and their heavily sintered structure.

Fireside corrosion can occur on both waterwall and superheater tube surfaces. Normal sulfates and pyrosulfates are frequently the cause of waterwall corrosion, although reducing conditions can also cause depletion of protective oxide coatings on tube surfaces. On higher temperature metal surfaces, (superheaters/reheaters) alkali-iron-trisulfates are often the cause of corrosion. Chlorine can also be a contributing factor toward superheater metal corrosion if sulfur content is low. While exact mechanisms can

be argued there have been examples of both liquid phase and gas phase corrosion when chlorides have been present (2).

Erosion of convective pass tubes, while not a function of deposits, is caused by the abrasive components in flyash. Flyash size and shape, ash particle composition and concentration, and local gas velocities play important roles concerning erosion phenomenon. Recent work has shown that quartz particles above a certain particle size are very influential in the erosion process and that furnace temperature history plays an important role in determining erosive characteristics of the particles (3,4).

#### FUNDAMENTAL CONSIDERATIONS IN ASH DEPOSITION

The coal ash deposition process involves numerous aspects of coal combustion and mineral transformation/reaction. The following all play a role in the formation of ash and the deposition process.

- Coal Organic Properties
- Coal Mineral Matter Properties
- Combustion Kinetics
- Mineral Transformation and Decomposition
- Fluid Dynamics
- Ash Transport Phenomena
- Vaporization and Condensation of Ash Species
- Deposit Chemistry - Specie Migration and Reaction
- Heat Transfer To and From the Deposit

Despite considerable research in these areas, there are gaps in our fundamental understanding of the mechanisms responsible for mineral matter behavior. The importance of furnace operating conditions on the combined results of each of the above areas must be stressed. For a given coal composition, furnace temperatures and residence times generally dictate the physical and chemical transformations which occur. The ash formation process is primarily dependent on the time/temperature history of the coal particle. The resultant physical properties of a given ash particle generally determine whether it will adhere to heat transfer surfaces. Local stoichiometries can also influence the transformation process and thereby the physical characteristics of ash particles; iron-bearing particles are a prime example of this.

Aerodynamics can play a role in the ash deposition process in all furnaces regardless of the type of firing; recent interest in micro-fine grinding of coal is testimony to this fact. It has been postulated that smaller ash particles will follow gas streamlines and be less likely to strike heat transfer surfaces. This is a logical hypothesis for those ash particles that cause deposition due to an impact mechanism. In addition to particle size, particle density and shape also affect aerodynamic behavior. Due to the difference in drag forces, molten, spherical particles will be less likely to follow gas streamlines than angular or irregular particles of the same mass.

Most coal ash will result in deposits which increase in severity with increasing gas temperature. This is not a linear relationship, as illustrated in Figure 2, but rather a progressively more severe ash deposit condition with increasing gas temperature (4). Boilers are normally designed so that cleanable, sintered deposits will be formed. This is a reasonable compromise between a very large, economically uncompetitive boiler that may produce very dry, dusty deposits and a very small, highly loaded boiler that would produce molten, running ash deposits.

One design objective is to determine how small a furnace can be, for a given MW output, and still result in deposits that are cleanable with conventional sootblowing equipment.

Because of the complexity of the ash formation and ash deposition process, it seems logical to deal first with those key coal constituents most responsible for ash deposition. The iron and sodium contents of an ash have typically been considered key constituents. Techniques have been developed to determine how these key constituents are contained in the coal, i.e., the particular mineral forms that are present or the grain size of the constituent in question. Obviously the remainder of the mineral matter has an effect, but depending on the concentration and form in which iron and/or sodium constituents are present, the remaining mineral matter often has second order effects.

As previously discussed, ash formation and the resulting ash size distribution is dependent on several factors including initial coal size, coal burning characteristics, mineral content, mineral grain size, volatile ash species, melting behavior of the mineral matter, and temperature history of the particle. Generally, coal containing lower melting mineral matter has a greater potential for ash agglomeration as the particle burns and yields fewer ash particles per coal particle. This results in coarser ash particles than those of coal with higher melting ash. Obviously things like ash quantity, and mineral grain sizes could influence this hypothesis. The way a coal particle burns may also influence the number of ash particles generated, i.e., a shrinking sphere burning mode may produce a different result from a constant diameter, decreasing density mode of burning; swelling coals may behave differently than non-swelling coals.

In reflecting on the above discussion, it becomes apparent that one cannot completely divorce the predictive techniques employed, from the particular coal burning application. Pulverized coal firing will require a sensitivity to different conditions than stoker firing, or a slagging combustor. Failure to address the specific conditions inherent in each type of firing system will lead to lower resolution in one's predictive abilities than desired.

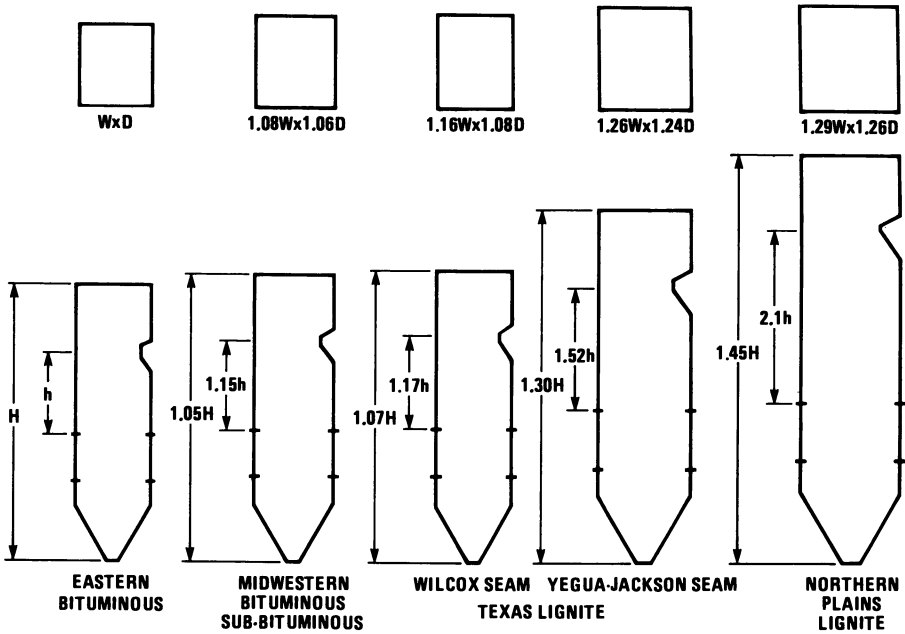


Figure 1. Effect of Coal properties on furnace size. Reproduced with permission from reference 11. Copyright 1978 C-E Publication.

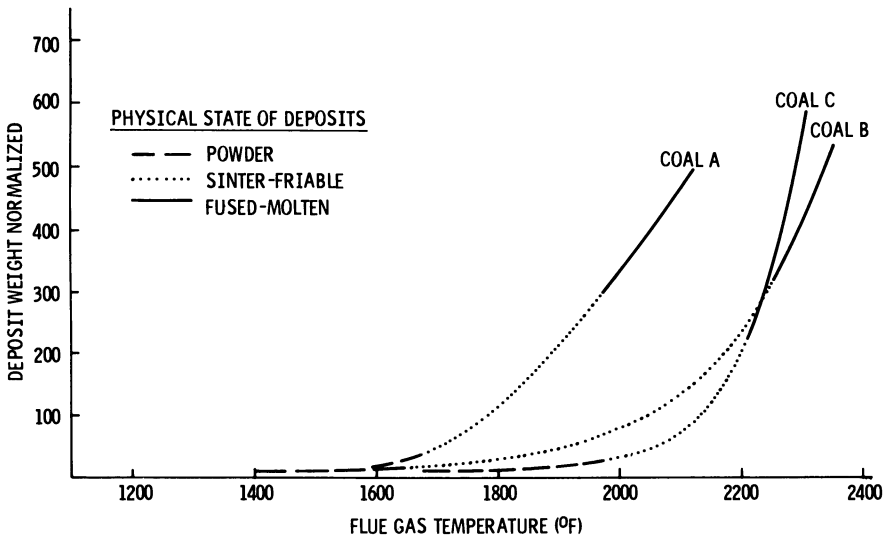


Figure 2. Superheater deposit buildup vs. flue gas temperature. Deposit collected in an 8-hour period. Deposit weight normalized: deposit weight/(ash input x surface area of collection). Reproduced with permission from reference 5. Copyright 1977 C-E Publication.

### ASSESSMENT OF TRADITIONAL PREDICTIVE METHODS

ASTM measurements such as ash fusibility (D1857) have formed the basis for traditional ash behavior predictive techniques. These bench-scale tests provide relative information on a fuel which is used in a comparative fashion with similar data on fuels of known behavior. Unfortunately, these commonly used tests do not always provide sufficient information to permit accurate comparison.

The fusibility temperature measurement technique attempts to recognize the fact that mineral matter is made up of a mixture of compounds each having their own melting point. As a cone of ash is heated some of the compounds melt before others and a mixture of melted and unmelted material results. The structural integrity or deformation of the traditional ash cone changes with increasing temperature as more of the minerals melt. However, more recent results indicate that significant melting/sintering can occur before initial deformation is observed (5). The fact that the time/temperature history of laboratory ash is quite different from conditions experienced in the boiler can result in differences in melting behavior. In addition, the ash used in this technique may not represent the composition of ash deposits that actually stick to the tube surfaces. Often there is a major discrepancy between the composition of as-fired ash and that which is found as deposits (See Table I). This is a major criticism of the ash fusibility test. The discrepancies between fusibility temperature predictions and actual slagging performance is usually greater on ashes that may look reasonably good based on fusibility temperature results. One can usually assume, with reasonable confidence, that the melting temperature of the waterwall deposits will be no higher than ASTM fusibility temperatures; but deposit melting temperatures can be and are often lower than ASTM melting temperatures. This is because selective deposition of lower melting constituents can and does occur with a resulting enrichment of lower melting material in the deposit.

Ash viscosity measurements suffer similar criticism with respect to the fusibility measurements. These tests are conducted on laboratory ash and on a composite ash sample. Viscosity measurements are less subjective and more definitive than fluid temperature determination for the assessment of ash flow characteristics. However, these measurements reflect the properties of a solution or liquid and precipitating crystals (pending temperature), of all the ash constituents and may not be representative of slag deposit properties in pulverized coal-fired boilers. During pulverized coal firing, a severe problem may already exist before slag deposits reach the fluid/running state. Generally, only a small quantity of liquid phase material exists in deposits and it is the particle-to-particle surface bonding which is most important.

Much use is made of the ash composition which is normally a compilation of the major elements in coal ash expressed as the oxide form. From this compilation of elements, expressed as oxides, judgments are often made based on the quantity of certain key con-

TABLE I  
 ENRICHMENT OF IRON IN BOILER WALL DEPOSITS  
 COMPARISON OF COMPOSITION OF ASH  
 DEPOSITS AND AS-FIRED COAL ASHES

UNIT SAMPLE	1		2		3	
	AS-FIRED COAL ASH	WATERWALL DEPOSIT	AS FIRED COAL ASH	WATERWALL DEPOSIT	AS-FIRED COAL ASH	WATERWALL DEPOSIT
Ash Composition						
SiO <sub>2</sub>	47.0	33.3	50.2	55.1	49.7	41.8
Al <sub>2</sub> O <sub>3</sub>	26.7	18.0	16.9	14.6	16.5	15.8
Fe <sub>2</sub> O <sub>3</sub>	14.6	43.5	5.9	18.3	12.0	28.5
CaO	2.2	1.2	12.8	7.2	6.5	9.0
MgO	0.7	0.5	3.5	2.0	0.9	0.9
Na <sub>2</sub> O	0.4	0.2	0.6	0.5	1.1	0.6
K <sub>2</sub> O	2.3	1.6	0.8	0.6	1.5	0.9
TiO <sub>2</sub>	1.3	0.8	0.9	0.8	1.1	0.7
SO <sub>3</sub>	1.1	0.5	12.0	0.1	2.0	0.2

stitutents like iron and sodium. Base/acid ratios are computed and used as indicators of ash behavior; normally lower melting ashes fall in the 0.4 to 0.6 range. It has been shown that base/acid ratios generally correlate with ash softening temperatures, so although base/acid ratios have helped explain why ash softening temperatures varied, it has not improved predictive capabilities in the authors' opinion. Other ratios such as Fe/Ca and Si/Al have been used as indicators of ash deposit behavior. Ratios like these have helped to explain deposit characteristics, but their use as a prime predictive tool is questionable especially since these ratios do not take into account selective deposition nor do they consider the total quantities of the constituents present. An Fe/Ca ratio of 2 could result from weight percent ratios of 6/3 or 30/15; the latter numbers would generally indicate a far worse situation than the former, but ratios don't show this.

Many slagging and fouling indices are based upon certain ash constituent ratios and corrected using such factors as geographical area, sulfur content, sodium content, etc. One commonly used slagging index uses Base/Acid ratio and sulfur content. Factoring in sulfur content is likely to improve the sensitivity of this index to the influence of pyrite on slagging. (As previously discussed, iron-rich minerals often play an important role in slagging.) However, the use of such "correction" factors is often a crude substitute for more detailed knowledge of the fundamental fuel properties. Another example of this is the use of chlorine content in a coal as a fouling index. This can be valid if the chlorine is present as NaCl (thereby indicating the concentration of sodium which is in an active form) and that the sodium will, in fact, cause the fouling. Chlorine present in other forms may or may not adversely affect fouling.

Sintering strength tests have been used as an indication of fouling potential. Assuming that correct ash compositions have been represented (which is less of a problem in the convection section than in the radiant section) worthwhile information may be obtained relative to a time/temperature vs. bonding strength relationship. In order for sintering tests to accurately predict actual behavior it is necessary that tests be conducted with ash produced under representative furnace conditions (time-temperature history). Fouling behavior is often greatly influenced by sodium reactions. Sodium which vaporizes in the furnace can condense in downstream convection sections thereby concentrating on flyash surfaces. Particle surface reactions are primarily responsible for convection deposit bonding.

In summary, traditional methods for prediction of ash deposit characteristics are heavily based upon ash chemistry. These conventional analyses do not provide definitive information concerning the mineral forms present in the coals and the distribution of inorganic species within the coal matrix. Such information can be extremely important in extrapolating previous experience, since the nature in which the inorganic constituents are contained in the coal can be the determining factor in their behavior during the ash deposition process.



ASSESSMENT OF NEW PREDICTIVE TECHNIQUES

Generally speaking the newer bench scale predictive techniques are far more sensitive to the conditions that exist in commercial furnaces than the older predictive methods. Selective deposition, for example, has been recognized as a phenomenon which cannot be ignored. More attention is being paid to fundamentals of the ash formation and deposition processes. New tools, such as Scanning Electron Microscopy (SEM), are being considered as ways to improve predictive capabilities. Other, more specialized bench scale apparatuses are being developed to simulate important aspects of commercial conditions and provide quantitative information on parameters that influence bonding strength.

Recent work has shown that pulverized coal, if separated by gravity fractionation, can yield important information relative to slagging potential due to the iron content. (6,7). Results of this work have shown that the percentage of iron in the heavy fractions correlates very well to the slagging behavior in commercial boilers. (See Figure 3). This technique appears to identify the proportion of relatively pure pyrites particles that are generated in the pulverized coal feed and that are capable of melting at relatively low temperatures and that would account for enrichment of iron in lower furnace waterwall deposits.

A method for measuring active alkalis has been developed as a means for improved prediction of fouling potential (8). Previous wisdom held that fouling potential was directly related to the total sodium content. Much of this early work was done on low rank coals in which case it was not uncommon for all of the alkalis to be present as an active sodium form (9). However, there were many occasions where the fouling potential was not adequately predicted by the total sodium content. (Table II provides some examples of anomalous fouling behavior.) The mechanism postulated for sodium-related fouling was one of a vaporization/condensation mechanism. Simple forms of sodium compounds resulted in the vaporization of sodium in the radiant zone of the furnace where peak temperatures are generated. Subsequent condensation of the sodium on the relatively cool tube surfaces effected a process for deposition of sodium. Sodium is a known, effective fluxing agent that can create hard, bonded deposits. The referenced method relied on the use of weak acid to preferentially leach out sodium from simple compounds like NaCl and/or organically-bound alkali as would be present in many of the lower rank coals. This method gives results that correlate well with field performance on coals having significant sodium contents (See Table II).

The use of new analytical techniques promises to give results that allow mineral matter to be identified according to composition, mineral form, distribution within the coal matrix, and grain size.

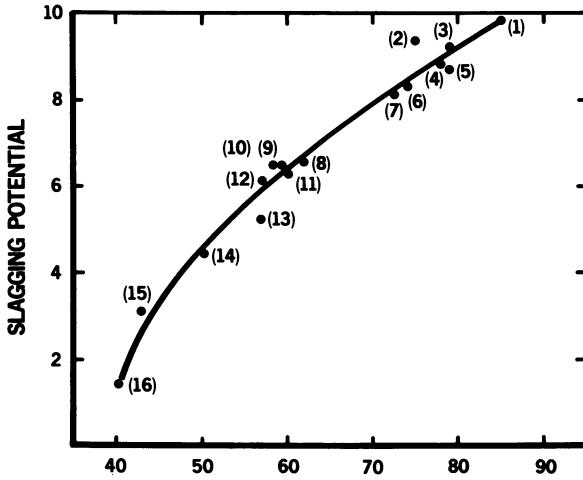


Figure 3. Effect of segregated iron on coal ash slagging. Presented as %  $\text{Fe}_2\text{O}_3$  in ash of 2.9 sp. gr. sink fraction. Reproduced with permission from reference 12. Copyright 1983 C-E Publication.

TABLE II  
ANALYTICAL DATA ON U.S. COALS

Rank Region	Lignite N. Dakota	Sub B Montana	Lignite Texas (Yegua)	Lignite Texas (Wilcox)	hvBb Utah	hvAB Penn	Lignite Texas (Wilcox)
(Dry Basis)							
Volatile.....	44.4	42.4	39.6	41.0	41.5	32.5	38.1
Fixed C.....	46.0	52.0	26.9	39.5	48.3	54.0	33.0
Ash.....	9.6	5.6	33.5	19.5	10.2	13.5	28.9
HHV (Btu/lb).... (Dry Basis)	10640	12130	7750	9710	12870	13200	8420
Ash Fusibility							
I.D.(°F).....	2130	1980	1940	2150	2190	2370	2210
S.T.....	2180	2020	2200	2250	2270	2510	2300
H.T.....	2190	2060	2430	2340	2390	2560	2420
F.T.....	2200	2170	2610	2530	2620	2660	2620
Ash Composition							
SiO <sub>2</sub> (%).....	20.0	33.9	62.1	52.3	52.5	51.1	57.9
Al <sub>2</sub> O <sub>3</sub> .....	9.1	11.4	15.1	17.4	18.9	30.7	21.8
Fe <sub>2</sub> O <sub>3</sub> .....	10.3	10.8	3.5	5.3	1.1	10.0	3.9
CaO.....	22.4	21.0	6.2	9.4	13.2	1.6	7.1
MgO.....	6.4	2.7	0.7	3.2	1.3	0.9	2.1
Na <sub>2</sub> O.....	5.0	5.8	3.6	0.9	3.8	0.4	0.9
K <sub>2</sub> O.....	0.5	1.6	2.1	1.2	0.9	1.7	0.8
TiO.....	0.4	0.7	0.9	1.2	1.2	2.0	1.1
SO <sub>3</sub> .....	21.9	12.0	6.1	9.6	6.2	1.4	4.4
Total Alkali, %, Ash Basis							
Na <sub>2</sub> O.....	5.0	5.8	3.6	0.9	3.8	0.4	0.7
K <sub>2</sub> O.....	0.5	1.6	1.9	1.2	0.9	1.7	0.8
Soluble Alkali, %, Ash Basis							
Na <sub>2</sub> O.....	5.58	6.45	3.88	0.71	1.49	0.15	0.16
K <sub>2</sub> O.....	-	-	0.44	0.04	0.08	-	0.05
Relative Soluble Alkali, %							
Na <sub>2</sub> O.....	112%	111%	108%	79%	39%	38%	23%
K <sub>2</sub> O.....	-	-	-	3%	9%	-	6%
Fouling Potential	Severe	High	High	Moderate	Moderate	Low	Low

Techniques such as computer-controlled scanning electron microscopy (CCSEM), scanning transmission electron microscopy (STEM), and X-ray diffraction can be used to characterize these properties on an individual particle by particle basis. New spectroscopies such as extended X-ray absorption fine structure spectroscopy (EXAFS), and electron energy loss spectroscopy, (EELS) are capable of determining the electronic bonding structure and local atomic environment for organically associated inorganics like calcium, sodium and sulfur. Other new techniques such as Fourier transform infrared spectroscopy (FTIR), electron microprobe, electron spectroscopy for chemical analysis (ESCA), etc. all provide methods of improving present capabilities. By development and application of these techniques a much better fundamental assessment of coal mineral matter behavior is possible. The authors believe these results, coupled with those of other existing methods, can make a significant improvement to predictive capabilities.

#### AREAS OF UNCERTAINTY

Prediction of ash deposit characteristics based solely on bench-scale fuel properties always requires substantial judgement and allows only a certain level of confidence. As discussed, the ash deposition process is so complex that detailed modelling of commercial systems based on fundamental data is presently unrealistic. However, current techniques can provide relative data which in most cases is sufficient to make accurate assessment of slagging and fouling potentials relative to other fuels.

There remain many areas of uncertainty where experienced judgements must fill the gap between good laboratory results/predictions and boiler design decisions. One of these areas concerns the extent of deposit coverage in a boiler. Though the fuels researcher may adequately characterize a given coal ash in terms of its potential deposit effects, he is often at a loss to adequately describe the extent of coverage of deposits in the boiler. It is necessary to accurately describe furnace conditions in order to assess resulting deposits in particular boiler regions. Though some good work is underway in this area, the question of bonding strength and cleanability remains a problem as far as its prediction from bench scale tests. Good correlations have been developed between iron content of heavy gravity fractions and slagging potential, but there does not exist a bench scale technique that can simulate what the local ash deposit composition shall be when burned in a commercial boiler.

It is possible to increase the level of confidence in prediction of deposit effects by conducting pilot-scale combustion studies in test rigs which simulate the conditions present in commercial boilers. Combustion testing allows evaluation of the ash formation and deposition process and permits detailed characterization of the deposits generated. Results can allow determination of deposit characteristics as a function of fundamental boiler design parameters (such as gas temperature, velocity, etc.). Combustion test

rigs also serve as valuable tools for assessment of fuels with very unusual properties and can significantly reduce uncertainties in extrapolation of their behavior from past experience.

Whenever test results are assessed and used to establish boiler design parameters, the representativeness of the test sample must be carefully considered. The degree of variability in the coal deposit and the impact of this variability on boiler performance must be evaluated. Judgements are also required on the effects of more gradual changes that could occur in coal properties as a function of time and location in the coal seam.

In summary, it can be stated that while significant progress has been made in predicting ash behavior, the ash formation and deposition process is not fully understood. Traditional ASTM analyses do not always provide information that can be used to make predictive judgements at the confidence levels desired. Newer techniques have been developed and are being developed that are more sensitive to the conditions that exist in the boiler environment, and that recognize the heterogeneity of the inorganic constituents in the coal matrix. There appears to be a recognition that no one test can adequately describe coal ash behavior; a combination of tests, each designed to focus on a particular aspect of ash behavior seems to be a logical approach. Based on the results from many of these newer tests, on coals that are presently being burned in existing units, the authors feel certain that significant improvements have been made in predicting ash behavior.

#### REFERENCES

1. G. J. Goetz, N. Y. Nsakala, and R.W. Borio, "Development of Method for Determining Emissivities and Absorptivities of Coal Ash Deposits," paper presented at the 1978 Winter Annual ASME Meeting, Dec. 1978, TIS-5890.
2. R. W. Borio, et.al., "The Control of High Temperature Fireside Corrosion in Utility Coal-Fired Boilers," OCR R&D Report No. 41 (1969).
3. F. Raask, "Flame Imprinted Characteristics of Ash Relevant to Boiler Slagging Corrosion and Erosion," presented at the 1981 Joint Power Generation Conference, ASME Paper No. 81-JPGC-Fu-1.
4. W. P. Bauver, J. D. Bianca, J. D. Fishburn, and J. G. McGowan, "Characterization of Erosion of Heat Transfer Tubes in Coal-Fired Power Plants," paper to be presented at 1984 Joint Power Generation Conference, Toronto, Canada, September 1984.
5. R. W. Borio, G. J. Goetz, and A. A. Levasseur, "Slagging and Fouling Properties of Coal Ash Deposits as Determined in a Laboratory Test Facility," paper presented at the ASME Winter Annual Meeting, December 1977, Combustion Engineering publication TIS-5155.

6. G. P. Huffman and F. E. Higgins, "Investigations of Partial Ash Melting by Phase Analysis of Quenched Samples," presented at 1981 Engineering Foundation Conference—Fouling and Slagging Resulting From Impurities in Combustion Gases, July 1981, Henniker, NH.
7. R. W. Borio, R. R. Narciso, Jr., "The Use of Gravity Fractionation Techniques for Assessing Slagging and Fouling Potential of Coal Ash," paper presented at the ASME Winter Annual Meeting, December 10-15, 1978, San Francisco, CA; available as Combustion Engineering publications TIS-5823.
8. R. W. Bryers, "The Physical and Chemical Characteristics of Pyrites and Their Influence on Fireside Problems in Steam Generators," ASME Paper No. 75-WA/CD-2, 1976.
9. G. L. Hale, A. A. Levasseur, A. L. Tyler and R. P. Hensel, "The Alkali Metals in Coal: A Study of Their Nature and Their Impact on Ash Fouling," paper presented at Coal Technology '80, November 1980, TIS-6645.
10. G. H. Gronhovd, W. Beckering, and P. H. Tlufte, "Study of Factors Affecting Ash Deposition from Lignite and Other Coals," an ASME publication presented at the ASME Winter Annual Meeting, November 16-20, 1969, Los Angeles, CA.
11. R. P. Hensel, D. A. Harris, "Properties of Solid Fuels and Their Impact on Boiler Design and Performance," TIS-5889, September 10-13, 1978.
12. W. H. Pollock, G. J. Goetz, E. Park, "Advancing the Art of Boiler Design by Combining Operating Experience and Advanced Coal Evaluation Techniques," Presented at American Power Conference, April 18-20, 1985.

RECEIVED October 10, 1985

## Deposit Constituent Phase Separation and Adhesion

Erich Raask

Technical Planning and Research Division, Central Electricity Generating Board,  
Leatherhead, Surrey, United Kingdom

The initial deposit material on coal fired boiler tubes consists largely of silicate, sulphate and iron oxide particles. The fused silicates and molten sulphates form immiscible phases at high temperatures first on the micro-scale in individual particles and subsequently as separate layers in the deposit. The adhesion of ash deposit constituents to boiler tubes starts with the small particle retention as a result of the van der Waals, electrostatic and liquid film surface tension forces. Subsequently a strong bond will develop between the oxidized metal surface and iron saturated layer of ash deposit.

The pulverized coal fired boilers at electricity utility power stations are designed for "dry" ash operation where the bulk of mineral matter residue is removed in the electrical precipitators in the form of particulate ash. However, it is inevitable that some deposits of sintered ash and semi-fused slag form on the heat exchange tubes and between 20 and 30 per cent of coal ash is discharged from the combustion chamber as clinker. The high temperature cyclone fired boilers are designed for "wet" ash operation and up to 80 per cent of coal ash is discharged from the furnace as molten slag.

The build-up of sintered ash and fused slag depends chiefly on the rate of ash particle impaction and the adhesive characteristics of the collecting surface. The initial deposit on the heat exchange tubes in pulverized coal fired boilers consists of ash particles of diameter ranging from less than 0.1  $\mu\text{m}$  to 100  $\mu\text{m}$ . Subsequently the deposited ash may be re-entrained in the flue gas or it may form first a sintered matrix and later a fused slag deposit chiefly by viscous flow. For the deposit formation the ash particles must be first held at the collecting surface and subsequently the deposit matrix bonded to the boiler tubes by adhesive forces sufficiently strong to overcome the gravitational pull, boiler vibration and eventually the sootblower jet impaction. This work sets out to examine the adhesive characteristics of different constituents of the flame heated ash and the formation of sintered deposits and slag bonded to the heat exchange tubes.

### Initial Deposit Constituents

The mineral matter in coal consists chiefly of silicate, sulphide, carbonate species, and chlorides and organo-metallic compounds associated with the fuel substance (1,2). The silicate mineral particles vitrify partially or completely, in the pulverized coal flame (3), and thus the silicate ash fraction of the initial deposit consists of particles of variable amounts of a glassy phase and crystalline species (4).

The sulphide, carbonate, chloride and organo-metal species dissociate and oxidize in the flame. The oxides may remain as discrete particles, chiefly iron oxide (magnetite), can dissolve in the glassy phase of silicates, and a fraction of calcium and sodium oxides are sulphated (5). Thus the initial deposit material will contain some calcium, sodium and potassium sulphate. The latter originates from the release of potassium in the flame heated aluminosilicate particles (6).

The relative concentrations of flame heated ash constituents, namely silicates, iron oxide and sulphate, can be estimated from the ash analysis. However, the composition of the initial deposit material can be markedly different as a result of selective deposition. In particular, the deposit material can be enriched in sulphate as shown in Figure 1. The relative concentrations of different deposit constituents were obtained by analysing the material on a cooled metal tube probe inserted in boiler flue gas for short, 2 to 15 minute, duration (7). The sulphate content of the flue gas borne ash and probe deposits in a cyclone fired boiler was higher than that in the pulverized coal fired boiler ash and deposits. This was because in cyclone boilers the bulk of silicate ash is discharged as molten slag but the residual ash is relatively rich in sulphate.

The rate of alkali-metal sulphate deposition will decrease when the temperature of collecting target surface exceeds 1075 K as shown in Figure 2. The decrease in the deposition of alkali-metal sulphates is related to the concentration of the volatile alkali-metals in the flue gas and the saturation vapour pressure of sodium and potassium sulphates (8). The initial deposit on cooled surfaces contains a small amount of chloride as shown in Figure 2.

In a reducing atmosphere the deposit material may contain iron sulphide (FeS) formed on dissociation of coal pyrite mineral. This is likely to occur on the combustion chamber wall tubes near the burners where the reaction time is short, below one second, for oxidation of FeS residue to the oxide. It has been suggested that calcium sulphide (CaS) may also be present in the ash material deposited from a reducing atmosphere gas stream as a result of sulphidation of calcium oxide (9).

### Thermal Stability of Sulphates and Immiscibility with Silicates

Bituminous coals usually leave a highly silicious ash on combustion. That is, fused aluminosilicates constitute an acidic media at high temperatures that is capable of absorbing large quantities of basic metals in the form of oxides, chiefly those of sodium, calcium and



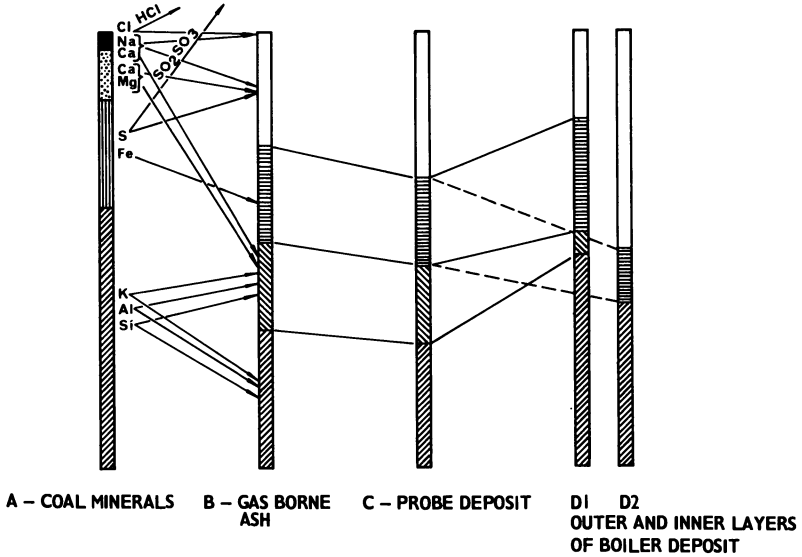


Figure 1. Ash composition changes on route from mineral matter to boiler deposits. insoluble silicates; soluble silicates; pyrites; iron oxides; carbonates; chlorides; sulphates.

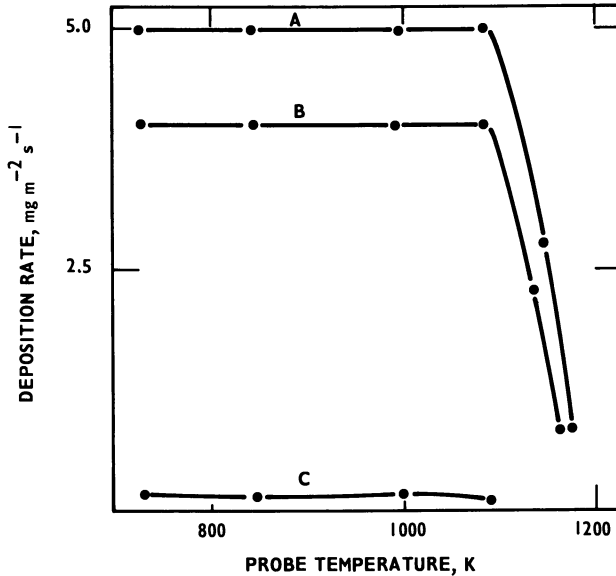


Figure 2. Deposition of sulphate and chloride in cyclone fired boiler, 0.28 per cent chlorine in coal. A, NaSO<sub>4</sub>; B, K<sub>2</sub>SO<sub>4</sub>; C, NaCl.

magnesium. At lower temperatures the corresponding sulphates are thermodynamically more stable in the presence of sulphur gases. The equilibrium distribution of alkaline oxides between molten sulphates and fused silicates at different temperatures can be calculated from the appropriate thermodynamic data. However, the residence time of the flame borne mineral species before deposition is short and the alkali-metal distribution does not reach the equilibrium state.

The fused silicate particles will absorb the flame volatilized sodium to the depth of about  $0.05 \mu\text{m}$  (10), and the remainder is converted to sulphate partly in the flue gas and partly at the surface of ash particles. The distribution of sodium in the silicate and sulphate phases can be expressed in a form:

$$m_{\text{sul}} = m_{\text{o}} - kw^{2/3} \quad (1)$$

$$\text{where } m_{\text{sil}} + m_{\text{sul}} = m_{\text{o}} \quad (2)$$

$m_{\text{sil}}$ ,  $m_{\text{sul}}$  and  $m_{\text{o}}$  denote the amount of sodium in silicate and sulphate fractions, and the total sodium in ash respectively;  $k$  is a constant and  $w$  is the ash content of coal.

When the ratio of sodium to ash in coal is below 1 to 100 (10) and the bulk of sodium is captured by the silicate particles Equation (2) reduces to:

$$m_{\text{sil}} = m_{\text{o}} \quad (3)$$

and consequently the amount of sodium available for the formation of sulphate is small.

The molten sodium sulphate/sodium silicate system of composition  $\text{Na}_2\text{SO}_4:\text{Na}_2\text{O}-\text{SiO}_2$  has one liquid phase at 1475 K, but as the proportion of silica increases, the melt separates into two layers (11,12). The change from the miscible to immiscible phase of the system has been explained by alterations in the silicate structure as the ratio of  $\text{Na}_2\text{O}$  to  $\text{SiO}_2$  decreases. In more basic, less viscous melts, the silicate ions exist in the form of  $\text{SiO}_4^{4-}$  tetrahedra which have the same mobility as sulphate ions, and thus homogeneity of the system is to be expected. As the silica content is increased the complexity of the silicate structure reaches a point where the silica anions become relatively immobile for a separation of sulphate from silica to take place.

The miscibility of the corresponding potassium sulphate-silicate system has been studied by the usual crucible method as well as by a technique of a hanging droplet (13). The droplets of potassium sulphate/silicate mixtures, 3 mm in diameter, were suspended from 0.5 mm platinum wire which had a semi-spherical head 1.5 mm in diameter. Separation of the silicate (internal) and sulphate phases in the droplets can be observed directly in the Leitz heating microscope which is used, in its conventional mode of operation, to assess the fusion characteristics of coal ashes (14). Figure 3 shows the two phase separation of  $2\text{K}_2\text{SO}_4-\text{K}_2\text{O}-2.1\text{SiO}_2$  system at 1575 K, having the transparent envelope of sulphate through which the platinum wire head (top) and globule of molten silicate (bottom) can be seen. As the temperature was increased to 1725 K the two phases became miscible because of the increased solubility of sulphate in the silicate melt at the higher temperature.

The  $K_2SO_4$ - $K_2O$ - $SiO_2$  phase diagram is depicted in Figure 4 which shows that the system is miscible at 1575 K when the molar ratio of  $K_2O$  to  $SiO_2$  is above 0.5. As in the corresponding sodium sulphate/sodium silicate system, less basic melts separate into two immiscible liquids. This is the case with most coal ash slags where the molar ratio of basic oxides (sum of  $Na_2O$ ,  $K_2O$ ,  $CaO$  and  $MgO$ ) to  $SiO_2$  is well below 0.5. Exceptions to this are the sodium and calcium rich ashes of some lignite and non-bituminous coals, which can have sufficient amounts of alkalis to form a single phase melt of miscible sulphates and silicates at high temperatures.

#### Adhesion by Van Der Waals and Electrostatic Forces

The ash particles deposited on boiler tubes are initially held in place by surface forces, i.e. van der Waals and electrostatic attraction forces. Van der Waals forces become important when molecules or solid surfaces are brought close together without a chemical interaction taking place. For a hemispherical particle of radius ( $r$ ) held at a distance of nearest approach ( $h$ ) from a plane, the resultant force ( $F$ ) is given by:

$$F = \frac{Ar}{6h^2} \quad (4)$$

where  $A$  is the Hamaker constant (15).

Equation 4 applies over short distances, up to 150 Å ( $1.5 \times 10^{-8}$  m) and for longer distances the "retarded" van der Waals forces decay rapidly (16). An equation based on the dielectric properties of solids for the retarded van der Waals forces ( $F'$ ) between a sphere of radius ( $r$ ) at the distance ( $h$ ) from a flat surface is (17):

$$F' = \frac{2B\pi r}{3h^3} \quad (5)$$

where  $B$  is the appropriate constant for the given material.

The changeover from the unretarded to retarded van der Waals forces occurs at a distance of about 150 Å ( $1.5 \times 10^{-8}$  m), and the corresponding value of the Hamaker constant ( $A$ ) in equation 4 was found to be  $10^{-19}$  N (Newton), and that of the Lifshitz constant ( $B$ ) in Equation 5 was  $8.9 \times 10^{-29}$  N m (16,18). These values have been used to compute the ratio of van der Waals forces to the gravitational force on small ash particles approaching a flat surface.

The gravitational force ( $F_g$ ) on an ash particle of radius ( $r$ ) and the density ( $D$ ) is given by

$$F_g = \frac{4\pi r^3 Dg}{3} \quad (6)$$

where  $g$  is the gravity acceleration constant ( $9.81 \text{ m s}^{-2}$ ). Thus, the ratio ( $F_r$ ) of the short distance van der Waals forces ( $F$ ) to the gravitational force ( $F_g$ ) on a particle is:

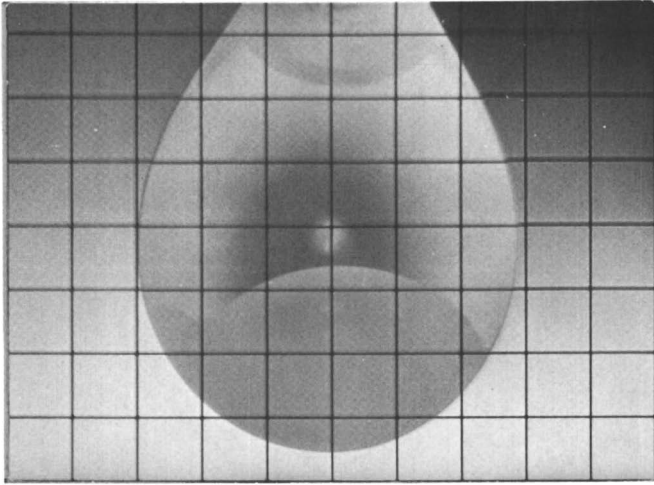


Figure 3.  $2K_2SO_4-K_2O-2.1SiO_2$  droplet in heating microscope. 0.5 mm grid. Two phases at 1575 K.

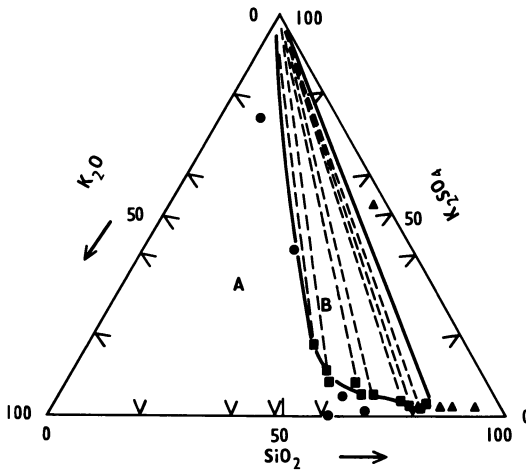


Figure 4. Miscibility gap in  $K_2SO_4-K_2O-SiO_2$  system at 1575 K. A, single phase; B, two phases.

$$\frac{F}{F_g} = F_r = \frac{A}{8\pi Dgr^2 h^2} = \frac{1.62 \times 10^{-25}}{r^2 h^2} \quad (7)$$

where the value of  $D$  for ash was taken to be  $2500 \text{ kg m}^{-3}$  and when  $h < 1.5 \times 10^{-8} \text{ m}$ . The corresponding ratio ( $F_r'$ ) of the retarded van der Waals forces ( $F'$ ) to the gravitational forces is given by:

$$\frac{F'}{F_g} = F_r' = \frac{B}{2Dgr^2 h^3} = \frac{2.04 \times 10^{-34}}{r^2 h^3} \quad (8)$$

where  $h > 1.5 \times 10^{-8} \text{ m}$ .

Figure 5 shows a comparison of van der Waals and the gravitational forces on small ash particles as these approach a collecting surface. Plots A and B indicate that the sub-micron sized particles are readily held on a surface by van der Waals forces. The capture of small particles of ash on boiler tube is further enhanced by surface irregularities of oxidized metal (19). Also, it has been suggested that electrostatic attraction forces enhance the transport and retention of sub-micron sized particles on steel probes inserted in the flue gas of coal fired boilers (7,20). A layer of electrically precipitated deposit of ash can have a cohesive strength between 5 and 40 times higher than that formed by sedimentation because particles in an electric field have permanent dipole characteristics which lead to these being oriented to form a cohesive layer of ash (21). It appears therefore that the combined effects of van der Waals and electrostatic forces of attraction, and surface irregularities are sufficient to hold the sub-micron diameter particles on the surface of boiler tubes for the subsequent liquid phase adhesion, and chemical and mechanical bond formation.

#### Adhesion by Surface Tension Force

The formation of strong adhesive bonds of enamel coatings and glass/metal seals on heating requires the presence of a liquid phase (22-24). The role of the liquid film is to provide the initial adhesion of solid particles as a result of surface tension. The work of adhesion ( $W_a$ ) is given by:

$$W_a = \pi + \gamma (1 + \cos \theta) \quad (9)$$

where  $\gamma$  is the surface tension of the liquid, and  $\theta$  is the contact angle at the solid/liquid interface. With perfect wetting, i.e. when  $\theta$  equals zero,  $W_a$  has the highest value:

$$W_a = \pi + 2\gamma \quad (10)$$

The work of cohesion of a liquid ( $W_c$ ) is given by:

$$W_c = 2\gamma \quad (11)$$

With wetting liquids, therefore,  $W_a$  can be higher than  $W_c$  and failure will take place within the liquid layer, whereas with non-wetting liquids the rupture occurs at the solid/liquid interface.

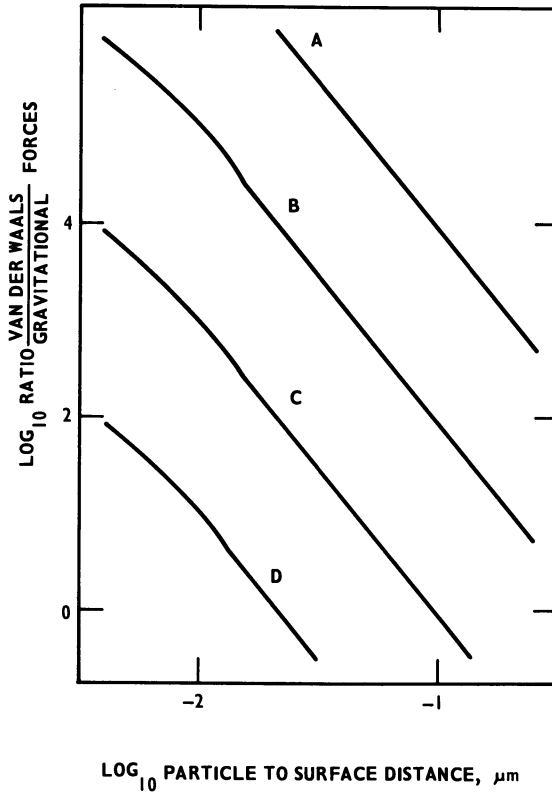


Figure 5. Comparison of van der Waals and gravitational forces on ash particles near collecting surfaces. Particle diameter ( $\mu\text{m}$ ): A, 0.01; B, 0.1; C, 1.0; D, 10. Reproduced with permission from reference 35. Copyright 1985 Hemisphere Publishing.

Alkali-metal sulphates frequently constitute a liquid phase in ash deposits, and the molten sulphates readily wet and spread on the surface of boiler tubes. In a reducing atmosphere and when in contact with carbon, sulphates are reduced to sulphides which wet and spread on any surface. The coefficient of surface tension of sulphates is fairly high,  $0.20 \text{ N m}^{-1}$  for  $\text{Na}_2\text{SO}_4$  and  $0.14 \text{ N m}^{-1}$  for  $\text{K}_2\text{SO}_4$  near their respective melting point temperatures (25,26). Thus work of cohesion of molten sulphate layer in boiler deposit is between  $0.3$  and  $0.4 \text{ N m}^{-1}$  and the work of adhesion is higher because of a low contact angle at the sulphate/tube surface interface. It is therefore to be expected and it is observed in practice that when the deposit is removed, e.g. by sootblowing, there remains a film of sulphate adhering to boiler tubes. The surface tension of coal ash slag has been measured previously by the sessile drop method (27) and a typical value was  $0.3 \text{ N m}^{-1}$ . It is about twice that of sulphates and thus the work of adhesion (Equation 9) and the cohesive bond strength are corresponding at the slag/solid interface.

Only a small amount of liquid, about a hundred molecule thick layer, is sufficient for the adhesion contact of sub-micron diameter particles (28). In the case of a volatile liquid, the equilibrium thickness of the film, and thus the adhesion, varies with partial pressure of the vapour in the surrounding atmosphere. When evaporation from a liquid film occurs, as a result of increased temperature, the adhesion first rises to a maximum value due to the meniscus effect but it breaks down as the film thickness is reduced to molecular dimensions. However, before the break-down of the surface tension chemical and mechanical bonds may develop between the deposited ash and boiler tube surface.

#### Mechanical and Chemical Bonding

Ash deposits on boiler tubes can be keyed to the surface of metal oxide by mechanical and chemical bonds. Mechanical bonding is enhanced by extending surface at the interface as shown in Figure 6a. Boiler tubes are not polished and thus have an extended surface that is further increased by oxidation and chemical reactions between the oxide layer and ash deposits. It is therefore evident that a comparatively rough surface of boiler tubes constitute an anchorage for keying ash deposits to the heat exchange elements.

Dietzel (29) and Staley (30) have proposed that the chemical reactions at an enamel/metal interface can be considered in terms of electrolytic cells set up between the metals of different electro-chemical potential. It has been suggested that cobalt or nickel precipitated in the enamel when in contact with steel surface, forms short-circuited local cells in which iron is the anode. The current flows from iron through the melt to cobalt and back to iron. The result is that iron goes into solution, the surface becomes roughened, and the enamel material anchors itself into the cavities as shown in Figure 6b.

The galvanic reactions will take place at a much faster rate in the low viscosity phase of sulphates in boiler deposit than in highly viscous silicate glass. However, rapid reactions at the tube surface/deposit interface may not be necessary or appropriate for development of a strong bond between the ash deposit and boiler

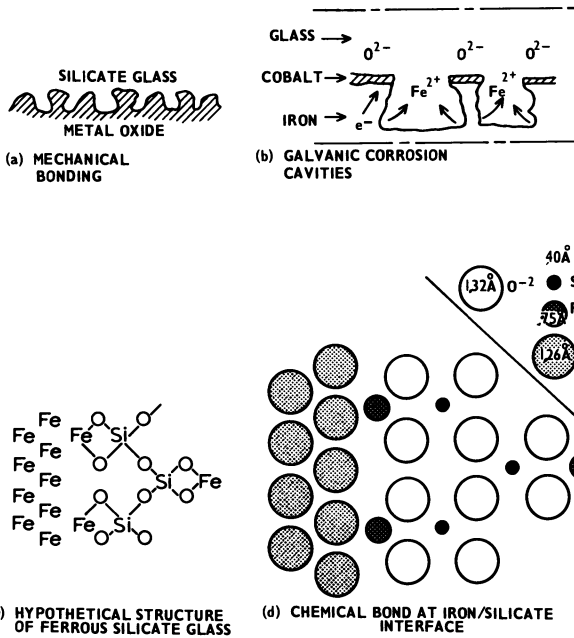


Figure 6. Schematic representation of mechanical and chemical bonds at boiler tube/ash deposit interface. Reproduced with permission from reference 35. Copyright 1985 Hemisphere Publishing.



tubes. In metal/glass seal and metal/enamel coating technology, the adhesive bonds formed on heating have to be completed in a few hours, whereas those in boiler deposits can form over a period of days or weeks. The adhesive bond between the metal surface and a silicate material can be high when there is a gradual rather than abrupt change in the glass phase composition near the interface (31).

When the ash deposit is brought in intimate contact with the surface of boiler tubes either by the action of surface tension or by the galvanic reactions, the controlling parameter in mechanical bonding is the strength of the glassy phase at the narrowest cross sectional area of contact cavities (Figure 6b). The annealed glass may have a tensile strength of around  $50 \text{ MN m}^{-2}$  giving a maximum bond strength of  $35 \text{ MN m}^{-2}$ . However, the glass at the interface may be stronger or weaker depending on whether the conditions in the keying cavities increase or decrease local flaws and resultant stresses.

Chemical bonds, covalent or ionic as shown in Figure 6c and d, at the metal oxide/deposit surface are potentially strong with theoretical values over  $10^9 \text{ N m}^{-2}$ . It is however, impossible to estimate the number of sites and the size of contact areas at the interface where the chemical bonds may be effective. In any case, the cohesive strength of the deposit matrix is the limiting factor since it is lower than that of chemical bonds by several orders of magnitude. In practice, this means that when a strongly adhering deposit is subjected to a destructive force, e.g. sootblower jet, failure occurs within the deposit matrix and there remains a residual layer of ash material firmly bonded to the tube surface.

#### Adhesion of Ash Deposits on Ferritic and Austenitic Steels

The adhesion bond strength of soda glass on a metal substrate has been determined by heating a glass disc sandwiched between two metal discs in a vertical furnace (32). The technique has been adopted for measuring the strength of the adhesive bond developed when a boiler deposit was sandwiched between two discs of ferritic or austenitic steels (33). The deposit material was taken immediately after boiler shut-down from the superheater tubes of a pulverized coal fired boiler fueled with a mixture of East Midlands, UK, coals. The flue gas temperature in the superheater prior to boiler shut-down was about 1300 K and the tube metal temperature was 850 K. The deposit material consisted of 30 per cent of alkali-metal sulphates in weight ratio of 2 to 1  $\text{Na}_2\text{SO}_4$  to  $\text{K}_2\text{SO}_4$ , the remainder being silicate ash. A layer of deposit, 3 mm thick, was sandwiched between two metal discs, 20 mm in diameter, made of boiler tube steels and then heated in a vertical furnace. After a time interval lasting from one to 25 days the bond was ruptured by applying a tensile force without prior cooling.

The results in Figure 7 show that the strength of adhesive bond between the ferritic steel sample and boiler deposit increased exponentially with temperature in the range of 775 to 900 K. Similar results were obtained by Moza et al. (34) who used a droplet technique to measure the adhesive bond of coal ash slag on a ferritic steel target in the temperature range of 700 to 950 K.

The results plotted in Figure 8 shows that the strength of adhesive bond of ash deposit on both the ferritic and austenitic steels.

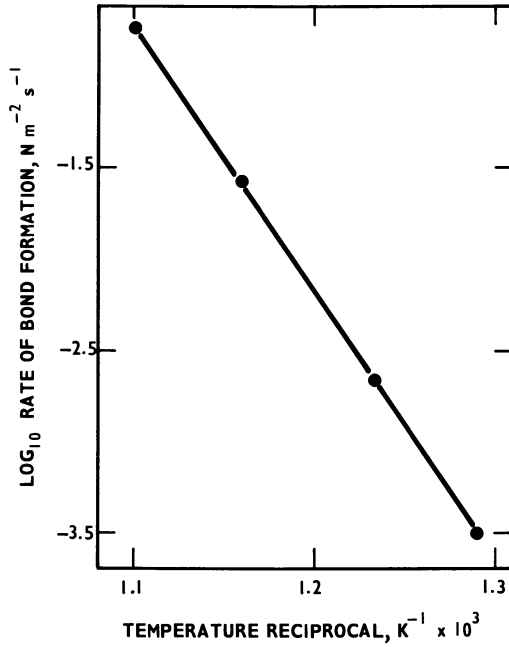


Figure 7. The effect of temperature on ash deposit/ferritic steel bond.

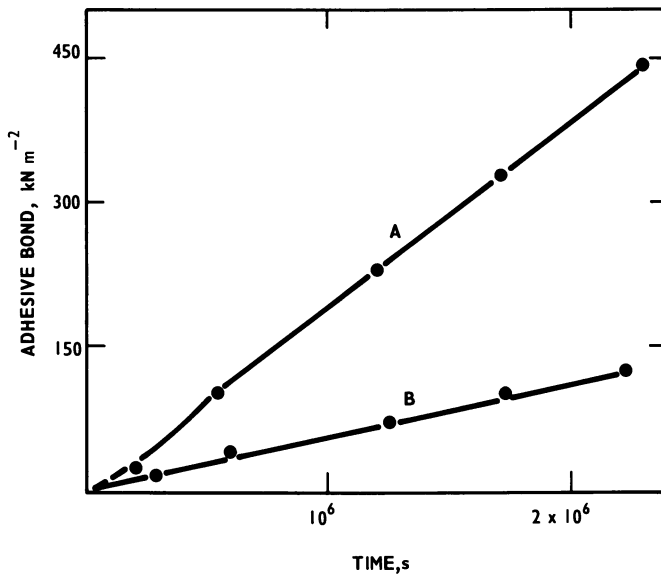


Figure 8. Bond strength between ash deposit and boiler steels at 900 K. A, ferritic steel; B, austenitic steel.

Table I. Coefficient of Thermal Expansion of Boiler Tube Steels, Oxides and Silicates

Material	Thermal expansion, $\frac{\Delta m}{m} K^{-1}$
<u>Steels</u>	
Mild steel and ferritic steels	11 to 12 $\times 10^{-6}$
Austenitic steels	16 to 18 $\times 10^{-6}$
<u>Oxides</u>	
Tube metal oxides ( $Fe_3O_4; Cr_2O_3; NiO$ )	8 to 10 $\times 10^{-6}$
<u>Deposit Constituents</u>	
Glassy material	6 to 9 $\times 10^{-6}$
Quartz (crystalline)	5 to 8 $\times 10^{-6}$
Silicates in fired brick	7 to 8 $\times 10^{-6}$

The data in Table I show that the coefficient of thermal expansion of mild steel and ferritic steels is not greatly different from that of their oxides and the ash deposit constituents. It is therefore evident that there is no gross incompatibility in the thermal expansion characteristics, and strongly bonded ash deposits once formed on mild steel tubes are not easily dislodged on thermal cycling.

In contrast, the thermal expansion of austenitic steel is significantly higher than that of the oxides and deposit material. In the absence of boiler deposit, the oxide material in the form of thin layer is able to absorb thermal stresses and the adhesive layer remains intact on cooling. However, it appears that the oxide layer is unable to absorb thermal stresses in a similar manner when contaminated and constrained by bonded ash deposits. It is therefore a usual occurrence that ash deposits peel off the austenitic steel tubes on cooling whereas the deposit formed on ferritic steels under the same conditions remain firmly attached to the tubes.

King et al. (22) have suggested that in order to obtain good adherence of enamel coatings on metals, the enamel material at the interface must become saturated with the metal oxide, e.g.  $FeO$  of ferritic steels. Coal ash deposit on boiler tubes contains between 5 and 25 per cent iron oxide and thus the layer at the tube/deposit interface becomes saturated with  $FeO$ . The chromium and nickel contents of ash deposit are low and thus the same chemical compatibility stage is not reached at the austenitic steel/deposit interface.

The adhesive bond between boiler ash deposit and the surface of ferritic steels can attain exceptionally high strengths. This was found on examining the deposits formed on different steel specimens tested in an experimental superheater loop. Favourable conditions for the formation of firmly bonded deposits were as follows:

- (a) The iron oxide content of coal was above 20 per cent expressed as  $Fe_2O_3$  giving an iron saturated layer of deposit on the tube specimens.
- (b) The ash collecting surface was a 5 per cent chromium ferritic steel which formed an oxide layer strongly adhering to metal for a firm anchorage of deposits.

- (c) The tube metal temperature was high, 950 K, which enhanced the formation of strong adhesive bond. The flue gas temperature at that position was approximately 1250 K.
- (d) The ferritic test piece in the experimental loop was sheltered from direct action of sootblower. Weak turbulence caused by the jet removed some of the unsintered silica ash leaving iron rich deposit firmly bonded to the tube. The iron rich deposit had grown in thickness to about 20 mm after nine months, and cohesive strength of the deposit material increased towards the surface of tube metal. The microscopic examination showed that there was no marked interface boundary between the ash deposit and metal oxide.

#### Formation of Layer Structure Deposits and Slag Masses

The coal ash deposits on boiler tubes have frequently a separate zone structure with a sulphate rich layer up to 2 mm thick under the matrix of sintered ash (35). The outer layer is porous and it constitutes a pathway for the enrichment of alkali-metals in the deposit layer next to tube surface. The diffusible species may be sulphate, chloride, oxide or hydroxide, but the thermodynamic data (8) and the results of deposition measurements in coal fired boilers (Figure 3) suggest that sodium and potassium sulphates are the principal vapour species which diffuse through a porous matrix of silicate ash deposit.

The relative amounts of  $\text{Na}_2\text{SO}_4$  and  $\text{K}_2\text{SO}_4$  which diffuse through the sintered matrix of silicate ash depend on the temperature gradient across the deposit layer, vapour pressure of the species and thermodynamic stability of the sulphates in the presence of silicates. Potassium sulphate has a higher temperature stability limit when compared with that of sodium sulphate and as a result  $\text{K}_2\text{SO}_4$  can be preferentially transported to the surface of cooled boiler tubes when there is a steep temperature gradient across the ash deposit. The  $\text{K}_2\text{SO}_4$  rich phase, when molten, can cause severe corrosion of tube metal.

The corrosion product, a mixture of oxide, sulphide at the metal interface and sulphate outside, has a weak adhesive bond to the metal surface and cannot support large deposit masses. It is therefore unusual to find excessive amounts of sintered ash deposits and fused slag in the exact localities where severe high temperature corrosion occurs. Conversely, a strongly adhering matrix of sintered ash deposit in the absence of sulphate, sulphide or chloride phases is not markedly corrosive.

The build-up of boiler tube deposits is a continuously changing process as depicted in Figure 9. When the deposit material reaches a thickness of 2 to 3 mm (Figure 9a) the separate sulphate and silicate phases occur (Figure 9b). Subsequently, the sulphate layer disappears in the middle section (Figure 9c) allowing a strong bond to be established between the sintered ash deposit and ferritic steel boiler tubes. This is the "classical" mode of formation of superheater tube deposit when the metal temperature is in the range of 750 to 900 K. Above 950 K the layer structured deposits are less likely to occur and a strong adhesive bond is rapidly formed between the silicate ash deposits and the high temperature tube surface.

A notable feature of slag formed in pulverized coal fired boiler

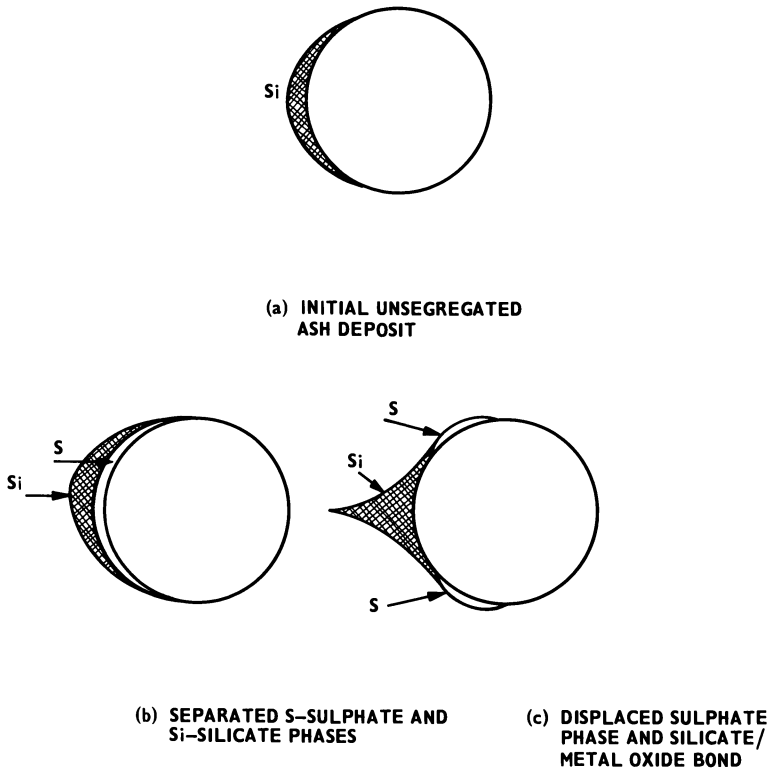


Figure 9. Sequential stages in the formation of layer-structured and firmly adhering superheater deposit. Reproduced with permission from reference 35. Copyright 1985 Hemisphere Publishing.

is its variable gas hole porosity. Burning coal particles are encapsulated in the deposit layer and generate CO and CO<sub>2</sub> inside the silicate material (27) resulting in a highly porous slag. The density of slag will increase when the encapsulated coal particles are consumed and gas bubbles have escaped.

It has been observed that new boilers have an "immunity" period lasting weeks or months before severe slag build-up occurs. This is partly due to the fact that during the commissioning period the boiler rarely reaches full load output. However, it may also be partly due to a slow rate of formation of the interface layer on boiler tubes which is able to have a strong adhesive bond to rapidly forming ash slag and thus able to support large masses of deposit.

## Conclusions

Initial Deposit. The initial deposit material on cooled tubes in coal fired boilers consists largely of flame vitrified silicate ash, iron oxide, and calcium and alkali-metal sulphates. Trace amounts of chloride will also deposit and under reducing conditions some iron and calcium sulphides can be present.

Phase Separation. Most coals leave an ash residue which is pyrochemically acidic, and the alkali-metals and calcium are distributed in the silicate and sulphate phases under oxidizing conditions. The fused silicates and molten sulphates are immiscible and separate into two phases. The phase separation enhances the adhesion of ash to boiler tubes and leads to the formation of layer structured deposits.

Initial Particle Adhesion. Initially the small particles of ash, below 1  $\mu\text{m}$  in diameter are held at the surface of boiler tubes by the van der Waals and electrostatic attraction surface/deposit interface and only a small amount of liquid, about one hundred molecules thick is sufficient for bonding.

Strong Adhesive Bond of Deposits on Ferritic Steels. Strong adhesive bonds can form between the oxidized surface of ferritic steels and iron rich ash because of the composition and thermal expansion compatibility of the metal oxide and silicate ash deposit. The adhesive bond strength increases exponentially with temperature of the target surface in the range of 750 to 950 K. The bond strength can reach high values, that is, higher than the cohesive strength of sintered ash deposits at temperatures above 850 K.

Weak Adhesive Bond of Deposits and Austenitic Steels. The adhesive bond between the austenitic steel surface and ash deposit is relatively weak as a result of the composition and thermal incompatibility of the steel oxide and the silicate material. The temperature fluctuations on changeable boiler load conditions can cause sufficiently high thermal stresses for deposit to skid off the austenitic steel tubes.

Boiler Tube/Ash Deposit Interface. The boiler tube/ash deposit interface layer which can support large masses of slag formed in the combustion chamber takes several months to develop. Thus the full extent of boiler slagging may not become evident during the commissioning period of new boiler plant.

## Acknowledgement

The work was carried out at the Central Electricity Research Laboratories and the paper is published by permission of the Central Electricity Generating Board.

## Literature Cited

1. Lowry, H.H. "Chemistry of Coal Utilization"; John Wiley and Sons: New York, 1963.

2. Francis, W. "Fuels and Fuel Technology"; Pergamon Press: London, 1965; Vol. I.
3. Raask, E. Fuel. 1969, 48, 366.
4. Raask, E.; Goetz, L. J. Inst. Energy. 1981, 54, 163.
5. Raask, E. Prog. Energ. Comb. Sci. 1982, 8, 261.
6. Raask, E. VGB Mitteilungen. 1968, 18, 348.
7. Raask, E. "Mechanism of Corrosion by Fuel Impurities"; Marchwood, UK; Butterworth: London, 1963; p. 145.
8. Halstead, W.D.; Raask, E. Inst. Fuel. 1969, 43, 344.
9. Hein, K. VGB Kraftwerkstechnik. 1979, 59, 576.
10. Hosegood, E.A.; Raask, E. unpublished data.
11. Kordes, E.; Zofelt, B.; Proger, H.J. Zeitschr. Anorg. Allgem. Chem. 1951, 264, 255.
12. Pearce, M.L.; Beisler, J.F. Am. Cer. Soc. 1965, 48, 40.
13. Raask, E. and Jessop, R. Phys. and Chem. Glasses. 1966, 7, 200.
14. DIN "Determination of Ash Fusion Behaviour"; German Standard: DIN 51 730, 1976.
15. Casimir, H.B.G.; Polder, D. Phys. Rev. 1948, 73, 360.
16. Tabor, D. Chem. Ind. 1971, No. 35, p. 969.
17. Lifshitz, E.M. Soviet Physics, JETP. 1956, 2, 73.
18. Tabor, D.; Winterton, R.S.H. Nature. 1968, 219, 1120.
19. Pfefferkorn, G.; Vahl, J. "Mechanism of Corrosion by Fuel Impurities"; Marchwood, UK; Butterworths: London, 1963; p. 366.
20. Steel, J.S.; Brandes, E.A. "Mechanism of Corrosion by Fuel Impurities"; Marchwood, UK; Butterworths: London, 1963; p. 374.
21. Penney, G.W.; Klinger, E.H. Trans. A.I.E.E. 1962, 81, 200.
22. King, B.W.; Tripp, H.P.; Duckworth, W.H. J. Am. Cer. Soc. 1959, 42, 504.
23. Holland, L. "The Properties of Glass Surfaces"; Champan and Hall: London, 1964.
24. Klomp, J.T. Am. Chem. Soc. Bull. 1979, 10, 887.
25. International Critical Tables. McGraw-Hill: New York, 1928; Vol. 4, p. 443.
26. Bertozzi, G.; Soldani, G. J. Phys. Chem. 1967, 71, 1536.
27. Raask, E. Trans. ASME for Power. 1966, Jan., p. 40.
28. Cross, N.L.; Picknett, R.G. "Mechanism of Corrosion by Fuel Impurities"; Marchwood, UK; Butterworths: London, 1963, p. 383.
29. Dietzel, A. Emailwaren-Industrie. 1934, 11, 161.
30. Staley, H.F. J. Am. Ceram. Soc. 1934, 17, 163.
31. Weyl, W.A. "Structure and Properties of Solid Surfaces"; University of Chicago Press": Chicago, 1953; p. 147.
32. Oel, H.J.; Gottschalk, A. Glastechnische Berichte 1966, 39, 319.
33. Raask, E. VGB Kraftwerkstechnik 1973, 53, 248.
34. Moza, A.K.; Shoji, K.; Austin, L.G. J. Inst. Fuel 1980, 53, 17.
35. Raask, E. "Mineral Impurities in Coal Combustion", Hemisphere: New York, 1985, p. 205.
36. Hodgman, C.D. "Handbook of Chemistry and Physics"; The Thermal Rubber Publishing: Ohio, 1962.

RECEIVED October 15, 1985

## Use of Glass for Modeling the Deposition of Coal Ash in Hot Cyclones

D. M. Mason<sup>1</sup>, A. Rehmat<sup>1</sup>, and K. C. Tsao<sup>2</sup>

<sup>1</sup>Institute of Gas Technology, Chicago, IL 60616

<sup>2</sup>University of Wisconsin—Milwaukee, Milwaukee, WI 53201

Tests have been conducted in a laboratory hot cyclone to obtain an estimate of the temperature below which spherical glass particles do not form a firmly attached deposit. A temperature of 800° to 850°C, corresponding to a viscosity between  $6.3 \times 10^5$  and  $2.9 \times 10^6$  poises, as calculated from the composition of the glass, was found. We take this viscosity to be approximately that of coal ash above which particles will not deposit in cyclones of fluidized-bed coal gasifiers.

A cyclone operating at temperatures near those of the fluidized bed of the reactor has been used in the ash agglomerating gasifier of the IGT U-GAS pilot plant to remove entrained char particles from the product gas and return them to the bed (1). Essentially pure coal ash has been found to deposit in this hot cyclone (2). The deposits have been analyzed chemically and examined by optical and scanning electron microscopy. Ferrous sulfide is responsible for deposition under adverse conditions, but deposition of iron-rich ferrous aluminosilicates is the more serious problem. In deposits from Western Kentucky coal, for example, whose ash contained about 23 wt. percent of ferric oxide, the selective deposition of high-iron siliceous particles is indicated by an  $\text{Fe}_2\text{O}_3/\text{Al}_2\text{O}_3$  ratio (calculated after excluding the iron contribution of iron sulfide) ranging from 2.2 to 4.6 in the ash of deposits, compared with a ratio of 1.2 in the ash of the coal. The effect of gas temperature (which equals particle temperature) and cyclone-wall temperature on the deposition of such particles was studied in a laboratory hot cyclone in the laboratories of the Mechanical Engineering Department of the University of Wisconsin at Milwaukee (2,3). The particles used in these tests were prepared from pilot plant deposits. The results indicated that the borderline temperature, below which the particles do not form a firm deposit, is about 900°C when gas and wall temperatures are equal.



We envision that the mechanism of deposition involves viscous or plastic flow following collision of particle and deposition surface to create a neck exerting enough surface tension to prevent rebound. We consider that the main cause of flow is impact. Flow driven by surface tension, as postulated by Raask (4) for hardening of coal ash deposits on heat exchange surfaces of boilers, constitutes an additional mechanism leading to firm adhesion. However, deposition at the inlet impingement area in the laboratory hot cyclone tests, massiveness of deposits at regions of high gas velocity and acceleration in or near the pilot plant cyclone, and virtual absence of deposits at low-gas-velocity regions of the gasification reactor all indicate that impact of deposition-prone particles plays an important role in the mechanism.

For both mechanisms the effect of temperature on deposition can be attributed to change in viscosity, as surface tension does not vary much with temperature. Investigation of the effect of viscosity with ash particles is difficult, because little is known about the viscosities of iron aluminosilicates and ferrous sulfide at temperatures from 850° to 1050°C and, in any case, the ash particles vary in composition and presence of high melting phases. Therefore, we have chosen to use glass spheres as a homogeneous model material of known viscosity in tests for a study of deposition. We assume that the two materials are sufficiently alike in relevant properties that their borderlines for deposition occur at the same viscosity although their temperatures there may be different. We report here a few results of a preliminary nature.

### Experimental

The test apparatus consists of a natural gas burner to provide hot flue gas, a dust feeder designed by one of the authors, and a 9.68-cm ID cyclone (Figure 1). Calculations indicate that the residence time of particles in the hot flue gas is sufficient to heat the particles to the temperature of the flue gas at the cyclone entrance, and in any case the glass particles were subjected to the same conditions as the particles prepared from pilot plant deposits. We expect to obtain experimental confirmation of the adequacy of heating in a more detailed future study.

The inlet section of the cyclone is jacketed to allow cooling of the wall; or alternatively, it can be heated to achieve substantially equal gas and wall temperatures. Temperature readings of the gas during a run are taken by a bare wire thermocouple projecting into the gas just upstream from the inlet section of the cyclone; it is calibrated before the run by an aspiration thermocouple in the inlet section. Temperature of the wall is measured by a thermocouple embedded in it at the spot where the entering gas impinges, where coherent deposits typically form (2,3). The surface of the inlet section is smoothed with No. 320-grit emery paper before each test.

The feed dust in these tests was supplied by the Cataphote Division of Ferro Corporation as Class IV-A uncoated Unispheres of soda-lime glass in a nominal 13-44  $\mu\text{m}$  diameter. A Coulter counter size distribution analysis indicated that the size ranged only between 20 and 51  $\mu\text{m}$ , with 14% greater than 40  $\mu\text{m}$  and 3% smaller than 25  $\mu\text{m}$ . These particle sizes are in the same range as those of the tests with particles prepared from pilot plant deposits. The burner

was operated to yield an oxidizing atmosphere at rates giving cyclone inlet velocities that ranged, in different runs, from 9 to 15 m/s; these velocities are comparable to those of our laboratory tests with particles of pilot plant deposits.

Our estimate of the borderline of deposition is based on eight runs with the glass spheres, of which seven were within about 50°C of a borderline region obtained by plotting wall temperature against gas temperature (Figure 2). Very light but firm deposits of the spheres were observed at the jet impingement area in three of these tests. We interpret the results to indicate that the borderline for firm deposition with equal gas and wall temperatures is between 800° and 850°C. This estimated temperature range depends very little on the slope of the borderline, because critical data points were obtained at nearly equal gas (particle) and wall temperatures. The slope shown on the graph was taken to be equal to the better-established borderline for the pilot plant deposits (2), which is also shown in Figure 2. In the future, we expect to make additional tests to establish the borderline more precisely and to determine the effect of variables such as velocity and size of particles.

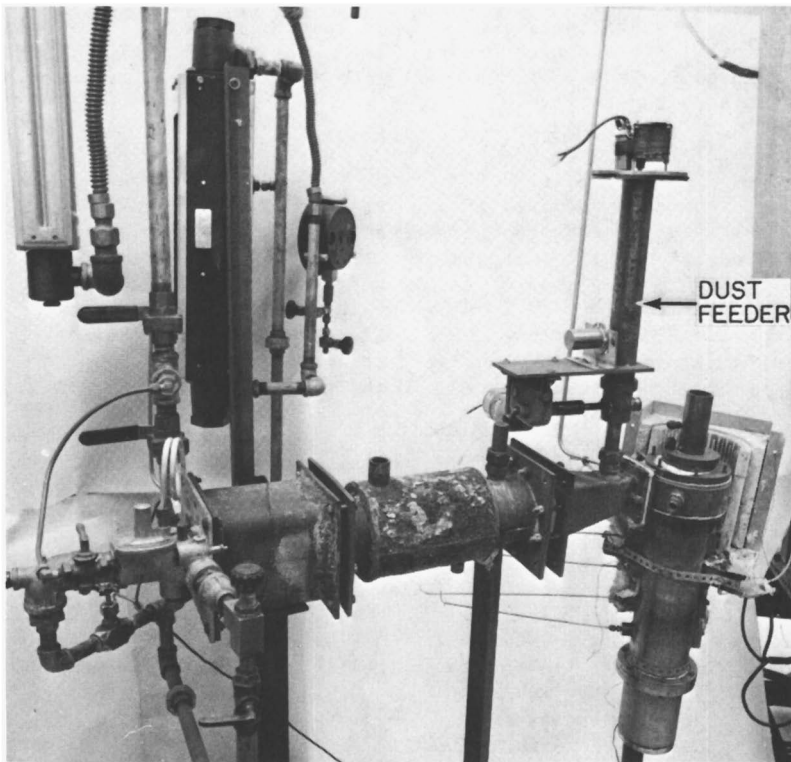


Figure 1. Laboratory Hot Cyclone Apparatus

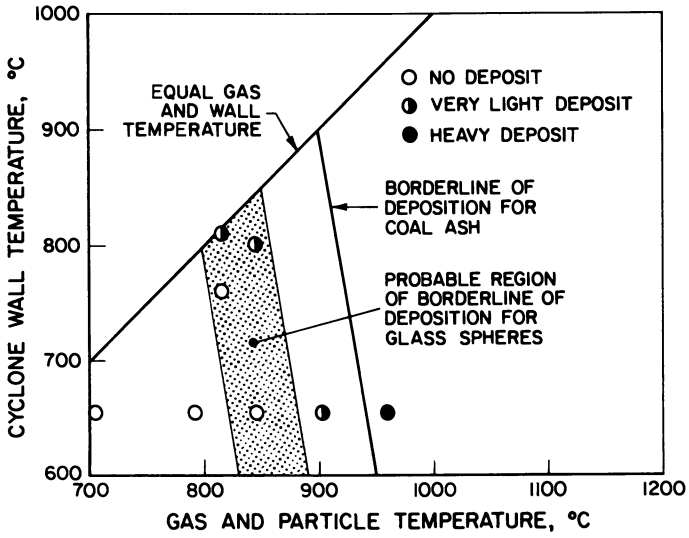


Figure 2. Borderline of Deposition

We have chemically analyzed the glass spheres and from this estimated the viscosity at 800° and 850°C by means of the correlation equations of Lyon (5). The range of viscosity thus obtained over the above temperature range is  $6.3 \times 10^5$  to  $2.9 \times 10^6$  poises. This is near the geometric mean of the viscosities at the softening and working temperatures of soda-lime glass (6).

### Discussion

According to Dietzel's correlation of the surface tension of glasses, glazes, and enamels with composition (7), the surface tension of the pilot plant deposits is up to about 25% higher than that of the glass used here. Neglecting this difference and the effect of particle shape, we may conclude that the effective viscosity of the pilot plant deposit for borderline deposition in the laboratory hot cyclone at equal gas and wall temperatures is in the range reported above for the glass spheres. In the pilot plant or in a commercial plant with much larger cyclones, considerable scale-up is required for application of our results, but we think it likely that they apply there also.

### Literature Cited

1. Mason, D. M.; Patel, J. G., Fuel Proc. Techn. 1980, 3, 181-206.
2. Mason, D. M.; Rehmat, A.; Tsao, K. C. in "Fouling of Heat Exchange Surfaces," Bryers, R. W., Ed. Engineering Foundation: New York, 1983, pp. 565-82.
3. Tsao, K. C.; Tabrizi, H.; Rehmat, A.; Mason, D. M. Am. Soc. Mech. Eng. [Pap], ASME Annual Meeting, November 1982, ASME Preprint No. 82-WA/HT-29.
4. Raask, E. VGB Kraftwerkstechnik 1973, 53(4), 248.
5. Lyon, K. C. J. Res. Nat. Bur. Stand. Section A, 78A, 1974, 497.
6. Boyd, D. C.; Thompson, D. A. in "Encyclopedia of Chemical Technology," 11, 807-80. Wiley: New York, 1980.
7. Scholze, H. "Glas-Natur, Struktur and Eigenschaften," 213-21. Vieweg: Braunschweig, 1965.

RECEIVED June 13, 1985

## Slag Deposit Initiation Using a Drop-Tube Furnace

M. F. Abbott<sup>1</sup> and L. G. Austin

Mineral Processing Section, The Pennsylvania State University, University Park, PA 16802

A drop-tube furnace was designed and constructed for the purpose of simulating the time/temperature environment for p.c. combustion in a utility furnace. The ash produced was impacted on oxidized boiler steel substrate at gas and metal temperatures similar to upper furnace waterwall tubes. Both fly ash and deposits were similar to those of a pilot-scale (7-9 kg/hr) combustor. Iron-rich slag droplets produced from pyrite-rich p.c. particles bonded strongly with the oxidized steel surface. These particle types were found at the base of ash deposits after removal of sintered and loose ash for both eastern and western coals. Adhesion of iron-rich droplets was a function of both flame and metal surface temperatures. Also, volatile species, i.e., alkali and exchangeable cations influenced the "sticking" behavior of the iron-rich droplets. These trends are in qualitative agreement with previous sticking test results.

Coals contain inorganic material, generally called mineral matter and when the coal is burned this mineral matter is converted to ash. The management of this ash constitutes one of the principal design limitations for a pulverized coal (p.c.)-fired electric utility boiler. The investigation reported here is part of an ongoing research program to gain a better understanding of the initiation of slag deposits on the upper walls of a boiler furnace enclosure. This paper reports on the development of a gas-fired vertical muffle tube (drop-tube) furnace as a new research tool.

The purpose of the drop-tube furnace was to simulate utility boiler combustion and ash forming and deposit conditions, in a laboratory-scale device. In particular, the furnace was used to

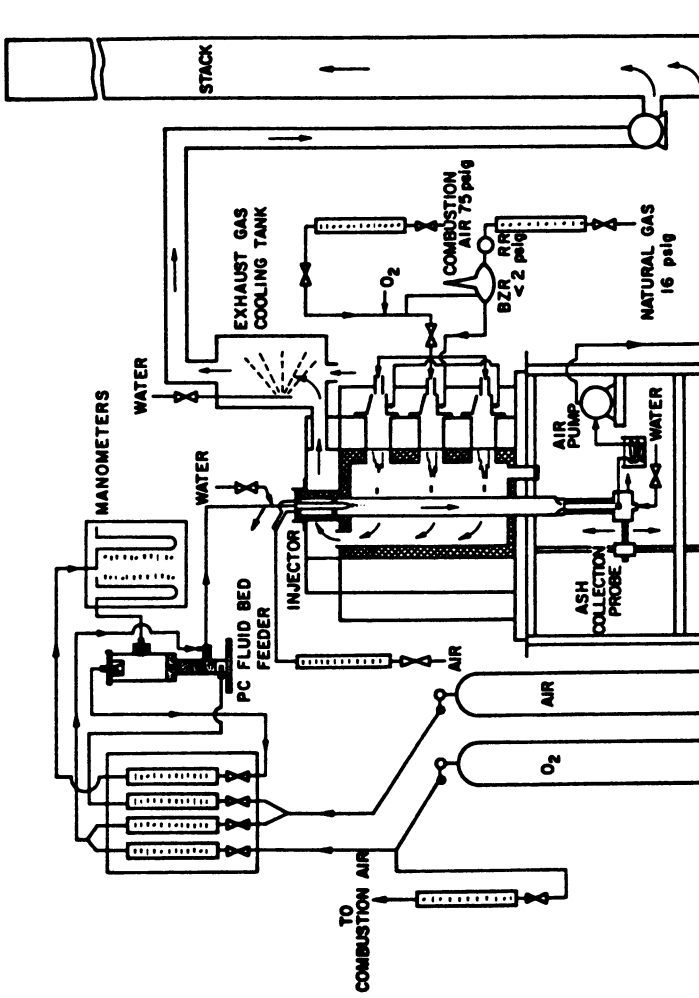
<sup>1</sup>Current address: Coal Research Division, Conoco, Inc., Library, PA 15129.

determine which inorganic constituents in coal gave ash particles that initiate slag deposits by adhering to relatively cold (e.g., 300 to 400°C) oxidized boiler steel surfaces. A previous laboratory test, the sticking test (1-6), led to a number of conclusions concerning the mechanism and chemistry of molten slag drop adhesion. However, this test has several inherent disadvantages. It required the use of relatively large molten ash drops 4 mm in diameter, and there was no proof that the conclusions could be applied to the smaller size droplets (normally less than 50  $\mu\text{m}$ ) produced in p.c.-fired furnaces. Also, the large drops formed from a coal ash contained all of the constituents of the ash (the mean ash composition), which do not accurately simulate the variety of mineral associations occurring on a particle-by-particle basis in a pulverized coal (7). Thus, the principal requirements of the drop-tube furnace were to produce coal fly ash particles under the same temperature-time-environment history experienced in full-scale boiler combustion, with impaction on an oxidized boiler steel substrate at a controlled temperature simulating a furnace waterwall.

#### Drop-Tube Furnace Description

Several drop-tube type furnaces were already in existence for conducting research on p.c. pyrolysis, combustion and mineral matter behavior (8-12). These were investigated in terms of their suitability, advantages and disadvantages for studying the slag deposition problem. It was decided that the simplest, least expensive and yet most versatile alternative was a vertical muffle tube (drop-tube) furnace externally heated by firing with natural gas and air. The drop-tube furnace system is shown in Figure 1. It consisted of four major component parts: (1) a hot zone section; (2) a preheat section and injector; (3) the fluidized-bed p.c. feeding system; and (4) a water-cooled ash collector probe. The necessary features incorporated into the hot zone design were: maximum gas temperatures of the order of 1500 to 1750°C; particle residence times between 1 and 2 seconds; and exit gas temperatures of 1000 to 1300°C. The preheat section and injector preheated the secondary air stream to about 1000°C and injected the cold p.c.-primary air stream into the hot combustion zone. The collector probe impacted the ash particles onto a boiler steel surface maintained at temperatures between 250 and 450°C to within  $\pm 5^\circ\text{C}$ .

A more detailed schematic of the drop-tube furnace hot zone is shown in Figure 2. It was heated by three tangentially-fired nozzle mix natural gas-air burners (101NM, Pyronics, Inc., Cleveland, Ohio). These were short flame, high capacity burner units designed for very wide turndown ranges, giving a great deal of operating flexibility in terms of heat input. The temperature was controlled by metering both the total quantity of natural gas and air (burner nozzle gas pressure), and the air-to-fuel ratio. The natural gas firing rate at an operating temperature of 1470 to 1550°C was 1.5 SCFM or 90,000 Btu/h (30,000 Btu/h for each of the three burners). The outside muffle tube wall temperatures were measured at three locations by embedded Pt/Pt-10% Rh type S thermocouples. The annular wall temperatures were also monitored in the same matter (see Figure 2).



BZR - BALANCE ZERO REGULATOR  
RR - REDUCING REGULATOR

Figure 1. Drop-tube furnace system.

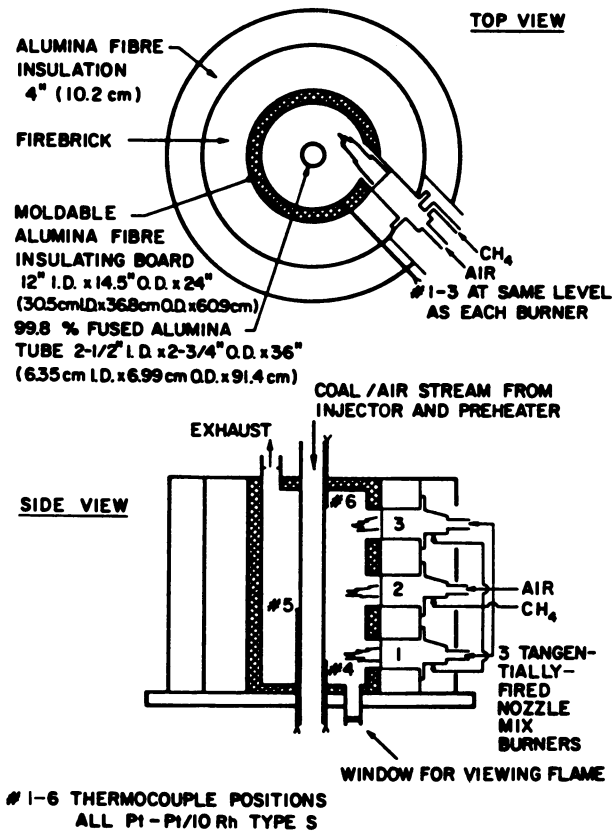


Figure 2. Drop-tube furnace hot zone.



Details of the preheat section and p.c. injector are shown in Figure 3. The heating coil on the injector isolated the cold injector from the preheated secondary air stream (approximately 2.5 liters/min) which entered through two channels at the top. The preheater coil and inner wall temperatures were also measured by type S thermocouples. The alumina honeycomb flow straightener distributed the air in streamlines across the muffle tube cross-section.

Fluidized bed feeders generally give more consistent homogeneous p.c. flow for low feed rates than other types of feeders (13-15). The fluid bed feeder used in this investigation is shown schematically in Figure 4. The feeder rested on a top loading balance in order to continuously monitor the p.c. feed rate. It delivered between 0.15 and 0.3 grams of coal with approximately 0.5 liters of air per minute. The p.c. particle size was kept between 60 and 325 mesh (250 to 45  $\mu\text{m}$ ) to insure consistent performance.

Figure 5 is a detailed diagram of the water-cooled collector probe. The constriction (0.5 inch diameter hole) above the steel substrate surface was used to accelerate the gas stream to about 2 m/sec in order to impact the particles on the surface with sufficient velocity to adhere. The steel substrate surface temperature was controlled by a combination of three methods: varying the substrate thickness; varying the thickness of the carbon steel plug; and varying the coolant (water) flow rate. The surface temperature was again measured by type S thermocouple as shown in Figure 5. Two boiler steels were used for substrate materials; 1040 carbon steel and Croloy 1/2.

### Experimental Procedures

Three Pennsylvania bituminous coals (designated Keystone, Montour and Tunnelton) and a Decker, Montana, sub-bituminous coal were studied in this investigation. The proximate and ultimate analyses for these coals were given in Table I. The mineralogical analysis of the low-temperature ash (LTA) from the Pennsylvania coals is listed in Table II and the elemental analysis of the ASTM high temperature (HTA) is given in Table III. In addition, pulverizer rejects from the Bruner Island Steam Generating Facility which burns the Tunnelton coal (among others) were tested. The mineralogical and elemental analyses of this material are given in Table IV. Table V gives the mineralogical and elemental analyses of untreated and acid-washed Decker coal samples. The three Pennsylvania coals were burned at three furnace temperatures. The other samples were all burned at 1500 to 1510°C furnace temperature.

The particle size distribution of the as received coal samples was measured by the Microtrac laser diffraction apparatus and size analyses for all samples are given in Table VI. The samples were sieved to remove any particles smaller than 45  $\mu\text{m}$  and larger than 250  $\mu\text{m}$ . The fluid bed feeder was loaded with a 20 to 30 gram coal or mineral sample. The feeder was operated at constant dilution or transport air flow and the coal flow was varied by changing the bed pressure (by either increasing the fluidizing air flow or decreasing the exhaust flow).

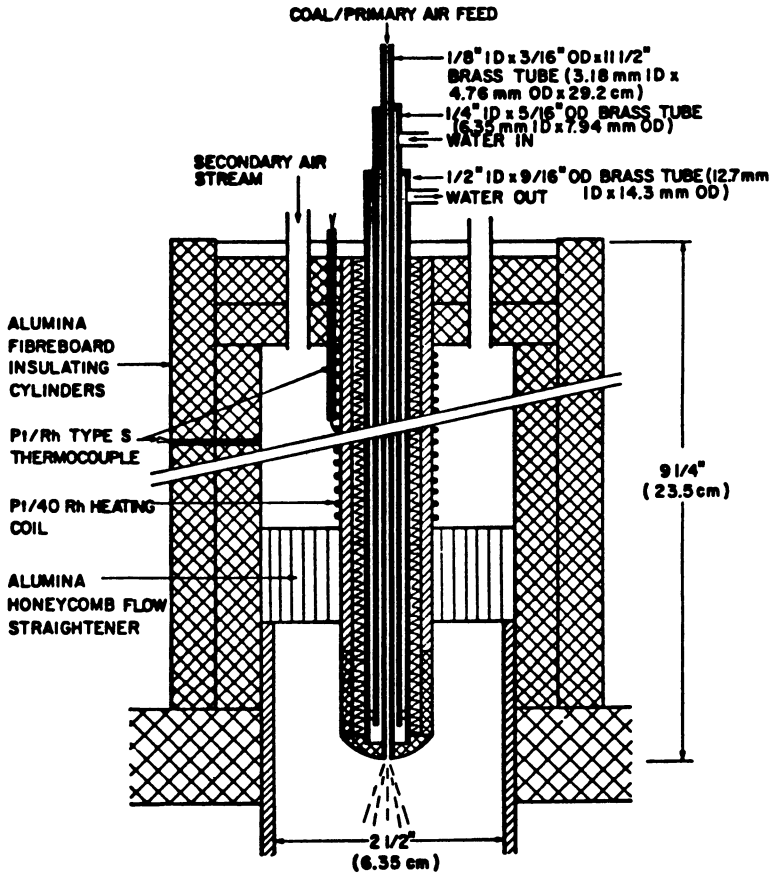


Figure 3. Drop-tube furnace injector and preheater section.

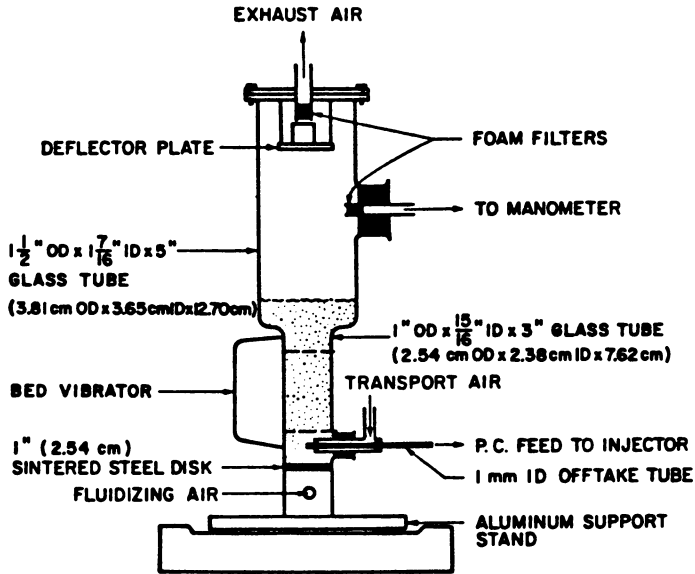


Figure 4. Drop-tube furnace pc fluid bed feeder.

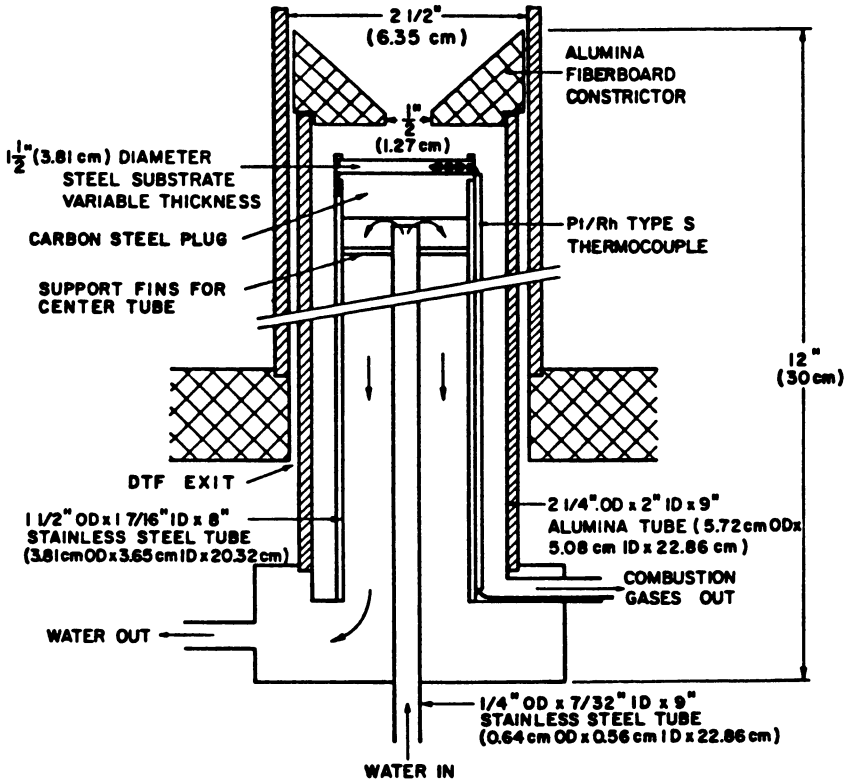


Figure 5. Drop-tube furnace water-cooled ash deposit collector probe.

Table I. Proximate and Ultimate Analyses of Test Coals  
(all on a dry basis with the exception of  
moisture determination)

Coal	Montour	Keystone	Tunnelton	Decker
<u>Proximate</u>				
Moisture	1.0	0.8	0.6	22.0
Volatilité Matter	25.9	29.9	26.4	43.8
Ash	16.0	18.1	21.9	4.5
Fixed Carbon	58.1	51.9	51.9	51.7
<u>Ultimate</u>				
Carbon	75.2	69.1	68.6	72.6
Hydrogen	4.4	4.3	4.1	5.1
Nitrogen	1.3	1.1	1.1	0.9
Sulfur	1.7	1.7	2.0	0.4
Ash	16.0	18.1	21.9	4.5
Oxygen	1.4	5.7	2.3	16.5

Table II. Semi-Quantitative Mineralogical Analysis  
of Low-Temperature Ash (LTA) for the  
Pennsylvania Coals

Coal	Montour	Keystone	Tunnelton
quartz	25	25	22
pyrite	15	10	15
calcite	5	n.d.	5
gypsum	n.d.	5	n.d.
kaolinite	17	30	18
illite	30	20	30-40
feldspar	n.d.	n.d.	5-10
n.d. = not detected in significant quantity.			
Wt. % LTA	18.0	21.6	22.9

The feeder and injector produced a thin pencil-like p.c. stream which passed down through the hot zone. The total combustion air supplied was approximately 3 liters/min for the bituminous coals, giving between 10 and 25 percent excess air for p.c. feed rates of 0.24 to 0.28 g/min. The flow and heat transfer conditions were modeled using the methods described by Pigford (16) for conditions of superimposed natural and forced convection at very low mass flow rates. Particle residence times were calculated by summing the centerline gas velocity and terminal velocity using Stokes's law (17). The error introduced using this method should never have exceeded 10 percent, even when pyrite was tested and particle Reynold's numbers approached one. The residence times thus calculated were found to be between one and two seconds.

Table III. Spectrochemical Analysis of ASTM High-Temperature Ash (HTA) Residues From the Pennsylvania Coals, Expressed as Weight Percent of Equivalent Oxides

Coal	Montour	Keystone	Tunnelton
SiO <sub>2</sub>	51.7	54.1	50.3
Al <sub>2</sub> O <sub>3</sub>	25.6	25.9	26.8
TiO <sub>2</sub>	1.3	1.3	1.3
Fe <sub>2</sub> O <sub>3</sub>	14.1	9.7	11.0
CaO	2.4	1.8	2.5
MgO	0.9	1.0	1.0
Na <sub>2</sub> O	0.2	0.3	0.4
K <sub>2</sub> O	2.4	2.9	2.9
SO <sub>3</sub>	1.5	1.1	2.3
P <sub>2</sub> O <sub>5</sub>	0.4	0.4	0.4
Totals	100.5	98.5	98.9
Wt. % HTA	15.3	18.3	20.1

Table IV. Semi-Quantitative Mineralogical Analysis and Spectrochemical Analysis for LTA and HTA of Pulverizer Rejects

<u>Mineralogical Analysis of LTA</u>	
Constituent	Wt. % LTA
quartz	15
pyrite	30
calcite	2-5
kaolinite	10
illite	30
siderite	2-5
iron sulfates	5-10
LTA (wt.% as received sample)	79.6
<u>Spectrochemical Analysis of HTA</u>	
Constituent	Wt. % HTA
SiO <sub>2</sub>	42.6
Al <sub>2</sub> O <sub>3</sub>	16.6
TiO <sub>2</sub>	0.9
Fe <sub>2</sub> O <sub>3</sub>	34.3
CaO	1.4
MgO	0.8
Na <sub>2</sub> O	0.2
K <sub>2</sub> O	2.1
Total	98.9
HTA (wt.% as received sample)	68.2

Table V. Semi-Quantitative Mineralogical Analysis and Spectrochemical Analyses for Two Decker Coal Samples; Untreated and Acid-Washed

<u>Mineralogical Analysis of LTA</u>		Wt. % LTA	
Constituent	untreated	acid-washed	
quartz	20	30	
pyrite	5	10	
calcite	5	n.d.	
gypsum (bassinite)	30	n.d.	
kaolinite	11	16	
illite	n.d.	n.d.	
LTA (wt.% as received coal)	6.3	3.3	
<u>Spectrochemical Analysis of HTA</u>		Wt. % HTA	
Constituent	untreated	acid-washed	
SiO <sub>2</sub>	28.0	53.0	
Al <sub>2</sub> O <sub>3</sub>	16.5	28.5	
TiO <sub>2</sub>	1.2	2.7	
Fe <sub>2</sub> O <sub>3</sub>	6.9	9.2	
CaO	19.0	4.1	
MgO	3.5	0.7	
MnO	0.03	0.01	
Na <sub>2</sub> O	7.7	0.4	
K <sub>2</sub> O	0.5	0.6	
SO <sub>3</sub>	15.8	-	
Total	99.1	99.2	
HTA (wt.% as received coal)	4.2	2.2	

Ash deposits were collected from an accelerated gas stream impacted on a water-cooled boiler steel substrate as shown in the probe of Figure 5. The sampling gas temperature was 1100°C and the 1040 carbon steel substrate was maintained at 340 ± 5°C for all tests except those with the Decker coal (sampling gas temperature was 1000°C and Croloy 1/2 substrate temperature was 425 ± 5°C). The ash deposits were then characterized by microscopic examination, using optical and scanning electron microscopes. Chemical characteristics were then sometimes determined by energy dispersive x-ray (EDX) fluorescence equipment associated with the scanning electron microscope.

### Experimental Results

The centerline gas temperatures were measured by shielded suction pyrometry at maximum wall temperatures ranging from 1450 to 1650°C. A comparison of gas and wall temperatures is given in Figure 6. In general, centerline gas temperatures were about 30°C lower than the corresponding wall temperatures at the same position on the muffle tube. A deposit collection zone with gas temperatures corresponding to upper furnace temperatures in a utility boiler was identified

Table VI. Particle Size Analysis (Sieve size)

Size ( $\mu\text{m}$ )	Keystone Coal	Montour Coal	Tunnelton Coal	Decker Coal	Brunner Island Pulverizer Tailings
500	100.00	100.00	100.00	99.70	100.00
355	98.06	99.65	99.86	99.21	100.00
250	96.61	98.82	99.17	97.93	100.00
176	93.78	96.54	95.30	94.29	100.00
125	88.94	92.12	87.42	88.68	97.63
88	81.34	86.59	75.81	77.76	91.86
62	75.67	79.06	68.41	64.47	83.68
44	65.72	68.83	56.12	57.81	80.87
31	59.35	58.05	45.80	43.52	75.88
22	53.17	47.83	37.18	32.76	68.76
16	45.81	38.67	30.06	24.67	60.16
11	38.12	30.78	24.23	18.57	50.92
7.8	30.79	24.21	19.47	13.98	41.92
5.5	24.28	18.86	15.61	10.52	33.72
3.9	18.82	14.59	12.50	7.92	26.63
2.8	14.36	11.28	9.99	5.92	20.74
2.0	10.85	8.59	7.97	4.49	15.97
1.4	8.12	6.56	6.36	3.38	12.19
1.0	6.05	4.99	5.07	2.55	9.25

Size analysis for  $-44 \mu\text{m}$  coal was determined by Microtrac with correction to equivalent sieve size.

between 15 and 20 cm before the tube exit. The carbon content of ash deposits collected at this position indicated that combustion was essentially complete (greater than 99.7%) if the maximum hot zone temperature was at least  $1420^\circ\text{C}$ .

The physical characteristics of the deposit collected from all four of the test coals and the pulverizer rejects were all similar. Figure 7 shows the typical ash deposit structure on both a macro and micro scale. The top photograph (Figure 7A) shows the outer sinter portion of the ash deposit collected from the Decker coal on a Croloy 1/2 steel substrate. The lower optical micrograph (Figure 7B) shows the strongly bonded material on the steel surface after the loosely adhering deposit has been brushed away. The opaque black droplets were found to be rich in iron (85-100 wt.%), whereas the light transparent spheres were predominantly aluminosilicates.

The deposit build-up mechanism appeared to be the same for all coal samples tested. All appeared to originate with the relatively strong bonding of iron-rich particles to the steel substrate oxide layer. In addition to these particles, there was always a layer of very fine particles (less than  $3 \mu\text{m}$ ) covering the entire substrate surface, which were not easily brushed or blown from the surface. A region of loosely bonded ash particles then built upon the more strongly adherent droplets. These particles were principally aluminosilicates, often containing some amounts of most of the



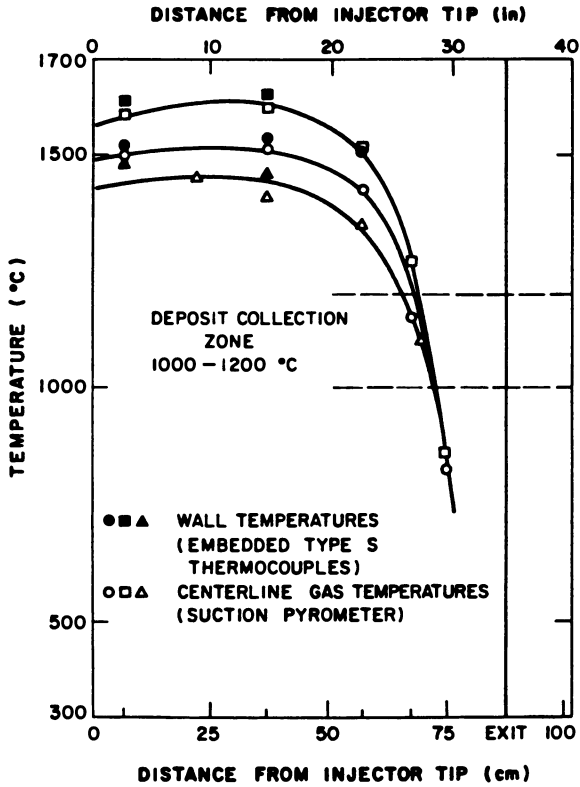


Figure 6. Drop-tube furnace temperature profiles.

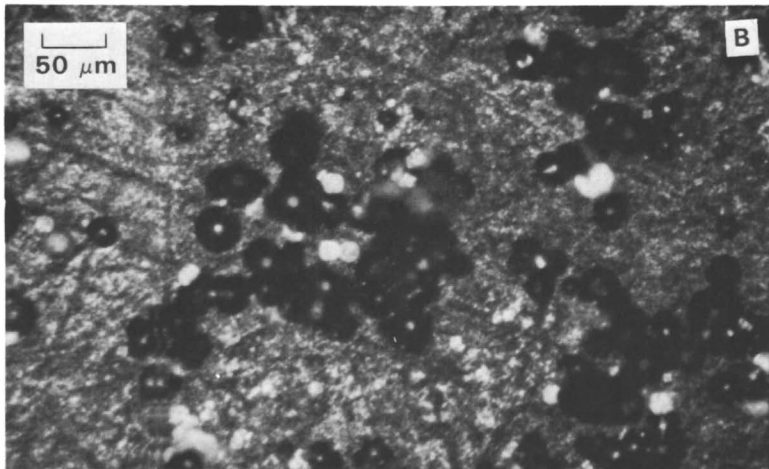
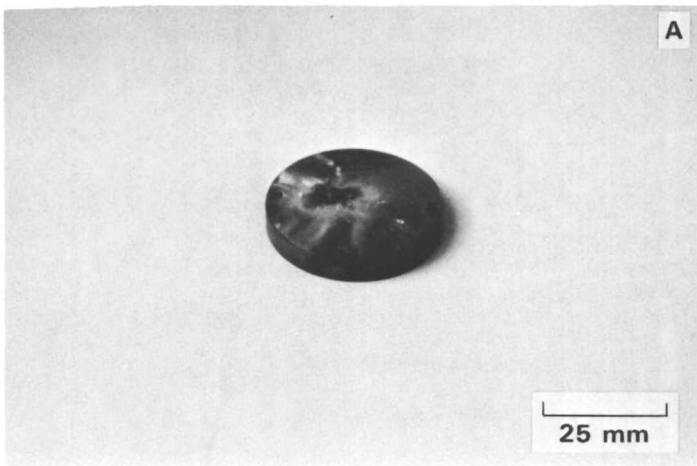


Figure 7. Ash deposit collected from the untreated Decker coal on Croloy 1/2 steel substrate: (A) Total deposit structure on a macroscale, and (B) Optical photomicrograph showing iron-rich particles.

major constituents of the ash. As the deposit grew from the steel surface these more loosely adherent particles began to sinter, and in some instances actually showed evidence of starting to form a fluid mass as shown in Figure 8.

The deposit mass and relative build-up rates on the medium carbon steel for the three Pennsylvania steam coals at different flame temperatures are given in Table VII, for a 12 minute time period for each test. As the flame temperature increased, the deposit mass also increased for all three coals. Most of this increase was due to a more rapid build-up of the sintered mass although there was a modest increase in the amount of deposit base material also. At the higher temperatures the fraction of coal ash collected in the deposit was one-third to one-half, (30% to 51%, Table VII) compared to the total amount of ASTM HTA.

The difference in the physical nature of the deposit base particles formed from the Keystone coal at flame temperatures of 1470 and 1500°C are shown in Figure 9. The concentration of iron-iron particles adhering to the oxidized steel substrate surface increased with increasing flame temperatures. Also, the particles flattened more on impact as the flame temperature was increased, possibly due to a decrease in particle viscosity. There appeared to be two different particle types in these deposits: a highly porous particle with a rougher surface texture, and a more glassy particle with a smooth surface texture. The EDX analyses for these two particle types showed that the porous particles were found to contain only iron, whereas the more glassy surface particles were also found to contain smaller amounts of silicon, aluminum and often potassium and/or calcium. Figure 10 shows that the iron-rich particulate deposit base grew in thickness to completely over the substrate surface in the selected viewing area when the flame temperature was 1560°C. This deposit was 130  $\mu\text{m}$  thick and covered an area 4.8 mm in diameter.

The deposit base particles collected from the Montour and Tunnelton coals at a flame temperature of 1510°C are shown in Figure 11. They exhibit much of the same physical and chemical nature as the Keystone coal deposits described above. Although the deposition rate was higher for the Tunnelton coal (see Table VII), the concentration of the more strongly adhesive particles was higher for the Montour coal. The greatest concentration of iron-rich particles ranged in size from 25 to 40  $\mu\text{m}$  for the Montour coal and 25 to 50  $\mu\text{m}$  for the Tunnelton coal. When the furnace temperature was increased to 1561°C the maximum size of the fly ash particles was reduced to about 15  $\mu\text{m}$  for the Montour ash, and the total concentration of adherent slag droplets did not appear to have increased as dramatically as it did with the Keystone coal.

Table VIII shows the change in deposition rate for the Keystone coal at a furnace temperature of 1500°C for two steel substrate surface temperatures. When the substrate temperature was increased from 310 to 340°C the deposition rate grew ten times.

The deposit mass and relative build-up rates for the pulverizer rejects are given in Table IX. The ash deposits were collected over a period of only 90 seconds. Once the sintered mass was removed, there remained a strongly bonded deposit of primarily iron-rich particles, roughly 1 mm thick and 8 mm in diameter. The composition

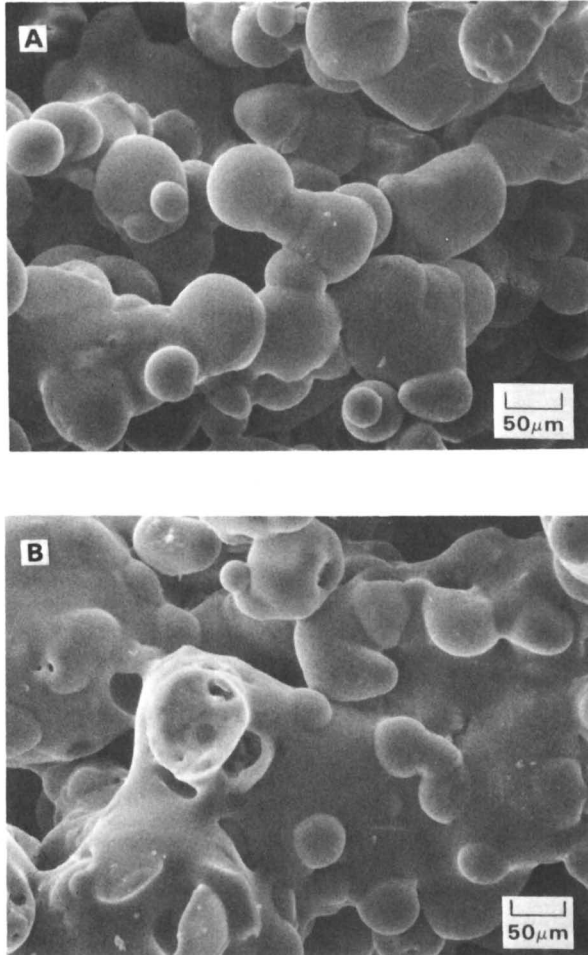


Figure 8. SEM photomicrograph of sintered ash deposit; (A) nearer substrate surface ( $\sim 1$  mm), and (B) at outer deposit surface (3-4 mm) from substrate surface.

Table VII. Deposit Mass and Relative Build-Up Rates for the Three Pennsylvania Steam Coals at Three Furnace Temperatures (Deposition Zone Gas Temperature, 1100°C; Substrate, 1040 Carbon Steel; Surface Temperature, 325±5°C)

Coal	Furnace (flame) temperature °C	p.c. feed rate g/min	Total feed g	Relative build-up rates mg/min	Deposit mass mg	Wt. % ASTM HTA
Montour	1465	0.20	2.4	2.2	26.5	6
	1518	0.24	2.9	5.4	64.5	15
	1561	0.24	2.9	11.1	133	30
Keystone	1470	0.28	3.4	2.0	24	4
	1500	0.24	2.9	9.8	118	22
	1560	0.28	3.4	23.8	286	46
Tunnelton	1467	0.28	3.4	3.3	40	6
	1510	0.28	3.4	21.1	253	37
	1568	0.24	2.9	24.8	297	51

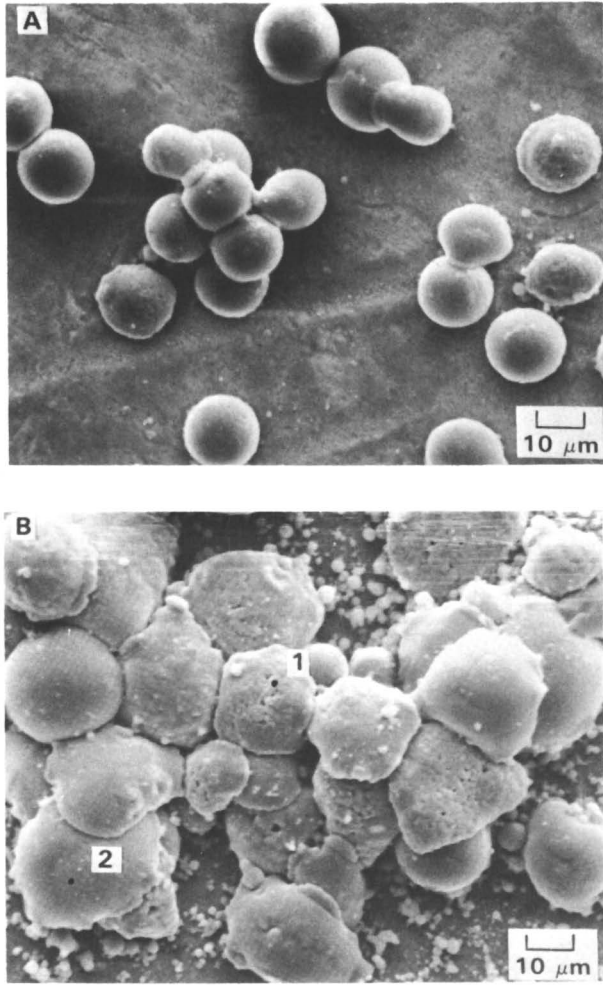


Figure 9. SEM photomicrographs of iron-rich deposit base particles collected from the Keystone coal at flame temperatures of: (A) 1470°C, and (B) 1500°C.

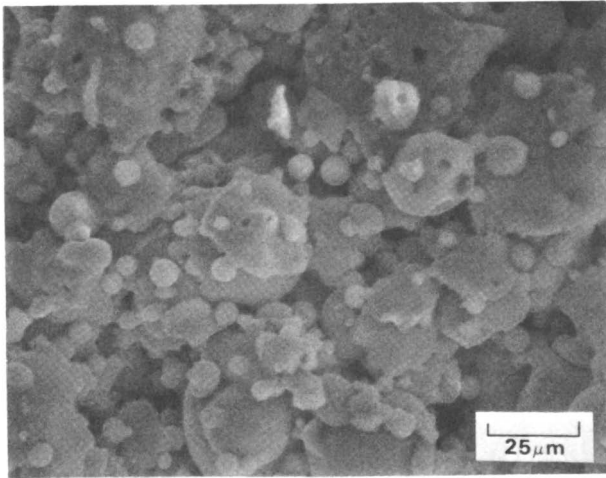


Figure 10. SEM photomicrograph of iron-rich deposit base particles collected from the Keystone coal at a flame temperature of 1560°C.

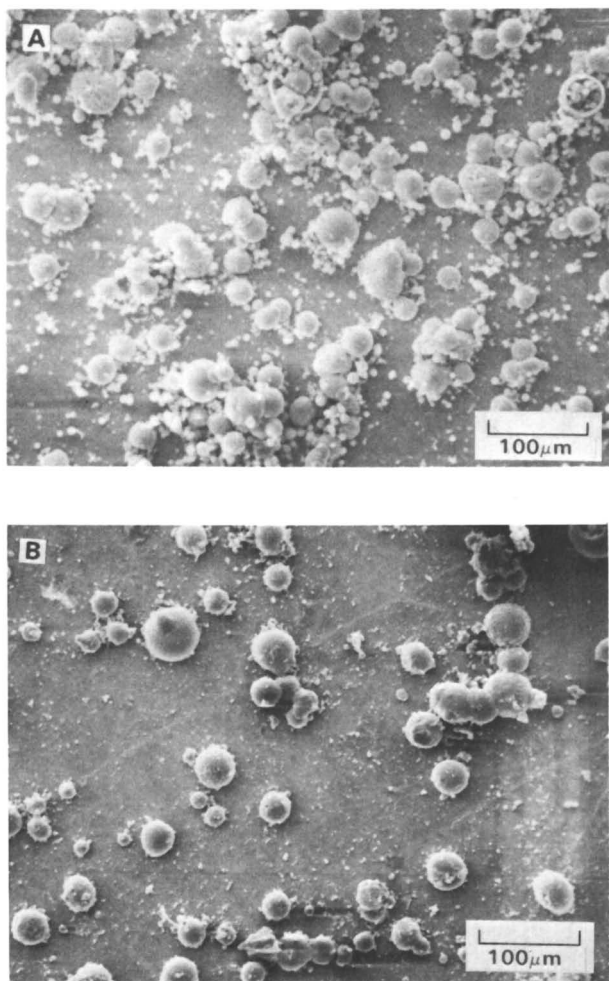


Figure 11. SEM photomicrographs of iron-rich deposit base particles collected at a flame temperature of 1510°C from: (A) Montour coal, and (B) Tunnelton coal.



Table VIII. Deposit Furnace Mass and Relative Build-Up Rates for Keystone Coal at a Furnace Temperature of 1500°C at Two Different Substrate Surface Temperatures (Deposition Zone Gas Temperature, 1100°C; Substrate, 1040 Carbon Steel).

Substrate temperature °C	p.c. feed rate g/min	Total feed g	Deposit mass mg	Relative build-up rates mg/min	Wt. % ASTM HTA
310	0.24	2.9	12	1.0	2
340	0.24	2.9	118	9.8	22

Table IX. Deposit Mass and Relative Build-Up Rates for the Pulverizer Rejects at a Furnace Temperature of 1515°C (Deposition Zone Gas Temperature, 1100°C; Substrate, 1040 carbon steel; surface temperature, 324°C)

Description	Deposit mass	Relative build-up rates mg/min
Total deposit	359	239
Sintered mass	319	213
Deposit base	40	26

of the base deposit particles was virtually the same as those collected from the three steam coals. However, when the collector probe was removed after so short a time period, there was a distinct sulfur odor, indicating that sulfur was escaping from the deposit at a relatively rapid rate, even though it was comparatively cool in temperature (less than 300°C). Figure 12 shows a perpendicular view of the deposit-steel oxide interface removed from the substrate surface. The average interface composition from x-ray fluorescence showed that there was a significant amount of sulfur in the depositing particles. Analysis of the substrate surface from which the deposit was removed showed regions which contained sulfur and sometimes traces of potassium, calcium and silicon. Thus bonding of the particles to the surface appeared to involve chemical transfer from the particle to the steel substrate.

Table X gives the relative build-up rates for two samples of the Decker coal: an untreated sample, and a hydrogen exchanged sample in which most of the ion exchange cations including  $\text{Ca}^{2+}$  and  $\text{Na}^+$  were replaced with  $\text{H}^+$  by acid washing. The deposition rates were somewhat lower than the three Pennsylvania coals at the same furnace temperature. The exchangeable cations removed from the untreated sample appeared to play a significant role in deposit build-up. The sintered material (yellow-brown in color) collected from the untreated coal was relatively strongly bonded together, requiring a force of 20 psi to break it up. The sinter (coral colored) from the acid-washed coal broke apart while removing the substrate from the collector probe. See Figures 7A and 13A for photos of ash deposits formed from untreated and acid-washed Decker coal samples, respectively.

The base layer of particles from the Decker coal were the same iron-rich drops seen in the Pennsylvania coal deposits (see Figure 7B). The concentration of these particles on the substrate surface decreased when the cations were removed from the coal. Compare Figures 7B with 13B. The total pyrite concentration in the untreated and acid-washed coal samples were the same, 0.3 weight percent in both instances. Thus, iron-rich particles may also initiate slag deposits from Western coals, even though the pyrite concentration in the coal is relatively low. The concentration of the exchangeable cations appeared to influence the deposition behavior of the iron-rich droplets, although the exact mechanism of this effect is unknown.

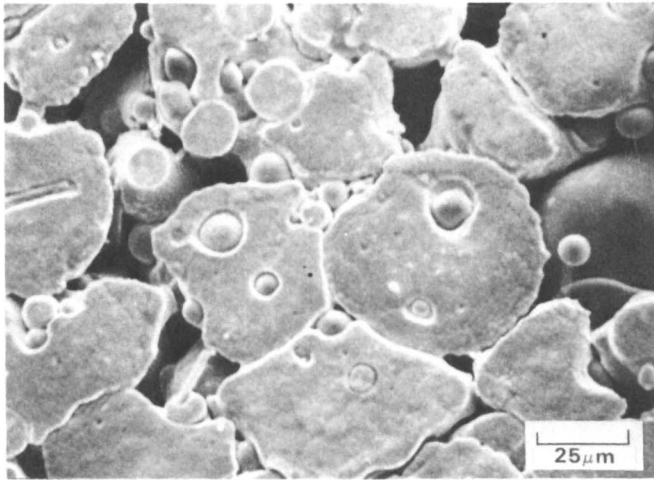


**Figure 12.** Perpendicular view of iron-rich deposit base oxide scale interface for deposit collected from pulverizer rejects (SEM photomicrograph).

Table X. Deposit Mass and Relative Build-Up Rates for the Decker Samples at a Furnace Temperature of  $1500 \pm 5^\circ\text{C}$  (Deposition Zone Gas Temperature,  $1050^\circ\text{C}$ ; Substrate, Croloy 1/2; Surface Temperature,  $425 \pm 5^\circ\text{C}$ ).

Test	p.c. feed rate g/min	Time, min	Total feed g	Deposit mass mg	Relative build-up rates mg/min	Wt. % ASTM HTA
1. Untreated coal sample	0.28	20	5.6	82	4.1	34
2. Acid-washed coal sample	0.24	20	4.8	25	1.3	24

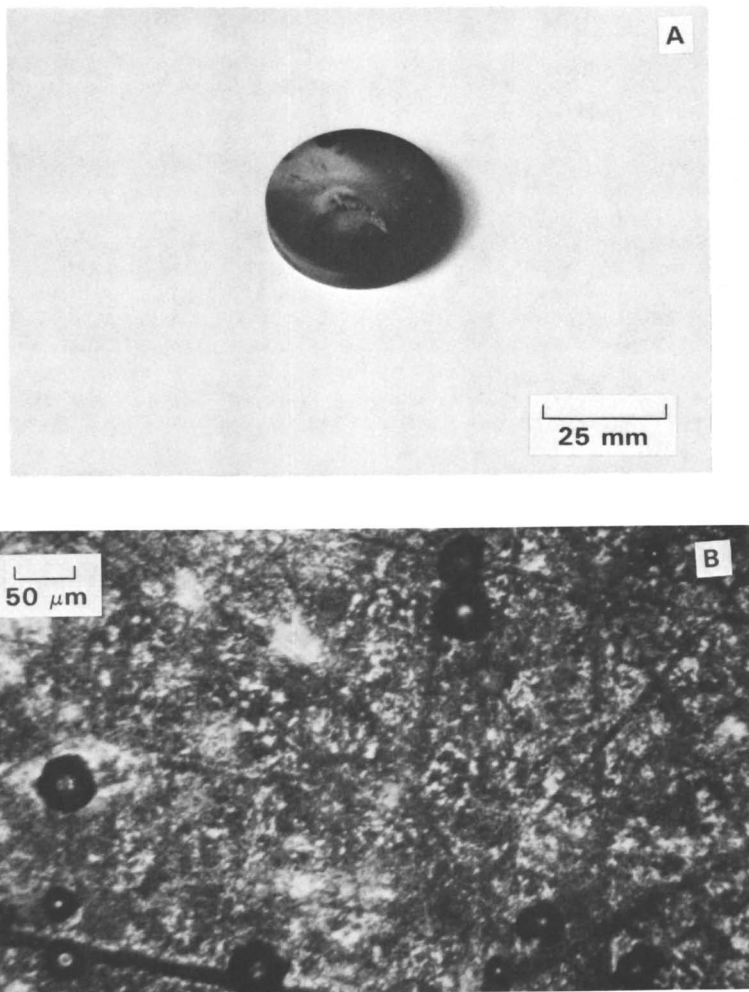


Figure 13. Ash deposit collected from the acid-washed Gecker coal on Croloy 1/2 steel substrate: (A) Total deposit structure on a macroscale, and (B) Optical photomicrograph showing iron-rich particles.

### Discussion and Conclusions

The mechanism of deposit formation for the three Pennsylvania steam coals and the Decker (Montana) sub-bituminous coal appeared to be as follows: (1) iron-rich molten slag drops formed from pyrite-rich mineral particles in the p.c. bonded to the oxidized boiler steel substrate; (2) concurrently a layer of fine particles (less than 3  $\mu\text{m}$ ) formed a thin layer on the steel coupon surface; (3) the initial layer of iron-rich drops then physically trapped or interacted with other ash particles reaching the substrate surface, and the build-up rate increased as deposition became less discriminatory with respect to ash particle composition or size; (4) finally, as the ash deposit grew and the temperature increased further from the substrate surface, sintering occurred between deposited particles until a semi-molten mass formed in the outermost region. Preferential deposition of iron-rich slags has been suggested by other investigators (18,19) and was also observed in a small scale p.c. test combustor on an air-cooled medium carbon steel probe (20). The fine particle layer formed on the substrate surface is due to condensation on or thermal diffusion to the relatively cold (300–350°C) steel substrate (21). Its role in deposit initiation is not yet known.

The weakest point in the deposit occurred in the zone between the initiating iron-rich particles and the sintered material. This allowed removal of the deposit down to the initial layer by brushing with a fine bristle paint brush or blowing with a high velocity air jet (25–30 m/sec). The fine particle layer was removed by using double-sided sticky tape. The strongly bonded, iron-rich particles had to be sheared from the substrate surface with a razor blade. This suggests that conventional sootblowing techniques in a utility boiler cannot remove a strongly bonded initiating layer formed from slag droplets bonded to the surface or fine particles deposited by condensation or thermal diffusion and held by Van der Waals forces. At higher flame temperatures the fly ash particle size appeared to be reduced, presumably due to a greater degree of breaking up of individual burning coal particles, and the base or iron-rich particles and overall deposit build-up rates were increased. The Keystone coal in particular gave drops which wet the surface better at higher flame temperatures. The Keystone coal formed the most extensive deposit base of the three coals at the highest flame temperature. The iron-rich particles adhered to the oxidized steel substrates at temperatures as low as 310°C. Surprisingly, the same layer of iron-rich base deposit particles was also observed with the low pyrite Decker coal. However, deposit initiation and build-up was reduced when the concentration of ion-exchangeable cations in the coal was reduced.

Slag deposit initiation and build-up were sensitive to both flame and steel substrate surface temperatures, even though the gas temperature of deposition was held constant. This suggests at least qualitative agreement between results from the drop-tube furnace and those from the sticking apparatus (1,5). It is hypothesized that a higher flame (melting) temperature gives a more homo-

geneous slag drop, which remains as a viscous, sticky, supercooled glass at deposition temperatures, whereas inhomogeneities in the melt at lower temperatures act as nuclei to give more crystallization on cooling. The high concentration of sulfur at the deposit-steel interface has been observed in p.c. utility boilers (22,23).

The principal questions posed by the results of this investigation were: (1) can ash deposits be formed in the drop-tube furnace in the absence of iron-containing minerals or slag drops?; (2) what role, if any, does the fine particle layer play in deposit formation?; (3) is there any significance to the high sulfur concentration at the deposit interface and what is the mechanism by which this sulfur enrichment occurs: does it originate from pyrite or from condensing sulfate?; (4) what influence do alkalis have on slag deposit initiation and build-up? To answer these questions, it is planned to test synthetic coal/mineral mixtures of controlled composition prepared by dispersing finely ground minerals in liquid organic polymer followed by setting and size reduction to p.c. grind.

#### Acknowledgments

This study was funded by a grant from the Department of Energy, Contract No. DE-FG22-80PC-30199. We would like to thank Babcock and Wilcox Alliance Research Center (Alliance, Ohio) for supplying the Croloy 1/2 steel for the test substrates.

#### References

1. Moza, A. K.; Austin, L. G. Fuel 1981, 60, 1057-64.
2. Abbott, M. F.; Moza, A. K.; Austin, L. G. Fuel 1981, 60, 1065-72.
3. Moza, A. K.; Austin, L. G. Fuel 1982, 61, 161-65.
4. Abbott, M. F.; Austin, L. G. Fuel 1982, 61, 765-70.
5. Abbott, M. F.; Conn, R. E.; Austin, L. G. "Studies on Slag Deposit Formation in Pulverized Coal Combustors. 5. The Effect of Flame Temperature, Thermal Cycling of the Steel Substrate, and Time on the Adhesion of Slag Drops to Oxidized Boiler Steels" Fuel, accepted.
6. Abbott, M. F.; Austin, L. G. *ibid* 6. The Sticking Behavior of Slag from Three Pennsylvania Steam Coals" Fuel, accepted.
7. Moza, A. K.; Strickler, D. W.; Austin, L. G., Proc. of Annual SEM Symp. Chicago, Ill., 1979.
8. Mims, C. A.; Neville, M.; Quann, R. T.; Sarofim, A. F. Proc. from the National AIChE Mtg., Boston, Ma., Aug. 1979.
9. Sarofim, A. F.; Howard, J. B.; Padia, A. S. Comb. Sci. and Tech., 1977, 16, 187-204.
10. Winegartner, E. J.; Lin, C. J. ASME Paper No. 79-WA/Fu-1, Dec. 1979.
11. Rees, D. "An Assessment of Pulverized Coal Fired Combustor Performance" DOE Combustion Contractors Mtg., Pittsburgh, Pa., March 1981.
12. Moza, A. K. Fouling and Slagging Resulting from Impurities in Combustion Gases, Eng. Foundation, NY, NY, 1983, 231-44.
13. Shiomoto, G. H.; Muzio, L. J.; Mansour, M. N. *ibid*, 363-73.

14. Hamor, R. J.; Smith, I. W. Fuel 1971, 50, 394-404.
15. Altenkirch, R. E.; Peck, R. E.; Chen, L. S. Powder Tech. 1978, 20, 189-96.
16. Pigford, R. L. Chem. Eng. Prog. Symp. Series 17, 1955, 51, 79-92.
17. Bird, R. B.; Stewart, W. E.; Lightfoot, E. N. Transp. Phenomena John Wiley and Sons, Inc., 1950.
18. Borio, R. W.; Narcisco, R. R. J. of Eng. for Power 1979, 101(4), 500.
19. Bryers, R. W. J. of Eng. for Power 1979, 101, 506.
20. Austin, L. G.; Abbott, M. F.; Kinneman, W. P. ASME 83-JPGC-Pwr-42, Sept. 1983.
21. Rosner, D. E.; Gokoglu, S.; Israel, R. Fouling and Slagging Resulting from Impurities in Combustion Gases, 1983, Eng. Found., N.Y., N.Y., 235-56.
22. Hazard, H. R. Final Report, EPRI CS-1418, June 1980.
23. Fessler, R. R.; Skidmore, A. J.; Hazzard, H. R.; Dimmer, J. P. ASME Paper No. 79-WA/CD-1 1979.

RECEIVED June 24, 1985



## Influence of Segregated Mineral Matter in Coal on Slagging

Richard W. Bryers

Foster Wheeler Development Corporation, Livingston, NJ 07039

The mineral content of any given rank of coal is a key factor in sizing and designing a steam generator or reactor. The mineral content becomes even more important as the premium solid fuels are consumed, leaving reserves with continually increasing mineral concentrations and lower quality ash. The problem of dealing with lower quality ash in coal is compounded by the increase in size of steam generators and refinements imposed by economic constraints. Empirical indices, based on coal ash chemistry and ASTM ash fusion temperatures or viscosities, are presently used to rank coals according to the fireside behavior of the mineral matter. Unfortunately, the indices are only marginally satisfactory, as they do not relate to operating or design parameters and frequently are based on a coal ash chemistry quite different from that deposited on the furnace wall. Frequently, different coals with identical ash chemistry produce decidedly different slagging conditions in steam generators of identical design operated in the same mode. Variations in composition of the slag, when compared with the coal ash, suggest specific minerals are being selectively deposited on furnace walls depending upon their specific gravity, size, composition, and physicochemical properties. It is quite apparent there is a need for a better understanding of the impact of mineral composition, its size, and its association with other minerals and carbonaceous matter on fireside deposits.

### Slagging and Fouling

The minerals in coal are converted to ash during combustion. The portion of the fly ash impacting on heat transfer surfaces, which is retained as deposits, depends on the particle size, its chemistry and its physicochemical behavior during combustion in the steam generator furnace, as well as subsequent cooling in the convective heat

0097-6156/86/0301-0353\$06.50/0

© 1986 American Chemical Society

recovery section. The type of deposit formed falls into one of two categories--furnace slag, or bonded convective heat transfer deposits. Slag is defined as a molten ash deposited on furnace walls in zones subjected to radiant heat transfer, as shown in Figure 1. Occasionally, when coal moisture levels approach 50 to 70 percent and the flame temperature becomes exceptionally low, bonded deposits instead of slag form on furnace walls. Fouling occurs in the convective heat transfer zones. The product of fouling is a bonded deposit consisting of an aggregate of dry particulate matter bound together by a molten phase that has wetted adjacent particulate and subsequently become frozen. The bonded deposit is frequently initiated by a melt on the tube side layers of deposit formed by the condensation of substances, such as alkali sulfate, with low vapor pressures and low melting temperatures. Bonding or sintering may also occur as a result of viscous or plastic flow between particles, a gas phase reaction, solution and precipitation, or diffusion transfer between adjacent particles. On occasion, when the furnace experiences a temperature excursion, slagging will occur in the high temperature gas passes.

### Mineral Matter in Coal

Minerals occurring in coal, which are responsible for fireside deposits, may be classified into five main groups. These include shale, clay, sulfur, and carbonates. The fifth group includes accessory minerals such as quartz and minor constituents like the feldspars [1].

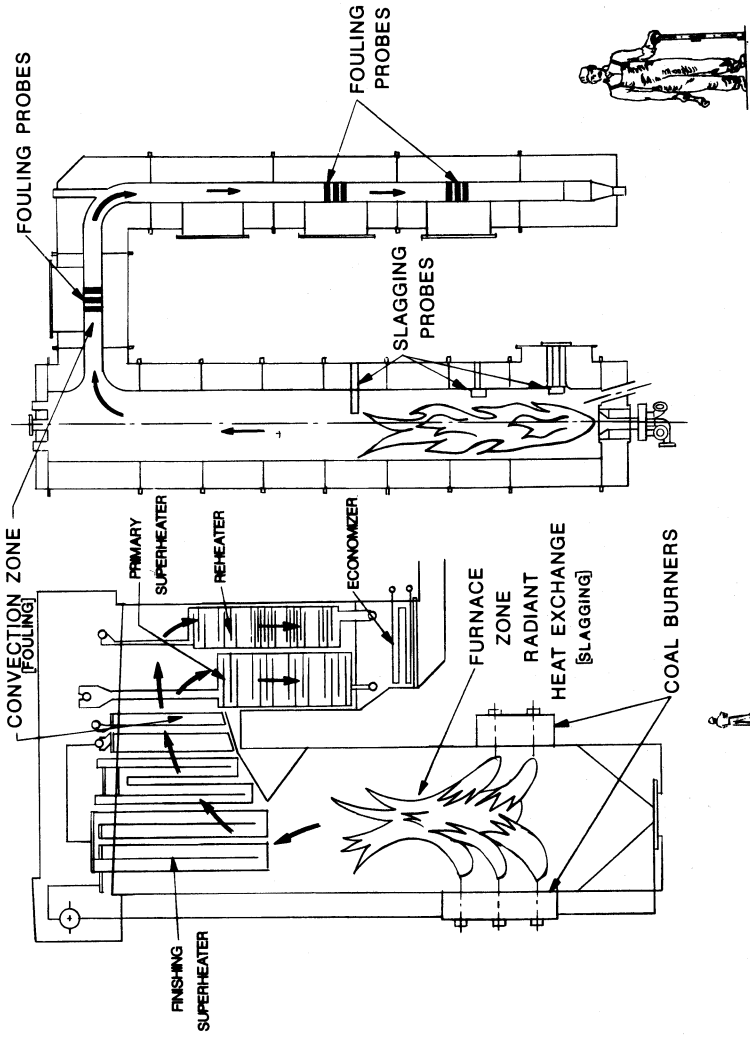
Shale, usually the result of the consolidation of mud, silt, and clay, consists of many minerals including illite and muscovite--these are forms of mica. Kaolinite is the most common clay material [1].

The sulfur minerals include pyrites with some marcasite. Marcasite has the same chemical composition as pyrites but a different mineralogical structure. Sulfur is also present as organic matter and occasionally as sulfate. The latter usually occurs in weathered coal such as in outcrops. The amount of sulfate sulfur in coal is generally less than 0.01 percent.

Generally, 60 percent of the sulfur in coal occurs as pyrite, particularly when the sulfur concentration is low. At higher concentrations it may run as much as 70 to 90 percent.

The mineral pyrite occurs in coal in discrete particles in a wide variety of shapes and sizes. The principal forms are [1-6]:

- o Rounded masses called sulfur balls or nodules an inch or more in size.
- o Lens-shaped masses which are thought to be flattened sulfur balls.
- o Vertical, inclined veins or fissures filled with pyrite ranging in thickness from thin flakes up to several inches thick.
- o Small, discontinuous veinlets of pyrites, a number of which sometimes radiate from a common center.
- o Small particles,  $2\mu$ , or veinlets disseminated in the coal. Microscopic pyrite occurs in five basic morphology types:



PILOT SCALE PLANT

FULL SCALE STEAM GENERATOR

Figure 1. Pilot Plant Slagging and Fouling Combustor Compared to a Full-Scale Steam Generator

- (a) framboids; (b) isolated, well-defined crystals;
- (c) nonspherical aggregates of well-defined crystals; (d) irregular shapes; and (e) fractured fillings [7].

The term, framboid, is derived from the French word for raspberry and thus refers to naturally occurring spheroidal clusters of hundreds of cubic or octahedral crystals of pyrites [9].

All coals contain some of the third and fifth forms of pyrites, and some coals contain all five of the principal forms [6, 8,9].

The carbonates are mainly calcite, dolomite, or siderite. The occurrence of calcite is frequently bimodal. Some calcite occurs as inherent ash, while other calcite appears as thin layers in cleats and fissures. Iron can be present in small quantities as hematite, ankerite, and in some of the clay minerals such as illite. In addition to the more common minerals, silica is present sometimes as sand particles or quartz. The alkalies are sometimes found as chlorides or as sulfates but probably most often as feldspars, typically orthoclase and albite. In the case of lignites, unlike bituminous and subbituminous, sodium is not present as a mineral but is probably distributed throughout the lignite as the sodium salt of a hydroxyl group or a carboxylic acid group in humic acid. Calcium, like sodium, is bound organically to humic acid. Therefore, it too is uniformly distributed in the sample [10].

The term, "mineral matter", usually applies to all inorganic, noncarbonaceous material in the coal and includes those inorganic elements which may occur in organic combination. Physically, the inorganic matter can be divided into two groups--inherent mineral matter and extraneous mineral matter. Inherent mineral matter originates as part of the growing plant life from which coal was formed. Under the circumstances, it has a uniform distribution within the coal. Inherent mineral matter seldom exceeds 2 to 3 percent of the coal [12].

Extraneous mineral matter generally consists of large bits and pieces of inorganic material typical of the surrounding geology. In some cases the extraneous matter is so finely divided and uniformly dispersed within the coal it behaves as inherent mineral matter. Coal preparation can separate some of the extraneous ash from the coal substance, but it seldom removes any of the inherent mineral matter.

The physical differences between inherent and extraneous ash are important not only to those interested in cleaning coal but also to those concerned with the fireside behavior of coal ash. Inherent material is so intimately mixed with coal that its thermal history is linked to the combustion of the coal particle in which it is contained. Therefore, it will most likely reach a temperature in excess of the gas in the immediate surroundings. The close proximity of each species with every other species permits chemical reaction and physical changes to occur so rapidly that the subsequent ash particles formed will behave as a single material whose composition is defined by the mixture of minerals contained within the coal particle. The atmosphere under which the individual transformations take place will, no doubt, approach a reducing environment. Figure 2 illustrates a model of the coal and mineral matter as fed to the combustor and the fate of the minerals after combustion [13].

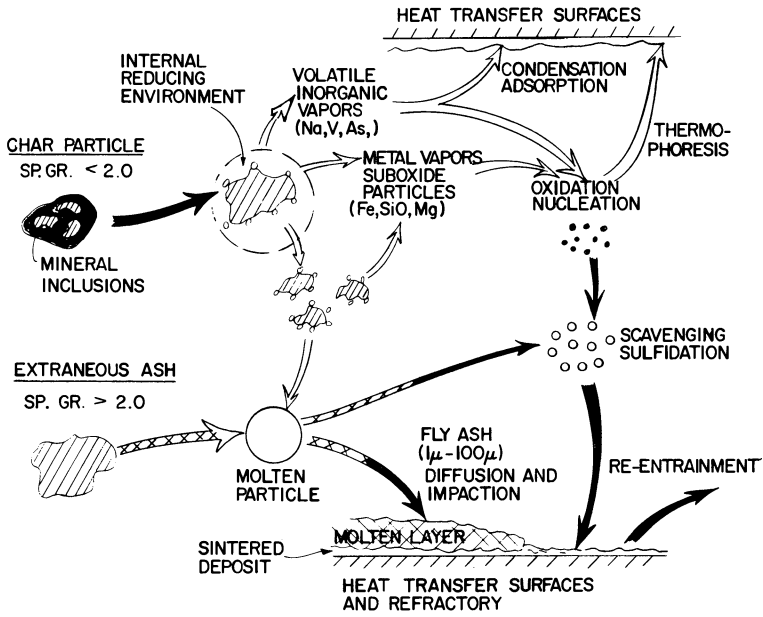


Figure 2. Fate of Mineral Matter in Coal During Combustion, as Proposed by Dr. Sarofim. Reproduced with permission from reference 23. Copyright 1982 The Combustion Institute.

Extraneous materials can behave as discrete mineral particles comprised of a single species or a multiplicity of species. As already indicated, a portion of this material may be so finely divided it can behave as inherent mineral matter. During combustion the larger particles respond individually to the rising temperature of the environment. In the absence of carbon or other exothermic reactants, the particle should always be at a temperature somewhat less than the local gas temperature. However, the particles may be subjected to either reducing or oxidizing conditions. As each particle rises in temperature, it loses water of hydration, evolves gas, becomes oxidized or reduced, and eventually sinters or melts, depending on its particular composition or temperature level.

It is evident, then, that there can be a great difference in the final state of each particle, depending upon its composition and whether it is inherent or extraneous ash. Figure 3 summarizes the phase transformations which pure mineral matter commonly found in coal undergoes during heating [12-18]. Since this data was developed primarily by mineralogists performing differential thermal analysis under air at slow heating rates, it must be used only as a guideline for predicting the thermal behavior of minerals in coal. Thermal shocking these minerals in the presence of carbon and other mineral forms at very high temperatures, no doubt, will alter some of these transformations and may defer others until postcombustion deposition on heat transfer surfaces.

Clays and Shale. The melting temperatures of most pure minerals are in the vicinity of or greatly exceed the maximum flame temperature encountered during combustion. Therefore, the fused spheroidal fly ash, generated from the mineral matter in coal, primarily forms as the result of the fluxing action between pure minerals contained within each particle. Illite and biotite appear to be an exception. Both minerals contain small concentrations of iron and potassium and form a glassy phase at 950°C and 1100°C, respectively. Depending upon its fluidity, this glassy phase could be responsible for surface deformation at a relatively low temperature and provide the necessary sticking potential to prevent reentrainment upon contacting heat transfer surfaces. Low-temperature ash of a gravity fraction containing illite was heated in a thermal analyzer under air to 600 and 1000°C, respectively, and compared to the low-temperature ash of a gravity fraction void of illite. The scanning electron photomicrographs, appearing in Figure 4, indicate the minerals containing illite did, indeed, show signs of the formation of a melt.

Quartz. The inherent silica retained in the char as quartz or silica released from kaolinite and illite at low temperatures (i.e., 950°C) is partially reduced to silica monoxide. Unlike silica, which boils at 2230°C, silica monoxide melts at 1420°C and boils at 2600°C [19]. The vapor pressure of silicon is low--in the range of temperatures experienced during combustion. Honig reports values ranging from 0.01m Hg at 1157°C to 1m Hg pressure at 1852°C [19-21]. The presence of other mineral matter and carbonaceous material appears to alter vapor pressure substantially. When a mixture of aluminosilicate and graphite was heated, the volatilization of silicon monoxide began at about 1150°C and reached a maximum at 1400°C. Mackowsky reports that volatilization of silicon monoxide starts at about 1649°C in

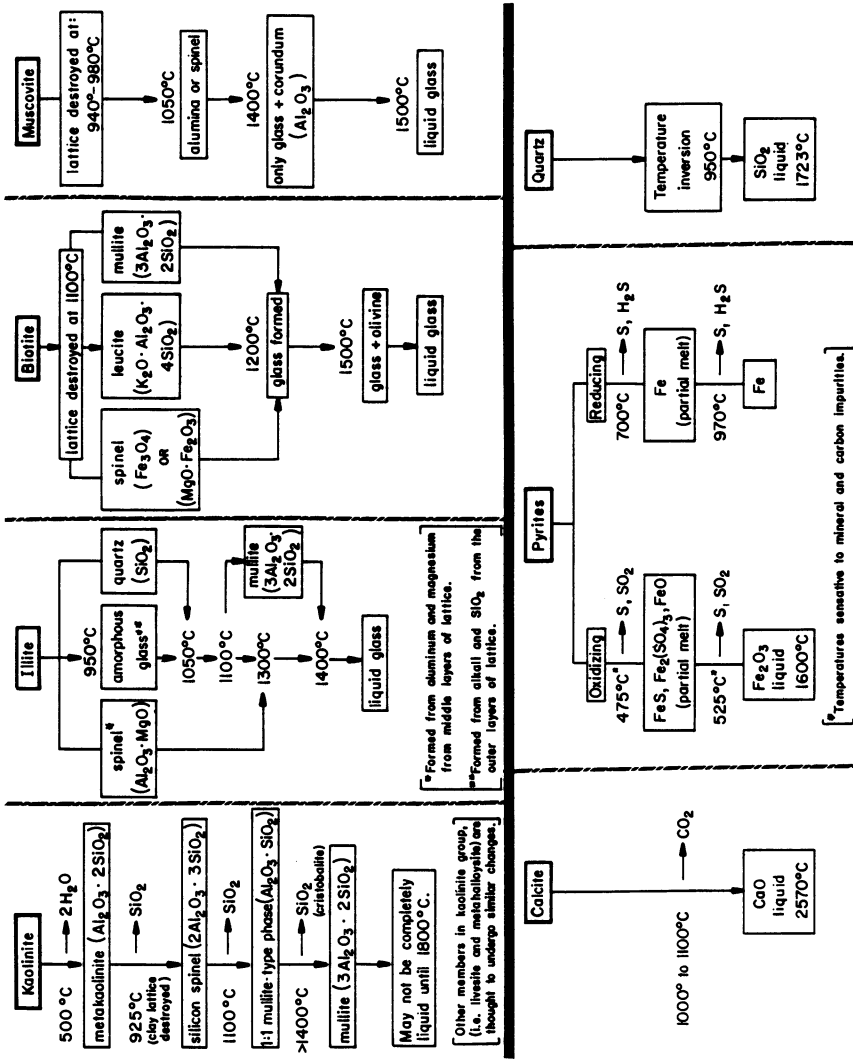


Figure 3. Phase Transformation of Some Mineral Matter Commonly Found in Coal. Reproduced with permission from reference 19. Copyright 1984 VGB.

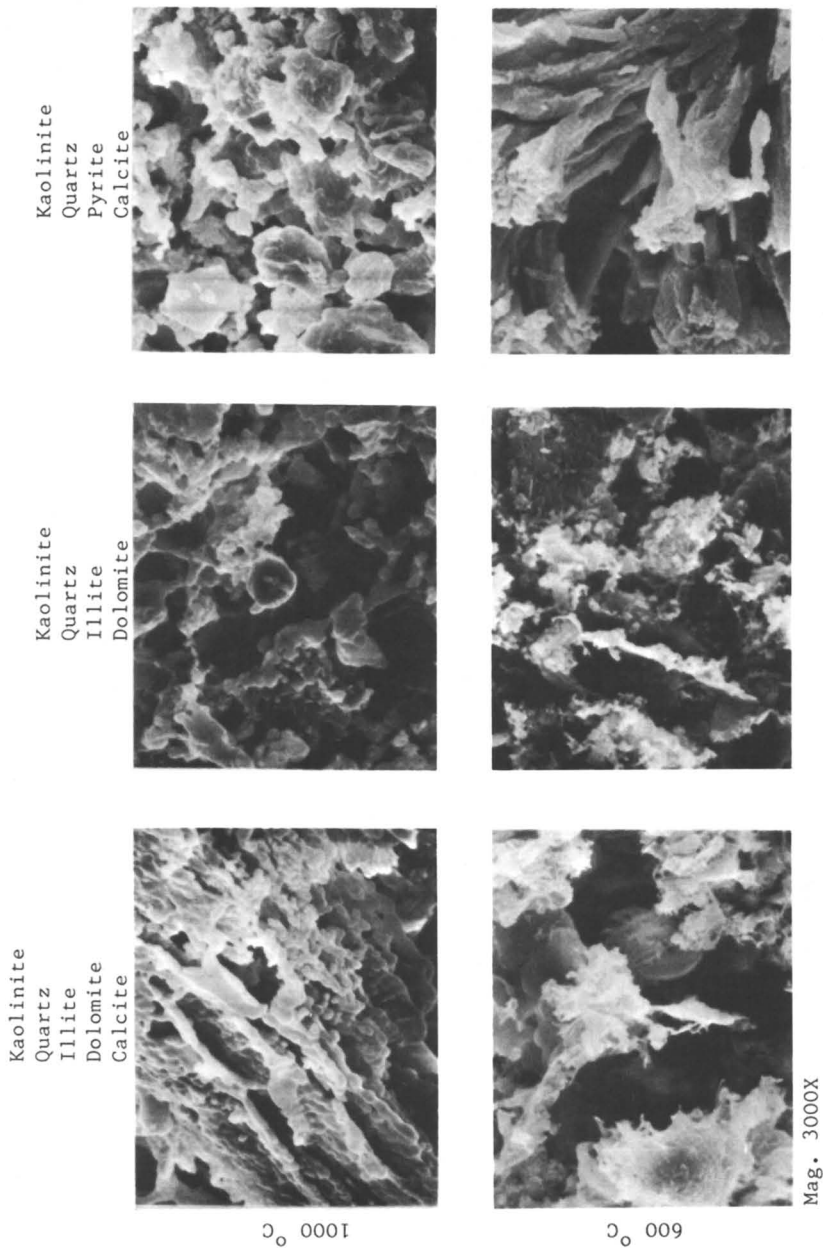


Figure 4. SEM Photomicrographs Showing the Impact of Illite on the Thermal Behavior of Low Temperature Ash. Reproduced with permission from reference 19. Copyright 1984 VGB.



the presence of carbonates and clays and reaches a maximum at 1704°C [22]. In the presence of pyrite or metallic iron, volatilization begins at about 1560°C and continues at a rapid rate as the temperature rises until practically all the silica in the mineral is volatilized. Sarofim has shown that about 1.5 to 2.0 percent of the ASTM ash in bituminous coals volatilize [23]. Approximately 35 to 40 percent of the volatilized material was silica. The next largest component was iron. Extraneous quartz appears to be relatively innocuous unless contaminated by  $\text{Fe}_2\text{O}_3$ ,  $\text{CaO}$ , or  $\text{K}_2\text{O}$ .

**Pyrites.** The decomposition of pyrite has been examined by numerous investigators under oxidizing, neutral, or reducing environments [1,11,16,17]. TGA, rather than DTA, has been used by most investigators (Figure 5). Acquisition of representative data is difficult, as the decomposition process is complex and sensitive to many variables including the chemical composition of pyrites, its grain size, its origin, and the presence of adventitious impurities, the composition of the local environment, and diffusion rates through sulfated layers. Under oxidizing conditions it is believed that pyrites decompose directly to an iron oxide and  $\text{SO}_2$  or  $\text{SO}_3$ , or iron sulfate and  $\text{SO}_2$ , depending upon the final temperature level. Under reducing conditions pyrrhotite and either sulfur or hydrogen sulfide form. Complete reduction results in elemental iron and carbon disulfide. There is also a possibility that pyrrhotite may form under oxidizing conditions as an intermediate step in the presence of sufficient adventitious carbon. Pure pyrites ignite at about 500°C in the thermal analyzer at 20°C/min and burn out by 550°C in a single-step process, as shown in Figure 6. Pure pyrites do ignite as readily as bituminous coal; however, the burnout time is comparable. Although pyrrhotite ignites readily, it requires as much time as anthracite to complete combustion. Pyrites containing small quantities of adventitious carbon, as might be found in the -1.80+2.85 gravity fraction, appear to form pyrrhotite deferring burnout until 800°C. Within the combustor the problem is compounded by the fact that pyrite particles do not shrink during the combustion process as do coal particles, and hence their burnout time is extended. The burnout time of particles in excess of 40 $\mu$  appears to exceed the residence time available in most combustors.

TGA reveals decomposition rates but tells little about the physical state during the combustion process. Phase diagrams for the Fe-S-O and FeS-FeO system, representing transitory states at the particle surface, imply the formation of a temporary melt at low temperatures. SEM photomicrographs, appearing in Figure 6, of pure pyrites heated to 600°C, 800°C, and 1000°C under reducing conditions, clearly reveal the formation of a melt at temperatures as low as 600°C. Large particles of partially-spent pyrites, which may be molten on contact with the heat transfer surface, complete the oxidation process *in situ*, forming a solid fused deposit with a very high melting temperature.

An examination of the thermal behavior of the mineral matter in coal indicates the mineral origin of the elements found in coal ash and their juxtaposition with regard to each other, as well as other mineral forms, and determines their physical fate during combustion. As indicated in Figure 2, the physical state (*i.e.*, vapor or solid) and the size of solidified ash will determine the mode

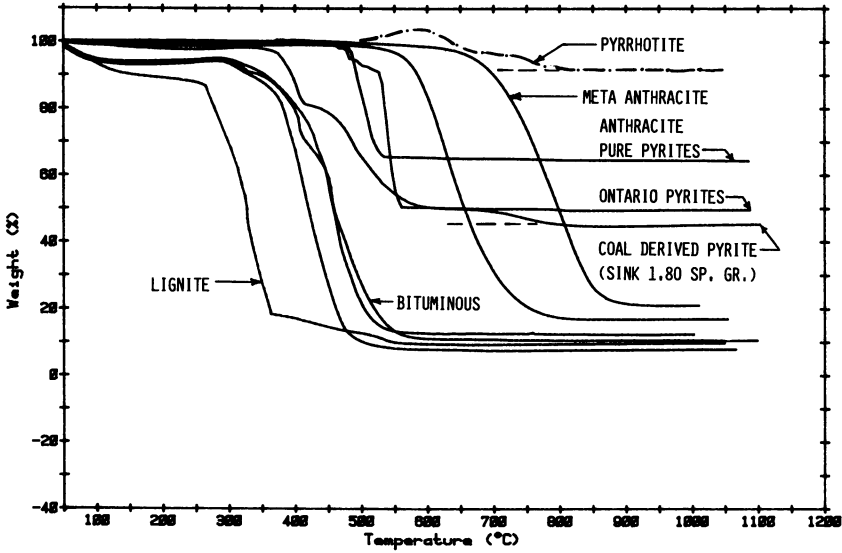


Figure 5. TGA Thermograms Comparing the Decomposition of Various Grades of Pyrites with permission from reference 19. Copyright 1984 VGB.

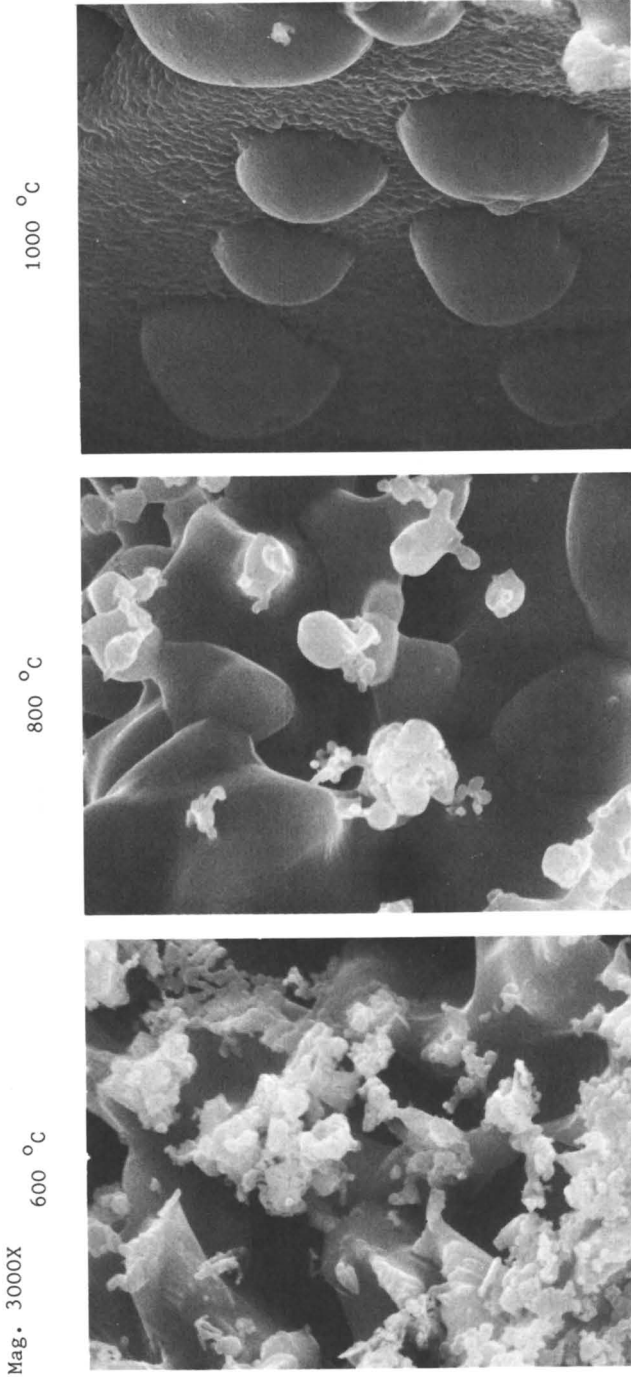


Figure 6. Pure Pyrites Heated Under Reducing Conditions to 600, 800, and 1000 °C. Reproduced with permission from reference 19. Copyright 1984 VGB.

and rates of migration to the heat transfer surface. The physical state at the tube surface will depend upon the local surface temperature and the composition of the particulate depositing. In the case of pyrites, residence time and environment, conditions may also play a significant role.

#### Characterization of Minerals in Coal

The fireside behavior of mineral matter in coal has been investigated by characterizing the mineral content of several bituminous coals, using size and gravity fractionation analysis of pulverized coal and then firing the coal in a vertically fired combustor. High sulfur coal containing pyrites of varying size and varying association with carbonaceous and other mineral forms were selected for examination. A comparison was also made with Western subbituminous coals to assess the impact of potassium in the mineral illite on furnace slagging.

Each coal was analyzed for proximate, ultimate, ash chemistry, and ash fusion temperatures to permit evaluation using conventional data. The pulverized coal samples were then divided into four sizes representing equal weights (i.e.,  $+105\mu$ ,  $-105\mu+74\mu$ ,  $-74\mu+44\mu$ , and  $-44\mu$ ). Each size fraction was separated into four specific gravity classes, thereby partitioning the coal into groups dominated by coal, nonpyritic mineral matter, and pyrites. The partitioned coal was analyzed for ash chemistry, ash fusion temperature, combustion profile, and mineral content.

The analytical data is summarized in Figure 7. The enclosed data points represent the composite analysis. The open data points represent the fractionated species. Ash softening temperatures and weight percent basic constituents were selected as the variables to characterize the coal, as they appear most frequently in the indices used to express the slagging or fouling potential of the fuel. It is quite evident the combustor is exposed to ash with a wide range of chemical compositions and melting temperatures not adequately identified by a composite coal analysis. Visual qualitative assessment of deposits in the slagging probes in the 100 lb/hr combustor indicates slagging was most severe with coals having the highest melting temperature and demonstrating the greatest degree of separation of ash from coal and pyrites from other mineral matter. The two coals with the lowest composite ash softening, having the highest slagging index by conventional evaluation, caused the least slagging. Liberation of mineral matter from these two coals was also the lowest.

The data was replotted on fusibility diagrams, appearing in Figure 8, typifying the coal with the greatest partitioning of mineral matter and highest degree of slagging and the coal with the least liberation of mineral matter and degree of slagging. The fusibility diagram illustrates the size and weighted contribution of each ash species. It also shows the degree of liberation of nonpyritic and pyritic mineral matter. By washing the worst coal at 1.80 sp. gr. and  $14M \times 0$ , thereby minimizing extraneous ash as well as total sulfur, the degree of slagging of the Upper Freeport coal was greatly reduced.

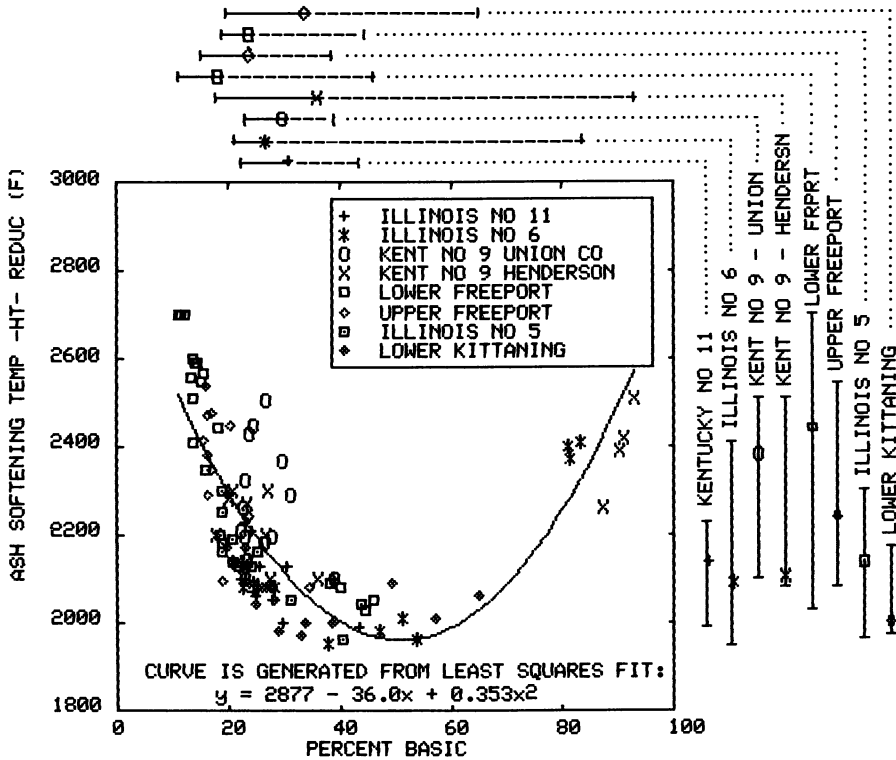


Figure 7. Ash Softening Temperature Vs. Percent Basic for Composite and Fractionated Coal Species

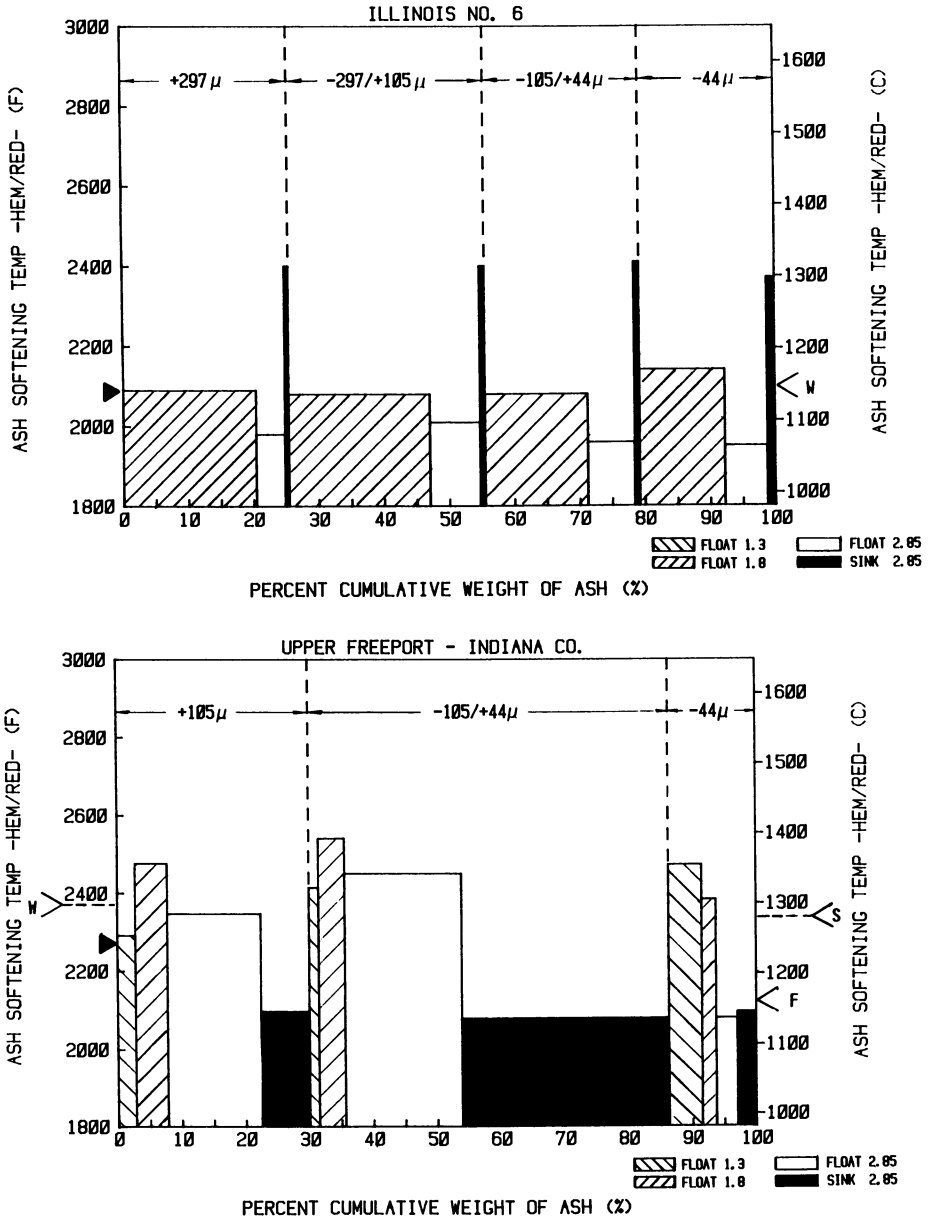


Figure 8. Fusibility Diagrams. Ash soft; temperature, °F. ▲, coal ash; F >, fouling probe deposit; S >, slagging probe deposit; and W >, furnace wall deposit.

### Combustion Testing

Deposits were removed from various locations in the combustor, illustrated in Figure 1, after firing each coal for 14 to 16 hours. Samples were removed from slagging probes at 750 to 950°C, fouling probes at 950 to 1000°C, and refractory surfaces at 1000 to 2200°C, and examined using the scanning electron microscope and energy dispersive x-ray. Fly ash samples were also examined for carbon loss, surface morphology, and chemical composition.

The deposits forming on the slagging probes were initiated by a thin layer of powdery fly ash,  $<8\mu$  in size, enriched with small quantities of potassium. Beads of slag formed on top of this thin layer when the surface temperature approached the initial deformation temperature of the deposit. Growth progressed with the formation of rivulets from which a continuous phase of molten slag formed. Deposits forming on the refractory surface represent an advanced stage of slag due to the higher surface temperatures which could only be achieved on the cooler probes after the initial dust layer formed. The composite ash chemistry and ash fusion temperatures of the slag resemble that of the heaviest gravity fraction (i.e.,  $>1.80$  sp. gr.) in most cases. Macrophotographs of the deposit formation on the furnace probes subjected to axial symmetric flow at low gas velocities (5 to 6 ft/s), illustrated in Figure 9, show that the initial layer of dust, upon which further slagging depends, formed only when firing coals whose ash contained more than 1-percent potassium. Continued deposit growth resulting in serious slagging is dependent upon the total pyrites liberated from the coal.

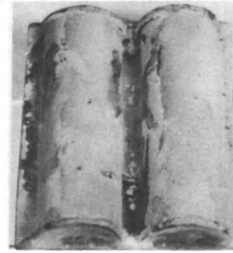
SEM microphotographs and EDAX scans of the cross section and outer surface of the slag deposit, illustrated in Figure 10, indicate the chemistry of the deposit is not uniform. The bulk of the fused material is rich in silica, low in iron, and virtually depleted of potassium. The outermost layers, no more than 2 to  $3\mu$  thick, are very rich in iron and frequently also rich in calcium. On occasion, the outer surface is covered with small particulate, several microns in diameter, or undissolved cubic or octahedral crystals whose origin is pyrites. Similar formations have been observed in full-scale operation. The evidence indicates deposits form under axial symmetric flow conditions in the furnace by the fluxing action at the heat transfer surface of small particles,  $<8\mu$  in diameter, of decidedly different chemical composition and mineral source. Migration of the fly ash to the surface is by means of eddy diffusion, thermophoresis, or Brownian motion.

Sintered deposits form at the furnace exit at lower gas temperatures and in zones subject to rapid changes in direction. The deposit is composed of spheroidal particles,  $<40\mu$ , bound together by a molten substance. In those cases where substantial quantities of coarse pyrites are liberated from the pulverized coal, the spheroids are nearly pure  $\text{Fe}_2\text{O}_3$ , as shown in Figure 11. The matrix contained silica, alumina, iron, and potassium, and has an initial deformation temperature of 1832°C, as determined by differential thermal analysis. The heavier pure iron spheroids deposit as a result of inertial impact. The mineral source of the molten phase is most likely illite.

Deposits also form on the leading edge of the first row of tubes in the convection pass when firing coals which liberate pure,

Ash Soft.  
Temp. (Red.) % Liberated  
and % Ash Fe<sub>2</sub>O<sub>3</sub> in Coal

2130°F      Kentucky  
14.9        No. 11  
              0.225



2080°F      Illinois  
9.4         No. 6  
              0.159



2443°F      Lower  
16.4        Freeport  
              1.56



2245°F      Upper  
23.5        Freeport  
              1.67



Figure 9. Slagging on Furnace Probes After 14 to 16 Hours Operation





<u>% K in Ash</u>	<u>Ash Soft. Temp. (Red.) and % Ash</u>
Western Fuel 1	2165°F
0.2	6.7



Western Fuel 2	2252°F
1.0	16.67



Western Fuel 3	2232°F
1.2	24.73



Lower Freeport	2443°F
1.56	16.4

Figure 9. Continued.

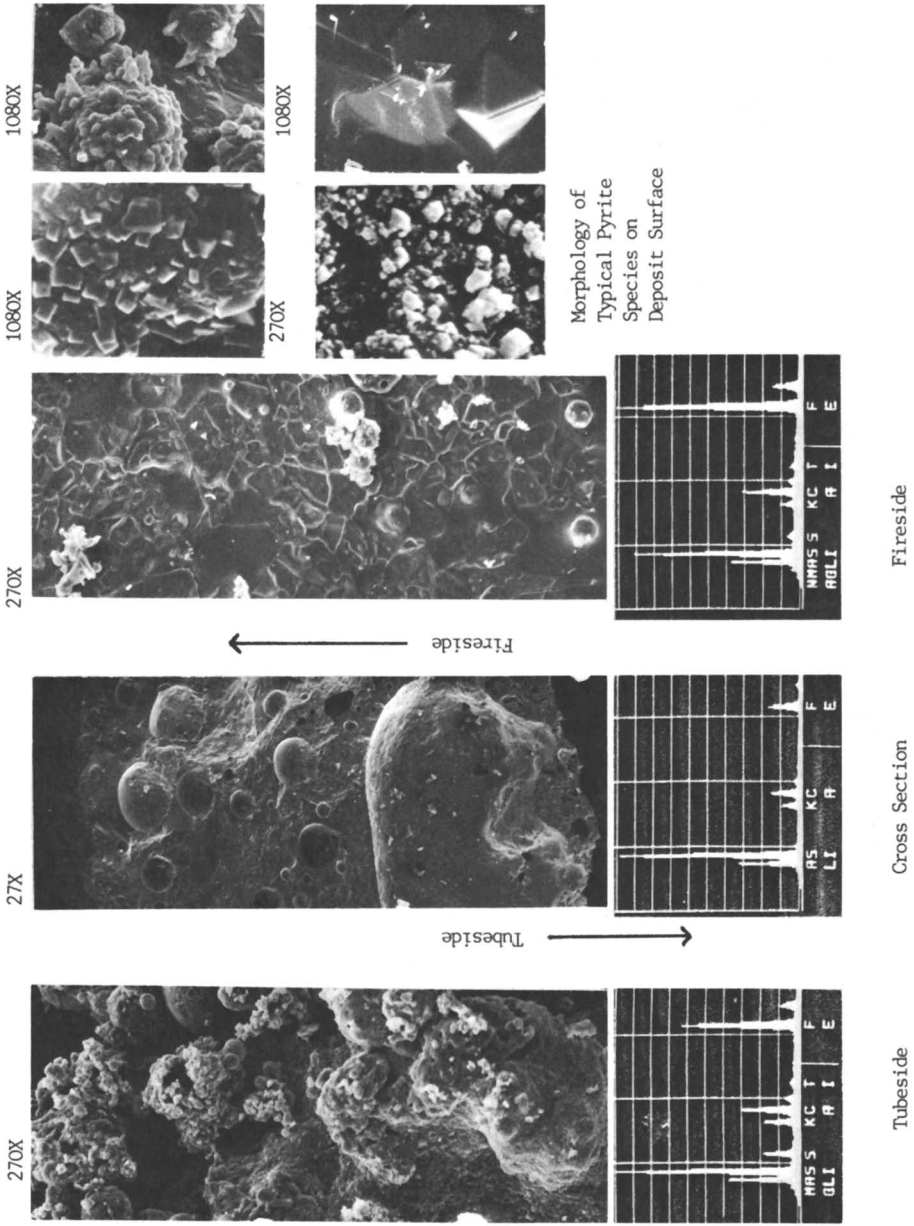


Figure 10. Slag Formation on Furnace Slag Probe

Publication Date: April 2, 1986 | doi: 10.1021/bk-1986-0301.ch025

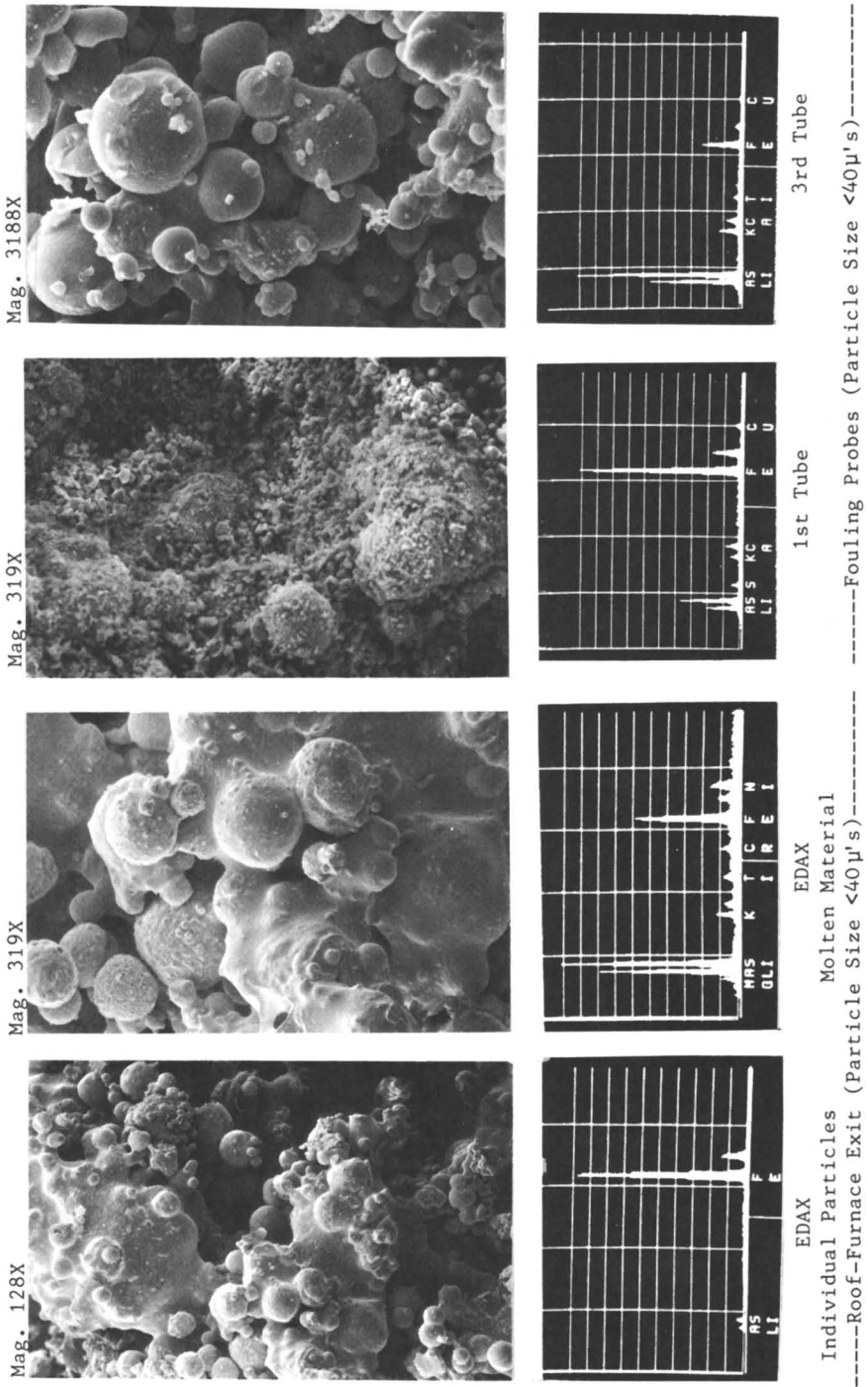


Figure 11. Iron-Rich Sintered Deposits Formed on Furnace Roof and 1st Tube of Convection Pass Probes by Coarse Pyrites. Reproduced with permission from reference 19. Copyright 1984 VGB.

coarse pyrites. These tubes are subjected to high gas velocities and have moderate-to-high collection efficiencies for particles between 40 and 100 $\mu$ . The deposits are nearly pure Fe<sub>2</sub>O<sub>3</sub>. They are hard and fused despite being at gas temperatures below their initial deformation temperature. No doubt the final stages of decomposition of the pyrites takes place at the tube surface.

### Conclusions

The formation of fireside deposits in furnaces depends on the composition, size and association of mineral matter liberated from the coal. Selective deposition of specific mineral species depends on their size, thermal behavior, the local gas temperatures, and their mode of transport to the surface. Consequently, the composition of the sintered deposit or molten slag may vary with time at a given location and will most probably vary throughout the combustor, depending on local temperatures and fluidynamics. The composition of the slag may be substantially different from the composite coal ash, depending upon its heterogeneity. Illite is a likely candidate as the mineral most responsible for initiating deposits. The molten phases are frequently part of the FeO-SiO<sub>2</sub> or FeO-CaO-SiO<sub>2</sub> system and depend on the interaction of quartz, calcite or pyrites at the heat transfer surface. Liberated pyrite crystals and small particles are primary candidates for slag formation subjected to parallel flow regimes at low velocities. Coarse pyrites can be selectively deposited and solely responsible for deposit formation on surfaces subjected to flue gas impingement at high velocities.

### Acknowledgments

Substantial portions of this study were sponsored by the U. S. Department of Energy, Pittsburgh Energy Technology Center, Contract DE-AC22-81PC40268, under the direction of Mr. J. Hickerson, Mr. H. Ritz, and Dr. R. Walker. I am grateful to Mr. O. R. Walchuk for supervising the combustion program; Mr. G. Lantos, who directed laboratory analyses; Messrs. G. Stanko and I. Dojcsanszky for SEM and EDAX analyses; and Mrs. J. Betyeman and Ms. S. Rowley for preparing the manuscript.

### References

- [1] Bryers, R. W., "The Physical and Chemical Characteristics of Pyrites and Their Influence on Fireside Problems in Steam Generators", Transactions of the ASME, Journal of Engineering for Power, October 1976.
- [2] Walker, F. E.; Hartner, E. F., "Forms of Sulfur in U. S. Coals", IC830, Bureau of Mines, U. S. Department of the Interior, 1966.
- [3] Gluskoter, H. J.; Simon, J. A., "Sulfur in Illinois Coals", Circular 432, Illinois State Geological Survey, Urbana, Illinois, 1968.
- [4] Nicholls, P.; Selvig, W. A., "Clinker Formation as Related to the Fusibility of Coal Ash", U. S. Bureau of Mines, Bulletin 364, 1932.

- [5] Barkley, J. F., "The Sulfur Problem in Burning Coal", Technical Paper 436, Bureau of Mines, U. S. Department of the Interior, 1928.
- [6] "Sulfur Codes Pose Dilemma for Coal", *Environmental Science and Technology*, Vol. 11, No. 12, December 1970.
- [7] King, H. M.; Renton, J.J., "The Mode of Occurrence and Distribution of Sulfur in West Virginia Coals", Carboniferous Coal Guide Book, (A. Donaldson, M. W. Presley, and J. J. Renton, eds.), West Virginia Geological and Economic Survey Bulletin B-37-1, 1929.
- [8] Deul, M., "Preliminary Observation of the Mode of Occurrence of Pyrite in Coal", Second Conference, Eastern American Anthrologists, University Park, Pennsylvania, May 26, 1958, p. 27.
- [9] King, H. M., "Sulfide Minerals in West Virginia Coals", *Mountain State Geology*, West Virginia Geological and Economic Survey, December 1980.
- [10] Hale, G.L., Levasseniz, A.A., and Tyler, A.L., "The Alkali Metals in Coal: A Study of Their Nature and Their Impact on Ash Fouling", *Coal Technology* 80.
- [11] Bryers, R. W., "Influence of the Distribution of Mineral Matter in Coal on Fireside Ash Deposition", *Transactions of the ASME, Journal of Engineering for Power*, October 1979.
- [12] Reid, W.T., "The Effect of Mineral Matter in Coal on Ash Behavior in Large Boiler Furnaces", Presentation to the ASME Committee on Corrosion and Deposits from Combustion Gases, September 29, 1971.
- [13] Flagan, R. C.; Sarofim, A. F., "Transformation of Mineral Matter in Coal", *Progress in Energy and Combustion*, to be published.
- [14] Hoy, H. R.; Roberts, A. G.; Wilkins, D. M., "Behavior of Mineral Matter in Slagging Gasification Processes", I.G.E. Journal, June 1965.
- [15] Jackson, P., "From Mineral Matter to Deposits in PF-Fired Boilers, Part I: The Behavior of Mineral Matter in the Flame", Pulverized Coal Firing - The Effect of Mineral Matter, T. Wall, ed., University of Newcastle, August 1979.
- [16] Watt, J. D., "The Physical and Chemical Behavior of the Mineral Matter in Coal Under the Conditions Met in Combustion Plants: A Literature Survey--Part II: The Occurrence, Origin, Identity, Distribution, and Estimation of the Mineral Species in British Coals", BCURA Industrial Laboratories, Leatherhead, Surrey, England, August 1979.
- [17] Borio, R.W.; Narcisco, R.R., "The Use of Gravity Fractionation Techniques for Assessing Slagging and Fouling Potential of Coal Ash", ASME Winter Annual Meeting, Paper 78-WA/CD-3, 1978.
- [18] Pollock, W.H.; Goetz, G.J.; Park, E.D., "Advancing the Art of Boiler Design By Combining Operating Experience and Advanced Coal Evaluation Techniques", American Power Conference, April 18-20, 1983.
- [19] Bryers, R.W.; Walchuk, O.R., "The Influence of Pyrites on Slagging in Steam Generators", International VGB Conference on Slagging, Fouling and Corrosion on Thermal Power Plants, VGB Technical Association of Large Power Plant Operators, Essen, West Germany, February 1984.

- [20] Nelson, H.W., et al, "A Review of Available Information on Corrosion and Deposits in Coal- and Oil-Fired Boilers and Gas Turbines", ASME, 1954.
- [21] Honig, R.E., "Sublimation Studies of Silicon in the Mass Spectrometer", Journal of Chemistry and Physics, Vol. 77, pp. 1610-1611, 1954.
- [22] Mackowsky, M.Th., "The Behavior of Coal Minerals at High-Combustion Temperatures with Consideration of Slow and Rapid Heating", Paper given at The Annual Meeting of the Association of Large Boiler Owners, Nurnberg, Germany, July 1955.
- [23] Quann, R.J.; Sarofim, A.F., "Vaporization of Refractory Oxides During Pulverized Coal Combustion", Nineteenth Symposium International on Combustion, The Combustion Institute, 1982.

RECEIVED October 24, 1985

# Influence of Thermal Properties of Wall Deposits on Performance of Pulverized Fuel Fired Boiler Combustion Chambers

W. Richter, R. Payne, and M. P. Heap

Energy and Environmental Research Corporation, Irvine, CA 92718

The properties which determine heat transfer through a deposit layer of given thickness are thermal conductivity, emissivity, and absorptivity. These properties vary with deposit temperature, thermal history, and chemical composition. Parametric studies and calculations for existing boilers were carried out to show the sensitivity of overall furnace performance, local temperature, and heat flux distributions to these properties in large p.f. fired furnaces. The property values used cover the range of recent experimental studies. Calculations for actual boilers were carried out with a comprehensive 3-D Monte Carlo type heat transfer model. Some predictions are compared to full-scale boiler measurements. The calculations show that the effective conduction coefficient  $(k/\Delta s)_{\text{eff}}$  of wall deposits strongly influences furnace exit temperatures.

The buildup of ash deposit layers on tube walls and superheaters in dry bottom p.f. boiler combustion chambers does not only deteriorate furnace and overall boiler efficiency, but also increases the temperature level in furnace and convective passages and aggravates existing deposit problems. This can finally lead to expensive outages when deposit formation cannot be controlled by soot blowing alone. Since errors in furnace design with respect to slagging and fouling or incorrect estimates of the impact of fuel conversion on deposit formation are so costly in large boilers, there is considerable financial incentive to develop analytical methods in order to predict furnace performance for a wide range of coal types and operating conditions. It is clear that such methods must take quantitatively into account, among other things, the thermal properties of ash deposits, i.e. thermal conductivity, emissivity, and absorptivity.

The current paper presents results from various studies carried out by the authors to show the influence of thermal properties of ash deposits on performance of large p.f. fired boiler furnaces. The paper is divided into three sections. In the first section, key

parameters of overall furnace performance are identified with the help of a sensitivity study and related to the ash deposit properties. The second section summarizes experimental data of thermal properties of deposits and defines the range of values probably occurring in boiler combustion chambers. In the third section, typical property values are used in combination with a sophisticated 3-D heat transfer model in order to demonstrate the effect of existing deposit layers on local temperature and heat flux distribution and performance of particular boiler furnaces.

### Parametric Study of Overall Furnace Performance

The parametric studies were carried out in order to identify the most important parameters influencing overall furnace heat absorption. These parameters are:

- o Adiabatic Flame Temperature
- o Firing Density
- o Total Emissivity
- o Temperature of Heat Sink Surfaces
- o Flow and Heat Release Patterns

Figure 1 shows how these quantities are related in a complex manner to each other, to fuel characteristics, to furnace operating conditions, and to wall deposits.

Some of the relationships in this figure were investigated utilizing a simple well-stirred furnace model (1) which assumed transport of gray radiation. This well-stirred analysis predicted qualitatively the dependence of furnace efficiencies  $\eta_f$  and exit temperature  $T_{ex}$ , both related by Equation 1

$$\eta_f = 1 - \frac{\dot{M}_o C_p \left| \begin{array}{c} T_{ex} \\ T_o \end{array} (T_{ex} - T_o) \right.}{\dot{Q}_o} \quad (1)$$

on furnace design and operating conditions. An important design parameter is the furnace height  $L$  required to obtain a desired efficiency or exit temperature (1 m of furnace height corresponds approximately to \$500,000). It was found that the height  $L$  depends considerably on the characteristics of the wall deposits, especially in large furnaces. This is shown in Figures 2 and 3 in which the efficiency  $\eta_f$  is plotted over the height  $L$  with surface temperature  $T_w$  of deposits and surface emissivities  $\epsilon_w$  as parameters. The calculations were carried out for a rectangular furnace box of width  $L/3$ . Other input parameters are listed in the figures. The strong impact of wall temperatures for larger sizes (Figure 2) is due to the fact that large furnace volumes approach black radiators and volume emissivities cannot be increased anymore by increase in size. For furnaces operated with the same thermal input at low efficiencies, the presence of wall deposits requires only a moderate increase in size.

A reduction of surface emissivities from 1 (clean "sooty" walls) to 0.4 which is the lowest range reported for ash deposits also causes a drop of  $\eta_f$  or requires an increase in height in order to maintain  $\eta_f$  (Figure 3). The size required varies nonlinearly



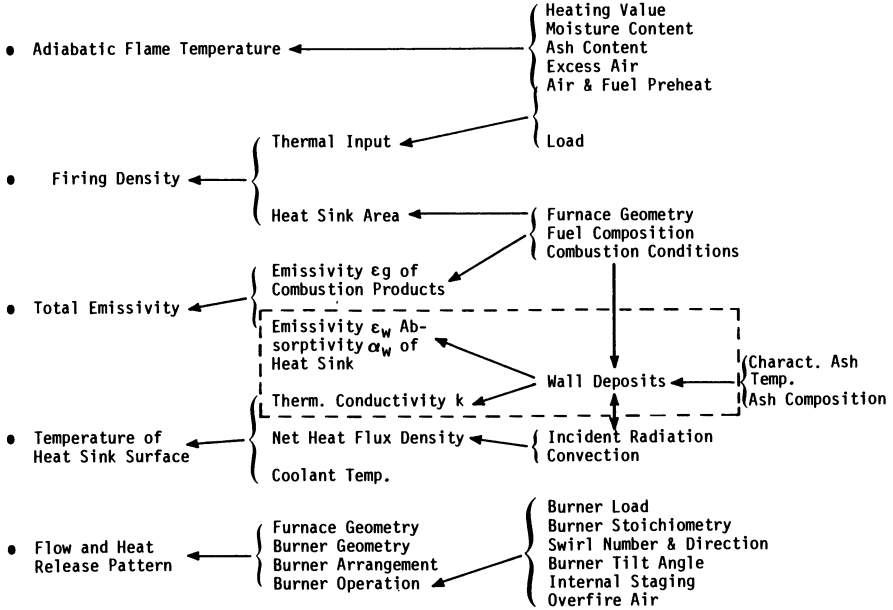


Figure 1. Major factors influencing thermal performance of furnaces.

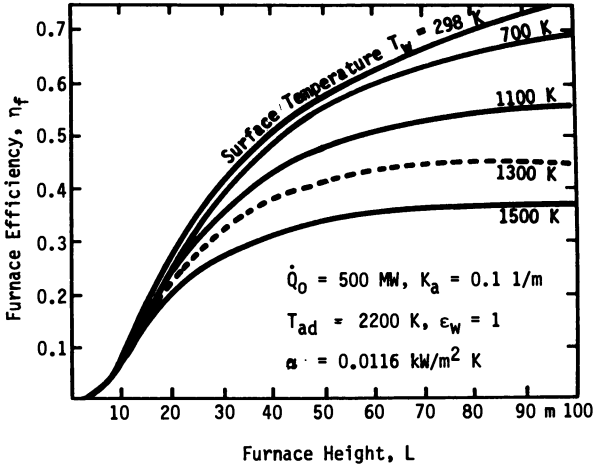


Figure 2. Dependency of furnace efficiency on furnace dimensions for various surface temperatures.

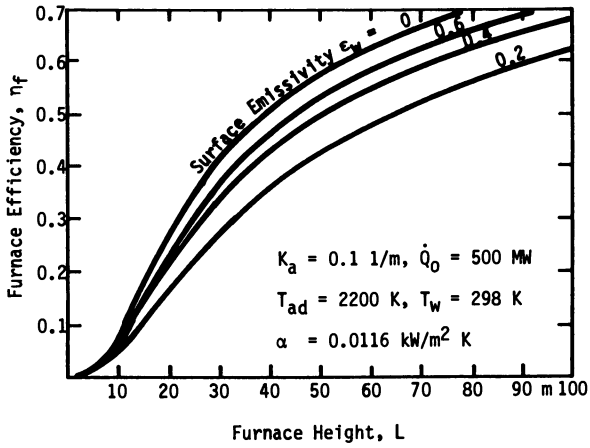


Figure 3. Dependency of furnace efficiency on furnace height with surface emissivity as parameter.

with changes of surface temperature but nearly linearly with  $\epsilon_w$  between  $\epsilon_w = 1$  and  $\epsilon_w = 0.5$ .

When a deposit layer is formed, surface temperature is increased and wall emissivity decreased. However, the superposition of these effects on  $\eta_f$  is less than a pure summation; since, by decreasing  $\epsilon_w$ , the net heat flux to the layer is reduced, thus retarding the increase of surface temperature to a certain extent. The simple well-stirred analysis, carried out for constant surface temperatures yields typically a drop of furnace efficiency  $\eta_f$  of 5.5 percentage points corresponding to an increase of furnace exit temperatures  $T_{ex}$  of 110 K for a decrease of  $\epsilon_w$  from 0.8 to 0.4. Detailed 3-D furnace heat transfer calculations carried out for the same decrease of  $\epsilon_w$  but allowing a variation of surface temperatures yield typically losses of  $\eta_f$  only 3.5 percentage points corresponding to increase of  $T_{ex}$  of only 70 K.

#### Available Data of Thermal Properties of Ash Deposits and Data Analysis

Thermal Conductivity. A comprehensive review of literature data for thermal conductivity  $k$  of ash deposits was published by Wall et al. (2). The thermal conductance,  $k$ , of the ash material increases reversibly with temperature until sintering or fusion occurs. At this stage, a rapid and irreversible increase of  $k$  is observed. Figure 4 shows schematically the range of measured values of  $k$  depending on mean temperature of the deposit layer and on the physical properties of the deposit. Typical values of  $k$  for nonsintered deposits from Australian coals in actual furnaces vary between  $0.1 \times 10^{-3}$  kW/mK at 500 K up to  $0.4 \times 10^{-3}$  kW/mK at 1300 K. The factors contributing to the thermal conductance in the powdered deposits are: conductance in the solid particles, gas conduction in the voids and radiative transfer through the voids. Fetters et al. recently measured  $k$  for boiler deposits of an Indiana coal (3) which demonstrated that the dominant mode of heat transfer through the deposit layer is by radiation at high temperature. The values of  $k$  measured for powdery deposits by Fetters et al. are about two times larger than those of Wall et al. (2) at the same temperature. This is contributed to relative large particle sizes in the Indiana coal ash deposits (75% in the 100 micron range) compared to the Australian coal ash deposits with weight mean particle diameters of 50 microns and less. Larger particles in a deposit layer increase the contribution of bulk particle conduction.

Thermal conductivity of sintered and fused deposits found by the Australian researchers range from  $0.5 \times 10^{-3}$  kW/mK at 800 K to  $2.0 \times 10^{-3}$  kW/mK at 1500 K. This is consistent with the recent findings of Fetters et al. (3) for crushed deposits from a boiler fired with Indiana coal and with other literature values (4). The increase of thermal conductivity of sintered and fused deposits is due to a decrease of void space and increased transmissivity of the material. Wall et al. emphasize that values of  $k$  obtained from ground deposits in laboratory studies are questionable since bounding of the deposit occurs in situ which leads to an increase of  $k$ . This agrees with our results for a 700 MW<sub>e</sub> boiler which yielded an overall value of  $k = 3.2 \times 10^{-3}$  kW/mK for deposits which could not be removed by soot blowing (see below).

**Emissivity and Absorptivity.** Reviews of emissivity data of ash deposits were given by Wall et al. (2) and recently by Becker (5). Figure 5 shows the range of data of surface emissivity depending on surface temperature obtained by Becker (5) and by Goetz et al. (6) for deposit probes prepared in various ways. Becker used predominantly probes prepared in the laboratory from precipitator ashes. In two cases, however, he studied also probes sampled in situ in boiler furnaces. Goetz et al. measured the emissivity of ash probes obtained directly or prepared from slag in a pilot scale furnace. The experimental data show, in general, a considerable spread of emissivity between values of  $\epsilon_w = 0.9$  and  $\epsilon_w = 0.3$  depending on temperatures, ash origin, and probe preparation. However, general agreement exists that for nonsintered material  $\epsilon_w$  decreases reversibly to higher values. The values reported by Goetz vary between 0.38 and 0.67 for powdery (initial) deposits, between 0.76 and 0.93 for sintered deposits, and between 0.65 and 0.85 for glassy or molten deposits.

The increase of emissivity with sintering and fusion is due to increased transmission of radiation into the surface of the deposit layer. In the range of surface temperatures of interest, namely between 800 K and 1400 K, measured total emissivities on probes of sintered real furnace deposits exhibit only slight variations with surface temperature (5), (6). However, measurements by Becker of spectral emissivities of deposits on laboratory prepared probes showed distinctive nongray behavior. For typical flame temperatures of 1700 K and typical surface temperatures of 1100 K, up to 0.2 higher values were found for emissivities than for absorptivities (Figure 6).

Nongrayness of emission and absorption is typical for glassy material and is due to the low spectral absorptivities at short wavelengths which becomes dominant for radiative transfer at more elevated flame temperatures. The assumption of gray radiation of furnace deposits and consequent use of gray emissivity values for determination of absorption may lead to errors in heat transfer calculations for furnaces with moderate deposits since at lower surface temperatures absorption is several times larger than re-emission. By performing detailed one-dimensional spectral calculations, Becker showed that for a 10 m path length, typical of furnaces, and relatively cool walls errors up to +30 percent in predicted net heat flux densities would result from the assumption that the deposits were gray. However, these findings are based on spectral values found for laboratory prepared probes. Spectral measurements of real furnace deposits show reduced nongray behavior (5), (6) and higher emissivities than the laboratory probes (6) (Figure 6). Moreover, coloring agents such as unburnt carbon as well as the rough surface structure of real deposits and tube curvatures tend to make boiler surfaces more closely approximate gray behavior. Thus, the importance of nongray deposits is uncertain in boiler chambers and, in any case, insufficient information is available to recommend replacing the assumption of gray radiation of deposits currently used in 3-D furnace models (see below) by expensive more rigorous spectral models.

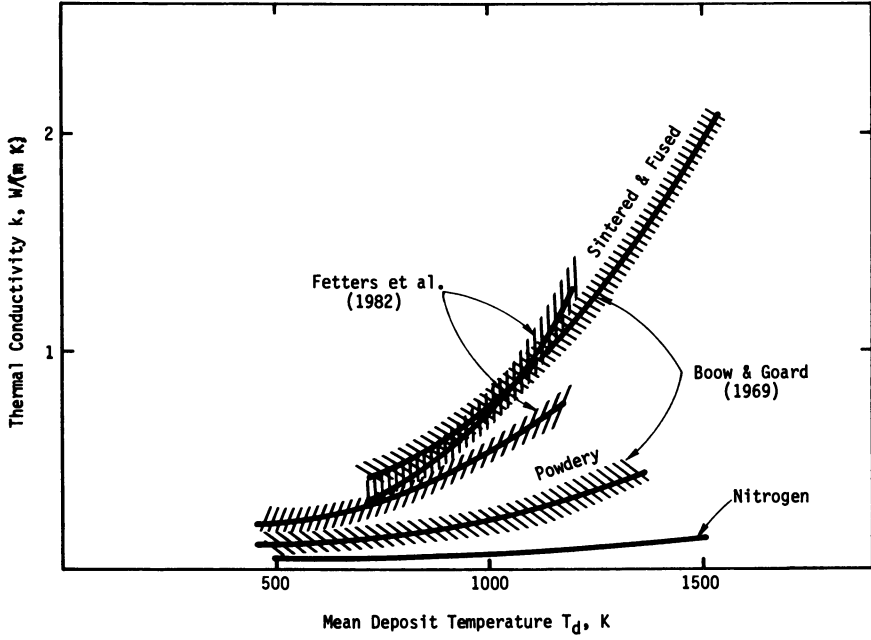


Figure 4. Range of measured thermal conductivities of deposits.

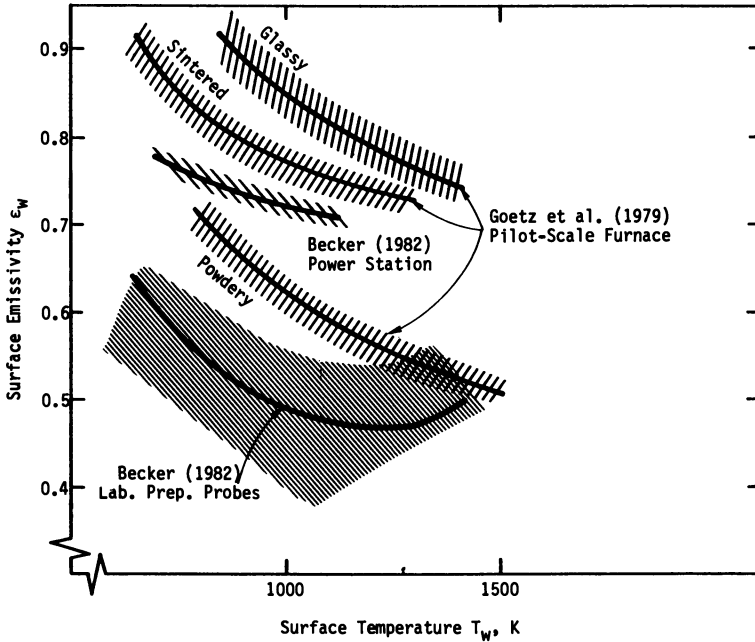


Figure 5. Range of measured values of emissivities of deposits.

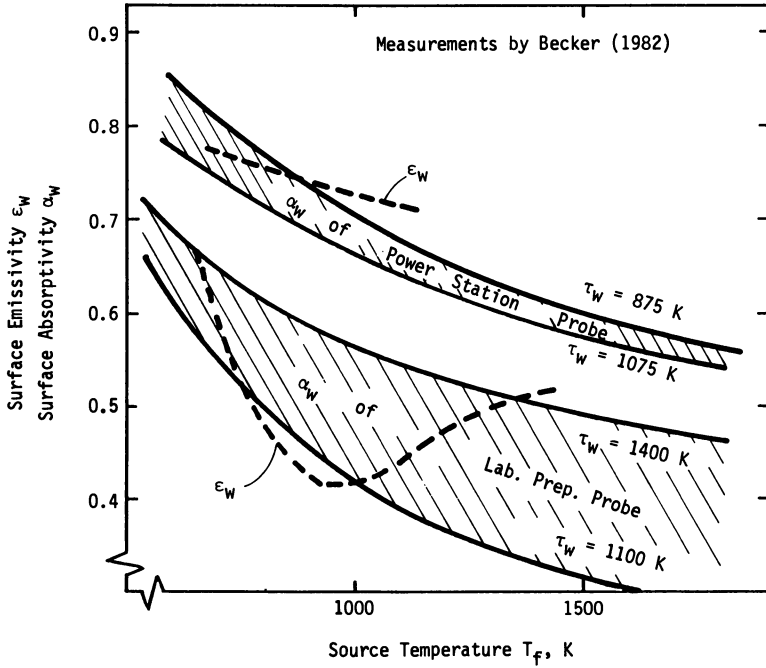


Figure 6. Comparison between measured emissivities and absorptivities of deposits.

Prediction of Influence of Wall Deposits on  
Heat Transfer in Existing Boilers

On the basis of the literature values of thermal properties discussed above a considerable number of performance predictions have been carried out for existing boiler combustion chambers in the past 2 years. Some results of those calculations with relevance to the impact of ash deposits on heat transfer follow. The tool used for the analysis is an extremely flexible 3-D Monte Carlo type zone model (7-9). In this model, the emissive power of each volume and surface zone is distributed into a discrete number of radiative beams. Taking multiple reflection at furnace walls into account, the beams are traced throughout the furnace volume until final absorption. Nongrayness of the combustion products is modeled with a weighted gray gas approach. The radiating species considered are H<sub>2</sub>O, CO<sub>2</sub> and particulates (soot, char, and ash). Currently, char and ash particles are treated as gray radiators. Scattering of radiation of ash particles which may be of some importance in large combustors fired with coal of high ash content can in principle be taken into account by the model but was neglected in the following examples. The model of radiative exchange is directly coupled with a total heat balance of volume and surface (deposit) zones with unknown temperatures. The calculation of convective heat fluxes through the furnace is based on mass flow vectors at the boundary of each zone obtained from isothermal modeling. The heat release pattern is based on this flow field. The heat release due to volatile combustion is based on observed visible flame length and the heat release due to burnout of char particles is calculated from carbon and oxygen balances solved simultaneously with the heat balance.

Example 1: Tangentially Coal-Fired Boiler

This study was carried out to investigate the influence of ash deposits in a boiler furnace originally designed to fire No. 6 oil at a net thermal input of 1000 MW<sub>t</sub>. However, the thermal input of the furnace was reduced to 590 MW<sub>t</sub> to investigate the prospects of firing coal in this unit. The coal considered was a Utah coal with 8.8 percent ash content fired with 30 percent excess air. Figure 7 shows the zoning of the furnace and the assumed flow patterns. The heat release assumed for combustion of volatiles is indicated by the shaded area. The surface conditions were specified by the following input data:

- Case A Clean surfaces, emissivity of tubes  $\epsilon_w = 0.9$ .
- Case B Powdery ash deposit,  $\epsilon_w = 0.6$ ,  $\Delta s = 0.5$  mm,  $k = 0.3 \times 10^{-3}$  kW/mK.
- Case C Properties of ash deposit layer in upper part of the furnace (above heat release zone) as specified for Case B; glassy ash deposit layer in lower part of the furnace with  $\epsilon_w = 0.8$ ,  $\Delta s = 7$  mm,  $k = 1 \times 10^{-3}$  kW/mK.

The properties for the powdery (primary) and for the glassy (molten) deposit layer of the Cases B and C correspond to average data from literature as cited above. The actual calculations were carried out with an effective emissivity of the tube walls taking the shadow effect of the gap between adjacent tubes into account.

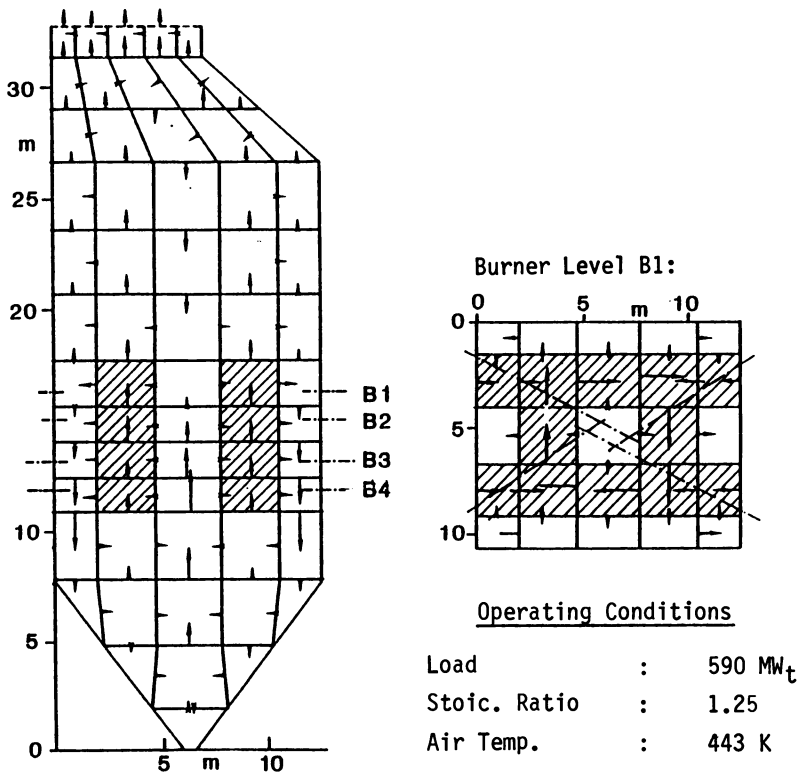


Figure 7. Geometry and zoning of tangentially fired boiler furnace originally designed for oil firing with 1000 MW<sub>t</sub> thermal input.



Table I and Figure 8 through 10 show that the buildup of ash deposits seriously affects overall and local heat transfer. The difference ( $\Delta\eta_f$ ) in computed furnace efficiencies for the extreme cases, A (clean walls) and C (highest thermal resistance), is 6.2 percentage points. The formation of a first initial deposit layer (Case B) has a stronger impact on heat transfer than subsequent increase of deposits in the lower furnace (Case C). The increase of the thickness of ash deposits opposite to the heat release zone displaces the peak heat fluxes up into the regions of the thinner deposits (Figure 9). This is one reason why the buildup of deposit layers, once started, spreads into adjacent wall zones. Once the deposit layers begin growing, surface temperature can soon reach values in the range between softening (1400 K) and fusion temperature (1500 K) as indicated by shaded areas in Figure 10. The furnace model is also able to predict, for a given coal ash fusion temperature approximately the development and extent of molten slag layers.

#### Example 2: Opposed P.F. Fired Boiler

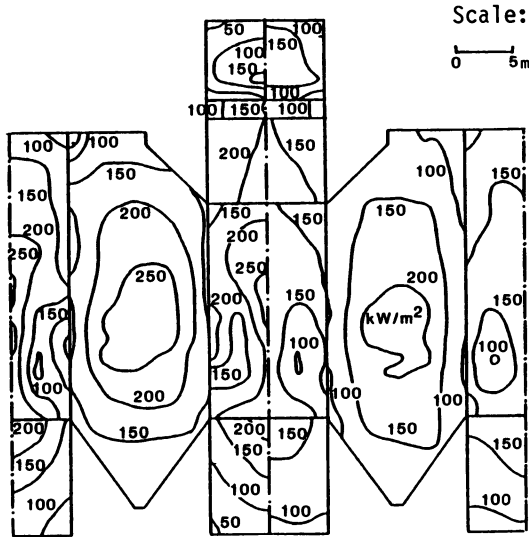
This study was carried out in order to verify the 3-D furnace heat transfer model with performance data available from a coal-fired, boiler combustion chamber of 1730 MW<sub>t</sub> fuel heat input (9). The coal had a medium volatile content, an ash content of 6.6 percent, and was fired with 28 percent excess air. In this case, the flow pattern was based on detailed distribution of mean mass flow vectors measured in a physical isothermal model. However, turbulent components were superimposed on these vectors with the help of a simple model of turbulence. Figure 11 shows a comparison of the profiles of gas temperatures measured and predicted for 100 percent load in one half of the furnace outlet plane. The difference between predicted and measured values was less than 25 K. The good agreement is partially due to a reasonable assumption of the effective heat conduction coefficient  $(k/\Delta s)_{eff}$  of the deposit layers. Figure 12 shows how the predicted mean furnace exit temperature varied with  $(k/\Delta s)_{eff}$  and compares those predictions with two data points obtained from measured heat balances of the boiler immediately after soot blowing and 20 h after soot blowing. Since measurements and observations yielded approximately a 2 mm deposit layer, which could not be removed by soot blowing an effective thermal conductivity of  $3.2 \times 10^{-3}$  kW/mK can be deducted. An assumed value of  $k = 0.8 \times 10^{-3}$  kW/mK for a dry partially sintered deposit would suggest the buildup of an additional layer of 1.5 mm, 20 h after soot blowing for a total layer of 3.5 mm thickness. Figure 12 also contains the relationship of  $T_{ex} = f(k/\Delta s)_{eff}$  for a similar boiler furnace of 1250 MW<sub>t</sub> heat input in which slagging and fouling problems were encountered.

#### Further Boiler Performance Predictions

The 3-D furnace heat transfer model has been verified several times in the past and has successfully predicted performance of gas, oil, coal, and slurry fired boilers located all over the world (9-12). The generalized performance predictions of the impact of wall deposits on heat transfer is shown in Figure 13 for a number of p.f.,

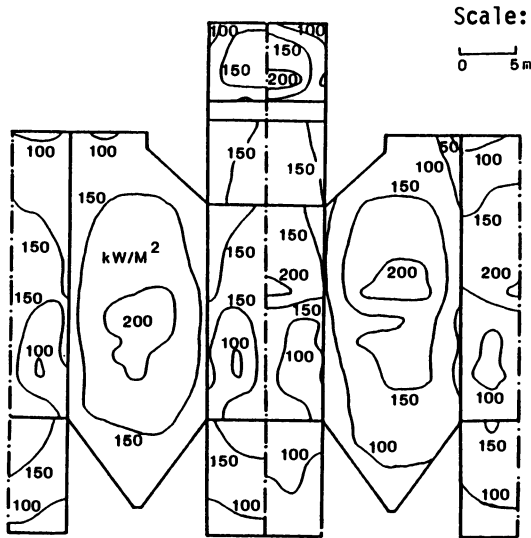
Table I. Thermal Performance of 590 MWt Coal-Fired Combustion Chamber for Various Slagging and Fouling Conditions

No.	Case	Fur-nace	Mean	Mean	Max. Net	Vertical	Max.	Un-	Carbon	
		Effi- ciency	Furnace Exit Temper- ature	Net Heat Flux Density	Heat Flux Density	Position of Max. Net Heat Flux Density	Flame Temp.	nace Exit Temp.	Content of Fly Ash	
		%	K	kW/m <sup>2</sup>	kW/m <sup>2</sup>	m	K	K	%	
A	Clean Surfaces	40.3	1436	168	304	14.9	1661	1515	1.35	6.43
B	Powdery Ash Deposit	35.6	1519	148	235	16.7	1728	1582	0.89	4.33
C	Slagging Lower Half	34.1	1541	143	239	19.2	1776	1610	0.75	3.68



(a) Clean Walls      (b) Thin Ash Layer  
 $\epsilon_w = 0.9$        $\Delta s = 0.5 \text{ mm}$   
 $\epsilon_w = 0.6$   
 $k = 0.3 \times 10^{-3} \text{ kW/mK}$

Figure 8. Influence of wall deposits on predicted net heat flux distribution in boiler combustion chamber fired with coal at a rate of  $590 \text{ MW}_t$ .



(a) Thin Ash Layer (b) Slagging Lower Half

$\Delta s = 0.5 \text{ mm}$

$\epsilon_w = 0.6$

$k = 0.3 \times 10^{-3} \text{ kW/mK}$

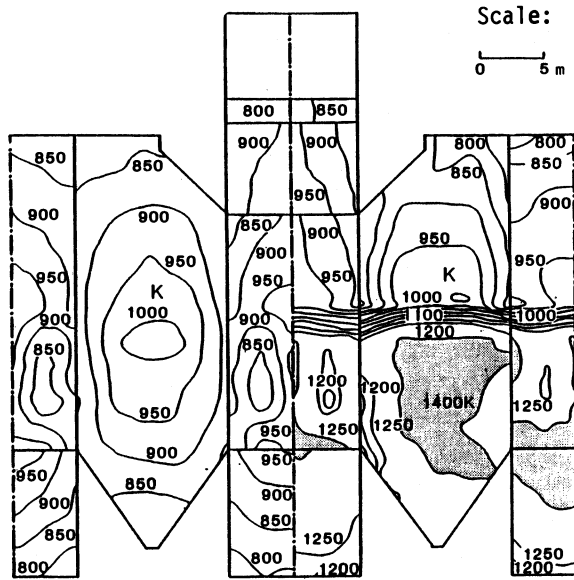
$\Delta s = 7 \text{ mm}$

$\epsilon_w = 0.8$

$k = 1 \times 10^{-3} \text{ kW/mK}$

Upper Half as in (a)

Figure 9. Influence of slagging in lower furnace half on predicted net heat flux distribution in boiler combustion chamber fired with coal at a rate of  $590 \text{ MW}_t$ .



(a) Thin Ash Layer      (b) Slagging Lower Half

$\Delta s = 0.5 \text{ mm}$

$\epsilon_w = 0.6$

$k = 0.3 \times 10^{-3} \text{ kW/mK}$

$\Delta s = 7 \text{ mm}$

$\epsilon_w = 0.8$

$k = 1 \times 10^{-3} \text{ kW/mK}$

Upper Half as in (a)

Figure 10. Influence of slagging in lower furnace half on predicted surface temperatures of deposits in boiler combustion chamber fired with coal at a rate of  $590 \text{ MW}_t$ .

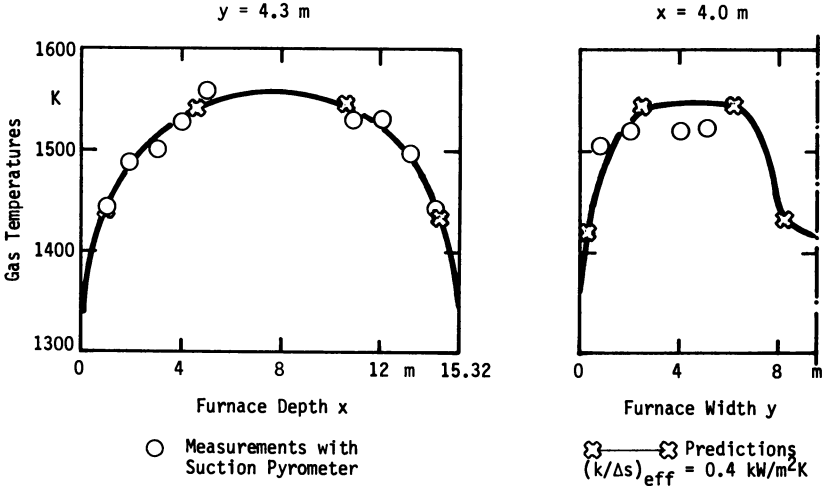


Figure 11. Comparison of temperature profiles predicted and measured near furnace exit ( $z = 68.6 \text{ m}$ ) of  $1730 \text{ MW}_t$  opposed coal-fired boiler combustion chamber.

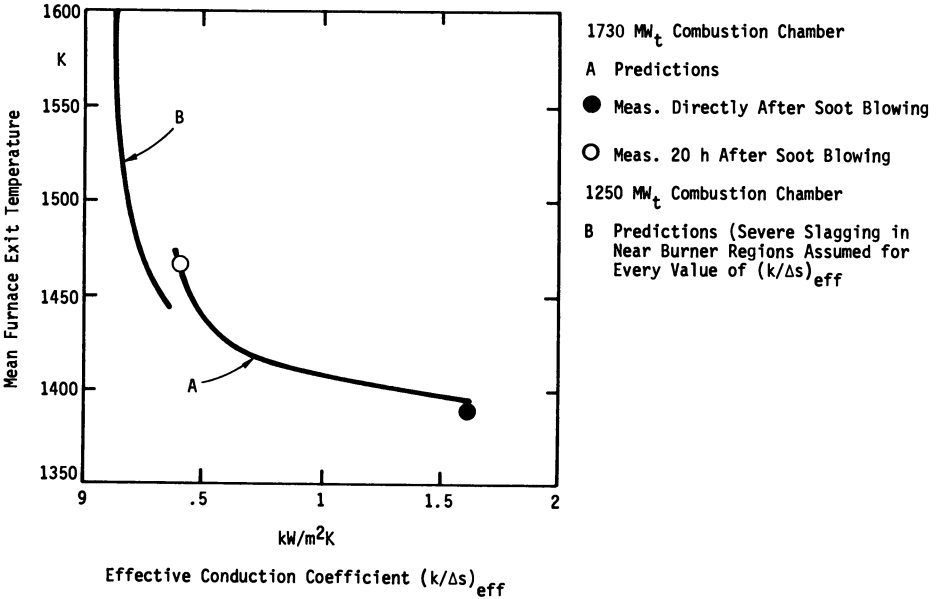
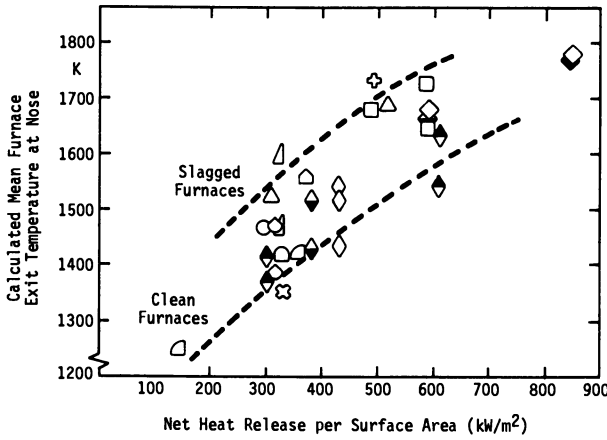


Figure 12. Influence of effective conduction coefficient on exit temperatures of opposed fired furnaces.



Furnace Nr. & Sym.	Firing Pattern	Fuel	Surface Area m <sup>2</sup>	(k/Δs)eff kW/m <sup>2</sup> K	Wet Slag Spots Pred.	Furnace Nr. & Sym.	Firing Pattern	Fuel	Surface Area m <sup>2</sup>	(k/Δs)eff kW/m <sup>2</sup> K	Wet Slag Spots Pred.		
1	◇	Tan.	Bit.	1748	0.8 0.32 Local	No	6	△	Front	Bit.	538	0.4	No
	◆	Tan.	CWM	1748	0.8 0.32 Local	No	7	◻	Opp.	Bit.	5254	1.6	No
2	□	Opp.	Bit.	3103	1.6 0.4 0.08 Local	No Yes	8	⊗	Tan.	Lig.	5120	1.6	No
							9	◻	Opp.	Bit.	2862	0.4	No
3	◇	Tan.	Bit.	1535	∞ 0.6	No No	10	△	Opp.	Bit.	2151	0.25 0.04 Local	Yes
	◆	Tan.	COM	1535	∞ 0.6	No No					0.1 0.04 Local	Yes	
	◆	Tan.	CWM	1535	∞ 0.6	No No	11	○	Opp.	Bit.	3080	1.6 0.4	No No
4	△	Front	Bit.	2109	0.4	Yes High Load	12	○	Tan.	Lig.	547	0.4	No
5	⊕	Tan.	Bit.	2407	0.4	Yes							

Figure 13. Furnace exit temperatures predicted for various boilers.

CWM and COM fired furnaces. In this figure, the mean exit temperature predicted for horizontal cross-sections through the tip of the furnace nose is plotted against the firing density (net heat release per projected surface area) of the furnaces. Different slagging and fouling conditions in the various furnaces were taken into account by specifying the distribution of the effective heat conduction coefficient at the furnace walls either based on observation in the actual furnaces or on engineering judgement. The exit temperatures can also clearly be correlated to the cleanliness of the furnaces. Despite the scatter in the data (largely due to different furnace design and operating conditions and to a minor extent to model assumptions) exit temperatures of furnaces with slagging are on the order of 100-150 K higher than those for clean furnaces.

### Conclusions

Thermal conductivity and emissivity of wall deposits have a considerable effect on heat transfer in large boilers. This results in temperature differences of furnace exit temperatures which influence furnace height, performance, and costs. More exact values of deposit thermal properties, which vary over a wide range of temperatures and conditions, than currently available are needed for detailed prediction of the initial formation of deposit layers. However, gross characteristics of thermal properties can be assumed and are sufficient to estimate the performance of furnaces, since the model contains other major uncertainties such as, thickness and inhomogeneous distribution of deposits at furnace walls and superheaters. This is especially true between soot blowing cycles. The 3-D heat transfer model used in the present study has the potential to form the basis of a more comprehensive model of slagging and fouling because it can provide reliable predictions of flame and deposit temperatures.

### Literature Cited

1. Richter, W. "Parametric Screening Studies for the Calculation of Heat Transfer in Combustion Chambers"; Topical Report, prepared for Pittsburgh Energy Technology Center, Department of Energy, Under Contract No. DE-AC22-80PC30297, 1982.
2. Wall, T. F.; Lowe, A.; Wibberley, L. J.; Stewart, McC. Prog. Energy Combust. Science, 1979, 5, p. 129.
3. Fetters, G. D.; Viskanta, R.; Incropera, F. P. 1982 ASME Winter Annual Meeting, 1982, Paper 82-WA/HT-30.
4. "Combustion: Fossil Power Systems"; Singer, J. G., Ed.; Combustion Engineering Inc.: Windsor, 1981, 3rd ed., p. C-16.
5. Becker, H. B. Ph.D. Thesis, University of Newcastle, Australia, 1982.
6. Goetz, G. J.; Nsakala, N. Y.; Borio, R. W. J. Eng. Power, 1979, 101, pp. 607-619.
7. Richter, W.; and Heap, M. P. Western States Section, The Combustion Institute, 1981 Spring Meeting, 1981, Paper 81-17.
8. Richter, W.; Heap, M. P., 1981 ASME Winter Annual Meeting, 1981, Paper 81 WA/HT27.
9. Richter, W.; Payne, R.; Thielen, W. Proc. 1st Annual Pittsburgh Coal Conference, 1984, Paper No. 86, pp. 592-611.



10. England, G. C.; Kwan, Y.; Richter, W.; Fujimura, K. 4th Int. Symp. on Coal Slurry Combustion, PETC, 1982, 3.
11. Payne, R.; Chen, S. L.; Richter, W. Proc. 5th Int. Symp. on Coal Slurry Combustion and Technology, PETC, 1983 Session VII.
12. Richter, W.; Pohl, J. H. Proc. 7th Int. Symp. on Coal Slurry Fuels Preparation and Utilization, PETC, 1985, Paper No. 12, pp. 443-462.

RECEIVED August 30, 1985

## Prediction of Slagging and Fouling Tendencies of European Lignites by New Statistical and Experimental Methods

Werner Altmann

Technical University Dresden, 8027 Dresden, German Democratic Republic

This paper reports the development of new statistical and experimental techniques to predict slagging and fouling of brown coal. The new statistical correlation relates the observed performance of brown coals in combustors to modified ash composition. The ash composition is modified by removing  $\text{SiO}_2$ , which does not contribute to slagging and fouling when present as quartz, and modifying the effect of iron and sulfur on ash composition. A pilot scale cyclone combustor is introduced to extend to larger particles and greater residence times, the conditions at which fouling and slagging can be experimentally observed.

Brown coal was already an important energy resource in Europe at the beginning of the 20th century. In spite of the many problems in process technology, the usable reserves of this low-value energy fuel (Figure 1) will surely be an indispensable basis of supply for another fifty years.

In addition to the traditional use in generation of electric power in large stations, application of brown coal has been extended to replace fuel oil in small heat generators and process furnaces.

After the reserves of high quality coal have been exhausted, it will be necessary to use brown coals with more impurities. Extremely high-ash coals with high alkaline contents must be used in some countries even though the performance of such fuels could not be controlled with the combustion technologies available in the past.

In addition to ignition problems, control of slagging and fouling, which depends on the properties of the mineral ash substance, is required.

These problems indicate the pressing need for methods to predict the deposition properties of solid fuels. This is required for operation and control of existing plants. However, this information is also significant in the planning of new plants to use difficult fuels or fuels on which little experience is available.

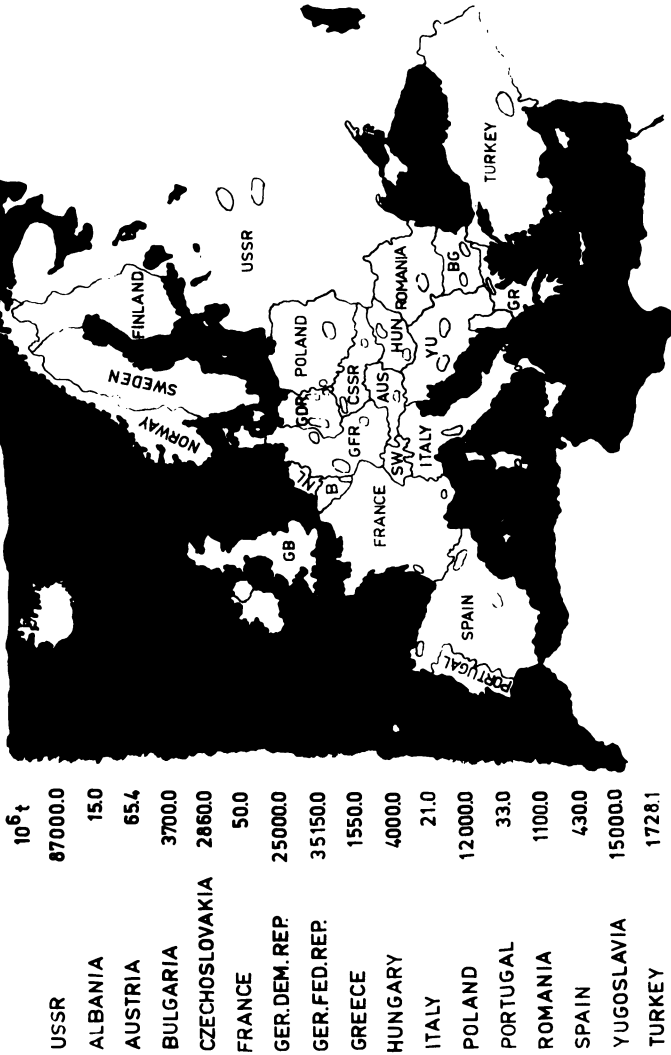


Figure 1. Lignite (Brown Coal) proved and recoverable reserves in Europe.

The information will also allow decisions to be made on whether to use:

- suspension firing
- fluid-bed firing or
- low-temperature combustion reactors

The slagging and fouling tendencies of coals largely differ according to the deposit but also differ within the deposit because of widely varying coal composition. Ash properties are so complex that evaluation of coal performance is extremely difficult. The performance of coals in furnaces are further complicated by the processes which control deposition on heat transfer surfaces in boilers. Based on these complications, we must neither deceive ourselves as to the possibility of reliable estimates nor deny the possibility of making a useful estimate of the performance of brown coal in boilers.

### Statistical Predictions

The known experimental methods include the determination of the characteristic temperatures for ash softening and melting using the heating microscope according to Radmacher (2) or use of ash viscosity-meters according to Gibbs (3) or Orgres (4). All are far from conditions representing processes in utility boilers. The estimate of ash performance by such methods has often been misleading and is uncertain.

Important performance characteristics of brown coal ash; however, have been observed in the temperature-dependent micro-changes in ash specimen using the Leitz equipment by Lustigova (5).

Ash oxide analyses are available and provide a wide base of data on coal ashes. Attig and Duzy (6) recommend calculation of a slagging index to increase the information available from such analyses. The index is based on the ratio between basic mineral components,  $Fe_2O_3$ ,  $CaO$ ,  $MgO$  and of alkalis to the acidic components  $SiO_2$ ,  $Al_2O_3$  and  $TiO_2$  and the sulfur content of the fuel. This method is closely related to the Teune index from 1912 which is used by many manufacturers and operators but is unsatisfactory in a great number of applications. Winegartner and Rhodes (7) made comprehensive analyses and investigated the relations between the chemical ash composition and the ash melting temperature measured in the laboratory. This activity resulted in the ability to predict melting points of ash, but these are not applicable to predict ash sintering or slagging of combustion chambers with dry ash removal.

In contrast to this, the course adopted by Garner (8) must be emphasized. The intensity of deposition for a great variety of Australian brown coals has been determined at conditions close to those in boilers using an experimental combustion chamber of 20 kg/h. The regression analyses using these test data offered valuable information on the different influences of elements contained in the ash. Transformation of the results is not yet fully satisfactory because the slagging-promoting aspects of fuel sulfur were not considered and the complicated processes are insufficiently represented by a simple linear regression. This analysis used oxide analyses comprising all ash components whereas only certain elements may be relevant to the slagging process. The investigations by

Schneider (9) with brown coals of different origin in a drop tube furnace similar to that used by Field clearly showed the influence of different mineral substances on ash deposition. Sand particles (Figure 2) maintained their former shape in combustion or showed changes only at their edges while other ash constituents fused together into dark brown or glassy-clear spheres.

This leads to the conclusion that the  $\text{SiO}_2$  content will not react with other ash constituents but will only alter the portion of slag-relevant constituents for coals in which  $\text{SiO}_2$  appears largely as quartz. The microspheres generated by fusion primarily determine the adhesion process in the liquid state and have a chemical composition different from the average ash analysis.

Obtaining useful information on the slagging tendency of solid fuels based on the above mentioned knowledge requires three prerequisites:

1. Availability of empirical data on the behavior of coals to be characterized from working plants or model combustion systems similar to those used in practical operation
2. Elimination of the  $\text{SiO}_2$  share of the ash which does not participate in the slagging process.
3. Finding significant parameters for ash properties which predict performance.

The first demand was met by exclusion of reference to quantities measured in the laboratory (heating microscope temperatures, viscosity measurements). These values were replaced by evaluation of the performance in operating boilers and results from pilot scale combustors. The tendencies used in this paper have been determined predominantly from the different behavior of coals from various mines fired in the same steam generators based on the opinions of experts.

The two other demands can be satisfied by laborious and analogous comparisons between oxide analyses and the coal properties found by experience or experiments which affect performance.

Purely statistical means (Figure 3) without consideration of chemical dependences first permitted two groups of ashes with a high risk of slagging to be identified:

- Coals with high  $\text{Al}_2\text{O}_3$  and low  $\text{SO}_3$  contents
- Coals with high  $\text{CaO}$  and high  $\text{SO}_3$  contents

The first class yields useful correlations by converting the oxide analysis to the mineral substance without  $\text{SiO}_2$ . The second class yields useful values when the relation  $\text{SiO}_2 = 1.8 \text{ Fe}_2\text{O}_3$  is used.

The ash types are established by a parameter  $\int \text{SO}_3$ ; group 1 when it is less than 0.06 and to group 3 when it is higher than 0.2. The transition range, group 2, can be described by  $\text{SiO}_2 = Y \cdot \text{Fe}_2\text{O}_3$ ; when the factor  $Y$  logarithmically increases with the parameter  $\int \text{SO}_3$ . This is also the range of uncertainty.

Regression analyses of ash oxide analyses converted with this relationship did not result in a useful correlation when the weight percentages of ash components were applied exclusively. Realistic dependencies could be found when an iron oxide parameter  $\int \text{Fe}$  was introduced in combination with the influence of the fuel sulfur: the sulfur influence decreased at high sulfur concentrations. There is a statistical relationship for a slagging tendency called  $f_g$  which refers to a predicate interval of

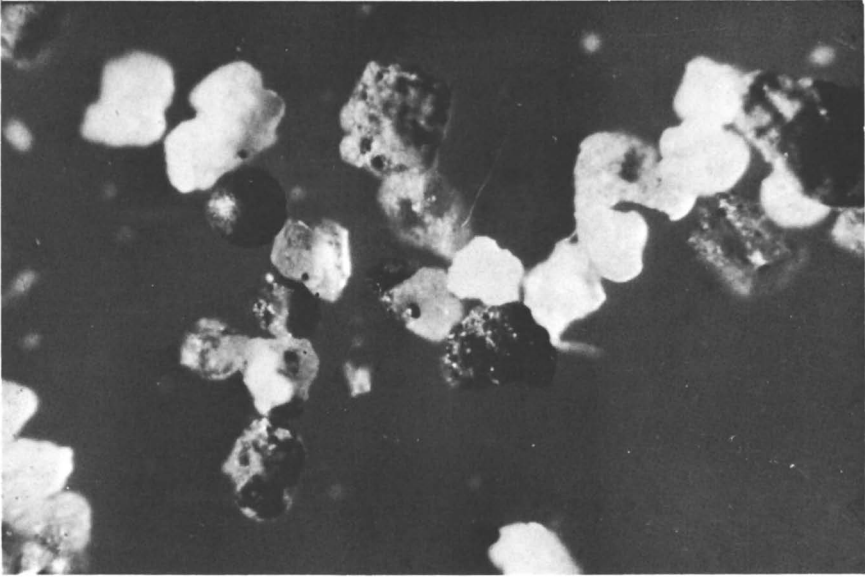
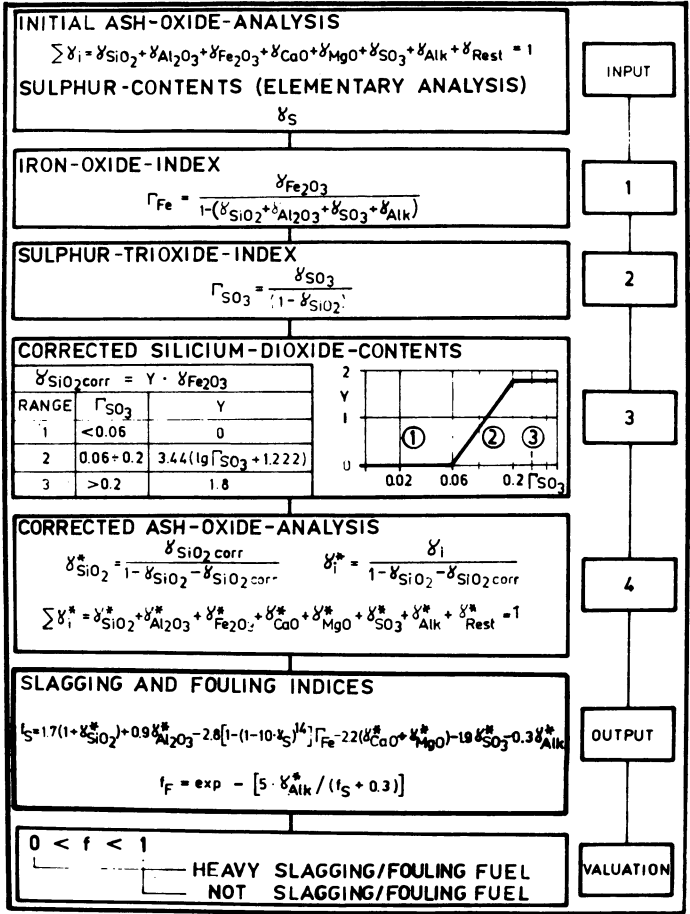
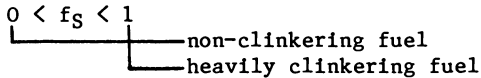


**Figure 2.** Differences in mineral matter constituents subjected to a combustion field.



Note:  $\gamma$  = Weight Fraction Ash

Figure 3. Statistical prediction of slagging and fouling behavior of solid fuels.



An exponential expression with the quotient of alkaline contents and slagging coefficient  $f_s$  is introduced for the extension of the evaluation to fouling of brown coals on heat exchanger surfaces in the temperature range of  $\vartheta < 1000^\circ\text{C}$  after Lautenschlager (10) as well as Below and Rundgin (11), but predominantly after interpretation of operational experience with salt coals (Kluge (12)).

The example of application of the statistical prediction method represented in Figure 4 contains a Czechoslovakian brown coal of group 1 which experience has shown to be a particularly vicious fouling coal and a GDR brown coal of group 3 which tends toward behavior of a salt coal but whose operational behavior, while complicated, can be controlled. The values calculated for  $f_s$  and  $f_p$  coincide with practical experience while the parameter  $R_s$  indicates that the Czechoslovakian coal is harmless whereas the GDR coal is characterized as uncontrollable by available technologies.

The ash analyses and estimated parameter shown in Table 1 refer to brown coals: from the GDR, Hungary, Poland, Czechoslovakia, FRG, Bulgaria, USSR, Yugoslavia, Austria, Spain and Turkey (13-17) and show good prediction of expected performance. The survey demonstrates that the number of brown coals without performance problems is distinctly smaller than those with performance problems. Calculation of the slagging tendency is highly sensitive to changes in the analytical data. Thus, analyses used should not be averages but should be individual analyses as a matter of principle. Values calculated for some cases indicate  $f_s < 0$  or  $f_s > 1$ . This indicates that there are even other components in addition to sulfur which act non-linearly at high concentrations. Reliability of the statistical method can be improved successively as more and more data are accumulated and used to interpret the correlation between the operational behavior of fuels and their ash analyses. As in all empirical methods, the relations must be repeatedly updated, and corrections must not be interpreted as necessarily proving uncertainty.

### Experimental Methods

Interpretation methods based on ash oxide analyses should always be understood as makeshift solutions to which experimental methods are preferred when they are similar to practical conditions. One example of the latter methods should be emphasized. It is a micro-method resulting from the cooperation between Dresden and Budapest (Schneider (18), Boross, Horvath, Voros (19)). A reaction pipe similar to that of Field (Figure 5) is used to observe the formation of deposits quantitatively on cooled or non-cooled heating surfaces which are subjected to the mineral substance of coal particles burnt completely or partially in the equipment at defined conditions (temperature, grain size and gas composition). The selected reaction time for these particles permits the degree of burn-out to be varied. This combustion reactor provides a method to avoid the great effort required by large scale test combustion chambers.



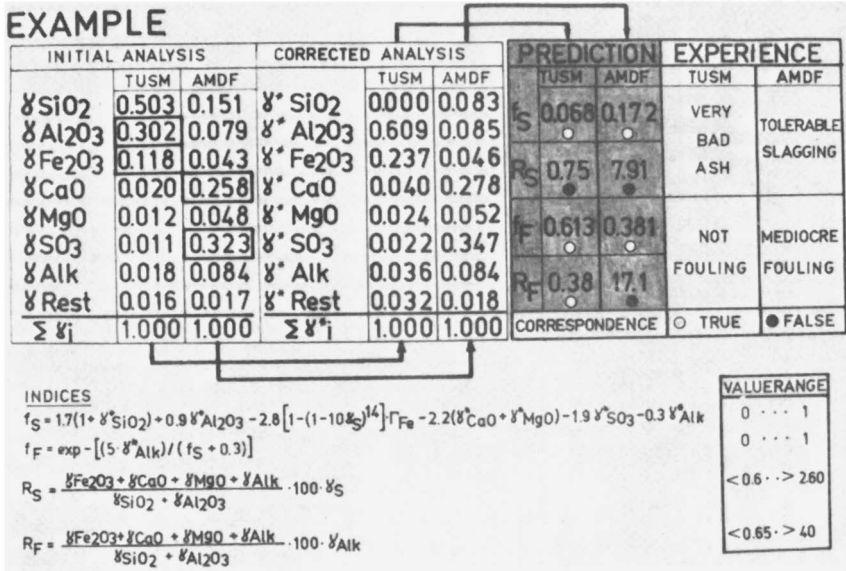


Figure 4. Comparison of predicted and observed performance.

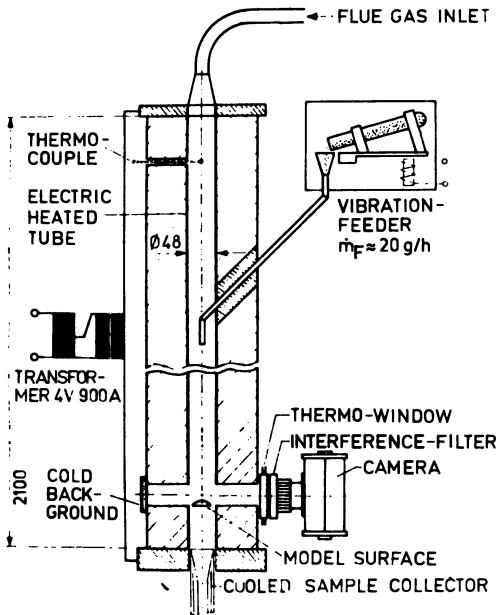


Figure 5. Field combustion tube furnace.

Table I. Calculated Parameters of Brown Coals

ORIGIN	GERMAN DEMOCRATIC REPUBLIC										HUNGARY					POLAND			CSSR		AUSTRIA	
	OBSL	NDLS	BIFD	LEPZ	PROF	MSBO	EGSM	NOGD	VISA	AJKA	OROS	JOWN	TURW	TUSM	LEDY	OBSL	FODF					
kg/kg	1	2	3	4	5	6	7	8	9	10	11	12	13	14	15	16	17					
$\delta$ SiO <sub>2</sub>	0.363	0.576	0.229	0.432	0.570	0.119	0.407	0.504	0.563	0.204	0.479	0.377	0.520	0.501	0.543	0.341	0.461					
$\delta$ Al <sub>2</sub> O <sub>3</sub>	0.208	0.058	0.066	0.068	0.034	0.030	0.039	0.191	0.155	0.139	0.261	0.074	0.358	0.291	0.318	0.385	0.230					
$\delta$ Fe <sub>2</sub> O <sub>3</sub>	0.124	0.149	0.142	0.081	0.038	0.069	0.064	0.089	0.071	0.070	0.086	0.085	0.050	0.126	0.059	0.067	0.172					
$\delta$ CaO	0.129	0.097	0.233	0.151	0.157	0.152	0.083	0.089	0.077	0.319	0.080	0.193	0.009	0.037	0.028	0.082	0.090					
$\delta$ MgO	0.020	0.048	0.019	0.038	0.020	0.022	0.021	0.021	0.022	0.036	0.017	0.039	0.013	0.011	0.012	0.019	0.012					
$\delta$ SO <sub>3</sub>	0.125	0.085	0.293	0.201	0.134	0.315	0.185	0.076	0.083	0.192	0.048	0.230	0.007	0.016	0.009	0.090	0.076					
$\delta$ Alk	0.002	0.003	0.005	0.012	0.005	0.220	0.201	0.027	0.014	0.030	0.020	0.001	0.039	0.018	0.031	0.016	0.009					
$\delta$ Rest	0.029	0.004	0.022	0.017	0.042	0.073	0.000	0.003	0.015	0.010	0.009	0.001	0.004	0.000	0.000	0.000	0.000					
$\Sigma \delta$	1.000	1.000	1.000	1.000	1.000	1.000	1.000	1.000	1.000	1.000	1.000	1.000	1.000	1.000	1.000	1.000	1.000					
$\delta$ S	0.010	0.011	0.039	0.018	0.018	0.042	0.037	0.040	0.030	0.032	0.044	0.017	0.009	0.038	0.012	0.015	0.075					
$\Gamma$ Fe	0.411	0.500	0.349	0.282	0.148	0.218	0.381	0.441	0.384	0.161	0.448	0.267	0.656	0.724	0.596	0.399	0.628					
$\Gamma$ SO <sub>3</sub>	0.196	0.153	0.380	0.354	0.312	0.358	0.312	0.153	0.190	0.241	0.092	0.369	0.015	0.032	0.020	0.137	0.048					
$\delta$ SiO <sub>2</sub> corr	0.219	0.209	0.256	0.146	0.068	0.124	0.115	0.125	0.122	0.126	0.055	0.153	0.000	0.000	0.000	0.000	0.000					
$\delta$ SiO <sub>2</sub>	0.256	0.330	0.254	0.205	0.137	0.123	0.163	0.201	0.218	0.137	0.096	0.197	0.000	0.000	0.000	0.112	0.000					
$\delta$ Al <sub>2</sub> O <sub>3</sub>	0.243	0.092	0.065	0.095	0.068	0.030	0.055	0.308	0.277	0.151	0.452	0.095	0.746	0.583	0.696	0.518	0.427					
$\delta$ Fe <sub>2</sub> O <sub>3</sub>	0.145	0.235	0.141	0.114	0.076	0.069	0.090	0.143	0.127	0.078	0.149	0.110	0.104	0.253	0.129	0.090	0.318					
$\delta$ CaO	0.151	0.153	0.231	0.211	0.316	0.151	0.117	0.143	0.138	0.345	0.139	0.250	0.019	0.074	0.061	0.111	0.167					
$\delta$ MgO	0.023	0.076	0.019	0.053	0.040	0.022	0.030	0.034	0.039	0.039	0.030	0.050	0.027	0.022	0.026	0.026	0.022					
$\delta$ SO <sub>3</sub>	0.146	0.103	0.290	0.281	0.269	0.313	0.261	0.122	0.149	0.208	0.083	0.296	0.015	0.032	0.020	0.121	0.048					
$\delta$ Alk	0.002	0.005	0.005	0.017	0.010	0.219	0.284	0.044	0.025	0.033	0.035	0.001	0.081	0.036	0.068	0.022	0.017					
$\delta$ Rest	0.034	0.006	0.021	0.024	0.084	0.073	0.000	0.005	0.027	0.011	0.016	0.001	0.008	0.000	0.000	0.000	0.000					
$\Sigma \delta$	1.000	1.000	1.000	1.000	1.000	1.000	1.000	1.000	1.000	1.000	1.000	1.000	1.000	1.000	1.000	1.000	1.000					
$\delta$ S	0.806	0.517	0.112	0.274	0.308	0.285	0.057	0.451	0.572	0.370	0.476	0.219	0.867	0.607	0.816	0.793						
$\delta$ F	0.991	0.970	0.941	0.862	0.921	0.154	0.019	0.746	0.867	0.782	0.798	0.990	0.707	0.549	0.708	0.906	0.925					

ORIGIN	GER. FED. REP.						YUGOSLAVIA						USSR			BULGARIA		SPAIN		TUR-KEY
	HESS	HELM	RHLD	RHLD	RHLD	RHLD	KOLU	KOSO	RASP	DJUR	PLOM	NASA	IBERI	ZAPN	TSHU	PUEN				
	18	19	20	21	22	23	24	25	26	27	28	29	30	31	32	33				
kg/kg																				
$\delta$ SiO <sub>2</sub>	0.342	0.029	0.362	0.530	0.161	0.422	0.262	0.103	0.387	0.043	0.300	0.150	0.237	0.574	0.450	0.644			0.425	
$\delta$ Al <sub>2</sub> O <sub>3</sub>	0.150	0.035	0.064	0.203	0.061	0.185	0.091	0.071	0.258	0.044	0.130	0.118	0.119	0.315	0.314	0.231			0.221	
$\delta$ Fe <sub>2</sub> O <sub>3</sub>	0.222	0.272	0.073	0.063	0.060	0.183	0.056	0.072	0.135	0.040	0.180	0.060	0.133	0.052	0.115	0.074			0.153	
$\delta$ CaO	0.112	0.286	0.260	0.070	0.257	0.110	0.405	0.410	0.065	0.437	0.330	0.582	0.256	0.025	0.051	0.015			0.061	
$\delta$ MgO	0.014	0.022	0.057	0.027	0.144	0.014	0.059	0.031	0.030	0.045	0.050	0.070	0.018	0.014	0.013	0.012			0.036	
$\delta$ SO <sub>3</sub>	0.136	0.340	0.160	0.087	0.261	0.081	0.109	0.295	0.077	0.362	0.000	0.000	0.237	0.020	0.038	0.002			0.051	
$\delta$ Alk	0.007	0.005	0.004	0.020	0.056	0.005	0.018	0.009	0.009	0.029	0.010	0.020	0.000	0.000	0.017	0.022			0.053	
$\delta$ Rest	0.017	0.011	0.000	0.000	0.000	0.000	0.000	0.009	0.039	0.000	0.000	0.000	0.000	0.000	0.002	0.000			0.000	
$\Sigma \delta_i$	1.000	1.000	1.000	1.000	1.000	1.000	1.000	1.000	1.000	1.000	1.000	1.000	1.000	1.000	1.000	1.000			1.000	
$\delta$ S	0.042	0.020	0.007	0.010	0.008	0.013	0.008	0.021	0.017	0.030	0.007	0.003	0.046	0.010	0.065	0.010			0.020	
fFe	0.608	0.460	0.187	0.394	0.131	0.596	0.108	0.138	0.502	0.077	0.321	0.084	0.327	0.571	0.635	0.733			0.612	
fSO <sub>3</sub>	0.207	0.350	0.259	0.185	0.311	0.140	0.148	0.329	0.126	0.378	0.000	0.000	0.311	0.047	0.068	0.006			0.089	
$\delta$ SiO <sub>2</sub> corr	0.400	0.490	0.131	0.106	0.108	0.234	0.076	0.130	0.150	0.072	0.000	0.000	0.239	0.000	0.024	0.000			0.090	
$\delta$ SiO <sub>2</sub>	0.377	0.335	0.175	0.184	0.114	0.288	0.093	0.127	0.197	0.070	0.000	0.000	0.238	0.000	0.042	0.000			0.135	
$\delta$ Al <sub>2</sub> O <sub>3</sub>	0.142	0.024	0.086	0.352	0.064	0.228	0.112	0.069	0.338	0.043	0.186	0.139	0.119	0.739	0.548	0.648			0.332	
$\delta$ Fe <sub>2</sub> O <sub>3</sub>	0.210	0.186	0.098	0.109	0.063	0.225	0.069	0.070	0.177	0.039	0.257	0.071	0.133	0.122	0.200	0.208			0.230	
$\delta$ CaO	0.106	0.196	0.346	0.122	0.271	0.136	0.437	0.399	0.085	0.424	0.472	0.684	0.255	0.059	0.089	0.042			0.092	
$\delta$ MgO	0.013	0.015	0.076	0.047	0.152	0.017	0.073	0.030	0.039	0.044	0.071	0.082	0.018	0.033	0.023	0.034			0.054	
$\delta$ SO <sub>3</sub>	0.129	0.233	0.214	0.151	0.277	0.100	0.134	0.287	0.101	0.352	0.000	0.000	0.237	0.047	0.066	0.006			0.077	
$\delta$ Alk	0.007	0.003	0.005	0.035	0.059	0.006	0.022	0.009	0.012	0.028	0.014	0.024	0.000	0.000	0.030	0.062			0.080	
$\delta$ Rest	0.016	0.008	0.000	0.000	0.000	0.000	0.000	0.009	0.051	0.000	0.000	0.000	0.000	0.000	0.000	0.000			0.000	
$\Sigma \delta_i$	1.000	1.000	1.000	1.000	1.000	1.000	1.000	1.000	1.000	1.000	1.000	1.000	1.000	1.000	1.000	1.000			1.000	
fS	0.258	0.153	0.404	0.901	0.224	0.435	0.310	0.114	0.566	<0	0.115	0.051	0.246	0.841	0.104	0.503			0.099	
fF	0.939	0.967	0.965	0.864	0.570	0.960	0.835	0.887	0.933	0.627	0.855	0.710	-	-	0.690	0.680			0.367	

Illuminating results are possible even when only small quantities (20 - 40 g per test) of substances may be available from prospect sampling in the exploration of new deposits. At the same time, this test equipment offers important information on the mechanism of deposit formation. Adherence of ash particles to the heating surfaces is a maximum when impact occurs after a combustion path in which the end of the burn-out of volatile components produces the highest temperature of coal grains over the surrounding gas atmosphere. Weser (20) improved the Field tube by installing thermophotographic equipment for measurement of particle temperature prior to deposition. Temperature differences between solid matter and flue gas of up to 400 K were found using this equipment.

Use of the Field tube for determining the performance of coals is limited by the short residence time of 0.3 seconds (2.1 m) and the inability to use particles larger than 0.14 mm. This limits the extent of particle size changes and the structure of the mineral substance relative to pulverized fuels or coarse-crushed brown coals used in utility boilers. This difference probably has an effect on the formation of deposits.

A newly introduced model cyclone firing unit (Figure 6) permits a longer retention time in the centrifugal field so that normal pulverized fuels and granular materials with maximum grain diameter of 3 mm can be burnt.

A quartz tube with diameter of 100 mm permits direct observation of the process with normal coal. The cyclone furnace produces steady combustion at gas temperature of 700°C but can also be extended to a temperature level of more than 1000°C. Combustion of salt coals is difficult to observe because the alkalines vaporize from the fuel and condense on the colder quartz tube wall to form an opaque layer. This problem is partially overcome by inserting a probe which measures gas and wall temperature and allows the slagging process to be determined as a function of temperature by weighing the deposit. Measurement of deposit hardness supplies additional information on the character of the clinker formed. The cyclone separator behind the reactor allows an analysis of structural changes which occur in the finest grain. The test results obtained indicate the cyclone reactor can be improved by automation (for easier operation) and by standardization to result in a piece of equipment capable of evaluating slagging tendencies.

### Boiler Processes

Operation with the experimental furnaces has shown that the material properties of coal or ash are only part of the clinkering processes. The geometric shape of the flame, reaction characteristics and heat transmission processes near the wall of the corresponding heating surfaces and on individual particles are coupled with melting, vaporization and condensation processes of mineral substance to form deposits.

The parameters shown in Figure 7 influence the mechanism of deposit formation and must be considered in the evaluation of processes expected of reducing furnace availability. The processes must be considered to be directly dependent on the properties of the fuel. The major influences on deposits in pulverized fuel firings

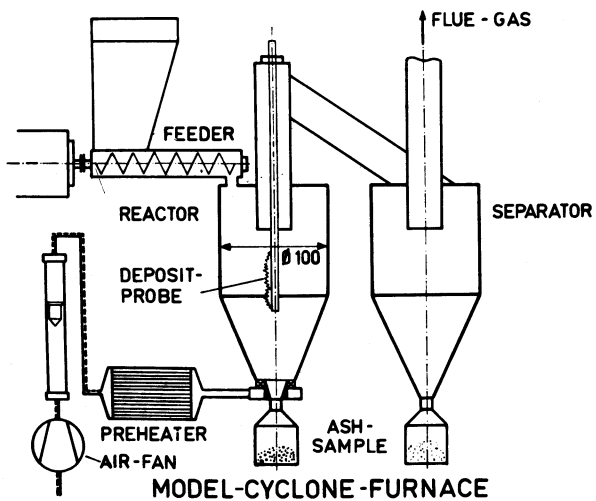


Figure 6. Model Cyclone furnace.



result from the aerodynamical properties of the flame jets, their influences on one another and their spatial positions in the combustion chamber.

Numeric calculation of three-dimensional flows in boilers are still difficult, but non-isothermal combustion chamber models operated with a test fuel of acetylene and nitrogen (Altmann (21)) can offer qualitative information on conditions leading to slagging and fouling. Large temperature fluctuations and profiles affect overheating and clinkering; jet deflection to the wall in combination with high temperatures of reacting pulverized fuel particles can initiate deposition in the combustion chamber; intense turbulence near the wall inhibits particle cooling below the critical adhesion temperature.

Information which can be derived from experiments on the thermal behavior of the ash-mineral substance and on the actual mechanism of deposits is, despite all imperfections, suitable for determining the applicability and application limits of fuels and selection of alternative combustion systems and their design.

### Conclusion

This paper developed new statistical methods for predicting slagging and fouling of brown coals. The method uses an empirical relationship between modified ash compositions and observations of slagging and fouling performance in boilers and pilot scale combustors. The ash composition is modified by calculating the ash constituents on a SiO<sub>2</sub> free basis; quartz is removed from the analysis since it does not participate in slagging or fouling. The value of quartz used to correct this ash composition is derived using a parameter which is a function of the sulfur and iron content of the ash. The performance estimated using the new indices agreed much better with observed boiler performance than that estimated from available indices. However, indices remain empirical and predicted and observed performance may disagree.

Pilot scale combustion techniques were also used to estimate the performance of brown coals. The Field tube is limited for estimating performance of brown coals and was supplemented by a cyclone combustor. The cyclone combustor allows combustion of the larger particles with longer residence times typical of brown-coal-fired boilers.

### Literature Cited

1. 11th World Energy Conference 1980, Survey of Energy Resources Part A.
2. Radmacher, W. *Brennst.-Chemie*, 1949 30, Nr. 21/22, 377-384.
3. Gibb, W. H. The Slagging Characteristics of Coal Ashes by Viscosity and Sintering Measurements, VGB-Konferenz "Rauchgasseitige Korrosionen und Verschmutzungen in Wärmekraftwerken" Essen, FRG 1977.
4. Zalkind, I. Ja.; Trojankin, Ja. W. *Feuerbeständige Stoffe und Schlacken in der Energietechnik* Moskow, USSR, 1953.

5. Lustigova, M. Tavitelnost popela a tvorba nanosu, Vyuzivani Popelnatych Hnedych Uhlí V Energetice Karlovy Varg 1978, 37-44.
6. Attig, R. C., Duzy, A. F. Coal Ash Deposition Studies and Application to Boiler Design, Amer. Power Conf., 1969, 290.
7. Winegartner, E. C.; Rhodes, B. T. J. of Engineering for Power July 1975, 395-436.
8. Garner, L. J. J. Inst. Fuel 40, 1967 107-111.
9. Schneider, W. Der Einsatz des Verbrennungs-rohres nach FIELD zur Ermittlung der Verschlackungs- und Ansatz- neigung von Braunkohlenaschen in Staubfeuerungen, Wiss.Z.TU Dresden 30, 1981, 6, 15-19.
10. Lautenschlager, F. W. Braunkohle, 1976, 6, 206-214.
11. Below, S. Ju.; Rundgin, Ju. A. Prognose der Verschmutzungsneigung fester Brennstoffe an Dampferzeugerheizflächen mit festen Ablagerungen, Tagungsbericht Tallinn, 1980, Sektion 1 Teil A, 145-150.
12. Kluge, K. H., Betriebsverhalten von Dampferzeugern für Salzkohle, in preparation.
13. Pomrehn, H.; Rodegast, M. Untersuchungsmethoden zur Charakterisierung von Kohlen I. Analysen von Kohlen und Aschen AdW-Informationen aus Wissenschaft und Technik Berlin 1981.
14. Jahns, H.; Schinkel, W., Energietechnik 1979, 29, 12, 464-469.
15. Beising, R., Die Minerale der niederrheinischen Braunkohle und ihr Verhalten bei der Verbrennung in Kraftwerken, N. Jahrbuch f. Mineralogie, Abhandlungen, 1971, 117, 96-115.
16. Ots, A. A. The Processes in Steam Generators in Burning Oil Shale and Kansk-Achinsk Basin Coals, Moscow "Energia" 1977.
17. Savic, D.; Opik, I. Fouling and Corrosion in Steam Generators, Beograd 1980.
18. Schneider, W. Untersuchungen zur Bewertung und Vorhersage des Verschlackungsverhaltens von Brennstoffen in Dampferzeuger-Feuerungen, Energietechnik, 1983, 33, 7, 254-256.
19. Boross, L.; Horvath, F.; Voros, F. Reaktionskinetik und Verschlackungseigenschaften von minderwertigen Braunkohlen bei Kohlenstaubfeuerung, Forschungsbericht VEIKI Budapest 1979.
20. Weser, A. Fotoradiografie und Thermografie als MeBverfahren in der Verbrennungsforschung, Energietechnik 1984 (in preparation).
21. Altmann, W. Nichtisotherme Modellierung von Flammen und Flammensystemen in Feuerraumen (in preparation).



## Mineral Matter Catalysis of Coal Conversion

Thomas D. Padrick and Barry Granoff

Sandia National Laboratories, Albuquerque, NM 87185

Since the 1920s, a variety of studies have investigated the effects of mineral matter on coal conversion processes. This interest accelerated greatly about 10 years ago. We have followed the development of this field from those investigations that screened the effects of various mineral types on coal conversion processes to those investigations that studied the detailed mechanism of a specific mineral on either coal gasification or coal liquefaction. As an outgrowth of this field of study, we have witnessed the development of both catalytic coal gasification and slurry phase catalytic coal liquefactions. We will review the field of mineral matter effects on coal processing and discuss the impact on the coal conversion industry.

In general, a catalyst consists of a support (alumina, silica, silica-alumina), an active catalytic metal and, in some cases, a promoter (1). The support is usually a high-surface-area (up to several hundred square meters per gram) porous solid. Gamma alumina, for example, has a surface area of 100-300 m<sup>2</sup>/g. The support is not necessarily inert and may play a significant role in chemisorption and oxidation state control. The active metal, which may be deposited by several techniques, is highly dispersed on the support. The promoter is an additive that can increase the activity of the metal and/or maintain the physical characteristics of the support.

A typical example is Co-Mo/Al<sub>2</sub>O<sub>3</sub>, which is used as a hydrodesulfurization catalyst. In this case, alumina is the support, Mo is the catalytically active metal and Co is the promoter. In actual practice, these catalysts must first be sulfided to convert the metals to metal sulfides. It is believed that these metal sulfides are the catalytically active species for hydrodesulfurization (2).

The need for clean liquid fuels from coal has led to the development of catalysts that had originally been used for

petroleum refining. In direct coal liquefaction, pulverized coal is mixed with a coal-derived solvent and treated with hydrogen at high temperatures (400–450°C) and pressures (1500–3000 psi) (3). At some stage in the conversion process, hydrotreating catalysts are used to improve the distillate yield, increase the hydrogen content and reduce the heteroatom (S, N, O) content of the liquid products.

Since coals contain aluminosilicates (clays), metal sulfides (e.g., pyrite) and numerous metal-containing species (4), it would seem reasonable to propose that a naturally occurring catalyst system exists within the inherent mineral matter in coal. This concept has been explored since the 1920's and several studies have focused on the catalytic effects of mineral matter on coal conversion (5). In recent years, we have witnessed an increase in the level of coal research and the development of new coal utilization processes. In parallel with this activity, there have been reports on the effects of coal minerals on coal liquefaction, coal gasification, in-situ coal gasification, and other areas of coal utilization (5–8). The terms minerals, mineral matter, and ash will be used synonymously. An attempt will not be made to review the effects of all classes of minerals, but will only consider those minerals which have shown a large effect on coal conversion processes.

### Coal Liquefaction

The Germans used coal liquefaction on a commercial scale from 1930 to the end of the second World War. They found that a catalyst could enhance liquid yields and help remove heteroatoms. The Bergius process used an iron oxide-aluminum catalyst at a 2–3% by coal weight concentration.

In recent years, it has been realized that mineral matter plays an important role in coal liquefaction (9–11), similar to the role of the added catalyst in the Bergius process. Several experimental techniques have been used to study the effects of minerals on coal liquefaction and to identify the specific catalytic phase (12). Most studies (12–14) strongly imply that the iron sulfides are the most active species, and the other minerals appear to have little effect on enhancement of liquid yield or quality.

The specific role of pyrite ( $\text{FeS}_2$ ) as a catalyst has been under investigation since pyrite was identified as the most active inherent mineral for coal liquefaction. Under liquefaction conditions,  $\text{FeS}_2$  is transformed into a nonstoichiometric iron sulfide,  $\text{Fe}_{1-x}\text{S}$  ( $0 < x < 0.125$ ). Thomas *et al.* (15) studied the kinetics of this decomposition under coal liquefaction conditions, and concluded that the catalytic activity of  $\text{FeS}_2$  is associated with radical initiation resulting from the pyrite-pyrrhotite transformation.

Several studies have investigated the possibility that defects in the pyrrhotite structure provide the sites for catalyst activity. A recent study (16) found a linear correlation between the conversion to benzene or THF solubles and the atomic percent iron in the liquefaction residues. Montano *et al.* (17) used

in situ Mössbauer spectroscopy to study transformation of  $\text{FeS}_2$  to  $\text{Fe}_{1-x}\text{S}$ . They observed a large pyrrhotite surface area at the reaction temperature (above  $350^\circ\text{C}$ ).

Stohl and Granoff (18) investigated the effects of pyrite particle sizes, pyrite defects and surface areas on coal liquefaction. They observed no effect due to surface area and concluded that the observed particle size effect was due to diffusional limitations in the transformation of pyrite to pyrrhotite.

While many studies indicate that pyrrhotites are probably involved in the liquefaction process, the exact mechanism by which pyrrhotite catalyzes the conversion of coal to oil is not clear. Based on the works of Thomas *et al.* (15) and Derbyshire *et al.*, (13) one can suggest that a possible role of pyrrhotite is as a hydrogenation catalyst. However, more work is necessary on the surface properties of the pyrrhotites and the interaction with model compounds before a definite catalytic mechanism can be proposed.

Pyrite has been shown to catalyze the hydrogenation of quinoline to tetrahydroquinoline (THQ) at  $325^\circ\text{C}$  and a 30 minute residence time (19). It has been known that THQ is a good hydrogen donor solvent for coal liquefaction (13). In experiments with Kentucky coal and quinoline, it was found that pyrite was required to maintain a sufficient concentration of THQ and prevent retrogressive reactions (19). It appears, therefore, that pyrite catalyzes the in situ regeneration of hydrogen donors, and allows more efficient hydrogen uptake from the gas phase to the solvent at lower temperatures than would be possible in the absence of pyrite.

It might be expected that coals high in pyrite (e.g., bituminous) would be more reactive than coals that have lower pyrite contents (e.g., subbituminous and lignites). Twenty coals of various ranks were tested by Gulf under SRC-II process conditions: 30 wt. percent coal,  $440\text{--}465^\circ\text{C}$ , 1800–2250 psia  $\text{H}_2$ , one-hr residence time. Coals which processed well had pyritic sulfur or iron contents greater than 1.5%, and were generally Eastern and Interior Province bituminous coals (20).  $\text{C}_5^+$  oil yields ( $875^\circ\text{F}$ ) ranged from 30–35% for coals with pyritic sulfur contents of 1.0 to 1.5% to 40–45% for coals with pyritic sulfur contents of 2.0 to 3.0%.

For these coals, addition of pyrite enhanced oil yields via conversion of asphaltenes and preasphaltenes, but did not affect the overall conversion of the coal to pyridine-solubles. Addition of pyrite to bituminous coals deficient in pyritic sulfur or iron increased oil yields to levels comparable to coals with naturally high concentrations of pyrite. For Ayrshire coal (Indiana VI) with 1.1% pyritic sulfur, the oil yield was 31%. Addition of 2.7% pyrite (based on coal) increased the oil yield to 50%.

The effect of pyrite removal was also clearly demonstrated (20). For Burning Star coal (Illinois No. 6), the oil yield for run-of-mine coal (4.8% pyrite) was 47%. Conventional cleaning to 1.5% pyrite resulted in an oil yield of 42%. Deep cleaning to 0.5% pyrite followed by addition of 5.3% pyrite to the clean coal produced an oil yield of 51%, even though the operating pressure (1800 psi) was lower than in the other runs (2250 psi).

For subbituminous coals, which are generally lower in pyrite than bituminous coals, it was impossible to achieve steady-state runs under SRC-II processing conditions without the addition of pyrite or other catalyst. For Belle Ayr coal (Wyodak-Anderson, WY), the pyritic sulfur content was 0.16% and the total oil yield was 40% at 450°C, 2250 psia H<sub>2</sub> and one-hr residence time. Addition of 5.2% pyrite resulted in an increase in oil yield to 54% and a corresponding increase in conversion to pyridine solubles from 91% (without added pyrite) to 96%.

For a Texas (Big Brown) lignite, SRC-II processing was possible without catalyst addition and resulted in an oil yield of 50% and a conversion (pyridine solubles) of 95.9%. When 2.9% pyrite was added, the oil yield increased to 61% and the conversion increased to 98.2%. The liquid quality was excellent and the performance with pyrite added as a catalyst was equal to or better than that observed with any bituminous or subbituminous coal.

In every case in which pyrite was added to a coal that was deficient in pyrite, the yield of oil under SRC-II conditions increased substantially.<sup>20</sup> The fact that pyrite actually is a catalyst was confirmed when similar results were obtained with catalysts that contained neither iron nor sulfur.

### Coal Gasification

The gasification of coal involves two distinct stages: (1) devolatilization and (2) char gasification. Devolatilization occurs quite rapidly as the coal is heated above 400°C. During this period, the coal structure is altered, producing a less reactive solid (char), tars, condensable liquids and light gases. Nominally 40% of the coal is volatilized during this period. The less reactive char then gasifies at a much slower rate. We will discuss the effects of coal minerals on both devolatilization and char gasification.

A large volume of work has been reported on rapid devolatilization of coal (heating rates approximating process conditions (21,22)). Recently, the effects of coal minerals on the rapid pyrolysis of a bituminous coal were reported by Franklin, *et al* (23). They found that only the calcium minerals affected the pyrolysis products. Addition of CaCO<sub>3</sub> reduced the tar, hydrocarbon gas and liquid yields by 20-30%. The calcium minerals also altered the oxygen release mechanism from the coal. Franklin, *et al.* attribute these effects to CaCO<sub>3</sub> reduction to CaO, which acts as a solid base catalyst for a keto-enol isomerization reaction that produces the observed CO and H<sub>2</sub>O.

Walker and co-workers at the Pennsylvania State University have investigated the reactivity of a variety of coals during gasification in air, CO<sub>2</sub>, H<sub>2</sub> and steam (24-27). Hippo and Walker (25) found a linear correlation between reactivity and CaO content in the ash. They also observed an increase in reactivity with MgO, up to about 1%. They found no correlation between reactivity and iron content or total K or Na content. In their studies on hydrogen and steam gasification, the Penn State group used coals demineralized by acid washing to study mineral matter effects. While changes were observed in these studies, it was

difficult to attribute these changes to catalytic effects or physical effects.

Mahajan *et al.* (28) observed that the presence of pyrite in coal had a beneficial catalytic effect on hydrogenation at 570°C. They suggested that the catalytic activity was due to pyrrhotite formation. Hüttinger and Krauss (29) reached a similar conclusion concerning the catalytic activity of pyrite, and showed that above 850°C, iron enhanced the methane formation if the H<sub>2</sub> pressure was sufficiently high.

Padrick *et al.* (30) observed enhancement of the hydrogasification rate of a Pittsburgh Seam coal at 1000°C when various iron-containing minerals were mixed with the coal. They investigated the chemical effect of the minerals by measuring H<sub>2</sub>/D<sub>2</sub> exchange rates, and also determined the physical effect of the mineral addition on the resultant surface areas and pore volumes of the chars. While the correlation of 1000°C hydrogasification rates with measured parameters was somewhat better including the chemical effects of the minerals, it was concluded that the gasification rates for the various sources of reduced iron were primarily due to the physical interaction of the minerals with the coal.

#### Acknowledgment

This work supported by the U.S. Dept. of Energy at Sandia National Laboratories under Contract DE-AC04-76DP00789.

#### References

1. Carberry, J. J., "Chemical and Catalytic Reaction Engineering," McGraw-Hill Book Co., New York, Chapter 8 (1976).
2. Gates, B. C., Katzer, J. R. and Shuit, G. C. A., "Chemistry of Catalytic Processes," McGraw-Hill Book Co., New York, Chapter 5 (1979),
3. Probststein, R. F. and Hicks, R. E., "Synthetic Fuels," McGraw-Hill Book Co., New York, Section 6.4 (1982).
4. Gluskoter, H. J., Shimp, N. F. and Ruch, R. R., in "Chemistry of Coal Utilization. 2nd Supplementary Volume," John Wiley and Sons, New York, NY, pp. 369-424 (1981).
5. Davidson, R. M., "Mineral Effects in Coal Conversion," Rept. No. ICTIS/TR22, IEA Coal Research, London, January 1983.
6. Otto, K., Bortosiewicz, L., and Shelef, M., *Fuel* 58, 85 (1979).
7. Fisher, J., Young, J. E., Johnson, J. E., and Jonke, A. A., Report ANL 77-7 (1977).
8. Plogman, H., and Kuhn, L., Proceedings of the International Conference on Coal Science, Dusseldorf, Germany, September 7-9 (1981).
9. Granoff, B. and Traeger, R. K., *Coal Process. Technol.* 5, 15 (1979).
10. Mukherjee, D. K. and Chowdhury, P. A., *Fuel* 55, 4 (1976).
11. Gray, D. *Fuel* 57, 213 (1978).
12. Gray, j. and Shah, Y. T. in "Reaction Engineering in Direct Liquefaction," Adison Wesley Pub. Co., New York, NY (1981).

13. Derbyshire, F. J., Varghese, P. and Whitehurst, D. D., Preprints, Amer. Chem. Soc., Div. Fuel Chem. 26, No. 1, 84 (1981).
14. Whitehurst, D. D., Mitchell, F. U. and Farcasiu, M., in "Coal Liquefaction. The Chemistry and Technology of Thermal Processes," Academic Press, New York, NY, pp. 163-177 (1980).
15. Thomas, M. G., Padrick, T. D., Stohl, F. V. and Stephens, H. P., Fuel 61, 761 (1982).
16. Montano, P. A. and Granoff, B., Fuel 59, 214 (1980).
17. Montano, P. A., Bommanavar, A. S., and Shah, V., Fuel 60, 703 (1981).
18. Stohl, F. V. and Granoff, B., 90th Annual Meeting of the AIChE, Houston, TX (1981).
19. Guin, J. A., Curtis, C. W. and Kwon, K. C., Fuel 62, 1412 (1983).
20. Tomlinson, G., Gray, D., and Neuworth, M., "Effect of Coal Rank on Direct Coal Liquefaction Processes: Solvent Refined Coal (SRC-II) Process Experience," The MITRE Corp., 84W00308, July 1984.
21. Anthony, D. B. and Howard, J. B., AIChE J. 22, 625 (1976).
22. Stangby, P. C. and Sears, P. L., Fuel 60, 131 (1980).
23. Franklin, H. D., Peters, W. A. and Howard, J. B., Preprints, Amer. Chem. Soc., Div. Fuel Chem. 26, No. 2, 121 (1981).
24. Jenkins, R. G., Nandi, S. P. and Walker, P. L. Jr., Fuel 52, 288 (1973).
25. Hippo, E. J. and Walker, P. L. Jr., Fuel 54, 245 (1975).
26. Tomita, A., Mahajan, O. P. and Walker, P. L. Jr., Fuel 56, 137 (1977).
27. Linares-Solano, A., Mahajan, O. P. and Walker, P. L. Jr., Fuel 58, 327 (1979).
28. Mahajan, O. P., Tomita, A., Nelson, J. R. and Walker, P. L. Jr., Fuel 56, 33 (1977).
29. Hüttinger, K. J. and Krauss, W., Fuel 60, 93 (1981).
30. Padrick, T. D., Rice, J. K. and Massis, T. M., Preprints, Amer. Chem. Soc., Div. Fuel Chem. 27, No. 3, 300 (1982).

RECEIVED October 10, 1985

## Iron Sulfide Catalysis in Coal Liquefaction

P. A. Montano, Y. C. Lee, A. Yeye-Odu, and C. H. Chien

Department of Physics, West Virginia University, Morgantown, WV 26506-6023

A diverse number of techniques has been employed to characterize the iron sulfides under coal liquefaction conditions. It is observed that the stoichiometry of the iron sulfides is determined by the  $H_2S$  partial pressure and that greater activity is observed when the surface is rich in vacancies. All the iron sulfides show great affinity toward oxygen-containing compounds. This activity was demonstrated both with low rank coals as well as model compounds. It is proposed that pyrrhotites can act as catalysts for the cleavage of oxygen bonds in coal.

The direct liquefaction of coal is a process that involves the interaction between coal, hydrogen, solvent, and catalysts. Mineral matter has been known to enhance the conversion of coal to liquid products (1,2,3). Addition of pyrite, pyrrhotite, and liquefaction residues (4) to coal has been shown to affect the coal conversion yields and the viscosity of the products (5). Of all the minerals present in coal, pyrite (and marcasite) are the most important for coal utilization, especially in direct coal liquefaction (1,5). However, one has to remember that under coal liquefaction conditions pyrite rapidly transforms to a nonstoichiometric iron sulfide  $Fe_{1-x}S$  ( $0 < x < 0.125$ ). It is noted that the sulfur formed as a result of the decomposition of pyrite is able to extract hydrogen from poor donor solvents. The stoichiometry of the pyrrhotite formed from  $FeS_2$  depends strongly on the partial pressure of  $H_2S$ .

A correlation between the conversion of coal to benzene soluble, and the stoichiometry of the iron sulfides was observed by Montano and Granoff (7). Higher conversion is accomplished by a more iron-deficient pyrrhotite (7). Stephens et al (8) studied the effect of additives to an IL#6 conversion to liquid products. Their work strongly suggests that  $Fe_{1-x}S$  and  $H_2S$  play a catalytic role in the conversion of coal to oils. These results are in good

agreement with the ones obtained from in situ Mössbauer measurements (6,9,10), where there was clear evidence of interaction between the iron sulfides and some coal components. Many questions remain unanswered concerning the catalytic roles of  $H_2S$  and  $Fe_{1-x}S$ . Lambert (11) suggested that the catalytic activity observed for pyrite is solely due to  $H_2S$  acting as a hydrogen-transfer catalyst. In a recent study by Anderson and Bockrath (12) on direct coal liquefaction, more conversion was obtained when the ratio of sulfur added to an iron solution (the catalyst) was equal to the one needed to obtain pyrrhotite ( $Fe_{1-x}S$ ). A very recent work by Ogawa, Stenberg, and Montano (13) reporting the hydrogenation of diphenylmethane in the presence of pyrrhotite clearly shows that maximum activity is obtained when the partial pressure of  $H_2S$  is enough to maintain an iron deficient surface. Too high a partial pressure of  $H_2S$  in the reactor moves the composition of the surface towards  $FeS_2$  and the conversion of diphenylmethane is reduced. Too low a partial pressure of  $H_2S$  leads to the formation of troilite ( $FeS$ ) and lower conversion. These results indicate that optimum conditions are obtained when the surface of the sulfide is rich in metal vacancies, where dissociation of  $H_2S$  can take place forming highly reactive species (13). It is obvious that the understanding of the catalytic role of the iron sulfides lies in the investigation of their surface properties. In the present paper we report such a study, where surface techniques were used to observe the reaction of gases found under liquefaction conditions with the sulfide surfaces. A special reactor was developed to study the surface composition of the iron sulfides after reaction with oxygen-containing compounds using Conversion Electron Mössbauer Spectroscopy (CEMS). Extended X-ray Absorption Fine Structure (EXAFS) and X-ray Absorption Near Edge Structure (XANES) were used for determining the environment of iron species in the residues obtained from the study of the interaction of iron sulfides ( $FeS_2$ ,  $Fe_7S_8$ ) with model compounds (14). The in situ reactions of iron with low rank coals are also presented. The results are compared with recent work on the hydrogenation of diphenylether in the presence of pyrrhotite (15).

### Experimental

Auger and electron energy loss spectroscopy measurements were performed using a UHV system with a base pressure of  $10^{-10}$  torr. The system was attached to a reactor cell where the samples were exposed to high temperatures and gases. The reactions of  $FeS_2$ ,  $Fe_7S_8$ , and  $FeS$  with  $CO$ ,  $H_2$ ,  $O_2$ ,  $NH_3$ ,  $CH_4$ ,  $C_2H_4$ , and higher hydrocarbons were studied between room temperature and  $450^\circ C$ .

The CEMS measurements were carried out in a specially designed reactor. In this reactor the samples of  $^{57}Fe$  foil were studied and treated with  $H_2/H_2S$  to obtain the iron sulfides. The detector employed for the detection of the electrons was a  $He/10\% CH_4$  flow counter connected in line with the reactor. The reactions of pure iron and iron sulfide with naphthoquinone were studied with this cell. The in situ Mössbauer measurements were performed using the system described in References 6 and 14. The coals used were a North Dakota lignite and an Australian Victorian Morwell Brown Coal



(16). The coals were studied at high pressure, 1500 psi of  $H_2$ , and in the presence of tetralin as a solvent (two ratios were studied-- 2:1 and 1:1, solvent to coal). The source used was a 150 mCi  $^{57}Co:Rh$ ; all the isomer shifts reported are given in reference to  $\alpha-Fe$ . The EXAFS and XANES measurements of the residues of the reactions of  $FeS_2$  and  $Fe_7S_8$  with model compounds were made at the Cornell High Energy Synchrotron Source.

### Experimental Results

Auger and Electron Energy Loss Measurements on  $FeS_2$ ,  $Fe_7S_8$ ,  $FeS$ . Natural crystals of  $FeS_2$  (pyrite) and  $Fe_7S_8$  (monoclinic pyrrhotite) were used for the measurements. The (100) face of pyrite and the (0001) face of pyrrhotite were studied in the reactor, and a polycrystalline sample of  $FeS$ . All the samples show a characteristic  $M_{2,3}VV$  Auger doublet with a separation of 5.0 eV (Figure 1). Two additional peaks (3 and 4 in Figure 1) are also observed for  $FeS$ . Peak 1 may correspond to transitions involving the s-3p ( $2\sigma$ ) valence band while peak 2 may correspond to transitions involving the d-band. A typical set of Electron Loss spectra for  $FeS_2$  is shown in Figure 2. Peak a is assigned to interband transitions from the Fe-3d band to an empty state above the Fermi level. Peaks b and c may be assigned to transitions for one s-3p-like valence band (peak b to  $1\pi_g \rightarrow 2\sigma_v$  and c to  $2\sigma_g, 1\pi_u \rightarrow 1\sigma_u$  transitions.) Peaks d and e are attributed to collective oscillations of the conduction or valence electrons. Peaks f and g are assigned to surface and volume plasmons respectively. Peaks j and k are transitions involving the Fe-3p electrons ( $M_{2,3}$  level). Peak l is due to transition from the  $M_1$  level. The EEL spectra for the other sulfides are similar but the position and intensities of the peaks vary (17). In our measurements we observed EEL peaks with strong iron or sulfur character. Damaged iron sulfur surfaces show evidence of reconstruction through migration of sulfur after heating to  $450^\circ C$ . For undamaged sulfides, heating results in changes in the chemical composition of the surface; migration of sulfur also occurs. There is clear evidence of the presence of elemental sulfur on the pyrite and pyrrhotite surface but not on troilite ( $FeS$ ). Since the maximum temperature attained was  $450^\circ C$  we do not expect that reduction of the  $FeS$  surface will take place. Essentially, if the partial pressure of  $H_2S$  is low in the reactor, the formation of  $FeS$  will occur by removal of sulfur from the  $Fe_{1-x}S$  surface. Once this state is reached no further loss of sulfur occurs and a fairly stable surface is obtained.

The interaction of the pyrrhotite with simple gases is more complex; damaged surfaces of  $FeS_2$  and  $Fe_7S_8$  react with CO at  $450^\circ C$ . We understand this phenomenon to be a result of the interaction of CO with Fe on the sulfide surface. This interaction is not detected with undamaged surfaces (pure single crystals) and with  $FeS$ . The formation of oxides on the surface is easily detected for  $FeS_2$ , and  $Fe_7S_8$  after reaction with CO. It has been observed that CO undergoes a disproportionation reaction on Fe,  $2CO \rightarrow C + CO_2$ , with the formation of surface oxide due to the dissociation of CO (18). The surface oxide is rapidly removed by  $H_2$ . The surfaces of the sulfides do not show any evidence in the Auger and EEL spectra of

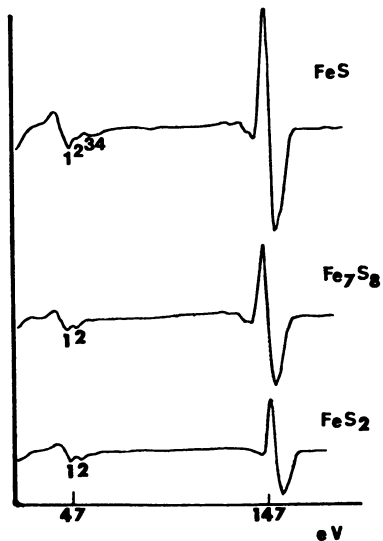


Figure 1. Low energy Auger spectra for the iron sulfides.

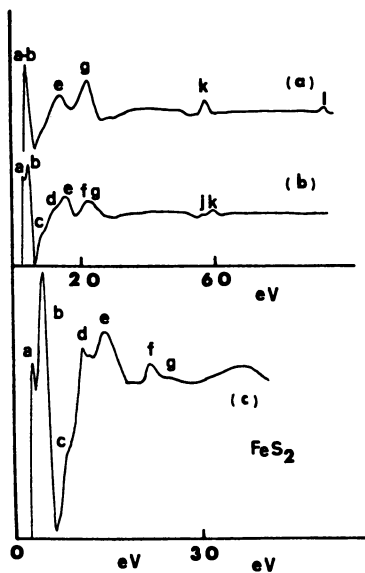


Figure 2. EEL spectra for  $\text{FeS}_2$  -- (a)  $E_{\text{primary}} = 300$  eV; (b)  $E_{\text{p}} = 150$  eV; and (c)  $E_{\text{p}} = 50$  eV.

reactions with  $\text{NH}_3$ ,  $\text{CH}_4$ , and  $\text{C}_2\text{H}_4$ . However, they interact strongly with molecular oxygen forming a surface oxide. Figure 3 shows the surface oxide formed on pyrite after interaction with oxygen; for comparison purposes the EEL spectrum for  $\alpha\text{-Fe}_2\text{O}_3$  is also shown. The present measurements indicate a high reactivity of the sulfide surfaces toward oxygen-containing compounds and very little toward light hydrocarbons and ammonia.

CEMS Measurements of the Surface Interaction of Naphthoquinone with Iron and Iron Sulfide Surfaces. A high purity  $^{57}\text{Fe}$  foil was used for these measurements; such a foil was necessary in order to record rapidly a Mössbauer spectrum (less than one-half hour). The sample was placed in the holder inside the reactor and  $\text{H}_2$  was flown for 2 hours at  $350^\circ\text{C}$  to reduce the surface and clean off any residual contamination. Figure 4a shows the Mössbauer spectrum at room temperature inside the reactor after cleaning. We studied the hydrogenation of naphthoquinone by introducing about 20 mg of the compound and flowing hydrogen at about 0.5 cc/sec. The temperature of the reaction was  $305^\circ\text{C}$  and  $405^\circ\text{C}$  and the time of reaction was about one-half hour. After reaction the CEM spectrum was taken inside the reactor. No evidence of the formation of any known oxide was detected (Figure 4b). The same experiment was repeated using a sulfided sample (produced from the  $^{57}\text{Fe}$  foil by flowing  $\text{H}_2/\text{H}_2\text{S}=0.1$  at  $350^\circ\text{C}$ ). The spectrum for such a sample is shown in Figure 5a before reaction. After reaction with naphthoquinone we see clear evidence of the formation of  $\text{Fe}_3\text{O}_4$  on the surface (Figure 5b). Magnetite is formed at the expense of the iron sulfide. This observation is in very good agreement with our earlier *in situ* Mössbauer work (14), where a less surface-sensitive technique was used for the measurements. We interpret these results as evidence of a greater reactivity of the iron sulfide surfaces toward oxygen-containing organic molecules than the pure metal. It is noted that magnetite can be easily removed by further flow of  $\text{H}_2/\text{H}_2\text{S}$ . The magnetite layer is formed in the first few surface layers of the iron sulfide (see Figure 5). This is suggestive of a possible catalytic role of the iron sulfides in the cleavage of oxygen bonds.

Interaction of Iron Sulfides with Low Rank Coal. *In situ* measurements were performed on low rank coals, one North Dakota lignite and one Australian Victorian Morwell coal. These two coals are characterized by their high oxygen content (as high as 24% for the Australian coal). Since the Australian coal is very low in mineral matter, a small amount of  $\text{FeCl}_2$  was added (16). In this case the amount of sulfur present is small and the partial pressure of oxygen is very high during reaction. Two charge states of iron are observed,  $\text{Fe}^{2+}$  and  $\text{Fe}^{3+}$ . Cassidy and co-workers explain the catalytic activity of iron in this coal as related to a redox mechanism. Figure 6 shows the Mössbauer spectra after reaction at  $300^\circ\text{C}$  and at  $440^\circ\text{C}$ . The spectra were taken inside the reactor and never exposed to air. The *in situ* Mössbauer measurements at  $300^\circ\text{C}$  show a similar spectrum to that shown in Figure 6a. At  $440^\circ\text{C}$  the spectrum is characteristic of  $\text{Fe}_3\text{O}_4$ . A similar result is obtained for the North Dakota lignite. Both coals are characterized for the

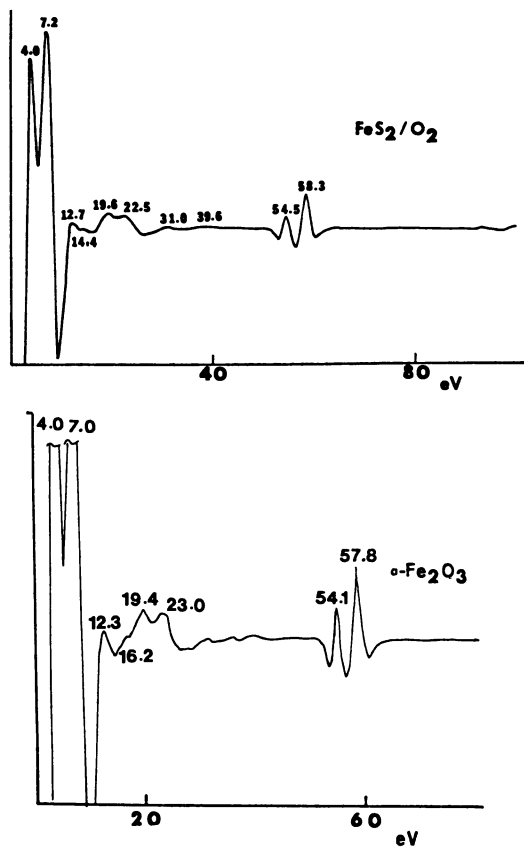


Figure 3. EEL spectra of FeS<sub>2</sub> after reaction with oxygen (a) and of  $\alpha$ -Fe<sub>2</sub>O<sub>3</sub> (b).

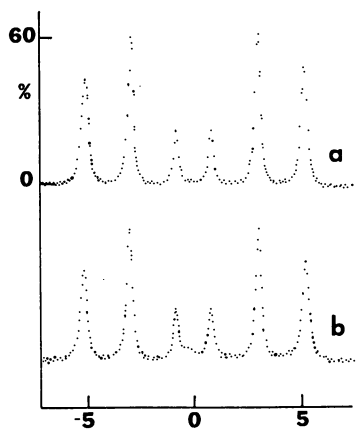


Figure 4. CEM spectra of <sup>57</sup>Fe foil (a) and after reaction with naphthoquinone (b). X-axis is in mm/sec.

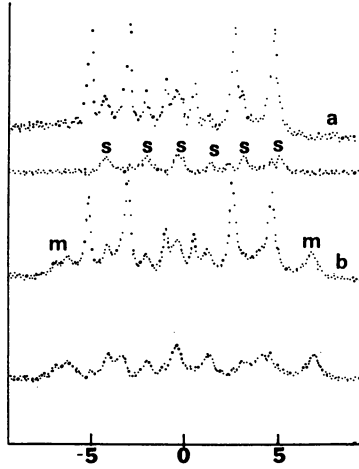


Figure 5. CEM spectra of (a) sulfided  $^{57}\text{Fe}$  foil, s: indicates the sulfide surface; (b) After reaction with naphthoquinone m: magnetic, bottom spectrum is the surface layers after reaction. X-axis is mm/sec.

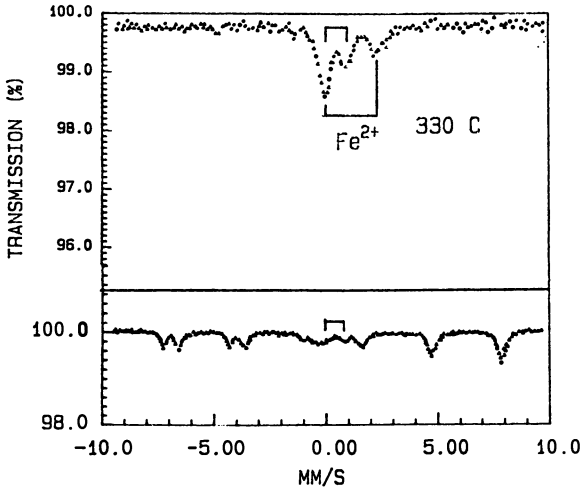


Figure 6. Mössbauer spectra after reaction (Australian Victorian Morwell coal) Top at  $330^\circ\text{C}$ , bottom at  $440^\circ\text{C}$ . In the bottom spectrum  $\text{Fe}_3\text{O}_4$  and small particles of iron oxides are identified; in the top spectrum  $\text{Fe}^{2+}$  and  $\text{Fe}^{3+}$  are clearly observed.

low sulfur content, however the residues of the North Dakota lignite show the presence of  $\text{Fe}_{1-x}\text{S}$ . Increasing the partial pressure of  $\text{H}_2\text{S}$  will improve the conversion to liquids, however we must remember that the surface of the iron sulfides will be easily oxidized during reaction in an environment rich in oxygen-containing compounds. This process of surface oxidation should be present also in bituminous coals although the detection of the surface species is more difficult in this case.

In a recent experiment we have demonstrated the catalytic activity of pyrrhotite in the hydrogenation of diphenylether (15). Diphenylether is converted mainly to benzene and phenol (see Figure 7). At low partial pressure of  $\text{H}_2\text{S}$ , magnetite was detected; for high partial pressure,  $\text{FeS}_2$  bands are visible and the amount of magnetite is strongly reduced. The conversion increases with  $\text{H}_2\text{S}$  partial pressure. We attribute this to the formation of a more iron deficient surface. These results also are in good agreement with our earlier studies in lignites and naphthoquinone and strongly point to the importance of iron sulfides in the cleavage of oxygen bonds in coal.

EXAFS and XANES Measurements. X-ray absorption measurements were performed on the residues of the reaction of  $\text{FeS}_2$  and  $\text{Fe}_7\text{S}_8$  with pyrene in the presence of hydrogen (14). Iron sulfide in the amount of 10% (200 US mesh) by weight was added and mixed with 1 g of the model compound. The reactions were carried out at 440°C and the initial hydrogen pressure was 250 psi; the reaction time was 1 hour. The residues were measured at room temperature. Figure 8 shows the XANES (X-ray Absorption Near Edge Structure) spectra for the residues of the reactions of pyrene with  $\text{Fe}_7\text{S}_8$  and  $\text{FeS}_2$ . Although the final product during both reactions is a nonstoichiometric iron sulfide ( $\text{Fe}_{1-x}\text{S}$ ), the spectra are remarkably different. Part of the difference in the XANES spectra is attributed to the presence of FeS (troilite) in the residues of the reaction with  $\text{Fe}_7\text{S}_8$ . The reason for the presence of FeS is related to the very low partial pressure of  $\text{H}_2\text{S}$  in the reactor during hydrogenation of pyrene. In the case of pyrite there is a high partial pressure of  $\text{H}_2\text{S}$  in the reactor resulting from the decomposition of  $\text{FeS}_2 \rightarrow \text{Fe}_{1-x}\text{S} + \text{H}_2\text{S}$ . We know that when the  $\text{H}_2\text{S}$  partial pressure is high, a nonstoichiometric pyrrhotite is always obtained during the reactions.

The EXAFS (Extended X-ray Absorption Fine Structure) spectra of the residues were analyzed and the Fourier transforms for pure  $\text{FeS}_2$  and  $\text{Fe}_7\text{S}_8$  are shown in Figure 9. The Fourier transforms of the EXAFS spectra after reaction are shown in Figure 10. The first prominent peak in all the spectra is due to Fe-S distances (2.26 Å for  $\text{FeS}_2$  and 2.44 Å for  $\text{Fe}_7\text{S}_8$ ). The second peak is due to the iron next-nearest neighbor—one for pyrite, but more complicated for  $\text{Fe}_7\text{S}_8$  since there are many iron distances present. For the residues of the reactions with  $\text{FeS}_2$  present, the Fourier transform is dominated by the Fe-S distance; Fe-Fe distances are difficult to identify. This is attributed to the fact that the iron atoms and vacancies in the  $\text{Fe}_{1-x}\text{S}$  structure (atomic % iron = 47.8) are extremely disordered and randomly distributed, in marked contrast to the residues of the reaction in the presence of  $\text{Fe}_7\text{S}_8$ . In the

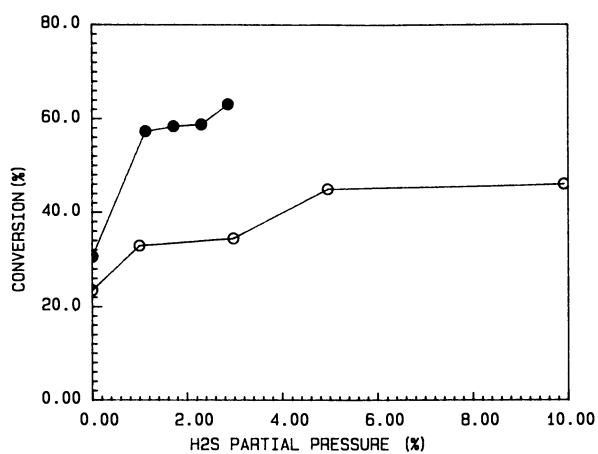


Figure 7. Conversion of diphenylether to benzene and phenol for 36% Fe<sub>7</sub>S<sub>8</sub> loading (top) and 10% Fe<sub>7</sub>S<sub>8</sub> loading (bottom). From Reference 16.

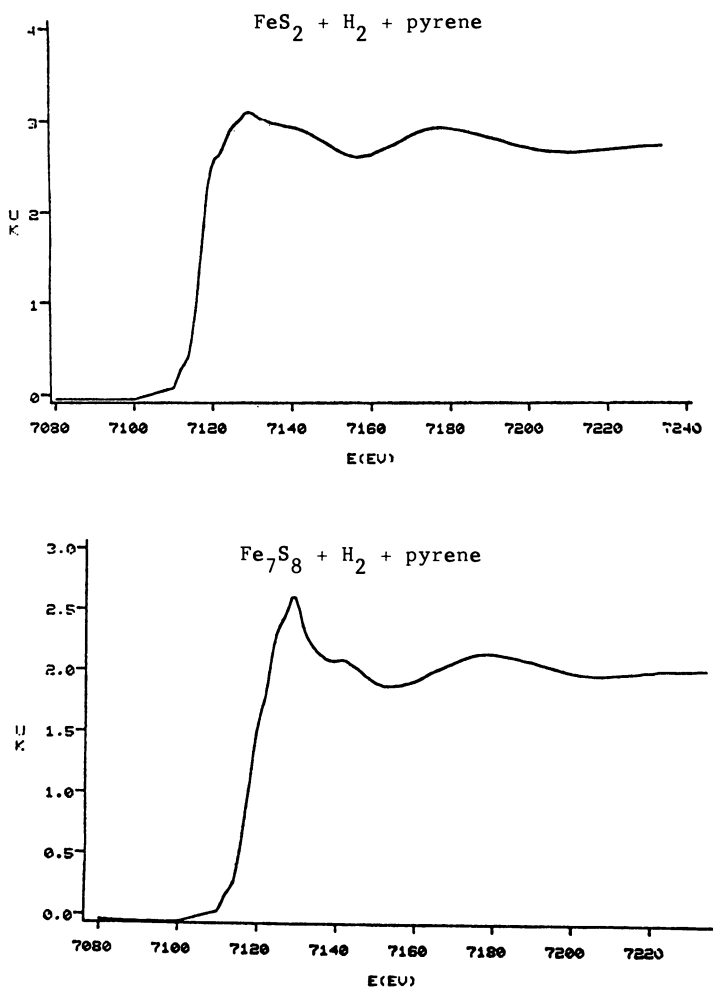


Figure 8. XANES spectra of the residues of the reactions of pyrene with (a) FeS<sub>2</sub> and (b) Fe<sub>7</sub>S<sub>8</sub>.



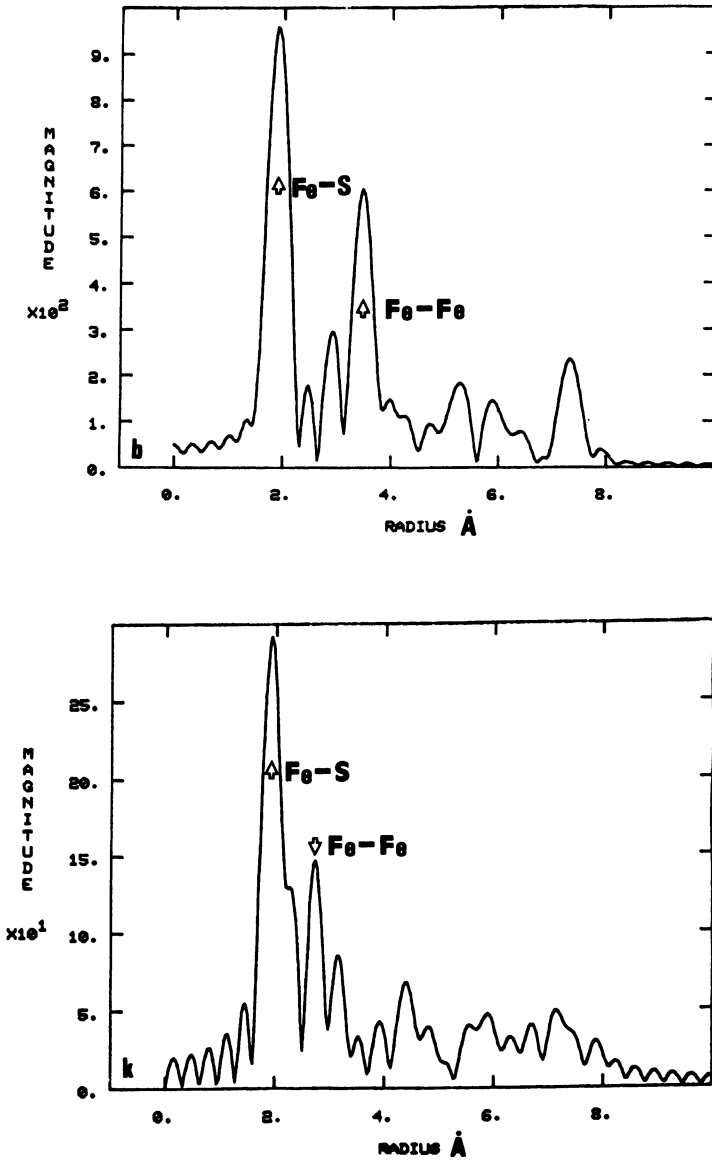


Figure 9. Fourier transforms of  $\chi \cdot k^3$ . Top:  $\text{FeS}_2$ ; bottom:  $\text{Fe}_7\text{S}_8$ .

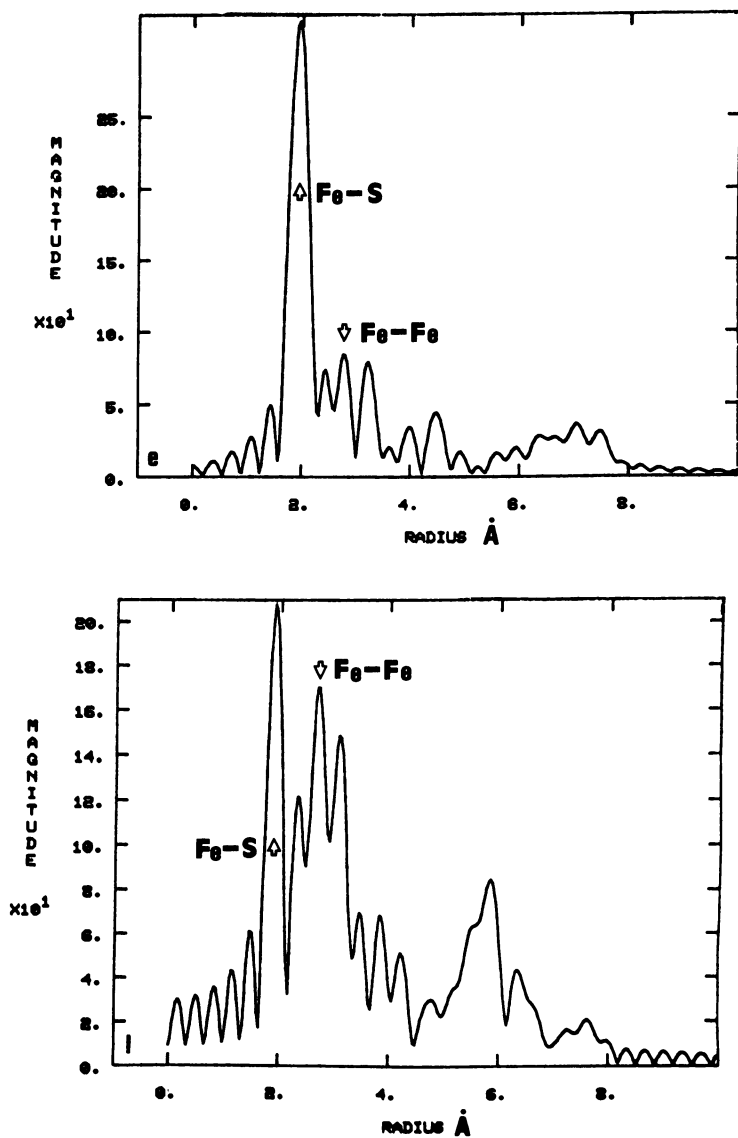


Figure 10. Fourier transforms of  $\chi \cdot k^3$ . Top: after  $\text{FeS}_2$  reaction at  $440^\circ\text{C}$  with pyrene; bottom: after  $\text{Fe}_7\text{S}_8$  reaction at  $440^\circ\text{C}$  with pyrene.

later case a rather rich spectrum of well-defined distances and strong peaks for Fe-Fe can be observed in Figure 10. The present results suggest that although Mössbauer spectroscopy and x-ray diffraction can give a good estimate of the average stoichiometry, the local environment of the iron can be quite different. These results indicate that a more microscopic approach should be employed in fully characterizing the sulfide surfaces, employing as many techniques as possible to really gain a deeper understanding of the active catalyst sites on the iron sulfide surfaces. The overwhelming evidence still points toward the metal vacancies as the major center for dissociation of  $H_2S$ , but the metal sites also can play a significant role in the catalytic activity of the iron sulfides.

### Conclusions

We have observed that the behavior of iron sulfide surfaces depends strongly on the stoichiometry. Iron deficient surfaces show a higher reactivity than the troilite surface. At high temperatures ( $450^\circ C$ ) there is elemental sulfur present on the iron sulfide surfaces. The metal vacancies can serve as centers for the dissociation of  $H_2S$  thus facilitating the transfer of hydrogen to organic entities. The pyrrhotite surface shows a great reactivity toward oxygen-containing compounds. The surface oxide formed on the pyrrhotite surface is reduced when  $H_2$  and  $H_2S$  are present in the reactor. The interaction between the pyrrhotite surfaces and light hydrocarbons is minimal. The local environment of the iron in the pyrrhotite residues is quite variable and depends strongly on the reaction conditions.

### Acknowledgment

The authors wish to thank the U.S. DOE for their financial support.

### Literature Cited

1. Davidson, R. M. "Mineral Effects in Coal Conversion," Report No. ICTIS/TR22, IEA Coal Research, London.
2. Mukherjee, D. K.; Chowdbury, P. B. Fuel 1976, 55, 4.
3. Hodek, W. Chemical and Physical Valorization of Coal Meeting, Liege, EUR-5954-d/e/f/i, Luxembourg, 87, 1978.
4. Granoff, B.; Thomas, M. G.; Baca, P. M.; Noles, G. T. Am. Chem. Soc. Div. Fuel Chem. Prepr. 23, 23 (1978).
5. Illig, E. "Disposable Catalysts in Coal Liquefaction," DOE, Albuquerque, NM (1978).
6. Montano, P. A.; Bommannavar, A. S.; Shah, V. Fuel, 1981, 60, 703.
7. Montano, P. A.; Granoff, B. Fuel 1980, 59, 214.
8. Stephens, H. P.; Stohl, F. V.; Padrick, T. D. Proc. Int. Conf. Coal Sci., Dusseldorf, Sept. 1981, Verlag Glück Auf Essen, p. 368.
9. Bommannavar, A. S.; Montano, P. A. Fuel 1982, 61, 1289.
10. Bommannavar, A. S.; Montano, P. A. Fuel 1982, 61, 523.

11. Lambert, J. M., Jr. Fuel 1982, 61, 777.
12. Anderson, R. R.; Bockrath, B. C. "Effect of Sulfur on Coal Liquefaction in the Presence of Dispersed Iron and Molybdenum Catalysts," PETC, Pittsburgh 1982.
13. Ogawa, T.; Stenberg, V. I.; Montano, P. A. Fuel (in press).
14. Montano, P. A.; Bommanavar, A. S. J. Molecular Catalysis 1983, 20, 393.
15. Montano, P. A.; Stenberg, V. I.; Sweeny, P. H. to be published.
16. The authors thank P. Cassidy for supplying this sample.
17. Lee, Y. C.; Montano, P. A. Surface Science 1984, 142, 27.
18. Jagannathan, K.; Srinivasan, S.; Hedge, M. S.; Rao, C. N. R. Surface Science 1980, 99, 309.

RECEIVED July 23, 1985

## Influence of Mineral Matter on the Rate of Coal Char Combustion

John H. Pohl

Energy and Environmental Research Corporation, Irvine, CA 92718

Large uncertainties exist in the apparent and intrinsic rate of char combustion. Estimates of the rate of char combustion within the range of uncertainties can result in over designed or under designed boilers. A review (2) has shown that one of the major uncertainties in the rate of char combustion is the catalytic influence of mineral matter. This paper reviews the available information on the catalytic effects of mineral matter and concludes that many coals contain sufficient sodium and calcium to increase the rate of char combustion by a factor of 100 at low temperatures. However, insufficient information is available to assess the influences of catalysis by mineral matter at combustion temperatures.

The rate of coal combustion can, in some instances, influence the design of boilers. The intrinsic rate of char combustion is, however, poorly known. Figure 1 shows that estimated intrinsic rate of char combustion can vary by a factor of  $10^4$  (1). The largest uncertainties are (2):

Property	Factor of Uncertainty
Surface Area	100
Effectiveness Factor	50
Catalysis	100
Crystal Structure	30

Other uncertainties account for less than a factor of four in the estimated intrinsic rate of coal char combustion.

Changes in the apparent rate of char combustion by a factor of 10 can influence the predicted performance of boilers. An example of these changes for a 660 MWe boiler is shown in Table I. These figures were calculated using a well tested model of boiler performance (3). Increasing the accepted apparent rate constant by a factor of 10 predicts slightly improved performance, but decreasing the accepted rate constant by a factor 10 predicts severely degraded and unacceptable boiler performance.

This paper assesses one of the major uncertainties in estimating intrinsic rate constants, the influence of catalysis of the combustion rate of coal char.

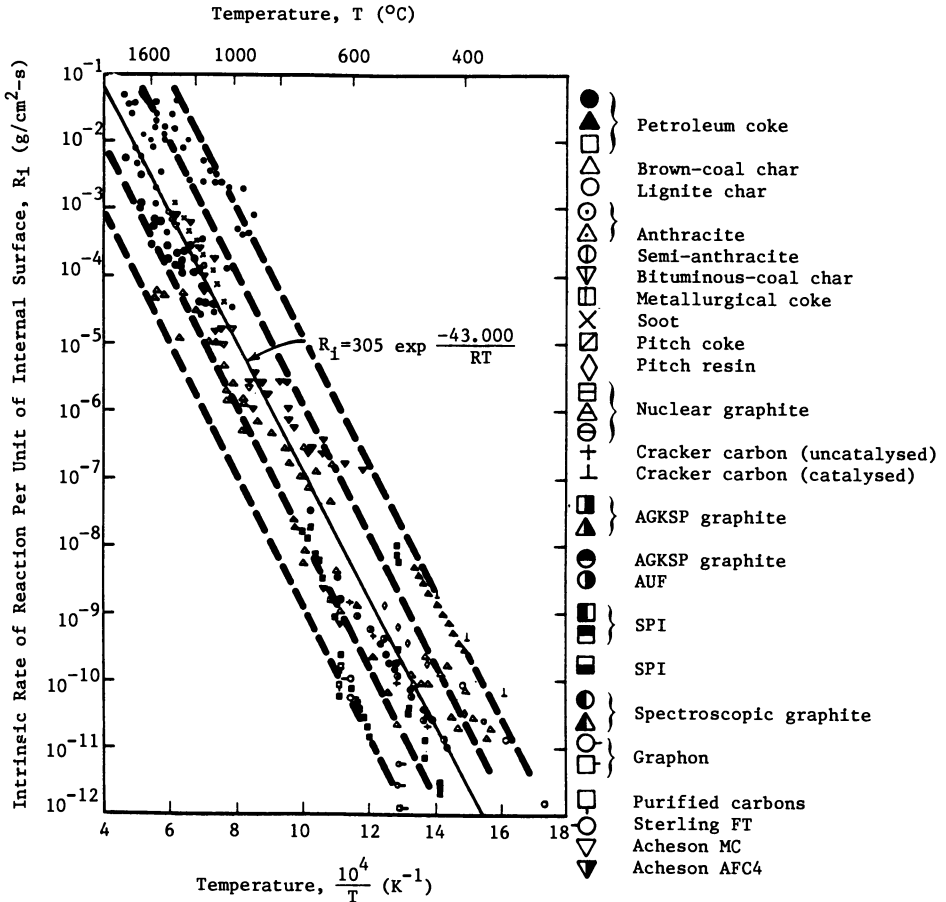


Figure 1. Intrinsic rate of reaction of chars. Reproduced with permission from reference 1. Copyright 1978 Butterworth.

Table I. Influence of Combustion Rate on Power Plant Performance  
for a 660 MWe Coal-Fired Boiler

Kinetic Constant, g/cm's Atmosphere	Furnace Efficiencies (%)	Mean Furnace Exit Temp of	Mean Net		Maximum Net Heat Flux Btu/ft <sup>2</sup> hr	Position of Maximum Heat Flux (ft)	Maximum Flame Temp. (°F)	Percent Unburned Fixed Carbon	Percent Combustibles In Ash (%)
			Heat Flux Btu/ft <sup>2</sup> hr	Heat Flux Btu/ft <sup>2</sup> hr					
40e <sup>-21</sup> ,450/RT <sup>a</sup>	43.1	2190	39,000	61,500	116	2650	0.66	5.97	
400e <sup>-21</sup> ,450/RT	44.2	2160	40,300	62,800	102	2670	0.04	0.38	
4e <sup>-21</sup> ,450/RT	33.6	2200	26,000	64,700	224 <sup>b</sup>	2350	32.17	69.03	

<sup>a</sup> Normal Value

<sup>b</sup> Boiler Exit Plane

Mineral Matter

Mineral matter contained in the coal could influence the rate of char combustion by blocking part of the coal surface or by catalytically increasing the rate of combustion. Figure 2 shows that the measured rate of combustion of purified nonporous graphites is uncertain by less than a factor of three. This is a small difference compared to the spread in the overall rate data and suggests that some of the scatter in the measured rates of coal combustion is caused by the mineral matter in the coal.

Blocking of the surface area of coal by ash is unlikely to significantly change the rate of char reaction. Calculations for a coal with 25 percent ash indicate that, except at high levels of burnout, much less than one percent of the surface area of char will be blocked with ash particles.

Experiments have shown that small amounts of certain metals can accelerate the rate of char combustion (4-9). A number of anions and cations have been shown to accelerate the combustion of carbons at concentrations of 10 to 1000 ppm. Table II shows the relative influence on the combustion rate of various salts added as solutions to purified graphite. Relatively small amounts of metals can accelerate the rate of combustion by many orders of magnitude. To effectively catalyze the combustion rate of coal, the metal which accelerates the rate must be distributed on nearly the molecular level, and be present in sufficient concentration to accelerate the rate. The range of relative acceleration of the combustion rate by different metals is shown in Figure 3. These estimates are made

TABLE II. Influence of Metals on the Rate of Graphite Combustion

Metal	ppm	Relative Reactivity
Be	120	1
B	80	1
Al	70	3
Ca	120	4
Mg	120	6
Sr	120	8
Ni	150	32
Cd	120	90
Ba	120	100
Na	120	230
Au	120	240
V	120	340
Cu	120	500
Ag	120	1,340
Cs	120	64,000
Mn	80	86,000
Pb	130	470,000

Source: Reproduced with permission from reference 9. Copyright 1966 Pergamon Press.



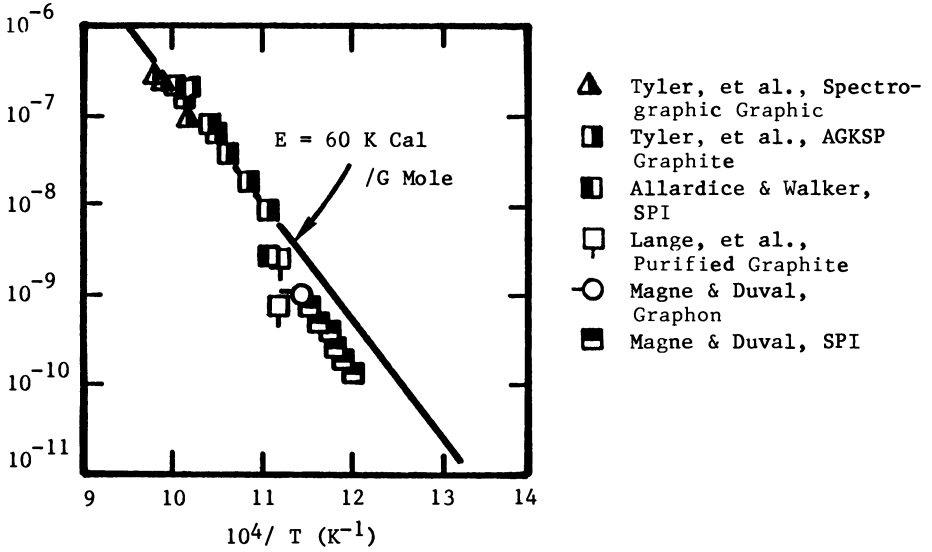
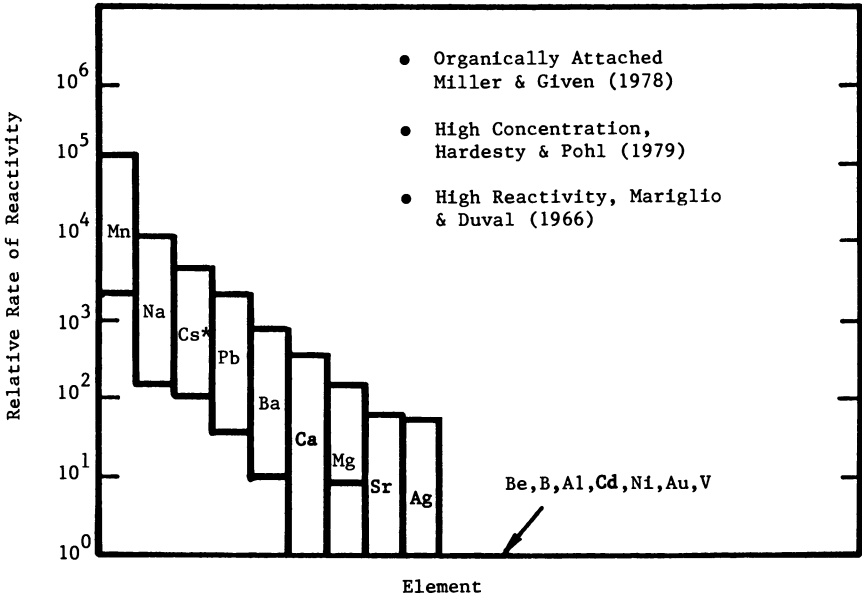


Figure 2. Combustion rates of highly purified graphite. Reproduced with permission from reference 4. Copyright 1972 Butterworth.



\* Assumed All Organically Attached

Figure 3. Estimate of the potential catalytic acceleration of coal combustion.

assuming the range of organic attachment of metals found by Miller and Given (10), the range of metals found in U.S. coals by Hardesty and Pohl (11), and the acceleration of the combustion rate determined by Mariglio and Duval (9). These may be over estimates as the influence of catalysis will decrease at higher loadings, the fraction of metals organically attached in high rank coals will be lower than found by Miller and Given, and the relative catalytic reactivity will be reduced at combustion temperatures.

The influence of relatively minor levels of sodium on the combustion rate of graphite is shown in Figure 4. Addition of sodium to a concentration of 15 ppm accelerates the reaction by one to two orders of magnitude; higher levels of sodium accelerate the reaction at a decreased rate.

The influence of catalysis will be less pronounced at the higher temperatures of combustion where noncatalytic combustion proceeds much faster. No data exists at these higher temperatures. The available data indicates that combustion of carbon is accelerated by up to two orders of magnitude by levels of sodium normally present in coals at temperatures only slightly lower than combustion temperatures.

#### Summary

Minerals present in coal can accelerate the rate of char combustion by as much as a factor of 100. Molecularly attached sodium and calcium compounds are likely to increase the char combustion rate substantially at low temperatures. However, information is not available and work should be undertaken to assess the acceleration of char combustion by minerals at the temperatures of combustion.

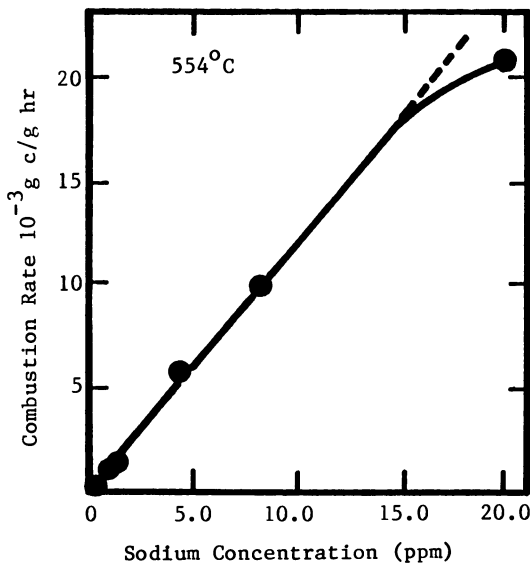


Figure 4. Catalysis of graphite combustion by sodium. Reproduced with permission from reference 9. Copyright 1966 Pergamon Press.

Literature Cited

1. Smith, I. W. Fuel, 1978, 57, 409-414.
2. Pohl, J. H.; Richter, R. W. ; Heap, M. P.; Folsom, B. A., "Influence of Coal Char Combustion Rate on Power Plant Performance," Special Report Prepared Under EPRI Contract EPRI RP 2256-1, 1983.
3. Richter, W.; and Pohl, J. H., "Scale-Up of coal Water fuels Experiments in Pilot Furnaces For Evaluation of Utility Boiler Performance," 7th Int. Symp. on Coal Slurry Fuels Preparation and Utilization, New Orleans Louisiana, May, 1985.
4. Smith, I. W.; Tyler, R. J., Fuel, 1972, 51, 312-321.
5. Essenhigh, R. H. Chemistry of Coal Utilization, Second Supplementary Volume. M. A. Elliott, Ed.: John Wiley & Sons: New York, 1981, p. 1153.
6. Patai, S., E. Hoffman, and L. Rajbenback. J. Appl. Chem., 1952, 2, 306-310.
7. Lang, F. M., P. Magnier, and S. May. 5th Proc. Conf. on Carbon, Vol. 1, 1961, p. 171.
8. Heuchamps, C. and X. Duval. Carbon, 1966, 4, 243-253.
9. Mariglio, H. and X. Duval. Carbon, 1966, 4, 323-332.
10. Miller, R. N.; and Given, P. H., Ash Deposits and Corrosion Due to Impurities in Combustion Gases, R. W. Bryers, Ed: Hemisphere Publishing Corporation: Washington, D.C., 1978, p. 39.
11. Hardesty, D. R.; and Pohl, J. H., "The Combustion of Pulverized Coals-An Assessment of Research Needs," Proceedings of the 10th Materials Research Symposium on Characterization at High Temperature Vapor and Gases, National Bureau of Standards Special Publication 561, 1979, p. 1407.

RECEIVED October 8, 1985

## Behavior of Mineral Matter during Coal Beneficiation

Harold L. Lovell

Department of Mineral Engineering, The Pennsylvania State University, University Park, PA 16802

Coal beneficiation involves a series of steps to separate the mineral matter from the combustible portion of the coal. Current coal characterization for beneficiation is usually limited to measurements of the particle specific gravity distribution (washability). It is further assumed that the properties of the coal feed stream and related mineral matter remain constant during the separation or cleaning process, but the compositions of the streams do change. These changes are important in understanding the lack of expected separations. The effects of specific mineral constituents on different unit operations are described. Better measurement and analytical systems will permit improved control of the processes and better separations.

Each coal beneficiation unit operation responds to the physical and chemical properties of its feed. The response of the beneficiation steps to the "collage" of the individual particles depends specifically on the frequency distribution of the component particle properties. The particle responses are not totally independent of particle property-process parameter interactions, but are also significantly controlled by the overall distribution of particle properties. Diligence is appropriately applied to establish the "collage" distribution by certain particle properties of the plant feed. This distribution provides the design bases for each unit operation in the flow sheet - including its capacity, flow rate, and unit loading - thus ultimately defining the separational performance, efficiency, and unit costs. Each unit operation should be sized and operated such that its optimum performance is well within the sensitivity range of its feed property distribution. The concern that the feed distributions may, at times, exceed the sensitivity range for some unit operation within

the system, is normally related to in situ coal variability, which can be extreme. The concern may extend to coal feeds from different seams and/or paleogeological origins, mining systems, or handling-storage systems. Unfortunately, seldom are the concerns extensive and rarely are the feed characterizations detailed to each downstream operation.

The plant feed characterization usually is limited to particle size distribution and, if detailed, will include a particle gravity distribution (washability) for several size groupings greater than 28 or 16 mesh. There is no generally accepted range for either the size or density groupings. The characterization of the individual particle fractions are usually limited to moisture, with temperature ash, and total sulfur content. In some unusual instances, the low temperature ash and sulfide sulfur content may be determined. Pragmatism, procedures, and economics prevent the direct determination of minerals whose concentrations will be modified in the process. These levels are expressed in terms of ash content. If there is any characterization of the individual macerals or minerals, they are evaluated on the basis of the "total-composite" feed sample. Should flotation processes be anticipated, some "laboratory floatability" studies (1) may be carried out on some minus 28 mesh or finer sized fraction. The particular fraction thus tested is seldom the same in all details as that which will exist within the plant flow sheet. Feed hardness or friability (Hardgrove Grindability Index, Drop-Shatter, etc.) may also be determined on the composite feed sample. If any comminution evaluations are made for the particular feed coal in the course of selecting a particular comminution device, they are usually made on a sample purported to be representative of the plant feed. Attempts to evaluate variations of particle strength or stability, maceral, mineral, or elemental composition, have been limited to research characterizations, as those reported by the author (2). We are almost totally devoid of pragmatic techniques to establish the particle sizes or volumes of individual components within a given individual coal particle (3).

These observations can but lead to the conclusion that in contrast to typical unit operations in chemical engineering, the coal processing engineer assumes a feed to each unit operation within the plant system based upon the defined plant feed. Further, it is assumed that the collage of particles entering the plant as feed DOES NOT CHANGE in passing through the processing system, and that the same number of particles 2 by 1-inch having densities between 1.40 and 1.45 gm/cc (or any other fraction) leave the plant as enter. We know that this is not correct even if we ignore the comminution operations within the plant designed to make such changes.

The composition of any individual coal beneficiation feed particle ranges from a nearly uniform metamorphized plant component through an almost infinite mixture series with macerals-minerals to an opposite end member as a nearly uniform mineral component. The behavior of a beneficiation feed during processing is determined by

compositions whose responses to process parameters are established by the particle properties such as size, shape, density, hardness, porosity, and gas-liquid-solid interfaces. The particle response establishes its direction and rate of movement toward one of the process product ports.

With coals as sedimentary rocks of paleobotanical origin, their plant inorganic contents incorporate those components which were part of the original plant system and associated substances, as well as those that have been introduced through all the subsequent geologic events. Accordingly, the mineral components found in coals reflect the nature of the originating plant systems, their environment, reduction conditions, temperatures, and pressures, as well as those conditions to which the coal-forming strata have been subject during all the ensuing geologic epochs, including past and current circulating ground waters. Thus, the observed complexity of the resulting physical characteristics is to be expected.

The minerals found in United States coals continue to be studied with the availability of improved instrumental procedures such as x-ray diffraction, infrared absorption, and scanning electron microscopy beyond the traditional optical and chemical mineralogical techniques as applied to thin sections, polished pellets, and isolated particles. The minerals may be grouped into the silicates (kaolinite, illite montmorillonite, and chlorite), the oxides (quartz, chalcedony, hematite); the sulfides (pyrite, marcasite, and sphalerite); the sulfates (jarosite, gypsum, barite, and numerous iron sulfate minerals); the carbonates (ankerite, calcite, dolomite, and siderite); and numerous accessory minerals (apatite, phosphorite, zircon, rutile, chlorides, nitrates, and trace minerals).

The greatest interest in mineral occurrences in coal particles for processing engineers relates to their potential liberation as an essential first step toward their physical removal. Further, the concern relates to the mineral behavior in each of the unit operations within the preparation plant and environmental implications within the preparation operations, for utilization of the clean coal product and the disposal of the refuse materials. The greatest attention has been given to the former interests, especially as applied to the liberation of pyrite in efforts to achieve the greatest possible sulfur reduction during processing.

#### Specific Responses of Coal Mineral Components during Processing:

The "collage" of particles entering a coal processing plant is subject to a series of unit operations designed to achieve the desired level of quality improvement. The development of the initial set of particles is determined by the mining and preprocessing storage and handling systems. Undoubtedly these operations introduce stresses within the coal particles that lead to subsequent fracture failures. Any potential control of the nature of this particle set is usually extremely limited - being

determined by production and economic factors. Situations which lead to oxidation, decrepitation, and absorption of excessive levels of moisture may be modified. The introduction of moisture prior to processing probably enhances clay swelling, tends to increase the amount of mineral fines (usually clays) into the plant stream, and may enhance localized heating, swelling, and oxidation. Initiation of dispersion of clays may begin here. Uncontrolled comminution during the handling and storage due to dropping from stackers, compaction by graders, etc. tend to create fines and probably selectively favors reduction of the softer particles, especially certain clays. Other handling steps such as particle movement through jigs, etc., tend to increase the production of fines. The oxidation of coal and temperature increases may favor the production of water soluble salts leading to acid plant waters and potential corrosion.

Primary crushing which usually involves breakers or single roll crushers may be preceded by a scalping operation to remove large particles of hard shales and sandstones. Such operations, though not rejecting large amounts of refuse, do prevent wear, save energy, and prevent the introduction of additional refuse into the plant feed. The primary comminution devices are designed to control top size rather than achieve particle liberation. Therefore, they offer an opportunity to minimize fines production and show some selectivity toward the large harder particles such as shales and sandstones. Pre-operational testing of comminution devices should minimize the production of fines. In coal processing systems where classifying rotating mills may be used, the selective buildup of harder components within the mill can affect system performance.

In coarse coal sorting equipment, such as jigs and heavy media vessels, the softer minerals will tend to comminute due to attritional actions of particle movement and result in further dispersion into the plant circulating water system. In jigs, the production of mineral fines may be desirable to enhance hindered settling effects. In the Haldex heavy media system (4) and water-only cyclones, the presence of mineral fines are essential to serve as an autogenous heavy media system. Operational care must be taken to prevent the buildup of unacceptable levels of fines leading to unacceptable fluid viscosity levels. Although quartz, clays, and other very fine mineral particles enhance these conditions, several types of clays, notably kaolinite and montmorillonite (those containing larger amounts of sodium), are especially responsible. Suspended clay levels above five percent in such systems are most undesirable and may limit control of the density in magnetite heavy media systems. The viscosity effect increases with decreasing particle size and with spherical shape which enhances settling rates. These concerns can also become critical in coal-water transport systems.

In fine coal sorting systems, such as heavy media cyclones, water-only cyclones, tables, and spirals, the density and viscosity responses of suspensions are even more critical. In froth

flotation, the presence of clay fines is undesirable and usually requires a desliming step ahead of flotation if their concentration becomes excessive.

It is in the water circuit that the buildup of fines, especially clays, must be controlled. The responses become evident in dewatering devices and as centrifuges and filters. In the latter case, clays may cause blinding resulting in unacceptable water contents in the filter cake, thin watery cakes, and unacceptable performance. Difficulties in the filtration of refuse fines has led recently to the introduction of expensive processes such as pressure and belt filters to meet environmental standards. In thickeners, excessive clay fines may reduce settling rates, minimize the formation of desirable underflow slurry densities, and lead to plant failure. It is in the dewatering stages and water circuit, those processes at the end of the flow sheet, that these responses become acute. Although the use of one or more polymeric flocculants can usually control these situations, unexpected changes in plant feeds may require feed rate reductions or plant shutdown.

Recent environmental regulations which essentially require closed water circuits make the problems of mineral fines buildup especially severe. Similar difficulties are associated with the disposal of refuse fines.

These examples describe some of the more prominent responses of mineral components in coal processing operations. Control of these problems can be achieved with better detection and analytical systems to identify the problems.

#### Literature Cited

- 1a. Cavallaro, J.A. and A.W. Deurbrouck, Froth Flotation Washability Data of Various Appalacian Coals using the Time Release Analysis Technique. Report of Investigations 6652. U.S. Bureau of Mines, 1965.
- 1b. Alderman, J.K., Evaluating Flotation Washability Data. Coal Mining and Processing, pp. 70-73, 1981.
2. Lovell, H.L., The Characteristics of American Coals, Final Report, U.S. Dept. of Energy, FE-2030-11, 1976.
- 3a. Richardson, D. and H.L. Lovell, Pyrite Liberation - Key to Sulfur Reduction during Beneficiation. Proceedings of Coal Conference and Expo V, Symposium on coal Preparation and Utilization, October 1979.
- 3b. Richardson, D.L. A study of the Occurrence of Pyrite in Coal and Its Relationship to Liberation in Coal Preparation and Mine Drainage Formation. M.S. Thesis in Mining Engineering, 1979, The Pennsylvania State University.
4. Anon. Investigation of the Haldex (Simdex) Process for Beneficiating Coal Refuse: Hungarian Practice - 1969. Special Report 80, The Coal Research Section, The Pennsylvania State University, University Park, Pennsylvania.



## Mineral Matter Analysis: A Technique To Improve Bituminous Coal Beneficiation

Richard B. Muter and William F. Lawrence

College of Mineral and Energy Resources, West Virginia University, Morgantown, WV 26506

Mineral matter analysis can provide a more accurate and complete representation of the minerals present in bituminous coal and the effects of beneficiation processes upon them. Comparisons with conventional analytical methods are made which demonstrate some of the potential advantages of this technique in the monitoring or design of coal cleaning operations.

As a new generation of coal cleaning technology becomes more commonly practiced, it is rapidly becoming apparent that a new generation of analytical methods to monitor the separation characteristics is also required. The analytical methods which are in present useage do not accurately report the materials which are being beneficiated; rather, they report elements which are within the materials. While this indirect measurement method is widely accepted, both because it is well known and because it has historically proven of value to the coal industry, it may provide a very false picture of what truly occurs during coal processing. Conventional coal cleaning or beneficiation is used to remove those materials within the coal seam which are deleterious to clean efficient combustion or conversion. However, a problem arises in that different mineral forms, even though they may contain the same elements, may react differently during cleaning. Most common analytical methods destroy the mineralogical structures and give the impression that coals are to a large extent homogeneous and consistent in mineral content. This is a false impression as coal is, in reality, heterogeneous in nature and its mineral content can change markedly from sample to sample taken from the same source. It is this variability in minerals content which reduces the effectiveness of common beneficiation methods.

Sulfur analysis provides a good example of the false conclusions which can be drawn based upon good analytical technique. It ignores mineralogical composition, although it can be improved if an analysis of sulfur forms is performed. However, knowing that "x" percentage of pyritic sulfur is present is still not sufficient for the design of the most effective cleaning process. Further information as to the size of the mineral grains

present and whether they are finely engrained within the coal material itself is needed; and a determination of the other sulfur minerals present, if any, could lead to further refinements in the cleaning methods employed and their improved effectiveness.

The analysis of silica, however, provides a better example of the problem which exists. Silicon is to mineralogy what carbon is to organic chemistry and appears in coal in many forms from simple quartz to complex clays (Table 1). However, most analytical methods destroy mineral forms through high temperature oxidation (ashing) and the results are determined as the amount of silicon present. Two coals may have the same  $\text{SiO}_2$  content when analyzed, but the physical properties of the parent minerals may be quite different. Different minerals, even of similar compositions, may require different cleaning processes and have different effects upon processing equipment. Sand might be easily removable through washing or froth flotation; whereas clay with a similar silicon content might adhere to the coal material or colloiddally disperse within the process waters and be difficult to remove.

Physical beneficiation is generally considered to be a "mature" subject in that most changes which have occurred over the past few years have been in terms of equipment design and refinement or in the order in which particular operations are performed. These operations are generally based upon differences in physical characteristics (eg. specific gravity, hardness or brittleness ) between the minerals of interest and the coaly materials. However these processes are still monitored using elemental analyses rather than specific mineral concentration measurements.

Froth flotation, considered to be a higher level of sophistication in beneficiation, is also based on differences in mineralogical properties. Based upon particle surface characteristics, the separation method is more chemical than physical in nature. Tendencies of specific mineral particles to be hydrophilic or hydrophobic are enhanced through the use of chemical additives and then a physical separation is made. However, it is still minerals and not elements which are being separated even though conventional analytical methods would imply otherwise.

The next level of sophistication in coal cleaning will most likely be that of chemical coal cleaning. It will also be the most costly level to date, especially when the large tonnage amounts involved in coal utilization are considered. In order to keep these costs to a minimum, while still attaining desired results, process operations will have to be carefully planned and closely monitored. Process designers will need to know which minerals are involved and whether any of them can be removed before employing chemical cleaning. Acquiring a better knowledge of what minerals occur in specific coals and how they are affected by less expensive physical beneficiation processes is an obvious first step.

As part of a much larger effort by the U.S. Department of Energy, the Coal Research Bureau of the College of Mineral and Energy Resources at West Virginia University has been characterizing the mineralogy and petrography of three major bituminous coals in an effort to determine whether the

mineralogical associations can be closely followed through common physical beneficiation processes. A listing of the minerals commonly present in bituminous coals is provided in Table 1.

#### Methodology

Representative samples of three major bituminous coals were obtained following ASTM sampling procedures. The specific coals chosen included a northern West Virginia high volatile coal, a southern West Virginia low volatile coal, and a northern Illinois coal. Head coal samples were split out for each coal and then screen and specific gravity (sink-float) separations were made. Screen fractions produced were +1", 1x1/4", 1/4"x8M, 8x28M, 28x100M and -100M. Gravity separations were performed on all but the -100M fraction at 1.30, 1.40, 1.60, and 1.80 (SG) and all samples were analyzed. Determinations were made of the ash, low temperature ash, and the elements Si, Al, Fe, Ti, Ca, Mg, Na, and K, among others. The concentrations of the minerals illite, kaolinite, quartz, calcite and pyrite were also determined.

Low temperature ashing techniques were employed to reduce the oxidation and decomposition of the minerals which would occur under normal ashing conditions. Mineralogical analyses were performed using X-ray powder diffraction, infra-red spectroscopy, optical petrography, and scanning electron microscopy. Elemental determinations were performed using atomic absorption spectroscopy.

Each of the mineral identification and quantification techniques mentioned met with varying degrees of success for each individual mineral. However, for ease of application accuracy and reproducibility, and the highest degree of quantification, X-ray analysis was determined to be the best method. Accordingly, the mineral values shown in the tables were obtained by this method. Pyrite was determined using ASTM procedures.

#### Results and Discussion

In this project, the first operations studied were size and specific gravity separations as they are the most common unit operations practiced. The mineralogical data obtained was then converted into washability tables similar to those produced using elemental analyses, e.g. ash washability tables. This data was then transferred to graphic form to produce a minerals washability diagram (Figure 1) for the head northern West Virginia coal. This figure is based on conventional sink-float specific gravity separations, but it could as readily have been produced by varying the processing parameters of a specific unit operation and monitoring the mineral separations which occurred. Such curves could be used as predictive tools to estimate the separations which would occur and also could provide a theoretical base line for monitoring the effectiveness of a particular cleaning operation.

Minerals were also followed through individual unit operations as part of the research project. The data obtained when coal was cleaned using a pilot scale Deister Table is presented in Table 2. An examination of the actual minerals contents versus those predicted by the washability data shows a lower yield of illite and a higher concentration of kaolinite and quartz reporting in the clean coal. This implies that the illite is being removed to a greater extent than expected and that the removal of quartz and kaolinite is being retarded relative to predicted values.

Conventional elemental analysis, in this case for Si, would not

Table 1

Minerals present in the northern West Virginia bituminous coal. The symbols indicate the analytical procedures available for each mineral and whether the procedure can be used for quantitative (Q), semi-quantitative (S), or identification (I) analyses only.

	X-ray Powder Diffraction	Infrared Spectroscopy	Normative Calculations	Optical Petrography	Scanning Electron Microscopy	Formulae
ILLITE	S		Q	S	I	Variable
KAOLINITE	Q	Q	Q	S	I	$Al_4(Si_4O_{10})(OH)_8$
QUARTZ	Q		Q	S	I	$SiO_2$
FELDSPARS	S				I	Variable
MUSCOVITE				S	I	$KAl_4(AlSi_3O_{10})(OH)_2$
CARBONATES		Q		S		Variable
CALCITE	Q	Q	S	I	I	$CaCO_3$
DOLOMITE	Q		S	I	I	$CaMg(CO_3)_2$
BASSANITE	S				I	$CaSO_4 \cdot 1/2H_2O$
GYPSUM		I		I		$CaSO_4 \cdot 2H_2O$
IRON DISULFIDES	Q		Q	S	I	$FeS_2$
PYRITE				S		$FeS_2$
MARCASITE				S		$FeS_2$
APATITE	S				I	$Ca_5(F,Cl,OH)(PO_4)_3$
HEMATITE				S		$Fe_2O_3$
RUTILE				S	I	$TiO_2$

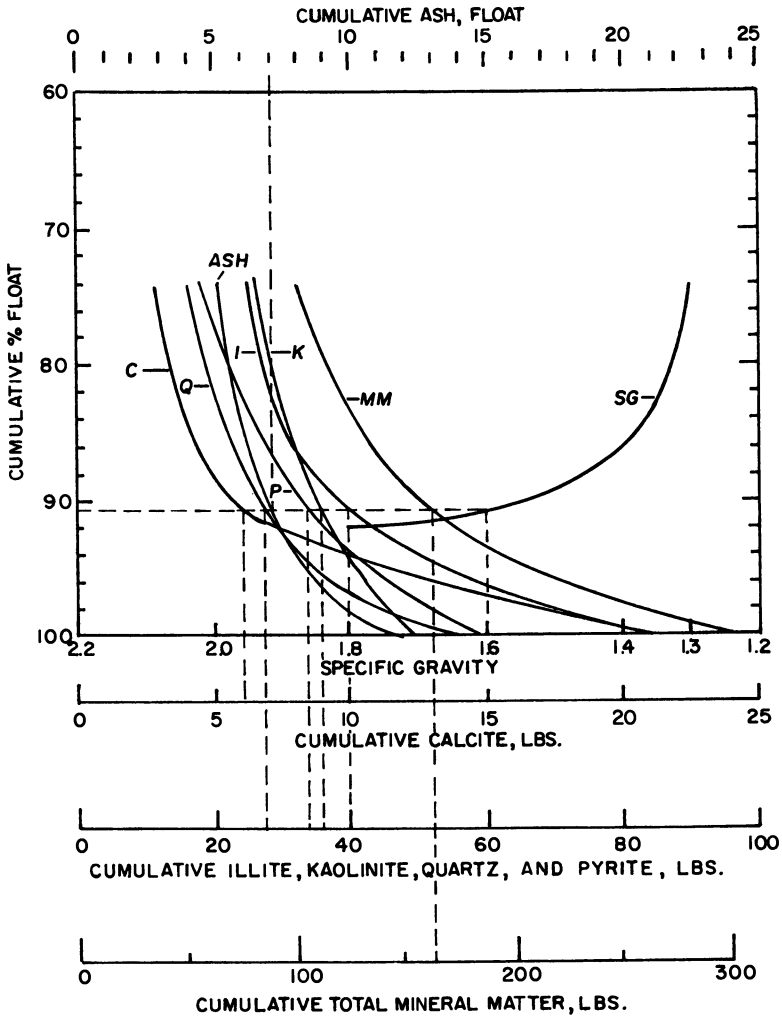


Figure 1. Washability Curves for the Most Common Minerals in a Northern West Virginia High Volatile Bituminous Coal.

show any changes occurring as the illite reduction would be offset by the greater than predicted amounts of the other two minerals. Further cleaning of this coal based upon removing quartz or kaolinite would be more effective than if a process to remove illite were used, but conventional analysis would not provide this type of planning information.

Table 2. Actual vs. predicted recovery (pounds per ton of feed coal) of products from a Northern West Virginia high volatile bituminous coal using a pilot scale Deister table.

	Actual	Predicted
Clean Coal	1705	1650
Ash	118	120
Mineral Matter	126	120
Illite	16	29
Kaolinite	34	30
Quartz	21	20
Calcite	13	4
Pyrite	30	23

#### Future Impact

Saying that mineralogical analysis may become as common as elemental analysis in the coal industry is not too strong a statement. Future preparation operations will be quite similar in complexity to current ore processing plants with advanced physical and chemical beneficiation methods being employed. The plant of the future will be designed based upon the properties of the specific coals being processed and will probably be a multiple unit operation, multiple end product, end use related plant. The economic success of such plants will depend upon the ability to monitor and closely control the materials which enter the individual processes while having the flexibility to handle coals from different seams. Such control will be difficult without an accurate identification of the minerals present and a knowledge of the changes which they undergo in specific cleaning operations.

#### REFERENCES

- Coal Preparation, 4th edition, AIME, New York, N.Y. 1979  
ASTM Standards, Section 5, Volume 05.05, 1982  
 Personal Communications: Dr. John Renton, William Grady, W. Va. Univ.

RECEIVED November 4, 1985

## **Analysis of Ash-Forming Mineral Matter in Raw and Supercleaned Coals by Automated Image Analysis-Scanning Electron Microscopy**

Warren E. Straszheim, Jay G. Yousling, and R. Markuszewski

Ames Laboratory and Department of Engineering Science and Mechanics, Iowa State University, Ames, IA 50011

Automated image analysis (AIA) was used in conjunction with scanning electron microscopy (SEM) and energy-dispersive x-ray (EDX) spectrometry to characterize directly the ash-forming mineral matter in raw and supercleaned samples of Illinois No. 6 and Pittsburgh No. 8 coals. The ground coals (70-80% less than 200 mesh) were cleaned to about 3% ash content by float-sink separation at 1.3 specific gravity. Samples of the raw and float material were analyzed for mineral matter phase and size distribution by the AIA-SEM technique. For the Illinois No. 6 coal, more than 90% of the mineral matter consisted of pyrite, kaolinite, illite or quartz, which were more or less uniformly distributed among the various particle sizes. The effectiveness of cleaning was gradually increasing with increase in mineral particle size. Removals of mineral matter ranged from 75% for the smallest particles (less than 4  $\mu\text{m}$  in diameter) to 100% for particles larger than 36  $\mu\text{m}$  in diameter. The Pittsburgh coal was significantly different in both the character of the raw sample and the extent of cleaning observed. Compared to the Illinois No. 6 coal, the pyrite in this sample was relatively more coarse, while the other minerals were more fine-sized. The cleaning process removed more of the large-size material, while the finely grained material was relatively untouched.

By using highly sophisticated and automated microscope techniques, together with powerful mini- and microcomputers, it is now possible to characterize the mineral components of coal *in-situ*. Combining automated image analysis (AIA) with scanning electron microscopy (SEM) and energy-dispersive x-ray (EDX) spectrometry allows detailed characterization of minerals in coal for chemical composition, particle size, and relation to the coal matrix. To evaluate coal particles produced by fine grinding for studying the liberation and removal efficiency, the AIA-SEM technique provides information on the elemental distribution among the various mineral phases. The

minerals are classified by using a chemistry definition file based on the relative amounts of elements present as determined by EDX spectrometry. For a statistically significant number of particles, both size distribution and volume fraction can be obtained and used to characterize the mineral matter content. The conventional chemical analyses for the bulk coal samples can be related to the AIA-SEM results for comparison of the data.

Other instrumental techniques, such as x-ray diffraction (XRD) and Fourier transform infrared spectroscopy (FTIR), can be used to identify the mineral phases present in coal. Sometimes they can be used to provide quantitative estimation, but their utility is limited to samples with large mineral contents. Furthermore, such techniques use bulk samples and provide only average values. Thus, when applied in coal preparation, they are limited to calculating only an "average" cleaning effectiveness and do not offer information on the size distribution of the mineral phases identified as removed or retained. On the other hand, AIA-SEM permits cleaning effectiveness to be evaluated with respect to both mineral phase and particle size distribution. Such information is important for any coal preparation process, especially since it can relate grinding and liberation of mineral particles to the effectiveness of a cleaning process (1). In practice, therefore, problems associated with removing a particle size or chemical class of particles could be detected and remedied for more effective cleaning.

The AIA-SEM technique has been used in Ames Laboratory to study the effect of grinding on the liberation of mineral matter from fine coal and its subsequent removal during cleaning. Several series of coals have been characterized by this technique in recent years, thus demonstrating its usefulness. In this work, the AIA-SEM technique was applied to determine the coal mineral character before and after cleaning by a float-sink technique.

### Experimental

Sample Description and Preparation. The two bituminous coals being tested for cleanability were from the Illinois No. 6 seam, Randolph County, Illinois, and from the Pittsburgh No. 8 seam, Lewis County, West Virginia. The coals were ground to a typical power plant grind (i.e., 70-80% less than 200 mesh or  $-75 \mu\text{m}$ ). The coals were then cleaned by float-sink separation (using halogenated hydrocarbons) at 1.3 specific gravity in a centrifuge to produce a very low-ash, clean coal fraction (ash content <3%). The raw and the superclean coal fractions thus produced were analyzed for moisture, ash, and sulfur forms by the usual ASTM procedures (see Table I). The apparent discrepancies in the organic sulfur determinations are probably artifacts of the indirect method; the deviations are within the anticipated error ranges of the ASTM procedures.

For the AIA-SEM analyses, the raw and clean coal samples were prepared by mixing 2 g of the sample with an epoxy resin and casting into molds 1 in. in diameter. The hardened pellets were polished to reveal a cross section and finished by polishing with  $0.3\text{-}\mu\text{m}$  alumina powder. Then the pellets were coated with approximately 500 Å of carbon to render sample surfaces electrically conductive for examination in the SEM unit.



Table I. ASTM Analyses of Raw and Supercleaned Coal Samples for Moisture, Ash, Forms of Sulfur, and Mineral Matter<sup>a</sup>

	Illinois No. 6		Pittsburgh No. 8	
	Raw	Clean	Raw	Clean
Moisture	16.90	1.95	1.97	1.12
Ash	16.11	2.61	6.75	2.97
Total S	5.10	2.54	3.17	1.82
Pyritic S	2.37	0.22	1.35	0.03
Sulfate S	0.36	0.04	0.41	0.12
Organic S	2.36	2.27	1.42	1.67
Mineral Matter <sup>b</sup>	19.32	3.05	8.26	3.37

<sup>a</sup> Values are expressed as wt. % on a dry basis, except for moisture.

<sup>b</sup> Calculated using the modified Parr formula:

Mineral Matter = 1.13 (ash) + 0.47 (pyritic sulfur), as defined in ref. (2).

**AIA-SEM Analysis.** The AIA-SEM system consists of a JEOL (Japan Electron Optics Laboratory) model JSM-U3 scanning electron microscope, a LeMont Scientific B-10 image analyzer, and a Tracor Northern TN-2000 energy-dispersive x-ray analyzer. The image analyzer is a software-based system with associated electronics for SEM beam control, image amplification, and thresholding. The software base for image analysis allows the appropriate analysis algorithm to be selected for the particular sample and image conditions encountered. The particle boundaries, or the so-called particle extents, are determined from the points at which horizontal scans cross a feature, and particle outline is reconstructed from these adjacent chords of a particle. Once the outline has been determined, the x-ray data are collected from the center of the particles.

Samples were analyzed in the SEM using 25-kV beam voltage, 1-2 nA sample currents, 300x magnification, and backscattered electron imaging. A point density of 1024 pixels across the screen was used to provide  $\pm 10\%$  accuracy on measurements as small as 1% of the field of view. EDX data were collected for 4 sec. per particle at a typical counting rate of 1000 counts per sec. Approximately 4000 particles were analyzed per sample at a rate of 200 particles per hour. Regions of interest were set to monitor the intensities of 30 elements. However, the only elements occurring with significant frequency were: Na, Mg, Al, Si, P, S, Cl, K, Ca, Ti, and Fe.

**Data Handling.** The particles were classified into one of nine mineral categories based on the relative amounts of the elements present and according to the definitions given in Table II. The categories were derived from previously established guidelines (3,4) and included the common coal minerals pyrite, quartz, calcite, siderite, kaolinite, and illite. Several other minerals were identified, but they occurred in such small amounts that they were classified together into one common category titled "MINORS". This category included the minerals gypsum, dolomite, rutile, alumina, and

apatite. In addition, several other categories were defined to accommodate particles not corresponding to any of the above definitions. For example, a "SILICATES" category was defined to include particles with significant silicon content, yet with the balance of the elements in such proportions that the particle would not fit into either the quartz, kaolinite, or illite categories. A "MISCELLANEOUS" category was provided to include those particles whose composition did not allow them to fall into any of the above-mentioned categories. Further descriptions of the instrumental, statistical, classifying, and processing techniques are given elsewhere (5).

Table II. Chemical Definitions for Mineral Phases

Mineral Phase	Definition by Chemical Composition (in % Range) <sup>a</sup>	Specific Gravity
PYRITE	S 10-80; Fe 10-70	5.00
KAOLINITE	Al 15-80; Si 15-85; Al/Si 0.33-3.0	2.65
ILLITE	Al 10-50; Si 20-85; Mg 0-15; Ca 0-35; Fe 0-40; Ti 0-15	2.75
QUARTZ	Si 65-100	2.65
CALCITE	Ca 70-100	2.80
SIDERITE	Fe 70-100; Mn 0-30; Ni 0-30	5.00
MINORS (includes the following categories)		
GYPSUM	S 10-80; Ca 10-70	2.30
DOLOMITE	Mg 10-60; Ca 60-100	2.90
RUTILE	Ti 70-100	4.50
ALUMINA	Al 65-100	4.00
APATITE	P 15-40; Ca 30-100	3.20
SILICATES	Si 20-80	2.70
MISCELLANEOUS	(no restrictions, all particles accepted)	2.00

<sup>a</sup>Specifications may be given for the amount of other elements that are allowed to be present. Such specifications allow minor amounts of elements not specifically listed in the class definition to be present, but they place an upper limit on the allowable amount.

Using the AIA procedures, mineral particles were classified into sizes and mineral phases. Area-equivalent diameter, i.e. the diameter of a circle with the same area as that measured for the mineral particle, was used as the size parameter for data presentation. Using available literature values for the specific gravity of the individual minerals, the data were then expressed as the weight fraction of the mineral matter within a given mineral/size category. The weight fraction data were then normalized using the mineral matter content to present the mineralogical estimates on a dry coal basis in order to provide a common base for comparing the coals before and after the cleaning process.

### Results and Discussion

ASTM analytical data presented in Table I indicate that the float-sink separation achieved an 84% and a 56% removal of ash from

the Illinois and Pittsburgh coals, respectively, with corresponding decreases in total and pyritic sulfur of 50 and 91% and of 43 and 97%, respectively. If expressed as a reduction in the total mineral matter content, based on using a modified Parr formula (2), the corresponding values are 84% for the Illinois coal and 59% for the Pittsburgh coal.

The AIA data for the Illinois coal and for the Pittsburgh coal are much more interesting. Results for the Illinois coal (Tables IIIa-c) show that pyrite, quartz, and two clays (kaolinite and illite in approximately equal proportions) make up the bulk of the mineral matter, 72% in the raw and 80% in the clean coal. Furthermore, all the mineral phases except pyrite are rather uniformly distributed in the raw coal over the entire range of particle size from less than 4  $\mu\text{m}$  to more than 36  $\mu\text{m}$  in diameter.

Table IIIa. AIA Results for Illinois No. 6 Raw Coal (200 x 0 Mesh), Expressed as Weight Percent of Dry Coal

Mineral Phase	Particle Size						Totals
	<4 $\mu\text{m}$	<7 $\mu\text{m}$	<12 $\mu\text{m}$	<21 $\mu\text{m}$	<36 $\mu\text{m}$	>36 $\mu\text{m}$	
Pyrite	0.14	0.84	1.31	1.86	1.43	2.29	7.86
Kaolinite	0.08	0.42	0.43	0.33	0.19	0.35	1.81
Illite	0.03	0.31	0.41	0.39	0.29	0.37	1.80
Quartz	0.10	0.62	0.80	0.58	0.27	0.13	2.51
Siderite	0.00	0.02	0.00	0.02	0.01	0.00	0.05
Calcite	0.00	0.03	0.10	0.10	0.16	0.47	0.87
Silicates	0.07	0.34	0.44	0.37	0.26	1.14	2.62
Minors	0.05	0.29	0.28	0.32	0.09	0.22	1.25
Miscellaneous	0.02	0.09	0.16	0.08	0.09	0.12	0.55
Totals	0.49	2.97	3.94	4.06	2.78	5.08	19.32

Table IIIb. AIA Results for Illinois No. 6 Coal Floated at 1.3 Sp. Gr., Expressed as Weight Percent of Dry Coal

Mineral Phase	Particle Size						Totals
	<4 $\mu\text{m}$	<7 $\mu\text{m}$	<12 $\mu\text{m}$	<21 $\mu\text{m}$	<36 $\mu\text{m}$	>36 $\mu\text{m}$	
Pyrite	0.19	0.28	0.42	0.21	0.07	0.00	1.17
Kaolinite	0.10	0.16	0.09	0.02	0.03	0.00	0.40
Illite	0.12	0.12	0.11	0.07	0.00	0.00	0.42
Quartz	0.16	0.19	0.18	0.09	0.01	0.00	0.63
Siderite	0.02	0.01	0.01	0.02	0.02	0.00	0.08
Calcite	0.00	0.00	0.00	0.00	0.00	0.00	0.01
Silicates	0.08	0.05	0.03	0.02	0.02	0.00	0.20
Minors	0.02	0.02	0.01	0.00	0.00	0.00	0.04
Miscellaneous	0.04	0.03	0.02	0.00	0.00	0.00	0.08
Totals	0.72	0.86	0.87	0.44	0.16	0.00	3.05

Table IIIc. Percent Removal of Minerals from Illinois No. 6 Coal, Based on Values in Tables IIIa and IIIB Before Rounding

Mineral Phase	Particle Size						Totals
	<4 $\mu\text{m}$	<7 $\mu\text{m}$	<12 $\mu\text{m}$	<21 $\mu\text{m}$	<36 $\mu\text{m}$	>36 $\mu\text{m}$	
Pyrite	--	66	68	88	94	100	85
Kaolinite	--	63	79	93	81	100	77
Illite	--	62	73	81	100	100	76
Quartz	--	69	77	84	94	100	75
Siderite	--	12	--	33	--	--	--
Calcite	75	90	95	95	100	100	98
Silicates	--	84	92	93	92	100	92
Minors	66	94	95	100	100	100	96
Miscellaneous	--	70	89	100	100	100	85
Total	--	71	77	89	94	100	84

In the supercleaned Illinois coal, the levels of almost all minerals have been reduced by 60-85% somewhat uniformly for most of the particle size ranges up to 21  $\mu\text{m}$ . Above that size, the removal increases sharply, with nearly complete removal for the larger sizes. This is depicted graphically for pyrite, kaolinite, illite, and quartz in Figures 1 and 2 and for pyrite alone in Figure 3.

The 21- $\mu\text{m}$  cut-off, very evident in Figure 3 for pyrite, seems reasonable when the following calculation is considered. A 21- $\mu\text{m}$  pyrite phase (specific gravity of 5.0) embedded in a 200-mesh (i.e., 75- $\mu\text{m}$ ) coal particle (specific gravity of  $\sim 1.25$ ) accounts for only 2.2% of the total volume. However, because it accounts for 8.2% of the total weight of such a particle, it increases the specific gravity of the total assemblage to over 1.33; it is thus rejected in the float-sink separation. A 12- $\mu\text{m}$  pyrite phase, however, accounts for about 1% of the volume of the 74- $\mu\text{m}$  assemblage, while the specific gravity is increased to only 1.29; thus it is carried along with the float fraction. Of course, since the size consist is 200 mesh x 0, there are many small pyrite particles completely liberated or attached to smaller sized coal particles; however, the cut-off at 21  $\mu\text{m}$  is still remarkably sharp. Furthermore, since the specific gravities for the other minerals are lower than for pyrite, similar calculations for the other minerals should yield a higher value for the particle size at the cut-off point.

The overall removal of 84% of the total mineral matter, when broken down by particle size, shows an expected trend of increasing with increasing particle size (see Figures 2 and 3, for example). The cleaning effectiveness ranges from  $\sim 70\%$  for the smaller particles (4-12  $\mu\text{m}$ ), to 89% at 21  $\mu\text{m}$ , and to 100% for particles larger than 36  $\mu\text{m}$ .

The AIA results for the Pittsburgh No. 8 coal (Tables IVa-c) show a distinctly different character of this coal. The mineral matter in the raw sample is more than 50% pyrite (see especially Figure 4). Although the total amount of clay plus quartz is only one-fourth that of the Illinois No. 6 coal, the clay-to-quartz ratio is much higher. In addition, a substantially larger fraction of

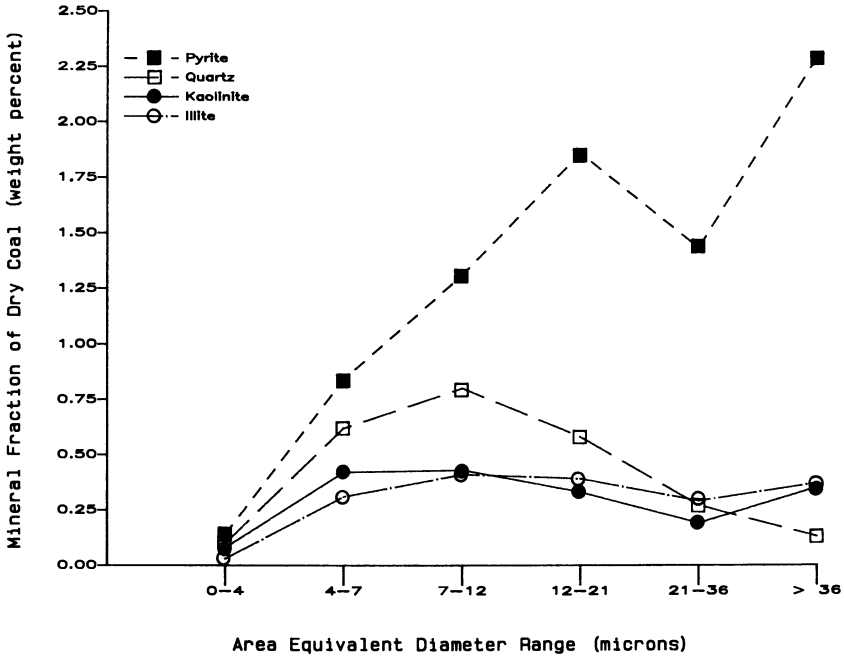


Figure 1. AIA results for Illinois No. 6 raw and (200 x 0 mesh).

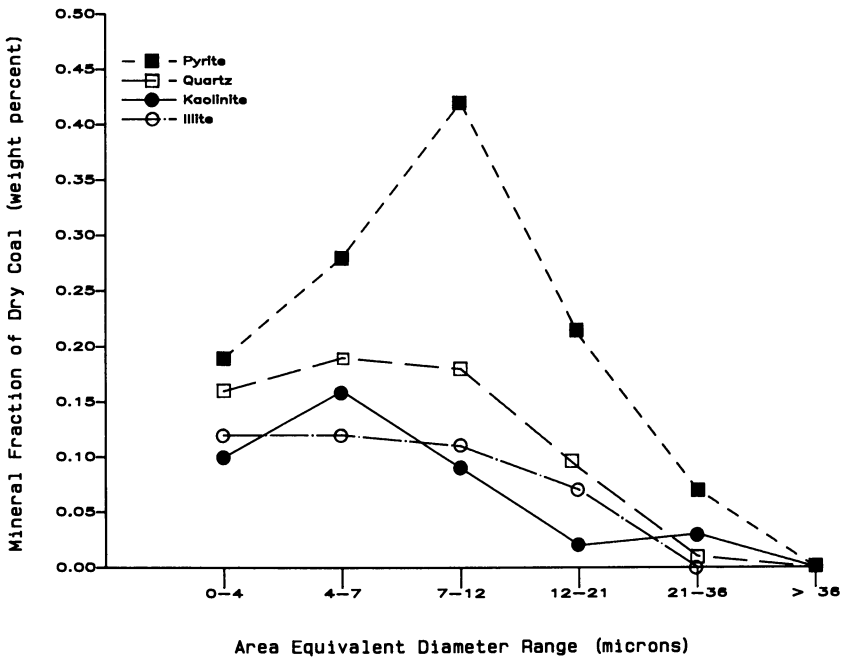


Figure 2. AIA results for Illinois No. 6 clean coal (200 x 0 mesh).

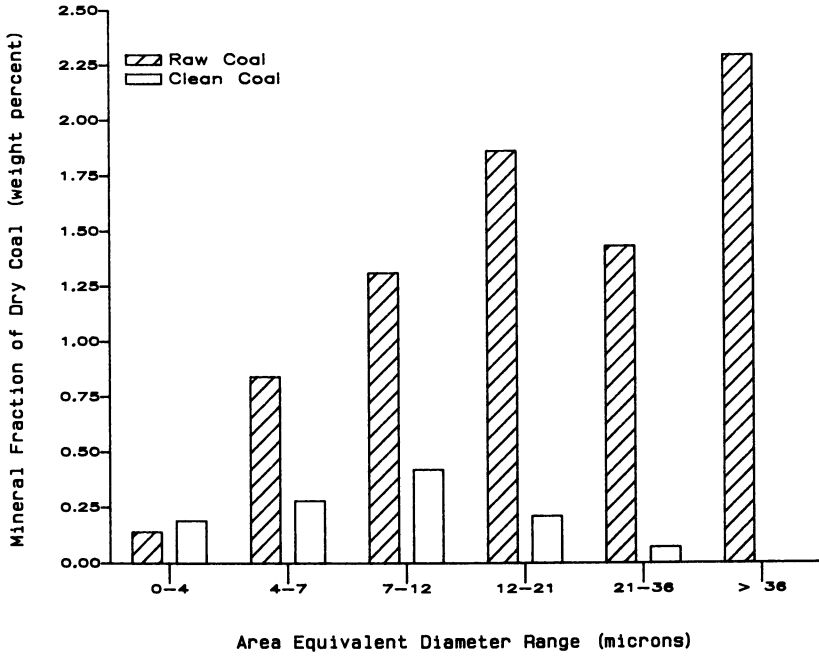


Figure 3. Pyrite distribution in raw and cleaned Illinois No. 6 coal (200 x 0 mesh).

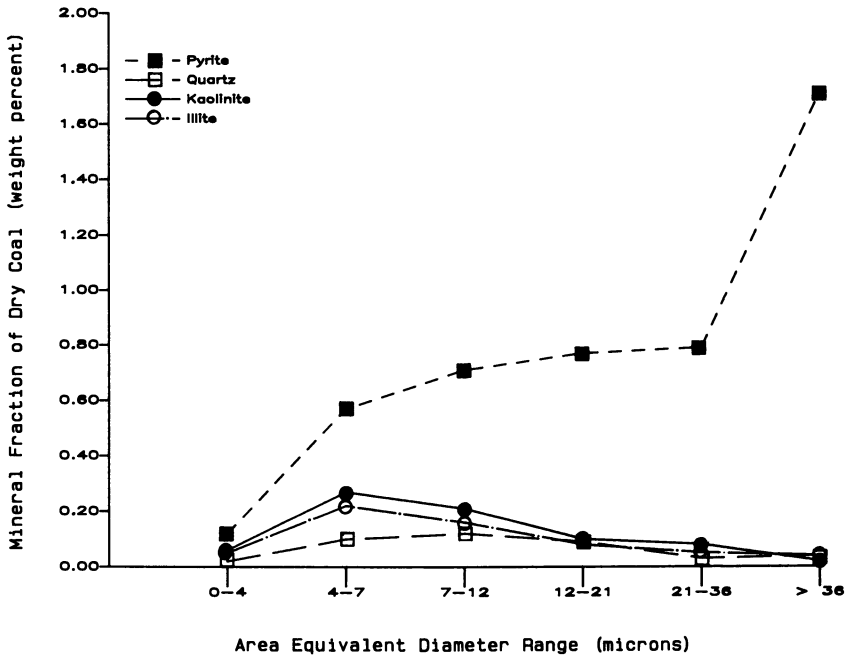


Figure 4. AIA results for Pittsburgh No. 8 raw coal (200 x 0 mesh).

Table IVa. AIA Results for Pittsburgh No. 8 Raw Coal (200 x 0 mesh), Expressed as Weight Percent of Dry Coal

Mineral Phase	Particle Size						Totals
	<4 $\mu\text{m}$	<7 $\mu\text{m}$	<12 $\mu\text{m}$	<21 $\mu\text{m}$	<36 $\mu\text{m}$	>36 $\mu\text{m}$	
Pyrite	0.12	0.57	0.71	0.77	0.79	1.71	4.67
Kaolinite	0.06	0.27	0.21	0.10	0.08	0.02	0.73
Illite	0.05	0.22	0.16	0.08	0.05	0.04	0.61
Quartz	0.02	0.10	0.12	0.09	0.03	0.04	0.39
Siderite	0.00	0.02	0.03	0.02	0.01	0.10	0.18
Calcite	0.00	0.01	0.01	0.01	0.01	0.00	0.04
Silicates	0.01	0.04	0.05	0.05	0.05	0.06	0.26
Minors	0.07	0.27	0.16	0.08	0.10	0.13	0.80
Miscellaneous	0.02	0.09	0.05	0.04	0.05	0.34	0.58
Totals	0.35	1.59	1.47	1.25	1.17	2.43	8.26

Table IVb. AIA Results for Pittsburgh No. 8 Coal Floated at 1.3 Sp. Gr., Expressed as Weight Percent of Dry Coal

Mineral Phase	Particle Size						Totals
	<4 $\mu\text{m}$	<7 $\mu\text{m}$	<12 $\mu\text{m}$	<21 $\mu\text{m}$	<36 $\mu\text{m}$	>36 $\mu\text{m}$	
Pyrite	0.21	0.33	0.35	0.08	0.00	0.00	0.96
Kaolinite	0.28	0.45	0.21	0.04	0.00	0.00	0.98
Illite	0.24	0.35	0.11	0.01	0.00	0.00	0.70
Quartz	0.07	0.17	0.07	0.02	0.00	0.00	0.34
Siderite	0.00	0.01	0.01	0.03	0.00	0.00	0.05
Calcite	0.00	0.01	0.01	0.01	0.00	0.00	0.02
Silicates	0.02	0.02	0.01	0.00	0.00	0.00	0.05
Minors	0.02	0.03	0.01	0.04	0.00	0.00	0.10
Miscellaneous	0.06	0.08	0.03	0.00	0.00	0.00	0.17
Totals	0.91	1.43	0.80	0.22	0.00	0.00	3.37

the mineral content is present in the larger size ranges. This coal exhibits a much sharper cut-off in the effectiveness of cleaning as a function of particle size. As shown in Figures 5 and 6 the super-clean coal fraction contains no mineral particles larger than 21  $\mu\text{m}$  in diameter. The smaller size fractions show only small amounts of mineral matter removed. For the two smallest sizes, even a slight enrichment can be seen for several mineral phases. This apparent enrichment is partially the result of a mathematical anomaly of the normalization process and partially due to the decrease in the total weight by the removal of other mineral matter from the larger fractions. In any case, the absolute mineral content in these very small size fractions is so minute that the allowed analytical errors can account for the discrepancy, and the overall differences become negligible.

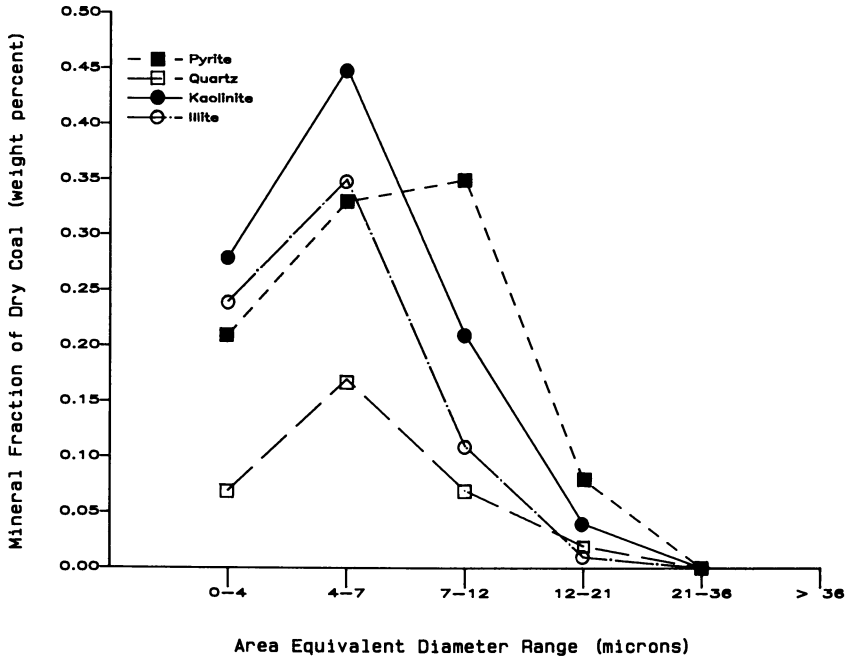


Figure 5. AIA results for Pittsburgh No. 8 clean coal (200 x 0 mesh).

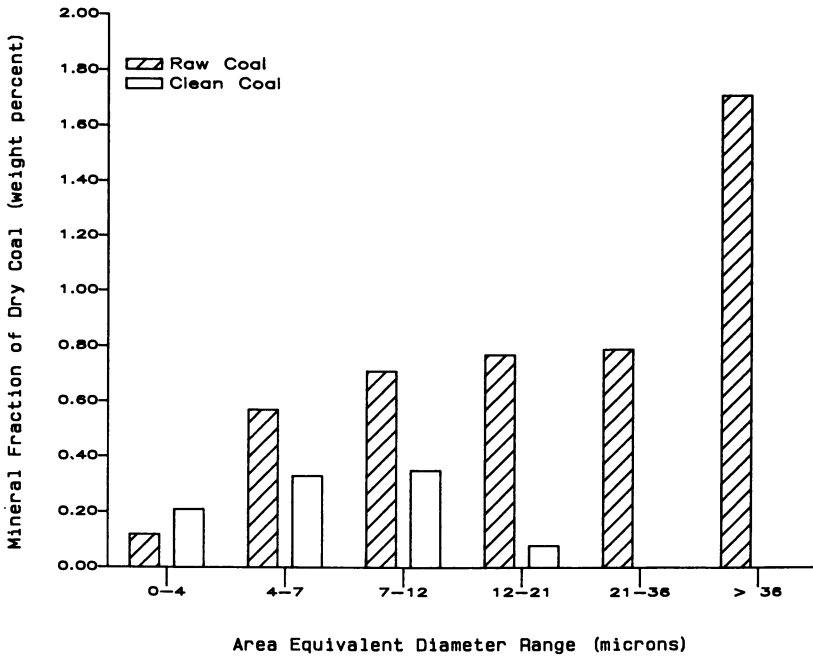


Figure 6. Pyrite distribution in raw and cleaned Pittsburgh No. 8 coal (200 x 0 mesh).



Table IVc. Percent Removal of Minerals from Pittsburgh No. 8 Coal, Based on Values in Tables IVa and IVb Before Rounding

Mineral Phase	Particle Size						Totals
	<4 $\mu\text{m}$	<7 $\mu\text{m}$	<12 $\mu\text{m}$	<21 $\mu\text{m}$	<36 $\mu\text{m}$	>36 $\mu\text{m}$	
Pyrite	--	42	51	89	100	100	79
Kaolinite	--	--	--	57	100	100	--
Illite	--	--	32	93	100	100	--
Quartz	--	--	39	76	100	100	14
Siderite	--	59	30	--	100	100	67
Calcite	70	39	--	55	100	--	45
Silicates	42	44	78	100	100	100	80
Minors	66	89	91	53	100	100	87
Miscellaneous	--	10	53	100	100	100	72
Total	--	9	45	82	100	100	59

Another observation, however, should be scrutinized more closely. In both coals, the content of pyrite as determined by AIA-SEM is consistently higher than that calculated from the pyritic sulfur values obtained by the ASTM procedure. Since the accuracy for ASTM analyses, i.e., reproducibility between different labs, can be within 0.30 or 0.40% for less than or more than 2.0% pyritic sulfur, respectively (6), part of the discrepancy could be explained by the possible analytical error. A more plausible interpretation can be given if the ASTM leachings with nitric acid do not remove all of the pyrite; for example, significant residues of pyrite have been observed previously in such leached coal samples (7). Another possible explanation can reside in the specific gravity of pyrite used. Although 5.0 is the literature value for mineral-grade pyrite, past work in this laboratory established that coal-derived pyrite can have a specific gravity significantly lower, ranging from about 3.60 for hand-picked samples to 4.25-4.50 for samples which have been extensively cleaned with hot hydrochloric acid (8).

Finally, since the intensity of the backscattered electron image used for AIA is highly dependent on the average atomic number of the material in view, pyrite particles with the heavy iron atom cross too often the signal threshold which has been set for a level characterized by clays, thus increasing the possibility of reading more pyrite. A similar bias has been observed previously (9), and an empirical factor of 0.75 has been suggested to scale down the inflated pyrite results.

Although the absolute values for the pyrite content are divergent, the relative amounts removed (on a wt. % basis) are relatively comparable for both methods of analysis. However, further work is in progress to resolve this issue of the pyrite content.

### Conclusions

Automated image analysis used in conjunction with scanning electron microscopy and energy-dispersive x-ray analysis has been shown to be an effective tool to characterize in-situ the mineral matter in raw

and cleaned coal. Both mineral phase analysis and particle size distribution were obtained for two coals (200 mesh x 0) before and after processing. For Illinois No. 6 coal, which contained mostly pyrite, quartz, kaolinite, and illite rather uniformly distributed among the various particle sizes, the cleaning effectiveness increased gradually with increasing particle size of the mineral phases. The levels of removal ranged from about 75% for the smallest particles to 100% for particles larger than 36  $\mu\text{m}$ . For the Pittsburgh coal, more than half of the mineral matter was pyrite, and the pyrite was relatively coarse. The other minerals were smaller in size. During cleaning of the Pittsburgh coal, most of the large-sized mineral matter was removed, while the finer-sized mineral matter was relatively untouched. The cut-off size was approximately 21  $\mu\text{m}$ .

### Acknowledgments

Ames Laboratory is operated for the U. S. Department of Energy by Iowa State University under Contract No. W-7405-Eng-82.

This work was supported by the Assistant Secretary for Fossil Energy, Division of Coal Utilization, through the Pittsburgh Energy Technology Center. The authors wish to thank Professor D. L. Biggs for collecting the coal samples and to J. Cavallaro (PETC) for cleaning the coal samples by float-sink separation.

### Literature Cited

1. Wheelock, T.D.; and Markuszewski, R. "Coal Preparation and Cleaning." In The Science and Technology of Coal and Coal Utilization, Cooper, B.R.; Ellingson, W.A., Eds.; Plenum Press: New York, 1984, pp. 47-123.
2. Given, P.H.; Yarzab, R.F. "Analysis of the Organic Substance of Coals: Problems Posed by the Presence of Mineral Matter." In Analytical Methods for Coal and Coal Products, Karr, C. Jr., Ed.; Academic Press: New York, 1978, Vol. II, pp. 3-41.
3. Huggins, F.E.; Huffman, G.P.; Lee, R.J. "Scanning Electron Microscope-Based Automated Image Analysis (SEM-AIA) and Moessbauer Spectroscopy -- Quantitative Characterization of Coal Minerals." In Coal and Coal Products: Analytical Characterization Techniques, Fuller, E.L. Jr., Ed.; ACS SYMP. SERIES 205, American Chemical Society: Washington, D. C., 1982, pp. 239-258.
4. Lebidzik, J., LeMont Scientific, Inc., State College, PA, personal communication, Fall 1980.
5. Straszheim, W.E.; Markuszewski, R. "Application of Scanning Electron Microscopy and Automated Image Analysis for Characterization of Mineral Matter in Coal," Am. Chem. Soc. Div. Fuel Chem. Preprints, 1985, 30(1), 47-55.
6. American Society for Testing and Materials, Annual Book of ASTM Standards, Section 5: Petroleum Products, Lubricants, and Fossil Fuels, Philadelphia, 1983, Method D2492.
7. Greer, R.T. "Organic and Inorganic Sulfur in Coal," Scanning Electron Microscopy/1979, Vol. I, pp. 477-485.

8. Chuang, K.C.; Chen, M.-C.; Greer, R.T.; Markuszewski, R.; Sun, Y.; Wheelock, T.D. "Pyrite Desulfurization by Wet Oxidation in Alkaline Solutions," Chem. Eng. Commun. 1980, 7, 79-94.
9. Huggins, F.E.; Kosmack, D.A.; Huffman, G.P.; Lee, R.J. "Coal Mineralogies by SEM Automatic Image Analysis," Scanning Electron Microscopy/1980, Vol. I, pp. 531-540.

RECEIVED August 19, 1985

## Behavior of Quartz, Kaolinite, and Pyrite during Alkaline Leaching of Coal

C.-W. Fan, R. Markuszewski, and T. D. Wheelock

Chemical Engineering Department and Energy and Mineral Resources Research Institute, Iowa State University, Ames, IA 50011

Most of the mineral matter was extracted from Illinois No. 6 coal, a representative bituminous coal, by first leaching it with a hot alkaline solution and then with a dilute mineral acid. The alkalis employed, in decreasing effectiveness, were: (1) NaOH, (2) Na<sub>2</sub>CO<sub>3</sub>, (3) NaHCO<sub>3</sub>. The results generally agreed with those obtained in leaching quartz, kaolinite, and iron pyrite individually under similar conditions. The quartz was solubilized by the stronger alkalis. Kaolinite was largely converted to sodium hydroaluminosilicates such as analcime, hydroxycancrinite, and natrodavynite. A portion of the iron pyrite was converted to hematite, the amount depending on alkali strength and temperature. The sodium hydroaluminosilicates and hematite were subsequently extracted by acid.

Previous work has shown that ash-forming mineral matter, including iron pyrites, can be removed from coal by leaching the finely divided material with a hot caustic solution under pressure followed by washing with a dilute mineral acid (1-6). Recently, similar results have been achieved in leaching fine-size coal with hot sodium carbonate solutions (7). In both cases, quartz appears to dissolve in the hot alkaline solution, while clay minerals and iron pyrite are converted into acid-soluble compounds which are removed in the acid washing step. Acid also removes any carbonate minerals which are present in the coal.

In the present study the behavior of some of the principal coal minerals was traced during alkaline leaching. This was accomplished by leaching several types of coal and by leaching individual minerals, which are commonly present in coal, with various alkalis. Different alkali concentrations and temperatures were employed. The solid reaction products were characterized by x-ray diffraction (XRD) and by dissolution in mineral acids. Results achieved with Illinois No. 6 coal are discussed, since they are representative, and the results of individually leaching quartz, kaolinite, and iron pyrite

are described because these minerals generally account for a major portion of the mineral matter in many coals.

#### Experimental Methods

Illinois No. 6 coal, obtained from the Elm Mine in Illinois, was dried under nitrogen at 90°C for 24 hr. and then ground to -74  $\mu\text{m}$  size. Analysis of the dry coal by ASTM methods (8) revealed the following composition: 12.75% ash, 1.32% pyritic sulfur, 0.24% sulfate sulfur, 1.68% organic sulfur, and 3.24% total sulfur. Examination by XRD showed the principal mineral impurities to be iron pyrite, quartz, kaolinite, and calcite (Table I). Iron pyrite nodules were obtained from refuse produced in cleaning coal from Mahaska County, Iowa. The nodules were crushed and then ball-milled to -38  $\mu\text{m}$  size; principal impurities determined by XRD are indicated in Table I. Part of the ground pyrite was treated for 1 hr. with excess 1.2 *M* hydrochloric acid at 70°C under nitrogen to remove acid-soluble impurities; it was then washed and dried. The acid-cleaned material contained 88% iron pyrite, based on total sulfur content, and significant amounts of quartz and kaolinite plus a trace of titania. In addition, the material seemed to contain a non-crystalline constituent which may have been coal. Quartz obtained for this study did not appear to contain significant amounts of any impurities when examined by XRD. On the other hand, the kaolin which was obtained seemed to contain a significant amount of quartz and trace quantities of illite and titania.

For the leaching experiments, a weighed amount of finely divided coal or mineral matter was mixed with 120 ml. of alkaline solution in a 300-ml. stainless steel (Type 316) autoclave equipped with a turbine agitator. The system was flushed with nitrogen and then heated to the desired leaching temperature. The mixture was stirred continuously while leaching was conducted at constant temperature and pressure for a specified period. After this treatment, the autoclave

Table I. Materials Which Were Chemically Treated

Material	Source	Size, $\mu\text{m}$	Impurities Indicated by XRD
Illinois No. 6 coal	Trivoli County (Ill.)	-74	$\text{FeS}_2$ , $\text{SiO}_2$ , kaolinite, $\text{CaCO}_3$
Raw pyrite	Coal, Mahaska County (Ia.)	-38	$\text{CaCO}_3$ , iron oxides, $\text{SiO}_2$ , kaolinite, $\text{TiO}_2$
Cleaned pyrite	Same as above	-38	$\text{SiO}_2$ , kaolinite, $\text{TiO}_2$
Quartz	Ottawa Sand (Ill.)	-38	None
Kaolin	Old Hickory No. 5 ball clay (Ky.)	-74	$\text{SiO}_2$ , Illite, $\text{TiO}_2$

was cooled quickly, and the contents of the autoclave were filtered to recover any undissolved solids. The solids were washed with water, dried in an oven, weighed, and divided into two parts. One part was analyzed by XRD or other means, and the other part was treated with acid to determine the proportion of acid-soluble material. For the acid treatment step, up to 3 g. of alkali-leached material was mixed with 300 ml. of mineral acid (approximately 2 M) in a stirred, three-neck Pyrex reaction flask fitted with a reflux condenser. The treatment was conducted for 30 min. either at room temperature (25°C) or at the boiling point (100°C). After the treatment the mixture was filtered, and any undissolved solids were washed with 600 ml. of water, dried, weighed, and analyzed by XRD or other means. XRD analysis was performed with a Siemens D500 diffractometer using copper  $K_{\alpha}$  radiation. The ash content of the treated coal was determined by ASTM Method D3174 (8), while the sulfur content was determined with a Fisher model 475 total sulfur analyzer.

### Results with Coal

The results of leaching Illinois No. 6 coal with different alkaline solutions followed by acid treatment are shown in Table II. In each leaching experiment 15 g. of coal was leached with 120 ml. of alkaline solution at 250°C for 1 hr. In some experiments the alkali-leached coal was washed with hydrochloric acid, and in other experiments the coal was washed with sulfuric acid. When hydrochloric acid was employed, the acid washing step was conducted at the boiling point and the final water washing step at room temperature. However, when sulfuric acid was used, the washing steps were conducted at various temperatures to study the temperature effect.

Table II. Results of Treating Illinois No. 6 Coal with a Hot Alkaline Solution Followed by Acid Leaching

Alkali Trtmt.		Acid Trtmt.		Washing	Product, %			Reduction, %	
Type	<u>M</u>	Type	T., °C	T., °C	Yld. <sup>a</sup>	Ash <sup>b</sup>	S <sub>t</sub> <sup>a</sup>	Ash <sup>b</sup>	S <sub>t</sub> <sup>a</sup>
NaHCO <sub>3</sub>	2.0	HCl	100	25	95	6.57	3.14	48	15
Na <sub>2</sub> CO <sub>3</sub>	1.0	HCl	100	25	94	2.61	2.40	80	35
NaOH	2.0	HCl	100	25	83	1.28	1.95	90	47
Na <sub>2</sub> CO <sub>3</sub>	1.0	H <sub>2</sub> SO <sub>4</sub>	25	25	94	3.40	2.72	73	27
Na <sub>2</sub> CO <sub>3</sub>	1.0	H <sub>2</sub> SO <sub>4</sub>	100	25	94	3.26	3.09	74	17
Na <sub>2</sub> CO <sub>3</sub>	1.0	H <sub>2</sub> SO <sub>4</sub>	100	100	94	2.93	2.55	77	31

<sup>a</sup>Yield and total sulfur content on a dry, ash-free basis

<sup>b</sup>Ash content on a dry basis

The results of the coal leaching experiments indicate that the ash and total sulfur contents of the coal were reduced substantially while the product yield was generally high. The results were affected by the type of alkali, and the effectiveness of the alkali decreased in the following order:  $\text{NaOH} > \text{Na}_2\text{CO}_3 > \text{NaHCO}_3$ . Although the greatest reduction in ash and sulfur contents was realized with sodium hydroxide, the product yield (84%) was the lowest. The 47% reduction in total sulfur content achieved with sodium hydroxide was equivalent to the reduction which would have been realized if all of the inorganic sulfur had been removed and none of the organic sulfur. Sodium carbonate appeared to be only slightly less effective than sodium hydroxide in reducing the sulfur and ash contents of the coal, but it provided a greater yield (94%). Sodium bicarbonate appeared considerably less effective than the other alkalis. For coal leached with sodium carbonate, slightly lower ash and sulfur contents were obtained when the material was washed with hydrochloric acid than when it was washed with sulfuric acid. However, the effectiveness of the sulfuric acid treatment was improved by using hot acid and by using hot water instead of cold water to wash the acid-treated coals.

#### Results with Individual Minerals

To explain the preceding results with coal, a series of leaching experiments was carried out with individual minerals. In the first set of experiments,  $-38 \mu\text{m}$  size quartz particles were leached with various hot alkaline solutions to study the effects of alkali type, alkali concentration, ratio of alkali to quartz, temperature, and leaching time on dissolution. After each leaching, the reactor contents were filtered with Whatman No. 40 filter paper using suction, and the residue was washed with cold water, dried at  $350^\circ\text{C}$  for 2 hr., and weighed. The percentage of material extracted was calculated using the following expression:

$$\text{Extraction (\%)} = 100 - \frac{\text{wt. of residue}}{\text{wt. of feed}} \times 100 \quad (1)$$

The results of leaching quartz with sodium carbonate solutions having different concentrations are shown in Figure 1. For each point, 2.0 g. of quartz was leached with 120 ml. of solution at  $250^\circ\text{C}$  for the indicated time. It can be seen that the amount of material extracted increased linearly with time for about the first hour. During this period the rate of extraction also increased with alkali concentration to approximately the 0.5 power. Following the constant rate period, no further material was extracted. Apparently the solubility limit was reached, and it seemed to be the solubility limit at room temperature rather than at the leaching temperature. The following evidence pointed to the lower temperature limit. The residue remaining after leaching quartz for 2 hr. or more was an amorphous, non-crystalline solid which was insoluble in hot hydrochloric acid. Examination of the residue for various chemical elements by energy dispersive x-ray analysis revealed a high concentration of silicon and only a trace of sodium. The results suggested that quartz had dissolved in the hot solution, and upon cooling some of the silica had reprecipitated as an amorphous or

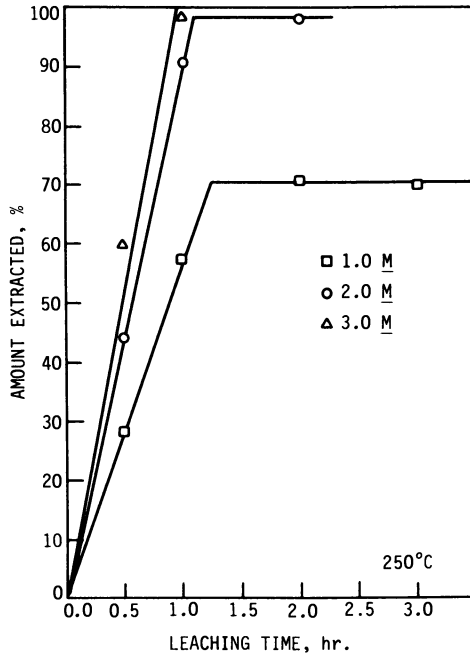


Figure 1. Dissolution of quartz (2.0 g.) by hot sodium carbonate solutions (120 ml.) having different concentrations.



glassy material. On the other hand, the residue remaining after quartz had been leached for less than 1 hr. appeared to be largely unreacted quartz. Furthermore, when quartz was leached for 1 hr. at the higher temperature of 300°C with a 1.0 M sodium carbonate solution, the amount of material extracted was only 69% which was no greater than the maximum amount extracted at 250°C. From published solubility data (9) for silica in various alkaline solutions, one would expect the solubility of quartz in a sodium carbonate solution to increase markedly with temperature.

Even though the amount of silica extracted seemed to be limited by the room temperature solubility limit, this limit was raised by increasing either the alkali concentration or the ratio of alkali to quartz. Thus by increasing the sodium carbonate concentration from 1.0 M to 2.0 M, the maximum amount extracted was raised from 70% to 98.5%. Moreover, when the quantity of quartz leached for 1 hr. with a 1.0 M solution at 250°C was reduced from 2 g. to 1 g., the percentage extracted increased from 58% to 95%.

Quartz was also leached for 1 hr. at 250°C with 2.0 M solutions of either sodium hydroxide or sodium bicarbonate. In each case 2.0 g. of quartz was leached with 120 ml. of solution. Most of the quartz (99.5%) was converted to soluble sodium silicates and extracted by the hot sodium hydroxide solution. On the other hand, only 10% of the quartz was extracted by the sodium bicarbonate solution, and the residue appeared to be entirely quartz. These values were noticeably different from the 58% extracted by 1.0 M sodium carbonate under similar conditions. Therefore, these solutions were not equivalent in leaching ability even though each provided the same number of moles of sodium. None of the residues remaining after leaching quartz with any of the alkalis were acid-soluble.

In a second set of experiments, -74  $\mu$ m size kaolin particles were leached with hot alkaline solutions to study the conversion of kaolinite to various sodium hydroaluminosilicate compounds (Table III) under different leaching conditions. In each experiment, 15 g. of kaolin was leached with 120 ml. of alkaline solution. The solid reaction product was recovered by filtration, washed with water, dried in an oven at 95°C, and analyzed by XRD. Although this method of analysis identified the minerals present, it could provide only an approximate indication of the relative proportions of the various minerals present. The amount of quartz was particularly difficult to assess because the method of detection was very sensitive to this mineral. Therefore, the results are reported only in terms of major, minor, and trace quantities present in the product as indicated by XRD (Table IV). Because the small amount of titania in the kaolin was apparently not affected by even the most rigorous leaching conditions, the product always contained a trace of this material and no further mention seems necessary.

When kaolin was leached with 1.0 M sodium carbonate at 200°C for 1 hr., most of the kaolinite was converted to the sodalite-type natrodavyne (NS) while the quartz and illite impurities were not affected noticeably (Table IV). Increasing the leaching temperature to 250°C resulted in the conversion of the kaolinite to a mixture of mixed-type natrodavyne (NCS) and analcime (A) and complete dissolution of the quartz impurity. The illite impurity was not affected. Leaching at 300°C and above resulted in the conversion of the

Table III. Various Sodium Hydroaluminosilicates Produced in Leaching Kaolinite with Hot Alkaline Solutions

Mineral	Chemical formula	Symbol
Analcime	$\text{Na}_2\text{O} \cdot \text{Al}_2\text{O}_3 \cdot 4(\text{SiO}_2) \cdot 2(\text{H}_2\text{O})$	A
Hydroxycancrinite	$\text{Na}_2\text{O} \cdot \text{Al}_2\text{O}_3 \cdot 2(\text{SiO}_2) \cdot \frac{2}{3}(\text{NaOH}) \cdot n(\text{H}_2\text{O})$	HC
Hydroxysodalite	(same as above)	HS
Natrodavyne (sodalite-type)	$\text{Na}_2\text{O} \cdot \text{Al}_2\text{O}_3 \cdot 2(\text{SiO}_2) \cdot \frac{1}{3}(\text{Na}_2\text{CO}_3) \cdot n(\text{H}_2\text{O})$	NS
Natrodavyne (cancrinite-type)	(same as above)	NC
Natrodavyne (mixed type)	(same as above)	NCS

kaolinite to the cancrinite-type natrodavyne (NC). Only at 350°C did the illite impurity appear to be affected.

A similar trend was observed when kaolin was leached for 1 hr. at 250°C with sodium carbonate solutions of different concentrations (Table IV). At the lowest concentration (0.2 M), part of the kaolinite was converted to the sodalite-type natrodavyne while the impurities were untouched. At the highest concentration of sodium carbonate (2.0 M), the kaolinite was converted to the cancrinite-type natrodavyne, and although the quartz was extracted, the illite remained.

Somewhat similar changes were observed when the leaching time was varied while holding the concentration of sodium carbonate at 1.0 M and the temperature at 250°C. With a leaching time of 0.5 hr. the kaolinite was converted to a mixture of analcime and sodalite-type natrodavyne, whereas with a leaching time of 2.0 hr. the kaolinite was largely converted to the cancrinite-type natrodavyne. Not all of the quartz was extracted when leaching was conducted for 0.5 hr., but all of the quartz appeared to be removed when leaching was conducted for longer periods. However, the illite remained even after 2 hr. of leaching.

When kaolin was leached with 1.0 M sodium hydroxide at 250°C for 1 hr., most of the kaolinite appeared to be converted to analcime (Table IV). Increasing the concentration to 2.0 M resulted in converting most of the kaolinite to hydroxycancrinite (HC). In either case the quartz impurity was extracted but the illite impurity remained. Leaching kaolin with 2.0 M sodium bicarbonate at 250°C for 1 hr. converted the kaolinite to the sodalite-type natrodavyne, but it had no apparent effect on the impurities.

To investigate the dissolution of the sodium hydroaluminosilicates produced by alkaline leaching, 3.0 g. portions of the leached product were treated with 300 ml. of acid in a stirred flask for 30 min. Either 2.0 M hydrochloric acid or 1.8 M sulfuric acid was utilized. While hydrochloric acid was always used at the boiling point, sulfuric acid was sometimes used at the boiling point and sometimes at room temperature. From XRD analysis of the solid

Table IV. Results of Leaching 15 g. Kaolin with 120 ml. Alkaline Solution

Leaching conditions				Mineral products excluding TiO <sub>2</sub> , type, (amount) <sup>a</sup>
Alkali	M	°C	hr.	
Na <sub>2</sub> CO <sub>3</sub>	1.0	200	1.0	NS(maj), SiO <sub>2</sub> (maj), kaolinite(min), illite(tr)
Na <sub>2</sub> CO <sub>3</sub>	1.0	250	1.0	NCS(maj), A(maj), illite(tr)
Na <sub>2</sub> CO <sub>3</sub>	1.0	300	1.0	NC(maj), A(min), illite(tr)
Na <sub>2</sub> CO <sub>3</sub>	1.0	350	1.0	NC(maj)
Na <sub>2</sub> CO <sub>3</sub>	0.2	250	1.0	SiO <sub>2</sub> (maj), kaolinite(min), NS(min) illite(tr)
Na <sub>2</sub> CO <sub>3</sub>	0.5	250	1.0	SiO <sub>2</sub> (maj), NS(maj), illite(tr)
Na <sub>2</sub> CO <sub>3</sub>	1.0	250	1.0	NCS(maj), A(maj), illite(tr)
Na <sub>2</sub> CO <sub>3</sub>	2.0	250	1.0	NC(maj), illite(tr)
Na <sub>2</sub> CO <sub>3</sub>	1.0	250	0.5	A(maj), NS(maj), SiO <sub>2</sub> (min), illite(tr)
Na <sub>2</sub> CO <sub>3</sub>	1.0	250	1.0	NCS(maj), A(maj), illite(tr)
Na <sub>2</sub> CO <sub>3</sub>	1.0	250	2.0	NC(maj), A(min), illite(tr)
NaOH	1.0	250	1.0	A(maj), HS(min), illite(tr)
NaOH	2.0	250	1.0	HC(maj), A(min), illite(tr)
NaHCO <sub>3</sub>	2.0	250	1.0	NS(maj), SiO <sub>2</sub> (maj), illite(tr)

<sup>a</sup>Amount: maj = major quantity, min = minor quantity, tr = trace quantity

residue remaining after the acid treatment, it was found that all of the sodalite-type and cancrinite-type compounds were dissolved by the acids whether hot or cold. On the other hand, analcime was completely dissolved only by the boiling acids.

In a third set of experiments,  $-38 \mu\text{m}$  pyrite particles were leached with hot alkaline solutions to study the conversion of iron pyrite to iron oxide and soluble sulfur species. In each experiment, 5 g. of acid-cleaned pyrite was leached with 120 ml. of alkaline solution for 1 hr. In addition to analyzing the solid residue by XRD, the total sulfur content of the leachate was determined in order to estimate pyrite conversion.

When pyrite was leached for 1 hr. with 1.0 M sodium carbonate at  $250^\circ\text{C}$ , only 12.7% of the pyrite was converted to iron oxide and soluble sulfur species (Table V). Increasing the leaching temperature to  $300^\circ\text{C}$  raised the conversion to 26.4%, and increasing the temperature to  $350^\circ\text{C}$  raised the conversion to 44.8%. In each case the solid residue consisted principally of hematite and unreacted pyrite.

Increasing the sodium carbonate concentration, while maintaining the leaching time at 1 hr. and temperature at  $250^\circ\text{C}$ , increased the pyrite conversion only slightly (Table V). On the other hand, when pyrite was leached with 2.0 M sodium hydroxide at  $300^\circ\text{C}$  for 1 hr., a conversion of 62% was achieved. Again, hematite appeared to be the principal solid reaction product.

When the pyrite residue from the alkaline leaching step was treated with acid, all of the hematite dissolved in either hot hydrochloric acid or hot sulfuric acid. However, the hematite appeared to dissolve incompletely or very slowly in cold sulfuric acid. Unreacted pyrite was not touched by the acids whether hot or cold.

#### Behavior of Mineral Matter During Coal Leaching

Following the preceding experiments with individual minerals, further consideration was given to the behavior of the mineral matter in coal

Table V. Results of Leaching 5 g. Acid-cleaned Pyrite with 120 ml. Alkaline Solution for 1 hr.

Alkali	Leaching conditions		Conv., %	Residue
	Conc., M	Temp., $^\circ\text{C}$		
$\text{Na}_2\text{CO}_3$	1.0	250	12.7	$\text{FeS}_2$ , $\text{Fe}_2\text{O}_3$
$\text{Na}_2\text{CO}_3$	1.0	300	26.4	$\text{FeS}_2$ , $\text{Fe}_2\text{O}_3$
$\text{Na}_2\text{CO}_3$	1.0	350	44.8	$\text{FeS}_2$ , $\text{Fe}_2\text{O}_3$
$\text{Na}_2\text{CO}_3$	1.0	250	12.7	$\text{FeS}_2$ , $\text{Fe}_2\text{O}_3$
$\text{Na}_2\text{CO}_3$	2.0	250	14.5	----
$\text{Na}_2\text{CO}_3$	3.0	250	15.8	----
NaOH	2.0	300	62.0	$\text{FeS}_2$ , $\text{Fe}_2\text{O}_3$

itself during leaching. The coal was examined by XRD after both the alkaline leaching step and the acid/water washing step. Leaching Illinois No. 6 coal with 2 M sodium bicarbonate at 250°C for 1 hr. appeared to convert essentially all of the kaolinite to natrodavyne and analcime and a small portion of the iron pyrite to hematite while not greatly affecting the quartz and calcite. However, it appeared that some of the quartz was converted to analcime since this mineral has a higher ratio of silica to alumina than is present in kaolinite. Following the subsequent acid washing step, the remaining mineral matter consisted mostly of quartz and pyrite. Leaching Illinois No. 6 coal with 1 M sodium carbonate under similar conditions also converted the kaolinite to natrodavyne and analcime and part of the pyrite to hematite; the quartz was either converted to soluble sodium silicates or analcime. After washing the alkali-treated coal with acid, pyrite seemed to constitute most of the remaining mineral matter. Leaching Illinois No. 6 coal with 2 M sodium hydroxide at 250°C for 1 hr. seemed to convert all of the kaolinite to hydroxycancrinite and a large portion of the pyrite to hematite; most of the quartz was extracted or converted. After washing the coal with acid, only a small amount of pyrite remained. These results were generally in good agreement with those observed in the leaching of individual minerals.

### Conclusions

Most of the mineral matter was removed from a representative coal (Illinois No. 6) by first leaching the finely ground material with a hot alkaline solution and then washing the product with a mineral acid and water. The effectiveness of various alkalis for converting or extracting mineral matter decreased in the following order:  $\text{NaOH} > \text{Na}_2\text{CO}_3 > \text{NaHCO}_3$ . Coal recovery, on the other hand, increased in the same order. Examination of the coal by XRD after each step and a study of the behavior of individual minerals when subjected to the same treatment indicated good agreement in results. In other words, the results were generally similar regardless of whether the minerals were leached individually or in a mixture with coal. The results of leaching several of the most prevalent minerals in coal on an individual basis are summarized below.

It was shown that fine-size quartz particles readily dissolve in 1-2 M sodium carbonate or sodium hydroxide at 250°C. However, when quartz is extracted by a hot solution which is then cooled, an amorphous, acid-insoluble material is produced under some conditions. A likely possibility is that amorphous silica precipitates when the room temperature solubility limit of the material is exceeded. Formation of the amorphous material is prevented by using higher concentrations of alkali or a higher ratio of alkali to silica.

It was also shown that kaolinite reacts with hot alkaline solutions to form various sodium hydroaluminosilicates which are acid-soluble. The particular sodium hydroaluminosilicate formed depends on the type of alkali employed, the alkali concentration, the treatment temperature, and length of treatment. When sodium carbonate is employed, kaolinite is largely converted to the sodalite-type natrodavyne under less rigorous conditions and to the cancrinite-type natrodavyne under more rigorous conditions. Under intermediate

treatment conditions, the mixed-type natrodavyne and analcime are produced. When sodium hydroxide is employed, kaolinite is largely converted to analcime and hydroxycancrinite with the latter being favored by higher alkali concentrations.

It was further shown that iron pyrite reacts with hot alkaline solutions to form hematite and soluble sulfur species. Sodium hydroxide is considerably more effective than sodium carbonate for this reaction. However, the effectiveness of sodium carbonate solutions can be increased by increasing the treatment temperature and to a lesser extent by increasing the alkali concentration. The hematite produced is readily dissolved by hot mineral acids.

#### Literature Cited

1. Crawford, A. The de-ashing of coal by combined jig washing, froth flotation, and extraction with caustic soda, BIOS Final Report No. 522, Item No. 30, Feb. 19, 1946, British Intelligence Objectives Sub-Committee, London, (A.T.I.-118668, Central Air Documents Office, Wright-Patterson Air Force Base, Dayton, Ohio).
2. Reggel, L.; Raymond, R.; Wender, I.; Blaustein, B. D. Am. Chem. Soc. Div. of Fuel Chem. Preprints 1972, 17(1), 44.
3. Reggel, L.; Raymond, R.; Blaustein, B. D. U.S. Patent 3 993 455, 1976.
4. Stambaugh, E. P. In "Coal Desulfurization: Chemical and Physical Methods"; Wheelock, T. D., Ed.; ACS Symposium Series No. 64, American Chemical Society: Washington, D.C., 1977; pp. 198-205.
5. Stambaugh, E. P.; Sachsel, G. F. U.S. Patent 4 055 400, 1977.
6. Yang, R. T.; Das, S. K.; Tsai, B. M. C. Fuel 1985, 64, 735-742.
7. Fan, C.-W.; Markuszewski, R.; Wheelock, T. D. Am. Chem. Soc. Div. of Fuel Chem. Preprints 1984, 29(1), 114.
8. American Society for Testing and Materials. "Annual Book of ASTM Standards"; Part 26 (Methods D 3174 and D 3177), Philadelphia, PA, 1975.
9. Iler, R. K. "The Chemistry of Silica"; John Wiley and Sons: New York, 1979.

RECEIVED August 12, 1985

## Separation of Mineral Matter from Pittsburgh Coal by Wet Milling

Douglas V. Keller, Jr.

Otisca Industries, Ltd., Syracuse, NY 13208

The fracture of massive Pittsburgh coal permits some of the entrained mineral matter to be released as a distinct phase. A study of the variables that affect the release of mineral matter during the wet (water) milling process of that coal indicated that the mineral matter exists as a distinct and separable phase to a content of at least 0.5 weight percent mineral matter in the product coal. The reduction of mineral matter by physical separation procedures of the free mineral matter phase from the coal phase is directly related to the log of the mode of the particle size distribution of the raw coal. That relationship also appears to be insensitive to some of the common chemical additives that are introduced to enhance the rate of milling.

The term "inherent mineral matter, or ash" is a commonly used phrase in the coal literature (1). The phrase refers to that fraction of the mineral matter bound organically to the carbonaceous structure of the coal and estimates of its content suggest that it is in the range of two weight percent of the whole mineral matter (1). Common classical physical separation schemes such as differential specific gravity separations or froth flotation which are directed at demineralizing the coal never approach that lower limit. For example, at the outset of this investigation one could receive a raw Pittsburgh seam coal at 30 weight percent ash and through careful float-sink processes reduce that ash content into the range of four to five weight percent. Practically reducing that ash content, however, to below three weight percent with a reasonable yield was quite unlikely (2). One consequence of the large weight fraction differential between the practical limit of demineralization, and if you like, the true "inherent" limit of demineralization was a total lack of understanding as to whether or not that mineral fraction could indeed be extracted by physical means. With this as a basis, further questions could be raised as to whether or not that retained mineral matter was a true distinct mineral phase, or if so, could it be bound chemically along the interfaces to the coal structure rendering those particles inseparable. Most simply, in all cases

one could ask the question does a separation of mineral matter from the coal take place in all cases when coal is fractured and to what extent, or limit, can the fracture process be utilized in the demineralization of coal.

A series of experiments was assigned to explore the extraction of mineral matter from coal in the size ranges below 0.25 mm. The raw coal samples were obtained from three different sources in the Pittsburgh seam which permitted a degree of comparison over a rather large geographic area. The results are interesting in that they allow a new perspective in the demineralization of coal.

### Experimental

The Pittsburgh seam coals used in this investigation have a nominal analysis as illustrated in Table I.

Lots of Pittsburgh seam coal in excess of 1000 pounds each were received from three different sources in Washington County: Mine (A) was located about 20 miles west of Pittsburgh; Mine (B) was located just south of Pittsburgh; Mine (C) was located about 40 miles south of Pittsburgh. Representative samples from each source were obtained by ASTM procedures and subjected to the following processing.

A raw coal sample was reduced to 250  $\mu\text{m}$  x 0 by dry mechanical crushing in a hammermill and then ground in a laboratory sample mill. The mechanically ground coal was then mixed with water to form one liter of slurry with 30 weight percent solids and placed in a standard 3 liter laboratory ball mill using 3/8" alumina grinding media. All of ball milling variables were held constant except for the duration of milling which permitted a variation of the particle size distribution. In the event that chemicals were employed during the ball milling operation, those chemicals were incorporated in an excess of the amount of the standard mill content.

The coal water slurry was removed from the mill, diluted with water to ten weight percent solids and the coal fraction removed utilizing the Otisca T-Process (OTP) (2,3). Separations by the T-Process are unique in that agglomeration results in the recovery of virtually all of the carbonaceous material leaving a fully dispersed mineral phase in the residue water. Many detailed investigations of this type have concluded that mineral matter recovered with the coal phase is included in the coal; that is the ash content of the product coal represents only that mineral matter mechanically attached to or enveloped by the coal.

Analytical procedures for ash (high temperature, HT) and sulfur contents were conducted according to ASTM procedures. Low temperature ash procedures were conducted at 550°C in an oven with an adequate supply of oxygen. The difference in mineral matter morphology and chemistry between this technique and the low temperature ashing method described by Gluskoter (3), can be anticipated from the paper by Mitchell and Gluskoter (4). Principally the higher temperature ashing process will convert pyrite to hematite and kaolinite to metakaolinite by the loss of water of crystallization. Between 30% and 50% of the mineral matter in the Pittsburgh coal is considered to be kaolinite (5), and in this investigation we presumed that the 550°C ashing procedure did not significantly alter the particle size distribution of the original kaolinite particles. The presumption was tested by comparing the size distribution of raw



mineral matter and that fired at 550°C. Little change in size was noted.

A Micromeritics 5500L unit was used to obtain the particle size distribution data for this investigation. Data from the Micromeritics unit using a one  $\mu\text{m}$  mode sample was compared with the data developed by the manufacturer from a Coulter Counter on the same sample to within ten percent. Even with this in hand, there was no attempt to characterize the particles or their shape on an absolute basis. The Micromeritics unit provides particle diameter data in terms of "area percent" which are readily converted to "mass percent" by a mathematical format developed by Micromeritics, cf the instrument handbook. The observed area percent data from the Micromeritics unit was transposed to a mass percent base at data points  $y$  (in  $\mu\text{m}$ ) for all of the points  $y = 2^x$  where  $x = n + 0.5$  and  $n = -3, -2.5, \dots, 0, \dots, +7, +7.5$ . The data point at  $y$  represents that mass fraction of material lying in the size range  $x \pm 0.25 \mu\text{m}$ . The data given below are plotted with the ordinate providing either the mineral matter, low temperature ash or coal, content in weight percent based on the coal or as  $(dw/d(\log x))$  which is the weight percent of mineral matter in that particular size range ( $\log x$ ) of all the mineral matter present in the system.

The following particle size distribution data are given as a log distribution in particle diameter ( $\mu\text{m}$ ) where the mass points are interconnected for convenience of comparison at the expense of rigor. Typical distributions are bell-shaped where the mode is defined as the particle diameter at that point of half width of the curve at the half height of the maximum. The Micromeritic unit is based on a Stokes' Law settling of the particles where one must choose an average specific gravity of particles under investigation before the data are recorded. In those cases where low temperature ash particles were investigated, the iron minerals with a density larger than 4 gms/cc were separated in a dense fluid from the clay minerals with densities less than 3 gms/cc. All densities were determined by pycnometric methods. The distributions were measured individually and then the size distributions were recombined mathematically. The product coals demonstrated a very narrow specific gravity distribution in the range of 1.33.

### Results and Discussion

Figure 1 illustrates the particle size distribution of the mineral matter that results from the low temperature ashing of three 5 cm cubes of bright coal that were hand-picked from the various samples. The ash contents were in the range of five weight percent. It is of interest to note that band of mineral matter particles that lie in the particle diameter range between one and 50  $\mu\text{m}$  with a mode between four and eight  $\mu\text{m}$ . The particle size distribution data from the low temperature ashing of the 5 cm cubes of coal show that raw coal from each source has a unique "fingerprint" of mineral matter particles distributed in the particle size range below 250  $\mu\text{m}$ . It should be noted that the distribution curves are reproducible to within plus or minus five percent of the designated ash, or coal, content values given for each particle diameter range ( $y$ ).

Investigations of many other coal seams and coals within a particular seam indicate that indeed the mineral matter distribution

Table I. Nominal Analysis of Pittsburgh Seam Coal

	Weight Percent (Dry Basis)
Volatile Matter	35
Fixed Carbon	58
BTU/lb	14,200
Carbon	77.3
Hydrogen	5.2
Nitrogen	1.5
Chlorine	0.1
Sulfur	1.5
Oxygen (diff)	7.6
Ash	6.8

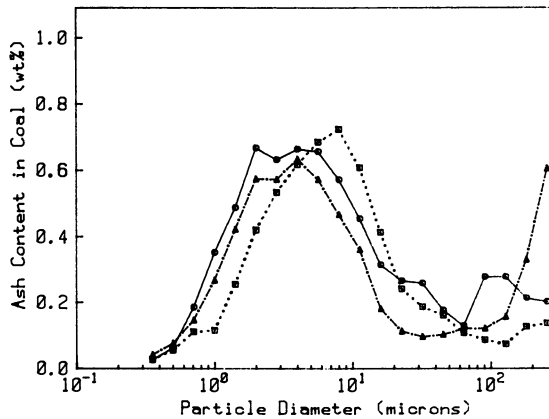


Figure 1. Particle size distributions of the low temperature ash products from three different 5 cm blocks of Pittsburgh seam coal: (○) Coal A; (▲) Coal B; and (□) Coal C.

varies widely both in shape and magnitude and as such cannot be anticipated from other coal properties. The mineral matter distribution is a fundamental property of that coal which is an uncontrolled natural variable in the extraction of mineral matter.

In order to demonstrate that the 5 cm cube was constituted of an accumulation of much smaller unit volumes, each of which represented the whole coal in mineral matter particle size distribution, a study of a series of size classified particles was undertaken. For example, if raw coal (C) were ground to  $250 \mu\text{m} \times 0$ , and then separated with standard sieves into the size fraction  $53 \times 44 \mu\text{m}$ , we would be afforded a dry mixture of raw coal particles and mineral particles with an average size of  $48 \pm 4 \mu\text{m}$ . Figure 2 illustrates the particle size distribution of the low temperature ash product of the product coal after the free mineral matter particles were removed. Again we have the characteristic curve very similar to the curve shown in Figure 1 (C). In fact, that portion of the curve that lies below  $3 \mu\text{m}$  can most usually be superimposed on other curves obtained in a similar manner from the other size fractions of coal (C). Providing, that is, that the original coal particle diameters are larger than  $10 \mu\text{m}$ .

The conclusion of that study indicated that product coal particles larger in diameter than the band of mineral matter microparticles seemed to contain the whole particle distribution of the small microparticles. That is, there appeared to be a relatively homogeneous distribution of particles throughout, limited in top size by the largest particle in the test. To explore that aspect in more depth, a raw coal was wet milled to smaller sizes.

When a raw coal is wet ball-milled for a sufficient time to produce a slurry with a particle diameter mode in the range of  $4 \mu\text{m}$  there results two forms of mineral matter: That fractured away from the coal and that which is still enveloped in the coal particles. Figure 3 illustrates a typical particle size distribution for the separated product coal as compared to the separated free mineral matter (90 weight percent ash) from one milling test. The separated mineral matter is clearly smaller in diameter than the coal which is probably due to its more brittle properties. Note that in Figures 3 and 4 an integration of the curves will yield 100% of the mineral matter (or ash) under consideration rather than the ash content of the coal as was the case in Figures 1 and 2.

When the product coal shown in Figure 3 was subjected to low temperature ashing as described above and that ash product subjected to particle size analysis, a curve as is illustrated in Figure 4 results. Clearly the enveloped mineral matter in the product coal particles is considerably smaller in diameter than the coal particles from which they came and as such are not available for separation by the T-Process. The T-Process separation rejects all particles of pure mineral matter and agglomerates as product coal all particles that have any fraction of coal exposed to the liquid system.

Two very important points are illustrated in Figures 1-4: Firstly, it appears that as coal fracture takes place in this system, mineral matter particles are ejected from the fractured coal system and most without attached coal. The implication is that the coal-mineral matter interfaces are not chemically bound. If those interfaces were chemically bound, one would observe mineral matter

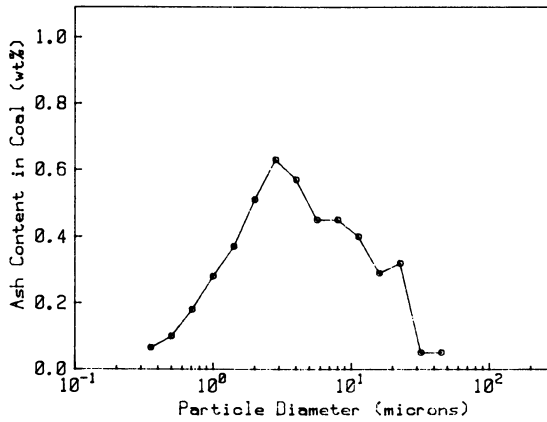


Figure 2. Particle size distribution of the low temperature ash product of a  $48 \pm 4 \mu\text{m}$  product coal after the free mineral matter was removed.

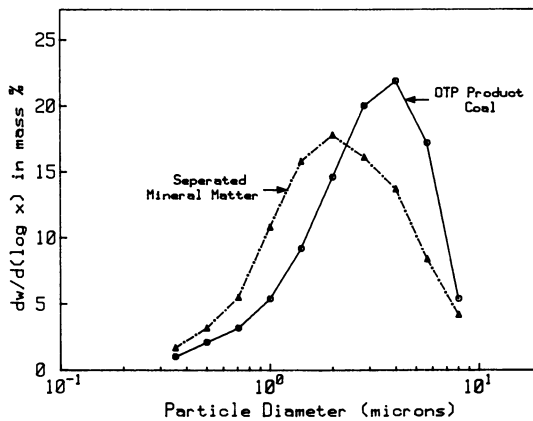


Figure 3. When the products of wet milling  $250 \mu\text{m} \times 0$  Pittsburgh coal (C) are separated, two products evolve: Product coal and separated mineral matter. The particle size distributions for each are illustrated.

rejection only when the particles were broken into smaller pieces. The result would be a large increase in the sub-micron particle population in the released mineral matter, cf. Figure 3, as well as that in the low temperature ash of the product coal. The latter is not observed as is illustrated below.

Secondly, given the low temperature ash size distribution of the raw coal and a knowledge of the raw coal particle size distribution after wet milling, we are in a position to predict the ash content of the product coal. Consider Figure 5 where a hypothetical low temperature ash particle size distribution is superimposed on a T-Process product coal size distribution. The product coal particles with diameters lying between  $x$  and  $dx$  contain no mineral matter particles larger than  $dx$  as those particles were removed during the separation process. The mineral matter retained in the product coal particles is the cumulative mineral matter content represented by the low temperature ash curve. Since the mineral content given on the ordinate in Figure 5 is based on 100%, the ash content in each size range can be estimated by multiplying the mass fraction of that point by the total ash content in the raw coal sample, i.e.  $250 \mu\text{m} \times 0$ , that was used to generate the low temperature ash curve.

A specific case is examined in Table II where the particle size distribution data from the low temperature ashing of a 5 cm cube of coal and 44-53  $\mu\text{m}$  coal was related to two product coal samples milled under different conditions all of which originated from the same source coal (C). The first column in Table II provides the average particle diameter points ( $y$ ) at which the data were observed i.e. the particles with diameters lying between  $x$  and  $x + dx$ . A comparison of the low temperature ash data for the 5 cm cube, column 2, and for the 44-53  $\mu\text{m}$  coal, column 3, illustrates that the fracture of coal from a 5 cm cube to 48  $\mu\text{m}$  does not significantly disturb the mineral matter particles lying in the range of diameters below 6  $\mu\text{m}$ . Since a 4  $\mu\text{m}$  particle of product coal ought to have the complete mineral matter particle distribution smaller than 4  $\mu\text{m}$  enveloped in that particle, a cumulative ash fraction of the lesser particle diameter ash should be equivalent to the ash content within the 4  $\mu\text{m}$  particles, that is, 2.67 weight percent ash, cf. column 4 at 4  $\mu\text{m}$ .

A test of this relationship is afforded in column 5 where we observe the mass fraction of particles at various diameters of a product coal from a standard mill run with no chemicals added. The predicted ash content of the product coal is determined by a summation, over all particle diameters of the product of the ash content of each diameter cumulated by increasing diameter, ( $X$ ), times the mass fraction of the product coal at the particular diameter, ( $y$ ). The predicted ash content for this case is 1.23 weight percent ash which can be compared to the observed value using ASTM procedures of 1.12 weight percent ash. Following identical milling procedures, except for the addition of 20 pounds per ton ligninsulfonate, a dispersant, we obtain a much finer size distribution as is illustrated in column 6, Table II. The predicted ash content in that case is 0.77 weight percent ash while the observed value was 0.91 weight percent ash. The large discrepancy in the finer coal case was probably due to imperfect separation procedures that were caused by the presence of the dispersant. The ability to predict ash contents using this procedure has been applied to

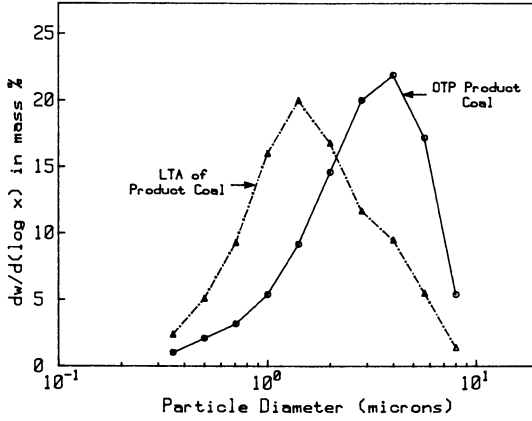


Figure 4. Particle size distribution of the low temperature ash product from the same product coal sample shown in Figure 3.

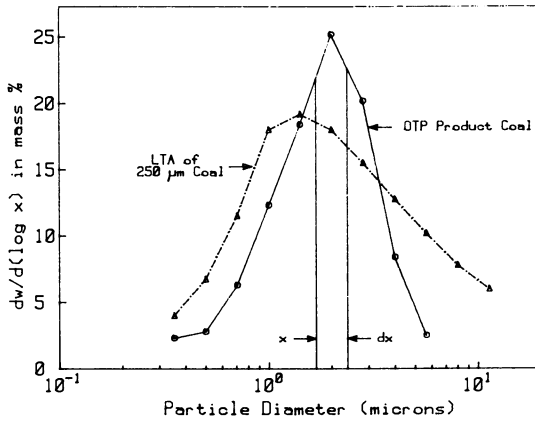


Figure 5. A hypothetical particle size distribution curve of low temperature ash and product coal.

several different coals from different seams and the same seam with results usually within ten percent. A careful examination of these data lends credence to the observation that for the most part the mineral matter included in coal to the micron particle size range is indeed a distinct separable phase capable of physical separation by fracture.

The extent to which milling can be carried out and still attain effective demineralization is to a degree limited by our knowledge of milling. Coal B was reduced in ash into the range of 0.5 weight percent, however, that limit appeared to be a function of milling phenomena as further milling did not allow further ash reduction. Clearly, according to the analysis shown in column 5 of Table II and the subsequent discussion, one might expect a monotonic decrease in product coal ash content with particle size distribution mode to zero mineral matter which has not been observed. What was not anticipated was the observation that the relationship appeared to be insensitive to what might be considered as rather severe changes in the chemical environment during the milling process even though some of the chemical additives made significant changes in the milling efficiency, i.e., specific area increase per unit input energy.

Consider the effect of three chemical additives: calcium hydroxide, sodium ligninsulfonate, and sodium sulfosuccinate, as compared to the case of no additives on the particle size distribution of the product coal from a standard mill run shown in Figure 6 where all conditions were identical. Clearly, there were no obvious effects. In the next series, shown in Figure 7, we investigated the additives ammonium hydroxide, sodium hydroxide, and a higher concentration of sodium ligninsulfonate. Clearly, a dynamic difference in specific surface area per unit input energy was observed. The explanation of the differences is beyond the scope of this paper, but what was interesting was the effect that the chemicals had on the fracture mechanism that affects the release of mineral matter. Figure 8 illustrates a plot of the ash content in the product coal versus the mode of the particle size distribution of the product coal. All of the tests utilizing chemical additives were milled under identical conditions utilized in the test which produced the "no additive" data with a 2  $\mu\text{m}$  mode. The three other "no additive" tests were milled for extended times to achieve smaller particle size distribution and these data are shown in Figure 8. Some of the chemical additives do alter the specific milling rate during the process, but that change does not alter the relationship between particle fracture and mineral matter released. Such lends support to the presumed model that the ultrafine mineral is to some degree homogeneously distributed and is only released with the fracture of the coal particle.

### Conclusion

High ranked bituminous coals like those of the Pittsburgh seam contain a distribution of discrete mineral matter particles in the size range from 50 to 1  $\mu\text{m}$  which can be released and physically separated from the coal by normal fracture mechanisms experienced in wet ball milling. Separation of the product coal from the mineral matter dispersed in water was achieved by agglomeration methods.

Table II. Particle Size Data For Low Temperature Ash Products and Product Coal

Data Point $\mu\text{m}$ (y)	Low Temperature Ash - Wt.%			Product Coal - Wt.%	
	5 cm Cube	44-53 $\mu\text{m}$	44-53 $\mu\text{m}$ (Cumulative X)	Standard No Additives (Y)	Standard 20 pounds/ton Ligninsulfonate (Z)
0.35	0.03	0.06	0.06	0.08	0.16
0.50	0.06	0.1	0.16	0.05	0.09
0.71	0.19	0.18	0.34	0.09	0.15
1.00	0.35	0.28	0.62	0.13	0.23
1.41	0.49	0.38	1.0	0.21	0.16
2.0	0.67	0.52	1.52	0.19	0.11
2.83	0.63	0.60	2.12	0.15	0.16
4.0	0.66	0.55	2.67	0.06	0.03
5.66	0.66	0.55	3.22	0.04	0.01

No Additives	$y = 5.66$	$\sum_{y=0.35} (X_y)(Y_y) = 1.23$ Wt.% Ash Predicted
		1.12 Wt.% Ash Observed
Ligninsulfonate	$y = 5.66$	$\sum_{y=0.35} (X_y)(Z_y) = 0.77$ Wt.% Ash Predicted
		0.91 Wt.% Ash Observed

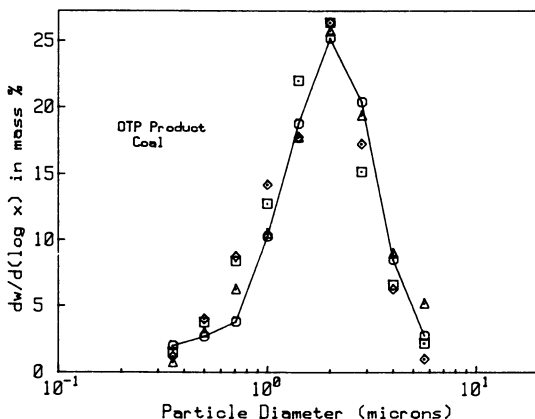


Figure 6. The effects of three chemical additives on product coal particle size distribution while milling at constant conditions, (O) No Additives; ( $\Delta$ ) 2 lbs/ton Calcium Hydroxide; ( $\square$ ) 2 lbs/ton Sodium Ligninsulfonate; and ( $\diamond$ ) 20 lbs/ton Sodium Sulfosuccinate.



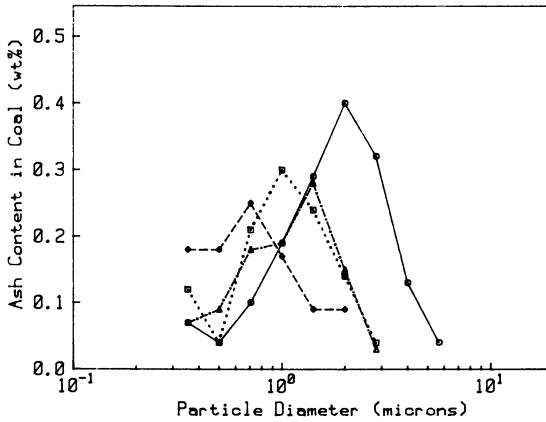


Figure 7. The effects of three chemical additives on product coal particle size distribution while milling at constant conditions, (O) No Additives; ( $\Delta$ ) 36 lbs/ton Ammonium Hydroxide; ( $\square$ ) 7.9 lbs/ton Sodium Hydroxide; and ( $\diamond$ ) 20 lbs/ton Sodium Ligninsulfonate.

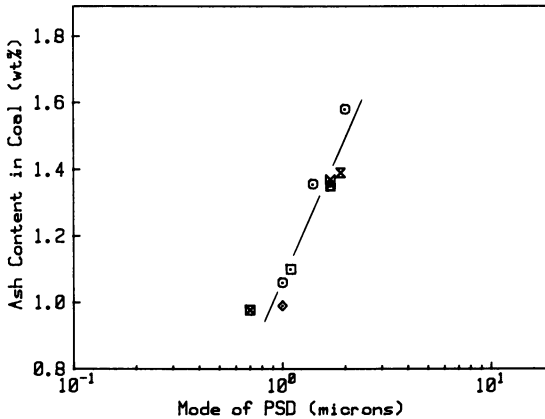


Figure 8. Weight percent ash in product coal versus the mode of the particle size distribution of the product coal, (O) No additives; ( $\diamond$ ) 7.9 lbs/ton Sodium Hydroxide; ( $\square$ ) 36 lbs/ton Ammonium Hydroxide; ( $\blacksquare$ ) 20 lbs/ton Sodium Ligninsulfonate; ( $\otimes$ ) 20 lbs/ton Calcium Hydroxide, ( $\otimes$ ) 2 lbs/ton Calcium Hydroxide and ( $\Delta$ ) 2 lbs/ton Sodium Ligninsulfonate.

Demineralization of coal by this mechanism appears to be a predictable process with an error in the range of 10 percent. The demineralization of Pittsburgh seam coal has been achieved to the range of 0.5 weight percent ash, a limit which appears to be controlled by the mechanics of the ball mill.

Application of the procedures used in this investigation to coals from other seams have resulted in product coals with ash contents below 0.3 wt. %. Further investigations are underway which focus on the mechanism of fracture during wet milling.

#### Acknowledgments

The author extends his sincere appreciation to W. Burry and D. S. Keller for their efforts in the development of the experimental procedures and data analysis.

#### Literature Cited

1. Leonard, J. W., "Coal Preparation", Amer. Inst. Mining Met. Pet. Eng., Inc., New York (1979).
2. Keller, Jr., D. V., "Otisca T-Process, A New Coal Beneficiation Approach for the Preparation of Coal Slurries", Coal Gasification, Liquefaction, and Conversion to Electricity Conference, University of Pittsburgh, August 1982.
3. Keller, Jr., D. V., "Coal Refining by Physical Methods for the Preparation of Coal Slurries With Less Than 1 wt. % Ash", Fifth International Symposium on Coal Slurry for Combustion and Technology, Tampa, Florida, April 1983, U.S. DOE, Pittsburgh, p. 269.
4. Gluskoter, H. L., Fuel, 44, 285 (1965).
5. Mitchel, R. S.; Gluskoter, H. L., Fuel, 55, 90 (1976).
6. O'Gorman, J. V.; Walker, P. L., "Mineral Matter and Trace Elements in U.S. Coals", U.S. Office of Coal Research, R & D Report No. 61, (1972).

RECEIVED July 23, 1985

## Decomposition of Pyrite in a Coal Matrix during the Pyrolysis of Coal

I. Stewart<sup>1</sup>, S. G. Whiteway<sup>1</sup>, P. J. Cleyle<sup>2</sup>, and W. F. Caley<sup>2</sup>

<sup>1</sup>Atlantic Research Laboratory, National Research Council, Halifax, NS B3H 3Z1, Canada

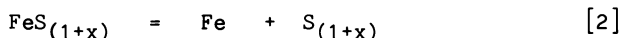
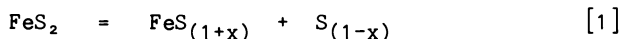
<sup>2</sup>Technical University of Nova Scotia, Halifax, NS B3J 2X4, Canada

The high levels of sulphur present in Nova Scotian coals may restrict their future use in power generation. A number of beneficiation strategies, aimed at reducing the sulphur levels, are currently under investigation in the Atlantic region; among these is pyrolysis. This work provides a better understanding of the fate of pyritic sulphur from the pyrite/pyrrhotite conversion during pyrolysis. Coal from collieries in Nova Scotia were pyrolysed under argon in a tube furnace at a variety of temperatures and times. Elements of interest in the resultant char were analysed using a scanning electron microscope, equipped with energy and wavelength dispersive spectrometers. The results indicate that sulphur originating from pyrite is transferred to the nearby surrounding organic matrix during the pyrolysis process. This sulphur is in a form which may be very difficult to remove. The possibility of using magnetic separation to reduce the sulphur levels in the char was explored.

The high sulphur content of Eastern Canadian coals, as much as 8%, has led to studies aimed at reducing these sulphur levels (1). In general about two thirds of the sulphur is pyritic, often occurring as small inclusions, and therefore difficult to remove by conventional means. One method which holds promise is pyrolysis followed by magnetic separation.

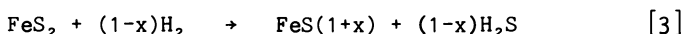
Pyrolysis involves the heating of coal in a non-oxidising environment producing char, liquid and gas. This publication deals with the reactions of pyrite in the coal, the partitioning of the pyritic sulphur during pyrolysis, and the effect this has on magnetic separation.

When mineral pyrite is heated under an inert atmosphere it decomposes, in two steps, to form firstly pyrrhotite and then at a higher temperature, iron.



Where  $0 \leq x \leq 0.22$ .

It is generally known that, in coal, reactions 1 and 2 proceed at a lower temperature, probably because hydrogen from the decomposing coal matrix aids the reaction:



Reaction [2] was not observed in this study because experimental temperatures were not high enough.

The fate of pyrite in coal has been the subject of a number of publications, particularly in the area of liquefaction, where pyrite or its products are thought to play an important catalytic role (2). In a previous publication (3) it was reported that the decomposition of pyrite to pyrrhotite occurred in the temperature range 500-550°C for a run-of-mine (ROM) Prince coal. This was within the range of 440-580°C reported by other workers for the decomposition of pyrite in coal (4,5). The current work extends the previous study to three washed coals and includes some preliminary work on magnetic separation.

Magnetic separation has been applied by other workers (6) who have shown that rejection of 95-99% of pyritic sulphur is possible, if advantage can be taken of the pyrite/pyrrhotite transformation. This latter process not only involves a loss of sulphur but concurrent 100-fold increase in magnetic susceptibility (7). It is this increase which makes magnetic separation attractive.

### Experimental

All the coals studied in the present work were washed commercially to free them of some of their mineral content. They were from three collieries of the Cape Breton Development Corporation: Prince, Lingan and No. 26. Lingan and No. 26 collieries are in different regions of the same coal seam: the Prince colliery is in a separate seam. All the coals are classed as high volatile bituminous A. Typical ash and sulphur contents are given in Table I.

The coal was crushed and sieved on Tyler screens to -8 +16 mesh (1-2.4 mm). Approximately 10 g of coal was placed in an alumina boat and pyrolysed under argon in a tube furnace for 20 hours at constant temperature in the ranges 410-645°C.

After pyrolysis pieces of the resultant char were mounted using Fisher Chemical Co. 'Quickmount' cold-mounting resin, and polished in preparation for scanning electron microscopy. The object was to analyse for sulphur by scanning across selected pyrite sections, and continuing out into the surrounding coal matrix.

Table I. Analyses of Coals

	Prince Coal	Lingan Coal	No. 26 Coal
Moisture	2.24	1.09	0.87
Volatiles	34.65	28.34	25.42
Ash	6.4	3.65	2.92
Carbon	58.95	68.01	71.66
Oxygen	5.0	5.6	5.0
Total sulphur	3.62	2.01	0.86
Pyrite sulphur	2.56	1.42	0.26
Sulphate sulphur	0.08	0.09	0.04
Organic sulphur	0.98	0.56	0.56

A Jeol-35 Scanning Electron Microscope equipped with energy- and wavelength- dispersive X-ray spectrometers was used for elemental analysis. Spot analyses were carried out; these covered approximately 0.5  $\mu\text{m}$  for the pyrite and 1  $\mu\text{m}$  for the coal. The standard atomic number, absorption and fluorescence (ZAF) corrections were applied to all analyses, using counting times of 200 seconds, an accelerating voltage of 15 kV and a pyrite crystal as standard.

In addition some of the samples were studied by Fe-57 Mossbauer spectroscopy. The spectrometer was an Apple IIe-controlled Ranger Scientific MS-900 operated in constant acceleration mode, using Co-57 in a matrix of rhodium as source. Spectral data were accumulated in 1024 channels.

### Results

The extent of pyrite decomposition was followed by obtaining S/Fe atomic ratios at various points across selected pyrite inclusions, the latter in the size range 10-20  $\mu\text{m}$ . Figure 1 is a plot of this ratio versus "distance from interface within pyrite" for each of the coals at different temperatures. The results indicate that, for pyrite of this size, decomposition to pyrrhotite occurs in the temperature range 450-500°C, for all the coals studied. The reaction essentially was complete at 500°C.

Mossbauer spectroscopy was used to examine the chars produced from the pyrolysis reaction. The results, which deal with bulk decomposition compared to the microscopic view obtained from SEM, tended to confirm those obtained above for the initial temperature of decomposition. However, a number of major differences were observed. Pyrite was always a component in the spectra, even those of chars produced at 650°C. In addition the three coals could be classed in two groups: Prince and Lingan behaved similarly with the formation of pyrrhotites at around 450-500°C; on the other hand No. 26 coal showed little sign of any reaction product even at 650°C (Figs. 2-4), an anomaly considering the fact that selected grains of size 10-20  $\mu\text{m}$  would have been completely reacted.

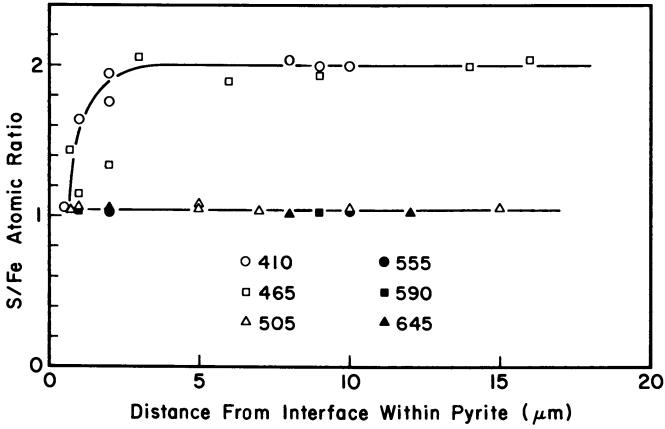


Fig. 1 S/Fe atomic ratio vs. distance from interface within pyrite for Prince, Lingan and No. 26 coals.

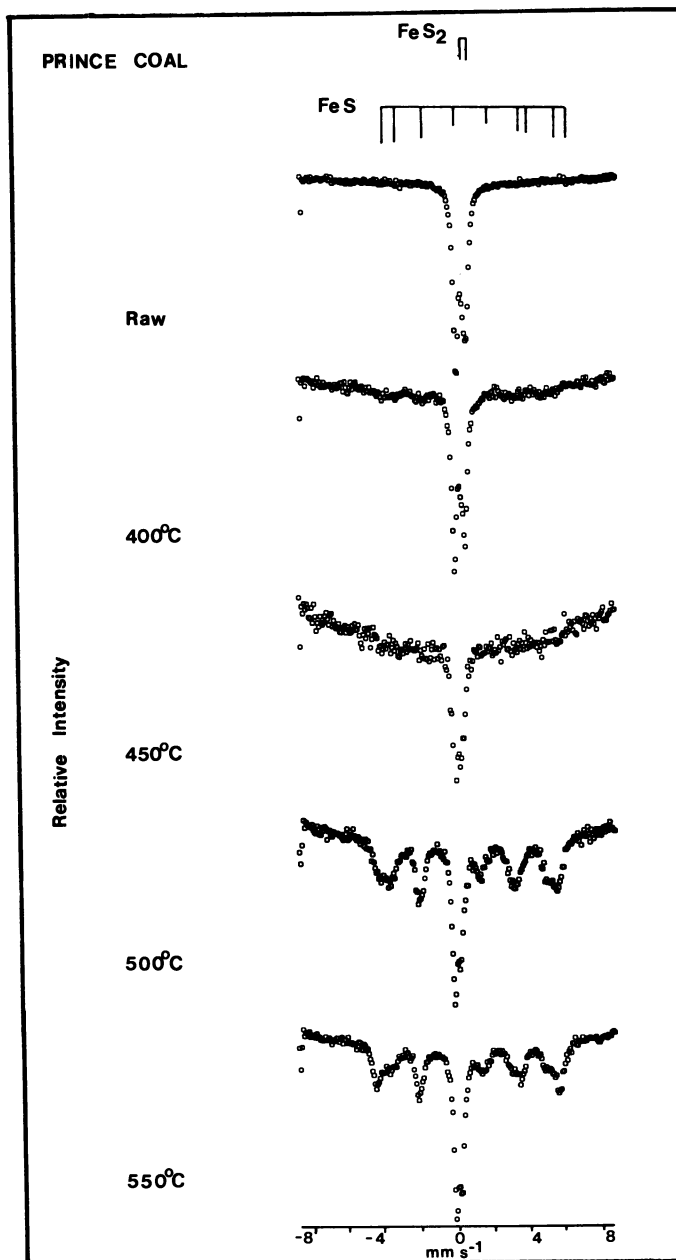


Fig. 2 Mössbauer spectra of Prince coal pyrolysed at different temperatures.

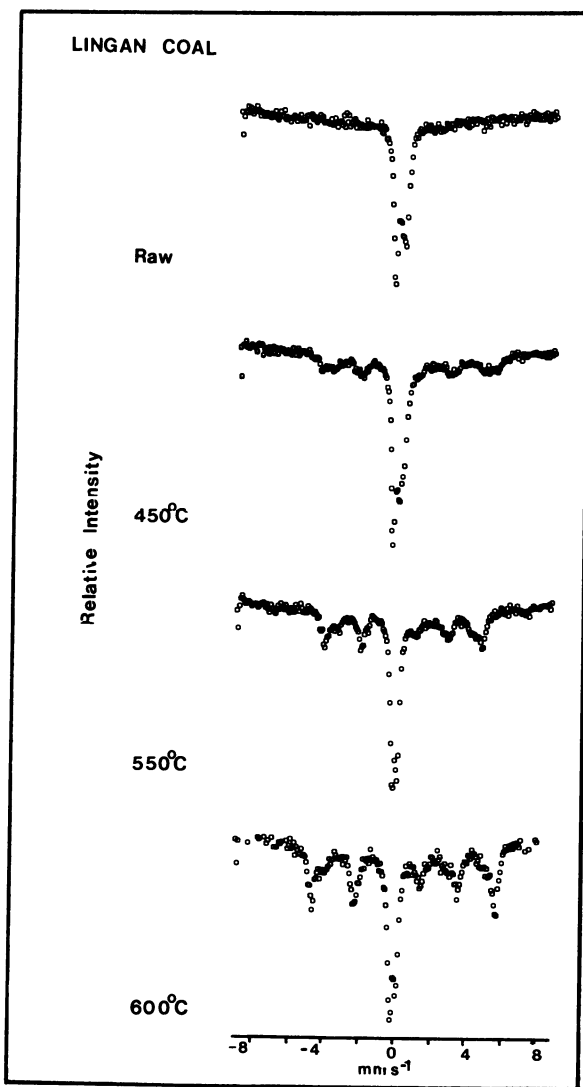


Fig. 3 Mössbauer spectra of Lingan coal pyrolysed at different temperatures.



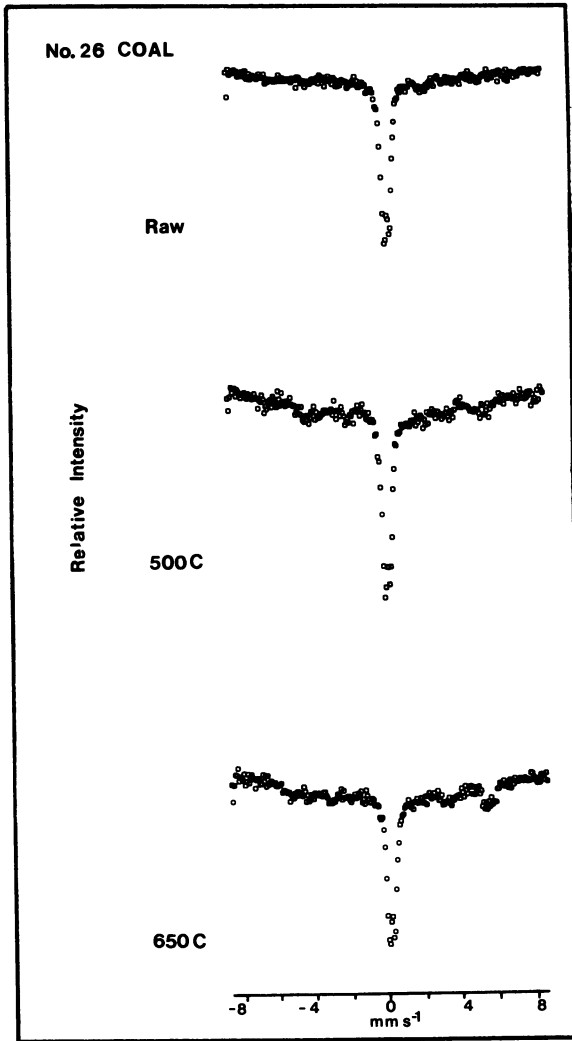


Fig. 4 Mössbauer spectra of No. 26 coal pyrolysed at different temperatures.

The incorporation of the sulphur from the decomposition of pyrite, into the surrounding coal matrix, was also followed by scanning electron microscopy. This involved spot analysis for sulphur out from the pyrite/coal interface into the surrounding matrix. These results follow the trend presented above for pyrite decomposition. At 400 and 450°C, little sulphur transfer was observed; at 500°C however, there was an observed increase in the % sulphur (Fig. 5), in the region around the decomposed particle.

Multiple runs were performed at each temperature in order to produce enough char for magnetic separation. The chars were crushed to an average size of 80% passing through 94  $\mu\text{m}$  and then 40-50 g were slurried with water and passed through a magnetic separator (Davis Tube Tester), using a field strength of 5.25 kG. No attempt was made to optimise the conditions and the separation was based on a single pass through the poles of the magnet. The results from these experiments are presented in figure 6. It appears the best reduction occurs using chars produced at about 450°C for Prince and Lingan coals, and at 550°C for No. 26 coal. In addition some of the products of magnetic separation were analysed by Mossbauer spectroscopy. The results were similar to those observed for the raw chars. Lingan and Prince coals showed an increase in Pyrrhotite content for the magnetic fraction and No. 26 coal showed iron oxide as the main product in the magnetic fraction (Figs 7,8).

### Discussion

Pyrite Decomposition. This study shows a slightly lower decomposition temperature for pyrite in washed coal (450-500°C) than was previously reported for ROM Prince coal, (500-550°C). The reason for this is as yet unclear, but is thought to reflect the lower ash content in the washed coals. Rostam-Abadi and Kruse (8) have reported a similar effect for the peak devolatilisation rates of coals with differing organic to pyritic sulphur ratios.

The anomalous behaviour of No. 26 coal may be related to the high oxygen:sulphur ratio, in this coal (Table I) and this is being investigated. In addition, it must be recognised that this SEM work was carried out on selected particles, which are not necessarily indicative of the bulk.

A number of kinetic models have been proposed for the decomposition of pyrite (9,10). There seems to be general agreement that the decomposition involves the reaction of  $\text{S}^{2-}$  sulphide ions with hydrogen, the latter originating with the decomposing coal matrix, to form  $\text{H}_2\text{S}$ . Alternatively it has been suggested that the organic hydrocarbon material may directly react with  $\text{S}^{2-}$  (9). As the reaction proceeds, a shell of pyrrhotite forms around the pyrite core with the  $\text{S}_2^{2-}$  ions now diffusing through the pyrrhotite to the pyrrhotite/coal interface. This has been described in the literature as the "shrinking core" model (5,10). A few pyrite particles formed from pyrolysis at 450°C, showed visible, as well as microchemical, evidence for this model (Fig. 9).

Sulphur Transfer. As previously reported there was no indication of increased sulphur levels around pyrite particles in the 'unreacted' coals (3,11). The increase in sulphur observed in the present study

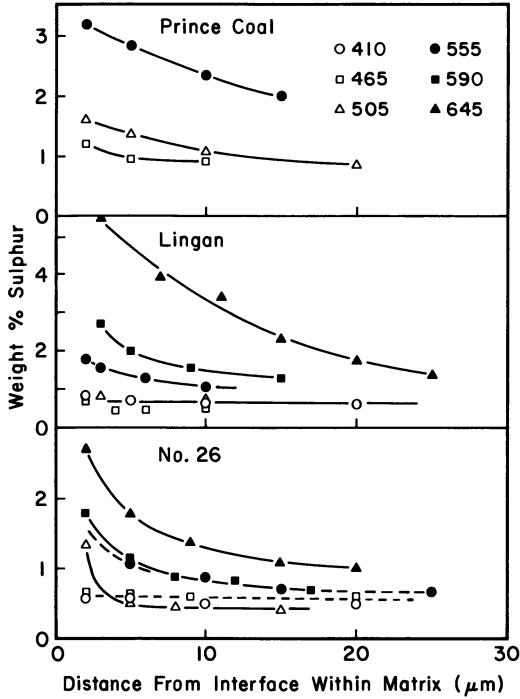


Fig. 5 Weight % sulphur vs. distance from interface within matrix for Prince, Langan and No. 26 coals.

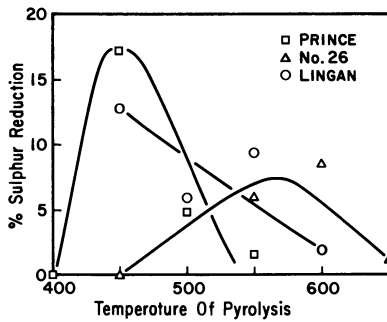


Fig. 6 % Sulphur reduction vs. temperature of pyrolysis for Prince, Langan and No. 26 coals.

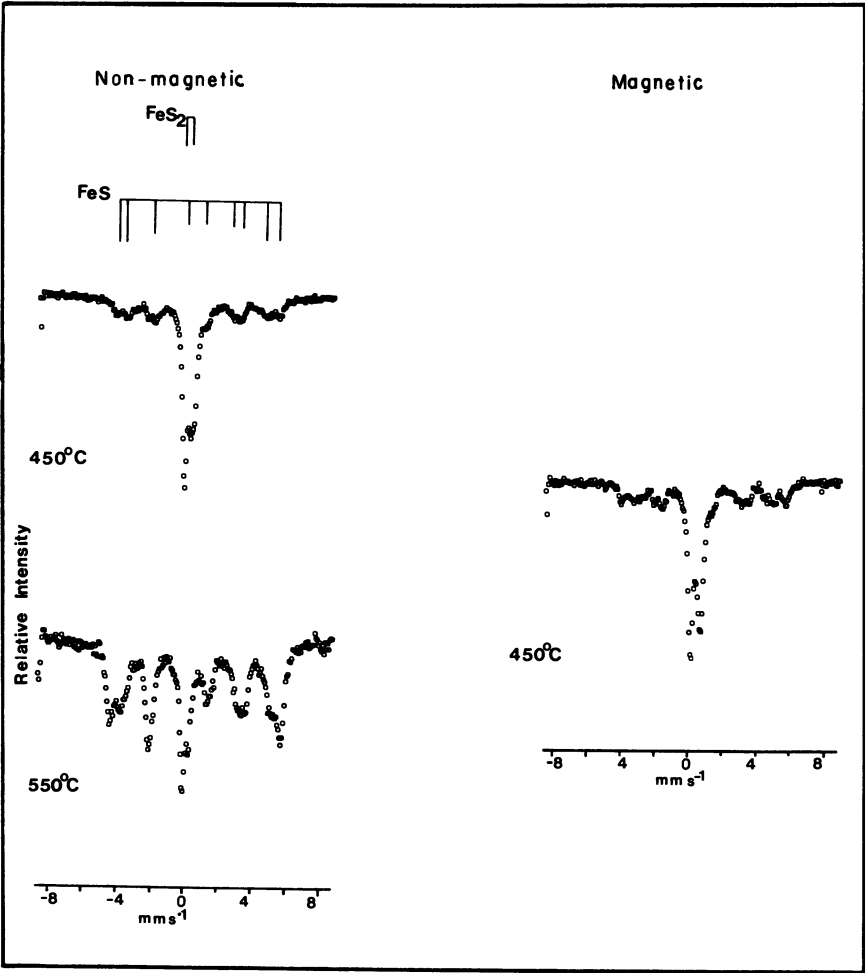


Fig. 7 Mössbauer spectra of non-magnetic and magnetic char fractions, after magnetic separation, for Prince coal.

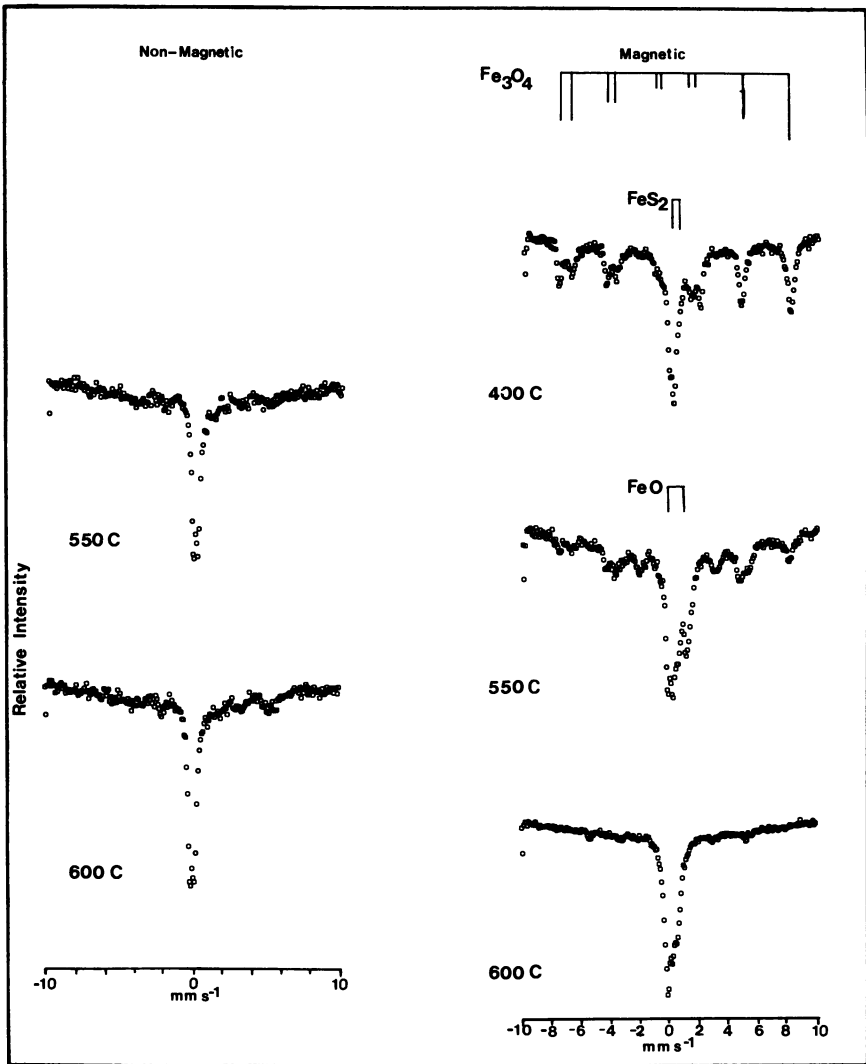


Fig. 8 Mössbauer spectra of non-magnetic and magnetic char fractions, after magnetic separation, for No. 26 coal.

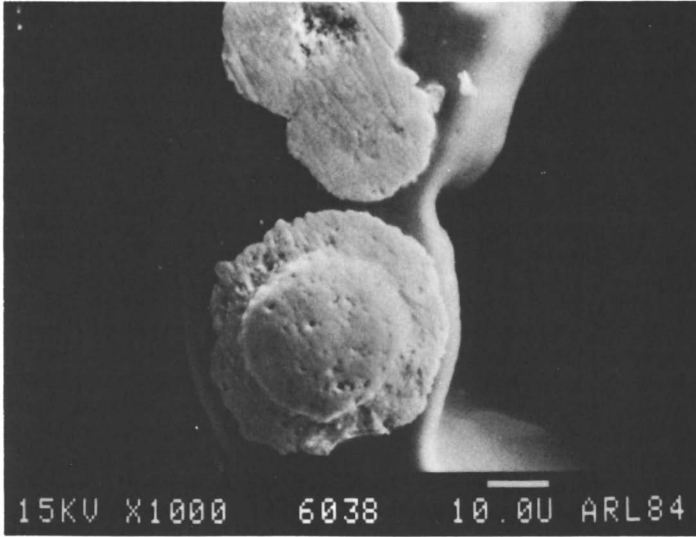


Fig. 9 Scanning electron micrograph of pyrite particle in Prince coal following pyrolysis.

originates as a result of the pyrolysis reaction, primarily from the decomposition of pyrite, as is evident from the local nature of the effect. The sulphur around the pyrite is thought to be formed by the reaction of  $H_2S$  with the surrounding coal matrix, rather than by the diffusion of  $S^{2-}$  through the matrix. This is based on our previous study, which showed no further increase in the size of the sulphur shell after a certain time.

It has been shown (12) that the thermal decomposition of coal probably involves a free radical process, providing active sites for the 'trapping' of  $H_2S$  formed as the result of pyrite decomposition. In this way the sulphur becomes incorporated into the coal matrix as organically bound sulphur. While the form of the trapped sulphur is unknown, it is clear that it is chemically bound into the char as part of a very stable organic group, presumably as part of a heterocyclic ring structure. Attar (9) has suggested that it is part of a highly graphitised, heterocyclic, thiophenic group.

Magnetic Separation. The future utility of pyrolysis as a process depends upon the successful use of the char. From the discussion on sulphur transfer, it is evident that as the result of pyrolysis some sulphur which is difficult to remove physically (well disseminated pyrite) is transformed to sulphur that is impossible to remove physically (organic sulphur). In addition it has been shown that this newly formed, organic sulphur is present in a very stable form. This would seem to be counter productive to any scheme which must include sulphur reduction as a primary goal. However, by carefully controlling the pyrolysis reaction conditions it should be possible to produce chars which are amenable to sulphur reduction by magnetic separation.

In the present work no attempt was made to optimise the magnetic separation conditions; rather the emphasis was on sulphur rejection as a function of pyrolysis temperature, to give information on the optimum pyrolysis temperature for separation. This work was based on a report (6) that pyrrhotite with the composition  $Fe_7S_8$  had the highest magnetic susceptibility and was therefore easiest to remove by magnetic separation.

The results indicated that maximum sulphur rejection occurs in the range 450-500°C for Prince and Lingan coals; there are two reasons for this. First, these results show that at this temperature the reaction is incomplete and therefore those pyrrhotite particles which are removed magnetically still have an appreciable pyrite core. The total sulphur content would be larger than that of a similar particle, with less residual pyrite, produced at higher temperatures. The second reason may be the formation of a pyrrhotite with a higher magnetic susceptibility, at this temperature, permitting a greater efficiency in particle removal.

The preceding indicates that in order to optimise sulphur rejection, the conditions of pyrolysis should be controlled so that the magnetic susceptibility becomes sufficient for particle separation, but also so that the transformation of pyrite to pyrrhotite should be kept to a minimum. For example, it has been shown that a 1% conversion of pyrite to pyrrhotite leads to an increase in magnetic susceptibility of two orders of magnitude (13). In addition, grinding could be controlled so that the sulphur

incorporated into the organic matrix could be liberated along with the pyrrhotite particles, making use of the localised nature of the effect.

### Summary

The work performed to date, has brought out a number of important points and raised several questions.

1. The decomposition temperature for pyrite in coal varies depending on the coal and its pre-treatment. The possible effects of particle size and maceral environment were not dealt with in the present study and are currently being investigated.
2. Sulphur transfer to the coal was observed to occur in a very localised shell. The exact nature of the newly formed organic sulphur remains elusive but it is probably as part of a heterocyclic ring.
3. Optimum pyrolysis conditions, for magnetic separation, were explored; preliminary results indicate that temperatures in the range 450-500°C may produce the highest sulphur rejection. This was thought to be due to the additive effects of optimum magnetic susceptibility and the high sulphur content of the rejected particles.
4. Pyrite was observed in the Mossbauer spectra of all the chars investigated, even though selected grains of size 10-20  $\mu\text{m}$  would indicate that all pyrite had decomposed to pyrrhotite.

### Acknowledgements

The authors wish to thank E. Dyer and C. Collings for the SEM analysis and D. Forgeron for the coal analysis. NRCC No. 24124.

### References

1. Nova Scotia Research Foundation Corporation, "A Series of Research Reports on Eastern Canadian Coals" (1979-1980), publ. 1981.
2. Montano, P. A., Bommanavar, A. S. and Shah, V. *Fuel*. 60, 703 (1981).
3. Cleyle, P. J., Caley, W. F., Stewart, I. and Whiteway, S. G. *Fuel*. 63, 1579 (1984).
4. Bommanavar, A. S. and Montano, P. A. *Fuel*. 61, 523 (1982).
5. Moneiro, J. L. F. *Can. J. Chem. Eng.* 59, 511 (1981).
6. Maxwell, E. and Kelland, D. R. *IEEE Trans Magn.* MAG-14(5), 482 (1978).
7. Tsai, S. C. p. 193 in "Fundamentals of Coal Beneficiation and Utilisation", Elsevier, New York, 1982.
8. Rostam-Abadi, M. and Kruse, C. W. Proceedings of the 12th North American Thermal analysis Society Conference, Sept. 25-29, Williamsburg, VA, p. 673-677.
9. Attar, A. *Fuel*. 57, 201 (1978).
10. Daugherty, D. F. *Coal Processing Technology*. 7, 108 (1981).
11. Raymond, R. and Hagan, R. C. *Scanning Electron Microsc.* 2, 619 (1982).



12. Retcofsky, H. L., Hough, M. R., Maguire, M. M. and Clarkson, R. B. p. 37 in "Coal Structure" ACS Advances in Chemistry Series No. 192 (Gorbarty, M. L. and Ouchi, K. eds) ACS, Washington, 1981.
13. Bluhm, D. D., Fenslow, G. E., Beck-Montgomery, S. and Nelson, S. O. p. 417 in "Chemistry and Physics of Coal Utilisation - 1980" AIP Conference Proceedings (Cooper, B. R. and Petrakis, L. eds) AIP, New York, 1981.

RECEIVED July 5, 1985

## Carbon Dioxide/Water for Coal Beneficiation

R. Sapienza, T. Butcher, W. Slegeir, and F. Healy

Brookhaven National Laboratory, Department of Applied Science, Upton, NY 11973

Pressurized carbon dioxide/water solvents affect the chemical and physical properties of coal to provide a method of simultaneous cleaning and fracturing. The synergistic interaction of these two inexpensive reagents causes the selective solubilization of the alkali and alkaline earth mineral matter in the coal and the swelling of the coal matrix which weakens the coal structure. Significant improvements in coal grindability with high retention of energy content have been achieved.

The chemical composition, physical size, and mode of distribution of the mineral matter in coal greatly affect the way in which coal minerals can be selectively removed. For any coal cleaning method to be applicable to a variety of coals, it should provide both physical liberation and chemical separation techniques. Brookhaven National Laboratory (BNL) has focused on this approach. The method involves the selective solubilization of coal mineral matter which also causes swelling of the coal. This swelling results in the fragmentation of the coal structure which affects coal grinding and facilitates the removal of mineral matter. With the proper selection of reagents, selective solubilization of mineral matter occurs. This work has clarified our understanding of the natural binding forces holding coal together and could be of value in improving and extending the capability of current cleaning processes and providing a basis for the development of new coal cleaning methodologies.

This approach to coal beneficiation is flexible and is applicable to a variety of coals because the nature of maceral-maceral and maceral-mineral interactions are similar for similar coals. The coal is modified both chemically and physically in a way which allows selected mineral components to be attacked. It is believed that improvements can be made which will be more effective in terms of degree and specificity for mineral matter removal, while potentially effecting a route to organic sulfur removal.

### The Concept

Coal is sedimentary rock composed of microscopically recognizable organic constituents (macerals) and inorganic constituents (minerals). Macerals are products of coalified remains of plants; they have been classified into groups, i.e. vitrinite, exinite, and inertinite. Coal minerals are believed to be located at maceral boundaries (1). The overwhelming majority of these minerals are in one of the following four groups, aluminosilicates, carbonates, sulfides, and silica (quartz). Hydrogen bonding may well be an important part of the forces that hold these minerals at the maceral boundaries. The most abundant element in coal, after carbon and hydrogen, is oxygen. Oxygen is found combined with other atoms in coal to form various functional groups, namely, carboxyl groups ( $\text{CO}_2\text{H}$ ), carbonyl groups ( $\text{C}=\text{O}$ ), and phenol ( $\text{OH}$ ) groups. One of the prominent features of the infrared spectra of most coals is an intense broad band associated with O-H vibrations. It is also worth noting that OH accounts for between one third and two thirds of the total oxygen in coal (2). These bonding features may contribute to hold the coal inorganic and organic aggregate together and are potential sites of further hydrogen bonding. Since the structure of coal shows many possible sites for hydrogen bonding, breaking hydrogen bonds along the maceral boundaries could result in the separation of the mineral matter from the coal matrix.

Conceptually, two routes are available for the disruption of the coal matrix. One method involves the use of reagents which attack the surface of coal and, during the chemical transformation, effectively "peel away" this surface to expose fresh surface to the reagent. This method appears to be operative during coal gasification. However, this technique, of necessity, involves radical transformations of the coal structure, resulting in extensive carbon-carbon bond cleavage. The second method involves the penetration of the coal structure with reagents that swell the coal. Such methodology allows for vastly greater surface area, effectively longer coal-reagent reaction times, and greater possibilities for selective cleavage of bonds.

Swelling strains the coal matrix, most probably leading to the rupture of hydrogen bonds. However, due to the high availability of hydrogen bonds, the reorientation of the coal matrix allows reorientation of the hydrogen bonding structure. It is believed that an appropriate hydrogen bonding agent, if allowed to penetrate the swelled coal structure, would be capable of "tying up" hydrogen bonding sites in the coal. The combined effects of swelling and bond breaking would appear to allow included mineral matter to drop out of the coal structure while physically weakening the coal matrix.

Unlike fracturing, this approach should cause only moderate disruption of the coal matrix and might not lead to complete comminution, but this method could be envisioned as a prelude to coal grinding. Removal of material from structural boundaries would yield a more friable, "soft" coal structure. The leaching of fine mineral particles from the coal matrix results in a more porous structure and should also improve the coal's grindability. The prior removal of some mineral matter would also reduce the coal's abrasiveness.

The treated coal should be more amenable to crushing and such crushing should occur along maceral boundaries due to the combined effects of external hydrogen bonding and swelling. This would release greater amounts of impurities of comparable particle-size distribution and reduce the cost of follow-on processing for separating impurities. This approach may also offer new ways of further coal clean-up because the coal structure is most susceptible to chemical attack during the swelling process.

A wide variety of chemical reagents are capable of blocking the internal hydrogen bonding of the coal. However, for a chemical coal beneficiation system to be practical this hydrogen bonding system must be readily available, inexpensive, be of sufficiently small molecular size, and not be expected to introduce unwanted chemical elements that will lead to corrosion or pollution problems with the processed, comminuted coal. These qualifications substantially limit the number of hydrogen bonding reagents. Our initial experiments were restricted to water combined with carbon dioxide to provide a reagent system which was tailored to the problems.

The process described is related to the unique effects carbon dioxide and moisture have on coal. Carbon dioxide readily and extensively penetrates the coal structure (3). In fact, this has led to the advocacy of employing carbon dioxide to measure the internal area of coals. It is likely the  $\text{CO}_2$  diffuses into the coal along the lines of mineral inclusion as has been seen for other gases (4). This is important since the diffusion of reagents through solid coal may be the rate-limiting step in many reactions. This diffusion has also been shown to cause a dimensional expansion of the structure.

Moisture adsorption-desorption cycles of coal causes weathering, a slow form of chemical comminution (5). Although a problem in coal storage, the loss of strength from the degradation of the coal could be practical for fracturing the coal structure if accelerated with better penetration of water. Additionally, the sorbed water can dissolve and serve as a transport medium for soluble minerals within the coal matrix. In this respect, the coupling of water with carbon dioxide to generate a weakly acidic solution would also be beneficial. The acid leaching of coal mineral matter has been employed to produce coals of unusually low ash content (6). Cleaning with acid offers an advantage over typical gravity cleaning methods in which chemical composition of the mineral matter does not influence its removal. Selective removal of mineral components that exert a deleterious effect is possible with acid cleaning. Acid attack of the mineral occurring in the cleats and partings of the coal is also the basis of a disintegration process for breaking down coal during mining (6).

Several bituminous coals have been employed during the course of this study. The method can be applied to relatively unprepared coals and seems to be very effective for the removal of alkali and alkaline earth metals which are related to boiler fouling. With modification, other mineral groups could be removed. Coal treated with  $\text{CO}_2/\text{H}_2\text{O}$  occasionally crumbles during processing. The system is flexible, may be modified both chemically and physically, and may be integrated into, or used to modify, an overall coal preparation

process. The method yields a more friable, "soft" coal structure and could significantly reduce the energy requirements and cost of follow-on coal grinding and separation process.

### Experimental Procedures

A variety of bituminous coals have been examined in the course of this work using  $\text{CO}_2/\text{H}_2\text{O}$ , including Kentucky #9 and Pittsburgh Seam coal. The treatment is carried out in a 2L stainless steel autoclave, equipped with a gauge, liquid sampling and gas venting valves and a thermocouple. The thermocouple is connected to a proportioning band temperature controller, which in turn is connected to a heating mantle. This system affords precise and reproducible temperature control of the autoclave contents.

Generally, a coal sample (typically 500g) of appropriate mesh size is added to the reactor followed by the appropriate amount of distilled water (typically 1L). After closure, the reactor is purged and then brought to the appropriate  $\text{CO}_2$  pressure; the weight of  $\text{CO}_2$  is then determined.

The reactor is heated to the desired temperature (typically  $80^\circ\text{C}$ ) and the pressure is again recorded. Once the temperature has stabilized, very little, if any, changes in pressure are observed. The temperature and pressure data may be used to calculate the amount of  $\text{CO}_2$  dissolved in the water.

At the end of the desired contact time, the reactor is removed from the heater, and the hot liquid phase is carefully transferred to a flask. After cooling, the coal is removed from the reactor and washed on a sintered glass funnel with distilled water. Final drying of the coal is carried out in a vacuum oven at  $110^\circ\text{C}$ . The cooled liquid phase, which frequently contains a small amount of powdered coal and precipitated mineral matter, is filtered. The water is evaporated to dryness to determine the quantity and nature of minerals leached from the coal.

The weight of the dried coal is compared with that of the feed coal. The dried coal is ashed by ASTM method D-3174-73 along with samples of untreated coal.

The gas phase was examined for  $\text{CO}$ ,  $\text{H}_2$ ,  $\text{CH}_4$ , and  $\text{SO}_2$  after some treatments, and in no cases were significant quantities of these detected. Within the liquid phase, a variety of inorganic materials are found (*vide infra*).

To assess quantitatively the effects of this treatment on grinding, a laboratory-scale grinding system was needed. Using a batch ball mill, the grindability of samples has been compared using an adaptation of the Bond Work Index (BWI) concept (7). The use of the BWI involves determining the energy input required to achieve a desired level of grinding with the Index being calculated by taking into account the energy input and the extent of size reduction. This approach is considered more flexible than other approaches, such as the Hardgrove, which are defined only for a given feed and product size. In addition the Hardgrove test requires only a small fraction of the coal to pass a given screen size and so may only reflect surface fracturing.

The actual grinding was carried out on a laboratory ball mill, using ceramic jars with dimensions of 5-13/16" internal diameter and 5-3/8" internal height. The overall volume is 1829cc. Initial experiments employed steel balls (seventeen of 3/4" diameter, eleven of 5/8" diameter and fifty of 1" diameter). The rate of jar rotation of the mill is nominally 80 rpm. The voltage and current feeding of the ball mill are measurable and constant; therefore, the grinding time is used as a measure of power input. Experiments employed 100 g of coal.

In the BWI test undersized coal is removed at calculated times and fresh feed is added to simulate closed circuit grinding. This procedure is repeated until a constant mass of undersized product is produced per revolution. Simpler approaches, however, involving batch grinding have been shown to provide accurate results, particularly for comparing the grindability of two materials (8). This later approach was used here for comparison of the grindability of treated and untreated coals. With the assumptions of constant power input to the mill, fixed feed size, a similar product size distribution curve, the change in BWI and hence grindability can be approximated by the difference in time required to achieve a fixed percentage of the product coal passing a given screen.

#### Condition Selection

Carbon dioxide pressures from 1 to 75 atmospheres and temperatures from 0° to 80°C were assessed. Since the liquid phase is in contact with the coal and is responsible for mineral matter dissolution, its composition would be expected to have a bearing on ash reduction in the coal. The solubility of CO<sub>2</sub> in the liquid phase increases as the CO<sub>2</sub> pressure increases and may be related to swelling of coal structure (although not linearly). Table I summarizes a set of experiments directed toward determining the effect of aqueous phase concentration of CO<sub>2</sub> on the treated product ash content for Pittsburgh Seam coal. At low CO<sub>2</sub> concentrations, little ash reduction is observed, consistent with poor matching of the solubility parameter of water with coal. As the CO<sub>2</sub> concentration is increased, a significant reduction in ash is observed. However, increasing the concentration above 24 g CO<sub>2</sub>/liter does not appear to result in significant ash reductions.

Table I. Effect of CO<sub>2</sub> Concentration on Ash Removal-Pittsburgh Seam Coal

Concentration CO <sub>2</sub> Dissolved g/L	Reduction in Ash, %
8	5
10	5
24	16
37	15
43	15

Initial tests were conducted with Pittsburgh Seam coal (NA1361 - Arkwrite Mine) sized to 1 3/8 inches x 3/8 inches. Reaction conditions studied for this sample included 75 - 80 atmospheres CO<sub>2</sub> at 80°C. These conditions were chosen because they are above the critical point of CO<sub>2</sub> yet below the boiling point of water. Super-critical pressure was chosen to maximize the amount of CO<sub>2</sub> present in the water.

Finally, we have found that simply treating the coal in water without CO<sub>2</sub> offers little change in mineral content or ease of grinding. Tests analogous to the CO<sub>2</sub>/H<sub>2</sub>O treatments, using either nitrogen or helium in place of the CO<sub>2</sub>, resulted in only small changes in the coal. These tests indicate that pressurized water alone is not important to the process. Rapid decompression tests using CO<sub>2</sub> in the absence of water were carried out to determine whether fracturing is due to pore-entrapped CO<sub>2</sub> causing stress on the coal structure during pressure release. Little change in the coal size or grinding time was observed for rapid CO<sub>2</sub> decompression. We believe these tests jointly point to pronounced synergy of water with carbon dioxide.

### Results

The compositional differences in treated and untreated samples of Pittsburgh Seam coal are presented in Table II. The 80°C, 1200 psi CO<sub>2</sub> treatment afforded a decrease in ash content and volatile matter. A significant decrease in sulfur was also observed. The small change in heating value supports the belief that this process does not drastically alter the coal structure.

Table II. PROXIMATE ANALYSIS OF TREATED AND UNTREATED PITTSBURGH SEAM COAL

	Untreated	Treated	Change
Ash	6.48%	5.93%	-8.5%
Volatile Matter	38.30%	37.67%	-1.6%
Fixed Carbon	55.06%	56.01%	+1.7%
Sulfur	2.49%	1.96%	-21.0%

Ultimate ash analyses for the treated and untreated Pittsburgh Seam coal are shown in Table III. In accordance with the results described, alkali and alkaline earth elements generally appear to be removed efficiently, although the results for sodium appear anomalous. Significant quantities of iron and titanium are also removed. The silicon concentration appears to remain constant while the aluminum concentration increases.

The data presented in Table IV can be used to evaluate the effect of treatment on the concentrations of several elements frequently encountered in coal mineral matter. Optical emission spectroscopy was used to obtain approximate measurements. The first two columns list concentrations found in the ash from untreated and treated samples, respectively, and the third column lists relative concentrations in the solid formed from evaporating the liquid

Table III. Ultimate Analysis of Ash From Treated and Untreated Samples of Pittsburgh Seam Coal

Component	Untreated	Treated
SiO <sub>2</sub>	40.45%	42.52%
Al <sub>2</sub> O <sub>3</sub>	23.08%	28.18%
Fe <sub>2</sub> O <sub>3</sub>	13.88%	11.83%
TiO <sub>2</sub>	1.11%	1.02%
CaO	8.27%	2.01%
MgO	1.30%	.59%
Na <sub>2</sub> O	1.60%	1.57%
K <sub>2</sub> O	1.37%	.43%

Table IV. Analysis of Leached Mineral Matter and Ash

Element	In Ash %		In Leached Mineral Matter, %
	Untreated	Treated	
Si	major	major	major
Al	major	major	major
Ca	major	0.03	major
Mg	1	0.05	major
Fe	1	1	1
Ti	0.5	0.08	1
Na	0.1	0.01	major
Mn	0.1	0.005	0.1
Ba	0.1	0.01	0.01
V	0.08	0.01	0.05
Ni	0.03	0.005	0.1



phase. The leached mineral matter contained very significant quantities of silicon, aluminum, calcium, magnesium, and sodium. This removal was also reflected in the retained ash. Although silicon and aluminum were removed from the coal, their percentage concentrations in the treated ash did not differ significantly from that of the untreated coal. It is important to note that the more corrosive elements, the alkalis and alkaline earths, appear to be particularly responsive to this treatment.

These results generally indicate a trend toward a reduced fraction of basic components in the ash. Figure 1 illustrates the effect which this might have on the fusion temperature of the ash. The curve in this figure (9) represents a correlation of data from an extensive number of coal fraction samples. For the case of the Pittsburgh Seam coal, treatment with  $\text{CO}_2/\text{water}$  reduced the percentage of basic components from 29.4% to 18.4% as shown on the figure. The curve in Figure 1 indicates that this reduction in percentage basic components should increase ash fusion temperatures. In very recent results (10) in which fusion temperatures have been measured, an increase has been confirmed.

The effect of reaction time on ash removal was also evaluated in a limited set of tests. After one hour 14.5% of the ash was removed and after 20 hours 18.8% was removed. This indicates that reaction times as short as one hour may be sufficient to adequately beneficiate coal.

Figure 2 compares dry grinding times required for Pittsburgh Seam coal (from Arkwrite Mine, NA1361) initially sized to 1-3/8" to 3/8". One curve depicts the weight of untreated coal remaining on a 18 mesh (US) screen after specified grinding times. The second curve is for the same coal treated with  $\text{CO}_2/\text{H}_2\text{O}$ . For these samples, the grinding and sieving process was repeated to afford an indication of deviation in these processes. The figure indicates a pronounced improvement in grinding. Two-thirds of the treated coal was below 18 mesh after about 5 minutes, while for the untreated coal about 70 minutes was required. Seven-eighths passage required 10 minutes for the treated coal and well in excess of 150 minutes for the untreated coal.

For finer final grind sizes, the treated coal also appears to require much less grinding power. Figure 3 depicts the amount of coal remaining on a 200 mesh sieve as a function of grinding time. Again an order of magnitude reduction in grinding time is afforded for the treated coal, with 45% of the coal passing through the 200 mesh sieve after 35 minutes. The untreated coal reached that level only at about 400 minutes.

The product size distribution after short grinding times is also very revealing. This allows better evaluation of the effect of feed coal size. The results for the 1" x 3/4" feed are shown in Table V. Comparison of the 10 minute grinding time results for treated and untreated results show that, as in our previously reported results, there is a significant improvement in grindability. This is particularly prominent at the minus-1/2" size which essentially means that the feed coal has been weakened. The difference is less significant, however, with a 200 mesh product.

Using this short grinding time approach comparisons of wet and dry grinding were also studied. Table VI shows that the diminishing improvement from  $\text{CO}_2/\text{water}$  treatment with finer coal sizes occurs for both wet and dry grinding.

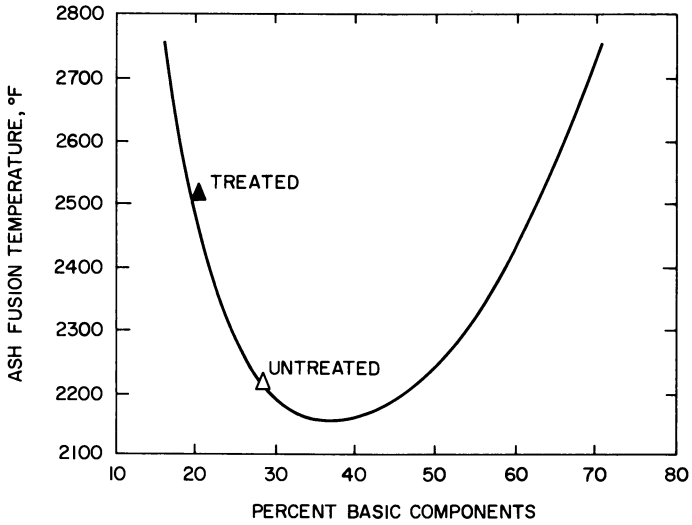


Figure 1. Effect of Ash Composition on Fusion Temperatures

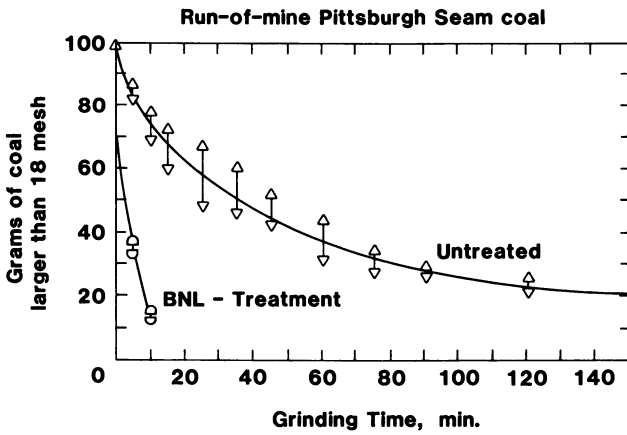


Figure 2. Initial Grinding Results - 18 Mesh Product

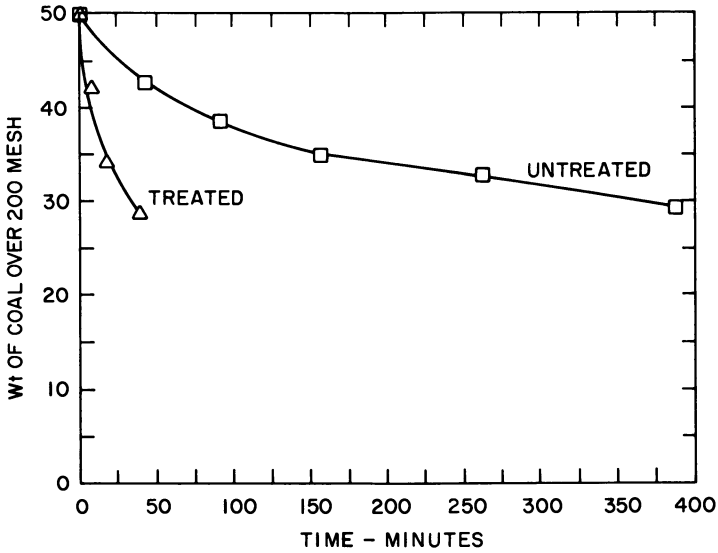


Figure 3. Initial Grinding Results - 200 Mesh Product

Table V. Product Size Distribution - 1" x 3/4" Feed - Short Grinding Times % of Product Less Than Screen Size - Dry Grinding

Screen Size	Run-of-Mine Coal 10 Min. Grind	Treated Coal		
		10 Min. Grind	6 Min. Grind	2 Min. Grind
1/2"	18.4	71.7	74	41.4
1/4"	14.9	68.3	63.1	32.1
6 mesh	14.7	61.3	57.8	25.4
40 mesh	14.1	57	48	14.3
120 mesh	12.8	45.3	32	7.6
400 mesh	11.4	19.4	21.1	4.7

Table VI. Comparison of Wet and Dry Grinding Summary -  
1/2" x 1/4" Feed Coal - 30 Second Grinding Time

	Weight % of Product Less Than Sieve Size Shown			
	1 Run-of-Mine Coal Dry Grinding	2 Treated Coal Dry Grinding	3 Run-of-Mine Coal Wet Grinding	4 Treated Coal Wet Grinding
6 mesh	17.1	32.9	14.1	24.0
40 mesh	4.9	8.2	5.8	7.9
80 mesh	2.9	4.3	4.0	4.1
120 mesh	2.2	3.2	3.3	2.9
200 mesh	1.6	2.1	2.6	3.2

Experiments were also performed to determine the initial breakage rate of untreated coal (no pressure), previously treated coal (no pressure while grinding), and under process conditions using an integrated reactor/grinder system. (After the exposure time, the mill was run as in the other tests while still under pressure.) The product size distributions are given in Table VII. The initial breakage rate for the integrated treatment/grinding systems was 3.7 times greater than that for the unpressurized wet grinding and 1.8 times greater than unpressurized wet grinding of previously treated coal. This demonstrates that the coal aggregate is weaker (more grindable) while in the CO<sub>2</sub>/water solvent system than it is when removed.

Table VII. Integrated Reactor Grinder Test Results  
1/2" x 1/4" Feed - 30 Second Grind

Sieve Size	Weight % of Products Less Than Sieve Size Shown		
	Untreated	Treated	Integrated System
-1/2	100.00	100.00	100.00
-1/4	15.80	31.60	58.20
-6 mesh	1.70	5.40	12.90
-40 mesh	0.67	2.15	3.50
-80 mesh	0.38	1.40	1.60
-120 mesh	0.28	0.98	1.00
-200 mesh	0.19	0.59	0.69

### Conclusions

The process of treating coal with CO<sub>2</sub>/water has been shown to remove as much as 15% of the ash. Ash removal apparently increases with increasing CO<sub>2</sub> concentration in the system up to approximately 24g/L and is invariant with higher concentrations. It has been shown that, in addition to ash, sulfur is removed with treatment and that the volatiles content and heating value are unchanged. Specific ash elements which have been shown to be removed include silicon, aluminum, calcium, magnesium, sodium, and iron. The overall effect is a reduction in the basic fraction in the ash which could be very beneficial in raising the ash fusion temperature.

From the results of the grinding tests with coal which was treated with CO<sub>2</sub>/water it is clear that the coal is more grindable. The results of the grindability tests, however, are apparently dependent upon mill feed coal size, and product coal size. With the 1-3/8" x 3/8" feed coal, exposure to the CO<sub>2</sub>/water environment reduced the time required for grinding through 18 mesh by a factor of 10. With a smaller feed coal and a finer product size the benefits gained by CO<sub>2</sub>/water exposure were significantly reduced in the initial series of tests. Further testing, however, showed a consistent reduction in both breakage rate improvement with treatment and improvement in the production rate of fine product with decreasing feed coal size. The production rate of fine (minus-200 mesh) coal which is most important since required power consumption is very high in this industrially significant size region.

Finally, results from the integrated-reactor grinder system showed a significant improvement in grindability even with the 1/2" x 1/4" feed coal. This confirms the suggestion that the coal is weakest while still in the presence of the CO<sub>2</sub>/water solvent system.

### Acknowledgments

This research was partially supported by a grant through the Morgantown Energy Technology Center from the U.S. Department of Energy under Contract No. DE-AC02-76CH00016 (11). Current support is being received from the Research Department of the Florida Power and Light Company.

Finally, the authors wish to thank Dr. Arden Walters of FPL for suggesting the writing of this paper and we also express appreciation for his presentation of our results as part of this Symposium at the ACS National Meeting in Philadelphia.

### Additional Note

Since the completion of this project other processes utilizing carbon dioxide and water beneficiation have been developed (12). Specifically, in this work liquid carbon dioxide near the critical point is used to coalesce the coal and leave behind ash components. The coal feed is a water slurry in this project. The coal is cleaned by the characteristics of two immiscible phases in sharp contrast to the miscible carbon dioxide water treatments described in this paper.

Literature Cited

1. Berkowitz, N. "An Introduction to Coal Technology"; Academic Press: New York, 1979.
2. Tschamler, R.; DeRuiter, E. "Chemistry of Coal Utilization"; Lowry, H., Ed.; John Wiley & Sons, New York, 1963; Chap. 2.
3. Fuller, E. L. "Coal Structure"; Gorbaty, M.; Ed., Am. Chem. Soc.: Washington, 1981; pp. 293.
4. Schmitt, R. J. of Inst. of Energy. 1981, 54,63.
5. Dryden, I. C. G.; op. cit. Ref. 3, Chap. 6.
6. Sustmann, H.; Lehnert, R. Brennstoff-Chemie. 1937, 18, 353.
7. Bond, F. C. AIME Trans. Mining Engineering, May 1952, pp. 484, 493.
8. Lowrison, G. C. "Crushing and Grinding"; Butterworths Monograph in Chemistry and Chemical Engineering, 1974, pp. 75-76.
9. Bryers, R. W.; Taylor, T. E. ASME Winter Annual Meeting, Houston, Nov. 30-Dec. 5, 1975, ASME 75-WA/CD-3.
10. Trinidad, R.; Sapienza, R.; and Butcher, T. "Effects of Carbon Dioxide on Low Rank Coal Grindability and Slurry Preparation," Final Report to Electric Power Research Institute, unpublished data.
11. Sapienza, R.; Slegeir, W.; Butcher, T.; Healy, F. "Coal Fracturing and Heteroatom Removal," Annual Report, Sept. 1983, Brookhaven National Laboratory, BNL-51749.
12. Morsi, B. I.; Klinzing, G. E. "Licado Process for Super-Clean Coal," Quarterly Report, December 1983, U.S. Department of Energy, DOE/PC-63048-TI.

RECEIVED August 30, 1985

## Effect of Caustic and Microwave Treatment on Clay Minerals Associated with Coal

C. K. Richardson, R. Markuszewski, K. S. Durham, and D. D. Bluhm

Ames Laboratory and Department of Earth Sciences, Iowa State University, Ames, IA 50011

Clay minerals typical of those occurring in coal (kaolinite, illite, and montmorillonite) were treated with 30 or 50% aqueous NaOH at room temperature for varying periods of time and then were either heated in a drying oven at 105°C or irradiated in a microwave unit for up to 3 minutes. The products were later washed with water or with 10% HCl. These experiments were performed to test and evaluate a chemical coal cleaning process based on reacting coal with aqueous NaOH, irradiating with microwave energy, and washing with acid to reduce the sulfur and ash content. X-ray diffraction analyses showed that no new reaction products were formed when these clay minerals were treated with NaOH solutions at room temperature. Heating in a drying oven at 105°C formed hydroxysodalite from kaolinite and a zeolite-like mineral from montmorillonite. Samples irradiated in the microwave unit underwent the greatest changes. Hydroxysodalite-hydroxycancrinite mixtures formed from kaolinite, nepheline formed from illite, and the montmorillonite dehydrated. The results suggest that the clay minerals selectively absorbed microwave energy and were heated to temperatures above the boiling point of the solution. The three clay minerals absorbed microwave energy to different degrees. Illite appeared to reach a higher temperature than either kaolinite or montmorillonite. The mineral products became more sodium-rich and less hydrated with increased microwave exposure time, suggesting that increasingly higher temperatures were attained. Acid washing of the treated samples resulted in the removal of all or part of the hydroxysodalite-hydroxycancrinite mixture and part of the nepheline. Because of the significant breakdown of clay minerals during the caustic and microwave treatment, this technique is promising for the removal of ash-forming minerals from coal.

One of the many processes being considered for chemically removing ash and sulfur from coal involves treatment of the coal with concentrated (30-50%) aqueous NaOH solutions, irradiating the coal with microwave energy, and then washing the coal with water and acid. Previous studies at the General Electric Company by Zavitsanos et al. (1-6) have shown that such a process can remove up to 80-90% of the sulfur and 40-50% of the ash content of the coal. The present study was initiated to try to determine the chemical and mineralogical changes that occur in clay minerals (commonly found in coal) during the alkali pretreatment, drying, microwave irradiation, and acid and water washing steps of the microwave process for cleaning coal.

A search of the literature yielded no other work on microwave treatment of clay minerals. Numerous studies, however, have looked into the solubility of various clay minerals in acid solutions (7-10) and in alkaline solutions (7,8,11-13), including many studies on the Bayer process. The solubility studies suggest that, in general, aqueous acid solutions remove the alkali metals, alkaline earth metals, and iron and aluminum from clay minerals (7). Alkaline solutions, on the other hand, preferentially remove silica from clay minerals (8). Acid solutions apparently first remove the exchangeable interlayer cations from the clays, and then they attack the octahedral layers. Alkaline solutions attack the tetrahedral layers, and if prolonged attack occurs, the structure of the clay is destroyed (8). Fan et al. (11,12) studied the reaction between clay minerals and aqueous sodium carbonate (1-3.0 M) and sodium hydroxide (1.0 M) in sealed autoclaves at 250°C. Although the conditions of these experiments were quite different from those employed in the present microwave process, they did show that prolonged high-temperature attack on clay minerals by alkaline solutions caused them to break down and form a series of hydrous sodium aluminum silicate minerals which could be removed by acid treatment. In the present work, it was expected that the mineral matter could absorb microwave energy and be therefore heated to temperatures in excess of 100°C. Thus, some clay alteration reactions were expected to occur at elevated temperatures, and, in the presence of caustic, reaction products -- perhaps similar to those seen in previous autoclave experiments -- were expected to form.

### Experimental

The clay minerals used in this study were kaolinite ( $\text{Al}_2\text{Si}_2\text{O}_5(\text{OH})_4$ ), illite ( $\text{K}_{1-x}\text{Al}_3\text{Si}_{3+x}(\text{OH})_2$ ), and montmorillonite which was approximately  $1/2 (\text{Ca}, \text{Na})_{0.7}(\text{Al}, \text{Mg}, \text{Fe})_4(\text{Si}, \text{Al})_8\text{O}_{20}(\text{OH})_4 \cdot n \text{H}_2\text{O}$ . The clays were natural samples purchased from Ward's Natural Science Establishment, Inc. The kaolinite sample was obtained from a kaolin deposit in Georgia. X-ray diffraction (XRD) patterns on this material showed peaks only for kaolinite, and scanning electron microscope-energy dispersive x-ray (SEM-EDX) analysis yielded peaks for Al, Si, and minor amounts of Ti. The illite was a green shale from New York which Ward's listed as 85% illite. XRD patterns of this



material contained peaks for illite and quartz, and SEM-EDX analysis showed presence of Si, Al, K, Fe, and some Ca. The montmorillonite sample was a powdered bentonite from Wyoming. XRD patterns showed peaks for montmorillonite and an illite-like material, and SEM-EDX analysis showed Si, Al, moderate Fe, and small Ca and K peaks. All materials were initially ground to a powder. Aqueous solutions of 30% or 50% NaOH were prepared from distilled, deionized water and reagent grade NaOH.

The experiments were set up in such a way that the alkali/mineral ratios, reaction times, drying temperature, and acid concentration were similar to those to be used later in the cleaning of coal with microwave irradiation. In the GE procedure described by Zavitsanos et al. (1-6), aqueous NaOH was added to coal to make a slurry with an alkali/coal ratio of 0.3 - 2.0. Their slurry had an initial moisture content of about 40% which was lowered to 20% by heating the slurry in a drying oven. Then the dried slurry was irradiated for 1 minute under inert atmosphere in a 2.45-GHz microwave apparatus at 1.0 or 2.0 kW. The mixture was then washed with water and acid (either 10% HCl or 10% H<sub>2</sub>SO<sub>4</sub>) to remove NaOH and acid-soluble products.

The present mineral experiments were designed to look at the mineralogical changes that occur as clay components are subjected to each step in this process. The microwave irradiation step in our experiments, however, was not entirely comparable to that in the GE experiments because a smaller, 500-watt unit was used while the 2.0-kW unit was being constructed. Future experiments in our laboratory will monitor clay reactions at higher microwave power levels.

Approximately equal amounts (usually 5 grams) of the clay mineral or clay mixture and 5 grams of 30% or 50% NaOH solution (alkali/clay ratio of 0.3 and 0.5, respectively) were placed in a beaker. Three different types of experiments were then performed:

- 1) The clay mineral or mixture was reacted with the NaOH solution at room temperature for varying periods of time, then filtered and water washed to remove excess NaOH, and finally air dried.
- 2) The clay mineral or mixture was reacted with NaOH for about 20 minutes and then placed in a drying oven at 105°C for 5 to 30 minutes to reduce the moisture content. The sample was then removed from the oven, filtered, water washed, and air dried. In a few experiments the caustic-treated clay mixture was filtered to remove excess moisture and then placed in the drying oven; the sample was again filtered and water washed. These two sets of experiments evaluated the effect of the treatment steps prior to microwave irradiation.
- 3) The clay mineral or mixture was reacted with the aqueous NaOH solution for about 20 minutes at room temperature and then was irradiated in a Microwave Drying/Digestion System (Model MDS-81, CEM Corporation, P. O. Box 9, Indian Trail, N.C. 28079) at 500 watts (2.45 GHz) for 30 seconds to 3 minutes. The sample was then filtered, water washed, and air dried.

All the samples were analyzed by standard XRD techniques. After initial XRD analyses of the treated samples were completed, many of the samples were acid washed with 10% HCl and re-analyzed to determine whether any acid-soluble products were removed.

### Results

The results of experiments on the individual clay minerals are summarized in Tables I-III. Kaolinite is unstable in alkaline (30% NaOH, alkali/clay = 0.3) solutions (7,14) and begins to break down even at room temperature. The first change noted in the XRD patterns in Table I was that the kaolinite peak intensities decreased, and the background increased somewhat. This may indicate a decrease

Table I. Treatment of Kaolinite with Caustic and Microwave Irradiation, Followed by Water or 10% HCl Wash

No.	NaOH Concn.	Reaction Time (min.)			Type of Wash	Products Observed by XRD
		Room Temp.	105°C	Micro- wave		
5-1	30%	41	--	--	H <sub>2</sub> O	kaol. only
5-2	30%	10	--	--	H <sub>2</sub> O	kaol. (peak intensities decreased)
5-3	30%	41	10	--	H <sub>2</sub> O	kaol. (peak intensities decreased)
5-4	30%	40	30	--	H <sub>2</sub> O	kaol., hydroxysodalite
5-4b	30%	40	31	--	acid	kaol.
10-1	30%	20	--	1	H <sub>2</sub> O	kaol., sodalite-cancrinite mix.
10-2	30%	20	--	0.5	H <sub>2</sub> O	kaol., cancrinite-rich cancrinite-sodalite mix.
10-2b	30%	20	--	0.5	acid	kaol., sodalite (peak intensities decreased)
10-3	30%	20	--	1.33	H <sub>2</sub> O	kaol., sodalite-rich cancrinite-sodalite mix.
10-4	30%	20	--	3	H <sub>2</sub> O	kaol., sodalite
10-4b	30%	20	--	3	acid	kaol., sodalite (peak intensities decreased)
13-1	50%	20	--	--	H <sub>2</sub> O	kaol. (peak intensities decreased)
13-2	50%	20	22	--	H <sub>2</sub> O	kaol. (peak intensities decreased), sodalite-cancrinite mix.
13-2	50%	20	22	--	acid	kaol., sodalite-cancrinite, (all peak intensities decreased)
13-3	50%	20	--	1	H <sub>2</sub> O	kaol., sodalite-cancrinite mix.
13-3	50%	20	--	1	acid	kaol., sodalite-cancrinite (all peak intensities decreased)

in the crystallinity of the kaolinite, possibly due to the formation of partially solubilized non-crystalline material. In the sample heated at 105°C for 30 minutes and in all of the microwave irradiated samples, kaolinite reacted to form the hydrous sodium aluminum silicates called hydroxysodalite  $[\text{Na}_8(\text{Al}_6\text{Si}_6\text{O}_{24})(\text{OH})_2]$  and hydroxycancrinite  $[\text{Na}_8(\text{Al}_6\text{Si}_6\text{O}_{24})(\text{OH})_{1-2} \cdot (1-5)\text{H}_2\text{O}]$ . In the microwave irradiated experiments, varying mixtures of hydroxycancrinite and hydroxysodalite formed. In the 30-second run, the hydroxycancrinite peaks predominated, but as the exposure time was increased, hydroxysodalite predominated. This change suggests that higher temperatures were attained in longer exposure runs and dehydration was occurring. The experiments performed with 50% NaOH (alkali/mineral = 0.5) yielded similar results with possibly one exception; in the XRD pattern for experiment 13-3 (44 minutes at room temperature and 1 minute in microwave oven) there was a new peak in addition to the hydroxysodalite-hydroxycancrinite peaks, suggesting that a new (as yet unidentified) mineral was forming. Acid washing the treated kaolinite in 10% HCl removed part of the hydroxysodalite-hydroxycancrinite mixture, demonstrating that these minerals are at least partially soluble in cold acid.

Illite, a mineral that forms in alkaline solutions (15), is more stable than kaolinite in 30% NaOH. The experiments (Table II) in which illite was reacted either at room temperature or at 105°C with 30% NaOH showed that no discernible reaction took place. In the microwave irradiated experiments, however, considerable changes occurred. Illite strongly absorbed the microwave energy, causing considerable heating of the sample. When illite was irradiated for

Table II. Treatment of Illite (Containing Quartz Impurities) with Caustic and Microwave Irradiation, Followed by Water or 10% HCl Wash

No.	NaOH Concn.	Reaction Time (min.)			Type of Wash	Products Observed by XRD
		Room Temp.	105°C	Micro- wave		
6-1	30%	16	--	--	H <sub>2</sub> O	ill. (+quartz)
6-2	30%	40	--	--	H <sub>2</sub> O	ill. (+quartz)
6-3	30%	22	35 <sup>a</sup>	--	H <sub>2</sub> O	ill. (+quartz)
6-4	30%	35	15	--	H <sub>2</sub> O	ill. (+quartz)
12-1	30%	20	--	1	H <sub>2</sub> O	ill. (+quartz), Na nepheline
12-1b	30%	20	--	1	acid	ill. (+quartz), nepheline (peak intensities decreased)
12-2	30%	20	--	0.5	H <sub>2</sub> O	ill. (+quartz), nepheline low-Na nepheline)
12-2b	30%	20	--	0.5	acid	ill. (+quartz), nepheline trace
12-3	30%	20	--	0.75	H <sub>2</sub> O	ill. (+quartz), Na-rich nepheline
12-4	30%	20	--	2	H <sub>2</sub> O	ill. (+quartz), nepheline

<sup>a</sup> Filtered before drying in oven.

2 minutes in the beaker, a reaction ring formed which was hot and glowing when the microwave unit was opened. XRD patterns showed that the anhydrous silicate nepheline  $[(Na,K)_4Al_4Si_4O_{16}]$  has formed. The position of the nepheline peaks shifted slightly with increasing exposure time, indicating that the nepheline was more potassium-rich (approximately  $KNa_2Al_3Si_3O_{12}$ ) initially and became more sodium-rich in 45-second and 1-minute runs. In the 2-minute microwave run, changes in peak intensities and additional peak shifts (in XRD) suggest that nepheline was beginning to convert to another mineral. Washing the microwave irradiated illites with cold HCl resulted in removal of only small amounts of the nepheline.

Montmorillonite began to break down in 30% NaOH solutions at room temperature (Table III). The first change noted, as with kaolinite, was that the peak intensities decreased in the XRD pattern. A decrease in peak intensities was also seen in the XRD patterns for samples heated to 105°C. Microwave irradiation of montmorillonite caused heating of the sample and some changes in the XRD pattern. The typical 13.6-Å peak disappeared and the 9.6-Å peak typical of illites and micas became stronger, indicating that the montmorillonite was undergoing dehydration and the layers were collapsing. Another montmorillonite peak split and formed two peaks, suggesting that other structural modifications were occurring. Although some structural modifications of the montmorillonite have occurred, the XRD pattern did not reveal the presence of a new mineral. Acid washing of the treated samples did not change the XRD pattern significantly, suggesting that any alteration product formed was not acid-soluble.

Table III. Treatment of Montmorillonite with Caustic and Microwave Irradiation, Followed by Water or Acid Wash

No.	NaOH Concn.	Reaction Time (min.)			Type of Wash	Products Observed by XRD
		Room Temp.	105°C	Micro- wave		
9-1	30%	40	--	--	H <sub>2</sub> O	mont. (peak intensities decreased)
9-2	30%	41	16 <sup>a</sup>	--	H <sub>2</sub> O	mont. (peak intensities decreased)
9-3	30%	40	16	--	H <sub>2</sub> O	mont.
11-1	30%	20	--	0.5	H <sub>2</sub> O	mont., dehydrated mont.
11-1b	30%	20	--	0.5	acid	mont., dehydrated mont.
11-2	30%	20	--	1	H <sub>2</sub> O	mont., dehydrated mont.
11-3	30%	20	--	1.33	H <sub>2</sub> O	mont., dehydrated mont.
11-3b	30%	20	--	1.33	acid	mont., dehydrated mont.

<sup>a</sup> Filtered before drying in oven.

The results of experiments in which binary and ternary mixtures of the three clay minerals were reacted with 30% NaOH and irradiated in the microwave oven are summarized in Tables IV and V, respectively. Reacting mixtures of these clay minerals did not result in the

Table IV. Treatment of Binary Clay Mixtures of Kaolinite, Illite, and Montmorillonite with 30% NaOH and Microwave Irradiation, Followed by Water or 10% HCl Wash

No.	Initial Sample	Reaction time (min.)		Type of Wash	Products Observed by XRD
		Room Temp.	Micro-wave		
14-1	kaol.-ill.	26	1	H <sub>2</sub> O	ill., kaol., neph., sodalite-cancrinite
14-1b	kaol.-ill.	26	1	acid	ill., kaol., neph., sodalite-cancrinite (little change from above samp.)
14-2	kaol.-ill.	22	2	H <sub>2</sub> O	ill., kaol., sodalite-cancrinite, neph. (peak shifting)
14-3	kaol.-ill.	7	0.5	H <sub>2</sub> O	ill., kaol., neph., sodalite-cancrinite
14-4	kaol.-ill.	24	0.5	H <sub>2</sub> O	ill., kaol. (peaks decreased), neph., sodalite-cancrinite
15-1	ill.-mont.	39	0.5	H <sub>2</sub> O	ill., mont., trace of neph., dehydrated mont.
15-2	ill.-mont.	35	1	H <sub>2</sub> O	ill., mont., neph., dehydrated mont.
15-3	ill.-mont.	36	2	H <sub>2</sub> O	ill., mont., neph., dehydrated mont.
16-1	kaol.-mont.	35	0.5	H <sub>2</sub> O	kaol., sodalite-cancrinite mix., mont.
16-2	kaol.-mont.	31	1	H <sub>2</sub> O	kaol., mont., sodalite-cancrinite, dehydrated mont.
16-3	kaol.-mont.	25	2	H <sub>2</sub> O	kaol., mont., sodalite-cancrinite, dehydrated mont.

formation of any minerals not already found in experiments with individual minerals. Reactions with kaolinite and illite resulted in the formation of both hydroxysodalite-hydroxycancrinite and nepheline. Reactions with kaolinite and montmorillonite resulted in the formation of hydroxysodalite-hydroxycancrinite and dehydrated montmorillonite, and reactions with illite and montmorillonite resulted in the formation of nepheline and dehydrated montmorillonite. When a ternary mixture of the clays (equal amounts of each mineral) was reacted with 30% NaOH solution and irradiated in the microwave oven, hydroxysodalite-hydroxycancrinite and traces of nepheline were found (Table V). The temperature did not appear to have risen as high in the ternary mixtures. Thus, nepheline was not found in 30-seconds experiments, and only small amounts were found in 1- and 2-minute experiments. The 13.6-Å montmorillonite peak remained in all patterns, suggesting that the montmorillonite did not dehydrate completely. Acid washing removed part of the reaction products from these mixtures.

Several tests were performed to increase solubilization by using warm (60°C) or hot (80°C) acid rather than cold acid. These

Table V. Treatment of Ternary Clay Mixtures of Kaolinite, Illite, and Montmorillonite with 30% NaOH and Microwave Irradiation, Followed by Water or 10% HCl Wash

No.	Reaction time (min.)		Type of Wash	Products Observed by XRD
	Room Temp.	Micro- wave		
17-1	23	0.5	H <sub>2</sub> O	kaol., ill., mont., trace sodalite-cancrinite
17-1b	23	0.5	acid	kaol., ill., mont. (peak intensities decreased), sodalite-cancrinite mix. (peak intensities decreased)
17-2	22	1	H <sub>2</sub> O	kaol., ill., mont., sodalite-cancrinite, trace neph., dehydrated mont.
17-3	22	2	H <sub>2</sub> O	kaol., ill., mont., sodalite-cancrinite, neph., dehydrated mont.
17-3b	22	2	acid	kaol., ill., mont., sodalite-cancrinite, neph., dehydrated mont. (peak intensities decreased)

runs indicate that considerably more product, although not all of it, was removed at 80°C. Fan et al. (11,12) were able to remove similar products completely by using boiling HCl or H<sub>2</sub>SO<sub>4</sub>.

### Discussion

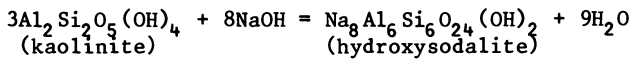
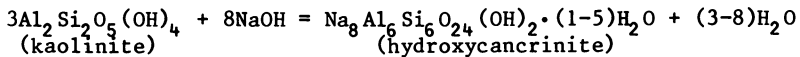
These experiments have allowed an evaluation of the extent of reaction between clay minerals and alkali solution during the pretreatment part of the microwave coal cleaning process. It is evident from these results that some reactions began to occur between the alkali solution and the clay minerals, particularly with kaolinite, before the microwave irradiation. The new product peaks, however, were small on the XRD patterns compared to the starting materials, suggesting that the amount of material that has reacted may be quite small. The visual appearance of the material also suggested that only a small reaction rim was forming in the container. Since overall the changes in the clay minerals during alkali pretreatment at room temperature were rather minor, very little ash removal can be expected during only the pretreatment part of the coal cleaning process.

On the other hand, substantial changes did occur under microwave irradiation. The clay minerals appeared to absorb microwave energy efficiently enough for considerable heating to occur. Complete dehydration of the clay-alkali slurry occurred within the first 30 seconds. No measurement of the temperatures attained was possible because temperature probes could not be inserted in the material during microwave heating without perturbing the microwave field. A probe was not inserted immediately after irradiation because considerable cooling took place as soon as the oven door was opened and because the reaction products formed a hard crust which was difficult to penetrate with a probe. These experiments also pointed out

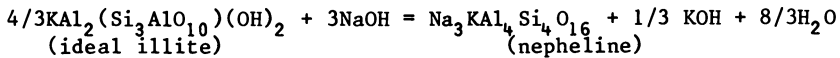
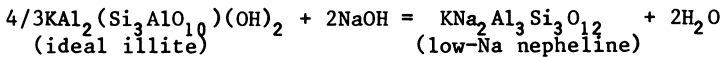
that not all clay minerals absorbed the microwave energy to the same extent. The illite samples were the only ones in which the product rim was glowing after opening the microwave unit, suggesting that illite absorbed microwave energy more strongly than the other clay minerals and reached higher temperatures. Also, anhydrous reaction products were formed in these experiments.

The reactions between clay minerals, NaOH solutions, and microwave irradiation showed that the clay mineral structures began to break down, and the released Al and Si (and some K) combined with Na from the solution to form new minerals. The exact reaction path could not be determined from the present experiments. Since the new minerals formed had approximately the same Al:Si ratio as the clay minerals, no excess Al (as  $\text{Al}_2\text{O}_3$  or  $\text{Al}(\text{OH})_3$ ) or quartz was expected, nor was any found in the XRD pattern. The following equations, arranged with increasing time, seem most reasonable to describe the reactions observed for kaolinite and illite:

kaolinite:



illite:



All of these reactions consume alkali and release water, reinforcing the observation that alkali (Na) addition and dehydration reactions were occurring, particularly with increased microwave exposure time. These products were similar to those observed in autoclave experiments run at 250-300°C for 1 hour (12). In our treated samples, however, XRD patterns for the starting clay materials were clearly visible, indicating that although high temperature reactions did occur, they did not go to completion. This implies that at the microwave power levels and irradiation times used in these experiments, not all of the clay minerals in a coal sample would be converted to soluble products. This conversion process, however, may be much more complete at the power levels to be used in the microwave coal cleaning process. Furthermore, the pretreatment, irradiation, and washing cycles can be repeated several times to improve the conversion. Still the results of these experiments are encouraging and suggest that most or all of the kaolinite and illite (the two most abundant clay minerals) in coal could be converted to soluble products and removed, reducing considerably the ash content of the coal.

These experiments are the first part of a program designed to evaluate each step of the microwave coal cleaning process. Additional experiments of the type reported here will be performed with

quartz and pyrite to complete our tests on the most abundant minerals in coal. All the minerals will be irradiated at higher power levels for varying periods of time in the larger microwave unit. These future experiments will help determine the optimum power levels and times necessary to get complete conversion of the mineral matter to soluble products. The results of these experiments will be used to guide our coal cleaning program and help us attain the highest levels of ash and sulfur removal.

### Acknowledgments

Ames Laboratory is operated for the U. S. Department of Energy by Iowa State University under Contract No. W-7405-Eng-82.

This work was supported by the Assistant Secretary for Fossil Energy, Office of Coal Utilization, through the Pittsburgh Energy Technology Center.

The unlimited use of an MDS-81 microwave unit on extended loan from the CEM Corporation is gratefully acknowledged.

Valuable discussions were held with Prof. G. Fanslow of the Electrical Engineering Department.

### Literature Cited

1. Zavitsanos, P.D.; Golden, J.A; Bleiler, K.W. "Coal Desulfurization by a Microwave Process," Tech. Prog. Report, Feb. - May 1981, General Electric Co., Philadelphia, PA, 1981.
2. Zavitsanos, P.D.; Golden, J.A; Bleiler, K.W. "Coal Desulfurization by a Microwave Process," Tech. Prog. Report, Jan. 1982, General Electric Co., Philadelphia, PA, 1982.
3. Zavitsanos, P.D.; Golden, J.A; Bleiler, K.W. "Coal Desulfurization by a Microwave Process," Tech. Prog. Report, May 1982, General Electric Co., Philadelphia, PA, 1982.
4. Zavitsanos, P.D.; Golden, J.A.; Bleiler, K.W. "Coal Desulfurization by a Microwave Process," Tech. Prog. Report, Sept. 1982, General Electric Co., Philadelphia, PA, 1982.
5. Zavitsanos, P.D.; Golden, J.A.; Bleiler, K.W. "Coal Desulfurization by a Microwave Process," Tech. Prog. Report, Dec. 1982, General Electric Co., Philadelphia, PA, 1982.
6. Zavitsanos, P.D.; Golden, J.A.; Bleiler, K.S.; Jain, K. "Coal Desulfurization by a Microwave Process," Tech. Prog. Report, March 1983, General Electric Co., Philadelphia, PA, 1983.
7. Carroll, D.; and Starkey, H.C. "Reactivity of Clay Minerals with Acids and Alkalies," J. Clays and Clay Minerals 1971, 19, 321-333,
8. Nutting, P.G. "The Action of Some Aqueous Solutions on Clays of Montmorillonite Group," U.S. Geological Survey, Prof. Paper, 197F, 1943, 219-235.
9. Gastuche, M.C. "Study of the Alteration of Kaolinite by Various Chemical Reagents," Silic. Ind. 1959, 24, 237-244.
10. Gastuche, M.C.; Delmon, B.; Vielvoye, L. "Kinetics of Heterogeneous Reactions. Attack on the Silicon-Aluminum Network of Kaolinite by Hydrochloric Acid," Bull. Soc. Chim. Franc. 1960, 1, 60-70.



11. Fan, C.-W.; Markuszewski, R.; Wheelock, T.D. "Process for Producing Low-Ash, Low-Sulfur Coal," Am. Chem. Soc. Div. Fuel Chem. Preprints 1984, 29(1), 114-119.
12. Fan, C.-W.; Markuszewski, R.; Wheelock, T.D. "Behavior of Mineral Matter During Alkaline Leaching of Coal," Am. Chem. Soc. Div. of Fuel Chem. Preprints 1984, 29(4), 319-325.
13. Eremin, N.I.; Tkacheva, L.V.; Makarenko, V.N. "Investigation of the Kinetics of the Decomposition of Kaolinite in Alkaline and Aluminate Solutions," Soviet Non-ferrous Metals Research 1978, 6(5), 197-199.
14. Montoya, J.W.; Hemley, J.J. "Activity Relations and Stabilities in Alkali Feldspar and Mica Alteration Reactions," Econ. Geol. 1975, 70, 577-582.
15. Deer, W.A.; Howie, R.A.; Zussman, J. "An Introduction to the Rock-Forming Minerals"; Longman:London, 1975.

RECEIVED August 30, 1985

## Author Index

- Abbott, M. F., 325  
 Altmann, Werner, 394  
 Apelian, D., 215  
 Austin, L. G., 325  
 Benson, S. A., 70  
 Biggs, Donald L., 128  
 Blander, Milton, 186  
 Bluhm, D. D., 513  
 Bohor, Bruce, 90  
 Borio, R. W., 288  
 Bryers, Richard W., 353  
 Butcher, T., 500  
 Caley, W. F., 485  
 Chien, C. H., 416  
 Cleyle, P. J., 485  
 Cook, L. P., 277  
 Davis, Alan, 41  
 DeYoung, David H., 170  
 Durham, K. S., 513  
 Falcone, S. K., 70,114  
 Fan, C.-W., 462  
 Finkelman, Robert B., 61  
 Granoff, Barry, 410  
 Greenberg, Sherman, 156  
 Harvey, Richard D., 10  
 Hastie, J. W., 277  
 Healy, F., 500  
 Heap, M. P., 375  
 Huffman, G. P., 100  
 Huggins, F. E., 100  
 Kalmanovitch, D. P., 234  
 Karner, F. R., 70  
 Keller, Douglas V., Jr., 473  
 Lawrence, William F., 443  
 Lee, Y. C., 416  
 Levasseur, A. A., 288  
 Lindahl, Peter C., 61  
 Lindsay, Curtis G., 128  
 Lovell, Harold L., 438  
 Markuszewski, R., 449,462,513  
 Mason, D. M., 320  
 McCauley, W. L., 215  
 Mills, K. C., 195,256  
 Montano, P. A., 416  
 Muter, Richard B., 443  
 Padrick, Thomas D., 410  
 Payne, R., 375  
 Pelton, Arthur D., 186  
 Piwinskii, A. J., 223  
 Poeppel, Roger, 156  
 Pohl, John H., 430  
 Raask, Erich, 138,303  
 Rehmat, A., 320  
 Renton, John J., 53  
 Richardson, C. K., 513  
 Richter, W., 375  
 Rimmer, Susan M., 41  
 Ruch, Rodney R., 10  
 Ryerson, F. J., 223  
 Sapienza, R., 500  
 Schobert, H. H., 70,114  
 Slegeir, W., 500  
 Stewart, I., 485  
 Straszheim, Warren E., 449  
 Triplehorn, Don, 90  
 Tsao, K. C., 320  
 Vorres, Karl S., 1,156  
 Weed, H. C., 223  
 Wheelock, T. D., 462  
 Whiteway, S. G., 485  
 Williamson, J., 234  
 Yeye-Odu, A., 416  
 Yousling, Jay G., 449

## Subject Index

- A
- Abrasion of metal parts, 11-12  
 Absorption coefficient  
   temperature effects, 258,260f  
   wavelength dependence, 258,259f  
 Absorption coefficient of slags,  
   calculation, 210  
 Absorptivity, comparison to  
   emissivity, 380,382f
- Acid cleaning, comparison to gravity  
   cleaning methods, 502  
 Alkali-rich slags  
   corrosive effects, 277  
   solid-liquid-vapor  
   equilibria, 277-284  
 Alkaline leaching  
   behavior of mineral matter, 470-471  
   determination of behavior of  
   minerals, 462-463  
   effectiveness, 465

## Author Index

- Abbott, M. F., 325  
 Altmann, Werner, 394  
 Apelian, D., 215  
 Austin, L. G., 325  
 Benson, S. A., 70  
 Biggs, Donald L., 128  
 Blander, Milton, 186  
 Bluhm, D. D., 513  
 Bohor, Bruce, 90  
 Borio, R. W., 288  
 Bryers, Richard W., 353  
 Butcher, T., 500  
 Caley, W. F., 485  
 Chien, C. H., 416  
 Cleyle, P. J., 485  
 Cook, L. P., 277  
 Davis, Alan, 41  
 DeYoung, David H., 170  
 Durham, K. S., 513  
 Falcone, S. K., 70,114  
 Fan, C.-W., 462  
 Finkelman, Robert B., 61  
 Granoff, Barry, 410  
 Greenberg, Sherman, 156  
 Harvey, Richard D., 10  
 Hastie, J. W., 277  
 Healy, F., 500  
 Heap, M. P., 375  
 Huffman, G. P., 100  
 Huggins, F. E., 100  
 Kalmanovitch, D. P., 234  
 Karner, F. R., 70  
 Keller, Douglas V., Jr., 473  
 Lawrence, William F., 443  
 Lee, Y. C., 416  
 Levasseur, A. A., 288  
 Lindahl, Peter C., 61  
 Lindsay, Curtis G., 128  
 Lovell, Harold L., 438  
 Markuszewski, R., 449,462,513  
 Mason, D. M., 320  
 McCauley, W. L., 215  
 Mills, K. C., 195,256  
 Montano, P. A., 416  
 Muter, Richard B., 443  
 Padrick, Thomas D., 410  
 Payne, R., 375  
 Pelton, Arthur D., 186  
 Piwinskii, A. J., 223  
 Poeppel, Roger, 156  
 Pohl, John H., 430  
 Raask, Erich, 138,303  
 Rehmat, A., 320  
 Renton, John J., 53  
 Richardson, C. K., 513  
 Richter, W., 375  
 Rimmer, Susan M., 41  
 Ruch, Rodney R., 10  
 Ryerson, F. J., 223  
 Sapienza, R., 500  
 Schobert, H. H., 70,114  
 Slegeir, W., 500  
 Stewart, I., 485  
 Straszheim, Warren E., 449  
 Triplehorn, Don, 90  
 Tsao, K. C., 320  
 Vorres, Karl S., 1,156  
 Weed, H. C., 223  
 Wheelock, T. D., 462  
 Whiteway, S. G., 485  
 Williamson, J., 234  
 Yeye-Odu, A., 416  
 Yousling, Jay G., 449

## Subject Index

- A
- Abrasion of metal parts, 11-12  
 Absorption coefficient  
   temperature effects, 258,260f  
   wavelength dependence, 258,259f  
 Absorption coefficient of slags,  
   calculation, 210  
 Absorptivity, comparison to  
   emissivity, 380,382f
- Acid cleaning, comparison to gravity  
   cleaning methods, 502  
 Alkali-rich slags  
   corrosive effects, 277  
   solid-liquid-vapor  
   equilibria, 277-284  
 Alkaline leaching  
   behavior of mineral matter, 470-471  
   determination of behavior of  
   minerals, 462-463  
   effectiveness, 465

- Alkaline leaching--Continued  
 experiment methods, 463-464  
 kaolinite leaching, 467,468-469t,470  
 minerals chemically treated, 463t  
 pyrite leaching, 470t  
 quartz leaching, 465,466f,467  
 removal of ash-farming mineral matter, 462  
 results for a bituminous coal, 464t
- Altered tuffs, definition, 91
- Aluminosilicate complexes  
 formation, 123-124  
 presence in low-rank coals, 123
- Apparent activation energies, coal slag, 228,230t
- Ash analysis  
 inorganic elemental variations, 62-68  
 instrumental methods, 62,63t
- Ash deposit constituents  
 adhesion on austenitic steel, 313,314f  
 adhesion on ferritic steel, 313,314f,315-316  
 adhesion by gravitational forces, 307,309,310f  
 adhesion by surface tension force, 309,311  
 adhesion by van der Waals forces, 307,309,310f  
 adhesive characteristics, 303  
 chemical bonding, 311,313  
 coefficient of thermal expansion, 315t  
 formation of layer structure deposits and slag masses, 316,317f,318  
 mechanical bonding, 311,313
- Ash deposit formation  
 determining factors of growth, 235  
 rate of growth of deposit, 235  
 sintering by viscous flow, 235  
 standard ash fusion test, 234-235
- Ash deposition in boilers  
 coal constituents,292  
 effect of coal properties on furnace size, 282,283f  
 effects of furnace operating conditions, 291  
 erosion of pressure parts, 291  
 fireside corrosion, 290-291  
 impedance to gas flow, 290  
 influencing factors, 291-292  
 physical damage to pressure parts, 290  
 reduced heat transfer, 290  
 superheater deposit buildup vs. flue gas temperature, 292,293f
- Ash deposits  
 deposition process, 6-7  
 thermal properties, 379-382
- Ash-fusion temperatures  
 determination, 103-105
- Ash-fusion temperatures--Continued  
 phase diagram, 103,104f
- Ash oxide analyses  
 advantages, 400,404  
 field combustion tube furnace, 400,401f,404  
 model cyclone furnace, 404,405f
- Ash-softening temperatures, phase diagram, 103,104f
- Authigenic, definition, 41
- Automated image analysis--scanning electron microscopy  
 advantages, 450  
 application, 449-450  
 chemical definitions for mineral phases, 451,452t  
 data handling, 450  
 description of system, 451  
 results for Illinois No. 6 coal, 453-454t,455-456f  
 results for Pittsburgh coal, 454-459  
 sample description and preparation, 450,451t  
 size and mineral phase classification, 452
- B
- Bassanite, formation, 122
- Bench-scale ash behavior predictive techniques  
 analytical data on U.S. coals, 297,299t  
 analytical techniques, 297,300  
 anomalous fouling behavior, 297,299t  
 areas of uncertainty, 300-301  
 effect of segregated iron on coal ash slagging, 297,298f  
 measurement of active alkalis, 297
- Beneficiation  
 changes in equipment, 444  
 chemical coal cleaning, 444  
 dependence on frequency distribution, 438-439  
 froth flotation, 444  
 inadequacies of many analytical methods, 443  
 physical and chemical techniques, 500  
 problems with silica analysis, 444  
 problems with sulfur analysis, 443-444
- Beneficiation feed, composition effects on behavior, 439-440
- Bentonites, definition, 91
- Binary clay mixtures, effect of NaOH and microwave irradiation, 518,519t

- Bituminous coals  
 analytical procedures for ash and sulfur contents, 474  
 chlorine content, 140-141  
 elemental analysis of  
   high-temperature ash, 329,334t  
 extraction of mineral matter, 474  
 inherent water content, 140  
 mineralogical analysis, 445-448  
 mineralogical analysis of  
   low-temperature ash, 329,333t  
 mineralogical and elemental analyses of pulverizer rejects, 329,334t  
 minerals, 444,446t  
 nominal analysis, 474,476t  
 particle-size distribution, 474-475  
 particle-size distribution of  
   low-temperature ash products, 475,476f,477,478f  
 particle-size analysis, 329,335,336t  
 proximate and ultimate analyses, 329,333t
- Blast furnace slags, thermal conductivity values, 269
- Boiler performance  
 effects of coal ash  
   properties, 288-289  
 problems, 289
- Bond work index, grindability of samples, 503-504
- Brown coal  
 application, 394  
 ash analyses and estimated parameters, 400,402-403t  
 ash oxide analyses, 396  
 deposition properties, 394,396  
 influence of different mineral substances on ash  
   deposition, 397,398f  
 intensity of deposition, 396  
 problems, 294  
 regression analyses, 396  
 reserves in Europe, 394,395f  
 slagging and fouling tendency of solid fuels, 397,399f,400  
 statistical predictions of behavior, 400,401f
- C
- Calcite, reactivity, 136  
 Calcium, reactions, 124  
 Calcium acetate, reaction with pyrite, 122  
 Calcium fluoride based slags, thermal conductivity values, 267,268
- Carbon dioxide/water beneficiation system  
 advantages, 502  
 analysis of leached mineral matter and ash, 506t,507  
 breakage rate for treatment grinding systems, 511t  
 comparison of wet and dry grinding, 507,510t  
 condition selection, 504-505  
 effect of ash composition on fusion temperatures, 507,508f  
 effect of carbon dioxide concentration, 504t  
 effect of feed coal size, 507,509t  
 effect of reaction time on ash removal, 507  
 effect of water, 505  
 grinding times, 507,508-509f  
 hydrogen-bonding blocking reagent, 502  
 procedure, 503  
 proximate analysis of treated vs. untreated coal, 505,506t  
 ultimate analysis of ash from treated vs. untreated coal, 505,506t
- Carbonates, description, 356
- Carbonization  
 description, 109  
 radial structure function, 109,110f  
 simulated spectrum vs. XANES spectrum, 109,110f
- Carnegietite, formation, 123
- Catalysts  
 definition, 410  
 example, 410  
 use in petroleum refining, 411
- Char gasification, catalytic effects of mineral matter, 413-414
- Chemical coal cleaning, problems, 444
- Chemical methods of analysis, examples, 21-22
- Chloride minerals  
 distribution, 140  
 formation, 140-141
- Classification by rank, 17,18t
- Clausius-Clapeyron equation, derivation, 218
- Clay minerals  
 changes during alkali treatment, 520  
 changes during microwave irradiation, 520-521  
 contents, 46,47f,48,49t  
 distribution in lower Kittanning coal, 48,49t,50  
 effect of drying in oven, 515  
 extent of metamorphism, 50  
 microwave irradiation, 515  
 origin, 46  
 solubility studies, 514

- Cleaning coal  
 chemical treatment, 8  
 choice of process, 7  
 density separation, 7
- Coal  
 analytical data, 364,365f  
 ASTM classification by rank, 17,18t  
 cleaning, 7  
 coal fields in the United States, 12,14f  
 composition of minerals, 19t,20-21  
 definition, 12,501  
 disruption of the coal matrix, 501  
 fusibility diagrams, 364,366f  
 geological age and rank of deposits, 12,14f  
 structure, 12,13f  
 weathering, 502
- Coalification, diagram, 15,16f
- Combustion, intrinsic rate, 430,431f
- Combustion testing of coal  
 deposit formation on furnace probes, 367,368-370f  
 sintered deposits, 367,371f,372
- Commercial use, problem, 5-6
- Composition of volcanic ash partings  
 primary composition, 92-93  
 secondary composition, 93-94
- Continuous-casting slags, thermal conductivity values, 269,270f
- Conversion processes  
 carbonization, 109,110f  
 gasification, 109,111f,112  
 liquefaction, 108
- Corrosive effects of alkali elements, 12
- Crystallization of ash melts  
 chemical compositions, 236t  
 crystallization behavior, 238,239t  
 crystallization process, 236
- Crystallization of  $\text{CaO-Al}_2\text{O}_3\text{-SiO}_2$ -iron oxide glasses, crystallization behavior, 242,243t
- Crystallization of  $\text{CaO-FeO-Al}_2\text{O}_3\text{-SiO}_2$  glasses, crystallization phases observed vs. predicted, 253,254t
- Crystallization of  $\text{CaO-MgO-Al}_2\text{O}_3\text{-SiO}_2$  glasses, crystallization behavior, 239,241t,242
- Crystallization of coal ash melts  
 deposition potential of ash, 253  
 observed vs. predicted behavior, 248,253t
- Crystallization of iron oxide glasses, crystallization behavior, 245,248t,249-252f
- Crystallization of MgO glasses, crystallization behavior, 245,246-247f
- Crystallization of model compositions of glasses  
 composition of  $\text{CaO-Al}_2\text{O}_3\text{-SiO}_2$  glasses, 237t  
 composition of  $\text{CaO-Al}_2\text{O}_3\text{-SiO}_2$ -iron oxide glasses, 238t  
 composition of  $\text{CaO-MgO-Al}_2\text{O}_3\text{-SiO}_2$  glasses, 237t  
 preparation of glasses, 239
- Crystallization of ternary composition of glasses  
 crystallization behavior, 239,240t  
 equilibrium phase diagram, 242,244f,245
- Crystallization sequence of molten basalt  
 experimental results, 226,227t  
 type formulas for the various mineral series, 226,227t  
 volume percentage of melt as a function of temperature, 226,228,229f
- Cyclone coal combustors, slag composition selection, 171
- D
- Density models  
 additive method, 199,202  
 partial molal volume model, 200,201f,202,203f
- Deposit formation of coals  
 mechanism, 350  
 temperature effects, 350-351
- Deposition of coal ash in hot cyclones  
 borderline of deposition, 322,323f  
 glass model, 320-324  
 mechanism, 321  
 test apparatus, 321,322f  
 viscosity, 324
- Detrital  
 definition, 41b  
 deposition of mineral matter, 17,19t,20
- Devolatilization  
 catalytic effects of calcium minerals, 413  
 description, 413
- Drop-tube furnace  
 deposit buildup mechanism, 336,339  
 deposit mass and buildup rates, 339,341t,345-346t,348t  
 description, 326,327f  
 injector and preheater section, 329,330f  
 photos of ash deposits, 346,349t  
 purpose, 325-326

- Drop-tube furnace--Continued  
 scanning electron photomicrograph of sintered ash deposit, 339,340f  
 scanning electron photomicrograph of iron-rich deposit base particles, 339,342f,344f  
 schematic of the hot zone, 326,328f  
 temperature profiles, 335-336,337f  
 typical ash deposit structure, 336,338f  
 view of the deposit-steel oxide interface perpendicular, 346,347f  
 water-cooled collector probe, 329,332f
- E
- Eastern coals  
 inorganic constituents, 101t  
 Mossbauer spectra of quenched ashes, 103,105,107f  
 reactions 103,104f  
 Electrical conductance measurements  
 description, 151  
 plot, 151,152f  
 Electron microscopy, 22  
 Electron spectroscopy for chemical analysis, 23  
 Electronic conductivity, 261  
 Elemental associations in lignites  
 analyses, 71  
 chemical fractionation, 75  
 correlation of lithologic layering in the vertical distribution of elements, 87  
 correlation with ash content, 81  
 correlation with ionic potential, 82-83t,85  
 direction determination of the chemistry of coal components, 87  
 distribution patterns of inorganic elements, 75,82-83t  
 electron microprobe analysis, 75,81,84f  
 influencing factors, 86  
 inorganic association, 85  
 organic association, 85-86  
 patterns of distribution for Beulah coals, 71-79  
 patterns of distribution for Beulah-Zap bed, 75,80f  
 patterns of elemental variation, 87,88f  
 qualification methods, 71  
 sample collection procedures, 71  
 unclassified elements, 86
- Emissivity  
 comparison to absorptivity, 380,382f  
 nongrayness, 380  
 values, 380,381f
- Emissivity of slags, definition, 211  
 Enthalpy, plot, 206-208,209f  
 Epigenesis of mineral matter, 17,19t,20  
 Extinction coefficient, 261  
 Extraneous mineral matter, definition, 356
- F
- Flame volatile sodium, distribution, 149  
 Forced outage, definition, 6  
 Fouling  
 analysis of deposits, 106,108t  
 definition, 6,11,105,289,354  
 influencing factors, 353  
 role of alkali sulfates, 105-106,108t  
 Framboid, definition, 356  
 Froth flotation, description, 444  
 Furnace performance  
 dependency fo furnace efficiency on furnace dimensions, 376,378f  
 dependency of furnace efficiency on furnace height, 376,378f,379  
 furnace exit temperatures, 385,391f,392  
 influencing factors, 376,377f  
 parameter influencing deposit formation, 404,406f,407
- G
- Gasification  
 catalytic effects of mineral matter, 413-414  
 description, 109,112  
 Mössbauer spectrum of a char residue, 109,111f  
 stages, 413  
 Gehlenite, formation, 123  
 Glasses, thermal conductivity values, 267,272f,274
- H
- Heat capacity, plot, 206-207,208t,209f  
 Heat transfer process, influencing factors, 274  
 Highly ordered binary solutions, thermodynamic analyses, 186-193  
 Hydrogen-bonding system, blocking reagents, 502

## I

- Illite  
 definition, 55-56  
 effect of caustic and microwave irradiation, 517t,518  
 structure, 136
- Illite/mica, distribution, 46,48,49t,50
- Inertinites, definition, 15
- Infrared spectroscopy, 22
- Inherent mineral matter,  
 definition, 15,356,473
- Initial ash deposit constituents  
 alkali-metal sulfate  
 deposition, 304,305f  
 selective, 304,305f
- Inorganic constituents of coal  
 classifications, 41-42  
 clay minerals, 46-50  
 distribution of depositional environments, 43,44f  
 eastern coals, 101t  
 fouling, 105-108  
 inorganic constituents, 101t  
 marcasite, 45  
 methods of analysis, 43  
 origins, 42  
 pyrite, 43,44f  
 quartz, 45-46,47f  
 sampling, 43  
 slagging behavior, 102-105,107  
 western coals, 101
- Inorganic elemental variations  
 ash-related variations, 63f,64f,t,65  
 concentrations of specific elements, 61  
 influencing factors, 61,68  
 rank-related variations, 65t,67f  
 variations due to geochemical factors, 65,66t  
 variations due to geologic factors, 66,67t
- Inorganic species, incorporation into low-rank coals, 114
- Iron sulfide catalysis in liquefaction  
 auger measurements, 418,419t  
 cleavage of oxygen bonds, 420  
 conversion electron Mossbauer spectroscopic measurements 420,421f,422f  
 electron energy loss measurements, 418,419t,420,421t  
 extended X-ray absorption fine structure  
 measurements, 423,426-427f,428  
 interaction with low rank coal, 420,422f,423,424f  
 measurement conditions, 417,418  
 reactivity toward oxygen-containing compounds, 420,421f  
 X-rays absorption near edge structure measurements, 423,425f

## K

- Kaolinite  
 alkaline leaching, 467,468t,470  
 content of the lower Kittanning seam, 46,47f  
 distribution, 48,49t  
 effect of caustic and microwave irradiation, 516t,517  
 presence in low-rank coals, 122  
 structure, 136

## L

- Lignite--See Brown coal
- Lignite-bearing strata, elemental distribution, 70-89
- Liptinite, definition, 15
- Liquefaction  
 activity of coals with catalysts, 412-413  
 description, 108,416  
 influence of iron sulfides, 416-417  
 role of mineral matter, 411  
 role of role of pyrite, 411
- Lithotypes  
 maceral composition, 56t  
 X-ray diffraction analysis, 56,57f,58
- Low-rank coals, X-ray diffractometer pattern sequence, 124-126
- Low-temperature ash  
 effect of illite on thermal behavior, 358,360f  
 effect of silica on volatilization, 358,361
- Low-temperature ashing, 23  
 description, 129  
 energy-dispersive spectra, 133,134f,135f  
 experiments with individual minerals, 131  
 geometric arrangement in heating-stage experiments, 131,132f  
 procedures, 117  
 samples and products, 130t  
 supporting experiments, 133,136t  
 techniques, 3

## M

- Macerals, classification, 501
- Magnetic separation  
 analyses of samples, 486,487t  
 maximum sulfur rejection, 497-498



- Magnetic separation--Continued  
 Mössbauer spectra, 492,494-495f  
 optimum pyrolysis temperature, 497
- Marcasite  
 description, 354  
 quantification, 58
- Marcastle  
 formation, 45  
 occurrence, 45
- Metakaolin, presence in low-rank coals, 122
- Microwave irradiation  
 description of procedure, 515  
 effect on binary mixtures, 518  
 effect on illite, 517t,518  
 effect on kaolinite, 515  
 effect on montmorillonite, 518t  
 effect on ternary clay mixtures, 519,520t  
 reaction path, 521  
 reaction with NaOH solutions at room temperature, 515
- Mineral analysis  
 mineralogical methods, 22-23  
 sampling procedures, 21
- Mineral composition of low-rank coals  
 phases, 117,120-121t  
 X-ray diffraction, 117,120-121t  
 X-ray fluorescence analysis, 116t,117
- Mineral matter  
 behavior during alkaline leaching, 470-471  
 catalyst, 7  
 catalyst system, 411  
 cations, 4  
 characteristics, 1  
 characterization, 11,364,449  
 classifications, 354  
 coarse coal sorting, 441  
 comparisons in other U.S. coals, 30-35  
 components, 90  
 definition, 10,356  
 effects of heating process, 3-4  
 elements, 2  
 environmental pollution, 12  
 fate during combustion, 356,357f,358  
 fine coal sorting, 441-442  
 geological dependence, 3  
 geological studies of distribution, 12  
 groups, 356,440,501  
 hydrogen bonding, 501  
 identification techniques, 3,130  
 initial set of particles, 440-441  
 instrumental procedures, 440  
 interfaces with coal, 477,479  
 low-temperature ashing, 129  
 mineral contents, 30,31t,32  
 minor elements, 32,33f,34t  
 nature, 2
- Mineral matter--Continued  
 origin, 17,19t,20  
 phase transformations, 358,359f  
 physical differences  
 between inherent and extraneous ash, 356  
 physical removal, 440  
 primary crushing, 441  
 problems, 11-12  
 removal by swelling and bond breaking, 501-502  
 removal from coal, 7-8  
 result of geologic events, 440  
 samples and analysis, 129t  
 specific responses during processing, 440  
 structure, 140,143f  
 trace elements, 35,36t  
 undesirable effects, 128  
 variation in Illinois basin coals, 23-30  
 water circuit, 442
- Mineral variation  
 benches of the Herrin (no. 6) coal, 23,24-25f,26  
 channel samples from the Herrin, Springfield coals, 26,27-28t,29f  
 coal seams in the Illinois basin, 30,33f
- Mineralogical analysis of bituminous coals  
 future impact, 445  
 minerals washability diagram, 445,447  
 recovery after cleaning, 445,448t  
 sampling procedures, 445
- Mineralogical methods of analysis  
 electron microscopy, 22  
 electron spectroscopy for chemical analysis, 23  
 infrared spectroscopy, 22-23  
 low-temperature ashing, 23  
 Mössbauer spectroscopy, 23  
 thermal analysis, 22  
 X-ray diffraction, 22
- Minerals in coal, 53,54t
- Mineral analysis, chemical methods, 21-22
- Models of slags surface tension  
 addition of the partial molar contributions, 202,203f  
 addition of partial molar contributions with surface-active component, 202,203f,204,205f  
 assessment of the model, 204,206  
 surface tension for non-surface-active constituents, 204t  
 surface tension for surface-active constituents, 204t
- Mold fluxes  
 description, 215

- Mold fluxes--Continued  
 uses, 215  
 viscosity, 215,222
- Molten basalt  
 apparent activation  
 energies, 228,230t  
 crystallization sequence, 224,229f  
 starting material, 224
- Molten coal ash systems, behavior, 4-5
- Montmorillonite,  
 effect of caustic and  
 microwave irradiation, 518t  
 structure, 136
- Mössbauer spectroscopy, 23
- Mullite, structure, 146f,147
- N
- Nepheline, formation, 123
- Non-steady-state methods for thermal  
 conductivity  
 laser pulse method, 262-263  
 line source method, 263  
 modulated beam method, 262  
 radial wave method, 262
- O
- Oldhamite, formation, 137
- Opposed pulverized fuel fired boiler  
 influence of effective conduction  
 coefficient on exit  
 temperatures, 385,390f  
 temperature profiles, 385,390f
- P
- Petrographic examination, 3
- Physicochemical property estimation for  
 slags  
 density, 199-202  
 melting range, 196-197  
 surface tension, 202-206  
 viscosity, 197-199
- Plant feed characterization  
 assumptions, 439  
 feed hardness or friability, 439  
 laboratory floatability studies, 439  
 particle gravity distribution, 439  
 particle size distribution, 439
- Potassium oxide, amounts in bituminous  
 coal mineral matter, 139
- Potassium sulfate, formation, 149
- Power generation,  
 magnetohydrodynamic, 5
- Product coal  
 ash content, 479,480f  
 ash contents vs. mode of particle-  
 size distribution, 481,483f  
 effect of chemical additives on  
 particle-size distribution, 477  
 interface with coal, 477  
 particle-size distribution of  
 low-temperature  
 ash, 477,449,480f,482t
- Promoter, definition, 410
- Pulverize fuel ash  
 structure, 141,142f  
 temperature vs. time plot, 142,145f
- Pyrite  
 alkaline leaching, 470t  
 content of the lower Kittanning  
 seam, 43,44f  
 decomposition, 361,362f,486  
 factors influencing  
 distribution, 43,45  
 factors influencing thermal  
 behavior, 361,364  
 formation, 45  
 forms, 56  
 heating under reducing  
 conditions, 361,363f  
 magnetic separation, 486  
 oxidation, 122  
 principal forms, 354,356  
 quantification, 56,58  
 reactivity, 136-137  
 role as catalyst in coal  
 liquefaction, 411-413  
 thermogravimetric analysis, 361
- Pyrite decomposition  
 atomic ratio vs. distance from  
 interface, 487,488f  
 kinetic models, 492  
 scanning electron  
 micrographs, 492,496f
- Pyrolysis  
 description, 485  
 Mossbauer spectroscopy, 487,489-491f  
 sulfur reduction vs.  
 temperature, 492,493f  
 sulfur transfer, 492,497
- Q
- Quantification by X-ray diffraction,  
 minerals in coals, 55-58
- Quartz  
 alkaline leaching, 465,466f,467  
 content of the Kittanning

- Quartz--Continued  
 seam, 45,47f  
 origin, 45,46
- Quasi-chemical theory  
 asymmetric approximation, 188-189  
 distribution of bonds, 188  
 excess free energy of mixing, 187-189  
 number of bonds, 187
- R
- Radiation conductivity  
 calculation, 257-258  
 mechanism, 257
- Rate of char combustion  
 effect of metals, 433t,434f  
 effect of sodium, 435f  
 effects of mineral  
 matter, 431,433,434f  
 influence on boiler  
 performance, 430,432t
- Raw coals  
 inorganic analysis, 115,116f  
 model mixtures of inorganic  
 compounds, 115,118-119t
- Rocks and minerals, thermal  
 conductivity values, 269,270f
- S
- Seams  
 mineral occurrences, 17,19t  
 origin, 15
- Shale, description, 354
- Silica, amounts in bituminous coal  
 mineral matter, 138,139t
- Silica minerals  
 coalescence products of ash in  
 flame, 147,148f,149  
 diagnostic features of flame-heated  
 ash, 142,156f  
 hydrofluoric acid  
 treatment, 142,146f,147  
 spherical shape  
 transformation, 142,144f  
 surface force tension, 141  
 viscosities for  
 spheridization, 141,142t  
 vitrification and  
 recrystallization, 147t
- Silicate, molar free energy of  
 mixing, 187
- Silicate mineral species, amounts in  
 bituminous coal mineral  
 matter, 138,139t
- Silicate particle, structure of surface  
 fused, 142,143f
- Silicates, correlation of thermodynamic  
 properties, 192
- Sintered ash deposits,  
 formation, 151,153
- Slag system  
 constituent system, 279,280t  
 potassium vapor pressure, 279,282f  
 representation of solid-liquid-vapor  
 equilibria, 279,281  
 subsolidus phase relations, 279,282f
- Slagging  
 definition, 11  
 influencing factors, 353  
 pilot plant slagging and fouling  
 combustor, 354,355f
- Slags  
 absorption spectra, 264,265f  
 additive, 171,172t  
 ash composition, 171,172t  
 definition, 289,354  
 desulfurization ability, 178  
 experimental conductivity  
 measurements, 271,273t  
 heat transfer model, 256-257  
 normalized compositions, 171,172t  
 phase equilibria, 278-281  
 physicochemical properties, 195-211  
 preparation, 174  
 properties, 196  
 seven-component system, 279,280t  
 sulfide capacities, 171,174  
 thermal  
 conductivities, 264,265-266f,267  
 thermal conductivity  
 values, 271,272f,274
- Sodium-enhanced sintering  
 electrical conductance  
 measurements, 151,152f  
 mechanism, 149-150  
 rate, 150-151  
 results from reaction between sodium  
 sulfate and silicates, 150t,151
- Solid-liquid-vapor equilibria of coal  
 slags, role for polymerization  
 theory, 281
- Solid-liquid-vapor interactions of  
 alkali-rich coal slags  
 high-temperature differential  
 thermal-thermogravimetric  
 method, 277-278  
 high-temperature quenching  
 method, 277  
 Rnuden effusion mass spectrometric  
 method, 277-278
- Solution model for the prediction of  
 alkali vapor pressures  
 application to  $K_2O$ -CaO- $Al_2O_3$ - $SiO_2$   
 system, 284,285f  
 basis of the model, 281-282

Solution model for the prediction of alkali vapor pressures--Continued  
 method of calculation, 284

Steady-state methods for thermal conductivity  
 linear heat flow method, 261-262  
 radial heat flow method, 262

Sticking test  
 application, 326  
 disadvantages, 326

Subbituminous coals  
 mineralogical and elemental analysis, 329,335t  
 particle-size analysis, 329,335,336t  
 proximate and ultimate analyses, 329,333t

Sulfates  
 miscibility of potassium sulfate-silicate system, 306-307,308f  
 miscibility of sodium sulfate-sodium silicate system, 306  
 thermal stability, 304,306

Sulfide capacity measurements of slags  
 additive effect, 178-179  
 capacities as a function of basicity, 174,177f,178  
 capacity vs. temperature, 179  
 comparison to other results, 179,181f  
 phases, 174,178  
 reactor, 174,175f  
 sulfur emission estimation from cyclone combustor, 179-182  
 ternary phase diagrams, 174,175f,177f  
 values, 174,177f,178

Sulfur emissions from a cyclone combustor  
 calculation, 180  
 sulfur removal, 180,181f,182

Sulfur minerals, constituents, 354

Sulfur removal  
 combustion kinetics effects, 180,182  
 hydrogen concentration effects, 180  
 plot, 180,181f  
 temperature effects, 180

Surface tension force, definition, 141

Syngeneses of mineral matter, subclasses, 17,19t,20

Synthetic coal ash slags  
 activation energies and temperature ranges, 165,166t,167  
 composition, 157,158t  
 difficulties in interpretation of viscosity-temperature behavior, 167-168  
 ionic potential, 165  
 logarithm of a rate constant vs. the reciprocal of the absolute temperature, 159,161f  
 logarithm of reciprocal viscosity vs. reciprocal temperature, 159,162-164f,165

Synthetic coal ash slags--Continued  
 logarithm of viscosity vs. temperature, 159  
 mole fractions of constituents, 166t,167  
 preparation, 157  
 viscometer for viscosity measurements, 157-158  
 viscosity behavior vs. composition, 159,165,167  
 viscosity vs. chemical composition, 156-168  
 viscosity measurements, 157-158  
 viscosity vs. temperature, 159,160f

## T

Tangentially coal-fired boiler  
 geometry and zoning, 383,384f  
 thermal performance for various slagging and fouling conditions, 385,386t,387-389t

Tephra, definition, 91

Ternary clay mixtures, effect of NaOH and microwave irradiation, 519,520t

Thermal analyses, 22

Thermal conduction mechanisms  
 absorption coefficient, 250  
 dependence of thickness of specimen, 257,259f  
 electron conductivity, 261  
 extinction coefficient, 261  
 radiation conductivity, 257-258  
 thermal phonon conductivity, 257  
 total thermal conductivity, 261

Thermal conductivity  
 experimental methods, 261-264  
 indirect measurements, 263

Thermal conductivity of ash deposits  
 comparison to sintered and fused deposits, 379  
 factors, 379  
 values, 379,381f

Thermal conductivity in slags, determination, 208,210

Thermal phonon conductivity, 257

Thermal properties of ash deposits  
 emissivity, 380,381f  
 thermal conductivity, 379,381f

Thermal properties of coal slags  
 absorption coefficient, 210  
 enthalpy, 206-209  
 heat capacity, 206-209  
 thermal conductivity, 208,210

Thermodynamic analyses  
 activities of FeO in binary system, 189,190f

Thermodynamic analyses--Continued  
 activities of FeO in ternary system, 189,191f,192  
 calculated phase diagram of the FeO-SiO<sub>2</sub> system, 189,190f  
 systems analyzed, 189t  
 Titanium peroxide based slags,  
 thermal conductivity values, 267  
 Tonsteins, definition, 91  
 Total thermal conductivity, 261  
 Trace elements, definitions, 61  
 Traditional ash behavior predictive techniques  
 ash viscosity measurements, 294  
 base/acid ratios, 294,296  
 composition of ash deposits and as-fired coal ashes, 294,295t  
 fusibility temperature measurement technique, 294,295t  
 sintering strength tests, 296  
 slagging and fouling indices, 296  
 Tuff, definition, 91

## V

Viscosity  
 definition, 216  
 influencing factors, 226  
 Viscosity determination of basalts  
 apparent viscosity, 230,231f,232t  
 calibration measurements, 225  
 experimental conditions, 225  
 flow curve, 228,229f  
 isothermal run, 225-226  
 log viscosity vs. log shear rate, 228, 229f  
 polythermal exploratory runs, 225-226  
 torque vs. rotational speed, 228  
 Viscosity of fluxes  
 Andrade-Arrhenius equation, 218,220,221t,222  
 compositional effects, 216  
 composition, 218,219t

Viscosity of fluxes--Continued  
 Kirchoff-Rankine equation, 218,220,222t  
 network-forming cation and anion effects, 216,217f  
 regression analysis, 218,220,221t,222  
 silica and alumina content effect, 216  
 temperature effects, 216,217f  
 summary of viscosities, 218,220t  
 Viscosity models  
 modification of Urbain's model, 198-199  
 Riboud's model, 197-199  
 Urbain's model, 198t,199  
 Vitrinite, definition, 15  
 Volcanic ash  
 origin, 91-92  
 composition, 90,91  
 Volcanic ash partings  
 composition, 92-94  
 definition, 91  
 distribution, 95-95,96f  
 field appearance, 92,96f  
 geological importance, 95,97

## W

Western coals, inorganic constituents, 101,102t  
 Wet milling, products, 477-478

## X

X-ray diffraction  
 description, 3,22,55  
 problems, 55-59  
 X-ray diffraction analysis  
 round-robin analysis, 59t  
 sample preparation and mounting, 58